

N. V. Churaev · B.V. Derjaguin
V.M. Muller

Surface Forces

SURFACE FORCES

SURFACE FORCES

**B. V. Derjaguin
N. V. Churaev**

and

V. M. Muller

Institute of Physical Chemistry
Academy of Sciences of the USSR
Moscow, USSR

Translated from Russian by

V. I. Kisín

Translation Edited by

J. A. Kitchener

SPRINGER SCIENCE+BUSINESS MEDIA, LLC

Library of Congress Cataloging in Publication Data

Derjaguin, Boris Vladimirovich.
Surface forces.

Translation of: Poverkhnostnye sily.

"Institute of Physical Chemistry, Academy of Sciences of the USSR,
Moscow, USSR."

Includes bibliographies and index.

1. Surface chemistry. I. Churaev, N. V. (Nickolai Vladimirovich) II.
Muller, V. M. (Vladimir Makovich) III. Kitchener, J. A. IV. Title.

QD506.D4213 1987 541.3'453 87-13599

ISBN 978-1-4757-6641-7 ISBN 978-1-4757-6639-4 (eBook)

DOI 10.1007/978-1-4757-6639-4

This volume is published under an agreement with the
Copyright Agency of the USSR (VAAP)

© 1987 Springer Science+Business Media New York
Originally published by Plenum Publishing Corporation, New York in 1987

All rights reserved

No part of this book may be reproduced, stored in a retrieval system, or transmitted
in any form or by any means, electronic, mechanical, photocopying, microfilming,
recording, or otherwise, without written permission from the Publisher

PREFACE

This monograph is devoted to long-range surface forces significant far beyond a single monolayer and felt over tens or even hundreds of molecular layers adjacent to an interface. The transition from the concept of short-range effects that reigned earlier to the concept of long-range forces simultaneously signified the transition from a two-dimensional world to a three-dimensional one, incomparably richer in physicochemical phenomena. This transition took many years and evolved through many steps. It began with the Gouy-Chapman theory of diffuse ionic atmospheres, which together with London's theory of molecular forces was used as a basis for the development (beginning in 1937) of the DLVO theory of stability of lyophobic colloids. Further elaboration of the theory involved the introduction of new types of force, and a generalization (in 1954) to the case of interaction between unlike particles (heterocoagulation). This theory is fundamental in such large-scale practical problems as flotation, water treatment, dyeing, soil science, microbiology, and interaction between biological cells.

This book is the first comprehensive monograph devoted to surface forces. This fact makes it easier to attract the reader's interest; yet, the reader's demands become all the more difficult to satisfy completely. Indeed, the research that we review and analyze here covers about 50 years of work. Much data has been amassed, so that the main problem was a careful selection and analysis. Fortunately, many aspects have been recently clarified, so that we were able, and felt entitled, to make a responsible selection of the most important topics.

Surface forces at interfaces are analyzed first, and then the thermodynamic properties of thin interlayers in which the fields

of long-range forces overlap and disjoining pressure is generated. This case is not covered in the classical work of Gibbs, who developed the thermodynamics of transition layers at the interfaces of bulk phases.

Both theoretical and experimental studies are treated, generalizing the results obtained both in the USSR and abroad. However, the theory of surface forces is treated preferentially, because the approach we elaborate here, constituting the basis of the modern physical chemistry of surface phenomena and disperse systems, cannot be practically applied without a clearly understood theoretical basis.

Special attention is paid to the properties of boundary layers of polar liquids. The obvious reason for this preference is the introduction of the structural component of disjoining pressure, resulting from the overlap of boundary layers whose structure is modified in comparison with that of the bulk liquid. The study of the specific behavior of boundary layers and of structural forces has been especially active during the last decade, when it has been understood that these phenomena are decisive factors in lyophilic colloids and films of polar liquids. Correspondingly, we give a brief exposition of the liquid-crystal state of boundary layers in certain nonmesogenic liquids, such as nitrobenzene.

The problem of steric forces that appear when the adsorption layers of surfactants and polymers overlap is not treated here, but not because steric effects in colloidal systems and films are insignificant — both theoretical and experimental research is quite intensive in this field — but rather because the problem has no relation to the concept of long-range surface forces that constitute the core of our monograph. The original publications and reviews by Hesselink, Napper, Lyklema, Sonntag, Klein, and some other well-known scientists who actively contribute to this field will give a good idea of the current status of this problem.

Both the static and the kinetic aspects of surface forces are discussed. Transport processes in microporous bodies and thin liquid films are treated in terms of nonequilibrium thermodynamics. Here surface forces lead to new kinetic effects — such as capillary osmosis, reverse osmosis, and diffusiophoresis — that are essential for a number of industrial processes. A joint analysis of heat and mass transfer processes has made it possible to develop both the theory of thermo-osmosis and the theory of thermocrystallization flow in nonfreezing interlayers and water films in frozen porous materials. The latter theory explains the effects of frost heaving of soil and frost cracking of porous materials.

Several important applications of the theory of surface forces are not discussed here because relevant books have been recently

published: B. V. Derjaguin and S. S. Dukhin, Electrokinetic Phenomena, Surface and Colloid Science, Vol. 7, Wiley, New York (1974); B. V. Derjaguin, N. A. Krotova, and V. P. Smilga, Adhesion of Solids, Consultants Bureau, New York (1978); P. M. Kruglyakov and Yu. G. Rovin, Physical Chemistry of Hydrocarbon Films, Nauka, Moscow (1978); B. V. Derjaguin and N. V. Churaev, Wetting Films, Nauka, Moscow (1984).

Linear tension, predicted by Gibbs and recently rejuvenated as a field of research, is another subject not reflected in our monograph. Fundamental work in this field is being carried out successfully in Bulgaria by A. D. Scheludko and his co-workers. The main results of these studies are presented in Scheludko's revised monograph Colloid Chemistry [Mir, Moscow (1984)].

Offering now the reader this first attempt at systematizing and summarizing the results of studying long-range surface forces, the authors will be grateful for critical comments and suggestions, and will take them into account later.

In conclusion, we wish to express our deepest gratitude to the colleagues and co-workers whose active participation in the theoretical and experimental studies of surface forces made the writing of this book possible.

Chapters 2 and 3 were written by B. V. Derjaguin. Chapters 4, 5, 7, 10, and 11 were written by N. V. Churaev and B. V. Derjaguin. Chapters 1, 6, 8, and 9 were written by B. V. Derjaguin and V. M. Muller.

B. V. Derjaguin

**FOREWORD
TO THE
ENGLISH EDITION**

Specialists in the chemistry and physics of interfaces need no introduction to the name of B. V. Derjaguin, for he is unquestionably the world's foremost colloid scientist. His numerous, varied, and highly original contributions have inspired many important developments. Yet the sheer versatility of his genius only becomes evident as these contributions are brought together in an integrated record of his researches. A glance at the table of contents of this book will show that Professor Derjaguin and his colleagues at the Institute of Physical Chemistry in Moscow have now written a unique and wide-ranging monograph about their special field. It must surely become a classic.

On the other hand, colloid science is still shamefully neglected in many academic departments of chemistry and physics, despite its great practical importance. Fortunately, there are now signs of a surging interest from many other quarters, including chemical engineering and biology. Journals of interface science are flourishing, with new work coming from a wide range of disciplines. For newcomers to this eminently interdisciplinary field of study, therefore, a brief explanation of the history of "surface forces" may be of interest, especially as the term is not yet to be found in traditional textbooks!

The physical chemistry of surfaces is often treated in elementary textbooks as deriving from the classical work of Langmuir and others on spread monolayers on water and partial monolayers of gases adsorbed on metals. Both phenomena seemed to indicate intermolecular forces of very short range. However, various observations gradually came to light that appeared more consistent with the idea of long-range effects of surfaces. By 1949 Henniker

was able to review a substantial body of evidence on "the effective depth of surfaces" (Rev. Mod. Phys., 21, 322). Yet much of it could still be dismissed by skeptics as circumstantial rather than proved. (Indeed, certain attempts to check some of Derjaguin's pioneering results were negative, though actually faulty.) The position was well stated by McBain in his textbook of "Colloid Science" (1950):

"One of the fundamental problems of science is to establish the effective ranges of molecular attractions. The classical physicists of the 19th century considered that there were direct forces of attraction over distances ... up to many microns. During the first decades of the 20th century, however, the recognition of the electrical structure of matter influenced scientific opinion to assume, without new evidence, that the direct range of molecular attraction amounted to only a few angstrom units; and an extreme view, under the influence of Langmuir, held that not adjacent molecules but only their adjacent atoms had any important influence upon each other. A third point of view recognizes the short range of direct attraction but considers that it must be relayed from molecule to neighboring molecule through impressive distances. The conflicting consequences of these beliefs are of the greatest importance."

Ever since 1932 and his first publication* on surface effects (yes, 53 years ago!) the Russian chemical physicist B. V. Derjaguin has been adamant in maintaining that solid surfaces can substantially modify the properties of liquids in contact with them. He has been tireless in devising ingenious new techniques for demonstrating and measuring the range of action of surfaces.

But how can one set about measuring, say, the minute forces that keep particles in stable colloidal dispersions from coagulating — or those that cause the same particles, when destabilized, to clump together? The key to this problem was given in a brilliant theoretical paper in 1934 (Kolloid-Z., 69, 155), which also provided the basis for much of the extraordinarily fruitful re-

*The 1932 paper was an experimental study of thin water layers between glass surfaces. It was followed by measurements of the friction between mica plates in various liquids. In 1935 a paper (written with Churaev) entitled "Inclusion of structural forces in the theory of stability of colloids and films" sets out the latest theoretical treatment of data for water films on glass, mica, and quartz. Between these dates lie several hundred Derjaguin publications dealing with many subjects besides surface forces.

searches of Derjaguin and his co-workers in the Laboratory of Surface Phenomena of the Institute of Physical Chemistry (Academy of Sciences of the USSR, Moscow). This paper showed that if there really are surface effects that extend to distances large compared with molecular radii (though still small compared with macroscopic objects), then it is possible to calculate shape factors for interactions of bodies of different geometry or size (such as sphere-sphere, plate-plate, sphere-plate, cylinder-cylinder). This meant that if measurements could be made with, say, macroscopic parallel plates, one could then calculate the forces of interaction of microscopic spheres or the adhesion of small particles to a plate, etc. Above all, a whole series of colloidal phenomena thus became related through the concept of forces of interaction between interfaces as they approach one another.

At first, such interactions were discussed in terms of the excess energy as a function of the separation of the interfaces. But by 1936 it was found more convenient to standardize the theory in terms of a force per unit area (for parallel planes) which was subsequently termed the "disjoining pressure." The physical concept is particularly clear for soap films, where the disjoining pressure can lead to the formation of equilibrium lamellae (as Derjaguin and Titiyevskaya proved in 1953), or to equilibrium "wetting films," as when a bubble of gas is pressed against a lyophilic plate in a liquid which does not form a contact angle (Derjaguin and Kus-sakov, 1939). On the other hand, interactions between interfaces are not always repulsive in character. In certain systems an attraction arises, corresponding to a "negative disjoining pressure." For example, a free film of any pure liquid is inherently unstable (because of dispersion forces) and collapses spontaneously. Another clear case is parallel solid plates in gas or vacuum; they are mutually attracted. The first successful measurements of this attraction were made by Derjaguin and Abrikossova in 1951 by an elegant new microbalance technique. These — and many other — consequences of the substantial "thickness" of interfaces are described in detail in this book.

Probably the best known achievement of all these researches is the modern theory of stability of lyophobic colloids. The qualitative principles were proposed in the 1930s. Derjaguin and Landau published their successful solution of the mathematical problem in the journal Acta Physicochim. URSS in 1941; but because of the War this paper was never received abroad. In the occupied Netherlands, Verwey and Overbeek solved the same problem independently by a slightly different route. Their substantially equivalent results were published in Trans. Faraday Soc. in 1946. Hence the theory is universally denoted "DLVO."

The present book is by no means simply a history of researches on surface forces throughout the world, though, in fact, it does

admirably set them in historical perspective right up to the present year. The form of presentation is essentially a logical unification of the whole field through a theoretical framework. The mathematical developments are outlined concisely throughout the book. The individual chapters take the form of self-contained reviews of their subjects, with crosslinks to the other chapters and slight overlap sometimes in material, which makes for convenient study.

For many years I personally have followed with admiration many of the pioneering researches of Derjaguin and his colleagues because they threw new light on my own interests in colloid stability, flocculation, and flotation. Consequently, I count it a privilege to have been invited to edit the translated edition of "Surface Forces." In the event, my contribution has only been to ensure that the text was as acceptable as possible for English-reading scientists of the world.

J. A. Kitchener
Imperial College, London
September 1985

NOTE ON THE RUSSIAN REFERENCES

For brevity, many of the Russian journal references cited in this book are given in short forms, as used by the authors. Several that appear frequently are identified more fully below; those currently available in cover-to-cover English translation are marked by an asterisk.

It seems hardly necessary to state, after references to monographs, that those published in the USSR are in Russian only. Where, exceptionally, an English translation is available — as with the classic monograph of Landau and Lifshitz — that will be obvious from its quoted place of publication.

One series of particular importance for the present book is Research in Surface Forces — a set of five collections of conference papers. These have been edited by D. V. Derjaguin (Deryagin) and published in English by Consultants Bureau, New York. In this book, page numbers of papers in this series refer to the English version.

Note that throughout this book the name of the distinguished senior author Professor Б. В. Дерягин is spelled in the form he prefers and has used for 50 years, viz., "B. V. Derjaguin." However, other spellings occur in the literature — notably, "Deryagin" (which incidentally approximates better to a phonetic pronunciation for English speakers).

AbbreviationFull title of journal

Dokl. Akad. Nauk SSSR*

Doklady Akademii Nauk SSSR (i.e., Proceedings of the Academy of Sciences of the USSR). English translations of the various sections of the Doklady are available, including Chemistry, Physical Chemistry, Physics.

Izv. Akad. Nauk SSSR,
Ser. Khim.*

Izvestiya Akademii Nauk SSSR, Seriya Khimicheskaya (i.e., Bulletin of the Academy of Sciences of the USSR, Division of Chemical Science). Similarly, Ser. Fiz.* is the Physical Sciences series.

Kolloidn. Zh.*

Kolloidnyi Zhurnal (i.e., Colloid Journal)

Usp. Fiz. Nauk

Uspekhi Fizicheskikh Nauk (i.e., Advances in Physical Science)

Usp. Khim.

Uspekhi Khimii (i.e., Advances in Chemistry)

Zh. Eksp. Teor. Fiz.*

Zhurnal Eksperimental'noi i Teoreticheskoi Fiziki (i.e., Journal of Experimental and Theoretical Physics)

Zh. Fiz. Khim.

Zhurnal Fizicheskoi Khimii (i.e., Journal of Physical Chemistry)

J. A. Kitchener

CONTENTS

Chapter 1. FORCES NEAR INTERFACES	1
Introduction	1
1.1. Molecular and Electric Forces in Interfacial Layers	4
1.2. Formation and Structure of Electrical Double Layers	8
1.3. Diffuse Part of the EDL. The Poisson-Boltzmann Equation	9
1.4. The Debye-Hückel Equation. Relation between Surface Potential and Surface Charge	12
1.5. Planar Double Layer. Some Exact Solutions of the General Poisson-Boltzmann Equation	13
1.6. More Complex Situations: Curved Surface, and Discreteness of Surface Charge	15
1.7. Adsorption of Ions in the Stern Layer	16
1.8. Charging of Surfaces by Dissociation of Ionogenic Groups	18
1.9. Testing of Models of Ionized Surfaces	18
References	19
Chapter 2. DISJOINING PRESSURE	25
2.1. Two Kinds of Surface Force	25
2.2. Definition of Disjoining Pressure	27

2.3.	Relationship between Disjoining Pressure and Other Thermodynamic Functions	31
2.4.	Pressure Distribution in the Interfacial Transition Zone	33
2.5.	Refinement of the Definition of Disjoining Pressure	36
2.6.	Equilibrium of Films under Gravity	40
2.7.	Hydrodynamics of Thin Films	44
2.8.	Thermodynamic Theory of Interaction between Bodies with Curved Surfaces	46
	References	51
Chapter 3.	THE THERMODYNAMIC THEORY OF STABILITY OF THIN FILMS	53
3.1.	Stability and Equilibrium of Interlayers between Parallel Plates	53
3.2.	Stability of Interlayers between Convex Bodies	55
3.3.	Stability of Wetting Films	57
3.4.	Stability of Interlayers between Two Identical Fluids	59
	References	83
Chapter 4.	DISPERSION FORCES IN THIN INTERLAYERS AND FILMS	85
4.1.	Historical Background of the Theory of Intermolecular Forces	85
4.2.	Direct Measurements of Molecular Attraction between Two Solids	88
4.3.	Experimental Results	93
4.4.	The Theory of Molecular Attraction between Macroscopic Objects	98
4.4.1.	Calculation of the Interaction be- tween Macroscopic Objects by Summing the Interactions between Micro- objects	98
4.4.2.	E. M. Lifshitz's Macroscopic Theory of Molecular Attraction between Con- densed-State Bodies	100

4.5.	Comparison of the Results of Early Experiments with the Theory	106
4.5.1.	Comparison with the Results of Calculations Carried Out by the Method of Summation of All Pairwise Molecular Interactions	106
4.5.2.	Comparison with the Macroscopic Theory of Molecular Attraction	106
4.6.	Current Status of the Macroscopic Theory of Molecular Forces	109
4.7.	Main Results of the Experimental Verification of the Theory of Molecular Interaction between Macroscopic Bodies	128
	References	146
Chapter 5.	THE ADSORPTION COMPONENT OF DISJOINING PRESSURE IN NONIONIC SOLUTIONS	151
	References	171
Chapter 6.	THE ELECTROSTATIC COMPONENT OF DISJOINING PRESSURE	173
6.1.	Methods of Calculation of Disjoining Pressure Π_e	173
6.2.	Interaction between Identical Layers. Boundary Conditions	179
6.3.	Interaction at Constant Charge or at Constant Surface Potential	181
6.4.	Interaction between Double Layers in Asymmetrical Electrolytes	183
6.5.	Some Approximate Formulas for Disjoining Pressure	185
6.6.	Gibbs Free Energy of the Interaction between Flat Double Layers under Different Boundary Conditions	189
6.7.	Interaction between Charged Spherical Particles	193
6.8.	Interaction between Unequally Charged Surfaces	198
6.9.	Effect of Discreteness of Surface Charge . .	210
6.10.	Disjoining Pressure in a Thin Free Film . .	218

6.11.	Experimental Verification of the Theory of Electrostatic Interaction	222
	References	228
Chapter 7.	THE STRUCTURE OF BOUNDARY LAYERS OF LIQUIDS AND THE STRUCTURAL COMPONENT OF DISJOINING PRESSURE	231
7.1.	Structural Changes in Thin Interlayers and Boundary Layers of Water	232
7.2.	Boundary Layers with Liquid-Crystal Struc- ture	244
7.3.	Boundary Layers of Nonpolar Liquids	252
7.4.	The Study of Boundary Layers of Liquids by the Blow-Off Technique	253
7.5.	Theory of the Structural Component of Dis- joining Pressure	264
7.6.	Experimental Isotherms of the Structural Component of Disjoining Pressure	271
	References	283
Chapter 8.	THE DERJAGUIN-LANDAU-VERWEY-OVERBEEK (DLVO) THEORY OF STABILITY OF LYOPHOBIC COLLOIDS .	293
8.1.	Effects of Electrolytes on Lyophobic Colloids	293
8.2.	Kinetics of Coagulation of Lyophobic Colloids	296
8.3.	Coagulation Criteria	297
8.4.	Exact Solution	300
8.5.	Effect of Charging Mechanism	302
8.6.	Further Development and Verification of the DLVO Theory	305
	References	308
Chapter 9.	THE THEORY OF HETEROFOAGULATION IN LYOPHOBIC SYSTEMS	311
9.1.	Destabilization Criteria for Heterodisper- sions with a Positive Hamaker Constant . . .	312
9.2.	Destabilization Criteria for Dispersions with a Negative Hamaker Constant	319
9.3.	Development and Verification of the Theory .	323
	References	325

CONTENTS	xix
Chapter 10. WETTING FILMS	327
10.1. Disjoining Pressure of Wetting Films	327
10.2. Experimental Methods of Determining the Disjoining Pressure Isotherms of Wetting Films.	330
10.3. Disjoining Pressure Isotherms of Wetting Films Formed by Various Liquids	338
10.4. Wetting Films on Nonflat Surfaces	359
References	364
Chapter 11. SURFACE FORCES IN TRANSPORT PHENOMENA	369
11.1. Capillary Osmosis	369
11.2. Reverse Osmosis	380
11.3. Diffusiophoresis	388
11.4. Thermo-osmosis, the Mechanocaloric Effect, and Thermophoresis	390
11.5. Thermocrystallization Flow in Thin Non-freezing interlayers	409
References	427
Conclusion	433
Index	435

Chapter 1

FORCES NEAR INTERFACES

INTRODUCTION

A monograph devoted to surface forces must begin with an explanation of what is meant by this term. We start by discussing the "micro-forces" acting on individual molecules and ions near interfaces. However, this notion remains vague unless micro-forces are averaged over a sufficiently long time for a certain fixed distance from the interface. In this way we obtain a macroscopic description of surface forces. Such a description forms the basis of the interpretation of surface tension and capillarity both in the older approach of Clairaut (1743) and Laplace (1806) and in the newer approach of Bakker (1928), based on introducing the pressure tensor in the interfacial region.

Consequently, we shall begin with remarks on the definition of interfacial energy at a boundary separating distinct phases. Next we pass to analyzing surface forces in the interfacial region. Then we take up a more complex case, viz., the situation in which two interfaces are so close to each other that their interfacial zones overlap. Attempts to treat this case in a systematic manner have been made only during the last 50 years. The subject is important; without an understanding of it many phenomena, such as the kinetics and dynamics of disperse and colloid systems (their stability and coagulation, peptization, structure formation, swelling, etc.) cannot be scientifically explained. A development of the relevant theory requires a thorough investigation of surface forces, of their specific features, and of the effects they produce. Particular attention is paid, for this reason, to the "disjoining pressure" of thin interlayers and films appearing when interfacial zones

overlap, and to the various components of this pressure, giving rise to different types of surface force.

The main body of the monograph is, therefore, devoted to studying the surface forces acting in the zones of overlapping interfacial regions, i.e., in the very thin interlayers and films that were excluded by Gibbs from his treatment of capillarity theory. Then we analyze, on the basis of this approach, the problems of stability of colloids, liquid films, and the phenomena of wetting.

Chapter 1 discusses forces acting near interfaces.

When two contiguous phases are fluids, their interfacial area can be extended against the resistance of surface tension (case I). When one of the phases is solid, the interface can only be elastically deformed; but a liquid may slip across a sufficiently smooth solid (e.g., mercury on glass or water on paraffin wax) (case II).

If both phases are solid (case III), the behavior of the interface is similar to that in case II; but a true phase contact can be realized either when surfaces are atomically smooth (e.g., the contact of two mica plates), or when it requires some plastic deformation, or preliminary melting, or evaporation followed by condensation and crystallization. A contact of two solids can only rarely be geometrically as perfect as that between two fluids.

Direct measurement of surface tension at an interface is possible only in case I. To a certain approximation, it is also possible for solids if the yield point in a specific temperature range is substantially reduced [1].

Determination of surface free energies of solids is possible for such materials as mica, by measuring the work of quasi-equilibrium cleavage along a cleavage plane. However, reversibility was not realized sufficiently closely in some reported studies. One of the main obstacles is the formation of opposite charges on the cleavage surfaces. These do recombine via surface conduction but only extremely slowly if no water vapor is present. But in the presence of water vapor the surface energy is reduced by adsorption. Some reliable results were reported by Derjaguin and Metsik [2] who also corrected previous errors in calculations of the work transformed into elastic strain [3].

There exists, however, a possibility of "indirect" determination of surface free energies from effects dependent on this quantity — for example, from the dependence on surface curvature of the phase equilibrium parameters, such as the pressure of saturated vapor over a curved surface.

In the standard thermodynamic treatment of case III, the interface is assumed to be ideally smooth, as with two fluids in contact. Consequently, caution is needed in applying the conclusions thus obtained to real situations. One of the features of crystalline materials is the anisotropy of surface tension - i.e., its dependence on the direction within a given face (in contrast to the surface free energy). Surface tension can also vary with the state of deformation of a solid. Rusanov [4] analyzed the corresponding effect on contact angle. It is possible to find such effects experimentally with elastic bodies, although the absolute values of the surface tensions cannot be determined.

The thermodynamic treatment of real crystalline surfaces can be refined by taking into account the line energy of edges. The logical necessity for line tension on three-phase contact boundaries, which can be either positive or negative, was already clear to Gibbs. This idea was recently elaborated by Scheludko et al. [5] who were able to demonstrate the important role played by line tension in processes of formation of two-phase contacts, for example, in wetting, adhesion of bubbles, and heterogeneous nucleation (e.g., in electrocrystallization). It was found possible to determine the values of line tension experimentally. The theory of line tension at a wetting perimeter has been developed by de Feijter and Vrij [6] and Starov and Churaev [7].

A correction for the effect of substrate roughness on the contact angle of wetting for real bodies was suggested in 1936 by Wenzel [8] and later derived more rigorously by one of us [9].

The main error in attempts to determine the surface energy of solids from the work of formation of new surface is caused by neglecting, first, the irreversible part of the work of cleavage transformed into heat or into the energy of residual strain and, second, the nonequilibrium high-energy state of the new surface of a solid. Such a surface may carry electric charge with a density up to 10^5 SGSE units of charge [$\sim 1 \mu\text{C} - \text{Ed.}$] per cm^2 . The electrostatic energy may absorb a substantial fraction of the excess work of cleavage. This fact was found in the work of Karasev, Krotova, and Derjaguin [10], and led to the discovery of the emission of high-energy electrons, not only in the process of cleavage of crystals but also through after-emission from a surface far removed from its counterpart [11].

Such surfaces are found to be covered by a mosaic of oppositely charged domains [12]. From a determination of the initial energy of the fastest electrons emitted and the domain size (the radius r of the equivalent circular area), it was possible to find the charge density σ . Then, when the potential at the center of a domain was determined (from the energy of the fastest electrons), it was possible to calculate the electrostatic energy of domains, and thus

the mean energy per unit area. This quantity was found to constitute an appreciable fraction of the apparent surface energy.

Freshly formed surfaces are special not only in their high energy but also in enhanced chemical activity. As a rule, the surface relaxes to its equilibrium state over a time of the order of 10 min, both through electron emission and through surface electric conduction. When a new surface appears as a result of breaking of a close contact of two dissimilar solids, each of the surfaces formed is covered with charge of one sign. In this case the electron after-emission drops off more slowly, over several hours, especially if surface conductivity is low.

1.1. MOLECULAR AND ELECTRIC FORCES IN INTERFACIAL LAYERS

No forces operate within a homogeneous bulk phase, in the absence of external fields, if it is described macroscopically. The points of a bulk phase are characterized only by the densities of its components, of free and total energy, and of entropy. The microscopic description operates with local electric and molecular fields as observables; but these vanish after averaging over a volume including a sufficiently large number of molecules and ions. However, in the transition zone between two phases there exists a field of electric and molecular forces that decreases with distance into each of the contiguous phases. We shall refer to these forces as surface forces (not to be confused with the term "surface forces" used in mechanics to denote forces applied to a surface). Correspondingly, such intensive quantities as densities of components within the phases, and densities of free and total energy and entropy vary across the interfacial zone. Gibbs's capillarity theory considers mostly the total excesses of extensive quantities, that is to say, excess amounts of components, excess free energy and entropy present in the system as compared with the values that would be realized if the transition zone were a geometric surface of zero thickness, and the bulk phases in contact at this surface had uniform properties up to the mathematical interface. The conditions of equilibrium of heterogeneous systems, obtained by taking into account the characteristics of transition zones, and expressed as the appropriate excesses, give correct results despite the uncertainty that appears because of the undefined localization of the geometrical boundary surface.

However, this correspondence fails if two phases of the system, 1 and 2, separated with a third phase, 3, approach one another so closely that in a certain region of the third phase the transitional interfacial layers of the phases 1-3 and 2-3 overlap. In this configuration the total amounts of free and total energy and entropy

differ from the sum of their values for the bulk phases and surface excesses. Such cases, not analyzed by Gibbs, will be treated in Chapter 2.

In the present chapter we follow Gibbs in limiting the analysis to cases in which the interlayer of phase 3 between phases 1 and 2 is of such thickness that the middle portion of the interlayer retains the intensive properties of phase 3. One of the corollaries and one of the attributes of this situation is that the tension in such an interlayer is equal to the sum of surface tensions of the interfaces 1-3 and 2-3.

"Surface forces" acting on molecules within transition interfacial zones must not be confused with electrostatic forces acting on ions. Ever since the classical works of Clairaut and Laplace and up to the mid-fifties of this century, it was a standard procedure to determine the forces applied to molecules at the interfaces by summing the pair forces of molecular attraction to the surrounding molecules. After London's theory of dispersion forces appeared [13], the energy of interaction between two atoms was invariably expressed by the formula

$$U = -\frac{\beta}{r^6}, \quad \beta = (3/4)\alpha^2\hbar\omega_0 \quad (1.1)$$

where α is the polarizability of the atom, \hbar is Planck's constant divided by 2π , and ω_0 is the characteristic frequency from the appropriate dispersion equation for a given sort of atoms. The energy $\hbar\omega_0$ is approximately equal to the ionization potential of the atom.

Casimir and Polder [14] later refined the theory of dispersion forces by taking into account that the electromagnetic fields mediating the interaction between molecules propagate at a finite velocity, viz. the velocity of light. As a result of the corresponding retardation, phase differences appear between waves emitted by a molecule and exciting another molecule, and the waves induced in this latter molecule when they reach the former one. This phase difference, called the electromagnetic retardation, weakens the molecular attraction. In the asymptotic limit, when the distance between molecules becomes much greater than the characteristic wavelength of dispersion interaction, the energy of attraction between molecules is given by a different formula, viz.

$$U = -\frac{23\hbar c\alpha^2}{2\pi r^7} \quad (1.2)$$

where c is the velocity of light. As a result, the exponent of distance in the denominator increases by unity. The polarizability

α in (1.2) can be simply expressed through the static dielectric constant ϵ_0 :

$$\alpha = \frac{3}{4\pi} \frac{\epsilon_0 - 1}{\epsilon_0 + 2} \frac{M}{\rho N_A} \quad (1.3)$$

where M is the molecular mass, ρ is the density, and N_A is Avogadro's number.

By assuming additivity and replacing, as a first approximation, the summation by integration for the force acting on a molecule of one phase (1) at the interface with the other phase (2), and neglecting the possible deviations of density at the interface from the bulk value, we obtain, for small distances between the molecule and the interface (when electromagnetic regardation can be neglected), the formula

$$f = -(\pi/2)q_2\beta_{12}/h^4, \quad \beta_{12} = (3/4)\alpha_1\alpha_2\hbar\omega_0 \quad (1.4)$$

where q_2 is the number of atoms per unit volume of the dispersed phase.

Another asymptotic formula holds for large distances h :

$$f = -\frac{23\hbar c\alpha_1\alpha_2 q_2}{5h^5} \quad (1.5)$$

After Lifshitz [15] gave a method for calculating the dispersion interaction between two macroscopic bodies as a function of the gap width, it became possible to carry out a macroscopic calculation of the force acting on a single molecule of a gas or of a solute in a dilute solution near an interface. The second, more general, case is treated as follows.

Consider an imaginary system in which the solution (phase 2) is separated from the adjacent solid phase 1 by a layer of pure solvent (phase 3) of thickness H . Since the forces of interaction f between individual molecules of the solute in a dilute solution and the contiguous solid phase are additive, the total force of interaction F between the solution and this phase per unit surface area is [16]

$$F(H) = \int_H^\infty Nf(h) dh = -Nu(H)$$

where N is the bulk concentration of the solute, and $u(H)$ is the energy of interaction between a dissolved molecule and the interface. This relation makes it possible to find the energy from an expression derived in [16], by using the general macroscopic theory for the interaction force $F(H)$ between two semiinfinite media across a flat liquid interlayer. To achieve this result, it is sufficient to expand the general formula for F into a series in N , and to retain only the leading term linear in N . The dielectric constants of the dilute solution, ϵ_2 , and of the pure solvent, ϵ_3 , are related by the following expression:

$$\epsilon_2 = \epsilon_3 + (\partial\epsilon_2/\partial N)_{N=0} \cdot N$$

Finally, we arrive at the following formula:

$$U = - \frac{\hbar}{16\pi^2 H^3} \int_0^\infty d\omega \frac{\epsilon_1(i\omega) - \epsilon_3(i\omega)}{\epsilon_3(i\omega)[\epsilon_1(i\omega) - \epsilon_3(i\omega)]} \left(\frac{\partial\epsilon_2(i\omega)}{\partial N} \right)_{N=0} \quad (1.6)$$

where $\epsilon_1(i\omega)$, $\epsilon_2(i\omega)$, and $\epsilon_3(i\omega)$ are the permittivities of the respective phases on the imaginary axis of frequency, and N is the concentration of the solute. As a limiting case, formula (1.6) gives the energy of a gas molecule at a surface of a condensed phase if the "solvent" is a vacuum [17].

Surface curvature makes the behavior of the corresponding fields and their theoretical interpretation much more complex. The field of dispersion forces at curved surfaces has been calculated by Belosludov and Nabutovsky [18-19] who used the macroscopic approach of Dzyaloshinsky, Lifshitz, and Pitayevsky [17].

Electric forces acting on ions near an interface produce a greater variety of effects but can be calculated on an elementary basis. The simplest case is that of a noncharged interface. In the macroscopic treatment the ion interacts with the surface only via the image force

$$F = \frac{z^2 e^2}{\epsilon_{20}(2x)^2} \frac{\epsilon_{10} - \epsilon_{20}}{\epsilon_{10} + \epsilon_{20}} \quad (1.7)$$

where ϵ_{10} and ϵ_{20} are the permittivities of the contiguous phase and the phase in which the ion is located, respectively, ze is the ion charge, and x is its distance from the interface. The force F is directed toward the phase with the greater value of ϵ .

In ionic crystals insoluble in the contiguous phase the positions of ions are fixed. If we neglect peculiarities in the structure of subsurface layers two to three atomic layers thick, the

calculation of the external electric field is an elementary, purely computational, problem. This field is rapidly damped out at a distance from the surface on the order of one lattice period. If this field acts on an electrolyte solution, the ions in this solution are redistributed so that the original field is substantially altered; this effect is discussed in the next section.

1.2. FORMATION AND STRUCTURE OF ELECTRICAL DOUBLE LAYERS

When an electrolyte solution is in contact with another phase (a solid, a gas, or another liquid immiscible with the electrolyte), a spontaneous redistribution of ions between the two phases takes place even in the absence of an external electric field. An ionic electrical double layer (EDL) is formed near the interface between the phases.

Mathematically, the simplest description of the buildup of a potential difference ψ_0 between the electrolyte solution and a solid phase is obtained when the solution principally contains ions that are constituents of the lattice of the solid phase. A typical example of such systems is silver iodide in solutions of AgNO_3 (or KI). As the chemical potentials of silver ions in a liquid medium,

$$\mu_\ell = \mu_1(T) + kT \ln c_{\text{Ag}^+} \quad (1.8)$$

and in a solid,

$$\mu_s = \mu_2(T) + e\psi_0 \quad (1.9)$$

are equal when the solution and the crystal are in equilibrium, we immediately arrive at the familiar Nernst equation:

$$\psi_0 = (kT/e) \ln (c_{\text{Ag}^+}/c_{\text{Ag}^+}^0) = 23(kT/e)(p_{\text{Ag}^+} - p_{\text{Ag}^+}^0) \quad (1.10)$$

Here μ_1 and μ_2 are functions of temperature, c_{Ag^+} is the concentration of silver ions far from the interface, and $c_{\text{Ag}^+}^0$ is the concentration of Ag^+ at the point of zero charge. The difference between unknown functions μ_1 and μ_2 is eliminated from the analysis by introducing into Eq. (1.10) the quantity $c_{\text{Ag}^+}^0$ which is determined experimentally. As the ratio kT/e at room temperature corresponds to a potential difference of ~25 mV, we find from (1.10) that a change in the concentration of potential-determining ions (silver ions in the case under discussion) by one order of magnitude, i.e., $\Delta p_{\text{Ag}} = 1$, must result in a change in ψ_0 by approximately 57 mV.

If experiments confirm this variation of ψ_0 , the Nernstian behavior of the interfacial charge is usually regarded as proved.

There are other factors that can trigger a spontaneous formation of an EDL - dissociation of ionogenic groups on the surface of oxide or latex particles, preferential specific adsorption of some ionic species from the solution onto the interface, and isomorphic substitution of ions in the lattice of the solid by ions of different charge from the solution.

By any of these mechanisms the interface may acquire a certain amount of charge of one sign, while in the adjacent layer of solvent there appears a diffuse counterpart of the double layer. This is a layer of greater concentration of oppositely charged mobile ions (counterions) along with a depletion in ions of like sign (co-ions).

The structure of an EDL as a whole depends on specific features of each system. It may be simple or complex. This structure is usually described by means of the simple Gouy-Chapman theory [20, 21], or by the theories of Stern [22] and Grahame [23] which make it possible to take into account the specific properties of particular materials. However, these specific features of an EDL structure are mostly connected with that part of the EDL which is very close to the interface and whose thickness does not exceed several angstroms. This part of the EDL includes the charge of the phase contiguous to the solution, and the charge of the specifically adsorbed ions (the dense part of EDL, or the Stern layer). On the other hand, the diffuse part of the EDL is independent of the mechanism of charging of the interface at moderate concentrations of ions in the solution. It depends only on the amount of charge, and has a well-known and relatively simple structure.

1.3. DIFFUSE PART OF THE EDL. THE POISSON-BOLTZMANN EQUATION

The structure of the diffuse part of the EDL is calculated on the basis of equations that describe the changes in the distribution of electric field and ionic concentration in the neighborhood of an interface. The fundamental electrostatic equation is that of Poisson (or rather, Maxwell):

$$\operatorname{div}(\epsilon \operatorname{grad} \psi) = -4\pi\rho \quad (1.11)$$

where ϵ , ψ , and ρ are the local values of the dielectric constant, electrostatic potential with respect to the bulk of the solution, and volume charge density, respectively. The last value is related to local concentration n_i of ions with the charge $z_i e$ by the obvious relation

$$\rho = \sum_i e z_i \tilde{n}_i \quad (1.12)$$

in which summation is carried out over all species of ions in the solution. In turn, local ionic concentrations are related to mean bulk values of n_i far from charged surfaces by the Boltzmann equation:

$$\tilde{n}_i = n_i \exp(-w_i/\theta) \quad (1.13)$$

where $\theta \equiv kT$ is the product of the Boltzmann constant and the absolute temperature, and w_i is the work of displacing the ion from the bulk of the electrolyte to a point within the diffuse part of the EDL. This work is the potential of the mean force acting on the ion, and can be calculated by means of the Bogolyubov-Born-Green-Yvon (BBGY) method of correlation functions [24] or by approximate equations of the theory of liquid state [25].

However, the usual method of closing the system of equations (1.8)-(1.10) is to set the quantity w_i , as suggested by Gouy, equal to

$$w_i = z_i e \psi \quad (1.14)$$

relating it thereby to the mean value of the potential at the point where the ion is located.

The local values of dielectric constant ϵ depend, in principle, on the properties of the solvent which, in turn, are functions of the distance to the interface and of local concentrations n_i , as well as of the local strength of electric field, $E = -\nabla \psi$ [26]. However, as a first approximation we can assume that ϵ in Eq. (1.11) is constant everywhere [27]:

$$\epsilon = \epsilon_0 = \text{const} \quad (1.15)$$

This assumption substantially simplifies the problem. Successive substitutions of Eqs. (1.12)-(1.15) into (1.11) yield the basic equation of the Gouy-Chapman theory, the so-called Poisson-Boltzmann equation:

$$\Delta \psi = (4\pi/\epsilon_0) \sum_i z_i e n_i \exp(-z_i e \psi / \theta) \quad (1.16)$$

where Δ is the Laplace operator.

Together with an appropriate boundary condition given by the mechanism of charge buildup at the interface, this equation completely defines the distribution of potential ψ in the space adjacent to the interface.

By virtue of Eqs. (1.14) and (1.13), solution of Eq. (1.16) simultaneously with the electrostatic potential determines the local concentration density of co-ions and counterions.

The Poisson-Boltzmann equation has important applications. Consequently, many theoretical papers have been devoted to analyzing its validity and to studying its possible modifications [28-44]. Many of them are discussed in well-known monographs and review papers (e.g., [45-48]). It is convenient to divide these papers into two large groups. The first covers work based on the methods of statistical mechanics [30-32, 34, 35, 38, 39, 41-44], mostly the BBGY correlation functions technique, while the second comprises papers based on the method of local thermodynamics [33, 36, 37, 40].

A consistent application of any of these techniques meets with considerable mathematical difficulties. As a result, most papers in this field analyze the effects produced in the structure of the diffuse ion layer by a single or several partial factors, such as image forces [35, 49, 50], the finite volume of ions [36, 50, 51-56], dielectric saturation [36, 55, 56], hydration of ions, and so on. The first of these effects is appreciable mainly for polyvalent ions [49], and the second is observed only at relatively high concentrations of electrolytes and at high potential of the interface [51]. The last two effects result in a slight reduction of the dielectric constant of the solution and of the concentration of counterions at the surface, provided the bulk ionic concentration and surface potential are high, and only at a distance of several angstroms from the interface [55, 56]. Grahame established, as early as 1950, that these two effects are very weak in the Gouy model of the EDL [26].

Other factors affecting the structure of the EDL at an interface have also been discussed - electrostriction [36, 37, 40], distortion of the atmospheres surrounding the ions [44], formation of ion pairs [29], and others. Calculations carried out by different authors indicate that some of these factors can cause a deviation from the Gouy theory by several percent in either direction, at a concentration of a 1-1 electrolyte up to 0.1 mole/liter. But conflicting trends operating simultaneously ultimately result in distribution curves that depart to only a negligible extent from the standard Poisson-Boltzmann solutions [34, 36, 37, 40]. At any rate, this is true in the range of concentrations up to 0.1 mole/liter (for 1-1 electrolytes) and diffuse layer potentials up to ~100 mV. The range of applicability of the Poisson-Boltzmann equation narrows considerably for polyvalent ions as their valence increases [49]. However, this range is still sufficiently broad, and corresponds with the conditions that occur in most real situations (with a possible exception of some electrochemical systems).

1.4. THE DEBYE-HÜCKEL EQUATION.
RELATION BETWEEN SURFACE POTENTIAL
AND SURFACE CHARGE

In some cases, electrochemical conditions are such that it is possible to use, instead of the general Poisson-Boltzmann equation (1.16), the linearized Debye-Hückel equation [57], which holds at low potentials ($z\psi < 25$ mV) and is based on expanding the exponentials in the Boltzmann equation (1.13) in powers of a small ratio w_i/θ , retaining the terms linear in ψ . The terms independent of potential cancel out in the sum because the solution is electrically neutral far from the interface.

The Debye-Hückel equation has a simple form:

$$\Delta\psi = \kappa^2\psi \quad (1.17)$$

where Δ is the Laplace operator and κ is the inverse Debye length characterizing the efficiency with which diffuse-layer counterions screen the surface field, and defined as follows:

$$\kappa = [(4\pi e^2/\epsilon\theta) \sum_i z_i^2 n_i]^{1/2} \quad (1.18)$$

The quantity $1/\kappa$ is a measure of thickness of the diffuse layer of counterions.

The solution of Eq. (1.17) at a uniformly charged plane is

$$\psi(x) = \psi_1 \exp(-\kappa x) \quad (1.19)$$

where x is the distance from the boundary of the diffuse layer into the bulk of the solution, and ψ_1 is the potential at this boundary. As follows from (1.19), the surface density in a planar diffuse layer is given by the Gauss theorem:

$$\sigma_d = - \frac{\epsilon}{4\pi} \left. \frac{d\psi}{dx} \right|_{x=0} = \frac{\epsilon\kappa}{4\pi} \psi_1 \quad (1.20)$$

This equation shows that in the Debye-Hückel approximation the differential capacitance of the planar double layer, $C = d\sigma_d/d\psi_1$, equals the capacitance of a plane capacitor with the distance between plates equal to the Debye length $1/\kappa$.

For a spherical double layer there is also a simple relation between potential and the distance r from the center of the sphere with radius a :

$$\psi(r) = \psi_1 \frac{a}{r} \exp[-\kappa(r - a)] \quad (1.21)$$

In this case the diffuse charge density per unit surface area of a spherical particle is

$$\sigma_d = - \frac{\epsilon}{4\pi} \left. \frac{d\psi}{dr} \right|_{r=a} = \frac{\epsilon\kappa}{4\pi} \psi_1 \left(1 + \frac{1}{\kappa a} \right) \quad (1.22)$$

For surfaces with radii of curvature large compared with the Debye screening length, Eq. (1.22) transforms into (1.20); i.e., a thin spherical layer can be treated locally as a planar one.

Similar relations for a cylinder with radius a are

$$\psi(r) = \psi_1 K(\kappa r) / K_0(\kappa a) \quad (1.23)$$

$$\sigma_d = (\epsilon\kappa/4\pi) \psi_1 K_1(\kappa a) / K_0(\kappa a) \quad (1.24)$$

where K_0 and K_1 are modified Bessel functions of the second kind of orders zero and one, and r is the distance to the cylinder axis. At large values of the argument these expressions also transform into Eqs. (1.19) and (1.20). It follows from Eqs. (1.22) and (1.24) that the differential capacitance of a curved surface is a function of the relation between the diffuse layer thickness and the radius of curvature of the surface.

1.5. PLANAR DOUBLE LAYER. SOME EXACT SOLUTIONS OF THE GENERAL POISSON-BOLTZMANN EQUATION

No serious difficulties stand in the way of deriving the solutions given above. But if we turn again to the nonlinear Poisson-Boltzmann equation (1.16), then even to solve it for a single uniformly charged surface would require, as a rule, much greater effort. For a binary electrolyte this equation is conveniently written in the following form:

$$\Delta\phi = [\kappa^2/(z_1 + z_2)] (e^{z_1\phi} - e^{-z_2\phi}) \quad (1.25)$$

where z_1 and z_2 are the valences of the counterion and co-ion respectively, and

$$\phi = e\psi/\theta \quad (1.26)$$

is the dimensionless potential. According to the general definition of the inverse Debye length (1.18), the quantity κ in (1.25) is

$$\kappa = [(4\pi e^2/\epsilon\theta)(z_1^2 n_1 + z_2^2 n_2)]^{1/2} \quad (1.27)$$

The concentrations of co-ions and counterions in the bulk of the solution are related by the electroneutrality constraint:

$$z_1 n_1 = z_2 n_2 \quad (1.28)$$

If the electrolyte is a symmetrical one ($z_1 = z_2 = z$), Eq. (1.25) is further simplified:

$$\Delta(z\psi) = \kappa^2 \sinh(z\phi) \quad (1.29)$$

$$\kappa = (8\pi e^2 z^2 n / \epsilon \theta)^{1/2} \quad (1.30)$$

The exact solution of this equation for a planar double layer ($\Delta = d^2/dx^2$) was given by Langmuir [58]:

$$\tanh(z\phi/4) = \tanh(z\phi_1/4) \exp(-\kappa x) \quad (1.31)$$

It can be obtained by multiplying the left- and right-hand sides of (1.29) by $2(d\phi/dx) dx$ and integrating it, taking into account that far from the charged surface

$$\phi = 0, \frac{d\phi}{dx} = 0 \quad (1.32)$$

and $\phi(0) = \phi_1 = e\psi_1/kT$ immediately at the boundary of the diffuse layer.

Exact solutions of Eq. (1.25) for a planar double layer can also be obtained for 2-1 and 1-2 electrolytes [59-61]. By introducing into this equation a new function

$$v_1(\phi) = \ln[3/(1 + 2e^{-\phi})] \quad (1.33)$$

for ϕ in the case of the 2-1 electrolyte (counterion valence $z_1 = 2$) or

$$v_2(\phi) = \ln[(2e^\phi + 1)/3] \quad (1.34)$$

for a 1-2 electrolyte ($z_1 = 1, z_2 = 2$), we can rewrite it in the form of (1.29) [60]:

$$\Delta v_i = \kappa^2 \sinh v_i \quad (1.35)$$

By virtue of definitions (1.33) and (1.34), the same conditions (1.32) hold for the functions v_i far from the interfaces as for the potential ϕ , so that the solution is of the type of Eq. (1.31) [60]:

$$\tanh(v_i/4) = \tanh(v_i(\phi_1)/4) \exp(-\kappa x) \quad (1.36)$$

where, by virtue of (1.27) and (1.28),

$$\kappa = (24\pi e^2 n_2 / \epsilon \theta)^{1/2} \quad (1.37)$$

and n_2 is the concentration of divalent ions (in cm^{-3}).

Obviously, the reversal of sign of surface charge transforms a co-ion into a counterion, and vice versa, so that the functions v_1 and v_2 change places. Equations (1.31) and (1.36) transform into the solution of the Debye-Hückel equation (1.37) at low potentials. But if the potential ψ_1 at the boundary of the diffuse layer is not low, then linearization in $\psi(x)$ is possible only far from the surface. In this case,

$$\phi(x) \approx (4/z) \tanh(z\phi_1/4) \exp(-\kappa x) \quad (1.38)$$

for z-z electrolytes [58], and

$$\phi(x) \approx 6 \tanh[v_i(\phi_1)/4] \exp(-\kappa x), \quad i = 1, 2 \quad (1.39)$$

for 2-1 and 1-2 electrolytes. The factor 6 in (1.39) instead of 4 in (1.38) appears because, by virtue of definitions (1.33) and (1.34), at small values of the argument

$$v \approx 2\phi/3 \quad (1.40)$$

The usefulness of the asymptotic representations (1.38) and (1.39) will be demonstrated later (see Chapter 6) in deriving explicit approximate formulas for disjoining pressure and free energy of interaction in planar and curved double layers, as well as in deriving approximate stability criteria in the framework of the DLVO theories of stability of hydrophobic colloids (Chapter 9).

1.6. MORE COMPLEX SITUATIONS: CURVED SURFACE, AND DISCRETENESS OF SURFACE CHARGE

No exact solutions are available for the general Poisson-Boltzmann equation in the case of curved surfaces. Only numerical or approximate analytical solutions for spheres [62] and cylinders [63] are known. The difference between the solutions obtained for the same surface geometry consists mostly in the physical meaning of the conditions that permit use of a specific approximation, or in the application of specific preliminary mathematical transformations that facilitate the solution. Among the latest achievements in this field is the work of Ohshima et al. [64], and an ingenious method of solving the linearized Poisson-Boltzmann equation, suggested in [65].

Considerable difficulties arise in solving various versions of the modified Poisson-Boltzmann equation for a sphere [55] and a plane [66]. The purpose of such modifications is to include in the

Poisson-Boltzmann equation various effects mentioned earlier (see p. 11). However, none of these effects produces a dramatic change in the diffuse part of the EDL, because at moderate concentrations all of them are felt only at a distance of several angstroms from the interface and, in fact, can be assigned to the Stern layer. But even within the framework of the standard unmodified Poisson-Boltzmann equation, the problem of finding the potential distribution within the diffuse layer grows considerably more complicated with a nonhomogeneous structure of charge on the interface itself. This transition to nonhomogeneous structures appears as a change in boundary conditions of the Poisson-Boltzmann equation. Instead of potential or charge uniformly averaged ("smeared") over the surface, these boundary conditions necessarily involve micro-potentials or micro-charges at the points where the ions are located on the interface or in the Stern layer. Alternatively, they may include some continuous or discrete distribution functions for the potential or charge density on the interface. In this case, a solution can be obtained only on the basis of the linearized Poisson-Boltzmann equation with boundary conditions representing a fixed, periodic, or random, distribution of discrete charge centers on the interface, or a continuous, periodic distribution of charge density on the interface. Calculations of such type, carried out for plane and cylindrical interfaces [67], show that the effect of nonuniform distribution of surface charge is appreciable at relatively short distances — not greater than either one period of the lattice of surface charges or the linear size of surface charge inhomogeneities.

A quite different approach in describing the discreteness, which takes into account the correlation in the positions of ions of both signs (due to their electrostatic interaction) on the interface, was suggested in [68]. But even this refinement shows that the effect of discrete distribution drops off very rapidly as we move from the interface into the solution (see Chapter 6).

1.7. ADSORPTION OF IONS IN THE STERN LAYER

The adsorption of ions from a solution in the Stern layer is usually described by the Stern isotherm [22]. For ions of only the i -th species adsorbed on the surface, this isotherm has the simplest form:

$$\tau_i = \frac{v_0 n_i \exp \frac{-\phi_i - z_i e \psi_\delta}{kT}}{1 + v_0 n_i \exp \frac{-\phi_i - z_i e \psi_\delta}{kT}} \quad (1.41)$$

Here τ_i is the coverage of the surface monolayer by ions of the i -th species with bulk concentration n_i , v_0 is the molecular volume

of the solvent, ϕ_i is the energy of specific (nonelectrostatic) adsorption of one ion, and ψ_δ is the potential in the adsorption plane (Stern potential). Usually, ψ_δ is identified with the potential ψ_1 of the boundary of the diffuse layer.

Equation (1.41) is readily derivable if the adsorption monolayer is treated as an individual phase whose ions are in equilibrium with the electrolyte solution. As compared to the standard expression for the chemical potential of the solid phase (1.9), in this model the chemical potential of an ion in a monolayer contains an additional entropy term $kT \ln[\tau_i/(1 - \tau_i)]$ that accounts for the coverage of the monolayer.

The Stern isotherm is, in fact, merely the Langmuir isotherm modified for adsorption of a charged component. It is generally used because its form is simple. Furthermore, it can be given a rigorous theoretical foundation at low coverages, when it transforms into the Henry isotherm. It is readily generalized to the case of adsorption of a mixture of ions, even if there is a competition between ions for sites in the monolayer. And, finally, it reproduces the effect of monolayer saturation at high concentrations of ions at the surface. However, despite its advantages, this isotherm cannot be given a solid theoretical foundation.

Aspects of a theoretical description of adsorption on a charged, structureless surface have been treated in a number of papers, for instance [35, 69]. The main conclusion to be drawn from the many papers is that a stringent, consistent approach, without additional simplifying assumptions, is impossible even if only one of the ionic components of the solution is adsorbed. In spite of the assumptions introduced, final results are usually unwieldy and, as a rule, do not make it possible to obtain explicitly an adsorption isotherm valid for all values of coverage. Consequently, it is difficult to use these results in studying the stability of disperse systems.

The fraction of the charge density of the monolayer, associated with a given ion species, is calculated by multiplying the coverage by the number of accessible adsorption centers on the surface and by the charge of an individual ion.

Usually, the Stern isotherm serves to describe adsorption of counterions on an already charged surface; but it can be used also, with equal success, when an initially noncharged surface adsorbs different ionic species and acquires a charge only because of preferential adsorption of one of the species [70].

1.8. CHARGING OF SURFACES BY DISSOCIATION OF IONOGENIC GROUPS

Problems of this sort are typical of inorganic oxides, polymer latexes, biological materials, minerals, etc., where electric charge appears as a result of dissociation of ionogenic groups located only on the interface. The electrokinetic, adsorptive, and energetic properties of such materials do not conform to the Nernstian scheme of charge buildup at a solid/electrolyte solution interface [71-73] (briefly outlined at the beginning of this chapter). In order to interpret some of the experimentally observed regularities, an approach was suggested [74] and subsequently developed independently and almost simultaneously by several authors [75, 76]. The basic model of this approach is known under various names: site-binding model, surface complexation, surface ionization, ligand exchange, ionized surface groups model, and so on.

Ionization of the surface is treated as a result of several (usually from one to four) surface chemical reactions, each of which is characterized by a specific equilibrium constant. Surface concentrations of charged reactants are assumed to be Boltzmann functions of the mean electrostatic potential of the plane in which the complex of a given type is formed. Among the models analyzed were those with active surface sites of a single type, for example with only acidic groups, and with sites of two types, covering materials with amphoteric properties. Here the discrete nature of the surface charge is taken into account only in the sense that the surface density of ionized groups is fixed for each group type. In the pure Gouy model an interface is thus characterized only by the number of dissociating groups and by equilibrium constants. In the Stern and Grahame models these characteristics are supplemented by the appropriate capacitances and adsorption constants. It can be readily shown that the dissociation or adsorption isotherms obtained in the simplest cases are completely equivalent to the standard Stern isotherm taking into account, or neglecting, the competition among the ions for the binding site, depending on the physical contents of a specific model.

1.9. TESTING OF MODELS OF IONIZED SURFACES

In order to test these various hypotheses, experimental data are usually compared with theoretical models by means of computers. As a rule, it is possible to achieve a satisfactory fit for adsorption or electrokinetic data [72, 77, 78], as well as for data on the two-dimensional surface pressure at a water/air interface [79] or data on the interaction between charged surfaces across an electrolyte interface [80]. However, caution is needed in interpreting the results of such procedures. Thus, numerical calculations carried out specially with various models of the double layer (the

Gouy, Stern, Grahame, and Helmholtz models) have demonstrated [81] that a limited sample of experimental data (in this case obtained by titration of oxides) can equally well fit different sets of parameters (having physically reasonable values in each case) for different models of the EDL.

In studies of the surface electric properties of silica, it was observed that under some conditions the specific surface charge appears to exceed the charge density that can be produced by a totally ionized monolayer. To explain this observation a model of a "porous layer" (or gel layer) was suggested, assuming, in contrast to the surface ionization model, that the charge exists within a layer of the solid of finite thickness [82]. This model is not universally accepted. Numerous data are available both supporting and contradicting it [78, 83]. The model needs to be further elaborated and, in this context, a paper by Martynov [84] should be mentioned, calculating the distribution of potential in a gel layer system in which adsorption of ions from the solution takes place.

The equations describing the distribution of ions in the diffuse part of a double layer and in its dense part (i.e., adsorption and dissociation isotherms) are merely starting points for the theory of stability of dispersions. The force and energy of interaction in colloid systems is the ultimate problem (see Chapter 6). In turn, these calculations still constitute only one component, though the most important one, of the analysis of stability and rates of aggregation and disaggregation of colloids (see Chapter 8). Consequently, it is often preferable to operate with less rigorous initial equations that yield numerical or analytical results (generally, as functions of several parameters) rather than with more rigorous but unwieldy initial equations representing the EDL structure. Approximate analytical results have advantages over numerical ones, because they point to those parameters that play the dominant role in concrete problems. They can also serve as useful reference points for more accurate numerical calculations.

REFERENCES

1. V. I. Likhtman, L. S. Brukhanova, I. A. Andreeva, and P. A. Rehbinder, Dokl. Akad. Nauk SSSR, 160, 867 (1965); L. S. Brukhanova, I. A. Andreeva, and V. I. Likhtman, Fiz.-Khim. Mekh. Mater., No. 2, 134 (1965); V. I. Likhtman, L. S. Brukhanova, I. A. Andreeva, and E. D. Shchukin, Fiz.-Khim. Mekh. Mater., No. 4, 433 (1969); I. A. Andreeva, L. S. Brukhanova, V. S. Yushchenko, E. D. Shchukin, and P. A. Rehbinder, Dokl. Akad. Nauk SSSR, 191, 373 (1970).
2. B. V. Derjaguin and M. S. Metsik, Fiz. Tverd. Tela, 1, 1521 (1959).
3. J. W. Obreimoff, Proc. R. Soc. London, A127, 290 (1931).

4. A. I. Rusanov, *Kolloidn. Zh.*, 37, 678 (1975).
5. A. Scheludko, B. V. Toshev, and D. T. Bojadjiev, *J. Chem. Soc., Faraday Trans. I*, 72, 2815 (1976).
6. J. A. de Feijter and A. Vrij, *J. Electroanal. Chem. Interface Electrochem.*, 37, 9 (1972).
7. V. M. Starov and N. V. Churaev, *Kolloidn. Zh.*, 42, 703 (1980).
8. R. Wenzel, *Ind. Eng. Chem.*, 28, 988 (1936).
9. B. V. Derjaguin, *Dokl. Akad. Nauk SSSR*, 51, 357 (1946); *C. R. (Dokl.) Acad. Sci. URSS*, 51, 361 (1946).
10. V. V. Karasev, N. A. Krotova, and B. V. Derjaguin, *Dokl. Akad. Nauk SSSR*, 88, 777 (1953).
11. V. V. Karasev, N. A. Krotova, and B. V. Derjaguin, *Dokl. Akad. Nauk SSSR*, 109, 728 (1956).
12. M. S. Metsik, *Physics of Cleavage of Mica*, Vost. Sib. Knigoizdat., Irkutsk (1967).
13. F. London, *Z. Phys.*, 63, 245 (1930).
14. H. Casimir and D. Polder, *Phys. Rev.*, 73, 360 (1948).
15. E. M. Lifshitz, *Zh. Éksp. Teor. Fiz.*, 29, 94 (1955).
16. B. V. Derjaguin, I. E. Dzyaloshinsky, M. M. Koptelova, and L. P. Pitayevsky, *Discuss. Faraday Soc.*, 40, 246 (1965).
17. I. E. Dzyaloshinsky, E. M. Lifshitz, and L. P. Pitayevsky, *Usp. Fiz. Nauk*, 73, 381 (1961).
18. V. R. Belosludov and V. M. Nabutovsky, *Dokl. Akad. Nauk SSSR*, 221, 570 (1975); *Zh. Éksp. Teor. Fiz.*, 68, 2177 (1975).
19. V. R. Belosludov, L. M. Korotkikh, and V. M. Nabutovsky, in: *Surface Forces in Thin Films*, Nauka, Moscow (1979), p. 152.
20. G. Gouy, *J. Phys.*, 9, 457 (1910); *Ann. Phys.*, 7, 129 (1917).
21. D. L. Chapman, *Philos. Mag.*, 25, 475 (1913).
22. O. Stern, *Z. Electrochem.*, 30, 508 (1924).
23. D. C. Grahame, *Chem. Rev.*, 41, 441 (1947).
24. N. N. Bogolyubov, *Problems of Dynamic Theory in Statistical Physics*, Gostekhizdat, Moscow (1946).
25. I. Z. Fisher, *Statistical Theory of the Liquid State*, Gosfizmatgiz, Moscow (1961).
26. D. C. Grahame, *J. Chem. Phys.*, 18, 903 (1950); B. E. Conway, J. O'M. Bockris, and I. A. Ammar, *Trans. Faraday Soc.*, 47, 756 (1951); P. Booth, *J. Chem. Phys.*, 19, 391 (1951).
27. J. Lyklema and J. Th. G. Overbeek, *J. Colloid. Sci.*, 16, 501 (1961).
28. J. G. Kirkwood and J. C. Poirier, *J. Chem. Phys.*, 58, 591 (1954).
29. M. J. Sparnaay, *Recl. Trav. Chim.*, 77, 782 (1958).
30. V. G. Levich and V. A. Kiryanov, *Dokl. Akad. Nauk SSSR*, 131, 1134 (1960).
31. V. S. Krylov and V. G. Levich, *Zh. Fiz. Khim.*, 37, 106, 2273 (1963).
32. G. A. Martynov, in: *Research in Surface Forces*, Vol. 2, Consultants Bureau, New York (1966), p. 75.
33. S. V. Nerpin and N. F. Bondarenko, in: *Research in Surface Forces*, Vol. 2, Consultants Bureau, New York (1966), p. 43.

34. V. S. Krylov, in: *Fundamental Aspects of Modern Theoretical Electrochemistry*. Proceedings of the 14th Conference of International Committee of Electrochemical Thermodynamics and Kinetics, Moscow, August 1963, A. N. Frumkin (ed.), Mir, Moscow (1965), p. 222.
35. F. P. Buff and F. H. Stillinger, *ibid.*, p. 141.
36. H. Hurwitz, A. Sanfeld, and A. Steinchen, *ibid.*, p. 174.
37. G. M. Bell and S. Levine, in: *Chemical Physics of Ionic Solutions*, B. E. Conway and R. G. Barradas (eds.), Wiley, New York (1966), p. 409.
38. V. P. Smilga and V. N. Gorelkin, in: *Research in Surface Forces*, Vol. 3, Consultants Bureau, New York (1971), p. 151.
39. G. A. Martynov, *Usp. Fiz. Nauk*, 91, 455 (1967).
40. A. Sanfeld, *Introduction to the Thermodynamics of Charged and Polarized Layers*, Wiley, New York (1969).
41. G. A. Martynov, *Teor. Mat. Fiz.*, 22, 85, 260 (1975).
42. S. Levine and Ch. W. Outhwaite, *J. Chem. Soc., Faraday Trans. II*, 74, 1670 (1978).
43. Ch. W. Outhwaite, *ibid.*, p. 1214.
44. G. A. Martynov, *Kolloidn. Zh.*, 41, 1105 (1979).
45. P. Delahay, *Double Layer and Electrode Kinetics*, Interscience, New York (1965).
46. S. S. Dukhin and B. V. Derjaguin, "Electrokinetic phenomena," in: *Surface and Colloid Science*, E. Matijevic (ed.), Vol. 7, Wiley, New York (1974), p. 49.
47. S. S. Dukhin and B. V. Derjaguin, *Electrophoresis, Chapters 1 and 4*, Nauka, Moscow (1976).
48. B. B. Damaskin and O. A. Petrii, *Fundamentals of Theoretical Electrochemistry*, Vysshaya Shkola, Moscow (1978).
49. G. A. Martynov, in: *Research in Surface Forces*, Vol. 2, Consultants Bureau, New York (1966), p. 84.
50. A. Sanfeld and R. Defay, *J. Chim. Phys. Phys.-Chim. Biol.*, 63, 577 (1966).
51. G. A. Martynov, in: *Research in Surface Forces*, Vol. 2, Consultants Bureau, New York (1966), p. 94.
52. S. Levine and G. M. Bell, *J. Colloid Sci.*, 20, 695 (1965).
53. C. Devillez, A. Sanfeld, and A. Steinchen, *J. Colloid Sci.*, 25, 295 (1967).
54. M. J. Sparnaay, *Electroanal. Chem. Interfacial Electrochem.*, 37, 65 (1972).
55. J. Frahm and S. Dickman, *J. Colloid Interface Sci.*, 70, 440 (1979).
56. S. Levine and G. M. Bell, *Discuss. Faraday Soc.*, 42, 69 (1966).
57. P. Debye and E. Hückel, *Phys. Z.*, 24, 185 (1923).
58. I. Langmuir, *J. Chem. Phys.*, 6, 873 (1938).
59. B. Abraham-Shrauner, *J. Colloid Interface Sci.*, 53, 496 (1975).
60. V. M. Muller, *Kolloidn. Zh.*, 38, 704 (1976).
61. A. Marmur, *J. Colloid Interface Sci.*, 71, 610 (1979).
62. N. E. Hoskin, *Trans. Faraday Soc.*, 49, 1471 (1953); A. D. Mac-Gilivray and J. D. Swift, *J. Phys. Chem.*, 72, 3575 (1968);

- J. R. Philip and R. A. Wooding, *J. Chem. Phys.*, 52, 593 (1970);
 S. S. Dukhin, N. M. Semenikhin, and L. M. Shapinskaya, *Dokl. Akad. Nauk SSSR*, 193, 385 (1970); V. I. Smirnov and B. Sh. Shapiro, *Dokl. Akad. Nauk SSSR*, 194, 867 (1970); B. Abraham-Shrauner, *J. Colloid Interface Sci.*, 44, 77 (1973); G. A. Martynov, *Kolloidn. Zh.*, 38, 1111 (1976); L. R. White, *J. Chem. Soc., Faraday Trans. II*, 73, 577 (1977); J. Bentz, *J. Colloid Interface Sci.*, 80, 179 (1981).
63. V. L. Sigal, S. S. Dukhin, and V. E. Shamanskii, in: *Surface Forces in Thin Films and Disperse Systems*, Nauka, Moscow (1972), p. 79; in: *Research in Surface Forces*, Vol. 4, Consultants Bureau, New York (1975), p. 83; D. Stigter, *J. Colloid Interface Sci.*, 53, 296 (1975); W. P. van der Drift, A. de Kaizer, and J. Th. G. Overbeek, *J. Colloid Interface Sci.*, 71, 67 (1979).
64. H. Ohshima, T. W. Healy, and L. R. White, *J. Colloid Interface Sci.*, 90, 17 (1982).
65. M. Teubner and J. Frahm, *J. Colloid Interface Sci.*, 82, 560 (1981).
66. P. L. Levine, *J. Colloid Interface Sci.*, 51, 72 (1975).
67. V. G. Levich and Yu. I. Yalamov, *Zh. Fiz. Khim.*, 36, 1096 (1962); Yu. I. Yalamov, *Zh. Fiz. Khim.*, 37, 1123, 1393, 1429 (1963); in: *Research in Surface Forces*, Vol. 2, Consultants Bureau, New York (1966), p. 104; P. Richmond, *J. Chem. Soc., Faraday Trans. II*, 70, 1066 (1974); 71, 1154 (1975); F. S. Kaplan, I. F. Efremov, and O. G. Us'yarov, in: *Surface Forces in Thin Films and Stability of Colloids*, Nauka, Moscow (1974), p. 171; F. S. Kaplan and O. G. Us'yarov, *Kolloidn. Zh.*, 36, 258, 672 (1974).
68. B. V. Derjaguin and V. M. Muller, *Dokl. Akad. Nauk SSSR*, 225, 601 (1975); V. M. Muller and B. V. Derjaguin, *Dokl. Akad. Nauk SSSR*, 228, 645 (1976); *Kolloidn. Zh.*, 38, 1117 (1976); *Izv. Akad. Nauk SSSR, Ser. Khim.*, No. 8, 1710 (1982); *J. Colloid Interface Sci.*, 61, 361 (1977); *Colloids Surfaces*, 6, 205 (1983).
69. S. Levine, G. M. Bell, and D. Calvert, *Can. J. Chem.*, 40, 518 (1962); G. A. Martynov and A. L. Muler, in: *Research in Surface Forces*, Vol. 3, Consultants Bureau, New York (1971), p. 236; J. Bockris and M. A. Habib, *J. Res. Inst. Catal. Hokkaido Univ.*, 23, 47 (1975); S. Levine and G. M. Bell, *J. Electroanal. Chem.*, 65, 415 (1975).
70. V. M. Muller and B. V. Derjaguin, *Kolloidn. Zh.*, 37, 1116 (1975); V. M. Muller, G. A. Martynov, G. L. Kuz'mina, and I. V. Bulatova, *Kolloidn. Zh.*, 38, 480 (1976).
71. R. Hunter and H. Wright, *J. Colloid Interface Sci.*, 37, 564 (1971).
72. M. P. Sidorova, J. Lyklema, and D. A. Fridrikhsberg, *Kolloidn. Zh.*, 38, 716 (1976).
73. M. P. Sidorova and D. A. Fridrikhsberg, *Kolloidn. Zh.*, 39, 1103 (1977); D. A. Fridrikhsberg, M. P. Sidorova, M. Fazilova, and N. B. Dmitrieva, in: *Surface Forces in Thin Films*, Nauka, Moscow (1979), p. 119; N. V. Churaev, I. P. Sergeeva, V. D. Sobolev, and B. F. Derjaguin, *J. Colloid Interface Sci.*, 84,

- 451 (1981); I.P. Sergeeva, V. L. Sobolev, and N. V. Churaev, *Kolloidn. Zh.*, 43, 918 (1981).
74. B. W. Ninham and V. A. Parsegian, *J. Theor. Biol.*, 31, 405 (1971); S. Levine and A. L. Smith, *Discuss. Faraday Soc.*, 52, 290 (1971).
75. H. Wright and R. Hunter, *Aust. J. Chem.*, 26, 1191 (1973); D. Chan, T. W. Healy, L. R. White, and D. E. Yates, *J. Electroanal. Chem.*, 80, 57 (1977); T. W. Healy and L. R. White, *Adv. Colloid Interface Sci.*, 9, 303 (1978); J. A. Davies, R. O. James, and J. O. Leckie, *J. Colloid Interface Sci.*, 63, 480 (1978); J. A. Davies and J. O. Leckie, *J. Colloid Interface Sci.*, 67, 90 (1978); 74, 32 (1980); D. G. Hall and M. J. Sculley, *J. Chem. Soc., Faraday Trans. II*, 73, 869 (1977); H. M. Rendall and A. L. Smith, *J. Chem. Soc., Faraday Trans. I*, 74, 1179 (1978); W. Stumm, R. Kummert, and L. Sigg, *Croat. Chem. Acta*, 53, 291 (1980).
76. D. Chan, J. W. Perram, L. R. White, and T. W. Healy, *J. Chem. Soc., Faraday Trans. I*, 71, 1046 (1975).
77. D. E. Yates, S. Levine, and T. W. Healy, *J. Chem. Soc., Faraday Trans. I*, 70, 1807 (1974); W. J. Wnek and R. Davies, *J. Colloid Interface Sci.*, 60, 361 (1977); R. O. James, J. A. Davies, and J. O. Leckie, *J. Colloid Interface Sci.*, 65, 331 (1978); W. Smit and C. Holten, *J. Colloid Interface Sci.*, 78, 1 (1980); L. Sigg and W. Stumm, *Colloids Surfaces*, 2, 101 (1981).
78. W. Smit, C. Holten, H. Stein, J. de Goeij, and H. Theelan, *J. Colloid Interface Sci.*, 63, 120 (1978); D. E. Yates, R. O. James, and T. W. Healy, *J. Chem. Soc., Faraday Trans. I*, 76, 1 (1980); D. E. Yates and T. W. Healy, *J. Chem. Soc., Faraday Trans. I*, 76, 9 (1980).
79. R. O. James, *Colloids Surfaces*, 2, 201 (1981).
80. R. M. Pashley, *J. Colloid Interface Sci.*, 80, 153 (1981); 83, 531 (1981).
81. J. Westall and H. Hohl, *Adv. Colloid Interface Sci.*, 12, 265 (1980).
82. T. F. Tadros and J. Lyklema, *J. Electroanal. Chem.*, 17, 267 (1968); J. Lyklema, *Croat. Chem. Acta*, 43, 249 (1971).
83. A. van Diemen and H. N. Stein, *J. Colloid Interface Sci.*, 67, 213 (1978).
84. G. A. Martynov, *Kolloidn. Zh.*, 40, 1110 (1978).

Chapter 2

DISJOINING PRESSURE

2.1. TWO KINDS OF SURFACE FORCE

Chapter 1 gave a general outline of the effects of long-range forces at interfaces. Surface forces of two kinds must be distinguished. First, there are the forces acting in the interfacial region on molecules, leading to departures of the appropriate intensive properties from their values in the bulk phase. These forces or effects are either of a dispersion nature (molecular or van der Waals forces, as will be discussed in Chapter 4), or originate with the macroscopic electrostatic field created by a nonuniform distribution of ions of both signs (formation of ionic double layers) or, finally, are functions of a special structure of interfacial layers. These forces and effects are responsible for the appearance and magnitude of the interfacial tension and potential jump. The study of interfacial molecular forces has a long history, but these forces are not discussed in detail in the present monograph.

However, when a system is not in thermodynamic equilibrium, these same forces give rise to effects that have not been investigated until recently, except for the electrokinetic phenomena. Among such relatively new effects are capillary osmosis, diffusio-phoresis, thermo-osmosis, thermophoresis, and some others analyzed in Chapter 11.

In contrast, there is a second class of surface force, which will be analyzed in more detail. This comprises long-range surface forces that arise when two interfacial regions overlap.

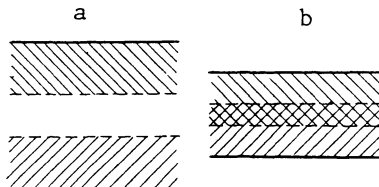


Fig. 2.1. a) Thin Gibbs layer; b) non-Gibbs layer.

As mentioned earlier, Gibbs capillarity theory treats only cases in which the mass of components of the system and extensive thermodynamic functions of the system (Helmholtz free energy, entropy, etc.) equal the sum of terms proportional to the volumes of the phases and terms proportional to the areas of interfaces between the phases. This approach presupposes that interfacial zones do not overlap anywhere in the system (Fig. 2.1a). Indeed, it was Gibbs's assumption that in the middle of a thin interlayer in equilibrium with the bounding phases there is a region (Fig. 2.1a) that retains the intensive properties of the bulk phase. This is equivalent to postulating that the zones in which surface forces of the first kind operate do not overlap. If such an interlayer constitutes a part of the bulk phase from which it was formed, then the presence of bulk properties within the interlayer is easily established by comparative experiments. If the interlayer is isolated from the bulk phase, as in a soap bubble freely floating in the air, local overlapping of the two subsurface zones results in departures from the originally uniform interlayer thickness, under external perturbation, no matter how small.

The presence of bulk phase in the interlayer can be detected, in principle, by studying the change in intensive properties (e.g., density or optical properties) along the normal to the interlayer surface if a sufficiently sensitive technique is used (e.g., an optical method). For a theoretical approach it is immaterial to what extent these tests are practically realizable. But a case of special interest, excluded from Gibbs's analysis, is that of two transition zones (i.e., fields of surface forces of the first kind) overlapping as a result of thinning of the interlayer of one phase sandwiched between the other two (Fig. 2.1b). A new set of phenomena appears. It is impossible to develop a theory of equilibrium and stability of colloids, foams and thin films, a theory of polymolecular adsorption, wetting, swelling of colloids, and intracrystalline swelling of laminated minerals without analyzing these phenomena. The theories of electrokinetic phenomena and of a number of mass transfer effects in disperse systems would also be incomplete. The modern theory of dispersion interaction also belongs to this field.

Until the interfacial fields overlap, a decrease in the interlayer thickness at constant phase volumes and constant areas of interfaces does not require work to be spent on a change in the free energy of the system; energy is dissipated only to overcome viscous and other passive resistance forces. The moment these fields overlap, the situation changes drastically (Fig. 2.1b). Now the interlayer thickness can be changed only by doing positive or negative work. Hence, the source of this work is a repulsive or attractive force appearing in the zone where the surfaces overlap. We shall refer to these forces induced by overlapping as surface forces of the second kind. Their theoretical analysis must be based on molecular or microscopic notions. In the general case, this constitutes an extremely complex problem, both physically and mathematically. To drastically simplify the problem, it is expedient to start with the simplest case, viz., the forces arising during thinning of a layer of uniform thickness h .

This simple case not only facilitates the theoretical calculation of the relevant forces but can also be used, as shown in [1], as a basis for an approximate calculation of the forces that act in interlayers of nonuniform thickness, and even in interlayers bounded by curved surfaces.

Finally, the plane-parallel layer model is convenient for an experimental study of surface forces of the second kind as functions of distance; and precisely this system arises in practice — for example, in the thinning of soap films.

This experimental problem was first formulated and solved for interlayers of uniform thickness between solid phases [2], a solid and a gaseous phase [3], and two gaseous phases [4]. The work led to the introduction of the concept of "disjoining pressure" in a thin interlayer, later considerably elaborated and widely applied.

2.2. DEFINITION OF DISJOINING PRESSURE

No departures from the laws of hydrostatics can be detected until the interfacial zones in a thin liquid film overlap; in the absence of external forces, the pressure in the layer is equal to the pressure of the bulk phase that formed the film. Thus, the interlayer thickness can change without change of free energy. The situation must change when overlapping sets in. This means that the hydrostatic pressure in a thin interlayer must differ from the pressure in the contiguous bulk phase from which the interlayer was formed when its thickness diminished. The additional (or supplementary) pressure in such a thermodynamically equilibrium interlayer was called the disjoining pressure [2, 3]. It is usually denoted by Π . The sign of this pressure can be either positive or negative — the latter when the surface forces of the second kind tend to reduce the thickness of the interlayer.

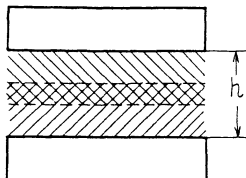


Fig. 2.2. Overlapping interfacial layers in the interlayer separating two parallel plates.

Clearly, a disjoining pressure could be measured by applying an external pressure just sufficient to keep the interlayer in mechanical equilibrium. Depending on the balancing method, the measure of a positive disjoining pressure is either the additional pressure on the surface of the interlayer or the drop in the pressure within the bulk phase that produced the interlayer. In both cases the disjoining pressure $\Pi(h)$ of the interlayer in thermodynamic equilibrium with the surrounding phases is equal to the difference between the pressure P_1 on the interlayer surface and the pressure P_0 in the bulk phase from which the interlayer extends:

$$\Pi(h) = P_1 - P_0 \quad (2.1)$$

where h is the interlayer thickness [5].

In order to give this general definition a concrete meaning, we shall discuss it for three particular cases.

Example 1. Consider an interlayer between two parallel plates (Fig. 2.2). Here the disjoining pressure equals the force per unit area N required to maintain the equilibrium thickness of the interlayer. The sign of N must coincide with that of $\Pi(h)$. In principle, this is sufficient, although the equilibrium must be a stable one for any practical realization of accurate measurements. The stability of the equilibrium is produced automatically, through the properties of the interlayer, if

$$\frac{\partial \Pi(h)}{\partial h} < 0 \quad (2.2)$$

If this condition is reversed, i.e., if

$$\frac{\partial \Pi(h)}{\partial h} > 0 \quad (2.3)$$

the interlayer is unstable. Condition (2.3) applies regardless

of thickness in the case of two plates separated by an interlayer of gas or vacuum.*

Under these conditions the pressure $\Pi(h)$ can be measured accurately at any thickness only if the external pressure N changes with h substantially more steeply than Π : in other words, it is necessary that

$$\frac{\partial N}{\partial h} > \frac{\partial \Pi}{\partial h} \quad (2.4)$$

The simplest way to realize this constraint is to link the plates by an elastic coupling of high stiffness, although this method necessarily reduces the sensitivity of measurements of force and, hence, of disjoining pressure. It is better to employ a negative feedback that acts as a very rigid spring; this achieves high sensitivity of force measurements and enables the experimenter to make stepwise changes in the interlayer thickness.

Example 2. Consider a liquid film of uniform thickness on a flat surface of an insoluble solid and in contact at its periphery with the bulk phase (Fig. 10.1). This case was realized in the earliest experiments with a liquid interlayer wedged between a glass plate and a gas bubble [3]. The disjoining pressure of the so-called "wetting film" is

$$\Pi(h) = P_1 - P_0 \quad (2.5)$$

or, with the difference $P_1 - P_0$ expressed via the Laplace-Young equation,

$$\Pi(h) = K\sigma \quad (2.6)$$

where σ is the surface tension of the liquid, and K is the curvature of the meniscus surface separating the gas bubble and the liquid phase. Therefore, in order to obtain the "disjoining pressure isotherm" – i.e., Π as a function of h – it is necessary to vary the surface curvature and measure the corresponding equilibrium values of film thickness. This is achieved, for instance, by changing the bubble diameter or by removing the liquid by suction from the bulk liquid surrounding the wetting film (Fig. 10.10).

If the liquid is appreciably volatile, the condition of chemical equilibrium through the vapor phase (adsorption) must also be

*Later in this chapter we shall explain how to interpret deviations from Pascal's hydrostatic law for a gas interlayer or vacuum, in terms of the generalized pressure tensor in interfacial zones and thin interlayers. It is usual (and natural) to speak here of molecular attraction between the plates. From our (general) point of view this is a negative disjoining pressure. However, it was shown in [6] that in a sufficiently dense gas the interaction between very thin plates can reduce to a positive disjoining pressure.

satisfied. For a one-component liquid this condition has the form

$$K\sigma = \Pi(h) = (RT/v_m) \ln(p_s/p) \quad (2.7)$$

where v_m is the molar volume of the liquid, p is the vapor pressure of the film and equal to the vapor pressure over the meniscus of the bulk phase, and p_s is the vapor pressure over a flat surface of this phase at the same temperature. If the bubble contains the vapor of the interlayer and a gas with a partial pressure p_1 , the condition of mechanical equilibrium of the film must be rewritten as follows:

$$P_1 = p(h) + p_1 = \Pi(h) + P_0 \quad (2.8)$$

By substituting $p(h)$ in (2.8) with the expression that follows from (2.7), we obtain

$$p_s \exp(-v_m \Pi(h)/RT) = \Pi(h) + P_0 - p_1 \quad (2.9)$$

By solving this equation with respect to $\Pi(h)$, we find that Π and h are functions of the difference $P_0 - p_1$. Hence, the function $\Pi(h)$, i.e., the disjoining pressure isotherm, is best determined by varying P_0 because in most experiments the values of p_1 are very close to the atmospheric pressure. In fact, it is more convenient to use Eq. (2.8) because the difference $P_1 - P_0$ is usually recorded by a manometer. If p_1 is varied in the experiments, Eq. (2.9) is more helpful.

Equation (2.7) must be used when the wetting film does not communicate with the bulk liquid phase – for instance, when it covers the surface of a sphere. In this case the thickness and uniformity of the film are essentially determined by the adsorption equilibrium with the surrounding vapor. The disjoining pressure isotherm $\Pi(h)$ can then be calculated through Eq. (2.7) by varying the relative pressure p/p_s and measuring the corresponding film thickness h . Since a correction must be introduced for the curvature of the substrate, if present, it is expedient, of course, to study a polymolecular adsorption film on a flat substrate; this also helps to improve the accuracy of measuring film thickness. Equation (2.7) can be used irrespective of whether there is a bulk phase communicating with the film. Clearly, once the vapor pressure is prescribed, the film thickness, and hence the surface forces of the second kind responsible for the disjoining pressure, are also fixed.

Example 3. A case of special interest is determination of the disjoining pressure of a liquid interlayer between two fluids, for example, between two gaseous phases; this system is referred to as a "free film," both surfaces of the film being ideally smooth.

A schematic diagram of the first measurements of this type is given in Fig. 3.5. The disjoining pressure is calculated, as in case 2, as the difference $\Pi(h) = P_1 - P_0$ between the pressures in the gaseous phase and in the bulk liquid from which the film extends. In order to reach a large value of Π , Mysels [7] used a setup with a porous diaphragm separating the free film from the bulk phase. However, this method makes it more difficult to prevent contamination and to maintain chemical equilibrium among all the components of the film and bulk phase.

The range of values of $\Pi(h)$ can be made especially wide by using the conditions of chemical equilibrium established through the vapor phase, if we use the normally acceptable assumption that the surfactants required to stabilize a free film are practically involatile. However, surfactants are soluble; consequently, p_s in (2.7) must be interpreted as the pressure of saturated vapor over a flat surface of the surfactant solution with concentration equal to that of the solution from which the free film was formed by thinning. If this film does not communicate with the bulk phase of the solution (e.g., a free soap bubble), the determination of p_s requires an additional equation that can be obtained, for instance, by measuring the tension of the free film. However, even if we forgo the unavoidable complications in the experimental procedure, the uncertainty caused by this factor cannot be large because the bulk concentrations of surfactants used to stabilize free films are usually very low.

Despite the diversity in the methods of measuring the disjoining pressure as a function of interlayer thickness, they are all based on the general definition of disjoining pressure, expressed by formula (2.1), which holds even if the interlayer between two phases is a vacuum. In fact, the disjoining pressure is the most important thermodynamic parameter of a thin interlayer.

2.3. RELATIONSHIP BETWEEN DISJOINING PRESSURE AND OTHER THERMODYNAMIC FUNCTIONS

Let us now show how the disjoining pressure is related to other thermodynamic functions. Consider the Gibbs free energy (thermodynamic potential) G of a system of several phases, containing a plane-parallel interlayer of thickness h of one of the phases. Take a reversible equilibrium change in a system at constant temperature T , constant chemical potentials of components μ_i , and constant pressure P , accompanied by a change in the interlayer thickness h by dh . In the course of this change the external forces (without which the thin layer could not be in equilibrium) do the following work on the system:

$$-\Pi(h) dh \quad (2.10)$$

This work must be equal to the increment dG of thermodynamic potential. Hence,

$$\Pi(h) = -(\partial G / \partial h)_{T, \mu_i, P} \quad (2.11)$$

It would be a mistake to express $\Pi(h)$ in terms of the derivative of the Helmholtz free energy F , because a change in the thickness of the interlayer (whose density differs from that of the mother liquid) would change the volume of the bulk liquid and hence of the system as a whole. The free energy F would then change not only as a result of external forces balancing out the disjoining pressure but also of the forces applied to the surface of the total volume of the system. This mistake unfortunately appeared in the definition of disjoining pressure as formulated in the IUPAC nomenclature [28].

An even greater shortcoming of this definition lies in the fact that an equation of the type of (2.11), without at the same time giving a direct dynamic determination of disjoining pressure (as we gave above), is found to be devoid of physical content; it merely represents a notation for the result of a mathematical operation. But even if we subsequently recall (which the nomenclature [28] fails to do) the physical meaning of $\Pi(h)$, the IUPAC commission's definition prompts theories first to calculate $G(h)$ on the basis of a specific molecular model, and then to find $\Pi(h)$ by taking the derivative. But it is clear that if we want to construct a theory of, for example, the electrostatic component of disjoining pressure, $\Pi_e(h)$, then the calculation of $G_e(h)$ requires that we know the potential or charge at the boundaries of the diffuse ionic layer as a function of thickness h . As this is a very complicated problem, any rigorous calculation of $\Pi_e(h)$ becomes questionable. But in fact $\Pi_e(h)$ depends only on the value of the potentials or charges at the boundaries of the diffuse ionic layer at a given thickness and state of this layer, and the calculation of $\Pi_e(h)$ is relatively simple and unambiguous. Furthermore, Muller [8] showed that $G_e(h)$ can be obtained analytically by integrating $\Pi_e(h)$ both at a constant potential and at a constant charge at the boundaries of the ionic atmosphere.

Finally, there is an important advantage in considering the direct definition of disjoining pressure as a primary one: it makes it possible to determine the disjoining pressure isotherm from experiments, leading to the thermodynamic potential as a function of interlayer thickness by integration. This last dependence is not always obtainable by a direct experiment.

The dynamic definition of disjoining pressure gains rigorous meaning only after a theoretical interpretation on the basis of a molecular model. Our preliminary step will therefore be to analyze the microscopic pattern of those departures from Pascal's law that find their

integral expression in the disjoining pressure as a function of interlayer thickness. This approach is a generalization and refinement of the treatment of surface tension in liquids developed by Bakker [9] and others.

2.4. PRESSURE DISTRIBUTION IN THE INTERFACIAL TRANSITION ZONE

In his treatment of equilibria of heterogeneous systems, Gibbs assumed that intensive quantities are identical at all points within each phase, except in transition layers at the interfaces. As for the pressure, in the transition zone it becomes a tensor, not only changing along the normal but simultaneously being anisotropic. Only the normal component $P_N = P_{zz}$ remains constant (in the case of a flat interface).

The interfacial transition layer is defined as the zone with thickness h_0 , all elements of which contribute to surface tension σ_0 , in accordance with Bakker's formula [9]

$$\sigma_0 = \int_{-h_0/2}^{h_0/2} (P_N - P_T) dz \quad (2.12)$$

where P_N and P_T are the normal and tangential components of the pressure tensor, respectively, and z is the coordinate perpendicular to the interface.

However, the situation changes if all elements with the properties of the original phase disappear as a result of overlapping of interfacial zones when the interlayer thickness diminishes. The pressure is then anisotropic everywhere within the thin interlayer, and its tension is not equal to $2\sigma_0$. The pressure in the thin interlayer differs from the pressure in the mother phase by the value of the disjoining pressure Π .

Therefore, when the interlayer thickness diminishes, the vanishing of its isotropic part and the appearance of the disjoining pressure are always simultaneous.

As an example, Fig. 2.3 shows the distributions $P_N(z)$ and $P_T(z)$ in a liquid interlayer 3 of thickness h bounded by two identical phases 1 and 2 (liquid or gaseous). The normal and tangential components of the pressure tensor in the anisotropic zone h_0 can differ in sign and magnitude. Under equilibrium conditions the equality $P_T = P_N = P$, where P is the isotropic pressure in the bulk of the phases contiguous with the interlayer, holds only beyond the zone h_0 .

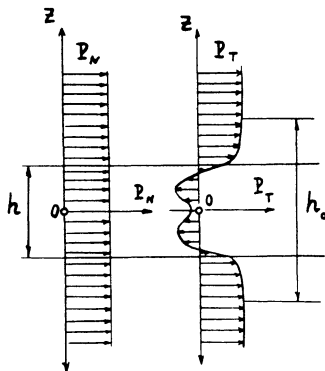


Fig. 2.3. Distribution of the pressure tensor components P_N and P_T in a thin liquid interlayer.

In equilibrium the normal component P_N does not change at the boundaries of a flat interlayer. The tangential component P_T changes in a complicated manner, depending on the nature of the forces acting in the interlayer and in the contiguous phases.

The constancy of P_N in the transition zone implies that the resultant of the volume forces acting on an elementary layer of thickness dz is zero (Fig. 2.3). These can be electrical forces acting on the charges of the diffuse double layers, or molecular attractive forces originating in the contiguous layers. Taking into account the electromagnetic nature of molecular forces, one can make use of the Faraday-Maxwell concept that electrostatic and electromagnetic forces are actually not long-range forces but are representable by equivalent forces of tension depending on the local values of electric and magnetic field strength. This idea was realized in the macroscopic theory of the van der Waals forces [10, 11]. This theory allows a replacement of the long-range molecular forces by the Lifshitz tensor [10], included together with the electrostatic field tensor [11] in the pressure field tensor.

This approach makes it possible to eliminate the bulk forces from the analysis. At the same time, such a generalization of the pressure concept removes the ambiguities and uncertainty of this notion as applied to interfacial transition layers and thin interlayers in which the characteristic range of the van der Waals-London forces is of the same order of magnitude as the scale of inhomogeneities in the direction of the normal to the interface. If we retain the "classical" approach, it is impossible to formulate correctly the equilibrium conditions for physically small volume elements dz within the interlayer (Fig. 2.3). It is only by eliminating the volume forces and replacing them with the equivalent stress

tensor that the solution of the problem becomes possible and rigorous conditions of hydrostatic equilibrium can be written.

Under the conditions of the z-axial symmetry of the fields ($E = Ez$, $Ex = Ey = 0$) the generalized tensor of hydrostatic pressure can be written in the form [11-13]

$$P_N = P_{zz} = P_t + P_h^N + \frac{E^2}{8\pi}(\epsilon_0 + \rho \frac{\partial \epsilon_0}{\partial \rho}) + \frac{\hbar}{16\pi kT} \times \int_0^\infty \overline{E^2(\omega)} [\epsilon(\omega) + \rho \frac{\partial \epsilon(\omega)}{\partial \rho}] d\omega \quad (2.13)$$

$$P_T = P_{yy} = P_{xx} = P_t + P_e^T - \frac{E^2}{8\pi}(\epsilon_0 + \rho \frac{\partial \epsilon_0}{\partial \rho}) - \frac{\hbar}{16\pi kT} \times \int_0^\infty \overline{E^2(\omega)} [\epsilon(\omega) - \rho \frac{\partial \epsilon(\omega)}{\partial \rho}] d\omega \quad (2.14)$$

The expression for the electromagnetic field tensor is approximate, being strictly applicable only to media without spatial dispersion [13].

Here E is the local strength of the electrostatic field, k is the Boltzmann constant, \hbar is Planck's constant, T is the absolute temperature, $\overline{E^2(\omega)}$ is the spectral density of the local mean squared strength of the fluctuation electromagnetic field [10, 11], ϵ_0 is the static dielectric constant of the medium, $\epsilon(\omega)$ is the permittivity of the medium taken along the imaginary axis of frequency $\omega = i\xi$, and ρ is the density of the medium. In keeping with standard procedure, expressions (2.13) and (2.14) neglect the magnetic field fluctuations.

The term P_t in Eqs. (2.13) and (2.14) represents the effect of thermal motion and Born's repulsive forces, while P_h^N and P_h^T represent the effect of hydrogen bonds and other forces that are not taken into account by Maxwell's stress tensor and the Lifshitz theory. If the molecules or atoms are spherically symmetrical, or if the molecules are not oriented (isotropic state),

$$P_h^N = P_h^T \quad (2.15)$$

Therefore, volume forces are eliminated if we neglect the action of gravity forces and other external forces on the system. This program was partially realized in [14]; it was possible, by using Scherbakov's idea [15], to generalize Bakker's approach to the tension σ of free films of electrolyte solutions.

An analysis of equilibrium of an elementary parallelepiped with edges of length dx , dy , and dz (dz being much less than the layer inhomogeneity scale) yields the condition $P_N = P_{zz} = \text{const}$; i.e., P_N must be independent of z .

On the other hand, the existence of film tension and of the interface requires that the pressure tensor be anisotropic and, hence, that P_{zz} be not equal to $P_{xx} = P_t$, where x is the direction along the layer. Furthermore, P_{xx} must be a function of the coordinate z . In the general case when, for instance, the surface possesses a tangential component of the dipole moment, regardless of the factor that produces it, the components P_{xx} and P_{yy} may not be equal (for a rigid dipole moment this is also true in zero external electric field).

By substituting expressions (2.13) and (2.14) for P_N and P_t into (2.12), we obtain

$$\sigma = \frac{h_0/2}{-h_0/2} \left[\frac{\epsilon_0 E^2}{4\pi} + \frac{\hbar}{16\pi kT} \int_0^\infty \epsilon(\omega) \overline{E^2(\omega)} \right] d\omega \quad (2.16)$$

The first term of this expression was derived earlier in [14].

2.5. REFINEMENT OF THE DEFINITION OF DISJOINING PRESSURE

Now we can refine the concept of the disjoining pressure. The pressure P on the surface of a thin flat plane-parallel layer is equal to the normal component $P_{zz} = P_N$ of the pressure tensor within this layer (Fig. 2.4). Consequently, a more general and more rigorous definition of disjoining pressure is needed, valid for any liquid or gaseous interlayer between any phases in an arbitrary state of aggregation, viz.: the disjoining pressure $\Pi(h)$ is equal to the difference, realized in mechanical equilibrium, between the component P_{zz} of the pressure tensor in the interlayer and the pressure P_0 in the phase from which the interlayer was formed as a result of its thinning:

$$\Pi(h) = P_{zz} - P_0 = P_N - P_0 \quad (2.17)$$

In the simplest case, when the phase and its thin interlayer are both one-component, mechanical equilibrium under isothermal conditions simultaneously implies total thermodynamic equilibrium. Then the disjoining pressure is a single-valued function of the interlayer thickness h (or, to be more definite, of the number of moles Γ per unit area) and represents an exhaustive thermodynamic characteristic of the thin interlayer, distinguishing it from the state of the mother bulk phase.

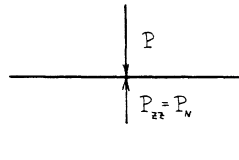


Fig. 2.4. Forces acting on a plane interface.

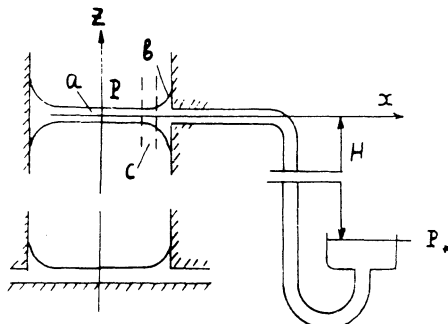


Fig. 2.5. Equilibrium between horizontal films and bulk liquid.

Let us illustrate the physical meaning of Eq. (2.17) with specific examples. Figure 2.5 shows free and wetting films formed by sucking the liquid away through a planar vertical slit. The liquid film a is in equilibrium with the adjacent capillary menisci. The pressure in the bulk of the contiguous gas phase is $P = P_N$. By definition, the pressure P_0 refers to the liquid under the capillary meniscus outside the transition zone c in which surface zones still overlap. The difference $P - P_0$ in the zone b of the bulk of the meniscus corresponds to a jump of pressure across a curved interface. In other words, $P - P_0$ outside the transition zone is equal to P_k , i.e., to the capillary pressure of the nonperturbed meniscus of constant curvature (assuming the effect of gravity to be negligible).

If a liquid plane-parallel interlayer is sandwiched between two solid plates, the normal pressure P_{zz} in the interlayer is found by dividing the force that must be applied to each of the plates for maintaining equilibrium by the plate area.

Obviously, it would be wrong to make the definition of disjoining pressure that follows from the above arguments and from formula (2.17) dependent on the sign of P_{zz} (pressure or tension) and on the type of interlayer. It is thus immaterial whether the interlayer is liquid or gaseous. But in the latter case P_{zz} is negative, indicating tension, not pressure. It retains its physical meaning, and so does the difference $P_{zz} - P_0$ in (2.17), at any degree of rarefaction of the gas and, hence, holds for plates in a vacuum.

No contradictions are encountered in this situation, because the pressure tensor $P_{zz}(h)$ in the interlayer includes the stress tensor $T_{zz}(h)$ of the fluctuating electromagnetic field taken with reversed sign. Indeed, the Lifshitz theory calculates the component of this tensor, $T_{zz}(h)$; the molecular attractive pressure A is assumed equal to

$$A = T_{zz}(h) - T_{zz}(\infty)$$

where $T_{zz}(\infty)$ is the pressure of electromagnetic fluctuations in the bulk of the vacuum. Evidently, A is at the same time equal to the disjoining pressure of the vacuum interlayer taken with the reversed sign:

$$A = -[P_{zz}(h) - P_0] = -\Pi(h)$$

because $P_{zz}(h) = -T_{zz}(h)$ and $P_0 = -T_{zz}(\infty)$. Therefore, the suggested definition of disjoining pressure is valid in all cases, including high vacuum and gaseous interlayers.

With $\Pi(\Gamma)$ known, it is also possible to find the excess tension in the film $\Delta\sigma$, as compared with the sum of surface tensions σ_{13} and σ_{23} (the subscript 3 refers to the film, and the subscripts 1 and 2 to the adjacent phases) [16]:

$$\Delta\sigma = \sigma - \sigma_{13} - \sigma_{23} = v_m \int_0^\Gamma \Gamma d\Pi \quad (2.18)$$

where σ is the film tension, and v_m is the molar volume of liquid in the interlayer, assumed to be constant. If the film thickness h is physically meaningful, the following substitution can be introduced into Eq. (2.18): $\Gamma v_m = h$. In contrast to the function $\Pi(\Gamma, T)$ the function $\sigma(\Gamma, T)$ can be used as the main thermodynamic characteristic only for films not in contact with a solid, since in this case σ cannot be measured in principle.

When the interlayer and the mother phase are multicomponent, a mechanical equilibrium between them does not imply total thermodynamic equilibrium because approach to total equilibrium may be a slow process, usually connected with diffusion. Thermodynamic equilibrium may be reached over a much longer time than that necessary for mechanical equilibrium. The latter may be reached rapidly for an interlayer between two solids — for example, if a rigid feedback is used. It would be instructive to show experimentally that the disjoining pressure in multicomponent systems can vary slowly over a long time at constant interlayer thickness.

A fast approach to mechanical equilibrium can also be assured when a thin interlayer is formed between surfaces of large cur-

vature - for instance, between thin crossed fibers. It was shown by one of us [17] that in this system also a slow change in the state of the interlayer separating the fibers does take place with a constant applied force. In this case, only a partial mechanical equilibrium is reached. Similar slow processes probably account for the reported kinetics of adhesion of disperse particles to flat quartz plates, studied by von Buzagh [18].

Presumably, such processes depend not only on the diffusion of components of the solution but also on structural transformations within the interlayer, due to the overlapping of two boundary layers having a special liquid structure and adjacent to the two solid surfaces. The structure may be modified in a single-component interlayer as well, so that even in this simplest case the disjoining pressure may change, reaching an equilibrium value only after a sufficiently long time.

To recapitulate, regardless of the number of components in an interlayer, its disjoining pressure corresponds either to a partial, mechanical equilibrium or to a total, thermodynamic one.

The available experimental data do not reveal slow structural transformations in liquid interlayers between lyophobic surfaces characterized by the absence of boundary layers with a special structure. The same conclusion follows from experiments with crossed metal wires in aqueous electrolyte solutions. These experiments [19] detected no slow variation of disjoining pressure. They agree quite well with the DLVO theory that takes into account only two components of disjoining pressure, viz., the component produced by the overlapping of diffuse ionic layers Π_e , and the component produced by the molecular force Π_m .

So far we have been discussing liquid interlayers bounded by plane-parallel interfaces. The case of curved surfaces is much more complicated. As a first approximation, we can limit ourselves to considering only the surface curvature K . However, since the main contribution to film tension σ comes from short-range forces concentrated at the two surfaces of the film, the film surface tensions do not differ greatly from the surface tension of each of the bulk phases: σ_{13} and σ_{23} . Consequently, we can again write for the layers within the film

$$P_{zz} = \text{const}$$

However, in contrast to a flat film, here P_{zz} differs from the pressures P_1 and P_2 in the phases, between which the interlayer 3 is sandwiched, by $K_1\sigma_{13}$ and $K_2\sigma_{23}$, respectively, where K_1 and K_2 describe the curvatures of the interfaces:

$$\begin{aligned} P_{zz} &= P_1 - K_1 \sigma_{13} \\ P_{zz} &= P_2 - K_2 \sigma_{23} \end{aligned} \quad (2.19)$$

Thus, according to (2.17), the following condition of mechanical equilibrium is obtained for a wetting film on an interface:

$$\Pi(h) = -K_1 \sigma_{13} + P_1 - P_0 \quad (2.20)$$

This equation must be used in such cases as the determination of a profile of a film — for instance, a film wetting a nonflat surface.

To the first approximation it can also be assumed that when a layer is bounded by curved surfaces but its thickness is a slowly varying function along the interlayer ($dh/dx \ll 1$), the local value of disjoining pressure $\Pi(h)$ is equal to the disjoining pressure of a flat film with the same thickness. This approximation finds fruitful applications of the concept of disjoining pressure to the statics and kinetics of systems involving thin liquid interlayers of nonuniform thickness.

The approach outlined above fails in the following cases:

- i) when interlayers separate surfaces with edges or angles, or when radii of curvature of the surfaces are of the same order as, or less than, the thickness of the layer in which the disjoining pressure has a significant magnitude, as we find in fine-dispersion systems;
- ii) in the transition zone close to large contact angles, where the layer thickness changes rapidly with distance and, therefore, the local disjoining pressure $\Pi(h)$ is not equal to the pressure of a plane-parallel interlayer. If a layer is sufficiently thick, its disjoining pressure is negligibly small, and classical equations of capillarity theory are valid.

2.6. EQUILIBRIUM OF FILMS UNDER GRAVITY

Consider now two examples of equilibrium of thin liquid interlayers in a gravitational field. Let a free film containing dissolved surfactant molecules be pulled out of a liquid by lifting a horizontal wetted wire or filament (Fig. 2.6). The force of gravity acting on an elementary segment of the film between the levels H and $H + dH$ is obviously balanced out by a difference $d\sigma$ between film tensions at the two levels, due to different thicknesses at the respective cross sections. Any extension of a film is known to perturb the adsorption equilibrium, changing the values

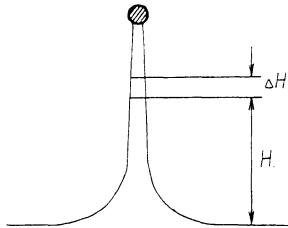


Fig. 2.6. The profile of a free film, drawn from a liquid containing a surfactant.

of adsorption at the liquid/gas interface. Hence, it produces unequal values of the surface tension σ_{13} on both surfaces of the film. Tension is higher in thinner segments.

This effect of "film elasticity" was already recognized by Gibbs [20]. It is evidently not related to the disjoining pressure in the film, because it is also observed in thick films in which subsurface layers do not overlap and the middle layer has the bulk-phase properties. However, this effect undergoes relaxation as a result of diffusion of components along the film. The system tends to thermodynamic equilibrium in which the chemical potentials μ_i of all components meet the condition

$$\mu_i + m_i g H = \text{const} = C_i \quad (2.21)$$

where m_i is the molar mass of the i -th component. However, the Gibbs equation

$$d\sigma_{13} = -\sum \Gamma_i d\mu_i = g dH \sum \Gamma_i m_i \quad (2.22)$$

which is valid for a film whose middle layers have the bulk-phase properties, implies that the difference between surface tensions can balance out only that part of the weight of the segment which lies in the adsorption surface layers. As for the middle "bulk-phase" film, it flows down until the surface layers overlap. Then the effects due to the disjoining pressure of the layer become dominant.

When a system is in total thermodynamic equilibrium, mechanical equilibrium of the film as a whole must be accompanied by a dynamic equilibrium for each elementary layer of the film, with unit width, thickness dz , and height dH . The corresponding equation is

$$dP_{HH}(z) = -\rho g dH \quad (2.23)$$

where z is the coordinate measured along the normal to the symmetry plane of the film, with $z = 0$ on this plane. This equation must hold for all values of z . Hence, if we neglect the dependence of film density ρ on film thickness and coordinate z , we find

$$\frac{\partial P_{HH}}{\partial H} = -g\rho = \text{const} \quad (2.24)$$

Simultaneously we have

$$P_{zz} = P_1 \quad (2.25)$$

where P_1 is the pressure in the external gas at the same level of H . Therefore,

$$\frac{\partial P_{zz}}{\partial H} = -\rho_1 g \quad (2.26)$$

where ρ_1 is the density of the ambient phase.

Furthermore, the condition of mechanical equilibrium must hold for the film as a whole:

$$\frac{\partial \sigma}{\partial H} = W \approx gh(\rho - \rho_1) \quad (2.27)$$

where σ is the tension of the whole layer, and W is the effective weight per unit area, taking into account both the adsorption of the surrounding phase and Archimedes' principle; h is the effective thickness of the film.

Using Eqs. (2.12), (2.24), and (2.26), we now integrate from $-\infty$ to $+\infty$ and obtain

$$\begin{aligned} \frac{d}{dH} \int_{-\infty}^{+\infty} [P_{zz} - P_{HH}(z)] dz &= \int_{-\infty}^{+\infty} (\rho - \rho_1)g dz \\ &= (\rho - \rho_1)gh \end{aligned} \quad (2.28)$$

At first glance, the integral conditions of equilibrium so obtained have no connection with disjoining pressure (like the differential conditions previously). However, this conclusion is incorrect, as a better analysis demonstrates.

Indeed, σ is a function of film thickness h and, hence, Eq. (2.27) can be used if we know how h varies with film height. By definition [see Eq. (2.17)], the disjoining pressure of a film at any point equals the difference

$$\Pi(h) = P_{zz} - P_0$$

In the presence of gravity, P_0 is the pressure of the bulk liquid phase with which the film can be in thermodynamic equilibrium, at the same level H . Obviously, the chemical potentials of this phase must satisfy Eq. (2.21) with the same values of constants C_i . Hence,

$$P_0 = P_* - \rho g H \quad (2.29)$$

where P_* is the pressure at the surface of the bulk liquid phase (from which the film was pulled), with height H measured from this surface (see Fig. 2.6). As follows from (2.17) and (2.29),

$$\Pi(h) = P_{zz} - P_* + \rho g H \quad (2.30)$$

By assuming

$$P_{zz} = P_1 = P_* - \rho_1 g H \quad (2.31)$$

and substituting it into (2.30), we find

$$\Pi(h) = (\rho - \rho_1) g H \quad (2.32)$$

With the form of $\Pi(h)$ known, we can find the film thickness h as a function of H for an equilibrium film under gravity. Conversely, with H known, we can find from (2.32) the disjoining pressure of horizontally oriented films (Fig. 2.5).

By differentiating Eq. (2.32), we obtain

$$d\Pi(h) = (\rho - \rho_1) g dH \quad (2.33)$$

By comparing this equation with (2.27), we arrive at a familiar relation

$$d\sigma(h) \approx h d\Pi(h) \quad (2.34)$$

This formula is derived for variations of film thickness dictated by gravity. This imposes certain constraints on the variation, following from Eq. (2.21), of chemical potentials and, hence, film composition. Relation (2.34) is unconditionally true for one-component films [21].

As a second example, we consider in detail the thermodynamic equilibrium under gravity for a film wetting a vertical surface of a solid. In this case, the concept of "film tension" becomes physically meaningless because we lack, even in principle, a recipe for its determination. The same is true for the "surface tension" of such a film, because it has no segments with the properties of the bulk phase.

However, Eq. (2.32) remains valid and makes it possible to find the film thickness h , for a known function $\Pi(h)$, as a function of elevation H of a point above the free surface of the liquid. Actually, $\Pi(h)$ is the function $\Pi(h, \mu_1, \mu_2, \dots, \mu_i)$ in which, for each elevation H , the quantities μ_i have values prescribed by Eq. (2.21). Such problems can be solved if Π is known as a function of all these variables. Therefore, Π acts as the characteristic function of a thin layer.

If the surface of a film is curved, it is necessary, through Eq. (2.20), to take into account also the capillary pressure in the film:

$$\Pi(h) = K_1 \sigma_{13} + (\rho - \rho_1) g H \quad (2.35)$$

where K_1 is the local value of curvature of the film/gas interface.

If the pressure of phase 1 at the film surface is not produced by gravity, we take into account that $P_0 = P_\infty - \rho g H$ and obtain from Eq. (2.20)

$$\Pi(h) = K_1 \sigma_{13} + P_1 - P_\infty + \rho g H \quad (2.36)$$

where P_∞ is the pressure in liquid phase 3 at $H = 0$.

2.7. HYDRODYNAMICS OF THIN FILMS

So far the analysis has been restricted to equilibrium in thin films. Assume now a slight perturbation of equilibrium, resulting in a flow. Assume also that this perturbation appears because of additional pressure $\delta P_{x,y}$ distributed over the film surface. This additional pressure produces increments, equal to $\delta P_{x,y}$, in the corresponding components of the pressure tensor:

$$\delta P_{xx}(h, z) = \delta P_{yy}(h, z) = \delta P_{zz}(h)_{x,y} = \delta P_{x,y} \quad (2.37)$$

If δP is distributed over the surface uniformly, the flow in the film is determined by the gradients of the additional pressure. The gradients can be found from relations (2.19), (2.20), and (2.36). We obtain

$$\delta P_{zz} = P - P_1 = P - P_{zz} + K_1 \sigma_{13} \quad (2.38)$$

or, by virtue of (2.37),

$$\begin{aligned} \text{grad } \delta P_{xx} &= \text{grad } \delta P_{yy} = \text{grad } (P - P_{zz} + K_1 \sigma_{13}) \\ &= \text{grad } [P - \Pi(h) + \rho g H + K_1 \sigma_{13}] \end{aligned} \quad (2.39)$$

where P is the distribution of pressure over the film surface.

If the film is horizontal and bounded by a gas, Eq. (2.39) simplifies still further because in a gas the pressure P is constant over all points of the surface and hence $\text{grad } P = 0$ and $\text{grad } H = 0$.

Equation (2.39) justifies a formal rule suggested earlier [22]. In order to calculate the flow in a film, driven by external pressure, one can assume that the local hydrodynamic pressure in the film is obtained by subtracting the local disjoining pressure from the external pressure, and then adding, as a first approximation (for moderately thin films), the capillary pressure dictated by the local surface curvature. Knowing the "hydrodynamic pressure" $P_i = P - \Pi(h) + K_1\sigma_{13}$, it is possible to find the velocity profile in the interlayer and the total flux, by integrating the Navier-Stokes equation of viscous liquid for specific boundary conditions.

The validity of this method is restricted to wetting films with slowly varying thickness, provided the change in film thickness during flow does not entail a change in relative concentrations of components. Otherwise, Π is not a well-defined function of film thickness h . Obviously, the composition is preserved if adsorption on the free surface of the film is either absent or changing only slightly with time; however, this is hardly ever realized. Hence, one must be very careful in employing dynamic methods of determining the disjoining pressure. The unavoidable presence of adsorption monolayers makes it essential to carry out a special analysis of the hydrodynamics of free film. A situation of this type was first discussed by Derjaguin and Nerpin in 1954 [22].

A local variation of thickness and surface curvature of a horizontal film produces a local variation in partial vapor pressure p over the given element of film surface:

$$p = p_s \exp [-v_m(\Pi - K_1\sigma_{13})/RT] \quad (2.40)$$

Consequently, one has to bear in mind that in volatile liquids a perturbed equilibrium can be restored not only by the flow of liquid through the film but also by vapor diffusion from thicker, convex segments of the film to thinner, concave ones.

If a liquid film is subjected also to volume forces (e.g., gravitational or centrifugal forces), or if a tangential force is applied to its surface (as in the blow-off method [23] or in thermo-capillary flow [24]), additional effects are found in complete analogy to the case of thick films. It is then sufficient to introduce into the equation of viscous flow the additional system of volume forces and shear stresses.

2.8. THERMODYNAMIC THEORY OF INTERACTION BETWEEN BODIES WITH CURVED SURFACES

The problem of interaction between bodies with curved surfaces at short distances was solved by one of us [1] in 1934. The solution gave the interaction force as a product of two factors, one being a function of the nature of the two bodies and of the medium in the gap, as well as of the gap width at the narrowest point, and the other being a function of only the curvature of the two surfaces and the mutual orientation of the principal normal sections of one surface with respect to the other. In the simplest case of two spheres in contact, the second factor depends only on their radii. The main advantage of the formula obtained – which is of considerable practical importance – is that, beside giving the force of interaction for one particular case, it makes possible the determination of this force for particles of different shapes and different sizes by a straightforward calculation. At the same time, the formula obtained reduces the problem of interaction between arbitrary particles to a calculation of the free energy of interaction per unit area of two parallel plane surface separated by a gap filled by the same ambient medium.

The theory developed in [1] is a phenomenological (in fact, thermodynamic) one. No special assumptions are made in it as to the nature and behavior of interaction forces between the surfaces, except that the forces rapidly decrease with distance and that reversible equilibrium is always maintained.

Consider the surfaces S_1S_1 and S_2S_2 (Fig. 2.7) of two solids. We denote by H_0 the shortest distance between them, given by a segment O_1O_2 of the common perpendicular to the surfaces. First we find how the distance H between the opposing points B_1 and B_2 of the two surface varies as they are moved in the neighborhood of the points O_1 and O_2 . We shall describe the surface S_1S_1 in a rectangular system of coordinates whose axis O_1Z_1 is perpendicular to the surface and the axes O_1X_1 and O_1Y_1 lie in the planes of principal normal sections whose curvatures are ε_1 and ε'_1 . Likewise, the second surface S_2S_2 will be described in a rectangular system whose axis O_2Z_2 coincides with the perpendicular, and the axes O_2X_2 and O_2Y_2 lie in the planes of the principal normal sections of the surface S_2S_2 , whose curvatures are ε_2 and ε'_2 .

Assuming that the surfaces S_1S_1 and S_2S_2 around the points O_1 and O_2 are smooth, we can write, to within terms of the second order of smallness in X and Y ,

$$\begin{aligned} Z_1 &= \frac{1}{2} \varepsilon_1 X_1^2 + \frac{1}{2} \varepsilon'_1 Y_1^2 \\ Z_2 &= \frac{1}{2} \varepsilon_2 X_2^2 + \frac{1}{2} \varepsilon'_2 Y_2^2 \end{aligned} \tag{2.41}$$

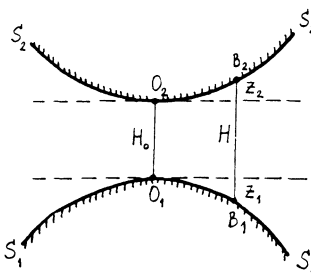


Fig. 2.7. Calculation of interaction force between curved surfaces.

Obviously,

$$H = H_0 + Z_1 + Z_2 \quad (2.42)$$

The quantities X_2 and Y_2 can be expressed through X_1 and Y_1 by the formulas for rotation of coordinate axes.

$$X_2 = X_1 \cos \omega + Y_1 \sin \omega$$

$$Y_2 = -X_1 \sin \omega + Y_1 \cos \omega$$

where ω is the angle between the axes O_1X_1 and O_2X_2 . By substituting these expressions into Eq. (2.41) and then into (2.42), we obtain

$$H = H_0 + \frac{1}{2}\alpha X_1^2 + \frac{1}{2}\beta Y_1^2 + \gamma X_1 Y_1 \quad (2.43)$$

where

$$\begin{aligned} \alpha &= \varepsilon_1 + \varepsilon_2 \cos^2 \omega + \varepsilon'_2 \sin^2 \omega \\ \beta &= \varepsilon'_1 + \varepsilon_2 \sin^2 \omega + \varepsilon'_2 \cos^2 \omega \\ \gamma &= (\varepsilon_2 - \varepsilon'_2) \cos \omega \sin \omega \end{aligned} \quad (2.44)$$

By choosing new coordinate axes O_1X and O_1Y rotated around the axis O_1Z_1 by a certain angle with respect to the axes O_1X_1 and O_1Y_1 , we can eliminate in expression (2.43), transformed to new coordinates, the term proportional to $X_1 Y_1$. This transformation gives

$$H = H_0 + \frac{1}{2} \varepsilon X^2 + \frac{1}{2} \varepsilon' Y^2 \quad (2.45)$$

The curves of equal thickness $H = \text{const}$ are thus similar concentric ellipses with principal half-axes

$$a_0 = \sqrt{2(H - H_0)/\varepsilon}, \quad b_0 = \sqrt{2(H - H_0)/\varepsilon'}$$

Making use of another invariant of the equations of second-order curves, we can write, in view of (2.43) and (2.45),

$$\varepsilon\varepsilon' = \alpha\beta - \gamma^2 \quad (2.46)$$

which yields, after substituting (2.44), and after an appropriate transformation, an expression for $\varepsilon\varepsilon'$ through the initial principal curvatures and the angle ω :

$$\begin{aligned} \varepsilon\varepsilon' &= (\varepsilon_1\varepsilon'_1 + \varepsilon_2\varepsilon'_2) + (\varepsilon_1\varepsilon_2 + \varepsilon'_1\varepsilon'_2) \sin^2 \omega \\ &+ (\varepsilon_1\varepsilon'_2 + \varepsilon'_1\varepsilon_2) \cos^2 \omega \end{aligned} \quad (2.47)$$

Now we shall calculate the resultant of the forces acting on the two bodies. We have assumed that the characteristic radius of these forces is small in comparison with the curvature radii of the surfaces, so that we can assume that the free energy U of the interaction can be set equal to the sum of the free energies dU of the interactions of all oppositely located segments dS_1 and dS_2 of the two surfaces. The quantity dU is a function of only the thickness H of the gap at a given point and is proportional to dS , i.e., the area of the corresponding segments of the surfaces S_1S_1 or S_2S_2 ; hence,

$$U = \int \int f(H_0 + \frac{1}{2}\varepsilon X^2 + \frac{1}{2}\varepsilon' Y^2) dX dY \quad (2.48)$$

where $f(H)$ is the specific free energy of interaction between two nearly parallel surfaces separated by an interlayer, with thickness H , of some phase. Infinite integration limits can be used in (2.48) because the function $f(H)$ decreases very sharply with increasing H . By replacing X and Y with polar coordinates ρ and φ ,

$$X = (\rho/\sqrt{\varepsilon}) \cos \varphi, \quad Y = (\rho/\sqrt{\varepsilon'}) \sin \varphi$$

we can rewrite the integral (2.48) in the form

$$U = \int_0^{2\pi} \int_0^\infty f(H_0 + \frac{1}{2}\rho^2) \frac{\rho d\rho d\varphi}{\sqrt{\varepsilon\varepsilon'}}$$

Changing the integration variable to $H = H_0 + \frac{1}{2}\rho^2$ and then integrating with respect to φ , we find

$$U = \frac{2\pi}{\sqrt{\varepsilon\varepsilon'}} \int_{H_0}^{\infty} f(H) dH \quad (2.49)$$

where expression (2.47) must be substituted for $\varepsilon\varepsilon'$.

The resultant force N of interaction between two bodies is obviously equal to

$$N = -\partial U / \partial H_0 = (2\pi/\sqrt{\varepsilon\varepsilon'})f(H_0) \quad (2.50)$$

Here $f(H_0)$ is the work, taken with reversed sign, of equilibrium isothermal removal of the flat surfaces to infinite separation from the initial separation of H_0 (per unit surface area). If this work is positive, N is an attractive force. Evidently,

$$f(H_0) = \int_{H_0}^{\infty} \Pi(H) dH \quad (2.51)$$

Formulas (2.49), (2.50), and (2.47) give the general solution of the problem formulated.

By assuming $\varepsilon = \varepsilon'_1 = 1/\alpha_1$, $\varepsilon_2 = \varepsilon'_2 = 1/\alpha_2$, we find from Eq. (2.47) that

$$\varepsilon\varepsilon' = (1/\alpha_1 + 1/\alpha_2)^2$$

When this expression is substituted into (2.49) and (2.50), it gives the force and energy of interaction between two spheres with radii α_1 and α_2 :

$$N = 2\pi \frac{\alpha_1 \alpha_2}{\alpha_1 + \alpha_2} f(H_0) \quad (2.52)$$

$$U = 2\pi \frac{\alpha_1 \alpha_2}{\alpha_1 + \alpha_2} \int_{H_0}^{\infty} f(H) dH \quad (2.53)$$

For two circular cylinders with radii r_1 and r_2 placed alongside with the angle ω between their axes, we have

$$\varepsilon_1 = \varepsilon_2 = 0, \quad \varepsilon'_1 = 1/r_1, \quad \varepsilon'_2 = 1/r_2$$

and thus obtain from (2.47)

$$N = \frac{2\pi\sqrt{r_1 r_2}}{\sin \omega} f(H_0) \quad (2.54)$$

$$U = \frac{2\pi\sqrt{r_1 r_2}}{\sin \omega} \int_{H_0}^{\infty} f(H) dH \quad (2.55)$$

The formulas so obtained are extensively used in problems of the theory of stability of colloids (see Chapters 6 and 9) and in experimental investigations of the forces of interaction between spherical surfaces and crossed cylindrical filaments [25]. It is these formulas that make possible the simulation of the interaction between colloidal particles in laboratory experiments with microscopic objects, such as crossed wires.

As follows from (2.50), the total adhesive force, i.e., the force that must be overcome to separate two surfaces in contact (the case of $H_0 = 0$), is equal to

$$N_0 = \frac{2\pi}{\sqrt{\varepsilon\varepsilon'}} f(0) \quad (2.56)$$

where $f(0)$ can be written in the form

$$f(0) = \sigma_{12} - \sigma_{13} - \sigma_{23} \quad (2.57)$$

The sign in (2.56) is changed in comparison with (2.54) in order to make the positive adhesive force correspond to attraction. In (2.57), σ_{12} is the free energy per unit area of the interface between phases 1 and 2 (two solids), σ_{13} is the free energy per unit area of the interface S_1S_1 between one solid and phase 3 that separates it from the other solid, and σ_{23} has a similar meaning. If phases 1 and 2 have identical properties, then σ_{12} reduces to σ_{11} , which vanishes for two liquid phases. Nevertheless, we shall assume that σ_{11} is nonzero for two solids in contact. Indeed, certain theoretical arguments and experimental facts indicate that the difference between the state of the surface and subsurface layers of solids cannot completely vanish even when identical surfaces are brought in contact. Hence, the interface with energy σ_{11} must physically exist after the contact is established. For this reason, the quantity $f(0)$ can be much smaller than twice the surface energy $2\sigma_{13}$, as measured by cleaving a solid.

Formula (2.56) has been subjected to thorough experimental scrutiny. The most conclusive data were obtained recently by Yaminsky et al. [26], who published the results on adhesive forces between identical fused methylated glass beads in air, water, in a number of organic liquids (alcohols, ethylene glycol, heptane), as well as in aqueous solutions of alcohols, ethylene glycol, and micelle-forming surfactants. The specific free energy of interaction, $f(0)$, between nonpolar surfaces of methylated glass in the media mentioned above was calculated from the data obtained by means

of Eq. (2.56). On the other hand, the same quantity was determined independently from data on surface tension at the methylated glass/medium interface. Good agreement between the two quantities demonstrated the correctness of Eq. (2.56).

In colloidal systems (such as gels), where thin liquid interlayers survive between particles, a certain effective disjoining pressure averaged over distances between particles can be introduced. This pressure can be found by compression techniques [29, 30] and by measuring the swelling pressure [27, 28, 31-34].

REFERENCES

1. B. V. Derjaguin, *Kolloidn. Z.*, 69, 155 (1934).
2. B. Derjaguin and E. Obukhov, *Acta Physicochim. URSS*, 5, 1 (1936).
3. B. V. Derjaguin and M. M. Kusakov, *Izv. Akad. Nauk SSSR, Ser. Khim.*, No. 5, 741 (1936); No. 5, 1119 (1937); *Acta Physicochim. URSS*, 10, 25, 153 (1939).
4. B. V. Derjaguin and A. S. Titiyevskaya, *Discuss. Faraday Soc.*, 18, 27 (1954); *Kolloidn. Zh.*, 15, 416 (1953); 22, 398 (1960); *Proceedings of the Second International Congress of Surface Activity*, Vol. 1, London (1957), p. 211; A. Sheludko, *Adv. Colloid Interface Sci.*, 1, 391 (1967).
5. B. V. Derjaguin, *Kolloidn. Zh.*, 17, 207 (1955); 38, 438 (1976); *Colloid Polym. Sci.*, 253, 492 (1975); B. V. Derjaguin and N. V. Churaev, *J. Colloid Interface Sci.*, 66, 389 (1978).
6. B. V. Derjaguin and G. A. Martynov, *Dokl. Akad. Nauk SSSR*, 144, 825 (1962).
7. K. J. Mysels, *J. Phys. Chem.*, 68, 3441 (1964).
8. V. M. Muller, *Kolloidn. Zh.*, 31, 427 (1969); in: *Research in Surface Forces*, Vol. 3, B. V. Derjaguin (ed.), Consultants Bureau, New York (1971), p. 236.
9. G. Bäkker, *Kappillaritat und Oberflächenspannung*, Handbuch der Experimental Physik, Bd. 6, Leipzig (1928).
10. E. M. Lifshitz, *Zh. Eksp. Teor. Fiz.*, 29, 94 (1955).
11. I. E. Dzyaloshinsky, E. M. Lifshitz, and L. P. Pitayevsky, *Zh. Eksp. Teor. Fiz.*, 37, 229 (1959); *Adv. Phys.*, 10, 165 (1961).
12. I. E. Tamm, *Fundamentals of Electricity Theory*, Nauka, Moscow (1966).
13. I. E. Dzyaloshinsky and L. P. Pitayevsky, *Zh. Eksp. Teor. Fiz.*, 36, 1797 (1959).
14. B. V. Derjaguin and Yu. V. Gutop, *Dokl. Akad. Nauk SSSR*, 171, 652 (1966); in: *Research in Surface Forces*, Vol. 2, Consultants Bureau, New York (1966), p. 17.
15. L. M. Scherbakov, *ibid.*, p. 26.
16. B. V. Derjaguin, G. A. Martynov, and Yu. V. Gutop, *ibid.*, p. 9.
17. B. V. Derjaguin and A. D. Malkina, *Kolloidn. Zh.*, 12, 431 (1950); B. V. Derjaguin, N. I. Moskvitin, and M. F. Futran, *Proceedings*

- of the 3rd USSR Conference on Colloid Chemistry, Izd. AN SSSR, Moscow (1956), p. 285.
18. A. von Buzagh, Kolloidn. Zh., 47, 370 (1929).
 19. T. N. Voropaeva, B. V. Derjaguin, and B. N. Kabanov, in: Research in Surface Forces, Vol. 1, Consultants Bureau, New York (1963), p. 116.
 20. J. W. Gibbs, The Scientific Papers, Longman, London (1906).
 21. B. V. Derjaguin, Acta Physicochim. URSS, 12, 181 (1940).
 22. B. V. Derjaguin and S. V. Nerpin, Dokl. Akad. Nauk SSSR, 100, 17 (1955).
 23. B. V. Derjaguin and V. V. Karasev, Kolloidn. Zh., 15, 46 (1953); Proceedings of the Second International Congress on Surface Activity, Vol. 3 (1957), p. 531.
 24. B. V. Derjaguin and M. K. Mel'nikova, in: A. F. Ioffe Festschrift Volume on 70th Anniversary of Ioffe's Birthday, Izd. AN SSSR (1950), p. 482; in: Highway Research Board, Special report 40, Washington, D. C. (1958), p. 43.
 25. I. I. Abrikosova and B. V. Derjaguin, Zh. Eksp. Teor. Fiz., 21, 945 (1951); B. V. Derjaguin et al., Discuss. Faraday Soc., No. 18, 24 (1954); B. V. Derjaguin, I. I. Abrikosova, and E.M. Lifshitz, Q. Rev., 10, 295 (1956); Usp. Fiz. Nauk, 64, 493 (1958); B. V. Derjaguin and I. I. Abrikosova, J. Phys. Chem. Solids, 5, 1 (1958); D. Tabor and R. H. Winterton, Nature, 219, 1120 (1968); J. N. Israelachvili and D. Tabor, Proc. R. Soc. London, A331, 19 (1972); B. V. Derjaguin, Ya. I. Rabinovich, and N. V. Churaev, Nature, Phys. Sci., 265, 520 (1977); 272, 313 (1978); H. Sonntag, B. Emke, R. Miller, and L. Knapschinsky, Adv. Colloid Interface Sci., 16, 381 (1982); R. M. Pashley, Adv. Colloid Interface Sci., 16, 57 (1982); J. N. Israelachvili, Adv. Colloid Interface Sci., 16, 31 (1982); Ya. I. Rabinovich, B. V. Derjaguin, and N. V. Churaev, Adv. Colloid Interface Sci., 16, 63 (1982).
 26. V. V. Yaminsky, E. A. Amelina, and E. D. Shchukin, in: Surface Forces in Thin Films, Nauka, Moscow (1979), p. 13; E. D. Shchukin, E. A. Amelina, and V. V. Yaminsky, Colloids Surfaces, 2, 221 (1981); E. D. Shchukin, A. V. Pertsov, and E. A. Amelina, Colloid Chemistry, Mosk. Gos. Univ. (1982), p. 252.
 27. P. F. Low, Soil Sci. Soc. Am. J., 44, No. 4, 667 (1980).
 28. Definitions, Terminology, and Symbols in Colloid and Surface Chemistry, Pure Appl. Chem., 31, 579 (1972).
 29. A. Homola and A. Robertson, J. Colloid Interface Sci., 54, 286 (1976).
 30. W. J. van Megen, I. K. Snook, and R. O. Watts, J. Colloid Interface Sci., 77, 131 (1980).
 31. P. F. Low and J. F. Margheim, Soil Sci. Soc. Am. J., 43, 473 (1979).
 32. J. P. Quirk, Israel J. Chem., 6, 213 (1968).
 33. N. Collins-George and J. M. Bozeman, Aust. J. Res., 8, 239 (1970).
 34. M. V. Serebrovskaya, O. G. Us'yarov, and V. M. Muller, Kolloidn. Zh., 34, 730 (1972).

Chapter 3

THE THERMODYNAMIC THEORY OF STABILITY OF THIN FILMS

The conditions of equilibrium of thin films essentially depend on the phases between which the film is sandwiched.

We shall consider four cases:

1. a thin (plane-parallel) interlayer between two solids;
2. a thin interlayer between two convex solids;
3. a thin plane-parallel wetting film;
4. a thin plane-parallel film between two identical nonsolid phases.

3.1. STABILITY AND EQUILIBRIUM OF INTERLAYERS BETWEEN PARALLEL PLATES

First we assume that the solubility of the bulk of both solids in the liquid interlayer and in the bulk liquid phase from which the interlayer is formed is negligible.

We have seen in Chapter 2 that a system is in equilibrium if

$$\Pi(h) = P - P_0 \quad (3.1)$$

where P is the pressure exerted by a solid on the interlayer, and P_0 is the pressure in the bulk phase of the liquid. The function $\Pi(h)$ is determined by the composition of the liquid and solid phases. For the equilibrium to be thermodynamically stable, it is necessary that

$$d\Pi(h)/dh < 0 \quad (3.2)$$

It is important to add that the derivative of the disjoining pressure with respect to thickness must be calculated with the constraint of constant equilibrium of the film and its bulk phase in the process of thinning. This equilibrium can be realized if the chemical potentials of all the components remain equal in the film and the bulk phase. When the film thickness changes because of simple draining, the chemical potentials of the film components may vary. The leveling-off may be quite slow because of relatively slow diffusion processes. Consequently, the derivative $d\Pi/dh$ in a rapid thinning of a film may have an essentially different value from that in a thermodynamically equilibrium state. And if departures from constant temperature are negligible, this value of the derivative must be less than the corresponding equilibrium value:

$$d\Pi/dh < (d\Pi/dh)_e$$

Indeed, when an irreversible change in thickness Δh is completed (assume the thickness to be reduced), the diffusional leveling of chemical potentials of the components in the film and the bulk of the liquid must result in establishing the final state of thermodynamic equilibrium. This process must be accompanied by a decrease in the free energy of the system. Hence, after an irreversible reduction in film thickness the free energy increases more than in a reversible process. This is only possible if the work consumed by film thinning is greater than

$$\frac{\Pi(h) + \Pi(h + \Delta h)}{2} \Delta h$$

Therefore, if the effective disjoining pressure at the beginning of this process were equal to the equilibrium value, at the end of the process it would be greater than the equilibrium value of $\Pi(h + \Delta h)$. This gives us the constraint on the effective value:

$$\Pi_{\text{eff}}(h + \Delta h) > (\partial\Pi/\partial h) \Delta h + \Pi(h)$$

In other words, if we take into account the negative sign in Δh , then

$$d\Pi_{\text{eff}}/dh < (\partial\Pi/\partial h) \quad (3.3)$$

It then follows that cases are possible in which the condition of film stability (3.2) is met for rapid changes in thickness while it is violated for slower changes. There is an analogy here to the stabilizing influence of the Marangoni-Gibbs effect when interlayers are stretched.

3.2. STABILITY OF INTERLAYERS BETWEEN CONVEX BODIES

The cases that must be considered here are the stability of an interlayer between two convex particles, and of an interlayer between a convex and a flat particle. The stability of the equilibrium is then determined not by the derivative of the disjoining pressure in the interlayer but by the derivative of the equilibrium interaction force N with respect to interlayer thickness at the narrowest point of the gap. However, we saw that if particles are not too small [as follows from Eqs. (2.50) and (2.51)], this derivative is

$$\frac{dN}{dH} = -g\Pi(H)$$

where

$$g = 2\pi/\sqrt{\epsilon\epsilon'}$$

Therefore, the condition of stability of the equilibrium

$$\frac{dN}{dH} < 0 \quad (3.4)$$

reduces to

$$\Pi(H) > 0 \quad (3.5)$$

and the necessary condition of thermodynamic equilibrium is

$$N = g \int_H^\infty \Pi(h) dh \quad (3.6)$$

After a fast isothermal change in the gap width caused by an external force, the system will not be at equilibrium, and the transition to equilibrium will take place, just as it did in the case of a plane-parallel interlayer, through a leveling of chemical potentials in the course of diffusion. The energy of the system must thereby decrease to the equilibrium value. When leveling started, the energy was, therefore, greater than the equilibrium value. This excess could only be produced by the average value of the external force \bar{N} being greater in the course of thickness reduction by ΔH than would correspond to the equilibrium value N in formula (3.6). Consequently,

$$\bar{N} = \frac{N + N_{eff}(H - \Delta H)}{2} > \frac{N + N(H - \Delta H)}{2}$$

or

$$dN_{\text{eff}}/dH < dN/dH$$

or, finally,

$$-dN_{\text{eff}}/dH > g\Pi(H) \quad (3.7)$$

As a result, the stability with respect to a rapid change in thickness may occur when the condition of thermodynamic stability (3.5) is violated, as in the case of plane-parallel films. The feasibility of such situations was confirmed by the experiments of Derjaguin et al. [1, 2], who reported a slow increase in the force necessary to separate crossed wires embedded in different solutions. The kinetics of adhesion so observed is explained by a slowly progressing thinning of the liquid interlayer and, hence, by a slow decrease of its equilibrium isotherm of disjoining pressure, as a result of relaxation of the "effective" disjoining pressure.

The general scheme of the phenomena described, outlined above, can be supplemented with some particular cases. When an interlayer of an electrolyte solution is rapidly thinned, the restructuring of the adsorption equilibrium of ions may be delayed, so that the charge density of the surface may remain constant. After the adsorption equilibrium is reached, the charge density diminishes, and with it diminishes the electrostatic component of disjoining pressure. A similar mechanism may explain the observations, reported by von Buzagh, that the adhesion of quartz particles to glass walls in electrolyte solutions becomes stronger with time (Chapter 2 of [17]).

However, a somewhat different mechanism of "adhesion kinetics" or relaxation of nonequilibrium disjoining pressure is possible. It can operate when boundary layers with a structure modified in comparison with that of the liquid phase in the bulk are formed at the surfaces of the interlayer. As the film thickness decreases and the "boundary layers" at its two surfaces overlap, the special structure of the peripheral parts of boundary layers must start to decay. Presumably, the remaining parts of these layers may subsequently be restructured as well. A delay in these processes of structural modification can explain the slow thinning of interlayers and the concurrent growth in adhesive forces in the experiments mentioned. (Elementary calculations show that these experimental results cannot be explained by viscous resistance to film thinning.)

The following arguments can establish an experimental distinction between the two mechanisms of relaxation, the diffusion and structural ones. The time of the diffusion mechanism of relaxation must be proportional to the square of the linear size of the interlayer, and must be very small for an interlayer separating two convex particles of colloidal size. Conversely, the time of structural relaxation must be independent of interlayer size. Nevertheless,

when we deal with the effectiveness of collisions between colloidal particles participating in Brownian motion, the period of diffusion relaxation, however small it may be, may prove much longer than the duration of a collision, and must therefore be taken into account.

The slow rate of diffusion makes it difficult to measure the equilibrium disjoining pressure of liquid interlayers between plane-parallel surfaces of two solids. It is therefore preferable to employ a technique based on measuring the equilibrium interaction between spheres or crossed cylinders. And although the values of $\Pi(h)$ must then be determined from the values of the derivative, in a number of cases we may be interested directly in the integral on the right-hand side of Eq. (3.6), which gives the excess free energy per unit area of a plane-parallel interlayer with thickness h .

3.3. STABILITY OF WETTING FILMS

At a given temperature, pressure, and chemical potentials of components, the interlayers between solids have only one additional degree of freedom, viz., their thickness. In contrast, a wetting film, even if originally it had a plane-parallel geometry, can change its profile and acquire a different thickness at different points. Moreover, it can exchange components with the contiguous gas phase, by evaporation or condensation.

Let us consider the conditions of equilibrium in a system consisting of a solid substrate covered by a bulk liquid phase and a thin plane-parallel wetting interlayer formed from the bulk phase with a gas over them. The substrate is solid and we assume that its surface cannot be stretched. Hence, the film area A is not one of the degrees of freedom of the system, as it was in the case of a liquid substrate. We begin with a system consisting of a single volatile component. If the liquid phase is separated from the gas by a meniscus whose curvature may vary, the system in equilibrium at constant temperature has a single degree of freedom. We can choose for this degree of freedom either the vapor pressure or the pressure difference between the vapor and liquid phases: $P_2 - P_1$. By definition,

$$P_2 - P_1 = \Pi(h) \quad (3.8)$$

where $\Pi(h)$ is the disjoining pressure of a film with thickness h .

Figure 3.1 is a schematic diagram of the system in the form in which it is possible to determine the isotherm of disjoining pressure of a film by changing the pressure P_1 in the liquid phase A in the neighborhood of the film S. The pressure P_1 can be reduced, for example, by lowering the left-hand elbow of the tube containing

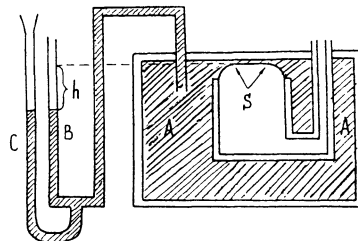


Fig. 3.1. Schematic diagram of the measurement of disjoining pressure of a wetting film.

the liquid, or by removing the liquid by suction through a segment C. The difference h between the level of the liquid in the wide tube B and the level of the film is obviously a measure of disjoining pressure. By measuring h at different values of $P_2 - P_1$ we can find function (3.8).

As follows from Kelvin's and Laplace's formulas, the pressure of an ideal vapor p in a system at equilibrium satisfies the relation

$$(RT/v) \ln(p/p_s) = P_2 - P_1 = \Pi(h) \quad (3.9)$$

where p_s is the vapor pressure over a flat surface, R is the gas constant, and T is the absolute temperature.

It is then obvious that the disjoining pressure isotherm of a wetting film can be obtained, without involving the bulk liquid phase, by determining the isotherm of (polymolecular) adsorption of vapor on the given substrate. The substrate can be either solid or liquid. However, the accuracy achieved in this way essentially diminishes as $p/p_s \rightarrow 1$. The principal advantage of this method is that it is valid when there is no bulk liquid phase. Now we shall consider the conditions under which the film equilibrium is stable.

Let the thickness of a film in equilibrium with vapor decrease by Δh . If this fall results in an increase in vapor pressure, the thinning will develop further and equilibrium will thus be unstable. But if the vapor pressure decreases, the film returns to the initial equilibrium. The necessary condition for stable equilibrium is therefore the inequality

$$dp(h)/dh > 0 \quad (3.10)$$

or, by virtue of (3.9),

$$d\Pi(h)/dh < 0 \quad (3.11)$$

If the film is nonvolatile, only condition (3.11) applies. By introducing the excess Gibbs free energy per unit area of the film $G(h)$, we obtain, instead of condition (3.11),

$$\frac{d^2G(h)}{dh^2} > 0 \quad (3.12)$$

Each of these conditions is at the same time the sufficient condition for the equilibrium to be stable at $T = \text{const}$. If these conditions hold for any h , a smooth transition to the bulk phase is obviously possible without jumps in thickness or slope. This means that the equilibrium contact angle of a droplet of a given liquid is zero.

Derjaguin and Zorin [2] reported cases in which the isotherm $p(h)$ [or $\Pi(h)$] gave a finite thickness $h = h_0$ at $p/p_s = 1$ [or at $\Pi(h) = 0$]. Frumkin, analyzing a film wetting a liquid phase, expressed the condition of partial wetting in terms of the dependence of tension in a wetting film on thickness [3], although this approach does not work in the case of a solid substrate.

3.4. STABILITY OF INTERLAYERS BETWEEN TWO IDENTICAL FLUIDS

Now we shall consider the case of a thin plane-parallel interlayer sandwiched between two fluid phases (liquid or gaseous) [4]. This is the most complicated case, because an additional degree of freedom appears owing to film stretchability. We shall discuss only the symmetrical case, in which two identical phases lie on the sides of the interlayer. This case is of special interest because the stability of such films determines the stability of foams and emulsions. The equilibrium and stability of such free, symmetrical films can be treated in a less ambiguous manner if we eliminate the arbitrary assignment of the geometrical Gibbs dividing surfaces [4]. The mathematical treatment will thereby be simplified.

Consider the case in which a free (or emulsion) film contains two nonvolatile components (e.g., a surfactant and an electrolyte) [5] in addition to two volatile components (e.g., water and gas).

The free energy F of the whole system, composed of the film and the phase surrounding it, is a function of absolute temperature T , the volume of the system V , the area of the dividing surface A (i.e., the area of the free film), and the total numbers of particles for each component, N_1 , N_2 , N_3 , and N_4 . The total differential of free energy dF , representing its increment under infinitesimal increments of independent variables describing the system, is

$$dF = -S dT - P dV + \gamma dA + \sum_{i=1}^4 \mu_i dN_i \quad (3.13)$$

where S is the entropy of the system, P is the pressure in the bulk phase at a large distance from the film, γ is the film tension, and μ_i is the chemical potential of the i -th component. In a sufficiently thick film, γ equals twice the surface tension of the film on its two surfaces.

Let us replace the volume V and the numbers of particles of volatile components N_3 and N_4 with new variables: the pressure in the bulk phase P , and chemical potentials μ_3 and μ_4 . These variables correspond to the interfacial characteristic function of state of the system:

$$F^S = F + PV - \mu_3 N_3 - \mu_4 N_4 \quad (3.14)$$

Its total differential is

$$\begin{aligned} dF^S = & -S dT + V dP + \gamma dA - N_3 d\mu_3 \\ & - N_4 d\mu_4 + \mu_1 dN_1 + \mu_2 dN_2 \end{aligned} \quad (3.15)$$

Not all of the variables in (3.15) are independent. The pressure P in the bulk component of the system is a function of temperature T and chemical potentials μ_3 and μ_4 . In the differential form this relation is given by the Gibbs-Duhem formula for the bulk phase:

$$-s^V dT + dP - n_3^V d\mu_3 - n_4^V d\mu_4 = 0 \quad (3.16)$$

where s^V , n_3^V , and n_4^V are the bulk densities of entropy and of particles of species 3 and 4.

By using (3.16) we can eliminate the pressure differential dP from the expression for the total differential dF^S , and obtain

$$\begin{aligned} dF^S = & -S^S dT - N_3^S d\mu_3 - N_4^S d\mu_4 + \sigma dA \\ & + \mu_1 dN_1 + \mu_2 dN_2 \end{aligned} \quad (3.17)$$

where S^S and N^S are the surface excesses of the corresponding quantities:

$$N_{3,4}^S = N_{3,4} - n_{3,4}^V V, \quad S^S = S - s^V V \quad (3.18)$$

or, if we divide by A ,

$$\Gamma_{3,4} = N_{3,4}^S / A, \quad s^S = S^S / A \quad (3.19)$$

We see from (3.18) that the surface excesses N_3^S , N_4^S , and S^S , and hence Γ_3 , Γ_4 , and s^S , are independent of the specific position of the dividing surface, in contrast to the usually analyzed cases in which, ever since Gibbs's work, one operates with the surface of discontinuity between two distinct phases.

Let us integrate (3.17) at constant values of the intensive quantities T , μ_3 , μ_4 , γ , μ_1 , and μ_2 . This will give us the expression for the characteristic function F^S :

$$F^S = \gamma A + \mu_1 N_1 + \mu_2 N_2 \quad (3.20)$$

At large values of the ratios N_1/A and N_2/A , when the film degenerates to the bulk phase, expression (3.20) for F^S transforms to

$$F_0^S = \gamma A + \varphi_1 N_1 + \varphi_2 N_2 \quad (3.21)$$

where

$$\varphi_{1,2} = \varphi_{1,2}(T, \mu_3, \mu_4, N_2/N_1) \quad (3.22)$$

are the chemical potentials of the first and second components in the bulk-phase film. In contrast to the case with a single nonvolatile component, the functions $\varphi_{1,2}$ depend on the ratios of the particles, and hence on volume concentrations. The chemical potentials μ_3 and μ_4 being fixed (as well as T and P), the bulk-phase film is monovariant and, therefore, the volume concentrations of particles at a given ratio N_2/N_1 are fixed as well, while in a thin film their surface concentrations are arbitrary. Consequently, film degeneration to the bulk phase is accompanied by a loss of one degree of freedom.

Another difference is that the intensive quantities characterizing a degenerate film can contain only volume concentrations, while in a thin film they contain quantities referred to unit area. We have to conclude that as a result of this degeneration the dependence of intensive quantities, such as μ_1 and μ_2 , on surface-intensive quantities (e.g., $N_{1,2}/A$) must transform to a dependence on volume-intensive quantities, i.e., on volume concentrations or mole fractions. As a result, the partial derivatives $(\partial\varphi_{1,2}/\partial N_{1,2})$ become meaningless for the bulk-phase film. In fact, they vanish even formally, according to (3.22), because N_1 and N_2 are very large.

By differentiating (3.20), subtracting the result from (3.17), and dividing by A , we arrive at the Gibbs-Duhem equation for the

film, relating in the differential form all intensive quantities characterizing the film:

$$s^S dT + d\gamma + \sum_{i=1}^4 \Gamma_i d\mu_i = 0 \quad (3.23)$$

where $\Gamma_i = N_i/A$. By differentiating (3.21), taking into account (3.17), and neglecting the term $A d\gamma$ in comparison with other terms proportional to the film volume, we arrive at the Gibbs-Duhem equation for the bulk-phase film in the form

$$\begin{aligned} s^S dT - V dP + N_1 d\varphi_1 + N_2 d\varphi_2 + N_3^S d\mu_3 \\ + N_4^S d\mu_4 = 0 \end{aligned} \quad (3.24)$$

In the above formalism the equation of state of a film appears as γ given as a function of temperature T , chemical potentials μ_3 and μ_4 , and adsorptions Γ_1 and Γ_2 :

$$\gamma = \gamma(T, \mu_3, \mu_4, \Gamma_1, \Gamma_2) \quad (3.25)$$

Expression (3.17) for the total differential dF^S yields

$$(\partial\gamma/\partial N_{1,2})_A = (\partial\mu_{1,2}/\partial A)_{N_{1,2}} \quad (3.26)$$

Since γ and $\mu_{1,2}$ are functions of only specific quantities Γ_1 and Γ_2 , after factoring out $1/A$ we can rewrite the last equality in the form

$$\frac{\partial\gamma}{\partial\Gamma_{1,2}} = - \frac{\partial\mu_{1,2}}{\partial\Gamma_1}\Gamma_1 - \frac{\partial\mu_{1,2}}{\partial\Gamma_2}\Gamma_2 \quad (3.27)$$

Dividing both sides of the equality by $-\Gamma_1$ gives

$$-\frac{1}{\Gamma_1} \frac{\partial\gamma}{\partial\Gamma_{1,2}} = \frac{\partial\mu_{1,2}}{\partial\Gamma_1} + \frac{\Gamma_2}{\Gamma_1} \frac{\partial\mu_{1,2}}{\partial\Gamma_2} \quad (3.28)$$

Assume now that a film with given values of Γ_1 and Γ_2 is formed from an infinitely thick, bulk-phase film with the same value of the ratio $N_2/N_1 = \Gamma_2/\Gamma_1 = k$ by a gradual thinning during which the ratio $\Gamma_2/\Gamma_1 = k$ is maintained constant. In such a process Γ_2 can be regarded as a function of Γ_1 , with $d\Gamma_2/d\Gamma_1 = \Gamma_2/\Gamma_1 = k$, the right-hand side of (3.28) being the total derivative with respect to Γ_1 :

$$-\frac{1}{\Gamma_1} \frac{\partial\gamma}{\partial\Gamma_{1,2}} = \frac{\partial\mu_{1,2}}{\partial\Gamma_1} \quad (3.29)$$

Let us integrate (3.29) with respect to $d\Gamma_1$:

$$\mu_{1,2} = \int_{\Gamma_1}^{\infty} \frac{1}{\Gamma_1} \frac{\partial \gamma}{\partial \Gamma_{1,2}} d\Gamma_1 + \varphi_{1,2} \quad (3.30)$$

where $\varphi_{1,2}$ are the values of the chemical potentials of the bulk-phase film at $\Gamma_1 \rightarrow \infty$, $\Gamma_2 \rightarrow \infty$. The functions $\varphi_{1,2}$ depend on $k = \Gamma_2/\Gamma_1 = N_2/N_1$. When integrating, Γ_2 in the integrand in (3.30) must be considered, after calculating the partial derivative, as a function of Γ_1 ($\Gamma_2 = k\Gamma_1$). After integration is completed, we have to substitute again the value $k = \Gamma_2/\Gamma_1$ into the final expression, as well as into the argument of the function $\varphi_{1,2}$.

Excesses of volatile components in the film are also found from expression (3.17) for the total differential dF^S . Together with (3.20) it gives

$$N_{3,4}^S = (\partial F^S / \partial \mu_{3,4}) = -(\partial / \partial \mu_{3,4}) [\gamma A + \mu_1 N_1 + \mu_2 N_2] \quad (3.31)$$

or, if we introduce specific surface excesses (adsorptions),

$$\Gamma_{3,4} = -(\partial / \partial \mu_{3,4}) [\gamma + \mu_1 \Gamma_1 + \mu_2 \Gamma_2]_{T, \Gamma_1, \Gamma_2, \mu_{4,3}} \quad (3.32)$$

This equation differs from the Gibbs adsorption equation in the presence of the terms $\mu_1 \Gamma_1$ and $\mu_2 \Gamma_2$. This distinction vanishes when there are no nonvolatile components ($\Gamma_1 = \Gamma_2 = 0$).

At constant temperature T , constant chemical potentials μ_3 and μ_4 , constant total amounts of nonvolatile components N_1 and N_2 , and constant film area A , the surface characteristic function F^S has a minimum at the equilibrium state. In this state any departure from equilibrium must increase the function

$$\sum F^S \quad (3.33)$$

where the summation is carried out over all segments of the film. Condition (3.33) is supplemented with three constraints:

$$\sum \Delta A = 0, \quad \sum \Delta N_1 = 0, \quad \sum \Delta N_2 = 0 \quad (3.34)$$

Let us divide the whole film into two parts, in order for the sums in (3.33) and (3.34) to contain only two terms each, the second term being much larger than the first. We assume at the same time that each of the two parts of the film is sufficiently wide in comparison with its thickness, in order that a departure from equilibrium in both parts of the film can be regarded as uniform

over the area, and the contribution to ΔF^S made by film inhomogeneities at the junction of its two parts be negligible. Varying the area A and the number of particles N_1 and N_2 , we can then write for the second part of the film

$$(\Delta F^S)_2 = \gamma(\Delta A)_2 + \mu_1(\Delta N_1)_2 + \mu_2(\Delta N_2)_2$$

In view of constraints (3.34), this expression can be rewritten in the following form:

$$(\Delta F^S)_2 = -\gamma(\Delta A)_1 - \mu_1(\Delta N_1)_1 - \mu_2(\Delta N_2)_1$$

so that the equilibrium condition (3.33) then gives

$$\Delta F^S = -\gamma \Delta A - \mu_1 \Delta N_1 - \mu_2 \Delta N_2 > 0 \quad (3.35)$$

All quantities in (3.35) refer to a small segment of the film.

By expanding ΔF^S in Eq. (3.35) into a series, we find, to within terms of the second order of smallness,

$$\begin{aligned} & \frac{\partial^2 F^S}{\partial A^2} (\Delta A)^2 + \frac{\partial^2 F^S}{\partial N_1^2} (\Delta N_1)^2 + \frac{\partial^2 F^S}{\partial N_2^2} (\Delta N_2)^2 \\ & + 2 \frac{\partial^2 F^S}{\partial A \partial N_1} \Delta A \Delta N_1 + 2 \frac{\partial^2 F^S}{\partial A \partial N_2} \Delta A \Delta N_2 \\ & + 2 \frac{\partial^2 F^S}{\partial N_1 \partial N_2} \Delta N_1 \Delta N_2 > 0 \end{aligned} \quad (3.36)$$

With the values of derivatives in (3.36) found from expression (3.17) for the total differential dF^S , the quadratic form transforms to the following expression:

$$\begin{aligned} & \frac{\partial \gamma}{\partial A} (\Delta A)^2 + \frac{\partial \mu_1}{\partial N_1} (\Delta N_1)^2 + \frac{\partial \mu_2}{\partial N_2} (\Delta N_2)^2 + 2 \frac{\partial \gamma}{\partial N_1} \Delta A \Delta N_1 \\ & + 2 \frac{\partial \gamma}{\partial N_2} \Delta A \Delta N_2 + 2 \frac{\partial \mu_1}{\partial N_2} \Delta N_1 \Delta N_2 \end{aligned} \quad (3.37)$$

The quantities γ , μ_1 , and μ_2 are functions of the ratios $N_1/A = \Gamma_1$ and $N_2/A = \Gamma_2$. Consequently, by virtue of Euler's theorem for homogeneous functions, these three satisfy the equalities

$$\begin{aligned} & A(\partial \gamma / \partial A) + N_1(\partial \gamma / \partial N_1) + N_2(\partial \gamma / \partial N_2) = 0, \\ & A(\partial \mu_1 / \partial A) + N_1(\partial \mu_1 / \partial N_1) + N_2(\partial \mu_1 / \partial N_2) = 0, \\ & A(\partial \mu_2 / \partial A) + N_1(\partial \mu_2 / \partial N_1) + N_2(\partial \mu_2 / \partial N_2) = 0 \end{aligned} \quad (3.38)$$

Equalities (3.38) taken together with expression (3.17) for the total differential dF^S make it possible to express six coefficients in the quadratic form (3.37) through only three of them. For instance, let us choose $\partial\gamma/\partial A$, $\partial\mu_1/\partial N_1$, and $\partial\gamma/\partial N_1$ for these three. Then

$$\begin{aligned} N_2 = \frac{\partial\mu_2}{\partial N_2} &= -A \frac{\partial\mu_2}{\partial A} - N_1 \frac{\partial\mu_1}{\partial N_1} = -A \frac{\partial\gamma}{\partial N_2} - N_1 \frac{\partial\mu_1}{\partial N_2} \\ &= \frac{A}{N_2} (A \frac{\partial\gamma}{\partial A} + N_1 \frac{\partial\gamma}{\partial N_1}) + \frac{N_1}{N_2} (A \frac{\partial\mu_1}{\partial A} + N_1 \frac{\partial\mu_1}{\partial N_1}) \\ &= \frac{A}{N_2} (A \frac{\partial\gamma}{\partial A} + N_1 \frac{\partial\gamma}{\partial N_1}) + \frac{N_1}{N_2} (A \frac{\partial\gamma}{\partial N_1} + N_1 \frac{\partial\mu_1}{\partial N_1}) \\ &= \frac{A^2}{N_2} \frac{\partial\gamma}{\partial A} + \frac{2AN_1}{N_2} \frac{\partial\gamma}{\partial N_1} + \frac{N_1^2}{N_2} \frac{\partial\mu_1}{\partial N_1}, \\ N_2 \frac{\partial\gamma}{\partial N_2} &= -A \frac{\partial\gamma}{\partial A} - N_1 \frac{\partial\gamma}{\partial N_1}, \\ N_2 \frac{\partial\mu_1}{\partial N_2} &= -A \frac{\partial\mu_1}{\partial A} - N_1 \frac{\partial\mu_1}{\partial N_1} = \frac{\partial\gamma}{\partial N_1} - N_1 \frac{\partial\mu_1}{\partial N_1} \end{aligned}$$

By substituting the coefficients written above into the quadratic form (3.37) and regarding the relative changes $\Delta A/A$, $\Delta N_1/N_1$, and $\Delta N_2/N_2$ as independent variables, we obtain

$$\begin{aligned} &A^2 \frac{\partial\gamma}{\partial A} \left(\frac{\Delta A}{A} \right)^2 + N_1^2 \frac{\partial\mu_1}{\partial N_1} \left(\frac{\Delta N_1}{N_1} \right)^2 + \left(A^2 \frac{\partial\gamma}{\partial A} + 2AN_1 \frac{\partial\gamma}{\partial N_1} \right. \\ &\quad \left. + N_1^2 \frac{\partial\mu_1}{\partial N_1} \right) \left(\frac{\Delta N_2}{N_2} \right)^2 + 2AN_1 \frac{\partial\gamma}{\partial N_1} \frac{\Delta A}{A} \frac{\Delta N_1}{N_1} - 2 \left(A^2 \frac{\partial\gamma}{\partial A} \right. \\ &\quad \left. + AN_1 \frac{\partial\gamma}{\partial N_1} \right) \frac{\Delta A}{A} \frac{\Delta N_2}{N_2} - 2 \left(AN_1 \frac{\partial\gamma}{\partial N_1} + N_1^2 \frac{\partial\mu_1}{\partial N_1} \right) \frac{\Delta N_1}{N_1} \frac{\Delta N_2}{N_2} > 0 \end{aligned} \quad (3.39)$$

or, by collecting like terms,

$$\begin{aligned} &A^2 \left(\frac{\partial\gamma}{\partial A} \right) \left[\frac{\Delta A}{A} - \frac{\Delta N_2}{N_2} + \frac{N_1}{A} \frac{\frac{\partial\gamma}{\partial N_1}}{\frac{\partial\gamma}{\partial A}} \left(\frac{\Delta N_1}{N_1} + \frac{\Delta N_2}{N_2} \right) \right]^2 \\ &+ \frac{N_1^2}{\frac{\partial\gamma}{\partial A}} \left[\frac{\partial\gamma}{\partial A} \frac{\partial\mu_1}{\partial N_1} - \left(\frac{\partial\gamma}{\partial N_1} \right)^2 \right] \left(\frac{\Delta N_1}{N_1} - \frac{\Delta N_2}{N_2} \right) > 0 \end{aligned} \quad (3.39')$$

The case $\partial\gamma/\partial A \rightarrow 0$, corresponding to a film degenerated to the bulk phase, will be analyzed later.

Let us assume $\Delta N_1/N_1 = \Delta N_2/N_2 \neq \Delta A/A$. The condition necessary for the quadratic form (3.39') to be positive is then

$$\frac{\partial \gamma}{\partial A} > 0 \quad (3.40)$$

Now we assume that $\Delta N_1/N_1 \neq \Delta N_2/N_2$, but with $\Delta A/A$ being such that the first quadratic term of the form (3.39') vanishes. This is always possible in the case under consideration because we leave for the future analysis the case of degeneration to the bulk phase, when there may be no suitable $\Delta A/A$. Then the necessary condition for the positively definite quadratic form (3.39') is

$$\frac{\partial \gamma}{\partial A} \frac{\partial \mu_1}{\partial N_1} - \left(\frac{\partial \gamma}{\partial N_1} \right)^2 > 0 \quad (3.41)$$

By using Euler's theorem on homogeneous functions, we can now transform (3.41) to intensive quantities:

$$-\left(\Gamma_1 \frac{\partial \gamma}{\partial \Gamma_1} + \Gamma_2 \frac{\partial \gamma}{\partial \Gamma_2}\right) \frac{\partial \mu_1}{\partial \Gamma_1} > \left(\frac{\partial \gamma}{\partial \Gamma_1}\right)^2 \quad (3.41')$$

Conditions (3.40) and (3.41) are simultaneously necessary and sufficient for the quadratic form (3.39') to be positive regardless of the variations of ΔA , ΔN_1 , and ΔN_2 (with the exception of the trivial case $\Delta A/A = \Delta N_1/N_1 = \Delta N_2/N_2$).

As follows from conditions (3.40) and (3.41),

$$\frac{\partial \mu_1}{\partial N_1} > 0 \quad (3.42)$$

The quantities γ , N_1 , and A being related by the equation of state (3.30) of the film, the following identity can be written:

$$\left(\frac{\partial \gamma}{\partial A}\right)_{N_1, N_2} \left(\frac{\partial A}{\partial N_1}\right)_{\gamma, N_2} \left(\frac{\partial N_1}{\partial \gamma}\right)_{A, N_2} = -1 \quad (3.43)$$

whence

$$\frac{\partial \gamma}{\partial A} = -\left(\frac{\partial \gamma}{\partial N_1}\right)_{\gamma, N_2} \left(\frac{\partial N_1}{\partial A}\right)_{\gamma, N_2} \quad (3.44)$$

The substitution of $\partial \gamma/\partial A$ given by (3.44) into (3.41) yields

$$-\left(\frac{\partial \gamma}{\partial N_1}\right)_{\gamma, N_2} \left(\frac{\partial N_1}{\partial A}\right)_{\gamma, N_2} \left(\frac{\partial \mu_1}{\partial N_1}\right) > \left(\frac{\partial \gamma}{\partial N_1}\right)^2 \quad (3.45)$$

In the general case the derivative $\partial \gamma/\partial N_1$ can be either positive or negative. If

$$\partial\gamma/\partial N_1 < 0$$

then

$$(\partial\gamma/\partial\mu_1)_{A,N_2} < 0$$

and by virtue of (3.43),

$$\partial N_1/\partial A > 0$$

Finally, we obtain from (3.45) that

$$(\partial N_1/\partial A)_{Y,N_2} > -(\partial\gamma/\partial N_1)_{A,N_2}/(\partial\mu_1/\partial N_1)_{A,N_2} \quad (3.46)$$

$$(\partial N_1/2A)_{Y,N_2} > -(\partial\gamma/\partial\mu_1)_{A,N_2} \quad (3.46')$$

If, however,

$$\partial\gamma/\partial N_1 > 0$$

then

$$-(\partial N_1/\partial A)_{Y,N_2} > (\partial\gamma/\partial N_1)_{A,N_2}/(\partial\mu_1/\partial N_1)_{A,N_2} \quad (3.47)$$

or

$$-(\partial N_1/\partial A)_{Y,N_2} > (\partial\gamma/\partial\mu_1)_{A,N_2} \quad (3.47')$$

In the last case the derivative $\partial\gamma/\partial\mu_1 > 0$, while the derivative $\partial N_1/\partial A$ is negative.

Likewise, by choosing the derivatives $\partial\gamma/\partial A$, $\partial\mu_2/\partial N_2$, and $\partial\gamma/\partial N_2$ for independent coefficients in the quadratic form (3.37), we find the conditions of stability in the form

$$\partial\mu_2/\partial N_2 > 0 \quad (3.48)$$

and

$$(\partial N_2/\partial A)_{Y,N_1} > -(\partial\gamma/\partial\mu_2)_{A,N_1} \quad (3.49)$$

if $\partial\gamma/\partial N_2 < 0$, and in the form

$$-(\partial N_2/\partial A)_{Y,N_1} > (\partial\gamma/\partial\mu_2)_{A,N_1} \quad (3.49')$$

if $\partial\gamma/\partial N_2 > 0$.

Finally, the set of independent coefficients $\partial\mu_1/\partial N_1$, $\partial\mu_2/\partial N_2$, and $\partial\mu_1/\partial N_2$ corresponds to the condition of stability

$$(\partial N_2/\partial N_1)_{\mu_1, A} > -(\partial\mu_1/\partial\mu_2)_{N_1, A} \quad (3.50)$$

if $\partial\mu_1/\partial N_2 < 0$, and to

$$-(\partial N_2/\partial N_1)_{\mu_1, A} > (\partial\mu_1/\partial\mu_2)_{N_1, A} \quad (3.50')$$

if $\partial\mu_1/\partial N_2 > 0$.

Only one of the three conditions (3.48), (3.49), and (3.50) is independent. Thus, condition (3.49) can be obtained from (3.41) by replacing the derivatives $\partial\gamma/\partial N_1$ and $\partial\mu_1/\partial N$ by their expressions in terms of $\partial\gamma/\partial N_2$, $\partial\mu_2/\partial N_2$, and $\partial\gamma/\partial A$ by means of Euler's theorem (3.38) and expression (3.17) for the total differential dF^S .

The limiting case of the bulk-phase film is best derived from (3.39). The tension γ then equals $\sigma = \sigma_0$, where σ_0 is independent of either Γ_1 or Γ_2 [$\sigma_0 = \sigma(\Gamma_1 \rightarrow \infty, \Gamma_2 \rightarrow \infty)$]. Consequently, all terms containing the derivatives $\partial\gamma/\partial A$ and $\partial A/\partial N_1$ vanish in expression (3.39), and its new form is

$$N_1^2 \left(\frac{\partial\mu_1}{\partial N_1} \right) \left(\frac{\Delta N_1}{N_1} - \frac{\Delta N_2}{N_2} \right)^2 > 0 \quad (3.51)$$

or

$$\frac{N_1^2}{N_2} \frac{\partial\varphi_1}{\partial b} \left(\frac{\Delta N_1}{N_1} - \frac{\Delta N_2}{N_2} \right)^2 > 0 \quad (3.52)$$

where

$$\varphi_1 = \varphi_1(T, \mu_3, \mu_4, N_1/N_2 = b)$$

is the value of the chemical potential of the film degenerated to the bulk phase.

The necessary and sufficient condition for the last inequality to hold is

$$\partial\varphi_1/\partial b > 0 \quad (3.53)$$

Since

$$\frac{\partial\varphi_1}{\partial N_1} = -\frac{N_2}{N_1} \frac{\partial\varphi_1}{\partial N_2} = -\frac{N_2}{N_1} \frac{\partial\varphi_2}{\partial N_1} = \frac{N_2^2}{N_1^2} \frac{\partial\varphi_2}{\partial N_2}$$

inequality (3.52) simultaneously indicates that

$$\partial\varphi_2/\partial(1/b) > 0 \quad (3.54)$$

or

$$\partial\varphi_2/\partial b < 0 \quad (3.55)$$

In the limiting case of a three-component film with a single nonvolatile component

$$\frac{\partial\gamma}{\partial N_1} = -\frac{A}{N_1} \frac{\partial\gamma}{\partial A} \quad \text{and} \quad \frac{\partial\mu_1}{\partial N_1} = -\frac{A}{N_1} \frac{\partial\gamma}{\partial N_1} = \frac{A^2}{N_1^2} \frac{\partial\gamma}{\partial A} \quad (3.56)$$

Consequently, the quadratic form (3.39) transforms to

$$A^2 \frac{\partial\gamma}{\partial A} \left(\frac{\Delta A}{A} - \frac{\Delta N_1}{N_1} \right)^2 > 0 \quad (3.57)$$

so that the necessary and sufficient condition for its positive definiteness is

$$\frac{\partial\gamma}{\partial A} > 0 \quad (3.58)$$

The stability condition (3.40) is identical to the condition of stability of a three-component film (with a single nonvolatile component). But condition (3.41), or its equivalent forms (3.46) and (3.47), is valid only for a four-component film.

The thermodynamic stability with respect to local fluctuations of film thickness (different on different segments of the film) was analyzed by Vrij [6]. He derived the stability condition which is necessary for a film with an arbitrary number of nonvolatile components. But this condition is sufficient only for films with a single nonvolatile component. In this last case there is a relationship between film thickness and the amount of the nonvolatile component, and fluctuations of film thickness are equivalent to the fluctuations of the amount of the nonvolatile component. But if the film contains several nonvolatile components, there is a possibility of fluctuations of these components along the film which will not affect the film thickness. Consequently, only an analysis of the fluctuations of each nonvolatile component along the film indepen-

dently of other components gives at the same time the sufficient conditions of equilibrium, their number being equal to that of non-volatile components in the film.

The criteria formulated above refer to the concept of thermodynamic stability, which significantly differs from the notion of stability of free films that are found in a number of relevant experimental and theoretical papers. These papers define stability as a quantity reciprocal to the probability of rupture of a film, either for a given film area or per unit area (provided the result is independent of the film size). This measure of stability is meaningful if the film is in a metastable thermodynamic equilibrium that can be broken in favor of a more stable state because of, for instance, film rupture or jumpwise thinning, caused by thermal fluctuations.

Consider now the equilibrium of a film with the peripheral bulk-phase liquid in the case of exchange by molecules of nonvolatile components. Assume that the system is maintained at constant T , μ_3 , μ_4 , P_1 , and A . The constraints imposed by the conservation of the number of particles are

$$\Delta n_1 + \Delta N_1 = 0, \quad \Delta n_2 + \Delta N_2 = 0 \quad (3.59)$$

The variables listed above correspond to the functions of state

$$F^S = F^S(A, N_1, N_2, T, \mu_3, \mu_4)$$

in the film and

$$\varphi = \varphi(P_1, n_1, n_2, T, \mu_3, \mu_4)$$

in the bulk liquid. In the equilibrium state the departures of the general function of state of the system ($F^S + \Phi$) from equilibrium must be positive:

$$\Delta F^S + \Delta \Phi > 0 \quad (3.60)$$

By expanding ΔF^S and $\Delta \Phi$ into a series, we obtain, to within quadratic terms,

$$(\mu_1 - \mu_1^V) \Delta N_1 + (\mu_2 - \mu_2^V) \Delta N_2 + \frac{1}{2} \left(\frac{\partial \mu_1}{\partial N_1} + \frac{\partial \mu_1^V}{\partial n_1} \right) (\Delta N_1)^2$$

$$+ \left(\frac{\partial \mu_1}{\partial N_2} + \frac{\partial \mu_1^V}{\partial n_2} \right) \Delta N_1 \Delta N_2 + \frac{1}{2} \left(\frac{\partial \mu_2}{\partial N_2} + \frac{\partial \mu_2^V}{\partial n_2} \right) (\Delta N_2)^2 > 0$$

where $\mu_{1,2}^V$ are the chemical potentials of the bulk liquid.

The requirement that the first-order terms vanish yields the condition of equality of chemical potentials:

$$\begin{aligned} \mu_1^V(P_1, n_1/n_2) &= \mu_1(\Gamma_1, \Gamma_2), \\ \mu_2^V(P_1, n_1/n_2) &= \mu_2(\Gamma_1, \Gamma_2) \end{aligned} \quad (3.61)$$

The necessary and sufficient condition of positive definiteness of the remaining quadratic form in (3.60) is given by the inequalities

$$\frac{\partial \mu_1}{\partial N_1} + \frac{\partial \mu_1^V}{\partial n_1} > 0 \quad (3.62)$$

$$\begin{aligned} &(\frac{\partial \mu_1}{\partial N_1} + \frac{\partial \mu_1^V}{\partial n_1})(\frac{\partial \mu_2}{\partial N_2} + \frac{\partial \mu_2^V}{\partial n_2}) \\ &- (\frac{\partial \mu_1}{\partial N_2} + \frac{\partial \mu_1^V}{\partial n_2})^2 > 0 \end{aligned} \quad (3.63)$$

Condition (3.63) is stricter than the corresponding equilibrium conditions for the film and the bulk liquid separately because it contains pairwise products that simultaneously contain the terms for the bulk liquid and the film.

When considering equilibrium with respect to the exchange of volatile components between the film and the surrounding gaseous phase, let us introduce, as a characteristic function of the film, a function H depending on T , A , N_1 , N_2 , N_3^S , and N_4^S :

$$\begin{aligned} dH = d(F^S + \mu_3 N_3^S + \mu_4 N_4^S) &= -S^S dT + \gamma dA \\ &+ \mu_1 dN_1 + \mu_2 dN_2 + \mu_3 dN_3^S + \mu_4 dN_4^S \end{aligned} \quad (3.64)$$

We choose the free energy F^V as the characteristic function of the bulk-phase part of the system:

$$dF^V = -S^V dT + \mu_3^g dN_3^V + \mu_4^g dN_4^V - P dV \quad (3.65)$$

where V is the volume of the system; S^V , N_3^V , and N_4^V are the entropy and the numbers of particles of the system, equal to their volume densities times the volume, respectively; and μ_3^g, μ_4^g are the chemical potentials in the bulk gaseous phase.

Let us assume that the exchange of volatile components between the film and the gaseous phase takes place at constant T, V, A, N₁, and N₂. Furthermore, the following conservation laws hold:

$$\Delta N_3^V + \Delta N_3^S = 0, \quad \Delta N_4^V + \Delta N_4^S = 0 \quad (3.66)$$

With the constraints mentioned above imposed on the system's equilibrium, the departures of the function (F^V + H) from the equilibrium value must be positive:

$$\Delta(F^V + H) > 0 \quad (3.67)$$

Expanding F^V and H, as before, into a series to within quadratic terms, we find

$$\begin{aligned} & (\mu_3^g - \mu_3) \Delta N_3^V + (\mu_4^g - \mu_4) \Delta N_4^V + \frac{1}{2} \left(\frac{\partial \mu_3^g}{\partial N_3^V} + \frac{\partial \mu_3}{\partial N_3^S} \right) (\Delta N_3^V)^2 \\ & + \frac{1}{2} \left(\frac{\partial \mu_4^g}{\partial N_4^V} + \frac{\partial \mu_4}{\partial N_4^S} \right) (\Delta N_4^V)^2 + \left(\frac{\partial \mu_3^g}{\partial N_4^V} + \frac{\partial \mu_3}{\partial N_4^S} \right) \Delta N_3^V \Delta N_4^V \end{aligned} \quad (3.68)$$

By requiring that the first-order terms vanish, we obtain

$$\begin{aligned} \mu_3(N_1/A, N_2/A, N_3^S/A, N_4^S/A, T) &= \mu_3^g(N_3^V/V, N_4^V/V, T) \\ \mu_4(N_1/A, N_2/A, N_3^S/A, N_4^S/A, T) &= \mu_4^g(N_3^V/V, N_4^V/V, T) \end{aligned} \quad (3.69)$$

The necessary and sufficient condition of positive definiteness of the remaining quadratic form in (3.68) is

$$\frac{\partial \mu_3^g}{\partial N_3^V} + \frac{\partial \mu_3}{\partial N_3^S} > 0 \quad (3.70)$$

$$\begin{aligned} & \left(\frac{\partial \mu_3^g}{\partial N_3^V} + \frac{\partial \mu_3}{\partial N_3^S} \right) \left(\frac{\partial \mu_4^g}{\partial N_4^V} + \frac{\partial \mu_4}{\partial N_4^S} \right) \\ & - \left(\frac{\partial \mu_3^g}{\partial N_4^V} + \frac{\partial \mu_3}{\partial N_4^S} \right)^2 > 0 \end{aligned} \quad (3.71)$$

Let the bulk-phase part of the system be an ideal gas. The chemical potentials of the two components of this gas are, respectively,

$$\mu_{3,4}^g = \theta \ln(N_{3,4}^V/V) + f_{3,4}(\theta) \quad (3.72)$$

where θ is the absolute temperature times the Boltzmann constant.

Therefore,

$$\partial\mu_3^g/\partial N_3^V = \theta/N_3^V, \quad \partial\mu_4^g/\partial N_4^V = \theta/N_4^V, \quad \partial\mu_3^g/\partial N_4^V = 0 \quad (3.73)$$

Consequently, for the ideal gas mixture inequalities (3.70) and (3.71) take the form

$$\partial\mu_3/\partial N_3^S > -\theta/N_3^V, \quad (3.73')$$

$$(\partial\mu_3/\partial N_3^S + \theta/N_3^V)(\partial\mu_4/\partial N_4^S + \theta/N_4^V) > (\partial\mu_3/\partial N_4^S)^2 \quad (3.73'')$$

It is clear from (3.73') that the strictest condition of stability is imposed on the film when the volume of the contiguous gaseous phase is infinite. In this case the numbers of particles N_3^V and N_4^V , proportional to the volume, are infinite, and (3.73') and (3.73'') transform to

$$\partial\mu_3/\partial N_3^S > 0 \quad (3.74)$$

$$(\partial\mu_3/\partial N_3^S)(\partial\mu_4/\partial N_4^S) - (\partial\mu_3/\partial N_4^S)^2 > 0 \quad (3.75)$$

or, by virtue of the equivalence of the third and fourth components,

$$(\partial\mu_3/\partial N_3^S)(\partial\mu_4/\partial N_4^S) - (\partial\mu_3/\partial N_4^S)(\partial\mu_4/\partial N_3^S) > 0 \quad (3.75')$$

The conditions so derived coincide with the conditions of stability with respect to the exchange of the molecules of volatile components between different parts of the film. Hence, this exchange being always allowed, the softening of stability conditions in the case of decreasing volume of the gaseous phase is only illusory. Condition (3.75') is again the necessary one.

Consider now a simpler particular case of a film with a single nonvolatile component, in the amount N_1 , and two volatile components with chemical potentials μ_2 and μ_3 . This gives us the film stability criterion

$$(\partial\gamma/\partial A)_{N_1, T, \mu_2, \mu_3} > 0 \quad (3.76)$$

The last inequality can be rewritten in two equivalent forms (taking into account that $\Gamma_1 = N_1/A > 0$):

$$(\partial\gamma/\partial\alpha)_{T, \mu_2, \mu_3} > 0 \quad (3.76')$$

$$(\partial\gamma/\partial\Gamma_1)_{T, \mu_2, \mu_3} < 0 \quad (3.76'')$$

where $\alpha = 1/\Gamma_1$.

Tension thus has to diminish as the surface concentration Γ_1 increases. Conditions (3.76) can hold only at such thicknesses of the film at which it contains no parts with the properties of the bulk phase, because in a "thick film" γ becomes equal to the surface tension of the film degenerated to the bulk phase and, hence, depends only on μ_2 and μ_3 , but not on Γ_1 . For this reason condition (3.76''), for instance, is essentially different from the Marangoni-Gibbs principle, where the derivative $\partial\sigma/\partial\Gamma_1$ is nonzero for a thick film because it is assumed that equilibrium between the solvent (water) and the surrounding phase is reached over a much longer time than the time of perturbation (stretching) of the segment of the film considered. Hence, in contrast to condition (3.76''), the Marangoni-Gibbs principle cannot ensure the stability of a free film with respect to prolonged perturbations, and it cannot explain the strictly uniform thickness of soap films on horizontal segments, observed in films that stay in equilibrium for a long time.

The coexistence of two film segments with uniform but different thicknesses is a spectacular phenomenon that also finds an explanation only within the approach outlined above. The condition of this coexistence is the equality of chemical potentials μ_1 , μ_2 , and μ_3 and tension γ of the two films, corresponding to different values of Γ_1 and, hence, to the values $\alpha = \alpha_1$ and $\alpha = \alpha_2$. This last situation is possible only if γ is a nonmonotonic function of α and, hence, has a form shown in Fig. 3.2. The expression for the chemical potential following from (3.30) is not convenient for such a function $\gamma(\alpha)$ because the inverse function $1/\Gamma = \alpha(\gamma)$ is not single-valued, so that the following equation must be used:

$$\mu_1 = \int_{\phi}^{\Gamma_1} \gamma d\frac{1}{\Gamma_1} - \frac{\gamma}{\Gamma_1} + \varphi_0 = \int_0^{\alpha} \gamma d\alpha - \gamma\alpha + \varphi \quad (3.77)$$

or

$$\mu_1 = \varphi - \int_{\gamma_0}^{\gamma} \alpha dy = \varphi - \int_0^{\gamma-\gamma_0} \alpha d(\gamma - \gamma_0) \quad (3.77')$$

By equating the chemical potentials μ_1 for the two films and assuming that the film tensions are identical (equal to γ' ; see Fig. 3.2), we obtain two equations to determine α_1 and α_2 :

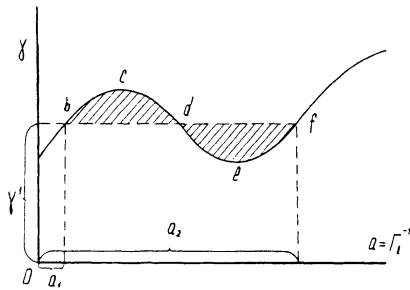


Fig. 3.2. Coexistence of films of unequal thickness.

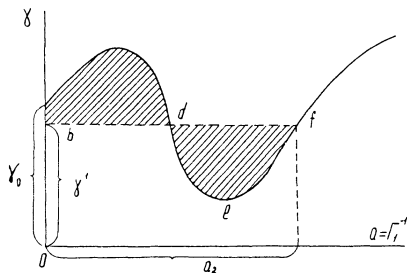


Fig. 3.3. Formation of a contact angle at a bulk phase-thin film boundary.

$$\gamma(\alpha_1) = \gamma(\alpha_2) = \gamma' \quad (3.78)$$

$$\int_{\alpha_1}^{\alpha_2} \gamma d\alpha - \gamma'(\alpha_2 - \alpha_1) = 0 \quad (3.78')$$

Geometrically this means that the areas bcd and def, hatched in Fig. 3.2, are equal. We can thus find the unknown quantities α_1 and α_2 for given values of temperature, pressure, and chemical potentials μ_2 and μ_3 .

The function $\gamma(\alpha)$ may be such that the equality of the hatched areas corresponds to the value $\alpha_1 = 0$ (Fig. 3.3), with the point b located on the ordinate axis below the curve $\gamma(\alpha)$. Then it is easy to see that in this case a film with $\alpha = \alpha_2$ can exist in equilibrium only with the bulk phase whose surfaces form with the film the contact angles θ satisfying the condition [4]

$$\cos \theta = \gamma'/\gamma^0 \quad (3.79)$$

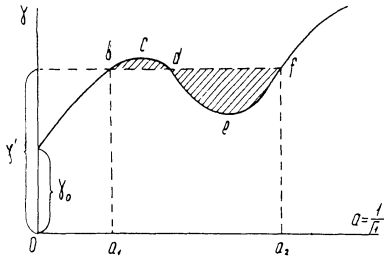


Fig. 3.4. The mechanical equilibrium of two films of unequal thickness.

The distinction of such contact angles is that their existence is completely determined by the specific properties of thin liquid films, viz., by the effects of overlapping of their interfacial zones. If there are two neighboring segments of the film satisfying only the conditions of mechanical equilibrium (3.78) but not condition (3.78'), the boundary between them will move. In the case shown in Fig. 3.4, it is obvious that $\mu_1(a_2) < \mu_1(a_1)$ and, hence, component "1" must convert into a thinner film whose area must grow at the expense of the simultaneously contracting thicker segment. This corresponds to a readily observable (and investigated by movie techniques) expansion of black spots which usually appear spontaneously on soap films, as well as to the displacement of the boundary between a "black" and a "gray" segment of the film [7, 9-11].

We thus find that in order to obtain the equation of state of a free film it is sufficient to establish experimentally the dependence of γ on T , Γ_1 , μ_2 , and μ_3 that determines the form of the fundamental equation. Two practical (but not principal) difficulties arise: i) measurement of the values of Γ_1 , and ii) measurement of γ with very high accuracy, which is required especially for thick films in which γ is very near to γ_0 , so that small variations of γ correspond to large variations in thickness and in the values of Γ_1 . The first difficulty can be overcome by introducing a radioactive tracer into the first component. The second difficulty can be partially overcome by observing the equilibrium of a vertical film under gravity and determining the excess surface density of the film ($m_1\Gamma_1 + m_2\Gamma_2 + m_3\Gamma_3$, where m_i denotes the mass of molecules) as a function of elevation z (e.g., by adsorption of β rays). Obviously,

$$\gamma - g \int (m_1\Gamma_1 + m_2\Gamma_2 + m_3\Gamma_3) dz = \text{const}$$

which gives the method of determining γ . Nevertheless, a different method of experimental investigation of the equation of state

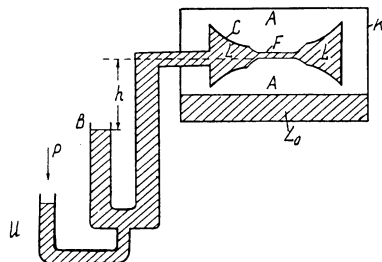


Fig. 3.5. Schematic diagram of the measurement of disjoining pressure in a free film.

is preferable for thick films. It is based on considering the equilibrium of a free film connected through its peripheral sections to the bulk liquid L separated from the surrounding gaseous phase by two identical menisci. The advantage of this technique is that the film has very small dimensions (with an area about 1 mm² or less) and its equilibrium with the bulk phase is maintained more easily and to better accuracy.

Let us specify the following experimental arrangement not completely identical to that used in [7, 8] but one better suited to a theoretical analysis (Fig. 3.5). A double concave hollow glass capsule C is equipped in its central portion with circular "windows" between which a free film F, surrounded along the periphery by a bulk phase L, is formed at a proper curvature of the menisci. The meniscus curvature and, hence, the disjoining pressure, the value of Γ_1 , and the film thickness are varied by changing the level of the liquid in the arm B of the siphon, through changing the pressure on the liquid in the arm U. The level difference h between the plane of the film and the meniscus of the liquid in the arm B determines the disjoining pressure Π of the film. The value of Γ_1 can be determined by radiotracers, and the film "thickness" by the light reflection coefficient, on the basis of the theory of light interference in a thin film. The value of μ_2 is maintained constant by placing within the chamber K a certain volume of a solution L₀ of constant concentration ("film degenerated to the bulk phase"). In principle, this liquid can maintain also the given value of μ_3 . This, however, is readily achieved by arranging in the lid T of the chamber K a small orifice that connects the contents of the chamber to the atmosphere. In equilibrium the chemical potentials μ_2 and μ_3 are identical in the two phases A and L and in the film F, while the chemical potential μ_1 is identical in the liquid phase L and the film F.

Since the surface of the menisci is curved, there is a pressure jump at the interface between the phases A and L, related to the meniscus curvature $K = 1/R_1 + 1/R_2$ by Laplace's equation

$$P_2 - P_1 = \sigma K \quad (3.80)$$

where P_2 is the pressure in the phase A, P_1 is the pressure in the liquid phase L, σ is the surface tension at the interface between the two phases, and R_1 and R_2 are the principal radii of curvature of the surface. As a result of this pressure jump the external pressure on the film surface at equilibrium exceeds the hydrostatic pressure in the phase L by a certain quantity Π . The film is part of this phase and connects to it through the peripheral sections. As with all other thermodynamic properties of the film, Π is a function of T , Γ_1 (or μ_1), μ_2 , and μ_3 . By changing the level of liquid in the arm B, we can change P_1 and, hence, can change to the same degree the pressure jump equal to Π , provided P_2 is maintained constant.

The potentials μ_2 and μ_3 in the film and in the bulk phase surrounding the film at its periphery are maintained constant because of the neighborhood of a gas volume A and the layer L_0 of a solution with strictly constant composition. Consequently, a change in P_1 must change the potential μ_1 in the film and near the peripheral region. The changes in the composition of the bulk liquid phase and, hence, the changes in the surface tension of its menisci, accompanying the changes in μ_1 and P_1 , are negligible. At the same time, the analysis can be made more rigorous by considering these changes in composition as resulting from the exchange of liquid components with the constant-composition phase L_0 .

As follows from the Gibbs-Duhem equation and from Eq. (3.77),

$$dP_1 = - d\Pi = \rho_1 d\mu_1 = - \alpha \rho_1 d\gamma \quad (3.81)$$

where ρ_1 is the molar concentration of the first component in the liquid phase.

By integrating (3.81) at $\mu_2 = \text{const}$ and $\mu_3 = \text{const}$ and neglecting the changes in ρ_1 , we find

$$\Pi \approx \rho_1(\varphi - \mu_1) = \rho_1 \int_{\gamma_0}^{\gamma} \alpha d\gamma \quad (3.82)$$

where φ [see Eq. (3.77')] equals the value of μ_1 for $\alpha \rightarrow 0$, $P_1 \rightarrow P_2$, and $\Pi \rightarrow 0$. By expanding α into a series in powers of $\gamma - \gamma_0$ and noticing that $\alpha \rightarrow 0$ when $\gamma - \gamma_0 \rightarrow 0$, we find from Eq. (3.82) that

$$\Pi = \frac{1}{2} \left(\frac{\partial \alpha}{\partial \gamma} \right)_{\gamma=\gamma_0} \rho_1 (\gamma - \gamma_0)^2 \quad (3.83)$$

Now we can find γ in terms of Π from Eq. (3.81) by means of the exact formula

$$\gamma - \gamma_0 \equiv \Delta\gamma = \int_0^{\Pi} \frac{d\Pi}{\alpha\rho_1} \quad (3.84)$$

where, again, $\mu_2 = \text{const}$, $\mu_3 = \text{const}$. In order to measure $\alpha = 1/\Gamma_1$, we can use, for instance, the radiotracer technique; Π is found from the measured level difference, and ρ_1 is nearly constant. Therefore, formula (3.84) makes it possible to find a very small difference $\gamma - \gamma_0$ as a function of Γ_1 , μ_2 , μ_3 , or μ_1 , μ_2 , μ_3 and, hence, to find the fundamental equation with a quite good accuracy, even for thick films in which $\Delta\gamma$ is very small and hardly measurable directly. Having found $\Delta\gamma$ as a function of Γ_1 , μ_2 , and μ_3 , we can find μ_1 , Γ_2 , and Γ_3 from the equations by means of the formulas

$$\begin{aligned} \mu_1 &= \varphi(T, \Gamma_1, \mu_2, \mu_3) - \int_0^{\Pi} \frac{d\Pi}{\rho_1} \\ &\approx \varphi(T, \Gamma_1, \mu_2, \mu_3) - \frac{\Pi}{\rho_1} \end{aligned} \quad (3.85)$$

$$\Gamma_2 = -\frac{\partial}{\partial\mu_2}(\gamma + \mu_1\Gamma_1) \quad (3.86)$$

$$\Gamma_3 = -\frac{\partial}{\partial\mu_3}(\gamma + \mu_1\Gamma_1) \quad (3.87)$$

Equations (3.86) and (3.87) differ from the Gibbs adsorption theorem in that σ is supplemented by the term $\mu_1\Gamma_1$. If a film is formed only of components "2" and "3" ($\Gamma_1 = 0$), this term vanishes. There remains, however, the distinction that formulas (3.86) and (3.87) give the absolute values of surface concentrations not related to the arbitrary drawing of the geometrical boundary surface, as was typical for the case of adsorption at an interface between two distinct phases. The possibility of expressing the unknown properties of the film — γ , μ_1 , μ_2 , and μ_3 — in terms of the prescribed values of Γ_1 , μ_2 , and μ_3 by means of formulas (3.84)-(3.87) after the function $\Pi(\Gamma_1, \Gamma_2, \Gamma_3)$ has been determined experimentally shows the fundamental role played by disjoining pressure in the thermodynamics of thin films.

The role played by disjoining pressure in the stability of free films with arbitrary thickness, including Perrin bimolecular films, follows from the fact that the necessary conditions of stability (or rather, metastability) of films, (3.76)-(3.76''), can be written in the following manner, by virtue of differential relation (3.81):

$$(\partial \Pi / \partial \alpha)_{T, \mu_2, \mu_3} > 0 \quad (3.88)$$

$$(\partial \Pi / \partial \Gamma_1)_{T, \mu_2, \mu_3} < 0 \quad (3.88')$$

These conditions are valid, however thin the films, because the stringent phenomenological definition of Π (in contrast to the intuitive one) holds without limitations for any films. The problem of the conditions of metastability of a free film must not be confused with that of the degree of stability and average lifetime of a film, determined by concrete rupturing mechanisms. There is no doubt, however, that regardless of the possible mechanisms of film rupturing and of the factors that are capable of slowing it down (e.g., enhanced viscosity), a violation of conditions (3.88), or of the equivalent conditions (3.76), must sharply reduce the average lifetime of the film because the state of the film becomes thermodynamically labile. Indeed, it is readily noticed that the violation of these conditions must have inevitable consequences. Any local spontaneous "thinning" of a film, in the sense of a lowered value of Γ_1 , must result in a local increase in γ and, hence, owing to a stretching of the film, in an unlimited decrease of Γ_1 , leading to a rupturing chain reaction. Therefore, in this sense the thermodynamic conditions of film stability are basic, although they do not completely determine the lifetime of the film.

The main contribution of the experimental method whose principle is illustrated in Fig. 3.5 lies in the possibility of studying the changes in the parameters of state of the film (thickness, disjoining pressure Π , the value of Γ_1 , etc.) produced by a change in μ_1 .

Thus, let us use theoretically the diagram of Fig. 3.6 and analyze how the film-bulk liquid equilibrium must be changed by a change in μ_1 produced by a change in the meniscus curvature (at $\mu_2, \mu_3 = \text{const}$). As follows from Eq. (3.85), at constant μ_2 and μ_3 the increment in μ_1 , approximately equal to

$$\Delta \mu_1 \approx -\Delta \Pi / \rho_1 \quad (3.89)$$

moves the representative point f to a new position f' , such that

$$-\int_f^{f'} \alpha d\gamma = \Delta \mu_1 \quad (3.90)$$

The corresponding value of the integral is shown in Fig. 3.6 by a hatched area. The shift of the point f increases the area per molecule of the first component and, hence, the film tension. Note that $\cos \theta = \gamma'/\gamma$, becoming a function of meniscus curvature,

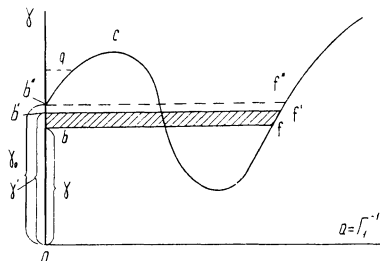


Fig. 3.6. Effect of meniscus curvature on the state of the adjacent film and on the contact angle.

will thereby increase, and at a certain point f'' corresponding to a certain value $\Delta\mu_1 = K$ the angle τ may become zero. As μ_1 further diminishes, the values of α and γ will continue to grow, always with zero contact angle. This will not violate the mechanical equilibrium of the film with the bulk phase contacting it at the periphery, because it can be shown that the equation

$$d\gamma = (\Gamma_1/\rho_1)d\alpha \quad (3.91)$$

contained in Eq. (3.81), is the condition of mechanical equilibrium for any small wedge-shaped segment of the film. Integration of Eq. (3.91) will prove that a film, for which $\alpha > 0$ for any value of Γ_1 , necessarily has the tension $\sigma > \sigma_0$. By referring to $\Gamma_1/\rho_1 \equiv H$ as the virtual thickness of the film, we can recast Eq. (3.91) in the form

$$d\gamma = H d\alpha \quad (3.91')$$

that was obtained earlier for single-component films. However, the notion of geometric thickness becomes uncertain for very thin films, while the ratio Γ_1/ρ_1 is always strictly defined and, in principle, measurable to any desired accuracy. A decrease in μ_1 results in a simultaneous decrease of Γ_1 and, hence, of film thickness.

A film represented by a point q on the segment of the curve $\gamma(\alpha)$ to the left of the maximum C can also exist in equilibrium with the menisci of the bulk liquid at $\theta = 0$. Obviously, the value of γ for this film will be higher than at some point to the right of f , corresponding to the same value of μ_1 . Therefore, a mechanical equilibrium is impossible in this coexistence. Since a greater γ corresponds to a film with a greater Γ_1 , a film with a smaller Γ_1 being stretched by the adjacent thicker film will rapidly thin out, while the thicker one will grow thicker and diminish its area. Since the chemical potential of the thicker segment of the film will at the same time increase, the decrease in the area

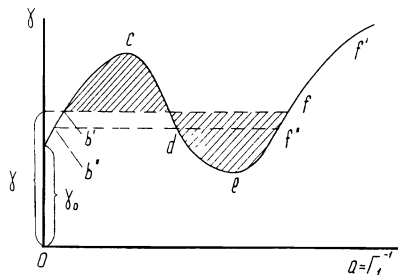


Fig. 3.7. Formation and growth of black (secondary) films.

of the thicker segment will be facilitated by an outflow of the first component owing to the difference in the chemical potential. The thicker segment thus inevitably decays. Nevertheless, it can be shown on the basis of the expression for the free energy of the film that a spontaneous fluctuation-induced formation of a thicker segment on a film has an extremely low probability.

The formation of a thicker segment on a film whose representative point lies to the left of f and that can be in equilibrium with convex menisci of the bulk phase is even less probable.

Films corresponding to the segment $b''b'$ in Fig. 3.7 can exist for prolonged periods in a metastable state, after they are formed by a gradual thinning of a thick layer of a solution, in the course of decreasing the value of μ_1 . However, as α increases, the probability of a jumpwise formation of a thinner (and stable) segment of a film, corresponding to the branch of the curve to the right of f , increases as well. The newly formed segment will gradually expand and cover the whole area of the film. This process may be accompanied by a formation of a nonzero "contact angle" if the change in μ_1 was not too large. Such phenomena of formation and growth of thinner black patches on soap films in experimental schemes close to that shown in Fig. 3.5 were reported in a number of papers [7-11]. In the case shown in Fig. 3.7, the contact angle of any film in equilibrium with concave menisci ($\Pi > 0$) is zero because it corresponds to points f' to the right of f for which the areas bcd and def are equal. The remaining characteristics and properties of the films respond to a change in μ_1 in a qualitatively similar manner to the case discussed earlier, including the probability of formation and growth of thinner black spots on "thick" films. However, in the case of a "thin" film whose representative point f'' lies to the left of the point f , it is also possible that a thicker "island" (point b'') suddenly appears and then covers the whole area of the original thinner film. However, it is then necessary for the ordinate of f'' to be greater than γ_0 , i.e., that the contact angle be zero.

REFERENCES

1. B. V. Derjaguin and A. D. Malkina, *Kolloidn. Zh.*, 12, 431 (1950); B. V. Derjaguin, N. I. Moskvitin, and M. F. Futran, Proceedings of the 3rd USSR Conference on Colloid Chemistry, Izd. AN SSSR, Moscow (1956), p. 285.
2. B. V. Derjaguin and Z. M. Zorin, *Zh. Fiz. Khim.*, 29, 1010 (1955); in: Proceedings of the 2nd International Congress on Surface Activity, Vol. 2, Butterworths, London (1957), p. 145.
3. A. N. Frumkin and A. V. Gorodetskaya, *Zh. Fiz. Khim.*, 12, 511 (1938).
4. B. V. Derjaguin and G. A. Martynov, *Kolloidn. Zh.*, 24, 480 (1962); B. V. Derjaguin, G. A. Martynov, and Yu. V. Gutop, in: Research in Surface Forces, Vol. 2, Consultants Bureau, New York (1966), p. 9.
5. B. V. Derjaguin and Yu. V. Gutop, loc. cit., Ref. 4, Research in Surface Forces Vol. 2, p. 23; ibid., Vol. 3, p. 122 (1971); *Kolloidn. Zh.*, 27, 674 (1965); *Dokl. Akad. Nauk SSSR*, 171, 652 (1966).
6. A. Vrij, *Discuss. Faraday Soc.*, No. 42, 23 (1966).
7. B. V. Derjaguin and A. S. Titiyevskaya, loc. cit., Ref. 2, Proceedings of the 2nd International Congress on Surface Activity, Vol. 1, p. 211; *Kolloidn. Zh.*, 22, 398 (1960).
8. B. V. Derjaguin and A. S. Titiyevskaya, *Discuss. Faraday Soc.*, No. 18, 27 (1954); *Kolloidn. Zh.*, 15, 416 (1953).
9. A. Scheludko, *Adv. Colloid Interface Sci.*, 1, 391 (1967).
10. K. J. Mysels, *J. Phys. Chem.*, 68, 3441 (1964).
11. D. Exerova and A. Scheludko, *C. R. Acad. Bulgare Sci.*, 24, 47 (1971).

Chapter 4

DISPERSION FORCES IN THIN INTERLAYERS AND FILMS

4.1. HISTORICAL BACKGROUND OF THE THEORY OF INTERMOLECULAR FORCES

The notion of attractive forces acting between molecules was introduced into science by Clairault [1], who treated the phenomenon of the rise of a liquid in a capillary by the same laws of hydrostatics that he had applied to the Earth, regarded as a liquid body. But Clairault mistakenly ascribed capillary rise solely to the action of attractive forces applied by the molecules of the wall and ignored the forces of interaction between the molecules of a liquid.

The correct explanation was given by Laplace [2], one of the creators of the classical capillarity theory, who is responsible for the notion of central attractive forces acting between molecules and differing from the gravitational forces in a steeper decrease with intermolecular distance. However, advances made in the development of theoretical and experimental studies of capillarity could not yield an exact law of molecular forces decreasing with increased separation between molecules, because the relevant effects proved hardly sensitive to this law. The equation of state of real gases was found equally insensitive to this factor.

One approach to elucidate the law would be to develop the theory of molecular forces. However, such work was started only at the end of the 19th century. It was at this time that P. N. Lebedev presented his doctoral thesis [3]. Lebedev's concepts of molecular forces were strikingly ahead of his time.

Discussing the ponderomotive action of waves on resonators, Lebedev wrote [3]: "Hertz's study, his interpretation of light

oscillations as electromagnetic processes, hides another problem, not yet approached, namely, that of the sources of light emission, of the processes that take place in a molecular vibrator when it emits light energy into the surrounding space; on the one hand, this problem leads us into the field of spectral analysis; but on the other, and rather unexpectedly, it brings us to one of the most complex aspects of modern physics, the field of molecular forces. This last aspect stems from the following argument. Having accepted the standpoint of the electromagnetic theory of light, we have to conclude that ponderomotive forces must exist between two light-emitting molecules as between two vibrators in which electromagnetic oscillations have been generated. They are caused by electrodynamic interactions between alternating electric currents in molecules (by Ampere's laws) or alternating charges in it (by Coulomb's laws). We have to state, therefore, that in this case there are molecular forces acting between molecules, the cause of these forces being directly connected with light emission processes..."

"...The most interesting and the most difficult situation is realized in a physical body in which many molecules act on one another simultaneously, and the oscillations of these molecules are not independent of one another because of the short distances separating them. If some day it is possible to solve this problem satisfactorily, then, using the data of spectral analysis, we shall be able to calculate in advance the magnitudes of intermolecular forces due to the emission of light by the molecules, to predict how these forces depend on temperature, and, comparing the calculated values with those observed in experiments, to solve a fundamental question of molecular physics: are the so-called 'molecular forces' reducible to the already known ponderomotive action of light emission (mentioned above), to the electromagnetic forces? Or are other forces, of hitherto unknown nature, also involved in them?"

The first quantitative theories of molecular forces, however, could be developed only after the structure of atoms and molecules was elucidated. The notion of molecular dipoles gave rise to Debye's theory of orientational forces and Keesom's theory of inductional forces. But the molecular interaction between nondipolar molecules remained unexplained, and especially the interaction between the molecules of noble gases with their spherically symmetrical structure of electron shells. Only by using the newly born quantum mechanics was London able to explain the existence of these forces [4] and to develop, to a first approximation, the general quantitative theory of molecular forces. This general theory was also able to refine the classical formulas for the interaction between polar molecules.

Where intermolecular spacings are large compared with molecular diameters (e.g., in gases), the theory shows that intermolecular attraction forces decrease in inverse proportion to the seventh power of the distance between molecules. In solids, where the rotation of molecules is frustrated, there can be forces that decrease with distance more slowly. At the same time, forces that decrease with distance more steeply - for instance, forces due to quadrupole moments - may become appreciable at the short intermolecular spacings typical of the condensed state. For these reasons, early attempts at testing the theory of molecular forces quantitatively were fundamentally incapable of providing accurate and conclusive results. Indeed, all these attempts were based on comparing the theory with integral effects in which the dominant terms are determined by the interaction between molecules at distances of the order of molecular radii.

For example, this is true for the methods of testing the theory on the basis of finding the constant α in the van der Waals equation, or finding the heat of sublimation and evaporation, and the adsorption or wetting energies. In all such cases a precise comparison with the theory is difficult because, strictly speaking, not one of the theories of molecular forces is applicable at such short distances. Furthermore, the result is the superposition of forces of different nature (e.g., quadrupole forces) that depend on (often unknown) orientation of molecules and on the asymmetry of their force fields.

The available theories of molecular forces can be tested much better by experimental investigation of effects dependent only on the action of molecular forces at distances large compared with molecular diameters. Measurements of molecular attraction between two solids separated by a gap much wider than one molecular diameter are especially pertinent, i.e., measurements similar to Cavendish's experiments with gravitational attraction and Coulomb's experiments with forces between electric charges. In contrast to measuring the adhesion force of bodies in contact, such experiments make it possible to verify a theory of intermolecular interaction at distances where forces of only one kind survive and the limitations on the validity of the theory can be ignored. Of course, the theory must be supplemented by a method of summation for molecules composing a given macroscopic body.

No experiments of such type, even qualitative ones, were reported until 1951, no doubt because of the experimental difficulties (discussed below). It is clear, however, that such measurements are of direct and fundamental importance for studying surface forces (the main subject of the present monograph). Such forces contribute to all interactions between phases, whether contiguous or separated by a gaseous, liquid, or solid interlayer of any thickness.

Direct investigation of the molecular attraction between macroscopic objects is particularly important because there are no simple, rigorous methods of transforming from a pairwise interaction of molecules (microscopic objects) to the interaction between macroscopic bodies by summation of microscopic interactions, although approximate procedures are frequently employed. We have seen that P. N. Lebedev clearly understood that this method of calculation would fail to give precise results for condensed bodies because of the mutual effects of "vibrations in neighboring molecules." In fact, the so-called additivity of molecular forces can be interpreted only as the difference between these forces and the chemical valence forces; valence forces reach saturation at short range, whereas the intermolecular fields do not. In the strict sense, additivity exists only for gases, where the distance between neighboring molecules is much greater than their diameters. Consequently, the study of macroscopic objects is a problem whose solution cannot be reduced to the elementary law of attraction between a pair of molecules.*

4.2. DIRECT MEASUREMENTS OF MOLECULAR ATTRACTION BETWEEN TWO SOLIDS

The experimental investigations now to be described were carried out by Derjaguin, Abrikossova, and Leib [5-7] on the basis of the following rationale. The exposition in the previous section illustrates the importance of developing a method for direct experimental determination of attractive forces between solids as a function of gap width. In order to solve this problem, it is necessary to make measurements with different gap widths H between the bodies, while maintaining H constant during each measurements, despite the molecular force $F > 0$, which tends to close the gap.

*These remarks should not be taken to imply that the concept of additivity of dispersion forces is totally misleading. As a first approximation it gives useful results, for example for the attractive force in simple systems (e.g., quartz/vacuum/quartz), as Sparnaay has pointed out [M. J. Sparnaay, *Physica*, 25, 217 (1959)]. Historically, it proved extraordinarily seminal in colloid science – as in Bradley's calculation of the attraction between spheres (1932), Kallmann and Willstätter's pioneering idea of colloid stability (1932), and London's first calculations of the energy of physical adsorption of gases on solids (1930, 1937). The present book later demonstrates, however, that the additivity approximation becomes increasingly unreliable, first where differences are involved, as with bodies embedded in another medium (especially if dubious "combining laws" have to be assumed), and, second, for interactions between materials of very different electronic properties – where it is useless – Editor.

If the position of one of the bodies is fixed, and the second body is rigidly coupled to a load gauge or balance to measure the force by recording a displacement ΔH from the equilibrium position, a major difficulty arises: as the dependence of molecular forces on distance is steep, an unstable equilibrium of the movable body may occur. Indeed, the condition of stability is

$$g + dF/dH > 0 \quad (4.1)$$

where g is the spring constant of the load gauge. Since dF/dH is always negative (assuming the attractive force positive), stability can easily be violated if g is small, i.e., if the sensitivity of the device is high. But if $|dF/dH| < g$ in the whole available range of H , $|dF/dH|$ will be much less than g at the upper boundary of this range. Since $F \sim H^{-m}$ and, hence, since

$$dF/dH = - mF/H$$

where $m \geq 2$, the displacement of the equilibrium position ($\Delta H = F/g$) caused by the force will constitute an inconveniently small fraction of the gap width H .

On the other hand, there are advantages in using a low-compliance load gauge or "crude" balance because this shortens the period of vibrations of the balance and reduces the effect of viscosity of the air in the gap between the two bodies, acting as a damper.

A way to satisfy these contradictory requirements was found (around 1950) by Derjaguin, Abrikossova, and Leib [5-7] in the use of electromagnetic feedback. Very small displacements of one body, resulting from the approach of the other, are used as an indicator to control a restoring force of correct magnitude to bring the body back to a "null" position. Thus it is possible to maintain the distance H constant automatically, say, by passing an electric current of proper magnitude and direction through a coil fixed to the body and placed in a magnetic field. The gap between the two bodies can be kept constant by such a "remote control" of the position of one of them. Then the molecular force to be measured is equal to the electromagnetic force applied.

It is obvious that a satisfactory stabilization of the gap width is not practicable if this balancing is done "by hand," with visual observation (e.g., by observing interference fringes in the gap between the bodies) because of a long response time of the experimenter and insufficient sensitivity to changes in the gap width. This problem is overcome by making the measurements automatic through a special circuit comprising a highly sensitive unit (sensor) tracking the changes in the position of the body and controlling the current supplied to the coil. This automatically balanced measuring circuit is at the same time a self-sustained oscillator

with negative feedback. If the electric current is regarded as a coordinate of the system affecting through the moment (proportional to this coordinate) the position of the body that is regarded as the dependent coordinate, then the tracking unit, which prescribes the current as a function of position of the body, produces a sort of negative feedback capable of maintaining the system in a stable equilibrium. The period of oscillations can easily be made small and the damping large, by introducing a phase-shifting circuit to make the current phase run ahead of the position phase. Thus the measuring circuit simultaneously maintains constant gap width and measures, through balancing, the force of molecular attraction. The technique provides many advantages. It is an early example of the applications of feedback to physical measurements.*

For several reasons, it is expedient to have one object flat and the other spherical. Derjaguin and Abrikossova used a plate 4×7 mm in conjunction with spherical lenses with radii of curvature R_0 from 5 to 26 cm. This arrangement facilitates geometrical adjustment (which is considerably more complex with two plates). The shortest distance between the bodies is readily and accurately calculable from the diameters of Newton's rings. This geometry also reduces the viscous resistance of the air interlayer (proportional to R_0^2). Furthermore, such objects make it possible to measure the force as a function of radius of curvature of the spherical surface, and thus separate the molecular force, which is proportional to this radius, from a number of masking effects, such as those produced by surface electric charge. The relation establishing the proportionality of the molecular attraction to the radius of the sphere (irrespective of the relevant law) was obtained in the form [11]

$$F(H) = - 2\pi R_0 U(H) \quad (4.2)$$

where $F(H) > 0$ is the force of attraction between a sphere and a flat plate, R_0 is the sphere radius, $U(H)$ is the energy of interaction, per unit area, between two infinite parallel plates of the same material in the same medium, and H is the shortest distance between the surfaces. This formula also shows that experiments measuring the attractive force between a sphere and a plate all yield the energy of interaction between two infinite flat plates per unit area — i.e., a result independent of the radius of curvature R_0 .

*Derjaguin et al. [8-10] also adapted the same principle to the design of an analytical microbalance — a forerunner of the modern, ubiquitous, electronic balances. Today's scientists are spared the tedium of weighing by the classical "method of swings"! — Editor.

Experiments began with objects made of quartz glass* because of its resistance to chemical reactants and because it can be polished very smooth. As the force of attraction between macroscopic objects is very small, it is desirable to study materials which are characterized by large interaction forces. Among the dielectrics with large expected attractive forces, the most suitable for our measurements were thallium halides. A series of measurements was carried out with a plate and a lens made of a mixed TlBr-TlI crystal (42.5% and 57.5%, respectively).

Metals are particularly interesting to study because of the maximum interaction force and simplicity of calculation (see below). A technically simpler case is a metal and a transparent dielectric, because it is then possible to retain the optical technique of measuring the gap width. Such experiments were run with a lens made of quartz glass, and a quartz plate coated by chromium (deposited by evaporation in vacuum). A relatively small coefficient of light reflection from the surface of chromium makes it possible to observe sufficiently sharply defined interference rings in the gap between the metal and quartz surfaces.

The attractive forces between the selected objects were measured in air and in vacuum. The interaction between two bodies should not depend appreciably on whether the gap is filled with air or not (although each system has experimental and methodological advantages and shortcomings). A comparison of results obtained with these two arrangements provides an important method of checking the correctness of measurements. Measurements in vacuum proved the more accurate and convenient. It was found that forces due to the viscosity of air in the gap between the surfaces may become comparable to the molecular forces investigated when the gap width is varied, even if the changes are slow. Readings had to be taken after waiting for a moment at which the gap width was constant. The procedure of measurement was therefore lengthened; often it was impossible to take a reading at a moment free of vibrations, even though the period of oscillations was sharply reduced by employing negative feedback. Moreover, it was not always possible to completely suppress the vibrations of the balance arm caused by convective flows in the air. These perturbations were much lower when experiments were carried out at a residual air pressure from 0.1 mm to several mm Hg.

The experimental setup was described in detail in [5-7]. It is shown schematically in Fig. 4.1. The main element of the system is a microbalance with negative feedback. The distance between

*That is, vitreous silica, density 2.21; later referred to simply as "quartz." Measurements by van Silfhout [73] with true, crystalline quartz (density 2.65) are mentioned on p. 192 - Editor.

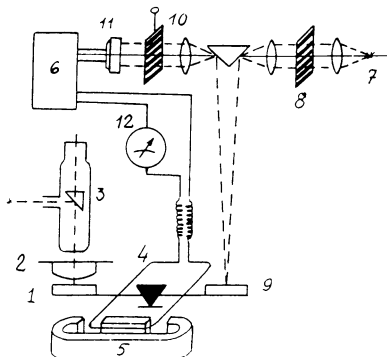


Fig. 4.1. Schematic representation of the first instrument for direct measurements of molecular forces between macroscopic bodies.

the plate 1 and lens 2 was determined by measuring the diameters of Newton's rings through a microscope 3. The forces of molecular attraction between the bodies 1 and 2 were compensated by passing a current J through coil 4 rigidly linked to the balance arm. The interaction between the current J and the field of a permanent magnet 5 produced the compensating torque. A tracking device consisting of a raster photoswitch and an amplifier 6 served as the current source. Light rays from a monochromatic source 7 passed through a raster 8 and were deflected by a prism onto a mirror 9 fixed to the right-hand arm of the balance. The reflected light again passed through the prism and then through an identical raster 10. Then this light fell on a photoelectric cell 11 that supplied the current J .

If no external force is applied, the tracking device sets the balance in a position corresponding to $J = 0$. Any departure from this state generates a coil current that restores the balance to the stable equilibrium position. Under an external force, such as the molecular attraction between the bodies 1 and 2, the equilibrium is possible only when the coil current $J \neq 0$. The current recorded by the microammeter 12 is proportional to the attractive force F . The proportionality coefficient is determined by a preliminary calibration of the instrument. The statistical error of measuring F did not exceed 10^{-4} dyn (10^{-9} N). The bodies 1 and 2 were brought together to within the range of molecular forces by shifting the raster 10 by a micrometer screw. The accuracy of measuring the gap width H was $\pm 0.01 \mu\text{m}$.

Successful experiments were possible only if the surface were carefully cleaned. Standard methods of chemical cleaning, such as

washing with potassium dichromate dissolved in sulfuric acid, were avoided in order not to spoil the polished glass surface. The plate and the lens were thoroughly cleaned by distilled alcohol and ether, with cotton wool degreased in a Soxhlet apparatus, and then subjected to glow discharge under a glass cover. Total wetting of a surface by water after cleaning operations indicated that it was indeed clean.

The most serious experimental difficulties were connected with dust particles on the surface to be investigated and with electric charging of surfaces when these particles were removed. The best results were obtained when surfaces were cleaned, after the glow-discharge treatment, by a degreased cotton wool slightly dipped in pure ether, the operation being monitored by visual control through a binocular microscope. After this treatment the surfaces remained clean and totally wetted by water.

Removal of dust particles from a surface by wiping results in an intensive charging of specimens, so that they interact with a force that may exceed the molecular attraction by a factor of several thousands. In order to remove the charge from the surfaces of the plate and the lens it was necessary to keep them at a distance of 1 to 10 mm and by some means ionize the air around the setup. Charge removal proved impossible if the surfaces were very close. For the ionization of air we used a β -radioactive preparation of sulfur isotope (S^{35}) placed close to the specimens. But when the surfaces were well separated, dust from the air often settled on them, necessitating renewed cleaning and charge neutralization, until we succeeded in getting rid of both dust particles and electrostatic interaction. It was found that dust cannot penetrate the gap if the gap is very narrow, so that it was essential to eliminate dust and surface charge once and then to separate the specimens by more than 5 to 10 μm .

4.3. EXPERIMENTAL RESULTS

Figure 4.2 plots $F(H)$ corresponding to the lowest attraction among all investigated quartz glass objects. This feature, together with a fairly good reproducibility of the effect in different experimental runs, points to its molecular nature. However, this assumption will be borne out only if we make sure that secondary effects — above all, electrostatic attractive forces — were indeed eliminated. If the attraction between bodies observed in the experiment was the molecular attraction, then it must be i) insensitive to repeated air ionization around the specimens, ii) proportional to the radius of the spherical surface [see formula (4.2)], iii) well reproducible both in magnitude and in the dependence of force on gap width, iv) well reproducible in experimental runs conducted at different points of the surfaces, and v) insensitive to evacuation of air from the gap between the bodies.

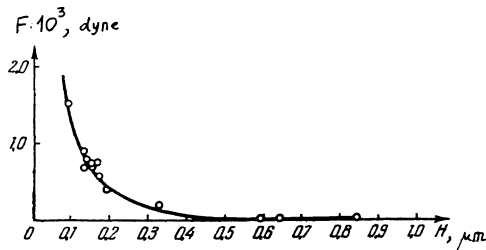


Fig. 4.2. Minimal attractive forces F between a quartz plate and a quartz lens ($R_0 = 10 \text{ cm}$) as a function of H (in air).

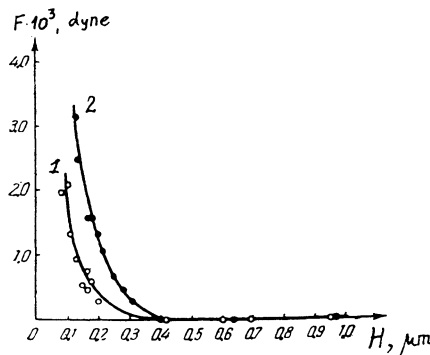


Fig. 4.3. Attractive force F between a quartz plate and a quartz lens ($R_0 = 10 \text{ cm}$ — curve 1, $R_0 = 26 \text{ cm}$ — curve 2) as a function of H (in vacuo).

Measurements in vacuum proved the most accurate and reproducible (Fig. 4.3). The data obtained in these measurements satisfy all the requirements listed above, to within the experimental error.

Figure 4.4 plots on a logarithmic scale the results of many experimental runs separated by long time intervals and conducted with different quartz specimens. Filled circles give the values obtained in measurements in air, and unfilled circles data obtained in vacuum. Nearly every run was preceded by intensive ionization of the air near the plate and lens (prior to evacuation).

According to relation (4.2), the ratio of $F(H)$ to $2\pi R_0$ is the energy of attraction U of two infinite plates, per cm^2 . Figure 4.5 plots U as a function of gap width H , with filled circles representing the data for a lens with $R_0 = 11.1 \text{ cm}$, triangles for $R_0 = 10 \text{ cm}$, and unfilled circles for $R_0 = 25.4 \text{ cm}$. This graph shows that

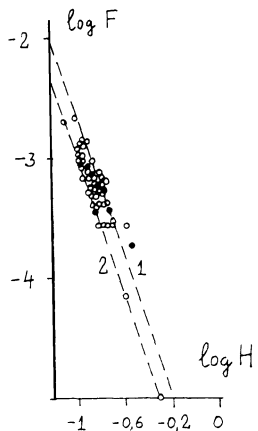


Fig. 4.4. $F(H)$ for different quartz specimens ($R_0 = 11.1$ cm). The dashed lines are curves of Lifshitz's theory for $\epsilon_0 = 3.6$ (line 1) and for $\epsilon_0 = n^2 = 2.13$ (line 2).

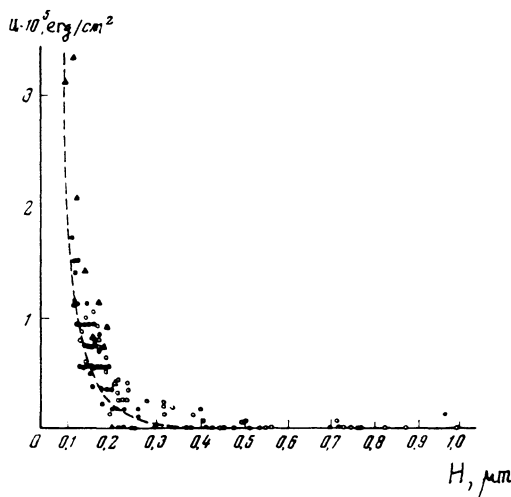


Fig. 4.5. Energy of molecular attraction $U(H)$ for lenses of different radii R_0 .

the energy of attraction between flat plates $U(H)$ is independent of the lens radius. Therefore, all conditions listed above have been met.

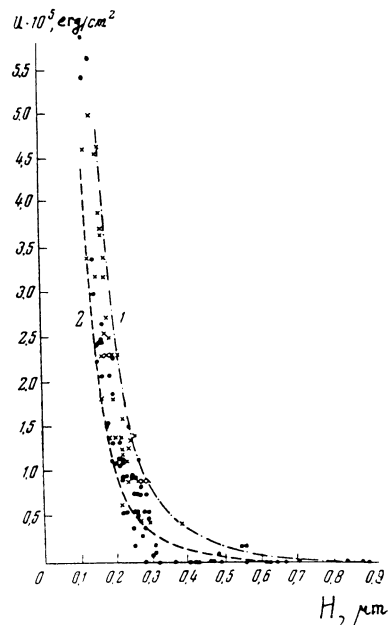


Fig. 4.6. $U(H)$ for thallium halides. Lens radius $R_0 = 12.5 \text{ cm}$ (filled circles) and $R_0 = 5.2 \text{ cm}$ (crosses).

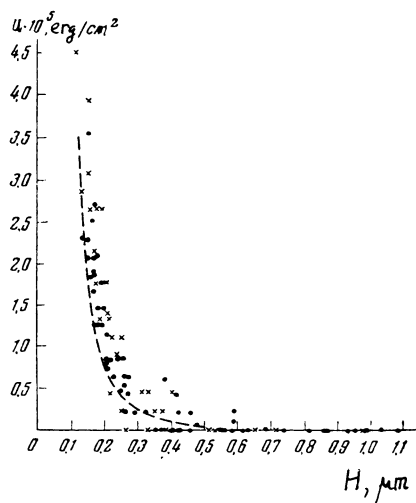


Fig. 4.7. $U(H)$ for a chromium-coated quartz plate and a quartz lens with $R_0 = 10 \text{ cm}$ (filled circles) and $R_0 = 5 \text{ cm}$ (crosses).

Figure 4.6 represents the results of experiments with specimens made of thallium halide. Likewise, Fig. 4.7 represents the results of measurements in which one of the surfaces (the plate) was coated with a sufficiently thick, mirror-smooth chromium layer.

Dashed curves plotted in Figs. 4.4-4.7 were calculated by the formulas of the Lifshitz theory (see later).

Since the results reported in [6, 7] concern the detection and measurement of an effect that was not previously confirmed by direct experiments, it is necessary to examine the results critically.

Since the results obtained in measurements in air and in vacuum coincide, the interaction is seen to be independent of convection currents, of the presence of a viscous air layer between the bodies, and of water vapor in the air.

Measures were taken to eliminate measurement errors due to mechanical influence of some elements of the system, such as the elastic resistance of current leads connected to the coil, friction between the knife-edge and the bearing plane, or dust particles left on the surfaces investigated. The elastic reaction of current leads was minimized by employing very thin annealed Wollaston wires. The agate prism and agate bearing plane met all requirements typical for the best analytical microbalances. Balance arms and pans weighing several tens of grams do not prevent good analytical microbalances from achieving the sensitivity of about 10^{-6} - 10^{-5} g. Friction is known to be roughly proportional to load. It is clear, therefore, why it was possible in a balance with the arm weighing about 0.1 g to neglect completely the friction between the knife-edge and the bearing plane in measurements with an accuracy of 10^{-7} g.

When dust particles capable of affecting the measurement were present on the surfaces they always produced repulsive forces appearing when the gap width was reduced. This repulsion could be recorded by the instrument with the same sensitivity as attractive forces were, but repulsion was never a smooth function of gap width. Measurements were carried out only if no forces except the attractive ones were detected when the gap was narrowed down to 0.05-0.1 μm .

There is no doubt that the observed attraction cannot be attributed to films left on the surfaces after cleaning. Adsorption films of water on quartz surfaces are unavoidable in measurements conducted in atmospheric or in moderately rarefied air; but they could not affect the results of measurements because, first, the distance between the interacting surfaces was much greater than the thickness of such layers and, second, the dielectric constant (closely related with molecular attraction) is nearly the same in adsorption films as in quartz. Furthermore, if the dielectric con-

stants of a film and quartz are not very different in magnitude, the presence of an adsorbed film about 10 Å thick changes the "effective" (optically measured) gap between quartz surfaces by approximately the same amount, i.e., by 10 Å, which nearly compensates for the change in molecular attraction.

4.4. THE THEORY OF MOLECULAR ATTRACTION BETWEEN MACROSCOPIC OBJECTS

4.4.1. Calculation of the Interaction between Macroscopic Objects by Summing the Interactions between Microobjects

According to London [4], the energy of interaction U between individual atoms and molecules at distances r large compared with atomic or molecular diameters is, according to (1.1),

$$U = - C/r^6$$

where C is a positive constant specific to each species of atom.

London's theory has limitations: the calculations are not valid at very small distances between atoms (when their wave functions overlap) or at large distances where the effect of electromagnetic retardation must be taken into account – as it was in the theory of Casimir and Polder [12]. According to their theory, the energy of interaction between two identical atoms is given by Eq. (1.2):

$$U = - \frac{23\hbar}{4\pi} \frac{c\alpha_0^2}{r^7} = - \frac{C_1}{r^7}$$

Theories thus have been developed, explaining the origin of intermolecular attraction and capable of calculating the interaction between free atoms and molecules.

The molecular attraction between objects consisting of a large number of molecules was then treated, as the resultant of London attractive forces between all pairs of molecules of which the objects are composed. For example, de Boer [13] and Hamaker [14] calculated the interaction between two identical bodies containing q molecules per unit volume, by integrating elementary interactions governed by London's law. Hamaker derived formulas for the energy and attractive force ($F > 0$) between two spherical bodies, between a sphere and an infinite planar wall, and between two parallel planar walls. If the shortest distance between surfaces is much less than their curvature radius R_0 , the energy of interaction between two spheres is given by the expression

$$U = - AR_0 / 12H \quad (4.3)$$

and the attractive force acting on them is

$$F = AR_0 / 12H^2 \quad (4.4)$$

For interacting sphere and plane the energy is

$$U = - AR_0 / 6H \quad (4.5)$$

and the force

$$F = AR_0 / 6H^2 \quad (4.6)$$

The energy per unit surface area of two infinite parallel plates is

$$U = - A / 12\pi H^2 \quad (4.7)$$

and the force acting on unit surface area is

$$f = A / 6\pi H^3 \quad (4.8)$$

where H is the distance between the bodies, and $A \equiv \pi^2 q^2 C$ is a constant, introduced by Hamaker, depending on the material of the bodies. These formulas have often been applied to calculate the interaction between identical colloidal particles and other macroscopic objects.

If similar calculations are carried out by taking into account electromagnetic retardation, the energy per unit surface area of parallel plates in the limiting case of sufficiently large distances becomes

$$U = - A_1 / 30\pi H^3 \quad (4.9)$$

and the force per unit area is

$$f = A_1 / 10\pi H^4 \quad (4.10)$$

where $A_1 \equiv \pi^2 q^2 C_1$.*

Actually, the additivity of the London forces in condensed states has not been substantiated either theoretically or experimentally. The assumption would be accurately valid only in the un-

*The coefficients A and A_1 , of course, have different dimensions. In this book, numerical values of the Hamaker coefficient A and the coefficient of retarded interaction B [Eq. (4.17)] ($= A_1 / 10\pi$) are given in cgs units, viz., ergs (10^{-7} J) and erg·cm, respectively.

feasible situation of two rarefied bodies (i.e., gases) separated by a gap. Furthermore, in condensed-state systems the atomic and molecular characteristics, including C and C_1 , are somewhat changed in comparison with the properties of isolated atoms and molecules because of the influence of neighbors. Consequently, the contribution of individual molecules to the resultant interaction depends upon their coordination and concentration, and for surface molecules depends also on the number of neighbors. In order to be consistent within the strict additivity approach, we would have to take the values of C and C_1 for isolated molecules, and thus certainly introduce an error. But if this approach is dropped, it is difficult to determine the "true" values of C and C_1 , hardly obtainable for the condensed state and frequently absolutely unknown.

It is thus impossible to calculate strictly the force of molecular attraction between condensed-state bodies on the basis of the law of interaction between individual molecules.

4.4.2. E. M. Lifshitz's Macroscopic Theory of Molecular Attraction between Condensed- State Bodies

In contrast to the "microscopic" approach, the problem can be treated in a quite different, purely macroscopic framework, in which the interacting bodies are regarded as continua. This approach is valid when the distance between the surfaces, although small, is still large in comparison with interatomic distances in the bodies.

The main idea of the theory is that the interaction between the bodies is treated as the effect of the fluctuational electromagnetic field. This field is always present within any medium owing to thermodynamic fluctuations, and also extends outside the medium. One well-known effect of this field is the thermal emission of bodies; but it must be emphasized that the fluctuational field outside a body is not limited to this emission. This is quite clear from the fact that electromagnetic fluctuations persist at the absolute zero of temperature when there is no thermal emission. At these temperatures fluctuations are of purely quantum nature and are caused by the so-called zero oscillations of electromagnetic field.

Let us choose for the two bodies two semiinfinite regions separated by a plane-parallel gap of width H . The calculations must determine the fluctuational electromagnetic field in this system and, in particular, in the volume of the gap. The force f acting on each of the two surfaces (per cm^2 of surface area) can then be found as the mean value of the appropriate component of Maxwell's stress tensor.

It is important that this approach to the problem is a general one and is valid at any temperature and for arbitrary bodies, irrespective of their molecular nature (ionic or molecular crystals, amorphous bodies, metals, dielectrics, etc.). The method has another important feature: the fields are calculated on the basis of the exact Maxwell equations, so that the effects of retardation, caused by a finite velocity of propagation of electromagnetic interactions, are automatically taken into account. These effects become appreciable at sufficiently large distances $H \gg \lambda_0/2\pi$, where λ_0 is the wavelength typical for absorption spectra of the interacting bodies.

The general method of calculating electromagnetic fluctuations was developed by S. M. Rytov; its description can be found in his monograph [15] (see also [16], Chapter 13). Here we shall not expound either this method or the fairly cumbersome calculations of Lifshitz relevant to our problem, but refer the reader to the original papers [17, 18]. Only the final results will be presented.

The formulas that will be given include a function $\epsilon(\omega)$, the permittivity of a body as a function of frequency of the field. (The formulas below are derived on the assumption that the magnetic permeability of the bodies equals unity; this is usually the case in actual situations.) In general, $\epsilon(\omega)$ is a complex quantity:

$$\epsilon(\omega) = \epsilon'(\omega) + i\epsilon''(\omega)$$

Its imaginary part is always positive and determines the dissipation of the energy of the electromagnetic wave propagating in a body. The function $\epsilon(\omega)$ is related to refractive index n and absorption coefficient κ by the well-known formula

$$\sqrt{\epsilon} = n + i\kappa$$

A formal treatment of $\epsilon(\omega)$ as a function of complex variable ω is known to yield certain integral relations between $\epsilon'(\omega)$ and $\epsilon''(\omega)$, represented by the so-called Kramers-Kronig relation (e.g., see [16]). A particular corollary of these integral relations is the formula

$$\epsilon(i\xi) = 1 + \frac{2}{\pi} \int_0^\infty \frac{\omega \epsilon''(\omega)}{\omega^2 + \xi^2} d\omega \quad (4.11)$$

which puts the values of the function ϵ of a purely imaginary argument $i\xi$ in correspondence to the values of the function $\epsilon''(\omega)$ of real arguments ω . The function $\epsilon(i\xi)$ is a real quantity monotonically decreasing from the value ϵ_0 (electrostatic value of permittivity at $\xi = 0$) to 1 at $\xi \rightarrow \infty$.

The theoretical formula for the attractive force between the bodies 1 and 2 in a vacuum, derived by Lifshitz, has the following form [17, 18]:

$$f = \frac{kT}{\pi c^3} \sum_{N=0}^{\infty} \int_{-1}^{\infty} p^2 \xi_N^3 \left\{ \left[\frac{(s_1 + p)(s_2 + p)}{(s_1 - p)(s_2 - p)} \exp\left(\frac{2p\xi_N H}{c}\right) - 1 \right]^{-1} + \left[\frac{(s_1 + \varepsilon_1 p)(s_2 + \varepsilon_2 p)}{(s_1 - \varepsilon_1 p)(s_2 - \varepsilon_2 p)} \exp\left(\frac{2p\xi_N H}{c}\right) - 1 \right]^{-1} \right\} dp \quad (4.12)$$

where k is the Boltzmann constant, T is the absolute temperature, p is the integration variable, $\xi_N = 2\pi kTN/\hbar$, where N is a natural number, $s = (\varepsilon - 1 + p^2)^{1/2}$, H is the width of the gap between the bodies, and $\varepsilon = \varepsilon(i\xi)$. The subscripts 1 and 2 refer to the bodies 1 and 2, respectively. The prime with the sum denotes that the first term must be taken with the weight 1/2.

Lifshitz showed [17, 18] that at low temperatures and at short separations H between the bodies (or both), i.e., if

$$H \ll \hbar c / kT \quad (4.13)$$

the summation in (4.12) can be replaced with integration. This yields a better-known expression for the dispersion attractive force between the bodies 1 and 2 in vacuum:

$$f = \frac{\hbar}{2\pi^3 c^3} \int_0^{\infty} \int_{-1}^{\infty} \left\{ \left[\frac{(s_1 + p)(s_2 + p)}{(s_1 - p)(s_2 - p)} \exp\left(\frac{2p\xi H}{c}\right) - 1 \right]^{-1} + \left[\frac{(s_1 + \varepsilon_1 p)(s_2 + \varepsilon_2 p)}{(s_1 - \varepsilon_1 p)(s_2 - \varepsilon_2 p)} \exp\left(\frac{2p\xi H}{c}\right) - 1 \right]^{-1} \right\} p^2 \xi^3 dp d\xi \quad (4.14)$$

We see from relations (4.12) and (4.14) that the attractive force f can be calculated, in principle, for any distance H if the functions $\varepsilon_1(i\xi)$ and $\varepsilon_2(i\xi)$ for the two bodies are known. Moreover, according to (4.11), $\varepsilon(i\xi)$ can be found from the function $\varepsilon''(\omega)$ known in a sufficiently wide spectral interval. Therefore, the imaginary part of the permittivity gives the unique characteristic of the macroscopic properties of bodies, determining the molecular attractive forces between them.

If condition (4.13) is satisfied, temperature can affect the attractive force f given by formula (4.14) only through the temperature-dependent imaginary part $\varepsilon''(\omega)$ of permittivity.

In two important limiting cases formula (4.14) can be substantially simplified [17-19].

We begin with the case of "short" distances $H \ll \lambda_0/2\pi$. By virtue of the exponentially growing factor $\exp(2p\xi H/c)$ in the denominators of the integrand in (4.27), the main contribution to the result of integration over p is made by those values for which $(p\xi H/c) \approx 1$. In this case, $p \gg 1$, and with sufficient accuracy we can set $s_1 \approx s_2 \approx p$. In this approximation the first term in braces in (4.14) vanishes. The second term, after a new variable $x = 2p\xi H/c$ is introduced, gives

$$f = \frac{\hbar}{16\pi^2 H^3} \int_0^\infty \int_0^\infty \frac{x^2 dx d\xi}{[(\varepsilon_1 + 1)/(\varepsilon_1 - 1)][(\varepsilon_2 + 1)/(\varepsilon_2 - 1)] \exp x - 1}$$

where the lower limit of integration over x is replaced, in this approximation, with zero. This formula can be further simplified, without introducing appreciable errors, by dropping the unity in the denominator of the integrand. The integration over x then finally gives

$$f = \frac{\hbar}{8\pi^2 H^3} \int_0^\infty \frac{[\varepsilon_1(i\xi) - 1][\varepsilon_2(i\xi) - 1]}{[\varepsilon_1(i\xi) + 1][\varepsilon_2(i\xi) + 1]} d\xi \quad (4.15)$$

Therefore, at $H \ll \lambda_0/2\pi$ the attractive force is inversely proportional to the cube of gap width, with a coefficient that can be calculated if the functions $\varepsilon_1(i\xi)$ and $\varepsilon_2(i\xi)$ are known. It has been mentioned above that the differences $[\varepsilon(i\xi) - 1]$ monotonically decrease when ξ increases, and tend to zero. Concurrently, the integrand in (4.15) also decreases, and beginning with a certain ξ_0 the values of ξ do not contribute appreciably to the integral; strictly speaking, the condition of smallness of H implies that $H \ll (c/\xi_0)$.

Now let us consider the opposite case of "large" distances, i.e., large in comparison with the main wavelengths in the absorption spectrum of the interacting bodies: $H \gg \lambda_0/2\pi$.

We again introduce a new integration variable $x = 2p\xi H/c$ in the general formula (4.27), but our second variable will be p , not ξ :

$$f = \frac{\hbar c}{32\pi^2 H^4} \int_0^\infty \int_1^\infty \frac{x^3}{p^2} \left\{ \frac{(s_1 + p)(s_2 + p)}{(s_1 - p)(s_2 - p)} e^x - 1 \right\}^{-1} \\ + \left\{ \frac{(s_1 + \varepsilon_1 p)(s_2 + \varepsilon_2 p)}{(s_1 - \varepsilon_1 p)(s_2 - \varepsilon_2 p)} e^x - 1 \right\}^{-1} \left\{ dp dx \right\}$$

where $\varepsilon = \varepsilon(i\xi) = \varepsilon(ixc/2pH)$. The denominators in the above integral contain e^x , so that the main contribution to the integral over

x is made in the range $x \approx 1$, and since $p \geq 1$, the argument of ε at large H is nearly zero in the whole significant range of x . Correspondingly, we can replace ε_1 and ε_2 simply by their values at $\omega = 0$, i.e., by electrostatic dielectric constants that we denote by ε_{10} and ε_{20} . In metals $\varepsilon(\omega)$ tends to infinity as $\omega \rightarrow 0$, so that we have to assume that $\varepsilon_0 \rightarrow \infty$.

We thus obtain

$$f = \frac{\hbar c}{32\pi^2 H^4} \int_0^\infty \int_1^\infty \frac{x^3}{p^2} \left\{ \left[\frac{(s_{10} + p)(s_{20} + p)}{(s_{10} - p)(s_{20} - p)} e^x - 1 \right]^{-1} + \left[\frac{(s_{10} + \varepsilon_{10}p)(s_{20} + \varepsilon_{20}p)}{(s_{10} - \varepsilon_{10}p)(s_{20} - \varepsilon_{20}p)} e^x - 1 \right]^{-1} \right\} dp dx \quad (4.16)$$

where $s_0 = (\varepsilon_0 - 1 + p^2)^{1/2}$.

The attractive force is found in this case to be inversely proportional to the fourth power of gap width. Its salient feature is that it is determined only by the static permittivities of the two bodies.

Let us consider some particular cases of formula (4.16). The result takes the simplest form for two metals. By assuming in (4.16) that $\varepsilon_{10} = \varepsilon_{20} = \infty$, we obtain

$$f = \frac{\hbar c}{16\pi^2 H^4} \int_0^\infty \int_1^\infty \frac{x^3 dp dx}{p^2(e^x - 1)} = \frac{\hbar c \pi^2}{240 H^4} = \frac{B}{H^4} \quad (4.17)$$

where B is the constant for fully retarded molecular forces.

Therefore, in the case of full retardation of molecular interactions, the force is completely independent of the kind of metal. This property ceases to be valid at "short" distances at which the force of interaction depends on the function $\varepsilon(i\xi)$ at all values of ξ , not only at $\xi = 0$. Formula (4.17) was derived earlier by Casimir by a different method [12].

For two identical dielectrics (i.e., $\varepsilon_{10} = \varepsilon_{20} = \varepsilon_0$) the result is obtained from (4.16) by numerical integration [17-19]:

$$f = \frac{\pi^2 \hbar c}{240 H^4} \left(\frac{\varepsilon_0 - 1}{\varepsilon_0 + 1} \right)^2 \varphi_{DD}(\varepsilon_0) = \frac{B}{H^4} \quad (4.18)$$

where $\varphi_{DD}(\varepsilon_0)$ is a function whose values are given in Fig. 4.8. As $\varepsilon_0 \rightarrow \infty$, this function tends to 1 [in accordance with (4.17)], and as $\varepsilon_0 \rightarrow 1$, it tends to 0.35. However, this limit is, in fact, reached at $\varepsilon_0 \approx 4$, after which φ_{DD} remains practically constant.

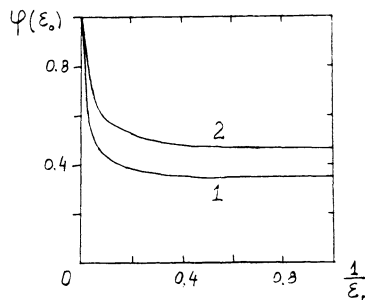


Fig. 4.8. Functions $\varphi_{DD}(\epsilon_0)$ (curve 1) and $\varphi_{DM}(\epsilon_0)$ (curve 2) in Eqs. (4.18) and (4.19).

A similar function $\varphi_{DM}(\epsilon_0)$ determining the attractive force between a metal and a dielectric, for $\epsilon_{10} = \infty$ and $\epsilon_{20} = \epsilon_0$,

$$f = \frac{\pi^2 \hbar c}{240 H^4} \left(\frac{\epsilon_0 - 1}{\epsilon_0 + 1} \right) \varphi_{DM}(\epsilon_0) = \frac{B}{H^4} \quad (4.19)$$

is shown in the same Fig. 4.8.

A question that naturally arises is the actual value of λ_0 with which the distance H is to be compared. It cannot be answered in a general form; the answer depends on concrete spectral characteristics of the interacting bodies, i.e., on concrete properties of the function $\epsilon''(\omega)$. This will be discussed in more detail in Section 4.6.

In view of the discussion of the results of the first experiments in Section 4.5, we shall mention here only the case of quartz, for the reason that it is to some extent specific because of the properties of its absorption spectrum [18]. Quartz is known to absorb strongly in the far ultraviolet (beginning approximately at 0.15 μm) and in the infrared (beginning with several μm) regions; it is transparent between them. The distances H employed in the experiments described above (Section 4.3) are in the transparency range, and it can be assumed for evaluation that H is small compared with $\lambda/2\pi$ at the right-hand, and large compared with $\lambda/2\pi$ at the left-hand, boundaries of absorption spectra. The contribution of absorption in the UV range to f can be evaluated if ϵ_0 in (4.35) is set equal to the square of refractive index n in the optical transparency region. The contribution of the IR region of absorption is much smaller. Therefore, a reasonable theoretical estimate of the attractive force f can be obtained by using formula (4.18) with the optical value of permittivity, $\epsilon = n^2$, for ϵ_0 (instead of the electrostatic value). This estimate is too small for large distances and too large for small distances.

4.5. COMPARISON OF THE RESULTS OF EARLY EXPERIMENTS WITH THE THEORY

4.5.1. Comparison with the Results of Calculations Carried Out by the Method of Summation of all Pairwise Molecular Interactions

In the framework of the "microscopic" summation of pairwise interactions of molecules the formula for a sphere and a plane is (4.6). With the results of the experiments described in Section 4.3, this formula gives $A = 5 \cdot 10^{-14}$ erg ($5 \cdot 10^{-21}$ J). However, the theoretical value of the constant A for quartz is roughly 10^{-12} erg, i.e., greater by a factor of 20 than the value obtained in the experiments. Actually, the methods of calculation used at first were not valid (at least at distances on the order of $0.1 \mu\text{m}$). Consequently, the results of the earliest experiments had only a general significance, as well as being limited to a few materials.

By using the same method of summation but taking into account the Casimir-Polder correction, we have to calculate the energy of interaction $U(H)$ by means of formula (4.9). By substituting into this formula the results of the first experiments, we obtain $A_1 \approx 3 \cdot 10^{-18}$ erg·cm. The formula $A_1 = \pi^2 C_1 q^2$ (where $C_1 = 251 e^2 \alpha_0^2$) gives $A' = 1 \cdot 10^{-18}$ erg·cm. The value of polarizability of quartz, α_0 , was taken from Margenau's paper [20]. It was obvious that again the theory and the experiment were in disagreement, although the discrepancy was much smaller than with summation of London interactions.

4.5.2. Comparison with the Macroscopic Theory of Molecular Attraction

A correct comparison with the Lifshitz theory calls for a detailed knowledge of the optical characteristics of the interacting bodies; otherwise, the function $\varepsilon(i\xi)$ cannot be constructed. However, an approximate theoretical evaluation could be made owing to the specific pattern of absorption spectrum of quartz [19].

In order to compare the theoretical estimates with directly measured quantities, we shall use several transformations. By integrating expression (4.18) for $f(H)$, we obtain a formula for the energy of attraction per cm^2 of surface area of two plates:

$$U(H) = - \frac{\hbar c \pi^2}{720 H^3} \left(\frac{\varepsilon_0 - 1}{\varepsilon_0 + 1} \right)^2 \varphi(\varepsilon_0) = - \frac{B}{3H^3} \quad (4.20)$$

Energy $U(H)$ is plotted in Fig. 4.5 (dashed line) according to (4.20), in which ε_0 is set equal to the square of the refractive index of quartz glass in the optical region: $\varepsilon_0 = n^2 = 2.13$. To

find now the force of interaction between a sphere with the radius R_0 and a plane, we use expression (4.2) given above:

$$f(H) = 2\pi R_0 B / 3H^3 \quad (4.21)$$

Dashed lines in Fig. 4.4 plot $f(H)$ for quartz specimens. The calculations assumed ϵ_0 equal to the static dielectric permittivity ($\epsilon_0 = 3.6$, curve 1) and to $\epsilon_0 = n^2 = 2.13$ (curve 2). Dashed curves in Fig. 4.6 correspond to theoretical calculations for thallium halides. Curve 1 corresponds to the static value of permittivity, $\epsilon_0 = 50$, of mixed thallium halide crystal and curve 2 to $\epsilon_0 = n^2 \approx 6$. As in the case of quartz, the second calculation can probably be regarded as more accurate.

The dashed curve in Fig. 4.7 is a similar dependence for chromium-quartz interaction. The formula given by the Lifshitz theory for estimating the metal-dielectric interaction across sufficiently wide gaps is (4.19). Taking into account again the transparency of quartz at wavelengths equal or close to H , we chose ϵ_0 equal to the square of refractive index of quartz in the optical region. Owing to the approximate nature of such theoretical evaluations, as well as to experimental errors, the agreement obtained could be considered satisfactory.

The agreement between the theory and the results of first experiments, shown in Figs. 4.4-4.7, can be regarded, on the one hand, as supporting the validity of the Lifshitz theory and, on the other hand, as important evidence of the molecular nature of the attraction measured in these experiments. This agreement of experiment and theory enables us to answer the question first posed by Lebedev in 1894 (see Section 4.1). The molecular attraction is indeed "reducible to ... electromagnetic forces," and does not involve any "other forces of as yet unknown nature."

About the same time that the experimental work described above was published, the Dutch scientists Overbeek and Sparnaay published a paper with essentially different results [21]. Overbeek and Sparnaay measured the attractive force between two fused quartz plates, one of which was fixed to a spring whose deformation was found from measured electric capacitance. The distance between the parallel plates was determined from the interference color in the gap. The effect of the air interlayer was minimized by evacuating the system to a pressure of 10^{-3} mm Hg. This study [21] was reported at the Faraday Society discussion in 1954 together with Derjaguin's paper [22]. The results of the Dutch authors were presented as a plot of force as a function of distance (on a logarithmic scale). The calculations, made under an assumption of the validity of Eq. (4.8), yielded an apparently overestimated value of the constant A : $3.8 \cdot 10^{-11}$ erg.

If the Lifshitz theory is used, the attractive force for the spacing $H = 1200 \text{ \AA}$ between quartz plates is equal to approximately $2 \cdot 10^{-4} \text{ dyn/cm}^2$, while in the experiments of Overbeek and Sparnaay this gap width corresponds to a force of 1 dyn. The experimental data thus exceeded the theoretical estimate by a factor of nearly 10^4 . Poor reproducibility of data in the experiment of Overbeek and Sparnaay, as well as the large attraction they observed, were undoubtedly caused by surface charging which the researchers did not take sufficiently into account.

Prosser and Kitchener soon afterwards reported [23] results of measuring molecular attraction between parallel borosilicate glass plates by a method similar to that of Overbeek and Sparnaay. Surface charges were effectively removed by ionization of the gas with a Tesla discharge. The method differed only in that the attractive force was found from the shift in the frequency of a quartz oscillator to which the lower movable plate was fixed. This somewhat improved the accuracy. Measurements were conducted in the range of H from 0.7 to 1 μm in a better vacuum (10^{-5} mm Hg). The results were close to those published by Derjaguin and Abrikossova.

Although one of the two first attempts to measure directly the molecular attraction between macroscopic bodies was unsuccessful, the methodological significance of study [21] was considerable. By the method developed there correct results (to be discussed below) were later obtained [24].

Overestimated results stimulated Overbeek and Sparnaay to modify the London-Hamaker theory in order to arrive at stronger forces [21]. In contrast to this approach, Derjaguin and Abrikossova explained their results in 1953 (underestimated with respect to the London-Hamaker theory) by resorting to Casimir's concept of molecular attraction weakened by electromagnetic retardation and by using the relevant approximate formula. At that time retardation was rigorously taken into account in the framework of macroscopic approach only for metals [12].

The results obtained in [6, 7] stimulated Lifshitz to construct the general macroscopic theory of molecular attraction [17, 18]. The most conclusive evidence of the correctness of the pioneer measurements of Derjaguin and Abrikossova is the close fit of their results of 1953-1954 to the formulas of the theory developed after the results were obtained, and containing no arbitrary empirical constants. This not only solved the problem of existence of long-range molecular attraction that had seemed doubtful to Langmuir, but also verified the rigorous macroscopic theory.

4.6. CURRENT STATUS OF THE MACROSCOPIC THEORY OF MOLECULAR FORCES

After Lifshitz formulated the basic ideas of the macroscopic theory of molecular forces [17, 18], its further development concerned application to more complex objects, such as absorbing liquid interlayers, multilayer systems, and nonplanar surfaces.

As the next step, Dzyaloshinsky, Lifshitz, and Pitayevsky [25] solved the problem of interaction between macroscopic bodies 1 and 2 through a thin liquid interlayer 3. The solution is limited to interlayers without spatial dispersion, i.e., to poorly conducting media. The solution obtained in [25] on the basis of thermal Green's functions differs from the case of vacuum interlayer [Eq. (4.12)] in that it takes into account the absorptive properties of the interlayer, and includes the frequency dependence of its permittivity $\epsilon_3 = \epsilon_3(i\xi_N)$:

$$\begin{aligned} -f = \Pi(H) = & -\frac{kT}{\pi c^3} \sum_{N=0}^{\infty} \xi_N^3 \epsilon_3^{3/2} \int_1^{\infty} p^2 \left\{ \left[\frac{(s_1 + p)(s_2 + p)}{(s_1 - p)(s_2 - p)} \right. \right. \\ & \times \exp \left(\frac{2p\xi_N H \sqrt{\epsilon_3}}{c} \right) - 1 \left. \right]^{-1} + \left[\frac{(s_1 + \alpha p)(s_2 + bp)}{(s_1 - \alpha p)(s_2 - bp)} \right. \\ & \times \exp \left(\frac{2p\xi_N H \sqrt{\epsilon_3}}{c} \right) - 1 \left. \right]^{-1} \left. \right\} dp \end{aligned} \quad (4.22)$$

where $s_1 = (\alpha - 1 + p^2)^{1/2}$; $s_2 = (b - 1 + p^2)^{1/2}$, $\alpha = \epsilon_1/\epsilon_3$; $b = \epsilon_2/\epsilon_3$, and Π is the disjoining pressure of the liquid interlayer ($\Pi < 0$ corresponds to attraction and $\Pi > 0$ to repulsion of the surfaces). The prime with the sum indicates that the leading term of the sum ($N = 0$) is taken with weight 1/2. When condition (4.13) is satisfied, the summation over frequencies $\xi_N = N \cdot 2\pi kT/\hbar$ can be replaced with integration. By setting $dN = (\hbar/2\pi kT) d\xi$, we obtain [25]

$$\begin{aligned} \Pi(H) = & -\frac{\hbar}{2\pi^2 c^3} \int_0^{\infty} \int_1^{\infty} p^2 \xi^3 \epsilon_3^{3/2} \left\{ \left[\frac{(s_1 + p)(s_2 + p)}{(s_1 - p)(s_2 - p)} \right. \right. \\ & \times \exp \left(\frac{2p\xi H \sqrt{\epsilon_3}}{c} \right) - 1 \left. \right]^{-1} + \left[\frac{(s_1 + \alpha p)(s_2 + bp)}{(s_1 - \alpha p)(s_2 - bp)} \right. \\ & \times \exp \left(\frac{2p\xi H \sqrt{\epsilon_3}}{c} \right) - 1 \left. \right]^{-1} \left. \right\} dp d\xi \end{aligned} \quad (4.23)$$

The corresponding asymptotes are

$$\Pi(H) = -\frac{\hbar}{8\pi^2 H^3} \int_0^\infty \frac{(\varepsilon_1 - \varepsilon_3)(\varepsilon_2 - \varepsilon_3)}{(\varepsilon_1 + \varepsilon_3)(\varepsilon_2 + \varepsilon_3)} d\xi = -\frac{A_{132}}{6\pi H^3} \quad (4.24)$$

$$\begin{aligned} \Pi(H) &= -\frac{\pi^2 \hbar c}{240 \sqrt{\varepsilon_{30}} H^4} \left(\frac{\varepsilon_{10} - \varepsilon_{30}}{\varepsilon_{10} + \varepsilon_{30}} \right) \left(\frac{\varepsilon_{20} - \varepsilon_{30}}{\varepsilon_{20} + \varepsilon_{30}} \right) \Phi \left(\frac{\varepsilon_{10}}{\varepsilon_{30}}, \frac{\varepsilon_{20}}{\varepsilon_{30}} \right) \\ &= -\frac{B}{H^4} \end{aligned} \quad (4.25)$$

Equation (4.24) is valid for short distances $H \ll \lambda_0/2\pi$ when electromagnetic retardation can be neglected. A_{132} is an analog of the Hamaker constant. Equation (4.25) holds when $H \gg \lambda_0/2\pi$, with the effect of retardation fully developed. In Eq. (4.25) and below, B stands for the coefficient of fully retarded molecular forces [Eq. (4.17)]. The values of Φ as a function of the ratio of static dielectric constants $\varepsilon_{10}/\varepsilon_{30}$ and $\varepsilon_{20}/\varepsilon_{30}$ were tabulated in [25].

Condition (4.13) of the applicability of Eq. (4.23) holds for most thin liquid interlayers, except liquids with high static dielectric constant, such as water ($\varepsilon_0 \approx 80$). The contribution of the zero term ($N = 0$) that is in fact omitted in integration can be quite substantial for water [26]. In this case expression (4.23) is sometimes simply supplemented by the zero term equal to

$$\Pi_0 = -\frac{kT}{8\pi H^3} \frac{(\varepsilon_{10} - \varepsilon_{30})(\varepsilon_{20} - \varepsilon_{30})}{(\varepsilon_{10} + \varepsilon_{30})(\varepsilon_{20} + \varepsilon_{30})} = -\frac{A_n}{6\pi H^3} \quad (4.26)$$

where A_n is a constant dependent on the static values of dielectric constants of the interacting bodies, and on temperature.

However, it is preferable to use the exact equation (4.22) of the theory of molecular forces. We shall discuss later the range in which the correction (4.26) to Eq. (4.23), and the asymptotes (4.24) and (4.25), is valid.

Temperature produces its effect not only directly through the value of T in (4.22) and (4.26), but mostly through temperature dependence of the permittivities of the interacting bodies.

It is obvious from Eqs. (4.24) and (4.25) that if two bodies are separated with a liquid interlayer, they can be either attracted owing to molecular forces (this was the case in vacuum) or repelled. Repulsion ($\Pi > 0$) occurs when the dielectric constant of one body is less than, and that of the second is greater than, the permittivity ε_3 of the interlayer. Evidently, the values of $\varepsilon(i\xi)$ that must be compared in Eq. (4.24) are those that give the largest contribution to the integral. These are usually frequencies on the order of 10^{16} rad/s in the UV range. The case of molecular repul-

sion is most often realized in such asymmetric systems as wetting films (see Chapter 10) when $\epsilon_2 = 1$, provided the substrate is more polar than the liquid in the film, i.e., if $\epsilon_1 > \epsilon_3$.

The microscopic theory of molecular forces employs for the interaction of three condensed bodies 1, 2, and 3 the so-called sum rule introduced by Hamaker [14]:

$$A_{132} = A_{12} + A_{33} - A_{32} - A_{13} \quad (4.27)$$

where A_{ik} is the vacuum Hamaker constant for the bodies i and k interacting across a vacuum interlayer. It was also assumed that the interaction constant for two different bodies equals the geometric mean of the constants for identical bodies [27]:

$$A_{ik} \approx \sqrt{A_{ii}A_{kk}} \quad (4.28)$$

For bodies interacting through vacuum, calculations by Eqs. (4.3)-(4.10) of the microscopic theory yield results that are only approximate, though correct in sign; but in the case of interaction through liquid interlayers the results may actually prove qualitatively incorrect (give the wrong sign of force).

It was shown in [28, 29] that expressions (4.27) and (4.28) are valid only in a limited number of cases because they neglect the variation of the dispersion force field when interaction proceeds through absorbing interlayers. Exact calculations of molecular forces in the theory of surface phenomena can be based only on Eqs. (4.22)-(4.25) that include, as particular cases, Eqs. (4.12) and (4.14)-(4.16) for the interaction across vacuum interlayers.

In colloid chemistry it is standard to use the approximation (4.24), assuming that the events most essential for the interaction between particles occur in the range of sufficiently short distances between them. However, the effect of electromagnetic retardation manifests itself already at a distance of 30-50 Å [30, 31]. It is therefore necessary to look for analytical expressions for the intermediate interval of distances (where electromagnetic retardation is already felt) that are simpler than (4.22) and (4.23) and more convenient for practical applications.

In systems composed of dielectrics we can assume $s \approx p$ in Eq. (4.23). Taking into account that the first term in square brackets is always greater than 1 in the range of frequencies significant for the interaction, we obtain [32]

$$\Pi(H) = -\frac{\hbar}{8\pi^2 H^3} \int_0^\infty \frac{\infty(x^2/2) + x + 1}{\exp x} \Delta_{31}\Delta_{32} d\xi = -\frac{A(H)}{6\pi H^3} \quad (4.29)$$

where $x = 2\xi H \sqrt{\epsilon_3}/c$, $\Delta_{ik} = (\epsilon_i - \epsilon_k)/(\epsilon_i + \epsilon_k)$, and the function $A(H)$ reflects the dependence of the "Hamaker constant" on interlayer thickness H , as a result of electromagnetic retardation.

The second integration of this equation is readily carried out graphically provided the dependences $\epsilon(i\xi)$ are known. When $H \rightarrow 0$, Eq. (4.29) transforms to the asymptote (4.24), and as $H \rightarrow \infty$, it transforms to the asymptote (4.25). Calculations demonstrated [31] that for systems such as water-vacuum-water the approximate equation (4.29) gives results (Fig. 4.9, curves 1 and 2) that practically coincide with computer simulations based on the exact equation (4.22).

Calculation of molecular forces acting at large distances between bodies require that we know only the static values of permittivity ϵ_0 (or $\epsilon = n^2$) (see Section 4.5). If the interlayer thickness is less than $0.1 \mu\text{m}$, molecular forces can be calculated only if complete information is available on the frequency dependence of permittivities of all the interacting bodies.

For some time it was difficult to use the equations of the macroscopic theory of molecular forces because the absorption spectra $\epsilon''(\omega)$ were not available in a sufficiently wide range of frequencies (from microwave to x-ray).

Krupp [33] and Parsegian and Ninham [34, 35] suggested a number of simplified methods for calculating the functions $\epsilon(i\xi)$ and thus paved the way to wider applications of the equations of the macroscopic theory. They were able to demonstrate that reliable results can be obtained by taking into account only several main bands in absorption spectra. As a first approximation it is sufficient to take into account the dipole relaxation corresponding to the frequency range $\omega_a \approx 10^{10}-10^{11} \text{ rad/s}$, the resonant absorption in the infrared ($\omega_b \approx 10^{13}-10^{14} \text{ rad}$) and in the near ultraviolet ($\omega_c \approx 10^{16} \text{ rad/s}$) bands of the spectrum [34, 35]:

$$\epsilon(i\xi) = 1 + \frac{\epsilon_0 - \epsilon_a}{1 + (\xi/\omega_a)} + \frac{\epsilon_a - \epsilon_b}{1 + (\xi/\omega_b)^2} + \frac{\epsilon_b - \epsilon_c}{1 + (\xi/\omega_c)^2} \quad (4.30)$$

where ϵ_0 is the static permittivity (at $\omega = 0$), ϵ_a refers to frequency ω_a , ϵ_b refers to frequency ω_b , and $\epsilon_c = 1$ refers to frequency $\omega \rightarrow \infty$.

For instance, in the case of water [35], $\epsilon_0 = 80$, $\epsilon_a = 5.2$, and $\omega_a = 1.06 \cdot 10^{11} \text{ rad/s}$; $\epsilon_b = n^2 = 1.78$ in the visible part of the spectrum, and $\omega_b(\text{mean}) = 5.66 \cdot 10^{14} \text{ rad/s}$; $\epsilon_c \approx 1$ at $\omega_c = 1.91 \cdot 10^{16} \text{ rad/s}$ corresponding to the first ionization potential of the water molecule; $I = 12.6 \text{ eV}$.

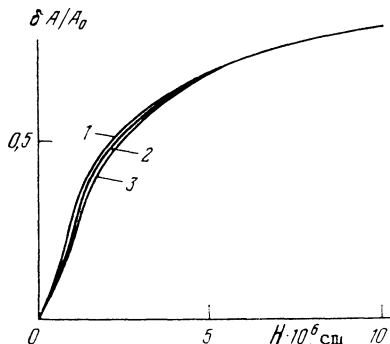


Fig. 4.9. $\delta A = [A_0 - A(H)]/A_0$ (A_0 is the value of A for $H \rightarrow 0$) plotted as a function of H for the water-vacuum-water system. 1) After Eq. (4.22); 2) after Eq. (4.29); 3) after Eq. (4.38).

In the frequency range $\omega > 10^{16}$ rad/s the energy of binding of the electrons furthest from the nucleus becomes less than the energy of the corresponding photon $\hbar\omega$. In the far ultraviolet and at still higher frequencies the so-called approximation of free electrons, or plasma equation, becomes valid [16]:

$$\epsilon(i\xi) = 1 + 4\pi Ne^2/m\xi^2 \quad (4.31)$$

where e is the electron charge, m is the electron mass, and N is the number of electrons per cm^3 that have a binding energy much less than $\hbar\omega$, i.e., these electrons interact with the quanta of electromagnetic field as free (not bound) electrons. As $\hbar\omega \rightarrow \infty$, N tends to the total number of electrons in an atom; when $\hbar\omega \sim 10^{16}$ rad/s, N corresponds to the number of the least bound valence electrons. In the case of light atoms, Eq. (4.31) is valid from $\hbar\omega = \infty$ down to the far ultraviolet, and in heavy atoms only down to x-ray frequencies.

A linear [35] or nonlinear interpolation [28] is used to transform from Eq. (4.30) to Eq. (4.31). Interpolation must in fact reflect the dependence $N(\hbar\omega)$, i.e., the number N of electrons per atom that can be considered free with respect to radiation quanta with a given energy $\hbar\omega$. The difficulty in calculating $N(\hbar\omega)$ lies in that there is no sharp boundary between free and bound electrons, and no equation is available to fill the gap between relations (4.30) and (4.31). Unfortunately, the largest contribution to the forces of molecular interaction is often made at frequencies corresponding to this "gap." Consequently, different methods of interpolation may lead to substantial differences both in the values of the function $\epsilon(i\xi)$ and especially in the values of the constant

A_{132} in Eq. (4.24) which includes differences between functions $\epsilon(i\xi)$ for the interacting bodies.

When spectral data $\epsilon''(\omega)$ are known up to high energies (50-100 eV), the functions $\epsilon(i\xi)$ can be calculated by means of the Kramers-Krönig equation (4.11) [36-38]. For instance, $\epsilon(i\xi)$ was calculated in this manner for quartz [36] on the basis of absorption spectra obtained by Wittmann et al. [39].

In principle, any number of absorption bands, not only two or three as in Eq. (4.30), can be taken into account. Parsegian and Ninham proposed the following more general expression [34, 35]:

$$\epsilon(i\xi) = 1 + \frac{\epsilon_0 - \epsilon_\alpha}{1 + (\xi/\omega)} + \sum_j^\infty \frac{C_j}{1 - (\xi/\omega_j)^2 + i\gamma_j(\xi/\omega_j)} \quad (4.32)$$

where C_j is a constant proportional to the strength of the j -th oscillator, and γ_j is the damping factor. In the case of narrow absorption bands typical for dielectrics, damping is negligible and just the first two terms can be retained in the denominator in the sum in (4.32). Well-known values of $\epsilon = n^2$ in the visible part of the spectrum can be used as the adjustment parameter in constructing the function $\epsilon(i\xi)$ [38].

In the case of nonpolar liquids and solids, the calculation is often restricted to taking into account the interaction at a single characteristic frequency ω_c in the UV band of the spectrum [35]:

$$\epsilon(i\xi) = 1 + (n^2 - 1)/[1 + (\xi/\omega_c)^2] \quad (4.33)$$

where n is the refractive index.

The values of ω_c can be found by means of the approximation

$$\omega_c \approx 1.52 \cdot 10^{15} I \text{ rad/s}$$

where I is the ionization potential, in eV. When determining the values of I for condensed matter, corrections must be made to the tabulated values of I_m of isolated molecules:

$$I = I_m + P$$

where P is the energy of polarization of a single charge in a dielectric material [40]. In many crystals $P = -1.5 \pm 0.5$ eV. This correction may prove considerable in liquids.

As an example, Fig. 4.10 shows $\epsilon(i\xi)$ calculated from spectral data and by means of Eqs. (4.30) and (4.31), and plotted on a semi-logarithmic scale. The inset in the upper right-hand corner of the

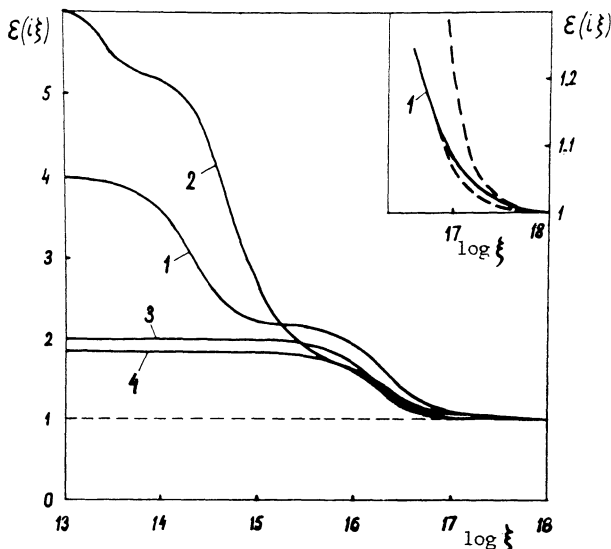


Fig. 4.10. Functions $\epsilon(i\xi)$ calculated from spectral data for quartz (1), water (2), decane (3), and pentane (4).

figure shows the range of interpolation for quartz between the spectral data and the plasma equation (4.31). We see from this figure that the shape of $\epsilon(i\xi)$ is different for polar and nonpolar media. As we find from Eqs. (4.22)-(4.24), the difference between the values of $\epsilon(i\xi)$ in the interacting bodies and in the separating interlayer is essential in the calculation of molecular forces. As a result, molecular forces reach maximum values when the polarity of the interlayer sharply differs from that of the interacting bodies. Other components of disjoining pressure may be more important if spectral properties are not very different.

The form of $\epsilon(i\xi)$ in metals is quite different because of strong absorption, including the range of low frequencies, owing to the presence of free electrons in the conduction band. The functions $\epsilon(i\xi)$ in metals are calculated from the Kramers-Krönig equation by using measured spectral data. Thus, they are known for gold and silver in the range from optical frequencies up to $\hbar\omega = 60$ eV and 100 eV, respectively [33, 41, 42]. The Drude equation can be used in the IR range [43]:

$$\epsilon''(\omega) = g\omega_c^2/\omega(\omega^2 + g^2) \quad (4.34)$$

where $\omega_c = (4\pi e^2 N/m_0)^{1/2}$ is the plasma frequency; N is the number of free electrons per cm^{-3} ; m_0 is the effective (optical) electron mass; and g is the reciprocal relaxation time of charge carriers.

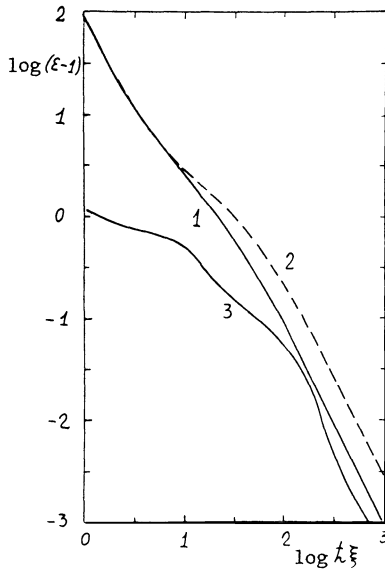


Fig. 4.11. Functions $\epsilon(i\xi)$ calculated from spectral data for gold (1), silver (2), and water (3).

Figure 4.11 plots $\epsilon(i\xi) - 1$ as a function of $\hbar\xi$ calculated by this method [44] for gold (curve 1) and silver (curve 2), on a double logarithmic scale. In the calculations we assumed: for gold, $m_0 = 1.03$ m, $\hbar\omega_c = 8.83$ eV, and $\hbar g = 0.176$ eV; and for silver, $m_0 = 1.04$ m, $\hbar\omega_c = 9.2$ eV, and $\hbar g = 0.113$ eV [33, 41, 42]. The values of g for $\omega \rightarrow 0$ were used, because relaxation is essential only at low frequencies. The figure shows that in metals the values of $\epsilon(i\xi)$ are higher than in polar water (curve 3). As we move to low frequencies, the difference between the functions $\epsilon(i\xi)$ in metals and dielectrics grows.

The following values of constants in Eq. (4.24) were obtained from the function $\epsilon(i\xi)$ for the gold-vacuum-gold and silver-vacuum-silver systems: $A_{101} = 4.1 \cdot 10^{-12}$ erg and $A_{101} = 5.4 \cdot 10^{-12}$ erg, respectively [44]. Parsegian and Weiss [38] employed spectral data reported in various publications, and obtained for gold the values of A_{101} from $2 \cdot 10^{-12}$ to $4 \cdot 10^{-12}$ erg, and for silver from $2 \cdot 10^{-12}$ to $5 \cdot 10^{-12}$ erg. Higher values of A_{101} obtained from more reliable spectral data appear to be more reasonable [45]. They are closer to the values of A_{101} reported in [44] and cited above. It is thus possible to obtain by different techniques closely agreeing values of the function $\epsilon(i\xi)$ and of molecular force constants if reliable spectral data are used. Parsegian and Weiss [38] calculated the function $\epsilon(i\xi)$ by means of Eq. (4.32), using three characteristic absorption bands for gold and four absorption bands for silver.

The linear behavior of $\log(\epsilon - 1)$ as a function of $\log \hbar \xi$ in the high-frequency range (Fig. 4.11) for gold and silver corresponds to the plasma equation (4.31) with the number of free electrons per atom $z = 11$ for gold and $z = 30$ for silver. It seems logical to relate the former result to the participation of one 6s and ten 5d electrons of the gold atom in the interaction with electromagnetic field quanta as free electrons. The higher value of z in silver indicates that electrons at deeper levels also participate in the interaction.

Calculations of $\epsilon(i\xi)$ can be further simplified and even presented in an analytical form by using an empirical expression suggested by Krupp [33]:

$$\Delta_{ik} = (\epsilon_i - \epsilon_k)/(\epsilon_i + \epsilon_k) = \alpha_{ik} \exp(-b_{ik}\xi) \quad (4.35)$$

where α_{ik} and b_{ik} are constants.

This equation gives a successful approximation of the function $\Delta_{ik}(\xi)$ in the frequency range 10^{16} - 10^{17} rad/s which gives the main contribution to dispersion forces. Equation (4.35) was verified for bodies interacting in vacuum in [33, 46, 47]. It proved possible to extend this equation also to the case of interaction through water interlayers [31]. The values of the constants α_{ik} and b_{ik} obtained for the interaction of identical bodies (i) through a vacuum or water interlayer (k) are listed in Table 4.1.

Equation (4.35) with the values obtained of the constants α_{ik} and b_{ik} can be used to find an analytical expression for the molecular component of disjoining pressure, valid in a relatively wide range of water interlayer thickness. It is then necessary to represent the function $\epsilon_3(i\xi)$ for water also in an analytical form. A successful approximation of $\epsilon_3(i\xi)$ for a water interlayer is [31]

$$\epsilon_3(i\xi) = [1 + (\ell/\xi)]^2 \quad (4.36)$$

where ℓ is a constant that in water equals $\approx 3.3 \cdot 10^{15}$ rad/s.

By substituting Δ_{31} and Δ_{32} into Eq. (4.29) with the appropriate expressions from (4.35) and substituting $\epsilon_3(i\xi)$ with the expression from (4.36), we obtain, after integrating (4.29), the following expression for $A(H)$:

$$A(H) = \frac{3\hbar}{4\pi} \frac{\alpha_{13}\alpha_{23}}{(b_{13} + b_{23})} \left[1 - \frac{1 + \ell(b_{13} + b_{23})}{\{1 + [(b_{13} + b_{23})c/2H]\}^3} \right] \quad (4.37)$$

A comparison with the exact solution shows that this equation holds for $H \leq 300 \text{ \AA}$, so that for the systems listed in Table 4.1 deviations do not exceed 5%. As $H \rightarrow 0$, $A(H)$ tends to the Hamaker constant

TABLE 4.1. Constants α_{ik} and b_{ik} in Eq. (4.35) Obtained from Spectral Data

Interacting substances, i	Interlayer, k	Values of constants	
		α_{ik}	$b_{ik} \cdot 10^{17}$ s/rad
Water	Vacuum	0.32	3.1
Quartz	"	0.44	3.1
Mica	"	0.49	2.9
Gold	"	0.96	3.0
Quartz	Water	0.12	3.1
Mica	"	0.17	2.4
Gold	"	0.80	3.4

$$A_0 = \frac{3\hbar}{4\pi} \frac{\alpha_{13}\alpha_{23}}{(b_{13} + b_{23})} \quad (4.37')$$

When two identical materials interact in vacuum (i.e., $b_{13} = b_{23} = b$, $\alpha_{13} = \alpha_{23} = \alpha$, $\epsilon_3 = 1 = \text{const}$, and $\ell = 0$), the equation is substantially simplified:

$$A = \frac{3\hbar}{4\pi} \frac{\alpha^2}{2b} \left[1 - \frac{1}{\{1 + [bc/H]\}^3} \right] \quad (4.38)$$

As $H \rightarrow 0$, this equation gives $A_0 = (3\hbar/4\pi)(\alpha^2/2b)$. At sufficiently large H we can assume

$$\{1 + (bc/H)\}^3 \approx 1 + (3bc/H)$$

which gives us the asymptote (4.25) of the Lifshitz theory:

$$A(\infty) = 6\pi B/H$$

where

$$B = 3\hbar\alpha^2 c / 16\pi^2$$

(details can be found in [31, 32]). As we saw in Fig. 4.9, Eq. (4.38), for instance in the water-vacuum-water system (curve 3), fits quite well the results of calculations based on Eq. (4.22) (curve 1).

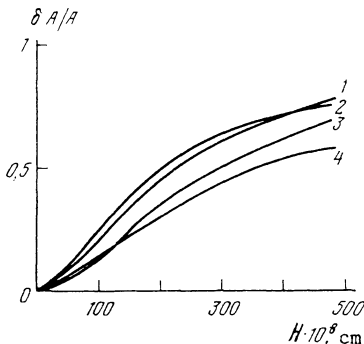


Fig. 4.12. $\delta A/A_0$ as a function of H for the mica-water-mica (curves 1 and 2) and gold-water-gold (curves 3 and 4) systems, obtained by numerical integration of Eq. (4.29) (curves 2 and 4) and by using Eq. (4.37) (curves 1 and 3).

When Eq. (4.37) is used in the case of bodies interacting through water interlayers, the departures from the results of numerical integration of the exact equation (4.29) are somewhat greater (Fig. 4.12). But the accuracy achieved is quite satisfactory for practical purposes. One advantage of using Eq. (4.37) is the possibility of presenting the law of molecular forces $\Pi(H)$ in an analytical form in the range of interlayer thickness from 0 to 300 Å:

$$\Pi(H) = -\frac{A_0}{8\pi^2 H^3} \left\{ 1 - \frac{E}{[1 + (D/H)]^3} \right\} \quad (4.39)$$

where E and D are constants found from Eq. (4.37).

Rabinovich used Eqs. (4.29) and (4.37) to calculate the constants A_0 for a large number of systems [48]. He was also able to obtain and analyze the exponent m in the equation $\Pi(H) = -C/H^m$ [approximating Eq. (4.39)] as a function of interlayer thickness H :

$$m(H) = 3 \left\{ 1 + \frac{d \cdot E}{(1 + d)[(1 + d)^3 - E]} \right\} \quad (4.40)$$

where $d = D/H$.

Good agreement was obtained for the mica-vacuum-mica system between the dependence $m(H)$ calculated by using (4.40) and the results of numerical calculations of Chan and Richmond [49] on the basis of the exact equation (4.22) of the Lifshitz theory.

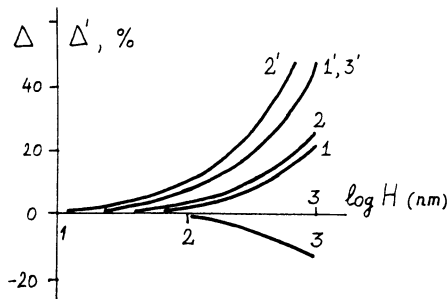


Fig. 4.13. Relative errors Δ (curves 1-3) and Δ' (curves 1'-3') produced by replacing summation with integration, plotted as functions of interlayer thickness H for the gold-vacuum-gold (curves 1 and 1'), gold-water-gold (curves 2 and 2'), and polystyrene-tetradecane-polystyrene (curves 3 and 3') systems.

The ranges where the asymptotes (4.24) and (4.25) are valid must be discussed in more detail because they are often used in practical calculations. Obviously, their wide use is justified by the simple analytical forms of the functions $U(H)$ that are conveniently included in calculations of colloid and film stability (Chapters 8 and 10).

With this in mind, the energy of interaction between two flat bodies 1 and 2 (per cm^2), i.e.,

$$U(H) = \int_{H_0}^{\infty} \Pi(H) dH \quad (4.41)$$

through an interlayer 3 was calculated by different methods, and the results were compared [50].

Let us consider first at what values of H and in what systems the differences between Eqs. (4.22) and (4.23) are appreciable — i.e., at what conditions the summation over frequencies ξ_N can be replaced with integration.

Figure 4.13 plots the discrepancy, or relative error $\Delta = (U_i - U_s)/U_s$ produced by the replacement of summation with integration, as a function of the logarithm of interlayer thickness H between the interacting objects (curves 1-3). Here $U_i(H)$ is calculated from Eq. (4.41) on the basis of (4.23), and $U_s(H)$ represents

the exact interaction energy calculated from (4.22) by summation over frequencies.

As we find from a comparison of curves 1-3, at $H \leq 1000 \text{ \AA}$ the discrepancies between different systems with vacuum, water, and non-polar liquid interlayers are small, i.e., below a few percent. This shows that in most cases encountered in colloid chemistry the replacement of summation with integration is quite justified. However, departures considerably increase if $H > 1000 \text{ \AA}$, and reach 10-20% for $H \approx 1 \mu\text{m}$. This growth of error is caused by an increase of the contribution to $U(H)$ at low frequencies, when the "weight" of the first terms of the series, which are not taken into account in the integration with sufficient accuracy, increases. This deviation is sometimes "corrected for" by adding to U_i the zero term of the series, U_z , equal to

$$U_z = A_z / 12\pi H^2$$

where the constant A_z is found from Eq. (4.26).

The relative error left after such a correction and equal to

$$\Delta' = (U_i + U_z - U_s)/U_s$$

is shown in the same Fig. 4.13 (curves 1'-3'). The illustrated results of calculations show that the discrepancy is only increased by adding the zero term. The reason for this is that the error is introduced by not only the zero term but also by several first terms of the series, and their sum departs from the integral corresponding to this range of frequencies. Lifshitz demonstrated [17, 18] that the magnitude and sign of this error are a function, respectively, of sign and magnitude of the first and third derivatives taken with respect to the summation index.

The situation is different for systems that include a polar liquid and either at least one dielectric or a vacuum interlayer. Figure 4.14 plots the relative values $\Delta = (U_i - U_s)/U_s$ and $\Delta' = (U_i + U_z - U_s)/U_s$ as functions of $\log H$ for a number of such systems: water-vacuum-water (curves 1 and 1'), polystyrene-water-polystyrene (curves 2 and 2'), water-tetradecane-water (curves 3 and 3'), and water-tetradecane-vacuum (curves 4 and 4'). For such systems, Eq. (4.23) yields a large error even in the range of narrow gaps between bodies. The error reaches 70% for tetradecane interlayers between water bulk phases (curve 3) even when $H \leq 100 \text{ \AA}$. In asymmetric systems the error rises sharply for $H \geq 100 \text{ \AA}$ (curve 4).

The cause of such discrepancies is that, in polar liquids (e.g., water), the zero term, practically neglected in integration, may constitute a significant fraction of the sum of the series. In the integration of (4.23) with respect to $d\xi$ an appreciable con-

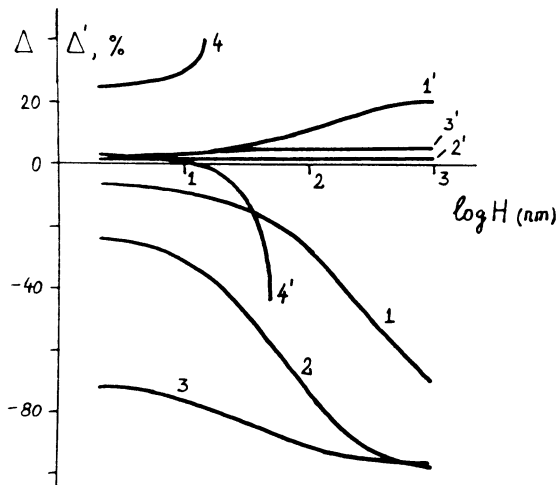


Fig. 4.14. Relative errors Δ (curves 1-4) and Δ' (curves 1'-4') plotted as functions of H for symmetrical systems water-vacuum-water (curves 1 and 1'), polystyrene-water-polystyrene (curves 2 and 2'), water-tetradecane-water (curves 3 and 3'), and for an asymmetrical system water-tetradecane-vacuum (curves 4 and 4').

tribution is made by the values of the integrand corresponding to frequencies $\xi > 10^{13}$ rad/s when the values of $\epsilon(i\xi)$ for water (and other polar liquids) already diminish to $\epsilon \approx 2$. As a result, the contribution of low-frequency interaction (when the values of ϵ are high) is ignored and U_i becomes less than U_s , resulting in the negative sign of Δ in symmetric systems. In this case, the addition of the zero term U_z to U_i (in symmetric systems) indeed considerably diminishes the discrepancy compared with the exact solution (curves 1'-3'). Discrepancies do not exceed 5-10% up to $H \leq 1000 \text{ \AA}$, and sometimes up to $H \leq 1 \mu\text{m}$. Consequently, the use of the equation

$$U = U_i + U_z = U_i + A_z / 12\pi H^2 \quad (4.42)$$

is then completely justified.

The introduction of the zero term in an asymmetric system (curve 4') can also diminish the difference between U and U_s , although in a much narrower range of interlayer thickness: $H \leq 300 \text{ \AA}$.

The state-of-the-art in computer simulations is such that computation with the exact equation (4.22) is not more complicated

than with Eq. (4.23) which was used more often until now (in fact, integration inevitably reduces to summation in computer simulation; the difference only consists in the choice of step). Therefore, it does not seem reasonable to go on using Eqs. (4.23) and (4.42).

The range of applicability of the asymptotes was also established by comparing the exact solution (4.22) with Eqs. (4.24) and (4.25) [50]. For systems represented in Fig. 4.13, Eq. (4.24) leads to errors above 25% for $H \geq 40\text{-}50 \text{ \AA}$. Equation (4.25) is valid for $H \geq 1 \mu\text{m}$ in metals (for $H < 1 \mu\text{m}$ the error is greater than 25%), and for $H \geq 300 \text{ \AA}$ in dielectrics.

In systems with a polar liquid the asymptote (4.24) works satisfactorily for interlayer thickness $H \leq 50 \text{ \AA}$ (if we choose the same maximum admissible error of 25%). However, the other asymptote, (4.25), for the full retarded forces proves to be completely unacceptable. It leads to large errors because Eq. (4.25) ignores the nonretarded zero term U_z . In systems with a polar liquid and a dielectric, this term (U_z) makes a contribution to the forces of molecular interaction of the same order of magnitude as all other terms of the series taken together.

The results of calculations plotted in Figs. 4.12-4.14 were based on the functions $\epsilon(i\xi)$ found from the data [38] for polystyrene, tetradecane, water, and gold. DESY spectral data were also used for gold [45].

A problem that arises rather often is the calculation of dispersion forces in nonplanar interlayers, for instance dispersion forces between spherical particles or those in multilayer systems. It proved possible to simplify considerably the calculation of dispersion forces after van Kampen et al. [51] developed a new method. The method is based on the approach applied by Casimir [12] to metals; it reduces the solution of the problem to the interaction between harmonic oscillators located not in the bulk but only on the surface of the interacting bodies (so-called surface plasmons). It was shown in [51-53] that the interaction between surface plasmons is equivalent to Lifshitz's dispersion forces. The expressions for dispersion forces coincide for planar interfaces. A more detailed exposition of the method of surface plasmons is given in the monograph by Mahanty and Ningham [26].

The problem of finding the disjoining pressure in a symmetrical five-layer system (Fig. 4.15) with a liquid interlayer of thickness H separated from identical bulk phases 1 by liquid or solid interlayers 2 of thickness δ was solved by Ningham and Parsegian [54]. The disjoining pressure of the interlayer 3 due to nonretarded dispersion forces is given by the following equation:

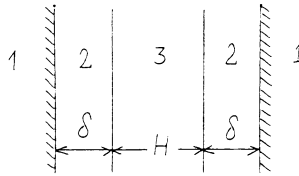


Fig. 4.15. An example of a symmetrical five-layer system.

$$\Pi(H) = -\frac{1}{6\pi} \left[\frac{C}{H^3} + \frac{D}{(H + \delta)^3} + \frac{E}{(H + 2\delta)^3} \right] \quad (4.43)$$

where

$$C = A_{232}, \quad D = -2A_{123}, \quad E = A_{121} \quad (4.44)$$

Here A_{ijk} are the constants of molecular forces, determined from Eq. (4.24).

This five-layer system is a faithful model of the interaction between, for example, solids coated with adsorption layers or with oxide films, as well as of molecular forces in free films ($\epsilon_1 = 1$) stabilized with surfactants.

Langbein [55] analyzed a more general case of n -layer, possibly asymmetric, systems, and took into account image forces of instantaneous dipoles generated by the presence of interfaces between layers with different dielectric properties. In the case of two bodies and one interlayer ($n = 3$) this method of calculating dispersion forces gives a solution coinciding with the Lifshitz theory of non-retarded forces. However, Langbein's method gives somewhat different expressions for the constants C , D , and E in Eq. (4.43). If mirror images of only the first order are taken into account [55],

$$C = \frac{3\hbar}{4\pi} \int_0^\infty \Delta_{32}^2 d\xi, \quad D = \frac{6\hbar}{\pi} \int_0^\infty \frac{\epsilon_2 \epsilon_3}{(\epsilon_2 + \epsilon_3)^2} \Delta_{32} \Delta_{21} d\xi,$$

$$E = \frac{12\hbar}{\pi} \int_0^\infty \frac{\epsilon_2^2 \epsilon_3^2}{(\epsilon_2 + \epsilon_3)^4} \Delta_{21}^2 d\xi \quad (4.45)$$

If second-order mirror images are included, additional small terms appear in the expressions for C and D and a new term $F/(2H + \delta)^3$ is added to Eq. (4.43). Equations (4.45) reduce to (4.44) only when the functions $\epsilon_2(i\xi)$ and $\epsilon_3(i\xi)$ are sufficiently close — i.e., when the dielectric properties of the layers 2 do not differ much from those of the liquid interlayer (Fig. 4.15). Later, Langbein

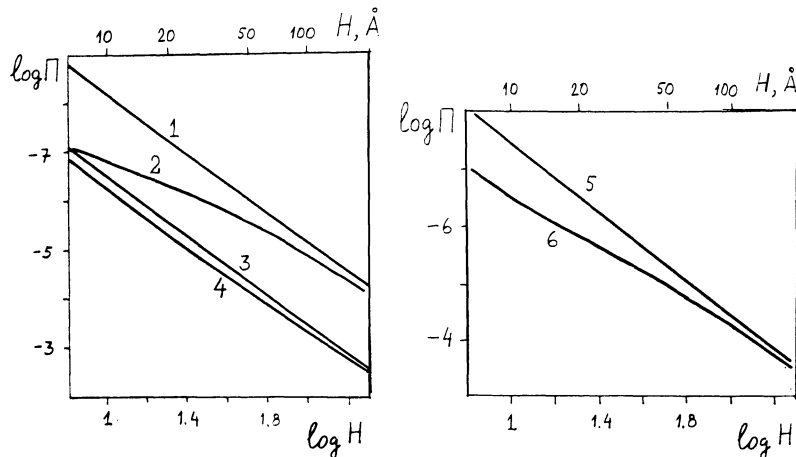


Fig. 4.16. The effect of adsorption layers on the molecular component of disjoining pressure Π of an interlayer with thickness H : no adsorption layer (curves 1, 3, 5); an adsorption layer of thickness $\delta = 10 \text{ \AA}$ (curves 2, 4, 6), for systems a) $\text{Au}-\text{H}_2\text{O}-\text{Au}$ (curves 1 and 2), $\text{SiO}_2-\text{H}_2\text{O}-\text{SiO}_2$ (curves 3 and 4); b) free water film (curves 5 and 6).

found an analytical solution of the dispersion forces problem in multilayer systems, having taken electromagnetic retardation into account [56].

Figure 4.16 illustrates the screening effect of surfactant layers ($\delta = 10 \text{ \AA}$) adsorbed on a metal surface (gold, curves 1 and 2) and on a dielectric (quartz, curves 3 and 4) [57]. The disjoining pressure of a water interlayer, $\Pi(H) < 0$, decreases even more, the smaller the interlayer thickness H . Screening is more pronounced on metals because of the greater difference between the dielectric properties of the substrates and adsorbed layers. The difference between the values of constants calculated by using Eqs. (4.44) and (4.45) is manifested only by D and E. This difference is greater for gold (D differs by 20%, and E by 5.6%) than for quartz (D differs by 7.6%, and E by 2.1%) [57].

An adsorbed layer of a surfactant produces an appreciable screening effect on free water films as well (curves 5 and 6, Fig. 4.16).

So far we have been discussing molecular forces in systems composed of layers homogeneous in their properties. The situation is more complex in, for instance, solutions whose composition and concentration within a thin interlayer become coordinate-dependent.

As we show in Chapters 5 and 6, in this case interaction forces are not reducible to molecular forces only, and additional components appear, because of an overlapping of diffuse layers composed of ions (electrostatic component of disjoining pressure) or of neutral molecules (adsorption component).

If diffuse adsorption atmospheres do not yet overlap but the interlayer of a solution or solvent is not uniform in its dielectric properties, the values of $\Pi_m(H)$ can be found by a further elaboration of the calculations of Dzyaloshinsky, Lifshitz, and Pitaevsky [25]. Different approaches are possible in this situation. The first is to divide a nonuniform interlayer into a number of layers with different values (but constant within each layer) of $\epsilon(i\xi)$. For instance, the five-layer model (Fig. 4.15) can be used, in which the layers δ refer to boundary layers of the solution with altered concentration, or to boundary layers of the solvent with altered density. Chan et al. [58] demonstrated, among other things, that a decrease in the density of boundary layers δ enhances the attraction through a nonuniform interlayer, while an increase in density results in a weakened attraction.

Parsegian and Weiss [59] realized the second approach, having calculated the forces of molecular attraction in a five-layer system (Fig. 4.15), having assumed that the values of $\epsilon_2(i\xi)$ vary along the normal to the interface within the boundary layers δ . The calculations demonstrated that an exponential decrease in the values of $\epsilon_2(i\xi)$ within the layers diminishes the forces of molecular attraction between the substrate as compared to the calculations with the five-layer model operating with mean values of $\epsilon_2(i\xi) = \text{const}$ for boundary layers δ . The nonuniformity of the dielectric properties of boundary layers thus changes appreciably the field of dispersion forces. Even now this important factor is mostly disregarded when the theory of molecular forces is applied to real objects.

In the case of electrolyte solutions it is also necessary to take into account the effect of electric conduction that results in the spatial dispersion of dielectric constant. However, the screening of dispersion interaction produced thereby leads to measurable effects only when interlayer thickness exceeds 0.1-1 μm [26, 60-62].

Lifschitz showed [17-19] that the anisotropy of permittivities of solids interacting in vacuum can result, in addition to attractive forces, in a rotation of crystals with respect to the axis perpendicular to surfaces bounding the planar interlayer. Equilibrium corresponds to such orientation of crystal axes that maximizes the energy of their interaction through the interlayer of a given thickness H , i.e., maximizes the drop in the free energy of the system. Kats [63] applied the Lifschitz theory developed for anisotropic

bodies to an analysis of stability of boundary layers and thin interlayers of liquid crystals characterized by anisotropic dielectric properties. The moment of forces was calculated by Barash and Ginzburg [53] for the case of weak anisotropy of the interacting bodies.

Using a strongly anisotropic uniaxial crystal of HgCl ($n_1 = 1.973$ and $n_2 = 2.656$), Parsegian and Weiss demonstrated [64] that the change in the energy of molecular attraction in vacuum does not exceed 1% in the whole range of possible rotation angles. The increment to the interaction energy due to the effect of anisotropy is equal in magnitude both in vacuum and in the case of interaction through liquid interlayers. Consequently, the contribution of anisotropy may become appreciable when molecular interaction forces are in themselves weak, for instance when the dielectric properties of the crystal and liquid interlayer are not very different. The anisotropy of dielectric properties may play an appreciable role for liquid crystals, by determining a preferred orientation at interfaces [63, 65, 66], and for crystals in their own melt.

Van Kampen's method was also successfully used for an exact solution of the problem of molecular attraction between small spherical particles in a liquid. Using this method, Mitchell and Ninham [67] derived the following expression for the energy of non-retarded dispersion interaction between two identical spheres 1 with radius $\alpha \gg H$ in a liquid 3:

$$U(H) = -\frac{1}{12} \left(A_1 \frac{\alpha}{H} - 2A_2 \ln \frac{\alpha}{H} \right) \quad (4.46)$$

where H is the shortest distance between spherical surfaces. The constants A_1 and A_2 are functions of the spectral characteristics $\varepsilon_1(i\xi)$ of the spheres and $\varepsilon_3(i\xi)$ of the liquid interlayer:

$$A_1 = -\frac{3\hbar}{4\pi} \int_0^\infty \Delta_{13}^2 d\xi; \quad A_2 = -\frac{3\hbar}{4\pi} \int_0^\infty (1 - \Delta_{13}) \times \ln(1 - \Delta_{13}^2) d\xi \quad (4.47)$$

Hamaker's solution [16], obtained on the basis of a microscopic theory by integrating pairwise interactions between molecules, has the following form:

$$U(H) = -\frac{A}{12} \left(\frac{\alpha}{H} - 2 \ln \frac{\alpha}{H} \right) \quad (4.48)$$

where $A = A_{131} = A_{11} + A_{33} - 2\sqrt{A_{11}A_{33}}$, and A_{11} and A_{33} are the corresponding "vacuum" Hamaker constants.

As we find by comparing expressions (4.46) and (4.48), they coincide only if $A_1 = A_2 = A$. But this equality occurs, as we see from (4.47), only if $\Delta_{13} \ll 1$, i.e., only if the dielectric properties of the particles differ very little from those of the liquid in which they are immersed. Quantitative calculations by Smith et al. [68] for spherical polystyrene particles in water, heptane, and vacuum confirmed that the Hamaker equation fails when the functions $\varepsilon(i\xi)$ of the particles and the surrounding medium are very different.

It was also shown [44] that Hamaker's formula (4.48) applied, for instance, to hydrosols of metals results in large errors. At $(H/\alpha) < 0.2$, the deviation in attraction energy exceeds $10 kT$. In fact, a change in the height of potential barrier by $10 kT$ may change the stability factor by several orders of magnitude.

Recently, Pailthorpe and Russel [71] carried out an analysis of the accuracy of solutions obtained by different authors [67-70] for the interaction energy of spherical polystyrene particles in water. The zero term ($N = 0$) was eliminated in numerical computations of [71]. It was assumed that this term is completely screened by the appropriate admixture of electrolyte to water. It was shown that, first, the effect of retardation becomes appreciable at $H \geq 50 \text{ \AA}$. An approximate expression (4.48) works quite well for the polystyrene-water system because here ε_1 is nearly equal to ε_3 . Deviations from the exact solution of Langbein [69] do not exceed 20% at $\alpha = 2500 \text{ \AA}$, and come to less than 10% at $\alpha = 1000 \text{ \AA}$. The Derjaguin equation (4.2) [11] correctly accounts for the geometric factor at $H/\alpha \ll 1$. This equation is considerably more convenient for calculations because the energy of interaction that enters it is that of interaction between plane surfaces; this makes the relevant calculations considerably simpler and more accurate.

4.7. MAIN RESULTS OF THE EXPERIMENTAL VERIFICATION OF THE THEORY OF MOLECULAR INTERACTION BETWEEN MACROSCOPIC BODIES

After the first measurements carried out by Derjaguin and Abrikossova [6, 7, 19], further attempts were made to measure directly the molecular forces between various model bodies. These experiments also confirmed the correctness of the macroscopic theory and of the calculations based on spectral characteristics of the interacting bodies.

At large spacings between bodies ($H > 0.1 \mu\text{m}$) when the effect of retardation of molecular interaction is fully developed, the results of direct measurements are in good agreement, not only qualitative but quantitative as well, with Eqs. (4.17) and (4.19)

of the macroscopic theory. Prosser and Kitchener, whose work was already cited [23], obtained for glass plates in vacuum that the constant B in Eqs. (4.18) and (4.20) is $B = (1.1 \pm 0.4) \cdot 10^{-19}$ erg·cm, falling between the theoretical values of B for quartz: 1.53×10^{-19} (taking the static value $\epsilon_0 = 3.6$) and $0.6 \cdot 10^{-19}$ erg·cm (taking $\epsilon_0 = n^2 = 2.13$). Figure 4.4 shows that the data reported by Derjaguin and Abrikossova also fall between these two theoretical estimates. However, the lowest experimental values of $F(H)$ and $U(H)$ (Figs. 4.4 and 4.5) should be regarded as more reliable (see Section 4.3).

In view of unsuccessful first experiments [21], when residual surface charge prevailed, Overbeek and co-workers, in their next paper [72], worked, as Derjaguin and Abrikossova had, with a quartz plate and quartz lens, and obtained for distances $H > 0.1 \mu\text{m}$ a correct value $B = 1.15 \cdot 10^{-19}$ erg·cm. This method was later improved by van Silfhout [73], who conducted still more accurate measurements on a torsion microbalance in a vacuum of 10^{-5} - 10^{-4} mm Hg. A shift in balance equilibrium was recorded by a change in the capacitance of a plane capacitor. The distance between a plate resting on three bellows supports and the lens was measured from the diameters of Newton's rings with an error less than 40 Å. Surface charges were removed by injection of water vapor whose adsorption on quartz surfaces forms well-conducting films. van Silfhout obtained for the quartz (vitreous silica)-vacuum-quartz system at $H > 0.1 \mu\text{m}$ the experimental value $B = 0.66 \cdot 10^{-19}$ erg·cm, quite close to the theoretical value of B calculated with $\epsilon_0 = n^2 = 2.13$. He obtained somewhat higher values for crystalline quartz: $B = 0.74 \cdot 10^{-19}$ erg·cm, because of a higher refractive index of quartz crystals ($n = 1.5$ and $\epsilon_0 = n^2 = 2.25$).

Still higher values of B were obtained, as in the experiments of Derjaguin and Abrikossova (Fig. 4.7), for the quartz-vacuum-chromium system: $B = 2.9 \cdot 10^{-19}$. The value given in this case by Eq. (4.19) is not very different: $B = 2.4 \cdot 10^{-19}$ erg·cm. In these measurements the surface of the quartz lens was coated by vacuum deposition with a chromium layer 1200 Å thick. Later measurements by Rouweler [74] with the same system gave a somewhat lower experimental value $B = 2.1 \cdot 10^{-19}$ erg·cm (for H from 0.1 to $0.28 \mu\text{m}$). However, the chromium coating was thinner in these experiments (540 Å).

Sparnaay was the first to measure molecular attraction between identical bulk metals (chromium) [75], with surface charge removed by short-circuiting the specimens. As a result, he obtained a correct value $B = 12.5 \cdot 10^{-19}$ in agreement with that calculated from the theory of Casimir and Polder [$B = 13 \cdot 10^{-19}$ erg·cm, Eq. (4.17)]. In these experiments the gap width H was measured off the electrical contact position ($H = 0$).

Later, van Blokland and Overbeek [76] measured molecular attraction between a quartz plate and a lens ($R_0 = 100$ cm) coated in vacuum by a chromium layer about 1000 Å thick. They also studied the effect of potential difference V applied to metal layers. The Volta potential spontaneously appearing between the metal layers was compensated for by applying a potential difference with reversed sign when molecular forces were measured. A new method was also employed to measure the gap between the bodies, viz., measuring the capacitance of the capacitor formed by the metal layers coating the two interacting bodies.

The results were compared with the Lifshitz equation (4.23) because measurements were carried out in a wide range of H , from 0.13 to 0.67 μm, where retardation could be appreciable. The functions $\epsilon(i\xi)$ were calculated by using Krupp's method [33] and the spectral data for chromium. Good agreement with the Lifshitz theory was found in the whole investigated range of H .

Nevertheless, it should be mentioned that at a prescribed potential difference the condition $V = 0$ did not exactly correspond to the minimum of the measured attractive force produced only by molecular forces; this may be connected with the presence of chromium oxide film on the surface.

Hunklinger et al. [77] used a dynamic method for measuring molecular forces. The method is based on transferring the vibration of the lens fixed to a low-frequency vibrator to a flat plate in a vacuum below 10^{-4} mm Hg through long-range forces. The vibration amplitude was much smaller than the lens-plate distance. The oscillatory motion of the plate connected to a microphone membrane produced an ac emf. The amplitude of the emf could be recalculated, after a preliminary calibration, into the amplitude of the driving force. This improved the accuracy of measuring the force F to 10^{-7} dyn. The distance H between a borosilicate lens ($R_0 = 25$ cm) and a borosilicate glass plate was varied from 0.08 to 1.5 μm and measured by recording the displacement of Newton's rings, from the position of electrical contact for which the authors assumed $H = 0$. The experimental curve $F(H)$ in the range from 0.08 to 0.8 μm fitted the theoretical equation (4.18) with $B = (0.86 \pm 0.15) \cdot 10^{-19}$ erg·cm. Results obtained at $H < 0.08$ μm were affected by roughness of the polished glass surface. At $H > 0.8$ μm, the values of F grew beyond the theoretical expectation because of the effect of the small residual surface charge. This charge remained despite very careful cleaning of the surface and injection of water vapor. The effect of electrostatic forces, with their characteristic slow decrease with distance, was felt only at distances H where molecular attraction sharply diminished (proportionally to $1/H^4$).

Possibly for the same reason, in repeated experiments Rouweler and Overbeek [78] and van Blokland and Overbeek [79] obtained

values slightly greater than those predicted by the theory for the same quartz-vacuum-quartz system [$B = (1.05-1.08) \cdot 10^{-19}$ erg·cm].

Dynamic techniques used in later research [80] revealed an interesting effect which directly confirms the dependence of molecular forces on spectral properties of the interacting bodies. A "metal-lization" of semiconductor silicon as a result of irradiation with white light (transfer of some electrons to the conduction band due to internal photoelectric effect) led to an increase in molecular attraction.

A considerable number of papers among those cited above reported deviations from the law $F(H)$ of full retarded forces when the gap width H was reduced to 500-800 Å. These deviations could be caused either by incompletely developed retardation or by surface roughness. Usually the roughness of polished surfaces is from 50 to 100 Å.

Obviously, smoother surfaces are needed for working in the range of smaller gap widths. Tabor and Winterton were the first to achieve this goal [81, 82] by using mica and by modifying the method of crossed fibers [22, 83]. The molecular attractive force F was measured between glass cylinders ($R_0 = 1$ cm) covered with sheets of muscovite mica several micrometers thick and crossed at right angles. The distance H between molecularly smooth mica surfaces was measured by the Tolansky method of multiple beam interferometry to an accuracy of about 3 Å, using white light and by observing fringes of identical color (identical wavelength) through optical filters. In order to observe multiple interference, the backs of the mica sheets were covered with semitransparent silver layers. This technique made it possible to determine not only the shortest distance H between the surfaces, but the shape of the gap as well.

Attractive forces were evaluated by the jump method introduced earlier by Overbeek and Sparnaay [21]. The method consists in finding a separation H_c between the objects that disturbs the stable equilibrium between the attractive force and the elastic resistance $F = \alpha x$ (x being the displacement) of a flat spring to which the upper glass cylinder is fixed. At this point, the gap between the plates "collapses." Replaceable springs with different stiffness α were used. The lower cylinder was fixed rigidly and could be shifted vertically in a controlled manner by short distances (up to 2 mm, to within 1 Å) by a micrometer screw and piezoelectric quartz in order to bring it closer to the upper cylinder [81, 82].

In this method the attractive force F could be found as a function of distance if the theoretical dependence $F(H)$ was chosen in advance. In the case of crossed cylinders of identical radius R_0 the expression for nonretarded forces was given by Derjaguin [11] as

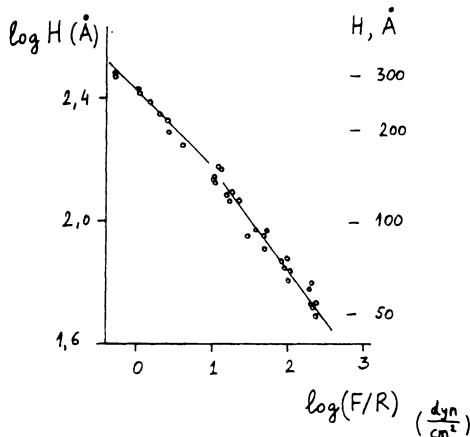


Fig. 4.17. The results of the first measurements of nonretarded molecular attractive forces between molecularly smooth mica surfaces [81].

$$F(H) = 2\pi R_0 U(H) = \frac{R_0 A_{101}}{6H^2} \quad (4.49)$$

where A_{101} is a constant found from Eq. (4.24) for the mica-air-mica system.

By equating the forces F and their derivatives $\partial F / \partial x$ at the jump point, we find

$$A_{101} = 3H_c^3 \alpha / R_0 \quad (4.50)$$

Correspondingly, in the range of full retardation we obtain

$$B = H^4 \alpha / 2\pi R_0 \quad (4.51)$$

Figure 4.17 shows the results of first measurements of Tabor and Winterton [81]. Values of $\log(\alpha/R_0)$, with $\log H$ on the ordinate axis, are marked on the abscissa axis. Experimental points correspond to the values of H_c obtained for different spring stiffnesses α . Figure 4.17 clearly shows that these points fall on two linear segments, one of which (at $H \leq 100 \text{ \AA}$) fits Eq. (4.48) with $A_{101} = 10^{-12} \text{ erg}$, and another (at $H \geq 200 \text{ \AA}$) fits Eq. (4.49) with $B = 0.87 \cdot 10^{-19} \text{ erg} \cdot \text{cm}$. The value obtained for the Hamaker constant is quite close to that theoretically calculated from Eq. (4.24) for mica: $A_{101} = 1 \cdot 10^{-12} \text{ erg}$ [28]. The value of A_{101} was found by means of Eqs. (4.30) and (4.31) using the following spectral characteristics of mica: $\epsilon_0 = \epsilon_\alpha = 5.4$, $\epsilon_b = n^2 = 2.43$, and $\omega_b = 7 \cdot 10^{14}$

rad/s. The chosen value of $\omega_c = 1.77 \cdot 10^{16}$ rad/s corresponds to the ionization potential of quartz. Richmond and Ninham used various spectral data and found that, depending on the calculation scheme, A_{101} of mica may be from $0.7 \cdot 10^{-12}$ to $6.4 \cdot 10^{-12}$ erg [84].

The constant B, first obtained by Tabor and Winterton for mica, perfectly coincided with the theoretical value given by Eq. (4.25) in which, as in experiments with quartz [19], ϵ_0 for mica was chosen as $n^2 = 2.43$.

Figure 4.17 demonstrates that the transition from full nonretarded molecular forces to full retarded forces is fairly sharp, taking place over a relatively narrow interval of about 100 Å. Measurements were carried out at H from 50 to 300 Å in air, with water vapor not removed. Consequently, interacting surfaces were covered with adsorbed water film 7 ± 2 Å thick. This film was regarded as "joined" to the solid, and H was measured off the film surface. Water film ensured the removal of surface charge in the course of measurements.

For cylinders of a different radius R_0 , the values obtained for A_{101} differed by not more than 15%, thus lying within the total error of the measurements.

Later this study was successfully extended by Israelachvili and Tabor [85], who were able to widen the experimental range of spacings between mica surfaces down to $H = 15$ Å and up to 1300 Å. The jump method was used to repeat the measurements of nonretarded forces (in the range $15 < H < 120$ Å). The constant obtained was $A_{101} = (1.35 \pm 0.15) \cdot 10^{-12}$ erg. This is somewhat higher than the result of the first experiments, but it was measured with greater accuracy and can be regarded as more reliable. Several replaceable springs were substituted with a single one whose stiffness was varied by changing the length by shifting the fixed point on the spring. This made possible continuous measurements without dismantling the setup.

The jump technique failed at distances above 200 Å, because the effect of vibration increased with reduced stiffness of the spring. In order to cover larger distances, Israelachvili and Tabor developed a novel technique [85]. Their method was based on measuring the frequency of vibrations of the upper cylinder, suspended on a stiff spring, which were induced by vibrations of the lower cylinder at a frequency f , and transferred to the upper one through the force of molecular attraction. Measurements were carried out in an evacuated chamber ($5 \cdot 10^{-5}$ mm Hg). The vibrations of the lower cylinder were driven at a predetermined frequency $f \approx 100$ Hz and small amplitude (about 1 Å). The force of molecular attraction $F_m = K/H^m$ was calculated from such distance H_0 and such frequency f_0 of the vibrations of the lower cylinder

for which $\partial F/\partial x = 0$ (where $F = \alpha x + F_m$), so that oscillations of the lower cylinder were not transferred to the upper one. The value of H_0 was related to the constants K and m via the equation

$$H_0 = (mK/\alpha)^{1/(m+1)} \quad (4.52)$$

The distance H between the bodies was slowly changed at a fixed frequency $f < f_D$ until the vibrations of the upper cylinder stopped, indicating that $H = H_0$. Then, knowing the stiffness of the spring α , and the exponent in the law of molecular force m , it was possible to find K . As before, the distance H_0 was measured by optical interferometry.

Among other things, the resonant technique made it possible to check the value of the exponent m in the law of molecular force written in the form

$$F_m = K/H^m \quad (4.53)$$

where $K = A_{101}R_0/6$ for nonretarded forces ($m = 2$), and $K = 2\pi BR_0/3$ for fully retarded forces ($m = 3$).

It was shown that $m = 2$ in the range $H \leq 120 \text{ \AA}$, and $m = 3$ when $H \geq 500 \text{ \AA}$. The value of m gradually increases in the transition region from 2 to 3 as H increases from 120 to 500 \AA . The constant B in the range of full retardation was found to be $(0.97 \pm 0.06) \times 10^{-19} \text{ erg}\cdot\text{cm}$, agreeing closely with the theoretical value calculated by Richmond and Ninham [84]: $B = 0.93 \cdot 10^{-19} \text{ erg}\cdot\text{cm}$.

These data were later reanalyzed [86] by employing more precise spectral data for mica. The analysis showed that the experimental results of Tabor and Israelachvili agree with the theory only if one assumes that the radius of curvature R_0 of cylindrical surfaces was overestimated by about 30%.

However, the possibility of such large local variation of surface curvature at the contact point seems hardly plausible. Consequently, deviations are most probably caused by inadequately studied spectral characteristics of the muscovite used in the experiments. Furthermore, optical properties of surface layers may deviate from the bulk properties of mica whose spectral characteristics were used in the calculations.

The effect of surface roughness on measured results also remains a matter of some doubt. Sparnaay recently demonstrated [87] that roughness manifests itself when it exceeds 10-20% of the gap width. The effect of 3 to 5 \AA molecular-scale roughness (or, what is the same, of surface heterogeneity) may be appreciable when non-retarded forces are measured at small distances $H \approx 30-50 \text{ \AA}$.

Czarnecki and Dabros [88] estimated the effect of surface roughness of a spherical particle on the energy of its attraction $U(H)$ to a plane by integrating molecular pair interactions. Roughness reduces $U(H)$ the more, the greater the particle radius and the lower H . The effect of the shape of the roughness is smaller than that of its height.

Experiments of Israelachvili and Tabor [85] with monolayers of stearic acid (of thickness $\delta = 25 \text{ \AA}$) deposited onto mica by the Langmuir-Blodgett method demonstrated that molecular attraction was the same as for bulk mica at $H > 50 \text{ \AA}$ (H being measured off the outer surface of the monolayers). Deposited monolayers affect the molecular interaction only when $H \leq 30 \text{ \AA}$.

This effect occurs because the main contribution to the dispersion interaction is made by surface layers of the interacting bodies, with thickness of the order of the separation H between the bodies. This conclusion follows directly from Eq. (4.43) if δ in this equation is treated as the thickness of the surface layer. As follows from (4.43), the main contribution to $U(H)$ at $H \leq \delta$ is made by the first term. This term is determined by the constant C , which depends only on the dielectric properties of the layers δ and of the interlayer H [see Eqs. (4.44) and (4.45)]. The effect of the material below the layer δ is the weaker, the smaller H is compared with δ .

Wittmann et al. [39] developed an ingenious technique for measuring molecular forces, consisting in observing the elastic deformation (sagging) of a thin quartz platelet supported at one end by a massive quartz slab and at the other end by a spacer only $0.16 \mu\text{m}$ thick. The platelet sags because of molecular attraction to the quartz slab. The profile of the gap $H(x)$ between the platelet and the slab depends on the distributed attractive force $F(x)$. Equations of elasticity theory make it possible to relate the profile $H(x)$ to the quartz elasticity modulus E_0 and the distributed force $F(x)$, i.e., to find the function $F(H)$. The gap profile $H(x)$ is determined by optical interferometry.

However, since $F(H)$ is found by determining the fourth derivative of profile $H(x)$ with respect to x , the accuracy of measuring $F(H)$ is rather poor. The value of A_{101} obtained for H from 80 to 150 \AA was $5.7 \cdot 10^{-13} \text{ erg}$, somewhat lower than the theoretical value for quartz, $A_{101} = 7.9 \cdot 10^{-13} \text{ erg}$ [32]. The constant B for H from 500 to 1000 \AA was found to be $1.2 \cdot 10^{-19} \text{ erg} \cdot \text{cm}$. This is approximately twice the theoretical value given above ($B = 0.6 \cdot 10^{-19} \text{ erg} \cdot \text{cm}$), because of the incompletely developed retardation at $H \leq 1000 \text{ \AA}$. Insufficient accuracy prevented further elaboration of this technique.

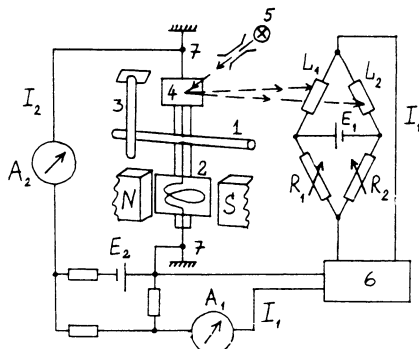


Fig. 4.18. Schematic representation of the experimental setup for direct measurements of molecular forces by the method of crossed fibers.

Coakley and Tabor [89] employed the jump technique to measure nonretarded forces ($H < 200\text{--}300 \text{ \AA}$) between 13 monolayers of calcium stearate (total thickness 340 \AA) deposited on each surface of mica by the Langmuir-Blodgett method, and also between mica and silver. In the latter case one of the mica surfaces was coated in vacuum with a silver film 500 \AA thick, on the outer side only. Measurements were conducted in air. The following constants were obtained: $A_{101} = (1.8 \pm 0.3) \cdot 10^{-12} \text{ erg}$ for the mica-mica system, $A_{101} = (1.1 \pm 0.3) \cdot 10^{-12} \text{ erg}$ for the stearate-stearate system, and $A_{102} = (3.3 \pm 0.5) \cdot 10^{-12} \text{ erg}$ for an asymmetric mica-air-silver system. All these Hamaker constants much exceed the theoretical predictions. Coakley and Tabor [89] connect this effect, as in [86], to a deformation (flattening) of the convex surface of mica in the neighborhood of the contact, and a slight increase in the local values of R_0 [see Eq. (4.50)]. They could not exclude the possibility of plastic or viscoelastic deformation in the interlayer of glue fixing a mica platelet to a glass cylinder. From this standpoint, experiments involving bulk solids with sufficiently smooth, for instance, fused surfaces are preferable.

In our laboratory we have developed a different method of direct measurement of molecular forces [90-94], based on the idea of modeling the contact between colloidal particles by means of thin crossed fibers (1-2 mm in diameter) [83, 22]. The experimental setup is shown schematically in Fig. 4.18.

A movable fiber 1 is fixed to the coil 2 of a mirror galvanometer, and the second fiber 3 is fixed. The galvanometer is in a photocompensation circuit with negative feedback. This circuit includes a mirror 4 fixed to the galvanometer coil, illuminated by a light beam from a source 5. The reflected beam falls on two photo-

resistors L_1 and L_2 in a bridge circuit. When the coil 2 with the movable fiber 1 rotates, the mirror 4 turns and the photoresistors are illuminated differently, thereby changing the resistances L_1 and L_2 . Two resistance boxes R_1 and R_2 make it possible to control the position of the mirror and the movable fiber. When R_1 and R_2 are such that the current in the bridge diagonal is zero, the coil 2 is at rest. Any fortuitous deflection of the coil causes the return to the equilibrium position because the current generated in the deflected coil interacts with the magnetic field and always rotates it in the direction opposite to the deflection.

The equilibrium position of the coil can be changed by varying one (or both) of the resistances R_1 and R_2 . This shifts the coil to a new position in which the ratio of photoresistors L_1 and L_2 is such that the current in the bridge diagonal again vanishes. Therefore, the stable position of the fiber 1 with respect to the fiber 2 can be changed in a controlled manner by varying R_1 and R_2 . After an appropriate calibration, it is possible to preset certain separations H between the fibers, choosing the contact position for the reference point, i.e., $H = 0$.

If the crossed fibers 1 and 3 are brought together to a distance H at which molecular forces are appreciable, the fiber 1 will be slightly shifted to a new equilibrium state, such that in this state there will be a current I_1 through the coil, proportional to the force of molecular attraction between the fibers. The out-of-balance current in the bridge is amplified by the amplifier 6 and measured with a microammeter A_1 . However, in order to preset the new separation between the fibers, the bridge must be brought to balance again, by passing through the coil and the bridge a counter-current from a controlled current supply unit E_2 . Then the resistances R_1 and R_2 at $I_{A_1} = 0$ yield the separation H , and the compensating current I_2 recorded by the microammeter A_2 yields the force. The readings of A_2 are converted to the values of force F by calibration.

One important advantage of the method is that measurements are possible not only with transparent but also with opaque objects, including metals.

Experiments were conducted with freshly drawn glass and fused quartz fibers with radii R_0 about 0.5 mm, and with electrochemically polished gold and platinum wires with radii from 0.15 to 0.5 mm. Figure 4.19 shows the results of measurements of the molecular interaction $F(H)$ between crossed fibers in air, converted via the Derjaguin equation [11] into values of specific energy of molecular attraction between flat surfaces, $U(H)$:

$$U(H) = F(H)/2\pi\sqrt{R_1 R_2} \quad (4.54)$$

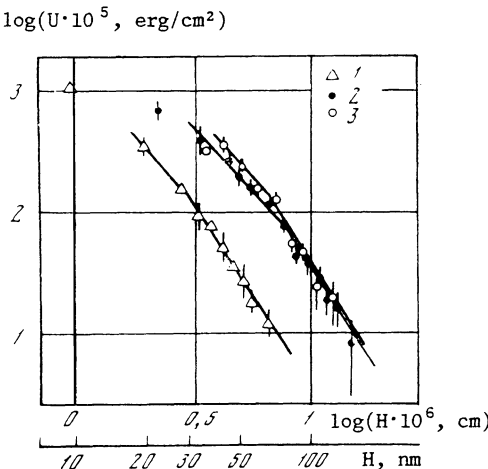


Fig. 4.19. Experimental curves for specific energy $U(H)$ of molecular attraction for quartz (points 1) and platinum (points 2 and 3) obtained by the crossed fibers technique: 1) $R_1 = 0.4$ mm, $R_2 = 0.57$ mm; 2) $R_1 = 0.5$ mm, $R_2 = 0.15$ mm; 3) $R_1 = R_2 = 0.15$ mm.

where R_1 and R_2 are the radii of the fibers. The range of spacings H covered by the measurements was from 100 to 1500 Å.

The curves $U(H)$ are plotted in Fig. 4.19 on a logarithmic scale. As in the experiments of Tabor et al., the experimental data can be approximated by two straight-line segments corresponding to nonretarded and fully retarded forces, and thus give the corresponding values of the constants A_{101} and B :

$$U(H) = A_{101}/12\pi H^2; \quad U(H) = B/3H^3 \quad (4.55)$$

The constants obtained for quartz were $A_{101} = 4.5 \cdot 10^{-13}$ erg and $B = 1 \cdot 10^{-19}$ erg·cm, close to the data reported by other authors. The values of A and B for platinum, not measured before, were: $A_{101} = 2 \cdot 10^{-12}$ erg and $B = 1 \cdot 10^{-18}$ erg·cm, respectively. The first value cannot be compared to prior results because no theoretical calculations of A_{101} were published for platinum. The constant B is quite close to the theoretical value for metals, viz., $1.3 \cdot 10^{-18}$ erg·cm.

Another confirmation of the validity of Eq. (4.54), and of the method of calculation of $U(H)$ according to Derjaguin [11], is the close agreement of the sets of points 2 and 3 in Fig. 4.19 obtained for the pairs of fibers of substantially different radii.

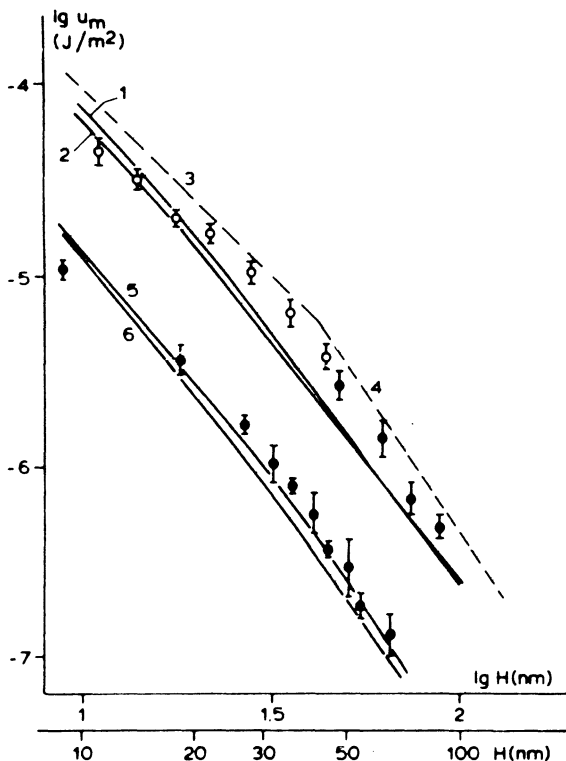


Fig. 4.20. Comparison of the experimental curves for specific energy $U(H)$ of molecular attraction for gold with theoretical calculations (curves 1-4).

Measurements become inaccurate at $H < 100 \text{ \AA}$ for quartz and at $H < 300 \text{ \AA}$ for platinum, owing to the effect of surface roughness, which is especially well pronounced for metal wires. For the same reason attempts to carry out accurate measurements of the constant A_{101} on gold wires were unsuccessful. The constant B for gold was found to be close to that for platinum.

Further modification of the measurement system by increasing the slope of feedback enabled us to improve the accuracy, mostly in the range of short distances in which the derivative $\partial F/\partial H$ is large. The advantages of the electronic feedback were especially manifested here because with mechanical stabilization of the body position an increase in spring stiffness diminishes the sensitivity of the setup.

In order to work in the range of short distances H fibers were replaced with smoother fused gold beads with radii from 0.3 to 0.75 mm. Figure 4.20 plots the force of molecular attraction between

spheres $F(H)$, recalculated according to Derjaguin [11] into specific energy of attraction

$$U(H) = F(H)(R_1 + R_2)/2\pi R_1 R_2$$

Filled circles in the range $H > 500 \text{ \AA}$ represent data obtained by the method of crossed gold wires and are taken from the preceding figure (Fig. 4.19). Unfilled circles represent the data for gold beads. It was possible to extend the measurements down to $H = 100 \text{ \AA}$, as with fused quartz (Fig. 4.19).

As in earlier experiments, it was again possible to evaluate A_{101} and B . For gold we find $A_{101} = 2.5 \cdot 10^{-12} \text{ erg}$, much lower than the theoretical value $A_{101} \approx 4 \cdot 10^{-12} \text{ erg}$ [44, 59]. (This discrepancy will be discussed below.) Naturally, the constant $B \approx 1 \cdot 10^{-19} \text{ erg} \cdot \text{cm}$ retained the same value as for crossed wires.

In view of the improved accuracy of measurements, it was expedient to compare the experimental results not only with the asymptotic formulas but also with more precise calculations using Eq. (4.22). Calculations were run on a computer, and up to $N = 3000$ terms of the series were taken, integration over p being from 1 to 500 [93]. A reduction of N and p by a factor of 1.5 left the results practically unaltered, giving a check for their accuracy.

The function $\epsilon(i\xi)$ for gold was calculated as follows. In the frequency range $\xi \leq 2 \cdot 10^{16} \text{ rad/s}$ the data of [44] were used. At higher frequencies we used, as before, the data of [31], and the plasma equation (4.31). Curve 1 in Fig. 4.20 plots $U(H)$ calculated with the exact equation (4.22) of the macroscopic theory. Curve 2 in Fig. 4.20 represents the calculations with a simplified equation taking into account electromagnetic retardation for metals [95]:

$$U(H) = - \frac{A_{101}}{12\pi H^2} \left\{ 1 - \frac{1}{[1 + (bc/H)]^2} \right\} - \frac{\hbar c}{16\pi^2 H^3} \left\{ 1 - [1 + (\xi_0 H/c)] \exp \left(- \frac{2\xi_0 H}{c} \right) \right\} \quad (4.56)$$

where $b = 3 \cdot 10^{-17} \text{ s/rad}$ (see Table 4.1), c is the velocity of light, and $\xi_0 = 8 \cdot 10^{14} \text{ rad/s}$ is the cut-off frequency at which the condition

$$\epsilon \xi \leq \xi_0 \gg \sqrt{\epsilon} \gg 1$$

is satisfied [95].

As seen from Fig. 4.20, this simplified equation yields results not very different from those of curve 1.

In the range from 120 to 250 Å curves 1 and 2 are in satisfactory agreement with the experimental data. At larger H , deviations are especially pronounced (up to 60%) at $H \approx 400$ Å. In all likelihood this discrepancy reflects insufficient accuracy of spectral data. Thus, the fit improves if absorption in the IR part of the spectrum for gold is somewhat raised.

Curves 3 and 4 in Fig. 4.20 are plotted by using the asymptotic equations (4.24) and (4.25), respectively. Curve 3 corresponds to the constant $A_{101} = 4.1 \cdot 10^{-12}$ erg theoretically calculated for gold [44]. In the range from 100 to 400 Å the experimental data yield a lower value $A_{101} = 2.5 \cdot 10^{-12}$, close to that obtained for platinum.

It appears reasonable to treat as more reliable not the value of A_{101} calculated in the range $100 < H < 400$ Å where electromagnetic retardation is appreciable, but that found by means of Eq. (4.56) where the constant A_{101} corresponds to the condition $H \rightarrow 0$. The best fit of the experimental points with Eq. (4.56) in the range $100 < H < 300$ Å yields the value $A_{101} = 3.8 \cdot 10^{-12}$ erg, in much better agreement with the theory.

For the constant B calculated by fitting the experimental points in the range $400 < H < 800$ Å to the asymptotic equation (4.25) we find $B = 0.91 \cdot 10^{-18}$ erg·cm, lower than the theoretical value $B = 1.3 \cdot 10^{-18}$ erg·cm for metals. Possibly, this discrepancy is a result of only partial retardation of the electromagnetic interaction in the range $400 < H < 800$ Å. As was shown above (Fig. 4.13), full retardation occurs when $H \geq 1$ μm.

The logical conclusion is that the results of measurements in the range of H from 100 to 1000 Å, plotted in Fig. 4.20, must not be compared with asymptotic solutions. Their interpretation must be based either on the exact equations of the theory, (4.22) and (4.23), or on simplified solutions (4.29) and (4.39), or on (4.56) taking into account electromagnetic retardation.

Measurements of molecular forces between model objects not in vacuum or air but in liquids are considerably more complicated and less ambiguous. This happens because the results are affected by other components of disjoining pressure acting simultaneously, as well as by the viscosity of the liquid which prevents rapid establishment of equilibrium. In order to determine molecular forces, it is necessary to subtract the electrostatic, structural, and adsorptional forces from the total force of interaction measured in the experiment. These components cannot always be found as functions of interlayer thickness with sufficient accuracy; consequently, the accuracy of deducing molecular forces is usually poor.

The effect of viscosity is effectively reduced by using the method of crossed fibers or cylinders. Viscous resistance is then quite small because of the nearly point-contact geometry.

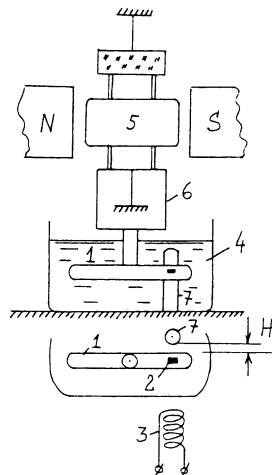


Fig. 4.21. Schematic diagram of the modified setup for direct measurements of long-range surface forces in liquid media.

Despite serious difficulties, it has been possible in some cases to carry out more or less reliable measurements of molecular forces by suppressing the electrostatic and structural components of disjoining pressure (e.g., by a high concentration of the electrolyte). Thus, Rabinovich et al. [31, 92, 96], and Israelachvili and Adams [97] were able to measure molecular forces in electrolyte solutions by employing essentially the same measurement techniques as in air or vacuum.

Israelachvili and Adams [97] made measurements for the mica-aqueous electrolyte solution-mica system in the range of concentration C of a 1-1 electrolyte, KNO_3 , from 0.1 to 1 mole/liter and a 2-1 electrolyte, $\text{Ca}(\text{NO}_3)_2$, from 0.01 to 0.1 mole/liter, when electrostatic forces are largely suppressed. Here the forces in the range $40 < H < 150 \text{ \AA}$ are mostly those of molecular attraction; this corresponds to the farther edge of the secondary potential well. The value obtained for the Hamaker constant $A_{131} = (2.2 \pm 0.3) \cdot 10^{-13} \text{ erg}$ was independent of the concentration of the electrolytes. Electromagnetic retardation became apparent for $H > 65 \text{ \AA}$.

While Israelachvili's setup required almost no design alterations for measurements in liquids, the setup for measuring molecular forces in liquids by the crossed fibers technique had to be substantially modified [92]. The new arrangement is shown in Fig. 4.21. The mobile quartz fiber 1 was made hollow, and a piece of permanent magnet 2 was inserted into it. This magnet interacted

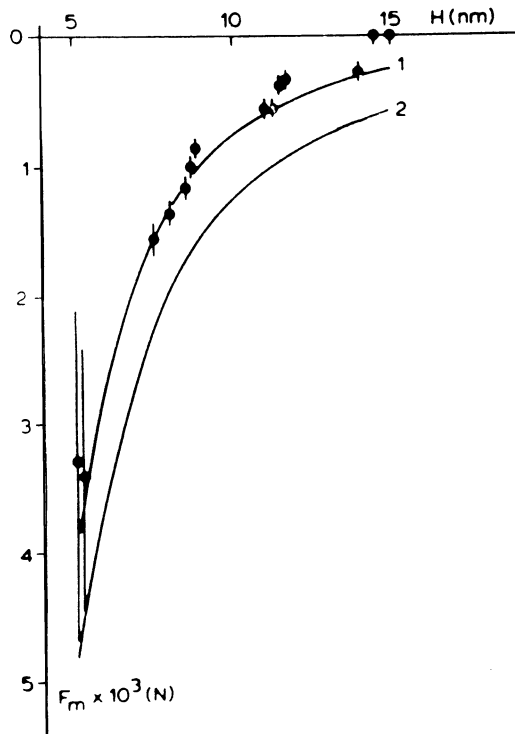


Fig. 4.22. Molecular attractive force F_m as a function of distance H between glass fibers ($R_0 = 0.5$ mm) in a 0.1 N KCl solution.

with the magnetic field of a solenoid 3 placed outside the container 4 with the solution. The quartz fiber 1 was fixed to the coil 5 of a galvanometer on a bracket 6; the fiber and the coil had a common axis of rotation.

As with measurements in air, the movable fiber 1 was moved away from the fixed fiber 7 by a tracking device to a distance greater than the radius of interaction forces. When the gap was then gradually reduced, interaction forces grew stronger, and were compensated and measured by a current I fed through the solenoid 3. The current I was increased until the current in the galvanometer coil vanished, indicating complete compensation of the interaction force F . This force could be determined from the current I , after a preliminary calibration.

Since the force acting on the magnet 2 in the modified setup is applied at the same point as that of the force of interaction between crossed fibers, the bending of the suspension 6, and hence

the error of measurements, was drastically reduced. A similar system for compensating a force was successfully applied earlier by Babak et al. [98].

Figure 4.22 shows the molecular attractive force F_m as a function of distance H between glass fibers in 0.1 N KCl solution in the range of H from 50 to 150 Å. The experimental points were obtained by subtracting the force of electrostatic repulsion F_e between fibers [31] from the measured force $F(H)$:

$$F_m = F - F_e = F - \frac{128CkTR_0}{\kappa} \tanh^2\left(\frac{e\psi_1}{4kT}\right) \exp(-\kappa H) \quad (4.57)$$

where C is the electrolyte concentration, R_0 is the fiber radius, κ is the reciprocal Debye radius, and ψ_1 is the potential of the fiber surface. Calculations involved the assumption of the independence of the potential ψ_1 of the distance between fibers.

The theoretical curve 1 in Fig. 4.22 plots Eqs. (4.29) and (4.37) assuming $A_0 = 1.35 \cdot 10^{-13}$ erg and $\psi_1 = -50$ mV. This last value was found from the equation for $F_e(H)$ using the experimentally obtained values of $F(H)$ in the range $30 < H < 50$ Å where the molecular attractive forces are small and $F \approx F_e$.

The theoretical curve 2 plots the asymptotic equation (4.24) for nonretarded forces, assuming the same value $A_{131} = A_0 = 1.35 \cdot 10^{-13}$ erg. The comparison of the curves 1 and 2 shows that the agreement with experimental data is improved by taking into account electromagnetic retardation in Eq. (4.29). The best-fit value $A_{131} = 1.35 \cdot 10^{-13}$ erg of Eq. (4.29) is close to that of Israelachvili and Adams for mica ($A_{131} = 2.2 \cdot 10^{-13}$ erg) [97].

The joint action of molecular and electrostatic forces manifests itself especially clearly in the range of the secondary potential well. Measurements of $F(H)$ are known to reflect the behavior of the potential energy curve $U(H)$ for the interaction of flat surfaces. Figure 4.23 plots the results of direct measurements of the total force F as a function of distance between glass fibers in a 10^{-1} mole/liter solution of KCl. The shape of the right-hand (farther) wall of the potential well is mostly determined by molecular attractive forces $F_m < 0$. The experimental points shown in Fig. 4.22 in fact referred (after a small correction for the effect of F_e) to this part of the $F(H)$ curve. Repulsive forces connected with the predominant effect of electrostatic forces sharply increase when $H < 50$ Å. The potential ψ_1 of the fiber surface was calculated precisely from this part of the curve $F(H)$.

The depth of the force well is seen from Fig. 4.23 to be about 10^{-3} dyn, and that of the potential well about $3 \cdot 10^{-3}$ erg/cm².

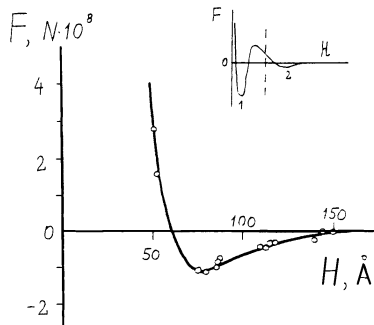


Fig. 4.23. Force F as a function of distance H between glass fibers ($R_1 = 0.5$ mm, $R_2 = 0.6$ mm) in a 0.1 mole/liter KCl solution.

Israelachvili and Adams obtained a similar well depth in 0.1 N solutions of KNO_3 [97], and these results have recently been confirmed by Knapschinsky et al. [99] in a 0.1 N solution of KCl, by means of a modified crossed-fibers technique.

Thin flat films, both wetting and free (see Chapter 10), constitute good objects for direct determination of molecular forces acting through liquid interlayers. Measurements are facilitated here because the disjoining pressure of a flat film Π is readily measurable at equilibrium from the capillary pressure of the meniscus, $P_k = \Pi$, with which the film is in contact. It will be shown in Chapter 10 that this method can also be used successfully for a direct test of the theory of molecular forces.

Concluding this chapter we can say that the macroscopic theory of molecular forces, whose development was initiated by Lifshitz [17, 18], has been reliably confirmed by direct experimental measurements by a number of techniques in various laboratories.

Discrepancies found in certain cases between theory and experiment probably result from incomplete information on the spectral characteristics of the interacting bodies. This raises an important question whether the spectral properties of bulk specimens are identical to those of the surface layers that contribute to the forces of molecular interaction; their influence is the greater, the thinner the interlayer between the bodies. Spectral characteristics of small particles are known to differ substantially from those of bulk specimens [100, 101]. This is especially significant for metals and semiconductors in which we are aware of special surface states of the electron gas; also, of course, oxide (dielectric) surface films of different thickness can be formed. Furthermore,

the surface layers of certain solids and liquids may be substantially altered in structure.

Another, no less important, problem is to take account correctly of the microscopic heterogeneity of the surface and of its roughness affecting the local curvature radii R_1 and R_2 at the nearest points of the approaching surfaces. Special model experiments must be carried out in order to deal with the regular roughness and heterogeneity of the surface.

The possibilities of controlling the forces of molecular interaction by external fields are not yet adequately known. For example, excitation of electron states by irradiating a semiconductor with visible or ultraviolet light; resonant absorption of x rays; application of electric fields to polar liquids, affecting the state of their polarization.

REFERENCES

1. A. C. Clairault, *Théorie de la Figure de la Terre*, Paris (1743).
2. P. S. Laplace, *Theorie de l'Action Capillaire*, Paris (1806).
3. P. N. Lebedev, *Wiedemann Ann.*, 52, 621 (1894); *Collected Works*, Moscow (1913), p. 56.
4. F. London, *Z. Phys. Chem.*, 11, 222 (1931).
5. B. V. Derjaguin, I. I. Abrikossova, and F. B. Leib, *Vestn. Akad. Nauk SSSR*, No. 6, 125 (1951).
6. B. V. Derjaguin and I. I. Abrikossova, *Zh. Eksp. Teor. Fiz.*, 21, 445 (1951); *Dokl. Akad. Nauk SSSR*, 90, 1055 (1953); 108, 214 (1956); *Zh. Eksp. Teor. Fiz.*, 30, 993 (1956); 31, 3 (1956); 33, 799 (1957).
7. B. V. Derjaguin and I. I. Abrikossova, *Discuss. Faraday Soc.*, 18, 24 (1954); *J. Phys. Chem. Solids*, 5, 1 (1958); *Sci. Am.*, 203, 47 (1960); B. V. Derjaguin, I. I. Abrikossova, and E. M. Lifshitz, *Q. Rev.*, 10, 295 (1956).
8. B. V. Derjaguin, *Dokl. Akad. Nauk SSSR*, 61, 275 (1948).
9. B. V. Derjaguin, K. K. Timofeev, I. I. Abrikossova, and Yu. N. Sachkov, *Inventor's Certificate* (USSR), No. 98706 (1951).
10. B. V. Derjaguin, K. K. Timofeev, I. I. Abrikossova, and Yu. N. Sachkov, *Mater. Tekh. NIIvesprom.*, No. 2, 78 (1952).
11. B. V. Derjaguin, *Kolloidn. Z.*, 69, 155 (1934); *Zh. Fiz. Khim.*, 6, 1306 (1935).
12. H. B. Casimir and D. Polder, *Phys. Rev.*, 73, 36 (1948); H. B. Casimir, *Proc. Nederl. Acad. Wetenschap.*, B51, 793 (1948).
13. J. H. de Boer, *Trans. Faraday Soc.*, 32, 16 (1936).
14. H. C. Hamaker, *Recl. Trav. Chim.*, 55, 1015 (1936); 56, 3 (1937); *Physica*, 4, 1059 (1937).
15. S. M. Rytov, *Theory of Electrical Fluctuations and Thermal Radiation*, Izd. Akad. Nauk SSSR, Moscow (1953).

16. L. D. Landau and E. M. Lifshitz, *Electrodynamics of Continuous Media*, Addison-Wesley, Reading, Mass. (1960).
17. E. M. Lifshitz, *Dokl. Akad. Nauk SSSR*, 97, 643 (1954); 100, 879 (1955).
18. E. M. Lifshitz, *Zh. Eksp. Teor. Fiz.*, 29, 94 (1955).
19. B. V. Derjaguin, I. I. Abrikossova, and E. M. Lifshitz, *Usp. Fiz. Nauk*, 64, 493 (1958); *Q. Rev.*, 10, 295 (1956).
20. H. Margenau, *Rev. Mod. Phys.*, 11, 1 (1939).
21. J. Th. G. Overbeek and M. J. Sparnaay, *J. Colloid Sci.*, 7, 343 (1952); *Discuss. Faraday Soc.*, 18, 24 (1954).
22. B. V. Derjaguin, A. S. Titijevskaia, I. I. Abrikossova, and A. D. Malkina, *Discuss. Faraday Soc.*, 18, 24 (1954); B. V. Derjaguin and I. I. Abrikossova, *Discuss. Faraday Soc.*, 18, 182 (1954).
23. A. F. Prosser and J. A. Kitchener, *Nature*, 178, 1339 (1956); *Proc. R. Soc. London*, A242, 403 (1957).
24. W. Black, J. G. V. de Jongh, J. Th. G. Overbeek, and M. J. Sparnaay, *Trans. Faraday Soc.*, 56, 1597 (1960).
25. I. E. Dzyaloshinsky, E. M. Lifshitz, and L. P. Pitayevsky, *Zh. Eksp. Teor. Fiz.*, 37, 229 (1959); *Usp. Fiz. Nauk*, 73, 381 (1961); *Adv. Phys.*, 10, 165 (1961).
26. J. Mahanty and B. W. Ninham, *Dispersion Forces*, Academic Press, New York (1976).
27. E. J. W. Verwey and J. Th. G. Overbeek, *Theory of the Stability of Lyophobic Colloids*, Elsevier, Amsterdam (1943).
28. N. V. Churaev, *Kolloidn. Zh.*, 959 (1972).
29. N. F. Owens and P. Richmond, *J. Chem. Soc., Faraday Trans. II*, 74, 691 (1978).
30. W. A. B. Donners, J. B. Rijnbout, and A. Vrij, *J. Colloid Interface Sci.*, 60, 540 (1977).
31. Ya. I. Rabinovich and N. V. Churaev, *Kolloidn. Zh.*, 41, 468 (1979).
32. N. V. Churaev, *Kolloidn. Zh.*, 37, 730 (1975).
33. H. Krupp, *Adv. Colloid Interface Sci.*, 1, 111 (1967).
34. V. A. Parsegian and B. W. Ninham, *Nature*, 224, 1197 (1969).
35. B. W. Ninham and V. A. Parsegian, *J. Chem. Phys.*, 52, 4578 (1970).
36. N. V. Churaev, *Kolloidn. Zh.*, 36, 318, 324 (1974).
37. R. Pashley, *J. Colloid Interface Sci.*, 62, 344 (1977).
38. V. A. Parsegian and G. H. Weiss, *J. Colloid Interface Sci.*, 81, 285 (1981).
39. F. Wittmann, H. Splittgerber, and K. Ebert, *Z. Phys.*, 245, 354 (1971).
40. R. Evans and D. H. Napper, *J. Colloid Interface Sci.*, 45, 138 (1973).
41. H. Ehrenreich and H. P. Philipp, *Phys. Rev.*, 128, 1622 (1962).
42. B. R. Cooper and H. Ehrenreich, *Phys. Rev.*, 138, 494 (1965).
43. T. S. Moss, *Optical Properties of Semiconductors*, Butterworths, London (1959).
44. V. M. Muller and N. V. Churaev, *Kolloidn. Zh.*, 36, 492 (1974).

45. H. J. Hagemann, W. Gudat, and C. Kunz, Optical Constants from the Far Infrared to the X-Ray Region, DESY SR-7417, Hamburg (1974).
46. J. Visser, Adv. Colloid Interface Sci., 3, 331 (1972).
47. C. S. Vassilieff and I. B. Ivanov, Colloid Polymer Sci., 254, 431 (1976); 256, 1142 (1978); 259, 772 (1981).
48. Ya. I. Rabinovich, Kolloidn. Zh., 41, 1146 (1979).
49. D. Chan and P. Richmond, Proc. R. Soc. London, A353, 163 (1977).
50. Ya. I. Rabinovich and N. V. Churaev, Kolloidn. Zh., 46, 69 (1984).
51. N. G. van Kampen, B. R. A. Nijboer, and K. Schram, Phys. Lett., A26, 307 (1968).
52. E. Gerlach, Phys. Rev., B4, 393 (1971).
53. Yu. S. Barash and V. L. Ginzburg, Pis'ma Zh. Eksp. Teor. Fiz., 15, 567 (1972); Usp. Fiz. Nauk, 116, 5 (1975).
54. B. W. Ninham and V. A. Parsegian, J. Chem. Phys., 53, 3398 (1970).
55. D. Langbein, J. Phys. Chem. Solids, 32, 133 (1971); J. Adhesion, 3, 213 (1972).
56. D. Langbein, J. Adhesion, 6, 1 (1974).
57. N. V. Churaev, Colloid Polymer Sci., 253, 120 (1975).
58. D. Y. C. Chan, D. J. Mitchell, B. W. Ninham, and B. A. Pailthorpe, Mol. Phys., 35, 1669 (1978).
59. V. A. Parsegian and G. H. Weiss, J. Colloid Interface Sci., 40, 35 (1972).
60. V. N. Gorelkin and V. P. Smilga, Kolloidn. Zh., 34, 685 (1972); Dokl. Akad. Nauk SSSR, 208, 635 (1973); in: Surface Forces in Thin Films and Stability of Colloids, Nauka, Moscow (1974), p. 206.
61. B. Davies and B. W. Ninham, J. Chem. Phys., 56, 5797 (1972).
62. D. J. Mitchell and P. Richmond, J. Colloid Interface Sci., 46, 118, 128 (1974).
63. A. E. Kats, Zh. Eksp. Teor. Fiz., 70, 1394 (1976).
64. V. A. Parsegian and G. H. Weiss, J. Adhesion, 3, 259 (1972).
65. H. Schröder, J. Chem. Phys., 67, 16 (1977).
66. M. Hitoshi and K. Shunsuke, Appl. Phys. Lett., 35, 4 (1979).
67. D. J. Mitchell and B. W. Ninham, J. Chem. Phys., 56, 1117 (1972).
68. E. R. Smith, D. J. Mitchell, and B. W. Ninham, J. Colloid Interface Sci., 45, 55 (1973).
69. D. Langbein, J. Phys. Chem. Solids, 32, 1657 (1971).
70. J. D. Love, J. Chem. Soc., Faraday Trans. II, 73, 669 (1977).
71. B. A. Pailthorpe and W. B. Russel, J. Colloid Interface Sci., 89, 563 (1982).
72. W. Black, J. G. V. de Jongh, J. Th. G. Overbeek, and M. J. Sparnaay, Trans. Faraday Soc., 56, 1597 (1960).
73. A. van Silfhout, Proc. Kon. Nederl. Akad. Wetenschap., B69, 501, 516, 532 (1966).
74. G. C. J. Rouweler, Chem. Phys. Lett., 8, 275 (1971).

75. M. J. Sparnaay, *Physica*, 24, 751 (1958).
76. P. van Blokland and J. Th. G. Overbeek, *J. Chem. Soc. Faraday Trans. I*, 74, 2637 (1978).
77. S. Hunklinger, H. Geisselmann, and W. Arnold, *Rev. Sci. Instr.*, 43, 584 (1972).
78. G. C. J. Rouweler and J. Th. G. Overbeek, *Trans. Faraday Soc.*, 7, 2117 (1971).
79. P. H. G. M. van Blokland and J. Th. G. Overbeek, *J. Colloid Interface Sci.*, 68, 96 (1979).
80. W. Arnold, S. Hunklinger, and K. Dransfeld, *Phys. Rev.*, B19, 6049 (1979).
81. D. Tabor and R. H. S. Winterton, *Nature*, 219, 1120 (1968); *Proc. R. Soc. London*, A312, 435 (1969).
82. D. Tabor, *J. Colloid Interface Sci.*, 31, 364 (1969).
83. B. V. Derjaguin and A. D. Malkina, *Kolloidn. Zh.*, 12, 431 (1952).
84. P. Richmond and B. W. Ninham, *J. Colloid Interface Sci.*, 40, 406 (1972).
85. J. N. Israelachvili and D. Tabor, *Nature, Phys. Sci.*, 236, 106 (1972); *Proc. R. Soc. London*, A331, 19 (1972).
86. L. R. White, J. N. Israelachvili, and B. W. Ninham, *Trans. Faraday Soc.*, 72, 2526 (1976).
87. M. J. Sparnaay, *J. Colloid Interface Sci.*, 91, 307 (1983).
88. J. Czarnecki and T. Dabros, *J. Colloid Interface Sci.*, 78, 25 (1980).
89. C. J. Coakley and D. Tabor, *J. Phys.*, D11, 77 (1978).
90. B. V. Derjaguin, Ya. I. Rabinovich, and N. V. Churaev, *Nature*, 265, 520 (1977); 272, 313 (1978).
91. Ya. I. Rabinovich, B. V. Derjaguin, and N. V. Churaev, *Dokl. Akad. Nauk SSSR*, 233, 349 (1977); in: *Surface Forces in Thin Films*, Nauka, Moscow (1979), p. 7.
92. B. V. Derjaguin, Ya. I. Rabinovich, and N. V. Churaev, *Adv. Colloid Interface Sci.*, 16, 63 (1982).
93. Ya. I. Rabinovich, M. B. Ryzhikov, V. D. Sobolev, and N. V. Churaev, *Kolloidn. Zh.*, 44, 977 (1982).
94. B. V. Derjaguin and Ya. I. Rabinovich, in: *Surface Forces and Boundary Layers of Liquids*, Nauka, Moscow (1983), p. 13.
95. Ya. I. Rabinovich, *Kolloidn. Zh.*, 44, 1096 (1982).
96. Ya. I. Rabinovich, *Kolloidn. Zh.*, 39, 1094 (1977).
97. J. N. Israelachvili and L. E. Adams, *J. Chem. Soc., Faraday Trans. I*, 74, 975 (1978).
98. V. G. Babak, S. P. Kozub, V. N. Sokolov, and V. I. Osipov, *Izv. Akad. Nauk SSSR, Ser. Fiz.*, 41, 2401 (1977).
99. L. Knapschinsky, W. Katz, B. Ehmke, and H. Sonntag, *Colloid Polymer Sci.*, 260, 1153 (1982).
100. Yu. I. Petrov, *Physics of Small Particles*, Nauka, Moscow (1982).
101. I. D. Morokhov, V. P. Petinov, L. I. Trusov, and V. F. Petrunin, *Usp. Fiz. Nauk*, 133, 653 (1981).

Chapter 5

THE ADSORPTION COMPONENT OF DISJOINING PRESSURE IN NONIONIC SOLUTIONS

An unequal molecular interaction energy of solute and solvent with the surfaces of a thin interlayer or film leads to a nonuniform distribution of concentration across the layer or film. For the same reason, the mean solution concentration in a thin interlayer or film may differ from that of the bulk solution in equilibrium with it.

In ionic solutions charged components are redistributed mainly because of the electric field of the surface charge. In nonionic solutions, neutral molecules are redistributed as a result of dispersion forces of the substrate, as a result of structural forces which change the solvent properties of the boundary layers of the solvent. The latter effect is not yet amenable to calculation. Quantitative calculations are possible for nonpolar solvents because there it is sufficient to take only dispersion forces into account [1-3].

Overlapping of such diffuse adsorption layers results in additional attractive or repulsive forces between surfaces bounding the interlayer. These forces have been termed the adsorption component of disjoining pressure [1-3].

The diffuse nature of adsorption layers of neutral molecules is indicated by the phenomena of capillary osmosis (see Section 11.2) investigated by one of us, and by reverse osmosis, which is widely used for separations by permeating solutions through micro-porous membranes (Section 11.3). Experimental studies of capillary and reverse osmosis demonstrate that the thickness of the diffuse adsorption layer of neutral molecules may extend to nanometers.

The overlapping of adsorption layers of surfactants and polymers in thin interlayers gives rise to another effect, known as the steric component of disjoining pressure. The concept of elastic repulsion between adsorption layers of surfactants and their mechanical strength as one of the reasons for high stability of colloids protected by surfactants, was proposed by Rehbinder [4] and subsequently developed [5, 6].

Adsorption layers of surfactants are sometimes regarded as mutually impenetrable because of the relatively abrupt outer boundary of a surfactant monolayer as compared with polymers. Of course, this is an oversimplification. While dispersion forces between particles may be weakened by adsorbed monolayers, they are capable of causing coagulation; and it is insufficient to take into account only steric repulsion.

Calculations of the steric component for overlapping adsorption layers of polymers is complicated. Mackor [7] suggested using for this purpose the equation relating the Gibbs free energy per unit area, G_s , to the adsorption Γ of the polymer in the bulk of the layer:

$$G_s = - \int_{-\infty}^{\mu} \Gamma d\mu + G_s^0 \quad (5.1)$$

where μ is the chemical potential of molecules of the solute, and G_s^0 is the Gibbs free energy of the layer of pure solvent. However, calculations of the adsorption of polymers in thin interlayers and films, and especially if they overlap, require a large number of factors to be taken into account simultaneously: conformation and elastic properties of polymer molecules, interaction of molecule segments with the surface of the interlayer and with other segments of the same polymer molecule, and of the adjacent molecules. Also, the presence of active centers on the bounding surfaces of the layer, and of groups of polymer molecules with different activities, ionogenic molecules among them, makes such calculations very complicated. Consequently, the theory of the steric component of disjoining pressure has to operate with some simplifying assumptions. For the introduction to the theory and experimental investigations of the steric component we refer the reader to well-known reviews on this subject [8-11].

In calculations of the adsorption component of the disjoining pressure we shall again use the expression for the Gibbs free energy, relating the free energy of a thin planar interlayer per unit area to the adsorption (i.e., excess) of the dissolved component Γ and the disjoining pressure of the layer Π :

$$dG + \Gamma d\mu + \Pi dh + SdT = 0 \quad (5.2)$$

where μ is the chemical potential of solute molecules, h is the interlayer thickness, S is the specific entropy, and T is the absolute temperature. Equation (5.2) is written in the approximation of negligible self-adsorption of the solvent, whose properties are treated as constant over the interlayer thickness. (In general, the adsorption Γ will not equal the sum of adsorptions of the two surfaces of the interlayer at zero overlap.)

If h and T are constant, we obtain

$$(dG)_{T,h} = -\Gamma d\mu \quad (5.3)$$

and

$$G(h) = - \int_{-\infty}^{\mu} \Gamma d\mu + G_0(h) \quad (5.4)$$

which is identical to Eq. (5.1). Here $G_0(h)$ is the energy of interaction through a layer of pure solvent.

As follows from (5.2),

$$\Pi(h) = -(\partial G / \partial h)_{\mu,T} \quad (5.5)$$

Then Eqs. (5.4) and (5.5) yield

$$\Pi(h) = \int_{-\infty}^{\mu} (\partial \Gamma / \partial h) d\mu + \Pi_{mo}(h) \quad (5.6)$$

where Π_{mo} is the disjoining pressure of the layer of pure solvent (for mole fraction of the bulk solution $C_\infty = 0$, and, correspondingly, $\mu = -\infty$). A similar expression was also derived by Everett et al. [12].

In the approximation of ideal solutions that we use here,

$$\mu = \mu_* + kT \ln C_\infty \quad (5.7)$$

where μ_* is a constant.

By substituting (5.7) into (5.6), we find

$$\Pi = kT \int_0^{C_\infty} \left(\frac{\partial \Gamma}{\partial h} \right) \frac{dC_\infty}{C_\infty} + \Pi_{mo} \quad (5.8)$$

The adsorption Γ (mole/cm²) is equal to the solute excess in a thin plane interlayer as compared with a layer of bulk solution of the same thickness h :

$$\Gamma = \frac{1}{v_m} \int_{\delta}^{h-\delta} [C(x) - C_\infty] dx \quad (5.9)$$

where v_m is the molar volume of the solvent. The distance x is measured along the normal to one of the surfaces bounding the thin interlayer, with $x = 0$ on this surface (Fig. 5.1a).

Since we are discussing effects associated with the overlapping of diffuse adsorption layers, the adsorption in a monolayer is not taken into account by Eq. (5.9): integration is carried out in the range of distances beyond the monolayer thickness δ . It is this factor that enables us to use, for adsorption calculations, the macroscopic theory of dispersion forces, applicable for distances exceeding the monolayer thickness [13].

In calculations of the forces of dispersion interaction between a molecule and a single substrate in vacuum, MacLachlan [14] derived equations involving a macroscopic characteristic of substrate, $\epsilon(i\xi)$ (see Chapter 4), and a frequency dependence of polarizability of individual molecules, $\alpha(i\xi)$.

Mahanty and Ninham [15] have taken into account the finite size of molecules in calculating physical adsorption on the basis of the macroscopic theory of dispersion forces. They assigned to each layer of molecules a thickness d_0 and a permittivity $\epsilon(i\xi)$ related to polarizability $\alpha(i\xi)$ of individual molecules by the following relation:

$$\epsilon(i\xi) = 1 + 4\pi N \alpha(i\xi) \quad (5.10)$$

where N is the number of molecules per unit volume.

Mahanty and Ninham concluded that Eq. (5.10) is valid in a wide range of values of N , not only for gaseous systems. However, since pair interactions are not additive, this equation cannot be used for solutions, where molecules of the solute are surrounded by those of the solvent.

This difficulty is overcome when the problem of interaction between solute molecules and the surface is solved by a method developed in [16]. Here, in contrast to other papers, the purely macroscopic approach is preserved, although interaction between molecules and the substrate is considered. The analysis is based on an artificial procedure introducing an imaginary situation in which the solution is separated from the substrate by a plane-parallel interlayer of pure solvent (Fig. 5.1b). The attractive force F per unit area, acting between the solution and the substrate across an interlayer of the solvent of thickness x , was calculated on the basis of the macroscopic theory. For dilute solutions

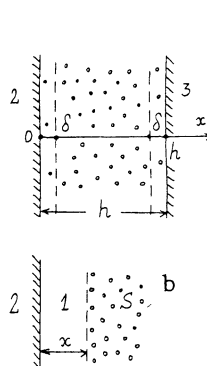


Fig. 5.1. Model for calculations of the adsorption component of disjoining pressure:
 a) solution interlayer between substrates 2 and 3; b) derivation of interaction energy between solute molecules and a single substrate (l — solvent, s — solution).

$$F = N \int_x^{\infty} f(x) dx = -NU(x) \quad (5.11)$$

where $f(x)$ is the effective attractive force between a molecule in a solution and the surface, and $U(x)$ is the corresponding interaction energy.

By definition, the disjoining pressure of an artificially defined interlayer of pure solvent between the solution and the substrate is $\pi = -F$. Then (5.11) yields the following relation:

$$U(x) = \pi(x)/N \quad (5.12)$$

The function $\pi(x)$ refers to the imaginary interlayer of pure solvent; x is the coordinate of the boundary that is conditionally defined within the solution. In what follows we also use another, more conventional definition of disjoining pressure $\Pi(h)$ acting within an interlayer of solution of thickness h bounded by two interfaces (solid or liquid substrates, or a gas) (Fig. 5.1a).

Major difficulties appear when the frequency dependence of permittivity $\epsilon_s(i\xi, C)$ is determined for a solution with coordinate-dependent concentration C that must enter the equations of the macroscopic theory of dispersion forces. In [16] the equation relating $\epsilon_s(i\xi)$ to the permittivity of pure solvent, $\epsilon_1(i\xi)$, and solution concentration was used:

$$\epsilon_s(i\xi) = \epsilon_1(i\xi) + (\partial\epsilon_s/\partial C)C \quad (5.13)$$

This equation holds quite well for dilute solutions to which the further analysis is restricted.

The following expression was finally obtained for the energy of (nonretarded) dispersion interaction between a solute molecule and a single substrate [16]:

$$U(x) = \frac{\hbar}{16\pi^2 x^3} \int_0^\infty \left(\frac{\Delta_{21}}{\epsilon_1} \right) \frac{\partial\epsilon_s}{\partial C} d\xi \quad (5.14)$$

Here \hbar is Planck's constant, $\Delta_{21} = (\epsilon_2 - \epsilon_1)/(\epsilon_2 + \epsilon_1)$, and x is the distance between the molecule and the substrate. The subscripts 1 and 2 refer to the solvent and the substrate materials, respectively.

For a thin layer (Fig. 5.1a) it is necessary to take into account the interaction between a solute molecule and both bounding surfaces. Assuming that force fields of the interlayer surfaces introduce into U an additive contribution, we obtain [1-3]

$$U(x) = \frac{\hbar}{16\pi^2 x^3} \int_0^\infty \frac{\Delta_{21}}{\epsilon_1} \left(\frac{\partial\epsilon_s}{\partial C} \right) d\xi - \frac{\hbar}{16\pi^2 (h - x)^3} \\ \times \int_0^\infty \frac{\Delta_{31}}{\epsilon_1} \left(\frac{\partial\epsilon_s}{\partial C} \right) d\xi = - \frac{A_2}{x^3} - \frac{A_3}{(h - x)^3} \quad (5.15)$$

where the subscripts 2 and 3 refer to different surfaces of the interlayer. In the symmetrical case $A_2 = A_3$.

When nonadditivity of dispersion interaction with two substrates (i.e., the many-body effect [17]) is taken into account, it does not affect to any significant degree the results of calculations of the isotherm of the adsorption component of disjoining pressure; this was shown in [18]. The corresponding corrections do not exceed a fraction of 1% for dielectrics, and 2-3% for metallic substrates.

The effect of adsorption monolayers on the forces of dispersion interaction of solute molecules can also be taken into account. In this case we introduce a thin layer on a substrate, with thickness δ , whose dielectric function $\epsilon_\alpha(i\xi)$ is assumed either identical to that of the macroscopic phase of the solute (in the case of positive adsorption) or identical to that of pure solvent (in the case of negative adsorption). The corresponding expression for $U(x)$ takes the form [3]

$$U(x) = - \frac{A_2}{(x - \delta)^3} - \frac{A_3}{(h - x - \delta)^3} \\ - \delta \left[\frac{B_2}{(x - \delta)^4} + \frac{B_3}{(h - x - \delta)^4} \right] \quad (5.15')$$

where

$$B_2 = \frac{3\hbar}{16\pi^2} \int_0^\infty \frac{\Delta_{a2}(1 - \Delta_{1a})^2}{(1 + \Delta_{1a} \Delta_{a2})} \left(\frac{\partial \varepsilon_s}{\partial C} \right) \frac{d\xi}{\varepsilon_1}$$

$$B_3 = \frac{3\hbar}{16\pi^2} \int_0^\infty \frac{\Delta_{as}(1 - \Delta_{1a})^2}{(1 + \Delta_{1a} \Delta_{as})} \left(\frac{\partial \varepsilon_s}{\partial C} \right) \frac{d\xi}{\varepsilon_1}$$

Here we use the standard notation $\Delta_{ik} = (\varepsilon_i - \varepsilon_k)/(\varepsilon_i + \varepsilon_k)$.

If $\delta \rightarrow 0$, expression (5.15') transforms to Eq. (5.15) described above.

In order to calculate the disjoining pressure of an interlayer of a nonionic solution by Eq. (5.8), it is necessary to know how the adsorption of the solute depends on the interlayer thickness h . Here we can make use of Eq. (5.9), with the Boltzmann equation establishing a functional relation between $C(x)$ and $U(x)$:

$$C(x) = C_\infty \exp[-U(x)/kT] \quad (5.16)$$

By substituting $C(x)$ from this equation into (5.9), we obtain

$$\Gamma(h) = \frac{C_\infty}{v_m} \int_\delta^{h-\delta} \{\exp[-U(x)/kT] - 1\} dx \quad (5.17)$$

Various approaches are possible to complete the solution of the problem. The simplest method, valid if the energy of adsorption is low ($U \ll kT$), is to use a linearized Boltzmann equation. In this case, the distribution of concentration over the thickness of the interlayer is

$$(C(x) - C_\infty)/C_\infty = A_2/kTx^3 + A_3/kT(h - x)^3 \quad (5.18)$$

which gives the following expression for $\Gamma(h)$:

$$\Gamma(h) = \frac{C_\infty(A_2 + A_3)}{2v_m kT} \left[\frac{1}{\delta^2} - \frac{1}{(h - \delta)^2} \right]$$

Having calculated the derivative $\partial\Gamma/\partial h$ for $\mu = \text{const}$ and $T = \text{const}$, we find the expression for disjoining pressure:

$$\Pi = (C_\infty(A_2 + A_3))/v_m(h - \delta)^3 - A_{213}/6\pi h^3 \quad (5.19)$$

The second term in this equation gives the force of dispersion interaction between the substrates 2 and 3 across the interlayer of pure solvent 1; A_{213} is the corresponding Hamaker constant (see Chapter 4).

Equation (5.19) shows that in the case of positive adsorption of a solute, when $A_2 > 0$ and $A_3 > 0$, the first term of the equation is positive. A positive adsorption produces additional positive disjoining pressure of the interlayer, reducing the magnitude of the usually negative disjoining pressure Π_{mo} which is related to the molecular attraction between the substrates 2 and 3. A negative adsorption of the solute changes the sign of the additional (adsorption) effect.

By setting (5.19) equal to zero, we can determine the interlayer thickness h_0 at which the second term of the equation is canceled out by the repulsion of surfaces due to the adsorption component of disjoining pressure in the interlayer:

$$h_0 = \delta/\{1 - [6\pi C_\infty(A_2 + A_3)/v_m A_{213}]^{1/2}\}$$

The thickness h_0 of an interlayer in equilibrium with the bulk solution (i.e., $\Pi = 0$ and $h = h_0$) is the greater, the higher the bulk solution concentration C_∞ , the higher the adsorption energy, and the lower the molecular attractive force between the surfaces.

Equation (5.19) thus takes into account two simultaneous components of disjoining pressure: adsorption and molecular components. The adsorption component $\Pi_a(h)$ per se can be singled out if we succeed in finding an exact expression for molecular forces $\Pi_m(h)$ acting across an interlayer of inhomogeneous solution. In general, a solution of this problem meets with considerable difficulties [19]. Calculation of the $\Pi(h)$ isotherms takes into account the combined effect of all components of surface forces. The thermodynamic approach outlined above enables one to determine precisely the required total disjoining pressure of an interlayer or film.

Calculations for films bounded on one side by a condensed phase and on the other by a gas differ only in that we can assume $\epsilon_3(i\xi) = 1$.

For low energy of adsorption [17, 18], a linearized Boltzmann equation is used; and if $h \gg \delta$, the values of $\Pi = \Pi_a + \Pi_{mo}$ are very close to the values of Π_{ms} for an interlayer of a homogeneous solution with bulk concentration C_∞ . Hence, in this case the values

of Π_α give the change in dispersion forces due to the change in the permittivity of a liquid interlayer. We can thus assume that Π_α equals the difference between Π_{ms} and Π_{mo} , where Π_{ms} is the force of dispersion interaction between bounding surfaces across an interlayer of a homogeneous solution in which the values of the function $\epsilon_s(i\xi)$ are constant throughout the interlayer. This constancy results from a low level of adsorption forces ($U \ll kT$).

For a symmetrical layer (when $A_2 = A_3$) we obtain the following expression for Π_α calculated from the difference between the forces of molecular attraction across an interlayer of homogeneous solution with $\epsilon = \epsilon_s(i\xi)$ and an interlayer of pure solvent with $\epsilon = \epsilon_1(i\xi)$:

$$\Pi_\alpha = \frac{\hbar C_\infty K}{2\pi^2 h^3} \int_0^\infty \frac{\epsilon_2(\epsilon_2 - \epsilon_1)}{(\epsilon_2 + \epsilon_1)^3} d\xi \quad (5.20)$$

Here $\epsilon_2(i\xi)$ is the dielectric function of substrates bounding the interlayer. In deriving this equation we made use of expression (5.13), in which the derivative $(\partial\epsilon_s/\partial C)$ is denoted by K .

As follows from Eq. (5.20), the adsorption component may have different signs, depending on the sign of K and the sign of the difference $(\epsilon_2 - \epsilon_1)$. Thus, if the solute is more polar than the solvent ($K > 0$) and the solvent is more polar than the substance of the substrates ($\epsilon_1 < \epsilon_2$), then $\Pi_\alpha > 0$; i.e., additional repulsive forces appear and reduce molecular attractive forces in comparison with the case of pure solvent. In general, the magnitude of Π_α is the greater, the higher the bulk concentration C_∞ and the larger K .

If we equated the value of Π_α to the excess osmotic pressure in the symmetry plane of the interlayer, by analogy to Langmuir's method [21] that he applied to take into account electrostatic repulsion, the result would be greater than the actual value by a factor of 8 [1].

The case of adsorption energies U comparable with kT is of greater interest. Here the nonlinearized equation (5.16) must be used, and an analytical solution can be obtained only as an approximation, under the condition $h \gg \delta$ [20]. To derive it, let us rewrite Eq. (5.9), by substituting for the concentration the expression obtained from the Boltzmann equation:

$$\Gamma(h) = \frac{2C_\infty}{v_m} \int_\delta^{h/2} \{\exp[-U(x)/kT] - 1\} dx \quad (5.21)$$

where the integral is taken, for reasons of symmetry, up to $h/2$. The lower bound of integration is cut off at a distance δ on the order of one monolayer thickness. This gives

$$\begin{aligned} \frac{\partial \Gamma}{\partial h} &= \frac{C_\infty}{v_m} \left\{ \exp[-U(h/2)/kT] - 1 \right\} \\ &- \frac{2C_\infty}{v_m} \int_{\delta}^{h/2} \frac{\exp[-U(x)/kT]}{kT} \frac{dU}{dh} dx \end{aligned} \quad (5.22)$$

By substituting the expression for $U(x)$ from (5.15) and considering first a particular case of $A_2 = A_3 = A$, we find

$$\begin{aligned} \frac{\partial \Gamma}{\partial h} &= \frac{C_\infty}{v_m} \left[\exp\left(\frac{16A}{kTh^3}\right) - 1 \right] \\ &- \frac{6C_\infty A}{kTv_m} \int_{\delta}^{h/2} \exp\left\{ \left[\frac{1}{x^3} + \frac{1}{(h-x)^3} \right] \frac{A}{kT} \frac{dx}{(h-x)^4} \right\} \end{aligned} \quad (5.23)$$

Integration by parts yields

$$\begin{aligned} \frac{\partial \Gamma}{\partial h} &= \frac{C_\infty}{v_m} \left[\exp\left(\frac{16A}{kTh^3}\right) - 1 \right] - \frac{2C_\infty}{v_m} \left\{ \exp\left\{ \frac{A}{kT} \left[\frac{1}{x^3} + \frac{1}{(h-x)^3} \right] \right\} \right\} \Big|_{\delta}^{h/2} \\ &- \frac{6C_\infty A}{kTv_m} \int_{\delta}^{h/2} \exp\left\{ \frac{A}{kT} \left[\frac{1}{x^3} + \frac{1}{(h-x)^3} \right] \right\} \frac{dx}{x^4} \end{aligned} \quad (5.24)$$

The integrand on the right-hand side of this equation increases sharply as x tends to δ . As a result, the main contribution to the integral is provided by the values of x in a neighborhood of δ . Hence, assuming that $h \gg \delta$, we can set in the exponent, without substantial error, that

$$(h - x) \approx (h - \delta) = \text{const} \quad (5.24')$$

The integration is then straightforward, and gives the following expression:

$$\begin{aligned} \frac{\partial \Gamma}{\partial h} &= \frac{2C_\infty}{v_m} \exp\left\{ \frac{A}{kT} \left[\frac{8}{h^3} + \frac{1}{(h-\delta)^3} \right] \right\} \\ &- \frac{C_\infty}{v_m} \left\{ \exp\left[\frac{16A}{kTh^3} \right] + 1 \right\} \end{aligned} \quad (5.25)$$

From Eqs. (5.8) and (5.25) we find the equation for the disjoining pressure of a solution interlayer:

$$\begin{aligned}\Pi &= \frac{2kTC_\infty}{v_m} \exp \left\{ \frac{A}{kT} \left[\frac{8}{h^3} + \frac{1}{(h - \delta)^3} \right] \right\} \\ &- \frac{kTC_\infty}{v_m} \left\{ \exp \left(\frac{16A}{kTh^3} \right) + 1 \right\} + \Pi_{mo} \quad (5.26)\end{aligned}$$

This expression can be used to calculate the adsorption component (together with the molecular component) of disjoining pressure if the interlayer thickness is not too small, so that the approximation (5.24') introduced in the integration is valid.

If the interlayer thickness is quite large (but not so large as to make the electromagnetic retardation effect appreciable), $h \gg \delta$, or if the adsorption energy is sufficiently low (i.e., A is small), the exponentials in (5.26) can be expanded into series, which gives Eq. (5.19). Let us analyze this equation, first replacing A with its expression from (5.15) and introducing the Hamaker constant A_{212} for a symmetrical interlayer of pure solvent:

$$\begin{aligned}\Pi &= \frac{2C_\infty A}{v_m(h - \delta)^3} - \frac{\hbar}{8\pi^2 h^3} \int_0^\infty \left(\frac{\epsilon_2 - \epsilon_1}{\epsilon_2 + \epsilon_1} \right)^2 d\xi \\ &\approx \frac{\hbar}{8\pi^2 h^3} \int_0^\infty \Delta_{21} \left[\frac{C_\infty}{v_m \epsilon_1} \left(\frac{\partial \epsilon_s}{\partial C} \right) - \Delta_{21} \right] d\xi \quad (5.27)\end{aligned}$$

This expression shows that in the following two cases the disjoining pressure of a solution interlayer can be positive:

$$i) \text{ if } \epsilon_2 > \epsilon_1 \text{ and } \frac{C_\infty}{v_m \epsilon_1} \left(\frac{\partial \epsilon_s}{\partial C} \right) > \Delta_{21} \quad (5.28)$$

$$ii) \text{ if } \epsilon_2 < \epsilon_1 \text{ and } \frac{C_\infty}{v_m \epsilon_1} \left(\frac{\partial \epsilon_s}{\partial C} \right) < \Delta_{21} \quad (5.29)$$

Relations (5.27) and (5.15) show that the necessary (but not sufficient) condition for Π to be positive is $A > 0$; i.e., adsorption must be positive and concentration C_∞ must be sufficiently high.

However, if the function $\epsilon_s(C)$ is very nearly linear, we can assume that

$$\frac{C_\infty}{v_m \epsilon_1} \left(\frac{\partial \epsilon_s}{\partial C} \right) \approx \frac{\epsilon_s - \epsilon_1}{\epsilon_1} \quad (5.30)$$

where ϵ_s is the permittivity of a solution with a given concentration C. By using (5.30), we can rewrite the conditions for $\Pi > 0$ [(5.28) and (5.29)] in the following form:

$$\text{i) if } \epsilon_2 > \epsilon_1, \text{ then } 2/\epsilon_s < 1/\epsilon_1 + 1/\epsilon_2 \quad (5.31)$$

$$\text{ii) if } \epsilon_2 < \epsilon_1, \text{ then } 2/\epsilon_s > 1/\epsilon_1 + 1/\epsilon_2 \quad (5.32)$$

Therefore, the quantity $1/\epsilon_s$ must be less in the first case and greater in the second case than the arithmetic mean of the inverse permittivity of the solvent and the substrates. In other words, ϵ_s must be greater or less, respectively, than the harmonic mean of ϵ_2 and ϵ_1 .

The quantities ϵ_s , ϵ_2 , and ϵ_1 in conditions (5.28), (5.29), or (5.31), denote, although somewhat conditionally, the values of the corresponding permittivity on the imaginary axis $i\xi$ in the range of frequencies important for the interaction. More strictly, one has to take instead of them the values of the appropriate integrals.

If

$$2A/kT\delta^3 > 1 \quad (5.33)$$

then it is obvious that while $h/2$ diminishes, still remaining greater than δ , the point will be reached at which the exponent

$$16A/kTh^3$$

will become very large. Then the term

$$-\frac{kTC_\infty}{v_m} \exp\left(-\frac{16A}{kTh^3}\right)$$

in (5.26) will exceed in magnitude the sum of the remaining terms, and Π will become negative.

If at large values of h the value of Π is positive because conditions (5.28), (5.29), or (5.31), (5.32) are satisfied, then as h diminishes, the disjoining pressure Π must change sign at a certain value of h corresponding to a nonequilibrium state of the system. However, there are several reasons why the calculation of Π cannot be exact when h tends to 2δ . First, formula (5.15) ceases to be exact. Second, the concentration of molecules in the immediate vicinity of the walls can be affected by forces other than dispersion forces; and third, the Boltzmann distribution can be violated at a high concentration of dissolved molecules. Even when $\delta \approx 3 \cdot 10^{-8}$ cm, condition (5.33) is satisfied at $T = 300$ K only with certain metals. However, it can be easily satisfied at a suffi-

ciently low temperature. The reverse condition will be more often satisfied at $T = 300$ K:

$$2A/kT\delta^3 \ll 1 \quad (5.34)$$

Hence, the treatment based on linearization of exponential functions in (5.26) remains valid.

Let us consider two particular cases.

1. If the interlayer is gaseous, then $\epsilon_3 = 1$ and the adsorption component $\Pi = \Pi_\alpha - \Pi_m$ for large values of h is equal, as follows from the first term in Eq. (5.27), to

$$\Pi = \frac{\hbar N}{2\pi(h - \delta)^3} \int_0^\infty \left(\frac{\epsilon_2 - 1}{\epsilon_2 + 1} \right) \alpha(i\xi) d\xi$$

where N is the number of molecules per unit volume of the gas, and $\alpha(i\xi)$ is the polarizability of the molecules of the gas. The expression for $(\partial\epsilon_s/\partial C)$ in (5.27) in terms of $\alpha(i\xi)$ is found from Eqs. (5.10) and (5.13). For small h and T the value of Π_α changes sign to minus, when condition (5.33), i.e., reversed (5.34), is satisfied. The thermodynamic treatment outlined above confirms the results of less rigorous calculations of Derjaguin and Martinov for large h [22]. Thus, Π_α can outweigh Π_m only for very dense gases (above their critical temperature); the disjoining pressure of the gas interlayer then becomes positive. But if substrates are very thin (e.g., the walls of two soap films), the net disjoining pressure Π can become positive already at atmospheric pressure, owing to an abrupt decrease in Π_m . This is a possible explanation of a phenomenon described by Dewar: two soap bubbles, one inside another, do not coalesce.

2. If a binary-solution interlayer forms a free film squeezed between two volumes of gas, then, assuming $\epsilon_3 = \epsilon_2 = 1$, we obtain the film instability condition ($\Pi > 0$) for large h in the form

$$\epsilon_s < 2\epsilon_1/(1 + \epsilon_1) < \epsilon_1 \quad (5.32')$$

where ϵ_1 and ϵ_s are the permittivities of the solvent and solution, respectively.

Therefore, for such a free film to be stable the solute must considerably reduce the permittivity of the solution. This conclusion probably explains the stability of free films of aqueous solutions of butyric acid, reported by Scheludko and Exerova [23].

A greater diversity characterizes systems in which an interlayer separates two different phases. The expression for the total

disjoining pressure of an asymmetrical interlayer (bounded by different bodies 2 and 3) at low adsorption energies ($U \ll kT$) can be represented, by analogy with (5.27), in the form

$$\Pi = \frac{\hbar}{8\pi^2 h^3} \left\{ \frac{C_\infty}{2v_m} \int_0^\infty \left(\frac{\partial \epsilon_s}{\partial C} \right) (\Delta_{21} + \Delta_{31}) \frac{d\xi}{\epsilon_1} \right. \\ \left. + \int_0^\infty \Delta_{21} \Delta_{31} d\xi \right\} \quad (5.35)$$

Here it is interesting to single out the case in which one of the substrates (say 2) and the solvent are spectrally nearly identical: $\epsilon_1 \approx \epsilon_2$. Then the second term in (5.35), characterizing the molecular component, vanishes: $\Pi_{mo} \rightarrow 0$. The disjoining pressure of the solution interlayer is totally determined by the deformation of the diffuse adsorption layer that forms only at one of the surfaces, viz., at the surface 3, because $A_2 = 0$. If $\epsilon_1 \approx \epsilon_2$, we obtain, instead of (5.35), the expression

$$\Pi_\alpha = \frac{\hbar C_\infty}{16\pi^2 v_m h^3} \int_0^\infty \left(\frac{\partial \epsilon_s}{\partial C} \right) \frac{\Delta_{31}}{\epsilon_1} d\xi \quad (5.35')$$

The situation discussed above makes it possible to study the effect of the adsorption component alone; an experimental confirmation would be of considerable interest. Candidates for objects with nearly identical spectral properties can be, for instance, solid hydrocarbon as the substrate and a hydrocarbon liquid as a solvent. The second substrate bounding the interlayer must be more polar than the solvent. Then repulsive forces can be detected in the interlayer for a polar solute ($\partial \epsilon_s / \partial C > 0$), due to the positive adsorption component $\Pi_\alpha \gg 0$ of the disjoining pressure.

An analytical solution of the problem for an asymmetrical interlayer can also be obtained without the condition of low adsorption energy $U \ll kT$. Then for the adsorption in the interlayer, instead of (5.21) we find that

$$\Gamma(h) = \frac{C_\infty}{v_m} \int_\delta^{h-\delta} \left\{ \exp \left[\frac{A_2}{kTx^3} + \frac{A_3}{kT(h-x)^3} \right] - 1 \right\} dx$$

where the constants A_2 and A_3 are given by Eq. (5.15).

The integral in the expression for adsorption can be separated into two parts, Γ_1 and Γ_2 , with integration limits δ and $h/2$ for the former and $h/2$ and $(h - \delta)$ for the latter:

$$\Gamma(h) = \Gamma_1(h) + \Gamma_2(h)$$

where

$$\Gamma_1(h) = \frac{C_\infty}{v_m} \int_{\delta}^{h/2} \left\{ \exp \left[\frac{A_2}{kT x^3} + \frac{A_3}{kT(h-x)^3} \right] - 1 \right\} dx$$

Replacing the variable x with $(h-y)$, we can recast the expression for $\Gamma_2(h)$ to the same form as $\Gamma_1(h)$, differing only in commuted A_2 and A_3 . Using now a familiar procedure [see Eqs. (5.22)-(5.26)], we find for h sufficiently large in comparison with δ :

$$\Pi \approx \frac{\hbar}{8\pi^2 h^3} \int_0^{\infty} \frac{(\epsilon_3 \epsilon_2 - \epsilon_1^2)(C_\infty/v_m \epsilon_1)(\partial \epsilon_s / \partial C) - (\epsilon_2 - \epsilon_1)(\epsilon_3 - \epsilon_1)}{(\epsilon_2 + \epsilon_1)(\epsilon_3 + \epsilon_1)} d\xi \quad (5.36)$$

In this general case the values of $\Pi = \Pi_\alpha + \Pi_{mo}$ can be positive or negative and in particular cases can change sign when the concentration of the bulk solution C_∞ is varied. One particular case of an asymmetrical interlayer is a wetting film bounded on one side by a gas phase, for which we must set in the above equations $\epsilon_3 = 1$.

The conclusions obtained in the analysis of the analytical solutions given above, involving either the assumption of low adsorption energy ($U \ll kT$), or the assumption of a thick interlayer ($h \gg \delta$), are confirmed by the results of exact numerical calculations. The values of $\Gamma(h)$ and $\Pi(h)$ were numerically calculated in a computer, from Eqs. (5.8), (5.9), and (5.16) in the range of interlayer thickness h from 12.5 \AA to 150 \AA , with a step $\Delta h = 2.5 \text{ \AA}$, for four values of the mole fraction of the bulk solution: $C_\infty = 0.01, 0.05, 0.1, \text{ and } 0.5$. Computations assumed $\delta = 5 \cdot 10^{-8} \text{ cm}$ and $T = 300 \text{ K}$. Quantitative estimates of A_2 and A_3 were obtained from frequency functions $\epsilon(i\xi)$ typical for metals and dielectrics.

As the values of $(\partial \epsilon_s / \partial C)$ were not known, they were computed from Eq. (5.10) written for dilute solutions:

$$\epsilon_s(i\xi) = \epsilon_1(i\xi) + 4\pi C \alpha_s(i\xi) \quad (5.37)$$

A comparison of (5.37) and (5.13) yields

$$\partial \epsilon_s / \partial C = 4\pi \alpha_s(i\xi) \quad (5.38)$$

Pitayevsky demonstrated [24] that the molecular polarizability $\alpha_s(i\xi)$ can be expressed through the permittivity of the solute, $\epsilon_s(i\xi)$:

$$\alpha_s(i\xi) = \frac{3v_0}{4\pi} \frac{(\epsilon_s - \epsilon_1)}{(\epsilon_s + 2\epsilon_1)} \quad (5.39)$$

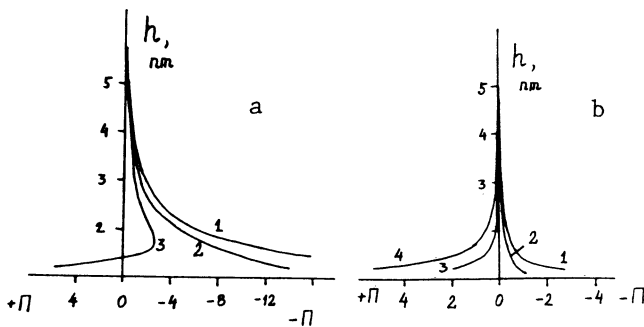


Fig. 5.2. Disjoining pressure isotherms $\Pi(h)$ in binary solution interlayers between identical plates positively adsorbing the solute: a) metal plates ($A_{213} = 10^{-12}$ erg, $A_2 = A_3 = 10^{-36}$ erg·cm³), $C_\infty = 0$ (1), 0.1 (2), 0.25 (3); b) dielectric plates ($A_{213} = 10^{-14}$ erg, $A_2 = A_3 = 10^{-37}$ erg·cm³), $C_\infty = 0$ (1), 0.01 (2), 0.05 (3), 0.1 (4).

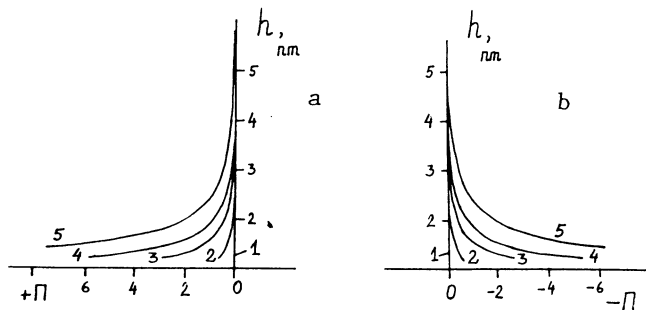


Fig. 5.3. Disjoining pressure isotherms $\Pi(h)$ in binary solution films on a solid substrate at $A_{213} = 0$; a) the solute is positively adsorbed at the liquid-gas interface ($A_2 = 0$, $A_3 = 10^{-36}$ erg·cm³), $C_\infty = 0$ (1), 0.01 (2), 0.05 (3), 0.01 (4), 0.25 (5); b) the solute is negatively adsorbed at the liquid-gas interface ($A_2 = 0$, $A_3 = -10^{-36}$ erg·cm³), $C_\infty = 0$ (1), 0.01 (2), 0.05 (3), 0.1 (4), 0.25 (5).

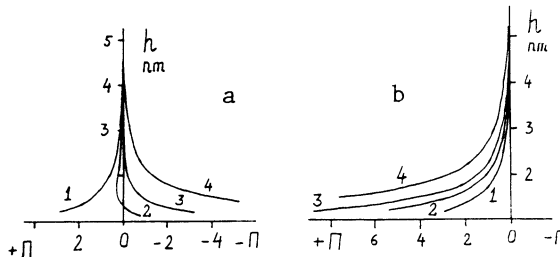


Fig. 5.4. Disjoining pressure isotherms $\Pi(h)$ in binary solution films on a solid substrate, $A_{213} = -10^{-13}$ erg: a) the solute is positively adsorbed at the substrate and negatively adsorbed at the liquid-gas interface ($A_2 = 10^{-37}$ erg·cm³, $A_3 = -10^{-36}$ erg·cm³), $C_\infty = 0$ (1), 0.01 (2), 0.05 (3), 0.1 (4), 0.25 (5); b) the solute is negatively adsorbed at the substrate and positively adsorbed at the film-gas interface ($A_2 = -10^{-37}$ erg·cm³, $A_3 = 10^{-36}$ erg·cm³), $C_\infty = 0$ (1), 0.05 (2), 0.1 (3), 0.25 (4).

where v_0 is the molecular volume. This equation enables us to calculate the values of $\partial \varepsilon_s / \partial C$ from macroscopic characteristics of the solute, $\varepsilon_s(i\xi)$, and of the solvent, $\varepsilon_1(i\xi)$. The results of computations are shown in Figs. 5.2-5.4. On all figures the origin corresponds to $h = 2\delta = 10 \text{ \AA}$, i.e., to twice the thickness of adsorption monolayers.

Consider first interaction forces between two identical metallic plates ($A_{212} = 10^{-12}$ erg) at different concentrations C_∞ (Fig. 5.2a) when the solute is adsorbed on the plates positively, owing to dispersion forces ($A_2 = A_3 = 10^{-36}$ erg·cm³). When $C_\infty = 0$ (curve 1), the negative disjoining pressure of the interlayer is caused only by the attractive dispersion forces between plates ($\Pi = \Pi_{mo}$), as follows from Eq. (5.8).

In solutions the isotherms $\Pi(h)$ are changed. Figure 5.2a shows that an increase in the solution concentration first results only in reduced attractive forces between plates (curve 2), and then, when $C_\infty = 0.25$ (curve 3), it reverses the sign of Π . Repulsive forces due to the interaction of the overlapping diffuse adsorbed layers of solute appear at small distances between the plates. The disjoining pressure vanishes ($\Pi = 0$) when $h = 14 \text{ \AA}$; this signifies, among other things, that with positive adsorption of the solute the plates can be stabilized at this distance.

The stabilizing action of the adsorbed component in the case of identical dielectric plates is even better pronounced ($A_{212} = 10^{-14}$ erg, $A_2 = A_3 = 10^{-37}$ erg·cm³). The isotherm $\Pi(h)$ intersects the abscissa axis (Fig. 5.2b) already at $C_\infty = 0.05$ at a point where $h \approx 45$ Å. At still higher concentrations ($C_\infty \geq 0.1$) the whole isotherm $\Pi(h)$ lies in the range of positive values of the disjoining pressure of the interlayer. This is explained by much smaller forces of molecular attraction between dielectric plates as compared with metal plates. Consequently, the stabilizing role of the adsorption component of disjoining pressure becomes more pronounced in colloids formed of dielectric particles.

On the contrary, negative adsorption of a solute ($\Gamma < 0$) on particles (plates) enhances coagulation of colloids because, in this case, the attractive forces can only become stronger.

Figures 5.3 and 5.4 give isotherms of the disjoining pressure of wetting films on solid substrates. Figure 5.3 plots isotherms for a particular case of identical dielectric functions $\epsilon(i\xi)$ of the substrate and solvent. Under this condition, $A_{213} = 0$ (the subscript 3 refers to the gas phase) and $\Pi_{\text{mo}} = 0$; i.e., films of pure solvent are unstable.

Let us trace how the adsorption of a solute on the surface of a film bounded by a gas affects the isotherms $\Pi(h)$. In our case, $\epsilon_2 = \epsilon_1$, so that $A_2 = 0$ and hence there can be no adsorption on the solid substrate due to dispersion forces. Estimates give $A_3 \approx 10^{-36}$ erg·cm³. Since $(1 - \epsilon_1) < 0$, adsorption can be positive ($A_3 > 0$) only if $\epsilon_1 > \epsilon_s$ (in the range of frequencies essential for the interaction), i.e., only if the solvent is less polar than the solute. Figure 5.3a shows that the positive adsorption of a solute at the film/gas interface leads to the formation of films that are stable owing to the adsorption component of disjoining pressure. No stable films can exist if $A_3 < 0$ (Fig. 5.3b). Similar conclusions follow from Eq. (5.35') when we set $\epsilon_3 = 1$.

Figure 5.4 shows the results of computations for wetting films, when the pure solvent forms stable films on the substrate. This situation requires $A_{213} < 0$, which is possible only if $\epsilon_2 > \epsilon_1$. For films of nonpolar liquids on a dielectric substrate we can assume $A_{213} = -10^{-13}$ erg. Equation (5.15) yields that, in the case $\epsilon_2 > \epsilon_1$ and $\epsilon_3 = 1$, the constants A_2 and A_3 have opposite signs, i.e., the solute is adsorbed at one of the surfaces positively, and at the other negatively. If the permittivities of the substrate and liquid are nearly the same, which is a normal situation for dielectrics, then $|1 - \epsilon_1| > |\epsilon_2 - \epsilon_1|$ and the constant A_3 is greater in magnitude than A_2 . The constants assumed for computations were: $|A_2| = 10^{-37}$ and $|A_3| = 10^{-36}$ erg·cm³. In the case $|A_3| > |A_2|$ the adsorption (both positive and negative) at the film/gas interface is greater than at the substrate, so that its role is dominant in

the stability of wetting films. Obviously, this is true only for the case of adsorption caused exclusively by dispersion forces.

The curves in Fig. 5.4 show that the stability of films increases if the solute is positively adsorbed on the liquid/gas interface (Fig. 5.4b, $A_2 = -10^{-37}$, $A_3 = 10^{-36}$). A negative adsorption at a free surface of the film (Fig. 5.4a, $A_2 = 10^{-37}$, $A_3 = -10^{-36}$) at a low concentration C_∞ reduces the positive values of Π , and at high C_∞ makes Π reverse the sign. Thus, for example, at $C_\infty = 0.1$ only solution films thicker than 30 Å can be stable. At $h = 30$ Å the isotherm $\Pi(h)$ intersects the abscissa axis, and for $h < 30$ Å the isotherm extends into the range of negative Π , i.e., into the range of unstable films.

Computations demonstrate that with the chosen values of the constants A_{213} , A_2 , and A_3 the effect of the adsorption component of disjoining pressure reaches appreciable levels for interlayers and films with $h \leq 50$ Å. The resulting forces of interaction depend on the energy and sign of adsorption, as well as on the bulk concentration of the solution. The appearance of repulsive forces in symmetrical systems is proof that the effect of overlapping of adsorption layers of dissolved molecules is quite real and can even exceed the forces of molecular attraction.

Figures 5.2-5.4 show that isotherms changing sign of $\Pi(h)$ can be obtained only when the nonlinearized Boltzmann equation is used. Such sign-alternating isotherms already appear at relatively low values of adsorption energy, $U(\delta) = (0.05-0.1) kT$. This demonstrates that nonlinear terms of the Boltzmann equation are of paramount importance for the problem under consideration. Linearization of this equation leads to a loss of some information on concentration distribution within the interlayer, and strongly affects the form obtained for $\Pi(h)$ curves. Apparently, the linearized Boltzmann equation is acceptable only for values of $U(\delta)$ much less than $(0.05-0.1)kT$.

The solutions obtained above are bounded from below by the condition $h > \delta$, and from above by the condition $h < 150$ Å because electromagnetic retardation was left out of the model.

Further elaboration of the theory will require that the adsorption in a monolayer and its dependence on h be taken into account. There may also be large departures from the above computations if the adsorption monolayer causes structural changes in the adjacent boundary layers of the solvent (see Chapter 7).

Conclusions similar to those presented in this chapter also follow from calculations reported earlier by Kuni, Rusanov, and Brodskaya of molecular distribution functions for multicomponent planar films and interlayers of a solution on the basis of the micro-

scopic approach [25]. In that paper intermolecular interactions were described by means of pair vacuum potentials with a renormalization factor taking into account the effect of the medium. The authors derived from the expression for the normal component of the pressure tensor P_N the equation of the isotherm of disjoining pressure $\Pi(h) = P_N(h) - P_0$, where P_0 is the pressure in the bulk phase of the solution. The expression obtained for $\Pi(h)$ contains, in addition to the main asymptotic term A/h^3 corresponding to attractive forces in the case of identical plates, also a term D/h^4 whose contribution becomes significant for sufficiently thin interlayers. The sign of D depends on the magnitude and sign of adsorption of molecules in the mixture, their concentration, and their polarizability. Under certain conditions D can be positive. Then, as the interlayer thins out, attractive forces can be replaced with repulsive ones; this corresponds to isotherms intersecting the thickness axis, as in Fig. 5.2. Kuni et al. [25] are of the opinion that the stable state of interlayers formed in this case can be explained only by taking into account the inhomogeneous concentration of the solution within the interlayer.

Vaslieff and Ivanov [26] combined the microscopic and macroscopic methods of the theory of molecular forces and obtained, by methods of statistical thermodynamics, expressions for calculating adsorption, concentration profiles, and disjoining pressure in films of a regular binary solution. The general solution obtained transforms, for low adsorption energy, into that of Kuni, Rusanov, and Brodskaya [25], and for low concentration of the solution into those of [1-3].

However, the microscopic approach enables one to achieve only a general analysis of the problem. It is difficult to obtain concrete results because the constants in the expressions for effective pair potentials of intermolecular interaction in different media are unknown. In contrast to this, the macroscopic theory of the adsorption component presented at the beginning of this chapter uses the physical characteristics of the solution, solvent, and substrate and, therefore, makes it possible to carry out quantitative calculations of the isotherms $\Pi = \Pi_\alpha + \Pi_{mo}$ for real systems.

Since the theory of the adsorption component Π_α has been developed only in recent years, a special experimental verification of the theory is still lacking. However, a number of experimental results obtained earlier that could not be explained can be interpreted now as resulting from this phenomenon.

For instance, Kusakov and Titiyevskaya [27] reported increased $\Pi(h)$ values for stable wetting films of n-heptane ($n_l = 1.39$) on steel as a result of adding caprylic acid ($n = 1.43$). The adsorption of caprylic acid takes place at the solid substrate because its surface tension is higher than that of heptane. As the compon-

ents of the solution are nearly identical in polarity (characterized by the value of the refractive index) and the adsorption is low, Eq. (5.19) holds in this case. This equation shows that the first term can be positive (resulting in a further growth of positive $\Pi(h)$ values because on the metal surface $\Pi_{mo} > 0$) provided i) $\Delta_{21} > \Delta_{13}$ and $\partial\epsilon_s/\partial C > 0$, and ii) $\Delta_{21} < \Delta_{13}$ and $\partial\epsilon_s/\partial C < 0$. Caprylic acid is more polar than heptane ($n > n_1$), so that $\partial\epsilon_s/\partial C > 0$. Consequently, the stability of a film is increased if the first condition which here we can rewrite in the form

$$(\epsilon_2 - \epsilon_1)/(\epsilon_2 + \epsilon_1) > (\epsilon_1 - \epsilon_3)/(\epsilon_1 + \epsilon_3)$$

is satisfied. For a metal substrate $\epsilon_2 \gg \epsilon_1$, and ϵ_3 corresponds to a gas (i.e., $\epsilon_3 = 1$ and hence $\epsilon_1 > \epsilon_3$), so that in this case the solution $\Pi(h)$ is greater than that in pure heptane, thus providing an explanation of the results of Kusakov and Titiyevskaya.

For free films the theory of the adsorption component of disjoining pressure predicts repulsive forces when $\partial\epsilon_s/\partial C < 0$ [see condition (5.32')], i.e., when a solute less polar than the solvent is introduced into the film. Indeed, Scheludko and Exerova [28] observed a slowing down in the draining of free films of aqueous solutions of butyric acid, and Manev and Buleva [29] reported the same for solutions of hexane in nitrobenzene. This damping of drainage could be associated with the appearance of a positive component of disjoining pressure $\Pi_a > 0$ against the background of attraction between film surfaces due to molecular forces, $\Pi_{mo} < 0$. The additional repulsive forces reported in [29] were proportional to $1/h^3$, in accord with Eq. (5.19).

Force barriers that prevent crossed wires from approaching were also detected in interlayers of aqueous solutions of butyric acid [30].

The theory of the adsorption component thus has been partly confirmed, even if only qualitatively. Special experiments are needed to test the theory quantitatively.

REFERENCES

1. B. V. Derjaguin and N. V. Churaev, Dokl. Akad. Nauk SSSR, 222, 554 (1975); Kolloidn. Zh., 37, 1075 (1975).
2. B. V. Derjaguin, B. M. Starov, and N. V. Churaev, Kolloidn. Zh., 38, 449 (1976).
3. B. V. Derjaguin and N. V. Churaev, J. Colloid Interface Sci., 62, 369 (1977).
4. P. A. Rehbinder, Izv. Akad. Nauk SSSR, Ser. Khim., 5, 639 (1936).

5. V. N. Izmailova and P. A. Rehbinder, *Structure Formation in Protein Systems*, Nauka, Moscow (1978).
6. E. D. Shchukin, A. V. Pertsov, and E. A. Amelina, *Colloid Chemistry*, Mosk. Gos. Univ., Moscow (1982).
7. E. L. Mackor, *J. Colloid Sci.*, 6, 492 (1951); *Recl. Trav. Chim. Pays-Bas*, 70, 717 (1951).
8. F. Th. Hesselink, *J. Phys. Chem.*, 75, 65 (1971); *J. Polymer Sci.*, 61, 439 (1977).
9. J. B. Smitham, R. Evans, and D. H. Napper, *J. Chem. Soc., Faraday Trans. I*, 71, 285 (1975).
10. D. H. Napper, *J. Colloid Interface Sci.*, 58, 390 (1977).
11. J. Lyklema, *Pure Appl. Chem.*, 53, 2199 (1981).
12. S. G. Ash, D. H. Everett, and C. Radke, *J. Chem. Soc., Faraday Trans. II*, 69, 1256 (1973).
13. J. Mahanty and B. V. Ninham, *J. Chem. Soc., Faraday Trans. II*, 71, 119 (1975).
14. A. D. MacLachlan, *Mol. Phys.*, 7, 381 (1964).
15. J. Mahanty and B. W. Ninham, *J. Chem. Soc., Faraday Trans. II*, No. 4, 637 (1974).
16. B. V. Derjaguin, I. E. Dzyaloshinski, M. M. Koptelova, and L. P. Pitayevski, *Discuss. Faraday Soc.*, 40, 246 (1965).
17. D. Y. C. Chan, D. J. Mitchell, B. W. Ninham, and B. A. Pailthorpe, *J. Colloid Interface Sci.*, 68, 462 (1979).
18. B. V. Derjaguin and N. V. Churaev, *J. Colloid Interface Sci.*, 87, 543 (1982).
19. V. A. Parsegian and G. H. Weiss, *J. Colloid Interface Sci.*, 40, 35 (1972).
20. B. V. Derjaguin, *Colloid Polymer Sci.*, 258, 433 (1980).
21. I. Langmuir, *J. Chem. Phys.*, 6, 873 (1938).
22. B. V. Derjaguin and G. A. Martynov, *Dokl. Akad. Nauk SSSR*, 144, 825 (1962).
23. A. Scheludko and D. Exerova, *God. Sofia. Univ.*, 54, (1959/60), Part 3, Sofia (1961), p. 205.
24. L. P. Pitayevsky, *Zh. Eksp. Teor. Fiz.*, 37, 577 (1959).
25. F. M. Kuni, A. I. Rusanov, and E. N. Brodskaya, in: *Research in Surface Forces*, Vol. 4, Consultants Bureau, New York (1975), p. 240.
26. Ch. S. Vassilieff and I. B. Ivanov, *God. Sofia Univ., Khim. Fak.*, 70, 111 (1979).
27. M. M. Kusakov and A. S. Titievskaya, *Dokl. Akad. Nauk SSSR*, 28, 333 (1940).
28. A. Scheludko and D. Exerova, *Izv. Khim. Inst. Bolg. Akad. Nauk Sofia*, 7, 105 (1960).
29. E. Manev and M. Buleva, *Colloid Polymer Sci.*, 256, 375 (1978).
30. B. V. Derjaguin, T. N. Voropaeva, and B. N. Kabanov, *J. Colloid Interface Sci.*, 19, 113 (1964).

Chapter 6

THE ELECTROSTATIC COMPONENT OF DISJOINING PRESSURE

Chapter 1 treated various mechanisms of spontaneous charging of interfaces between two phases, one of them an electrolyte solution. This phenomenon leads to an equilibrium diffuse ionic atmosphere. If two such interfaces are brought together, their ionic atmospheres overlap, giving rise to the electrostatic component Π_e of disjoining pressure.

6.1. METHODS OF CALCULATION OF DISJOINING PRESSURE Π_e

Several approaches are known for calculating Π_e . The earliest, developed by Derjaguin [1], consists in directly determining the electrostatic disjoining pressure acting on the surfaces of parallel plates embedded in an electrolyte solution. Derjaguin assumed that at equal potentials of the external and internal (with respect to the interlayer) surfaces of the plate the hydrostatic pressure applied to them is identical, and concluded that, in this case, the disjoining pressure is determined by the difference between the Maxwell stresses at the internal and external surfaces of either of the plates:

$$\Pi_e = \epsilon E_{ex}^2 / 8\pi - \epsilon E_{in}^2 / 8\pi \quad (6.1)$$

where E_{in} and E_{ex} denote the strength of electric field at the internal and external surfaces, respectively, found from the solution of the Poisson-Boltzmann equation with appropriate boundary conditions, and ϵ is the permittivity of the solution. Somewhat later, Langmuir [2] gave, or rather postulated (see below), the formula

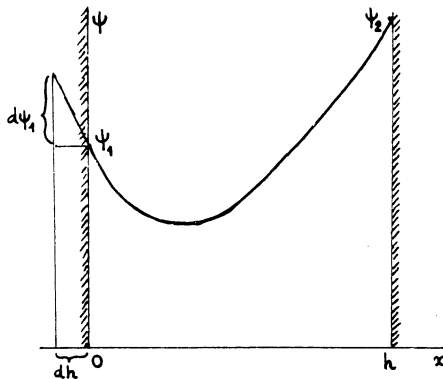


Fig. 6.1. Model for the derivation of the expression for Π_e . Potential distribution in the gap between plates.

$$\Pi_e = kT(n^+ + n^- - 2n_0) \quad (6.2)$$

where the ion concentrations n^+ and n^- must be taken in the plane in which the potential has the extremum and the electric field is zero, and n_0 is the bulk concentration of ions.

For clarity and rigor in the calculation of Π_e , the formula will be derived on the basis of general thermodynamic arguments, without additional assumptions.* Let us analyze the expression for the differential of Gibbs free energy, taking into account the work of external forces that maintain the equilibrium thickness h of the electrolyte interlayer, and of charge sources maintaining the equilibrium charge densities σ_1 and σ_2 on the two surfaces:

$$dG_{T,P,\mu_i} = S\Pi_e dh + S(\psi_1 d\sigma_1 + \psi_2 d\sigma_2) \quad (6.3)$$

where μ_i are the chemical potentials of the components of the system, T is the temperature, P is the pressure, S is the surface area of each of the plates, and ψ_1 and ψ_2 are the surface potentials with respect to the bulk of the solution (Fig. 6.1). By subtracting from the two sides of this equation the differential of the expression

$$S(\psi_1 \sigma_1 + \psi_2 \sigma_2)$$

we obtain

$$dG_{T,P,\mu_i} - Sd(\psi_1 \sigma_1 + \psi_2 \sigma_2) = -S\Pi_e dh - S(\sigma_1 d\psi_1 + \sigma_2 d\psi_2)$$

*See also B. V. Derjaguin, in: Modern Theory of Capillarity, Akademie Verlag, Berlin (1981), p. 35.

The left-hand side is a total differential; hence,

$$\partial \Pi_e / \partial \psi_1 |_{h, \mu_i, \psi_2} = \partial \sigma_1 / \partial h |_{\mu_i, \psi_1, \psi_2} \quad (6.4)$$

In order to obtain Π_e from (6.4) by integrating $\partial \Pi_e / \partial \psi_1$, we have to transform $\partial \sigma_1 / \partial h$. Our initial equation will be the Poisson equation for an electrolyte interlayer, (1.11):

$$d^2\psi / dx^2 = (4\pi/\epsilon)\rho \quad (6.5)$$

in which the potential ψ is a function of the coordinate x measured from the left-hand surface of the interlayer perpendicularly to it (Fig. 6.1). The volume charge density ρ is found from Eq. (1.12):

$$\rho = \sum_i e z_i \tilde{n}_i$$

in which the local concentrations of ions \tilde{n}_i are determined by the concentrations of ions in the bulk n_i and by the work of their transfer from the bulk into the interlayer,

$$w_i = z_i e \psi$$

Hence, the local volume density is a function of local potential ψ :

$$\rho = \rho(\psi) \quad (6.6)$$

In the bulk of the solution where $\psi = 0$, $\tilde{n}_i = n_i$, the solution is locally electroneutral ($\sum_i e z_i n_i = 0$) and $\rho(0) = 0$. By multiplying the left- and right-hand sides of the Poisson equation (6.5) by $2 \frac{d\psi}{dx}$ and integrating, we obtain

$$\frac{\epsilon}{8\pi} \left(\frac{d\psi}{dx} \right)^2 = - \int_0^\psi \rho(\psi) d\psi + C \quad (6.7)$$

The integration constant C is a function of interlayer thickness h ; it is obvious from (6.7) that as $h \rightarrow \infty$ (which means that $d\psi/dx \rightarrow 0$ and $\psi \rightarrow 0$), the constant $C \rightarrow 0$. For the left-hand plate we can replace (6.7) by

$$\frac{2\pi\sigma_1^2}{\epsilon} = C - \int_0^{\psi_1} \rho d\psi \quad (6.8)$$

because, by virtue of Gauss's theorem,

$$\sigma_1 = - \frac{\varepsilon}{4\pi} \left(\frac{d\psi}{dx} \right)_{x=0}$$

and $\psi(0) = \psi_1$. In what follows we consider the potential of the right-hand plate constant: $\psi_2 = \text{const}$. By differentiating (6.8) we obtain

$$\frac{4\pi\sigma_1}{\varepsilon} \left(\frac{\partial\sigma_1}{\partial h} \right)_{\psi_1} = \left(\frac{\partial C}{\partial h} \right)_{\psi_1} \quad (6.9)$$

By resorting to the identity

$$\left(\frac{\partial C}{\partial h} \right)_{\psi_1} \left(\frac{\partial h}{\partial \psi_1} \right)_C \left(\frac{\partial \psi_1}{\partial C} \right)_h = -1$$

and an obvious relation (see Fig. 6.1)

$$\sigma_1 = \frac{\varepsilon}{4\pi} \left(\frac{\partial \psi_1}{\partial h} \right)_{C, \psi_2}$$

we derive from Eq. (6.9)

$$\left(\frac{\partial \sigma_1}{\partial h} \right)_{\psi_1, \psi_2} = - \left(\frac{\partial C}{\partial \psi_1} \right)_{h, \psi_2} \quad (6.10)$$

By substituting this last equality into (6.4) and integrating we find

$$\Pi_e(h) = -C \quad (6.11)$$

where we take into account that $\Pi_e(\infty) = 0$ and $C(\infty) = 0$. Taking C from (6.7), we finally obtain, instead of (6.11),

$$\Pi_e(h) = - \int_0^\psi \rho(\psi) d\psi - \frac{\varepsilon E^2}{8\pi} \quad (6.12)$$

where the potential ψ and its derivative E can be taken in any plane x parallel to the surfaces of the interlayer. The most general derivation of the formula for Π_e considered above, based on thermodynamics and electrostatics, holds both for symmetrical and for asymmetrical double layers in electrolyte solutions of arbitrary composition, and is free of any a priori assumptions on the law that relates local values of volume charge density ρ to those of potential ψ in the electrolyte layer. In general, this relationship depends on the conditions of electrochemical equilibrium for all charged dissolved components in the layer. To determine this relationship is a complicated independent problem. We have already mentioned, in Chapter 1, that in the Gouy-Chapman theory this re-

lation is prescribed by the Boltzmann equation, which immediately yields the Poisson-Boltzmann equation already mentioned. However, it is not necessary to resort to the Poisson-Boltzmann equation in order to derive the general formula for Π_e . It is sufficient to know that a relation $\rho(\psi)$ exists. As we see from (6.12), the electrostriction effect does not influence, contrary to the statements made in [3], the disjoining pressure in the electrolyte interlayer. (This conclusion has been confirmed in [4, 5].)

In order to clarify the derivation, let us derive formula (6.12) by using the principles of hydrostatics and electrostatics. The following equality holds in equilibrium electrolyte layers [6]:

$$\text{grad } p + \rho \text{ grad } \psi + \frac{1}{8\pi} \text{ grad } \left(E^2 \frac{\partial \epsilon}{\partial \rho_l} \rho_l \right) = 0, \quad (6.13)$$

where $p(x, h)$ is the local hydrostatic pressure, E is the electric field strength, and ρ_l is the density of the solution. The second term in this equation is the electric force acting on the volume charge, and the third term is the electrostriction term. As in Chapter 1, we neglect the polarization of the medium resulting in ϵ being a function of E and, hence, of x .

Equation (6.13) can be written in the differential form

$$dp + \rho d\psi + \frac{1}{8\pi} d \left(E^2 \frac{\partial \epsilon}{\partial \rho_l} \rho_l \right) = 0 \quad (6.14)$$

While in the bulk of the solution $p = p_0$ (hydrostatic pressure in the bulk liquid), $\psi \equiv 0$, and $E \equiv 0$; in the interlayer $\psi(x) \neq 0$, $p \neq p_0$, and $E \neq 0$, and we obtain from (6.14) the following relation:

$$p_0 = p(x, h) + \int_0^{\psi(x, h)} \rho d\psi + \frac{1}{8\pi} E^2(x, h) \frac{\partial \epsilon}{\partial \rho_l} \rho_l \quad (6.15)$$

On the other hand, we immediately obtain an equivalent relation by substituting the Poisson equation (6.5) into (6.13):

$$\frac{\partial}{\partial x} \left[p(x, h) - \frac{\epsilon E^2(x, h)}{8\pi} + \frac{E^2(x, h)}{8\pi} \frac{\partial \epsilon}{\partial \rho_l} \rho_l \right] = 0$$

It follows from this that the pressure normal to the surfaces in any transverse cross section of the film, i.e.,

$$p_1 \equiv p(x, h) - \frac{\epsilon E^2(x, h)}{8\pi} + \frac{E^2(x, h)}{8\pi} \frac{\partial \epsilon}{\partial \rho_l} \rho_l \quad (6.16)$$

is constant; it is a function only of h , independent of x . It is composed of the hydrostatic pressure, Maxwell stress, and striction

pressure. The difference between $p_1(h)$ and p_0 is precisely the disjoining pressure $\Pi_e(h)$, constant at a given gap width. Indeed, by subtracting (6.15) from (6.16) we immediately obtain (6.12) with the electrostriction term eliminated. Therefore, the only result of the electrostriction effect is that the hydrostatic pressure p becomes, by virtue of (6.15), a function of the local value of the electrostatic potential ψ and of the local value of the field E . (This was first shown by one of us in [4].) The derivation given above does not require a knowledge of what happens with charges and potentials of interfaces when double layers overlap, and of the mechanism of surface charging. Integration of Π_e over the distance h between the interfaces of diffuse layers makes it possible to obtain an important characteristic of overlapping diffuse atmospheres, viz., their Gibbs free energy of interaction, $V_e \equiv \Delta G_e$.

Another method of calculating Π_e is based on a preliminary calculation of the free energy G_e of overlapping electrical double layers. The energy of interaction V_e is found as the difference between the sums of free energies of the overlapping and distant double layers, so that the disjoining pressure is then found by differentiating V_e with respect to distance. Calculations of free energy usually involve considerable difficulties not only in computations but also in principle. The problem was first pointed out by one of us in [7] where two possible methods of calculating V_e were given, and a correct expression for V_e in the Debye-Hückel approximation was obtained, coinciding with that obtained by integrating the disjoining pressure found in the framework of the direct-force approach [1]. The first of the methods for calculating free energy, suggested in [7], is thermodynamic, while the second is a modification of the charging method employed by Debye in the theory of strong electrolytes. Both methods were later used in the development of the theory of stability of lyophobic colloids [8-10]. Specific features of different techniques for calculating the free energy of double layers are discussed in detail in the review [11] where, among other things, the complete equivalence of the thermodynamic method and the charging method is proved.

The general statistical-mechanical derivation of the integral relations for the free energy of double layers was given by Ikeda [12] who analyzed, as in [9, 10], two different boundary conditions for the overlapping of double layers: constant potential ψ_1 , and constant surface charge density. It was found that each of these conditions (and hence, any other possible condition) yields a distinct integral expression for free energy. This is a shortcoming of this method of calculating the interaction between double layers. (Ikeda chose not to go beyond deriving the general integral formulas from which the free energy of overlapping electrical double layers can be calculated only after the corresponding electrostatic problem had been solved. Obviously, the final calculation formulas for $\psi = \text{const}$ and $\sigma = \text{const}$ must be different.)

6.2. INTERACTION BETWEEN IDENTICAL LAYERS. BOUNDARY CONDITIONS

If the overlapping diffuse layers are identical, the system necessarily has a symmetry plane $x = d = h/2$ corresponding to $\psi = \psi_d$ and $E = 0$. In this case, Eq. (6.12) yields a well-known formula [9]:

$$\Pi_e(\psi_d) = - \int_0^{\psi_d} \rho d\psi > 0 \quad (\rho\psi < 0) \quad (6.17)$$

which allows derivation of the desired function $\Pi_e(h)$ after the dependence of ρ on ψ has been established and boundary conditions at the interfaces formulated. In the Gouy-Chapman approach, the volume charge density of a binary asymmetric electrolyte is (see Chapter 1)

$$\rho = e(z_1 n_1 e^{z_1 e\psi/\theta} - z_2 n_2 e^{-z_2 e\psi/\theta}) \quad (6.18)$$

where z_1 and z_2 are the valences of counterions and secondary ions, respectively, n_1 and n_2 are their volume concentrations, $\theta = kT$, and, by virtue of the electroneutrality condition, $z_1 n_1 = z_2 n_2$. Substitution of (6.18) into (6.17) and integration yield the isotherm

$$\Pi_e(\phi_d) = \frac{1}{2}(z_1 n_1 + z_2 n_2)\theta f(\phi_d) \quad (6.19)$$

where, in accord with the definition introduced in Chapter 1,

$$\phi_d = e\psi_d/\theta$$

The function $f(\phi)$ in Eq. (6.19) depends on the value of potential and the valences of the ions:

$$f(\phi) = \frac{1}{z_1} e^{z_1 \phi} + \frac{1}{z_2} e^{-z_2 \phi} - \frac{1}{z_1} - \frac{1}{z_2} \quad (6.20)$$

and, obviously, $f(0) = 0$.

With two identical layers in a symmetrical electrolyte, Eq. (6.19) becomes

$$\Pi_e = 2n\theta(\cosh \phi_d - 1) \quad (6.21)$$

This formula was first derived by Langmuir [2] from Eq. (6.2), by considering the excess osmotic pressure of ions in the symmetry plane of an electrolyte film where the strength of electric field is zero. However, in strong electrolytes the osmotic pressure is given by the formula [13]

$$P_{os} = \theta(n_1 + n_2) - \frac{e^2 \kappa}{6\epsilon} (z_1^2 n_1 + z_2^2 n_2) \quad (6.22)$$

where the second term on the right-hand side constitutes a considerable fraction of the first term, even for univalent ions at relatively low electrolyte concentrations ($C \approx 0.1$ mole/liter). Formally, Eq. (6.21) can be derived from (6.12), provided we neglect the second term in (6.22) in comparison with the first. However, the relationship between disjoining pressure and osmotic pressure is in fact an arbitrary assumption that cannot be proved. Moreover, it was shown in [14] that a similar use of excess osmotic pressure in the calculation of the component of disjoining pressure that depends on the overlapping of nonionic diffuse adsorption atmospheres gives results much greater than the true values. At the same time, the Langmuir equation (6.21), giving Π_e as a function of excess volume density of the energy of ionic thermal motion in the zone of zero field strength, remains completely valid. However, Langmuir's method cannot be used if the potential within the interlayer has no minima. Such cases are possible even if the surface potentials are of like sign but differ in magnitude [15-20]. In this case we have to use the general formula (6.12) that yields, in certain conditions, negative values of Π_e corresponding to attraction of the surfaces. Attraction may take place even for surfaces with like sign [15]. Correct derivations of formula (6.21) were given by Frumkin [21] for wetting films with noncharged surfaces, and by Derjaguin and Landau for the symmetrical case [8].

The result of immediate practical importance is not the function $\Pi_e(\psi_d)$ but Π_e as a function of the distance h between the interfaces of diffuse layers. In contrast to the former, the latter is not invariant with respect to boundary conditions [22] which reflect the specific features of the charging mechanism. It is this mechanism that determines, via the electroneutrality condition for a system of double layers, the changes in the potential ψ_1 of the interfaces of these layers when the thickness of the separating interlayer is varied. In a planar gap the electroneutrality condition is

$$\sigma_s(\phi_1) + \sigma_d(\phi_1, \phi_d) = 0 \quad (6.23)$$

where σ_s is the surface charge density, including the charge of the surface per se and that of the Stern monolayer, and σ_d is the density of the diffuse charge between the surface and the symmetry plane. The first of these quantities is determined by the equation that corresponds to a specific mechanism of surface charging, and the second by the general relation representing the first integral of the Poisson-Boltzmann equation (1.16). In the notation introduced above, this integral is

$$\frac{d\phi}{dx} = - \kappa \sqrt{\frac{2}{z_1 + z_2} [f(\phi) - f(\phi_d)]} \quad (6.24)$$

where $1/\kappa$ is the Debye screening length (1.27). Now we readily find the surface charge of the diffuse atmosphere:

$$\sigma_d = - \frac{\epsilon}{4\pi} \frac{d\psi}{dx} \Big|_{x=0} = \frac{\epsilon \theta \kappa}{4\pi e} \sqrt{\frac{2}{z_1 + z_2} [f(\phi_1) - f(\phi_d)]} \quad (6.25)$$

The last equation necessary to find $\Pi_e(h)$ relates the quantities ϕ_1 and ϕ_d directly to the distance h , and constitutes the second integral of the Poisson-Boltzmann equation:

$$\frac{\kappa h}{2} = \sqrt{\frac{z_1 + z_2}{2}} \int_{\phi_d}^{\phi_1} d\phi / \sqrt{f(\phi) - f(\phi_d)} \quad (6.26)$$

If the dependence

$$\sigma_s = \sigma_s(\phi_1) \quad (6.27)$$

is known or fixed a priori, the set of equations (6.9), (6.23), (6.25)-(6.27) define the function $\Pi_e(h)$ for a given composition of the solution.

6.3. INTERACTION AT CONSTANT CHARGE OR AT CONSTANT SURFACE POTENTIAL

We have seen that the $\Pi_e(h)$ curves are different for systems which have the same potential of the lone (isolated) double layer $\psi_\infty = \psi_1(h \rightarrow \infty)$ but differ in the mechanism of charging of the interface. However, one factor makes it possible to evaluate how large this difference can be. In fact, all possible $\Pi_e(h)$ curves fall within a "fork" formed by the $\Pi_e(h)$ curves calculated for constant potential of diffuse layer interfaces ($\psi_1 = \psi_\infty = \text{const}$) and for constant charge density [$\sigma_s = \text{const}$ and, hence, $\sigma_d = \text{const}$ by (6.23)]. Repulsion is minimal in the first case, and maximal in the second. These two cases allow for the exact parametric solution of the problem for symmetrical electrolytes of arbitrary valence [9], for asymmetrical electrolytes of the types 1-2 and 2-1 [23], and also for some mixtures [24] – i.e., for conditions in which the second integral of the Poisson-Boltzmann equation, given by Eq. (6.26), can be calculated analytically. Introduction of new variables

$$\begin{aligned} \vartheta &= \arcsin(1/\cosh(z\phi_d/2)) \\ \varphi &= \arccos(\sinh(z\phi_d/2)/\sinh(z\phi_1/s)) \end{aligned} \quad (6.28)$$

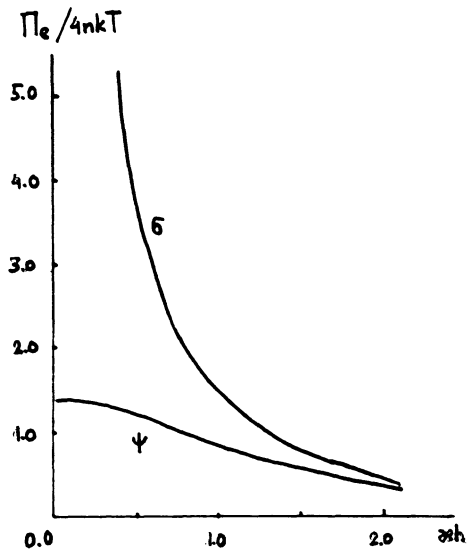


Fig. 6.2. Π_e as a function of kh in a symmetrical electrolyte at $\psi_1 = \text{const}$ (lower curve) and at $\sigma = \text{const}$ (upper curve). The single layer potential is $50/z$ mV.

for symmetrical electrolytes transforms Eqs. (6.21) and (6.26) to a simple form [25]:

$$\Pi_e / 4nkT = \cot^2 \vartheta \quad (6.29)$$

$$\kappa h = 2 \sin \vartheta \cdot F(\varphi, \vartheta) \quad (6.30)$$

The relation between the parameters φ and ϑ in these equations is dictated by boundary conditions. If $\phi_1 = \text{const}$,

$$\cos \varphi = \cot \vartheta / \sinh(z\phi_1/2) \quad (6.31)$$

and if $\sigma = \text{const}$,

$$\tan \varphi = \tan \vartheta \cdot \sinh(z\phi_\infty/2) \quad (6.32)$$

The function $F(\varphi, \vartheta)$ in Eq. (6.30) is an elliptic integral of the first kind with modulus $\sin \vartheta$ and amplitude φ . Figure 6.2 presents some calculated results of $\Pi_e(kh)$ to illustrate the difference between the cases $\sigma = \text{const}$ and $\psi_1 = \text{const}$. This figure shows that the difference is especially marked at small distances h between the surfaces. Thus, if $\psi_1 = \text{const}$, the potential ψ_d of the symmetry plane tends to ψ_1 as $h \rightarrow 0$, and disjoining pressure Π_e tends, by (6.21), to a finite limit.

$$\lim_{h \rightarrow 0} \Pi_e^\psi = 4nkT \sinh^2(\phi_1/2) \quad (6.33)$$

When h is reduced at $\sigma = \text{const}$, it results not only in increasing the potential ϕ_d but also in a theoretically unlimited growth of ϕ_1 , by Eq. (6.25). As a result, ϑ in (6.28) becomes very small, φ tends to $\pi/2$ and, hence, $F(\varphi, \vartheta) \rightarrow \pi/2$. According to Eqs. (6.29) and (6.30), $\Pi_e/4nkT \approx 1/\vartheta^2$ and $\kappa h \approx \pi\vartheta$. When the parameter ϑ is eliminated from the last two approximate equalities, a simple relation holds:

$$\Pi_e/4nkT \approx \pi^2/(\kappa h)^2 \quad (6.34)$$

In view of the definition of the reciprocal Debye length (1.30), (6.34) transforms into the well-known Langmuir formula [2]:

$$\Pi_e \approx \pi \epsilon (kT)^2 / 2z^2 e^2 h^2 \quad (6.35)$$

If $\sigma = \text{const}$, this formula holds at least for $h \ll 1/\kappa$. It signifies that disjoining pressure increases indefinitely when the interlayer thins out, being independent of the potential $\phi_\infty = \phi_1(\infty)$ of the double layers prior to the onset of the interaction. Actually, as $h \rightarrow 0$, the dependence of Π_e on distance is modified to $\Pi_e \sim \sigma/h$ (see [19] and Eq. (6.149) in Section 6.10). At high values of ϕ_∞ and ϕ_1 formula (6.35) can be approximately valid at large distances as well, not only at $\sigma = \text{const}$ but even in the case $\psi_1 = \text{const}$. However, in this last case it definitely fails at very short distances as $h \rightarrow 0$ because then it contradicts the exact equality (6.33).

6.4. INTERACTION BETWEEN DOUBLE LAYERS IN ASYMMETRICAL ELECTROLYTES

It has been mentioned earlier that exact formulas for $\Pi_e(h)$ are also available for electrolytes consisting of mono- and bivalent ions [23]. These formulas are more cumbersome than those given above. In accordance with (6.19) and (6.26) we find for 2-1 electrolytes (with a bivalent counterion)

$$\Pi_e = n_2 kT (1/b^2 + 2b - 3) \quad (6.36)$$

$$\kappa h = 2 \sqrt{\frac{6}{\alpha + c}} F(\mu, q) \quad (6.37)$$

where n_2 is the concentration of bivalent ions (in cm^{-3}), $\kappa = (24\pi \times e^2 n_2 / \epsilon kT)^{1/2}$,

$$\mu = \arcsin \sqrt{\frac{(\alpha + c)(b - v)}{(b + c)(\alpha - v)}}, \quad q = \sqrt{\frac{b + c}{\alpha + c}} \quad |$$

$$\left. \begin{aligned} b &= e^{-\phi d}, \quad v = e^{-\phi_1}, \\ a &= (\sqrt{1 + 8b^3} + 1)/4b^2, \quad c = (\sqrt{1 + 8b^3} - 1)/4b^2 \end{aligned} \right\} \quad (6.38)$$

For $\phi_1 = \text{const}$ the only independently varying quantity in (6.38) is ϕ_d ($0 \leq \phi_d \leq \phi_1$), i.e., the parameter b , because v remains constant. If $\sigma = \text{const}$, these equations must be supplemented by another following from (6.25):

$$f(\phi_1) - f(\phi_d) = f(\phi_\infty) \quad (6.39)$$

i.e., by the definition (6.20),

$$\begin{aligned} 1/2v^2 + v - 1/2b^2 - b &= 1/2w^2 + w - 3/2 \\ w &= e^{-\phi_\infty} \end{aligned} \quad (6.40)$$

If the potential of a single layer ϕ_∞ is known, Eq. (6.40) enables one to calculate for any prescribed value of ϕ_d (or b) the corresponding value of ϕ_1 (in terms of v) and thus find the sought pair of values of $\Pi_e/n_2 kT$ and κh . Now it is ϕ_d that at short distances can reach values greater than ϕ_∞ .

For 1-2 electrolyte (with a univalent counterion)

$$\Pi_e = n_2 kT(2\alpha_1 + 1/\alpha_1^2 - 3) \quad (6.41)$$

$$\kappa h = 2 \sqrt{\frac{6}{\alpha_1 + c_1}} F(\mu_1, q_1) \quad (6.42)$$

where n_2 is again the concentration of the bivalent ion (in cm^{-3}), and $\kappa = (24\pi e^2 n_2 / \epsilon kT)^{1/2}$,

$$\begin{aligned} \mu_1 &= \arcsin \sqrt{\frac{v_1 - \alpha_1}{v_1 - b_1}}, \quad q_1 = \sqrt{\frac{b_1 + c_1}{\alpha_1 + c_1}}, \\ \alpha_1 &= e^{\phi d}, \quad v_1 = e^{\phi_1} \end{aligned} \quad (6.43)$$

$$b_1 = (\sqrt{1 + 8\alpha_1^3} + 1)/4\alpha_1^2, \quad c_1 = (\sqrt{1 + 8\alpha_1^3} - 1)/4\alpha_1^2$$

If $\phi_1 = \text{const}$, the parameter v_1 is constant and the degree of overlapping is determined directly by the parameter α_1 related to ϕ_d . If $\sigma = \text{const}$, Eq. (6.39) transforms to

$$\begin{aligned} 1/2v_1^2 + v_1 - 1/2\alpha_1^2 - \alpha_1 &= 1/2w_1^2 + w_1 - 3/2 \\ w_1 &= e^{\phi_\infty} \end{aligned} \quad (6.44)$$

which is analogous to (6.40). The procedure for calculating the pairs of values of Π_e and κh is the same here as for 2-1 electrolytes. Although the exact relations given above are extremely unwieldy and call for using special functions, their application is in fact unavoidable in a number of cases. Indeed, accurate recent experiments made it possible to establish that structural forces do act in very thin electrolyte interlayers [26-28] (see Chapter 7) but the dispersion and electrostatic forces being also high in these conditions, the determination of structural forces is possible only by finding the difference between the measured effect and the sum of calculated electric and molecular components. Figure 6.2 shows how important for this problem is the choice of boundary conditions that reflect the physical content and mathematical treatment of the mechanism of interface charging. Indeed, at small distance, Π^σ may be several times greater than Π^ψ , and there is a danger that electrical effects due to the constancy of charge on approaching interfaces will be assigned to structural forces.

However, some specific features of the interaction in asymmetrical electrolytes can be evaluated without involving complicated calculations. Thus, formulas (6.19) and (6.20) make it possible to demonstrate immediately the effect of the valence of the co-ion with the same counterion on disjoining pressure when the surfaces are in close contact, i.e., when $\phi_d \rightarrow \phi_1$. By comparing disjoining pressures at identical potential ψ_1 and identical concentration n_{z_1} of counterions, we obtain

$$\frac{\Pi_{2-1}^\psi}{\Pi_{2-2}^\psi} = \frac{e^{2\phi_1} + 2e^{-\phi_1} - 3}{e^{2\phi_1} + e^{-2\phi_1} - 2} = \begin{cases} 3/4 & \text{at } \phi_1 \ll 1 \\ 1 & \text{at } \phi_1 \gg 1 \end{cases}$$

$$\frac{\Pi_{1-1}^\psi}{\Pi_{1-2}^\psi} = \frac{2(e^{\phi_1} + e^{-\phi_1} - 2)}{2e^{\phi_1} + e^{-2\phi_1} - 3} = \begin{cases} 2/3 & \text{at } \phi_1 \ll 1 \\ 1 & \text{at } \phi_1 \gg 1 \end{cases}$$

Hence, an increase in the valence of the co-ion at constant concentration of counterions results in a relatively small enhancement of disjoining pressure at close contact, and therefore, in enhanced stability of films. In general, the pressure $\Pi^\psi(0)$ at low potentials is directly proportional to the sum of valences $z_1 + z_2$ if the values of ψ_1 and n_{z_1} are fixed.

6.5. SOME APPROXIMATE FORMULAS FOR DISJOINING PRESSURE

In many cases it is sufficient to work with relatively simple approximations for $\Pi_e(h)$. Such approximations are valid mainly if

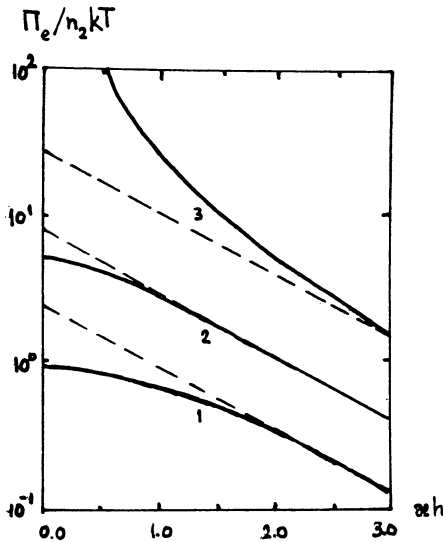


Fig. 6.3. Π_e as a function of κh in a 2-1 electrolyte (with a bivalent counterion). Solid curves plot formulas (6.36)-(6.38), and dashed curves plot formulas (6.48) and (6.49). The diffuse layer potential: 12.5 (1), 25 (2), 150 mV (3).

the surface charge is small and the linearized Poisson-Boltzmann equation is acceptable. Formula (6.12) then gives

$$\Pi^\psi = \frac{1}{4}(z_1 + z_2)(z_1 n_1 + z_2 n_2)kT\phi_1^2/\cosh^2 \kappa d \quad (6.45)$$

$$\Pi^\sigma = \frac{1}{4}(z_1 + z_2)(z_1 n_1 + z_2 n_2)kT\phi_\infty^2/\sinh^2 \kappa d \quad (6.46)$$

However, at short distances $\kappa d \ll 1$ the second of these equations is not valid because formally the potential in the symmetry plane, $\phi_d = \phi_\infty/\sinh \kappa d$, undergoes unlimited growth and thus violates the condition of applicability of the linearized Debye-Hückel equation. Nevertheless, the dependence of Π^σ on distance remains correct; i.e., $\Pi^\sigma \sim h^{-2}$ in accordance with the Langmuir formula (6.35), but Π^σ ceases to be independent of surface potential.

Important approximate expressions for $\Pi_e(h)$, valid for interlayers that are not too thin, can also be obtained on the basis of simple physical arguments, even in certain cases in which the equation cannot be linearized. If the distance between surfaces is rel-

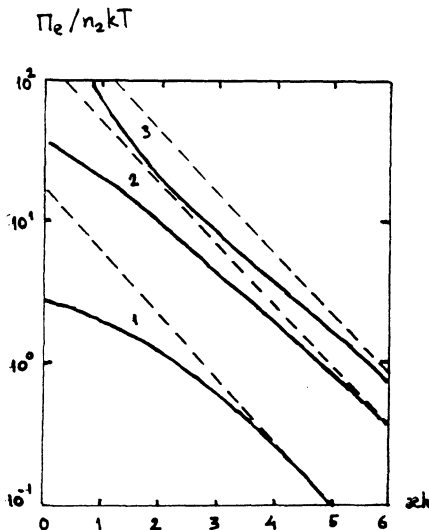


Fig. 6.4. Π_e as a function of z/h in a 1-2 electrolyte (with a univalent counterion). Solid curves plot formulas (6.41)-(6.43), and dashed curves plot formulas (6.48) and (6.50). The diffuse layer potential: 25 (1), 75 (2), 150 mV (3).

atively large, we can make use of the fact that the electrostatic potential of the interlayer close to its symmetry plane is nearly equal to the sum of potentials of each surface calculated under the assumption that the other surface is removed to infinity [8-10]. Taking into account that both potentials are small, expanding formula (6.19) into a series in potential ϕ_d , and using formulas (1.38) and (1.39) for $x = d = h/2$, we obtain for symmetrical electrolytes a well-known formula [9]:

$$\Pi_e = 64n_2 k T \gamma^2 e^{-\kappa h}, \quad \gamma = \tanh(z\phi_1/4) \quad (6.47)$$

An explicit dependence of Π_e on distance for 2-1 and 1-2 electrolytes is obtained in the same way [23]:

$$\Pi_e = 432n_2 k T \tanh^2[v_i(\phi_1)/4]e^{-\kappa h}, \quad i = 1, 2 \quad (6.48)$$

where n_2 is the concentration of bivalent ions (in cm^{-3}) and the functions $v_i(\phi_1)$ are defined by Eqs. (1.33) and (1.34). We recall that

$$v_1(\phi) = \ln[3/(1 + 2e^{-\phi})] \quad (6.49)$$

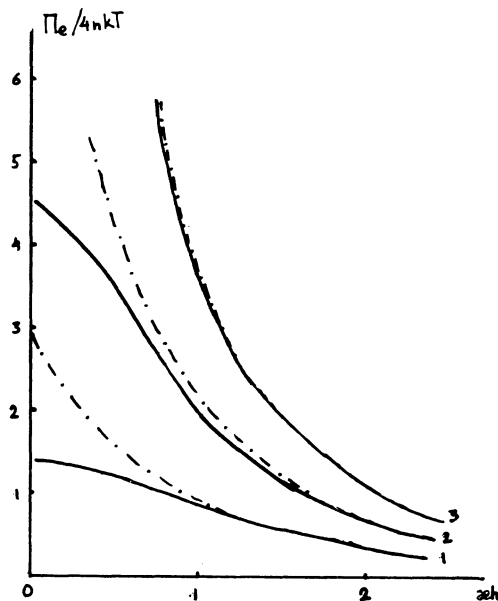


Fig. 6.5. Exact ($\psi_1 = \text{const}$) and approximate curves $\Pi_e(kh)$ in symmetrical electrolytes. Solid curves plot Eqs. (6.29)-(6.31), and dashed curves plot Eqs. (6.51) and (6.52); $z\psi_1 = 50$ (1), 75 (2), and 100 mV (3).

in electrolytes with a bivalent counterion, and

$$v_2(\phi) = \ln [(2e^\phi + 1)/3] \quad (6.50)$$

in electrolytes with a univalent counterion.

The regions in which these formulas are valid can be established only by comparing them with the results of calculations employing the exact equations given above. An analysis shows that Eq. (6.48) fits the function $\Pi_e(kh)$ very well for $kh \geq 2$ in 2-1 electrolytes (with a bivalent counterion), even if $\phi_1 \gg 1$. As potential decreases, this equation becomes more accurate, and can be used for practically any kh when $\phi_1 \approx 1$ (Fig. 6.3). At smaller ϕ_1 , formula (6.45) can be reliably used. In the case of 1-2 electrolytes the accuracy of formula (6.48) is considerably lower (Fig. 6.4), but even here it can serve as a basis for quantitative calculation of the energy of interaction between flat and curved double layers at relatively large distances (see below).

Finally, formulas (6.29) and (6.30) yield another useful approximate parametric relation for $\Pi_e(h)$ of a symmetrical electro-

lyte. By expanding the last of these formulas in a small parameter related to potential ϕ_1 we find [25]

$$\kappa h/2 \approx qK(q) - 1/\sinh(z\phi_1/2) \quad (6.51)$$

$$\Pi_e/4nkT = 1/q^2 - 1, \quad q < 1 \quad (6.52)$$

Here $K(q)$ is the complete elliptic integral of the first kind. This formula is a good representation of $\Pi_e(h)$ for $\phi_1 \gtrsim 2$ ($z\phi_1 \gtrsim 50$ mV) in the range of distances of the order of the Debye length (see Fig. 6.5). Curiously enough, the curves $\Pi_e(\kappa h)$ for different values of ϕ_1 are obtained by parallel transfer of the curve calculated for $\phi_1 = \infty$ along the horizontal axis by $2/\sinh(z\phi_1/2)$ toward the origin. This parametric relation proves useful, for instance, in the derivation of criteria of stability breakdown in the framework of the DLVO theory (see Chapter 8).

6.6. GIBBS FREE ENERGY OF THE INTERACTION BETWEEN FLAT DOUBLE LAYERS UNDER DIFFERENT BOUNDARY CONDITIONS

The direct integration of disjoining pressure Π_e over distance h is definitely the best way to calculate the free energy of interaction V_e between flat double layers. However, the method was rarely used, owing to the following misunderstanding. An opinion was advanced [9] that even in the simplest case of constant potential of diffuse layers, $\psi_1 = \text{const}$, the exact integration of Π_e over h at an arbitrary value of ψ_1 is impossible. Having derived the equation for the disjoining pressure in the planar case in the form

$$P = 2nkT(\cosh u - 1) \quad (41)$$

(notations as in [9]), Verwey and Overbeek remark, on p. 95 of [9]: "A remarkable point about Eq. (41) is that it contains neither the electric surface potential (ψ_0 or Z) nor the plate distance $2d$, but only the electric potential midway between the plates (ψ_d or u). But the relation between Z , u , and d being rather complicated (cf. Chapter IV), it is impossible to integrate Eq. (41), for a given value of ψ_0 , with respect to the distance. Hence there is no advantage in using this force equation to evaluate the repulsive potential V_R , for a system of two plane double layers, on the basis of the complete differential equation (3)" (i.e., the Poisson-Boltzmann equation). This statement is not correct. Later, exact expressions for the energy of electrostatic interaction were derived in this way [25], not only at $\psi_1 = \text{const}$ but also at $\sigma = \text{const}$ in symmetrical electrolytes. The first of them proved completely equivalent to the corresponding expression derived by Verwey and Overbeek by the charging method in terms of free energy [9].

The second was derived for the first time. (Later it, too, was derived by the charging method [29, 30].) Then it was shown in [31], again for symmetrical electrolytes, that the direct force approach gives the exact expression for $V_e(h)$, regardless of the mechanism of surface charging, provided the relation between surface charge density σ_s (including the Stern layer charge) and the diffuse layer potential ψ_1 is known.

In addition to the cases of $\psi_1 = \text{const}$ and $\sigma = \text{const}$, the interaction energy was found in [31] in the cases where the Stern layer charge is described by the Stern isotherm for the ion mixture, and when double diffuse layers exist on both sides of the interface between two immiscible liquids. And, finally, the general solution for $V_e(h)$, valid for symmetrical and asymmetrical electrolytes and an arbitrary prescribed dependence $\sigma_s(\psi_1)$, was obtained in [23] in quadrature by using Eqs. (6.19), (6.20), (6.23), (6.25), and (6.26). This solution can be written in the form

$$V_e = V_1(\psi_1, \psi_\infty, \psi_d) + 2 \int_{\psi_\infty}^{\psi_1} \sigma_s(\psi_1) d\psi_1 \quad (6.53)$$

$$\kappa h = f_1(\psi_1, \psi_d) \quad (6.54)$$

where f_1 is the integral on the right-hand side of Eq. (6.26). Exact integration is possible when the second integral of the Poisson-Boltzmann equation (6.26) can be found, i.e., can be reduced to known functions. In the notations of (6.28), for symmetric electrolytes we have [31]

$$\begin{aligned} \frac{\kappa}{16nkT} V_1(\phi_1, \phi_\infty, \phi_d) = & - \frac{\cosh(z\phi_d) - 1}{4 \cosh(z\phi_d/2)} F(\varphi, \vartheta) \\ & + \cosh\left(\frac{z\phi_d}{2}\right) E(\varphi, \vartheta) + \cosh\left(\frac{z\phi_\infty}{2}\right) - 1 \\ & - \coth\left(\frac{z\phi_1}{2}\right) \left(\frac{1}{2} [\cosh(z\phi_1) - \cosh(z\phi_d)] \right)^{1/2} \end{aligned} \quad (6.55)$$

where $E(\varphi, \vartheta)$ is an elliptic integral of the second kind, of modulus $\sin \vartheta$, with amplitude φ . In order to find $V^\psi(h)$ at $\psi_1 = \text{const}$, it is sufficient to set $\phi_1 = \phi_\infty$ in formula (6.55), and make use of formulas (6.28), (6.30), and (6.31). The second term on the right-hand side of Eq. (6.53) is then zero. But if $\sigma = \text{const}$, the corresponding dependence $V^\sigma(h)$ is obtained by adding to (6.55) the term

$$\frac{1}{2} z(\phi_1 - \phi_\infty) \sinh(z\phi_\infty/2)$$

and then applying formulas (6.28), (6.30), and (6.32) [31].

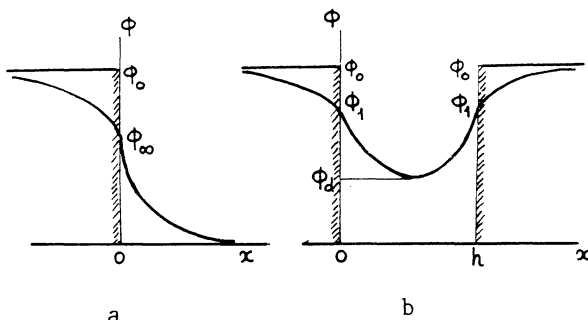


Fig. 6.6. Double layers in emulsions: a) single interface; b) two interfaces.

Formula (6.53) can also be used when double layers are formed not only in the interlayer but also in the contiguous immiscible phases (the situation typical for oil/water or water/oil-type emulsions) (Fig. 6.6). In this case, Eq. (6.43) is supplemented by the term

$$\frac{\sinh(z\phi_\infty/2)}{\sinh[z(\phi_0 - \phi_\infty)/2]} \left[\cosh \frac{z(\phi_0 - \phi_\infty)}{2} - \cosh \frac{z(\phi_0 - \phi_1)}{2} \right]$$

[31] which yields the formula for $V_e^{\text{em}}(h)$ in which the potential ϕ_∞ is found from the equation

$$\sqrt{\varepsilon_1 n_1} \sinh \left(\frac{z\phi_\infty}{2} \right) = \sqrt{\varepsilon_2 n_2} \sinh \left[\frac{z(\phi_0 - \phi_\infty)}{2} \right] \quad (6.56)$$

Here ϕ_0 is the difference in dimensionless potentials between the bulks of two immiscible liquids (oil and water), ε_2 and n_2 are the permittivity and the concentration of ions in the dispersed liquid, respectively, and ε_1 and n_1 denote the same quantities in the continuous phase. Much more cumbersome expressions are obtained for asymmetrical 2-1 and 1-2 electrolytes [23], not given here. Figure 6.7 illustrates the difference in the energy of electrostatic repulsion in two limiting cases, $\psi_1 = \text{const}$ and $\sigma = \text{const}$. Both in this figure and in Fig. 6.8 we give the results for $V_e(h)$ obtained by means of the formulas derived by direct integration of the approximate functions $N_e(h)$ given above. In a symmetrical electrolyte [9, 10]

$$V_e = \frac{n k T}{\kappa} \tanh^2 \left(\frac{z\phi_1}{4} \right) e^{-\kappa h} \quad (6.57)$$

and in 1-2 and 2-1 electrolytes [23]

$$(\alpha/16\pi\theta)V_e$$

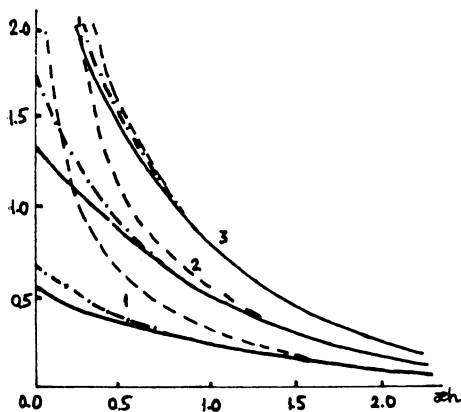


Fig. 6.7. Exact and approximate dependences $V_e(\alpha h)$ in symmetrical electrolytes:
 —) $\psi_1 = \text{const}$; - - -) $\sigma = \text{const}$;
 - · -) formulas (6.52) and (6.61);
 $z\psi_1 = 50$ (1), 75 (2), 100 mV (3).

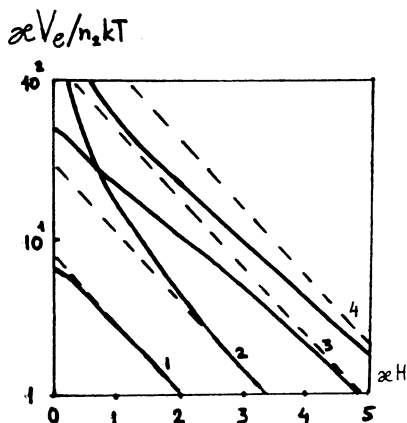


Fig. 6.8. Exact (solid curves) and approximate (dashed lines) dependences $V_e(\alpha h)$ in asymmetrical electrolytes for $\psi_1 = \text{const}$: 2-1 electrolyte: $\psi_1 = 25$ mV (1), 150 mV (2); 1-2 electrolyte: $\psi_1 = 75$ mV (3), 150 mV (4). Dashed lines plot formula (6.58).

$$V_e = 432 \frac{n_2 kT}{\kappa} \tanh^2 \left[\frac{v_i(\phi_1)}{4} \right] e^{-\kappa h} \quad (6.58)$$

where the functions v_i are defined by Eqs. (6.49) or (6.50). As before, the accuracy of formula (6.58) in systems with a bivalent counterion is much better than in systems with a univalent counterion. Integration of formulas (6.45) and (6.46) for low potentials yields simple relations:

$$V^\psi = \frac{1}{2}(z_1 + z_2)(z_1 n_1 + z_2 n_2) \frac{kT}{\kappa} \phi_1^2 \left[1 - \tanh \left(\frac{\kappa h}{2} \right) \right] \quad (6.59)$$

$$V^\sigma = \frac{1}{2}(z_1 + z_2)(z_1 n_1 + z_2 n_2) \frac{kT}{\kappa} \phi_\infty^2 \left[\coth \left(\frac{\kappa h}{2} \right) - 1 \right] \quad (6.60)$$

As the distance between the surfaces diminishes, the difference between V^σ and V^ψ can become very large because $V^\sigma/V^\psi = \coth(\kappa h/2)$. When $\kappa h \gtrsim 3-4$, V^σ and V^ψ practically coincide. Finally, integration of the disjoining pressure (6.52) over distance (6.51) at constant ϕ_1 yields an approximate formula [25]

$$\frac{\kappa}{8nkT} V_e \approx \frac{2}{q} E(q) - \frac{1}{q} (1 - q^2) K(q) - 2 \quad (6.61)$$

where $E(q)$ is a complete elliptic integral of the second kind. This formula can readily be obtained by expanding the exact formulas for V^ψ and V^σ [25]. Taken together with (6.51), this formula gives a faithful description of $V^\psi(\kappa h)$ at potentials above 50 mV. This formula was first derived for maximally charged surfaces by Derjaguin and Landau [8].

6.7. INTERACTION BETWEEN CHARGED SPHERICAL PARTICLES

Objects used to measure surface forces often have a curved (spherical or cylindrical) surface [26-28, 32]. It is also very rare for the particles of disperse systems whose stability critically depends on surface forces, to be plate-shaped. Their shapes are usually nearly spherical, ellipsoidal, or cylindrical. The "ring zones" formula (2.49) makes it possible to relate the force of interaction of such objects to their curvature and to the free energy of interaction between interfaces. It is only necessary for the characteristic radius of surface forces to be much smaller than particle curvature radii. Derjaguin's method yields for the force and energy in the case of two identical spheres [33] (see Section 2.8)

$$F(h) = \pi a V(H) \quad (6.62)$$

$$U(H) = \int_H^{\infty} V(h) d(h) \quad (6.63)$$

where

$$V = \int_H^{\infty} \Pi dh$$

is the free energy of interaction between planes, a is the radius of the spheres, and H is the shortest distance between them. Therefore, the formulas obtained above for the energy of repulsion of plane interfaces give simultaneously, to within a constant factor, the force of interaction between spheres.

No exact formulas are available for the energy of repulsion between spheres, not even in the framework of the linear Debye-Hückel approximation, although McCartney and Levine [34] were able to derive, in a complicated way, a quite good and at the same time simple approximate formula that holds for low double layer potentials [34]:

$$U^\psi = \epsilon a \psi_1^2 \frac{a + H}{2a + H} \ln \left(1 + \frac{a}{a + H} e^{-\kappa H} \right) \quad (6.64)$$

Derjaguin's method used together with formulas (6.59) and (6.60) immediately yields simpler relations:

$$U^\psi = \frac{\epsilon a \psi_1^2}{2} \ln(1 + e^{-\kappa H}) \quad (6.65)$$

$$U^\sigma = -\frac{\epsilon a \psi_\infty^2}{2} (1 - e^{-\kappa H}) \quad (6.66)$$

Here, again, the difference between the conditions $\psi_1 = \text{const}$ and $\sigma = \text{const}$ appears at small κH as a sharp increase in U^σ when the interlayer thickness is reduced. If $H \ll a$, the McCartney-Levine formula (6.64) is identical to Derjaguin's formula (6.65), and for $H \sim a \gg 1/\kappa$ it transforms into another well-known formula derived specially for this case [1]:

$$U^\psi = \epsilon a \psi_1^2 \frac{a}{2a + H} e^{-\kappa H} \quad (6.67)$$

The advantage of the "rings" method is that, in contrast to all other methods, it imposes no restrictions on surface potential either from above or from below. Thus, when double layers slightly

overlap, so that the difference between the cases $\sigma = \text{const}$ and $\psi_1 = \text{const}$ is insignificant, this method gives for symmetrical electrolytes of arbitrary valence z [see formula (6.57)]

$$U_e = \frac{8\alpha\varepsilon(kT)^2}{z^2e^2} \tanh^2 \left(\frac{z\phi_1}{4} \right) e^{-\kappa H} \quad (6.68)$$

For asymmetrical 2-1 and 1-2 electrolytes [see formula (6.58)] we obtain

$$U_e = \frac{18\alpha\varepsilon(kT)}{e^2} \tanh^2 \left[\frac{v_i(\phi_1)}{4} \right] e^{-\kappa H} \quad (6.69)$$

Differences in the valence type of electrolytes affect the functions v_i whose dependence on surface potential is determined by Eqs. (6.49) and (6.50). If double layers slightly overlap ($\kappa H > 2-3$) and surface potentials are low, all formulas (6.65)-(6.69) yield the same result:

$$U_e = \frac{\varepsilon a \psi_1^2}{2} e^{-\kappa H} \quad (6.70)$$

In the case of asymmetrical electrolytes we must take into account when considering low potentials that $v = (2/3)\phi$, by (1.40).

If it is necessary to evaluate the energy of interaction for strongly charged spherical surfaces at short distances, the approximate parametric relations (6.61) and (6.51) can be used. Derjaguin's method for symmetrical electrolytes yields [25]:

$$U = \frac{2\alpha\varepsilon(kT)^2}{z^2e^2} \left[(1 - q^2)K^2 + 2K(q - E) + \int_q^1 \frac{KE}{q} dq \right] \quad (6.71)$$

where $K(q)$ and $E(q)$ are complete elliptic integrals of the first and second kind, respectively, and

$$\int_q^1 \frac{KE}{q} dq \approx -\frac{\pi^2}{4} \ln q \quad (6.72)$$

Together with (6.51), these formulas fit quite well the dependence of the electrostatic component of interaction energy of two spheres on the distance between them, provided $\psi_1 \geq 50/z$ mV; indeed, the resultant curves $U(\kappa H)$ coincide with those obtained in [9, 10] by numerical integration (Fig. 6.9).

When the characteristic radius of surface forces becomes comparable with the size of the particles, the rings method fails be-

$$(z^2/a) U_e \cdot 10^7, \text{ ergs/cm}^2$$

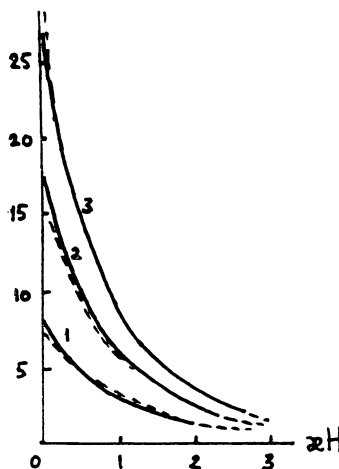


Fig. 6.9. U_e as a function of κH . Solid curves plot Eqs. (6.51), (6.71), and (6.72), and dashed curves represent numerical integration [9, 10]: $\psi_1 = 50$ (1), 75(2), 100 mV (3).

cause the potential distribution in the gap considerably deviates at each point from the distribution in the planar gap. However, an acceptable approximate relation can be obtained even in this case if potentials at the symmetry plane are low and can be approximated by a superposition of single-sphere potentials [35, 36]. The potential distribution around weakly charged particles [see (1.21)] is

$$\psi(r) = \psi_1 \frac{\alpha}{r} e^{-\kappa(r-\alpha)} \quad (6.73)$$

and the integration of electric field pressure in the symmetry plane in which the field vector lies yields a simple formula (6.67). Du-khin et al. [35] have shown for particles with arbitrary potential that the Poisson-Boltzmann equation can be linearized far from the particle surface, where potential drops to values below 10-15 mV, so that the potential distribution also has a form similar to (6.73):

$$\psi(r) = \frac{kT_B}{e} \frac{\alpha}{r} e^{-\kappa(r-\alpha)} \quad (6.74)$$

The only departure from (6.73) lies in a constant preexponential factor with a rather complicated structure.

$$\begin{aligned}
 B &= 4 \tanh \frac{\phi_1}{4} \left[1 + \frac{1}{2\kappa\alpha} \tanh \frac{\phi_1}{4} \right. \\
 &\quad \left. + \frac{1}{16\kappa\alpha} \int_0^{\phi_1} F(f_0) \frac{f_0^2(f_0) \sinh f_0}{\rho(f_0)} df_0 \right] \\
 f_1 &= \sinh \frac{f_0}{2} \left[\tanh^2 \frac{\phi_1}{2} - \tanh^2 \frac{f_0}{2} + 2(\kappa\alpha - \rho(f_0)) \right] \\
 F(f_0) &= \frac{\cosh \frac{\phi_1}{2}}{\sinh^2 \frac{\phi_1}{2}} - \frac{\cosh \frac{f_0}{2}}{\sinh^2 \frac{f_0}{2}} + \rho(f_0) - \kappa\alpha \\
 \rho(f_0) &= \kappa\alpha - \ln \left(\tanh \frac{f_0}{4} / \tanh \frac{\phi_1}{4} \right)
 \end{aligned} \tag{6.75}$$

Dukhin, Derjaguin, and Semenikhin [36] used linearization and showed that in this case the energy of interaction between two identical spheres can again be obtained by the method used to derive Eq. (6.67), i.e., by integrating the field pressure in the symmetry plane. By analogy to (6.67), the final result can be written immediately, by replacing the potential ψ_1 in (6.67) with a constant $(kT/e)B$ from relations (6.75):

$$U(H) = \epsilon \left(\frac{kT}{e} \right)^2 B^2 \alpha^2 \frac{e^{-\kappa H}}{2\alpha + H} \tag{6.76}$$

This formula holds for $\kappa\alpha > 1$ and $\kappa H > 2-3$. Therefore, it also holds for $\kappa\alpha \gg \kappa H > 2-3$ and hence is valid if $H/\alpha \ll 1$; thus, the energy of interaction between spheres can be found simply by summing up the energies of ring zones. Hoskin and Levine [37] found by this method [i.e., by using (6.63)] that for $\kappa\alpha \gg \kappa H > 1.5$

$$U = 8\epsilon \left[\frac{kT}{e} \right]^2 \alpha A_1 [1 - A_1 (\kappa H - 1 + 2\delta + \dots)] \tag{6.77}$$

where

$$A_1 = \tanh^2 \left(\frac{\phi_1}{4} \right) \exp(-\kappa H), \quad \delta = \cosh \left(\frac{\phi_1}{2} \right) / \sinh^2 \left(\frac{\phi_1}{2} \right) \tag{6.78}$$

It can be readily shown that in the case $\kappa\alpha \gg \kappa H \gg 1$ the higher-order terms of (6.76) and (6.77) coincide. Consequently, formula (6.76) is also a generalization of (6.67) for arbitrary potentials, and of (6.77) for $H/\alpha \sim 1$.

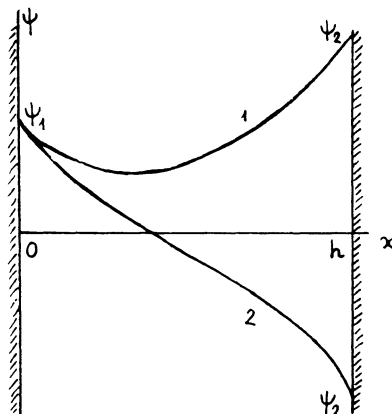


Fig. 6.10. Nonidentical double layers. Potential distribution within the interlayer: 1) for potentials of like sign; 2) for potentials of unlike signs.

6.8. INTERACTION BETWEEN UNEQUALLY CHARGED SURFACES

Many colloidal disperse systems of considerable practical significance consist of mixtures of particles of different nature. Evidently, the problem of calculating their electrostatic interaction is more difficult than similar calculations for two identical interfaces. For asymmetrical systems, the single parameter ψ_1 is replaced by two potentials, ψ_1 and ψ_2 , that differ not only in magnitude, but at certain compositions of the continuous phase may even have opposite signs (Fig. 6.10). These differences are caused by different mechanisms of charge formation on the surfaces or by different positions of points of zero charge for two interfaces with the same mechanism of surface ionization. In fact, the situation is even more complicated if we take into account that, owing to differences in charging mechanisms, in addition to the situations corresponding to constant potential or constant charge of a thinning interlayer already analyzed, "mixed" cases are possible in which one of these conditions holds on one interface and the other holds on the second interface.

The general parametric solution of the problem of disjoining pressure as a function of distance between surfaces in an asymmetrical system can be expressed, for symmetrical electrolytes, in terms of elliptic integrals. The free energy of interaction, which was found in 1963 by Devereux and de Bruyn by the charging method for constant potentials ψ_1 and ψ_2 [18], is even more complex. How-

ever, one of us had suggested earlier a very general method [15] of graphical analysis of the electrostatic interaction between non-identical surfaces (the so-called "method of isodynamic curves"). This method revealed all the specific effects of heterointeraction in the conditions of constant potentials of ionic diffuse layers. The most interesting of these features is that the disjoining pressure of the interacting surfaces with unequal charges of like sign reaches a maximum as the interlayer is thinned, and is then replaced by an "unlimited" growth of attraction. The maximum repulsion Π_e^{\max} is determined in this case only by the magnitude of the smaller of the particle potentials (e.g., ψ_1 in Fig. 6.10). In symmetrical electrolytes Π_e^{\max} is

$$\Pi_e^{\max} = 4nkT \sinh^2 (ze\psi_1/2kT) \quad (6.79)$$

The essence of the method of isodynamic curves is as follows. The first integration of the Poisson equation (6.5) with volume charge density ρ given by the Boltzmann equation (6.18) was shown to result in Eq. (6.7) which relates the electric field strength $E = -d\psi/dx$ to the potential ψ at each point within the interlayer. The integration constant C appearing in (6.7) is directly expressed in terms of disjoining pressure Π_e by means of Eq. (6.11). The subsequent integration of Eq. (6.7) with boundary conditions $\psi(0) = \psi_1$ and $\psi(h) = \psi_2$ yields a complicated parametric dependence of Π_e on ψ_1 , ψ_2 , and h [15, 16]. Instead, it was proved considerably simpler to choose Π_e in Eq. (6.7) directly as the integration constant, and then construct and analyze series of integral curves $\psi = \psi(x, \Pi_e)$ by solving (6.7) (Fig. 6.9), having prescribed a certain sequence of values of Π_e (hence, the term isodynamic curves). The interlayer thickness h for a given Π_e is found from the difference in the abscissas of the points with coordinates (x_2, ψ_2) and (x_1, ψ_1) . Figure 6.11 shows, among other things, that if $\Pi_e > 0$ and $\psi_1\psi_2 > 0$, there are always two distances h' and h'' corresponding to the same disjoining pressure. This means that $\Pi_e(h)$ has a maximum. Another advantage of the isodynamic curves method is that these curves, once plotted, are valid for analyzing any problem that involves heterointeraction. The difference lies only in the values of ψ_1 and ψ_2 . The method of isodynamic curves is undoubtedly convenient, and sometimes even the only one practicable, for studying heterointeractions. However, if both surfaces are weakly charged, a simple analytical solution relating Π_e directly to the distance between surfaces is also possible.

For low potentials the solution of the linearized Poisson-Boltzmann equation (1.17) satisfying the boundary conditions of Fig. 6.10 is

$$\psi = \frac{\psi_1 \sinh \kappa(h - x) + \psi_2 \sinh \kappa x}{\sinh \kappa h} \quad (6.80)$$

where κ is defined in the general case by Eq. (1.18). The volume charge density is then directly proportional to potential:

$$\rho = -\frac{\epsilon \kappa^2}{4\pi} \psi \quad (6.81)$$

so that the general formula for disjoining pressure (6.12) becomes quite simple (see also [19]):

$$\Pi_e(h) = \frac{\epsilon}{8\pi} (\kappa^2 \psi^2 - \psi'^2) \quad (6.82)$$

and the values of the potential and its derivative can be taken at an arbitrary point within the interlayer. By substituting here the potential ψ from (6.80) and its derivative, we obtain

$$\Pi_e = \frac{\epsilon \kappa^2}{8\pi} \frac{2\psi_1 \psi_2 \cosh \kappa h - (\psi_1^2 + \psi_2^2)}{\sinh^2 \kappa h} \quad (6.83)$$

This formula reveals all peculiarities in the behavior of $\Pi_e(h)$ when surfaces approach at constant potentials ψ_1 and ψ_2 . If the surfaces have unlike signs of charge, then $\psi_1 \psi_2 < 0$ and, hence, $\Pi_e < 0$; i.e., the surfaces are attracted to each other at all distances (curve 2 in Fig. 6.12). If the surfaces carry charges of

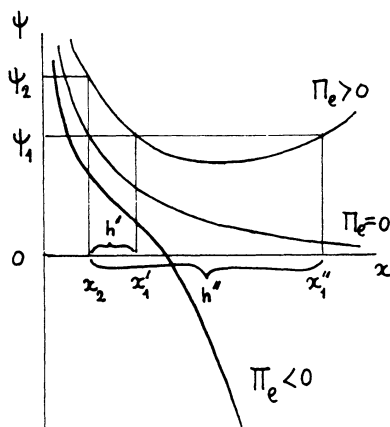


Fig. 6.11. Isodynamic curves.

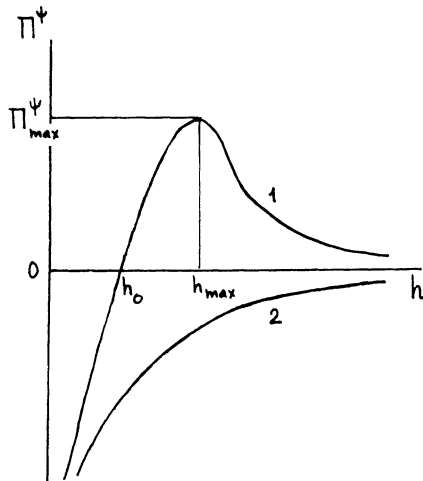


Fig. 6.12. $\Pi_e(h)$ plotted for $\psi = \text{const}$ and unequal potentials: 1) $\psi_1\psi_2 > 0$; 2) $\psi_1\psi_2 < 0$.

like signs ($\psi_1\psi_2 > 0$) but of unequal magnitudes, then at relatively large distances where $\cosh \kappa h \approx \sinh \kappa h \gg 1$ they are repelled, obeying the law (curve 1 in Fig. 6.12)

$$\Pi^\psi \approx \frac{\varepsilon \kappa^2}{2\pi} \psi_1 \psi_2 e^{-\kappa h} \quad (6.84)$$

but the repulsion is replaced with attraction at a distance h_0 , found from the solution of the equation

$$\cosh \kappa h_0 = (\psi_1^2 + \psi_2^2)/2\psi_1\psi_2 > 1, \text{ i.e., } \kappa h_0 = \ln(\psi_2/\psi_1) \quad (6.85)$$

As the interlayer thins out further, $\cosh \kappa h \rightarrow 1$, $\sinh \kappa h \rightarrow \kappa h$, and attraction grows steeply, obeying the law

$$\Pi^\psi \approx -\frac{\varepsilon}{8\pi} \frac{(\psi_1 - \psi_2)^2}{h^2} \quad (6.86)$$

This formula holds both at low and at high potentials [15]. The distance h_{\max} at which maximum repulsion Π_{\max}^ψ is reached is found by setting the derivative $d\Pi^\psi/dh$ equal to zero:

$$\cosh \kappa h_{\max} = \psi_2/\psi_1 > 1 \quad (6.87)$$

and Π_{\max}^ψ is found to be

$$\Pi_{\max}^\psi = \frac{\varepsilon \kappa^2}{8\pi} \psi_1^2 \quad (6.88)$$

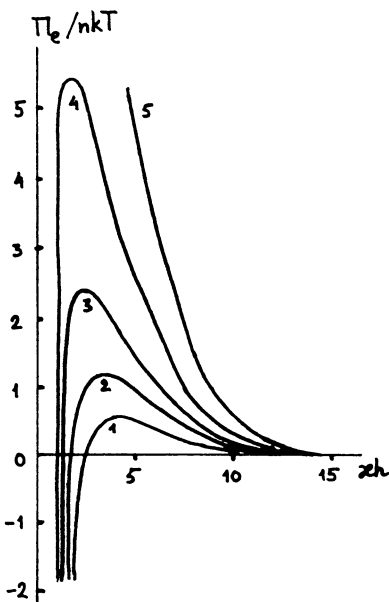


Fig. 6.13. The effect of the lower potential ψ_1 on $\Pi_e(h)$: $\psi_1 = 17.5$ (1), 25 (2), 35 (3), 50 (4), 250 mV (5); $\psi_2 = 250$ mV [15].

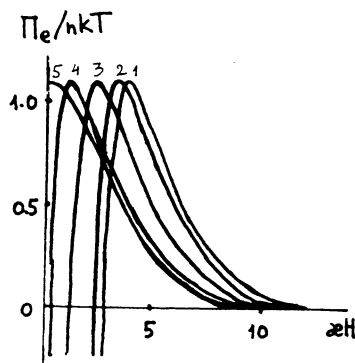


Fig. 6.14. The effect of the higher potential ψ_2 on $\Pi_e(h)$: $\psi_2 = 250$ (1), 100 (2), 50 (3), 30 (4), 25 mV (5); $\psi_1 = 25$ mV [15].

For a symmetrical electrolyte this formula coincides with that derived from the general relation (6.79) for low potentials. Figures 6.13 and 6.14 plot the results of exact calculation of $\Pi^{\psi}(h)$ for $\psi_1\psi_2 > 0$.

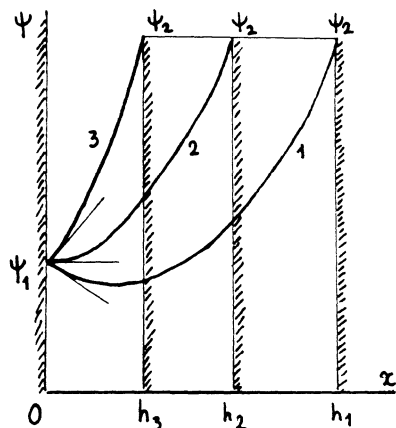


Fig. 6.15. Model for the interpretation of the dependence $\Pi_e(h)$ at $\psi_1\psi_2 > 0$ (curve 1 in Fig. 6.12).

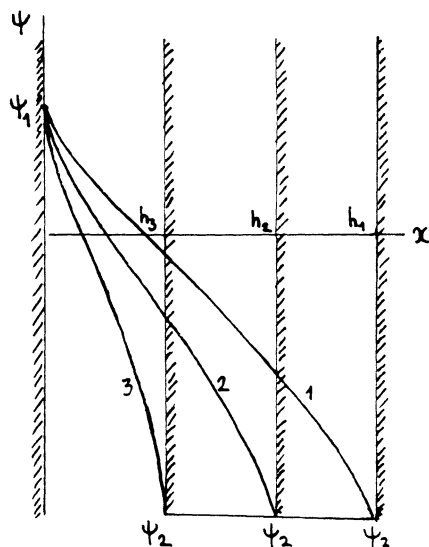


Fig. 6.16. Model for the interpretation of the dependence $\Pi_e(h)$ at $\psi_1\psi_2 < 0$ (curve 2 in Fig. 6.12).

The extremum on the curve $\Pi^\psi(h)$ in the case $\psi_1\psi_2 > 0$ is best understood if we analyze in more detail what happens on the less-charged surface when h diminishes (Fig. 6.15). Its potential ψ_1 is fixed, so that the hydrostatic repulsive pressure remains constant and is determined solely by the value of ψ_1 . The potential

of the second surface, ψ_2 , influences the electric field strength at the first surface, i.e., the slope of the curve $\psi(x)$ and with it Maxwell's stress. As h diminishes, the field here first decreases (Fig. 6.15, curve 1), then vanishes (curve 2) (this occurs when Π_{\max}^{ψ} is reached), and then increases again (curve 3), this growth being formally unlimited because the slope of $\psi(x)$ tends to 90° at full contact. Obviously, at some point Maxwell's stress exceeds the hydrostatic repulsion, and the resultant force is attractive. When the approaching surfaces have charges of unlike sign, the attraction generated at large distances, also given by (6.84) (for $\psi_1\psi_2 < 0$), continues to operate and increases because of the monotonic increase of field stress at each surface (Fig. 6.16). Obviously, for very thin interlayers it is described by the same asymptotic formula (6.86) as for $\psi_1\psi_2 > 0$.

The mechanism of surface charge formation may be such that, instead of potentials, charge densities σ_1 and σ_2 will remain constant during the process of thinning. Formula (6.83) remains valid; but in order to make use of it account has to be taken of how surface potentials ψ_1 and ψ_2 change under electroneutrality conditions when the interlayer thins out:

$$\begin{aligned}\sigma_1 &= - \frac{\epsilon}{4\pi} \frac{d\psi}{dx} \Big|_{x=0} = \frac{\epsilon\kappa}{4\pi} \psi_{1\infty} = \text{const} \\ \sigma_2 &= \frac{\epsilon}{4\pi} \frac{d\psi}{dx} \Big|_{x=h} = \frac{\epsilon\kappa}{4\pi} \psi_{2\infty} = \text{const}\end{aligned}\quad (6.89)$$

where $\psi_{1\infty} = \psi_1(\infty)$ and $\psi_{2\infty} = \psi_2(\infty)$ are the initial potentials of isolated surfaces. Substitution of the distribution $\psi(x)$, (6.80), into Eq. (6.89) makes it possible to find first the two functions $\psi_1(h)$ and $\psi_2(h)$:

$$\begin{aligned}\psi_1 &= (\psi_{1\infty} \cosh \kappa h + \psi_{2\infty}) / \sinh \kappa h, \\ \psi_2 &= (\psi_{1\infty} + \psi_{2\infty} \cosh \kappa h) / \sinh \kappa h\end{aligned}\quad (6.90)$$

and then to derive from them the formula for disjoining pressure at $\sigma = \text{const}$:

$$\Pi^{\sigma} = \frac{\epsilon\kappa^2}{8\pi} \frac{2\psi_{1\infty}\psi_{2\infty} \cosh \kappa h + \psi_{1\infty}^2 + \psi_{2\infty}^2}{\sinh^2 \kappa h} \quad (6.91)$$

or, in view of (6.89),

$$\Pi^{\sigma} = \frac{4\pi}{\epsilon} \frac{2\sigma_1\sigma_2 \cosh \kappa h + \sigma_1^2 + \sigma_2^2}{\sinh^2 \kappa h} \quad (6.92)$$

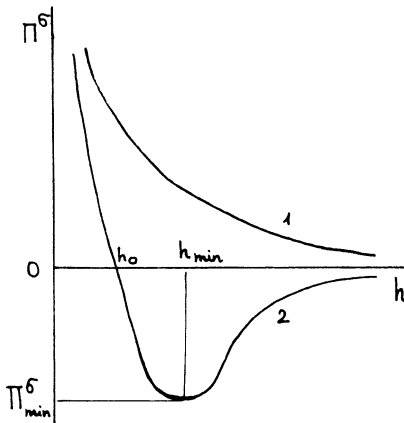


Fig. 6.17. $\Pi_e(h)$ at $\sigma = \text{const}$ for nonidentical charges: 1) $\sigma_1\sigma_2 > 0$; 2) $\sigma_1\sigma_2 < 0$.

As follows from (6.90), ψ_1 and $\psi_{1\infty}$, and ψ_2 and $\psi_{2\infty}$ are practically indistinguishable at large distances. Formula (6.91) then changes to (6.84), or into one equivalent to this last,

$$\Pi^\sigma = \frac{8\pi}{\epsilon} \sigma_1 \sigma_2 e^{-\kappa h} \quad (6.93)$$

regardless of the signs of surface charges. But the sign of the product $\sigma_1\sigma_2$ will determine whether the result is repulsion or attraction.

The curve $\Pi^\sigma(h)$ is obviously monotonic for charged surfaces of like sign because the numerators and denominators of the fractions in (6.91) and (6.92) are positive (Fig. 6.17, curve 1). As $\kappa h \rightarrow 0$, repulsion increases as follows:

$$\Pi^\sigma = \frac{\epsilon}{8\pi} \frac{(\psi_{1\infty} + \psi_{2\infty})^2}{h^2} = \frac{4\pi}{\epsilon \kappa^2} \frac{(\sigma_1 + \sigma_2)^2}{h^2} > 0 \quad (6.94)$$

The same pattern is observed when $\sigma_1\sigma_2 < 0$ as $\kappa h \rightarrow 0$ (unless $\sigma_1 = -\sigma_2$). But since in this case ($\sigma_1\sigma_2 < 0$) $\Pi^\sigma < 0$ at large distances, the extremum on the curve at constant charges is observed even for charged surfaces of unlike sign (Fig. 6.17, curve 2). The coordinates of the minimum of $\Pi^\sigma(h)$, found from the equation $d\Pi^\sigma/dh = 0$,

$$\begin{aligned} \Pi_{\min}^\sigma &= (4\pi/\epsilon)\sigma_1\sigma_2, \quad \kappa h_{\min} = \operatorname{arcosh}(-\sigma_2/\sigma_1) \\ &= \operatorname{arcosh}(-\phi_{2\infty}/\phi_{1\infty}) \end{aligned} \quad (6.95)$$

and attraction is replaced by repulsion at a distance

$$\kappa h_0 = \ln(-\sigma_2/\sigma_1) = \ln(-\psi_{2\infty}/\psi_{1\infty}) \quad (6.96)$$

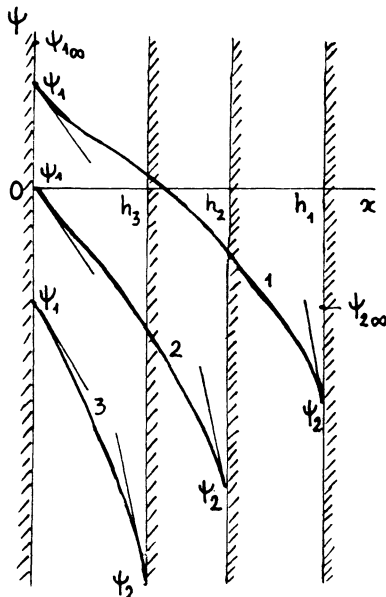


Fig. 6.18. Interpretation of $\Pi_e(h)$ when $\sigma_1\sigma_2 < 0$.

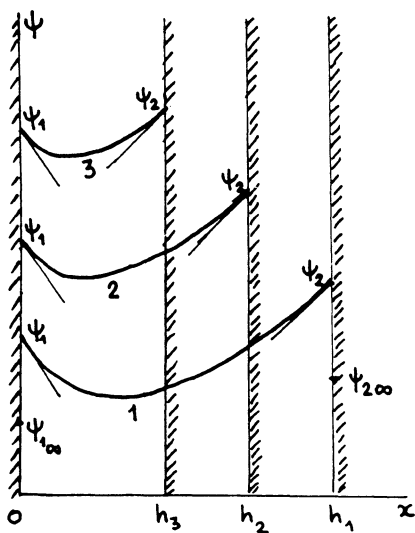


Fig. 6.19. Interpretation of $\Pi_e(h)$ when $\sigma_1\sigma_2 > 0$.

The same factors as were discussed above cause reversal in the sign of interaction when h diminishes. However, in contrast to the preceding case, now the constancy of charge at the interface maintains constant field strength at the surface (Fig. 6.18) and, hence, con-

stancy of Maxwell's stress tensor, so that only the hydrostatic pressure at the surface is changed when interfaces approach [because the surface potential obeys Eqs. (6.90)]. The lower of the two potentials ψ_1 first diminishes in magnitude (curve 1), then vanishes (curve 2); this reduces the hydrostatic pressure at the left-hand wall (see Fig. 6.10), which becomes equal to its bulk value, and attraction reaches the maximum; finally, the potential ψ_1 reverses sign in accordance with Eqs. (6.90) and sharply increases proportionally to $1/h$ (curve 3); this enhances repulsion owing to the increase in hydrostatic pressure. If $\sigma_1\sigma_2 > 0$, no sign reversal occurs in potential (Fig. 6.19).

The corresponding formulas for the energy of interaction between two nonidentical flat diffuse layers are obtained by integrating the formulas for disjoining pressure. They are simply

$$V^\Psi = \frac{\epsilon\kappa}{8\pi} \left[\frac{2\psi_1\psi_2}{\sinh\kappa h} - (\psi_1^2 + \psi_2^2)(\coth\kappa h - 1) \right] \quad (6.97)$$

$$V^\sigma = \frac{\epsilon\kappa}{8\pi} \left[\frac{2\psi_{1\infty}\psi_{2\infty}}{\sinh\kappa h} + (\psi_{1\infty}^2 + \psi_{2\infty}^2)(\coth\kappa h - 1) \right] \quad (6.98)$$

For $\psi_1\psi_2 > 0$ and $\psi_1\psi_2 < 0$ these functions of distance have the same peculiarities as the corresponding curves $V_e(h)$; but, other conditions being equal (potentials or charges, and concentrations), the abscissas of extrema and the zeros of the functions are shifted to smaller distances. At larger thickness the expansions of (6.97) and (6.98) yield simple exponentials:

$$V_e \approx (\epsilon\kappa/2\pi)\psi_1\psi_2 e^{-\kappa h} \approx (8\pi/\epsilon\kappa)\sigma_1\sigma_2 e^{-\kappa h} \quad (6.99)$$

which can be obtained by straightforward integration of (6.84) or (6.93).

Integration by the rings method [see (6.63)] also gives simple formulas for the energy of electrostatic interaction between two spherical layers with radii a_1 and a_2 :

$$\begin{aligned} U^\Psi = & \frac{\epsilon a_1 a_2}{4(a_1 + a_2)} [(\psi_1 + \psi_2)^2 \ln(1 + e^{-\kappa H}) \\ & + (\psi_1 - \psi_2)^2 \ln(1 - e^{-\kappa H})] \end{aligned} \quad (6.100)$$

for constant potential [38], and

$$\begin{aligned} U^\sigma = & -\frac{\epsilon a_1 a_2}{4(a_1 + a_2)} [(\psi_{1\infty} + \psi_{2\infty})^2 \ln(1 - e^{-\kappa H}) \\ & + (\psi_{1\infty} - \psi_{2\infty})^2 \ln(1 + e^{-\kappa H})] \end{aligned} \quad (6.101)$$

for constant charge [20]. At "large" distances ($\kappa H \gtrsim 3$) these two formulas for energy are practically identical:

$$U^\psi \approx U^\sigma \approx \frac{\epsilon \alpha_1 \alpha_2}{\alpha_1 + \alpha_2} \psi_1 \psi_2 e^{-\kappa H} \approx \frac{16\pi^2 \alpha_1 \alpha_2}{\kappa^2 (\alpha_1 + \alpha_2)} \sigma_1 \sigma_2 e^{-\kappa H} \quad (6.102)$$

In general, the behavior of $U_e(H)$ curves is the same as that of $\Pi_e(h)$ curves. They have extrema for $\psi_1 \psi_2 > 0$ and $\sigma_1 \sigma_2 < 0$, and are monotonic for $\psi_1 \psi_2 < 0$ and $\sigma_1 \sigma_2 > 0$.

To conclude this section, it is noteworthy that any one of the formulas given above indicates simple exponential decay of the interaction at large distances. The same type of decay is realized when the potentials of the interfaces of double layers are not low. As mentioned earlier, this effect is caused by the possibility of linearization of the Poisson-Boltzmann equation because the potential is low almost everywhere in the gap (except in the regions directly adjacent to the surfaces), so that the solution far from each of the surfaces has the form

$$\psi(x) = A_1 e^{-\kappa(h-x)} + A_2 e^{-\kappa x} \quad (6.103)$$

i.e., represents a superposition of the potentials generated by each surface independently. Consequently, the constants A_1 and A_2 in Eq. (6.103) are determined only by the potentials of isolated surfaces and by the type of the electrolyte (see Chapter 1). Now we can find the disjoining pressure between the surfaces directly from formula (6.82) derived for low potentials. By substituting (6.103) into (6.82), we obtain

$$\Pi_e(h) = (\epsilon \kappa^2 / 2\pi) A_1 A_2 e^{-\kappa h} \quad (6.104)$$

Since the expression for $\Pi_e(h)$ is the same in any plane parallel to the surface, the formula gives the pressure acting on each of the surfaces. Obviously, the arguments used above never referred to, or assumed the existence of, a minimum in the distribution of potential between the surfaces [9, 39], so that (6.104) holds both for like-sign and for unlike-sign charged surfaces. The constants A_j for symmetric electrolytes are [see (1.38)]

$$A_j = (4kT/ze) \tanh(ze\psi_j/4kT), \quad j = 1, 2 \quad (6.105)$$

For 2-1 and 1-2 electrolytes they are [see (1.39)]

$$A_j = (6kT/e) \tanh[v_i(\psi_j)/4], \quad j = 1, 2; i = 1, 2 \quad (6.106)$$

where the functions $v_i(\psi)$ are defined by (6.49) or (6.50). Therefore, the generalization of (6.84) to the case of arbitrary potential for symmetrical electrolytes is

$$\Pi_e \approx \frac{\epsilon \kappa^2}{2\pi} \left(\frac{4kT}{ze} \right)^2 \tanh \left(\frac{z\phi_1}{4} \right) \tanh \left(\frac{z\phi_2}{4} \right) e^{-\kappa h} =$$

$$= 64nkT\gamma_1\gamma_2e^{-\kappa h}, \quad \gamma_i = \tanh\left(\frac{z\phi_i}{4}\right) \quad (6.107)$$

$$\phi_i = e\psi_i/kT, \quad i = 1, 2$$

and for 2-1 and 1-2 electrolytes it is

$$\begin{aligned} \Pi_e &\approx \frac{\varepsilon\kappa^2}{2\pi} \left(\frac{6kT}{e}\right)^2 \omega_1\omega_2 e^{-\kappa h} \\ &= 432n_2kT\omega_1\omega_2 e^{-\kappa h}, \quad \omega_j = \tanh\left[\frac{v_i(\psi_j)}{4}\right] \end{aligned} \quad (6.108)$$

For charged surfaces of unlike sign, one of the functions v_i must be used for one of the surfaces, and the other one for the second surface. Indeed, in an electrolyte consisting of uni- and bivalent ions the bivalent ion is a counterion at one surface and a co-ion at the other one.

These expressions represent a generalization of formulas (6.47) and (6.48) to two different double layers. Integration of Eqs. (6.107) and (6.108) over distance first gives the corresponding expressions for the free energy of interaction between flat plates in symmetrical electrolytes,

$$V_e = (64nkT/\kappa) \gamma_1 \gamma_2 e^{-\kappa h} \quad (6.109)$$

and in asymmetric 2-1 and 1-2 electrolytes,

$$V_e = 432(n_2kT/\kappa)\omega_1\omega_2 e^{-\kappa h} \quad (6.110)$$

Then, after a second integration, for the energy of interaction between spheres in symmetrical electrolytes,

$$U_e = \frac{16\varepsilon\alpha_1\alpha_2(kT)^2}{(\alpha_1 + \alpha_2)z^2e^2} \gamma_1\gamma_2 e^{-\kappa H} \quad (6.111)$$

and in asymmetrical 2-1 and 1-2 electrolytes,

$$U_e = \frac{36\varepsilon\alpha_1\alpha_2(kT)^2}{(\alpha_1 + \alpha_2)e^2} \omega_1\omega_2 e^{-\kappa H} \quad (6.112)$$

Here we use the definition of the reciprocal Debye length for symmetrical electrolytes [(1.30)],

$$\kappa^2 = 8\pi e^2 z^2 n / \varepsilon kT \quad (6.113)$$

and for asymmetric electrolytes comprising uni- and bivalent ions [(1.37)],

$$\kappa^2 = 24\pi e^2 n_2 / \epsilon kT \quad (6.114)$$

The asymptotic formula (6.104) makes it possible to calculate the disjoining pressure, and with it the energy of interaction, in all cases in which the asymptotic behavior of the potential of an isolated layer is known or can be found. One particular case in which this situation can occur is a mixture of a symmetrical and an asymmetrical electrolyte (containing no trivalent or higher-valent ions). In each specific situation the accuracy of the formulas thus obtained should be checked by comparing them with accurate numerical results. Certainly they must work quite well for $kh \gtrsim 3$.

6.9. EFFECT OF DISCRETENESS OF SURFACE CHARGE

As in most of the published papers devoted to calculation of electrostatic interaction between two charged interfaces, the presentation in the preceding sections is based on the assumption that charge is uniformly spread on a surface with average density σ . This assumption is certainly justified when the distance h between the interacting surfaces is much larger than the mean distance ℓ between two adjacent charges on the surface. But if h is of the same order as, or less than, ℓ , a different approach is required, based on treating the interactions between individual charges. Ultimately we deal with macroscopic surfaces, each of which carries a great number of charges, so that these pair interactions must be summed and averaged. Obviously, the result of averaging must depend first on the pair correlation between the positions of charges on the surfaces. In general, the result may differ appreciably from that obtained by assuming uniform smearing of surface charge.

Two possible sources of correlation are recognized. The first is generated by a prescribed arrangement of charges - for instance, when the two charged surfaces are obtained by cleaving a single crystal (without rotating the crystal fragments) along the cleavage plane. The fact that such surfaces are almost always charged was confirmed, in particular, by the discovery of the emission of fast electrons (up to 200 keV) in the process of destruction of crystals (e.g., quartz, gypsum, or mica) in vacuum [40]. However, a change in the orientation of the axis of one half of the crystal with respect to those of the other by displacement and rotation cancels the configurational correlation. On the other hand, correlation can arise spontaneously if the axes of identical small crystals suspended in a liquid continuous phase get aligned in parallel owing to a torque of the van der Waals forces when the crystals slowly approach each other [41].

Another example of such systems is the interaction of elementary planes of montmorillonite swelling in aqueous media. The effect of the configurational correlation of charges on the forces of interaction between "crystalline" surfaces ("parquetry") was analyzed for different types of lattice in a number of papers, both for a simple dielectric interlayer [42] and for an electrolyte layer [43, 44]. In addition, the interaction between charged surfaces on which the potential or charge density varied periodically along one or two directions was calculated in [45-48]. In all cases, without exception, it was found that at very short distances on the order of the correlation length the intensity of interaction must be substantially different, owing to the configurational correlation, from that dictated by the smeared-charge concept. Furthermore, the results of calculations for electrolyte solutions depend on the ratio of the Debye length to the period of the two-dimensional surface lattice of ions. The obvious weak points of this model are the assumption of strictly periodic arrangement of ions on the surfaces and the assumption of no rotation and no relative displacement of the approaching 2D lattices.

The second source of pair correlation of charges results from their electrostatic interaction. It is most strongly pronounced when the charges are completely free to move along the interface; then the calculations are the least difficult. This situation arises in a nonlocalized adsorption of ions or when the binding energy of localized adsorption is low and the Boltzmann distribution can be used to calculate the probability of occupancy of adsorption centers. The essential features of such calculations, reported by the authors in a number of papers [49-51], are as follows.

The simplest case for calculations is when the concentration of ions on the two surfaces is not high and the probability of finding a charge at a given site can be regarded as approximately independent of the positions of its neighbors in the same plane. The following approach will be used for determining the mean force of interaction between surfaces (Fig. 6.20). We choose axis z directed perpendicularly to the interfaces I and II, and place a charge q_1 at the point of intersection of the axis z and the plane I. With the given assumptions, the number of charges q_2 in the plane II within a ring of radius r and width dr is

$$dw = 2\pi r dr n_2 \exp[-q_2 \varphi_1(r, h)/kT] \quad (6.115)$$

where n_2 is the mean surface concentration of charge q_2 , and φ_1 is the electric potential produced by the charge q_1 and all its mirror images in the planes I and II at the points of the circle of radius r in the plane II. The component of the force of interaction between the charges q_1 and q_2 , perpendicular to the planes, is

$$f_z = -q_2 \partial \varphi_1(r, h) / \partial h \quad (6.116)$$

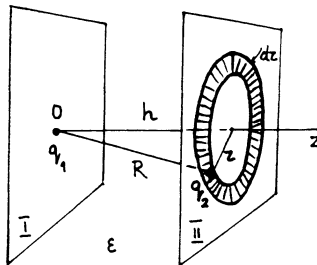


Fig. 6.20. Model for the calculation of the interaction force between charges.

The mean force of interaction F_1 between one charge q_1 and all charges q_2 in the plane II is

$$F_1 = \int_S f_Z dw$$

where S is the surface area of the interface, and the mean interaction force applied to a plane (per cm^2 of the surface) equals $F = n_1 F_1$, where n_1 is the surface concentration of the charges q_1 . Therefore,

$$F(h) = -2\pi n_1 n_2 q_2 \int_0^\infty \frac{\partial \varphi}{\partial h} e^{-q_2 \varphi_1 / kT_r} dr \quad (6.117)$$

The problem reduces to finding the potential $\varphi_1(r, h)$. The solution of this electrostatics problem for two media with unequal permittivities ϵ_1 and ϵ_2 separated by an interlayer with permittivity ϵ was obtained in [49]. However, the main features of the problem as formulated are best shown if we immediately neglect, for simplicity, the effects resulting from image forces due to differences between permittivities. In this case,

$$\varphi_1 = q_1 / \epsilon R, \quad R = (r^2 + h^2)^{1/2} \quad (6.118)$$

so that by substituting (6.118) into (6.117) we immediately arrive at a simple formula

$$F = 2\pi n_1 n_2 k T_h (1 - e^{-q_1 q_2 / \epsilon k T_h}) \quad (6.119)$$

The distance h_B at which the energy of electrostatic interaction between two elementary charges ($|q_1| = |q_2| = e$) equals, in air and in room temperature, the energy of thermal motion kT is nearly 600 Å, and in water ($\epsilon = 80$) nearly 7 Å. Expanding the exponential in (6.119) in a series for $h \gg h_B$ in powers of a small parameter $q_1 q_2 / \epsilon h k T$ gives

$$F = F_\infty = 2\pi n_1 n_2 q_1 q_2 / \epsilon = 2\pi \sigma_1 \sigma_2 / \epsilon = E_1 \sigma_2 = E_2 \sigma_1 \quad (6.120)$$

This result could be expected for the force acting on unit surface area if we took into account that $\sigma_1 = q_1 n_1$ and $\sigma_2 = q_2 n_2$ are surface charge densities, and that by virtue of Gauss's theorem the field strength E_1 produced by an infinite plane I is $E_1 = 2\pi \sigma_1 / \epsilon$. Thus, at $\sigma_1 = -\sigma_2 = \sigma$ the force $F_\infty = F_C = -2\pi \sigma^2 / \epsilon$ is nothing more than the ordinary force of attraction between the plates of a flat capacitor. At smaller distances h the expansion (6.119) yields

$$F \approx F_\infty (1 - q_1 q_2 / 2\epsilon k Th + \dots) \quad (6.121)$$

and the behavior of force as a function of distance is determined, as we see from (6.121), by the combination of signs of surface charges. For surfaces with charges of like sign ($q_1 q_2 > 0$, $F_\infty > 0$) the repulsive force must decrease with decreasing h because the charges are displaced to keep maximum possible distance from the charges on the approaching plane, at constant mean density. As $h \rightarrow 0$, the normal component of the force must tend to zero. This indeed follows from (6.119). For charged planes of unlike sign ($q_1 q_2 < 0$, $F_\infty < 0$) the attractive force must increase as surfaces approach because the attraction between pairs of charges on opposite planes is enhanced and, hence, the probability for charges to be at a minimum possible distance becomes correspondingly greater.

The correctness of this approach was checked by considering a plane-parallel electrolyte interlayer between two interfaces with surface charges formed through nonlocalized adsorption of like-sign ions. At a large interlayer thickness h much greater than the characteristic separation ℓ between ions on the surface, the disjoining pressure is completely determined by the concentration and type of the electrolyte, its temperature, and by the "macroscopic" potential in the symmetry plane of the film [see (6.19)]. When interfaces are brought to distances below the Debye screening length, the macropotential of the layer becomes almost independent of the distance to surfaces, i.e., of the coordinate z , and the disjoining pressure reaches a maximum while the charge density of each interface tends to zero. This occurs because the adsorption of ions of both charge signs on the surface tends to equal values, owing to an increase in the Stern potential as a result of decreasing h . At the same time, the diffuse charge per unit surface area also tends to zero, because of electroneutrality (since ions together with the solvent are squeezed out of the gap). Consequently, the two surfaces become practically electroneutral although each carries a large number of charges of both signs [52]. An analysis of the properties of such two-dimensional electrolyte solutions was given in [53].

If the thickness h becomes comparable to ℓ , it is necessary to allow for the correlation in the mutual arrangement of all

charges on the two interfaces (not only for pairs of charges located on the opposite interfaces, as we did above). In this case the interaction between interfaces can be evaluated qualitatively by using formulas (6.119) or (6.121). Assuming the concentration of cations and anions in the two planes to be identical and equal to n_s , and the charges to be $\pm q$, we find the force of interaction between the positive charges in the plane I (Fig. 6.20) and all charges in the plane II by adding (6.19) for $q_1 q_2 = -q^2 < 0$ with itself for $q_1 q_2 = q^2 > 0$. The same force is applied to the negative charges in the plane I. As a result, the total interaction force is attractive and equals

$$F_{\text{cor}} = -16\pi n_s^2 k T h \sinh^2(q^2/2\epsilon k T h) \quad (6.122)$$

This force, caused exclusively by the correlation in charge arrangement on interfaces, is added to the "macroscopic" repulsion between surfaces (6.19), produced by the hydrostatic pressure in the interlayer enhanced in comparison with that in the bulk of the electrolyte.

In order to calculate the "microscopic" disjoining pressure more accurately we used a method [50, 51] similar to that employed in the Debye-Hückel theory of strong electrolyte solutions [13]. As in electrostatics, the energy of a system of charges q_j is

$$W = \frac{1}{2} \sum_j q_j \tilde{\varphi}_j \quad (6.123)$$

where $\tilde{\varphi}_j$ is the potential produced at the point of location of charge q_j by all other charges. The summation in (6.123) runs over all the charges of the system. Obviously, $\tilde{\varphi}_j$ is a function of distance between adsorption planes; hence, the corresponding pressure is

$$\Pi_{\text{cor}}(h) = -\frac{1}{S} \frac{\partial W}{\partial h} = -\frac{1}{S} \sum_j q_j \frac{\partial \tilde{\varphi}_j}{\partial h} \quad (6.124)$$

where S is the surface area of the interface. All charges of the system being equivalent, the problem as formulated and the one discussed above reduce to finding the micropotential φ around an ion q that we place for convenience at the origin of coordinates (on surface I; see Fig. 6.20). The potential distribution in the interlayer is described by the Poisson equation with volume charge density

$$\rho = q \delta(x) \delta(y) \delta(z) + \sigma_1(x, y) \delta(z) + \sigma_2(x, y) \delta(z - h) \quad (6.125)$$

where $\delta(x)$, $\delta(y)$, ... are the Dirac delta functions. The surface charge densities σ_i ($i = 1, 2$) are expressed, via the Boltzmann

equation, in terms of the concentrations of ions of both signs on each of the surfaces, depending on local values of the potential: $\varphi(x, y, 0)$ and $\varphi(x, y, h)$. The expansion of the Boltzmann factors into series (in analogy to the Debye-Hückel approximation), taking into account the surface electroneutrality far from the charge q , yields a linear equation for potential φ :

$$\Delta = -\frac{4\pi}{\epsilon} q \delta(x) \delta(y) \delta(z) + 2\kappa_s [\delta(z) + \delta(z-h)] \varphi \quad (6.126)$$

where

$$\kappa_s = \pi(z_+ + z_-) e^2 (z_+ n^+ + z_- n^-) / \epsilon k T \quad (6.127)$$

and n^+ and n^- are the mean surface concentrations of cations and anions, respectively. Its solution, obtained by means of the Fourier transform, is

$$\varphi(r, 0) = \frac{q}{\epsilon} \int_0^\infty \frac{[(\kappa_s + k) - \kappa_s e^{-2kh}] k J_0(kr) dk}{(\kappa_s + k)^2 - \kappa_s^2 e^{-2kh}} \quad (6.128)$$

where J_0 is the Bessel function of order 0. Here we again neglect the effect of mirror-image forces that were, in fact, taken into account in [50, 51].

In order to find the potential $\tilde{\varphi}$, we have to subtract from $\varphi(r, 0)$ the potential of the charge q itself, equal to $\varphi_0 = q/\epsilon r$, and calculate the limit of this difference for $r \rightarrow 0$. However, since we are interested only in the force, not in the interaction energy, and since φ_0 is independent of h , it is sufficient to begin by substituting (6.128) into (6.123), carry out the differentiation, and then, setting $r = 0$, carry out the summation over all ions of both signs located on a unit surface area of each of the two interfaces. In view of the definition of κ_s [(6.127)], the "correlational" disjoining pressure is found to equal

$$\Pi_{\text{cor}} = -kT \kappa_s^2 Q(2\kappa_s h) / 2\pi h \quad (6.129)$$

where

$$Q(\xi) = \int_0^\infty \frac{(t + \xi)t^3 e^{-t} dt}{[(t + \xi)^2 - \xi^2 e^{-t}]^2} \quad (6.130)$$

Clearly, Π_{cor} is attractive. The quantity $r_s = \kappa_s^{-1}$ plays the role of the characteristic correlation radius in the plane [53], analog-

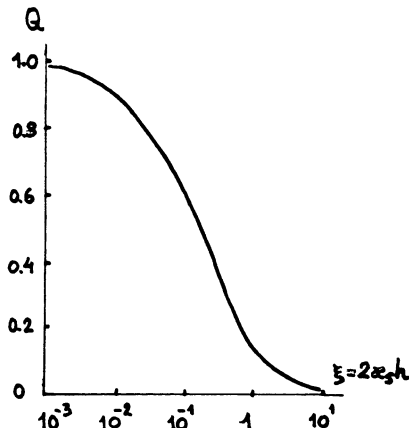
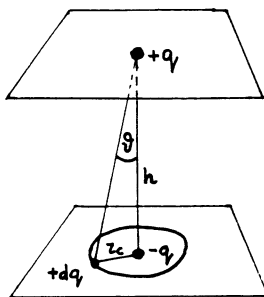
Fig. 6.21. Correction factor Q to Eq. (6.131).

Fig. 6.22. Model for the derivation of formula (6.133).

gous to the Debye screening radius in the bulk of the electrolyte, although the type of screening — i.e., the dependence of potential and interaction force on distance h — is given in this case by power, not exponential, functions (as will be shown below). At very short distances ($\xi = 2\kappa_s h \ll 1$) $Q(\xi) \rightarrow 1$, and

$$\Pi_{\text{cor}} = -kT\kappa_s^2/2\pi h = -\pi e^4(z_+ + z_-)^2(z_+ n^+ + z_- n^-)^2/2\epsilon^2 k T h \quad (6.131)$$

This formula gives for $z_+ = z_-$ and $n^+ = n^-$ a result exactly twice that obtained for small values of argument from the formula (6.122) that takes into account only pair correlations, and even those only among charges located on opposite surfaces. The results of numerical calculations of the correction term $Q(2\kappa_s h)$ by using Eq. (6.130) are shown in Fig. 6.21; they give a measure of correct-

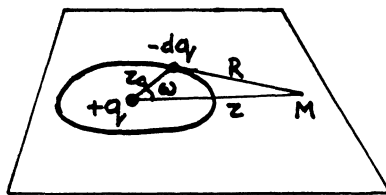


Fig. 6.23. Model for the derivation of the formula (6.137)

ness of Eq. (6.131) for different values of $\xi = 2\kappa_s h$. Evidently, this equation fails to give the correct order of magnitude to Π_{cor} for $h \gtrsim r_s$.

At still larger distances $h \gg r_s$, we obtain from Eqs. (6.129) and (6.130) [50, 51] that

$$\Pi_{\text{cor}} = -3\zeta(3)kT/8\pi h^4\kappa_s \quad (6.132)$$

where $\zeta(3) \approx 1.202\dots$ is the Riemann zeta function. The screening of correlational forces in this approximation thus indeed displays power behavior, not an exponential one. This result has a simple physical interpretation. Indeed, dependence (6.132) can be readily derived if we assume that the oppositely charged ions on each of the surfaces form "pairs" ("dipoles"), being separated by a distance r_c roughly equal to the correlation radius $r_s = \kappa_s^{-1}$; on average, each charge interacts with a charge of opposite sign located directly across the gap in the second plane, and with a charge of like sign uniformly smeared around this charge in the second plane along a circumference with a radius r_c of the same order as r_s (see Fig. 6.22). As we see from this figure, at $r_c \ll h$, the force of interaction of the charge q with this "dipole" is

$$\begin{aligned} f &= q^2/\epsilon h^2 - (q^2/\epsilon R^2) \cos\varphi = q^2/\epsilon h^2 \\ &- q^2 h/\epsilon (h^2 + r_c^2)^{3/2} \approx -3q^2 r_c^2/2\epsilon h^4 \end{aligned} \quad (6.133)$$

i.e., is attractive regardless of the sign of the considered charge q . The total force f_d acting on a unit surface area is then equal to $2nf$ because the total number of charges is $2n$. A substitution $r_c = r_s$ yields

$$F_d = -3\epsilon(kT)^2/16\pi^2 q^2 n_s h^4, \quad q = ze \quad (6.134)$$

which coincides with (6.132) to within a factor $\zeta(3)/2 \approx 0.6$.

The concept of circular dipoles in a plane is supported by the results following from the theory of two-dimensional electro-

lytes, mentioned above [53]. The electrostatic potential in the plane at a large distance r from any charge q in such an electro-neutral ion "solution" is

$$\varphi \approx qr_s^2/\epsilon r^3 \quad (6.135)$$

and represents the potential of just such a circular dipole. Indeed, the potential created by the central charge q and a circular charge $-q$ at a point M (Fig. 6.23) is

$$\varphi_M(r) = q/\epsilon r - \int dq/\epsilon R = q/\epsilon r$$

$$= \int_0^{2\pi} q d\omega / 2\pi\epsilon(r^2 + r_c^2 - 2rr_c \cos\omega)^{1/2} \quad (6.136)$$

The expansion of the denominator in a series in powers of small ratio r_c/r , for $r_c \ll r$, gives

$$\varphi_M \approx -qr_c^2/4\epsilon r^3 \quad (6.137)$$

which coincides with (6.135) for $r_c \approx 2r_s$.

An evaluation of the ratio of the correlational correction to the maximum macroscopic disjoining pressure in the gap as given by (6.33) shows that at very small distances (i.e., at fractions of the Debye length) the electrostatic repulsion of interfaces can be substantially weakened by the correlational attraction and, in principle, can alter the balance of forces acting in very thin layers of dilute electrolytes. Thus, for interfaces with potential 25 mV in a 10^{-3} M aqueous solution of a univalent electrolyte, $|\Pi_{\text{cor}}/\Pi_e^{\text{max}}| \approx 0.5$ for $h = 20 \text{ \AA}$ (the Debye radius $\sim 100 \text{ \AA}$) if the ion concentration at the surface is 10^{12} cm^{-2} , i.e., if the surface coverage with ions is below 0.1% and the correlation radius is approximately 110 \AA . As the surface potential and electrolyte concentration increase, the relative contribution of the correlation increment decreases; this increment becomes appreciable at distances where structural effects inevitably become strong (see Chapter 7).

6.10. DISJOINING PRESSURE IN A THIN FREE FILM

As already mentioned in Section 6.2, boundary conditions must be correctly formulated in the integration of the Poisson-Boltzmann equation when the disjoining pressure is found as a function of film thickness. The usual constraint of constant potential at the boundaries of the diffuse ion layer is acceptable only as long as

the interlayer thickness considerably exceeds the thickness of the Debye ion atmospheres (see Fig. 6.2). However, the situation changes when the interlayer thickness becomes much less than the Debye length. This situation occurs in secondary black free films or emulsion films, or in aggregates of colloidal particles when they retain a liquid interlayer. This may possibly come about if particles approach one another too rapidly for ionic equilibrium to be maintained. Consequently, the final stage of approach proceeds rather at constant charge. The subsequent relaxation possibly explains why no peptization is observed experimentally after particles stay in the aggregated state for a long time.

However, this explanation fails for the stability of secondary black films; they appear when primary films thin out slowly and sometimes last for years. Here we need an approach based on a concrete mechanism of surface charging to enable us to calculate the charge and potential of the surface as functions of interlayer thickness. Ninham and Parsegian [54] investigated the changes in the degree of ionization at the surface of a film containing dissolved uni- and bivalent ions when the film thins out; but the study was restricted to a numerical analysis of complicated parametric equations. Here we consider, for simplicity, only a dilute solution with a single ionogenic surfactant component, for instance anion-active sodium oleate.

If the thickness of the solution interlayer is sufficiently small (much less than the thickness of the ionic atmosphere), the amount of anions in the bulk of the interlayer can be neglected. All the anions must be in specifically adsorbed monolayers on the interfaces. Some anions are blocked by cations, and only the remainder of the anions determines the surface charge per unit area σ . In view of electroneutrality, this charge is compensated by cations in the bulk of the film:

$$2\sigma = \int_{-h/2}^{h/2} c(x) dx \quad (6.138)$$

where $c(x)$ is the cation concentration at a distance x from the symmetry plane of the film, and h is the film thickness (minus the thickness of the adsorbed monolayer). The adsorption isotherm is now found by writing the condition of dynamic equilibrium of the processes of adsorption and desorption of cations:

$$c_1\sigma = b(\sigma_0 - \sigma) \quad (6.139)$$

where c_1 is the cation concentration directly at the adsorption monolayer, σ_0 is the surface charge density in the absence of adsorbed cations (in other words, when the monolayer is completely dissociated), and b is the equilibrium constant with the dimension

of concentration. The difference $\sigma_0 - \sigma$ is proportional to the number of adsorbed cations (or to the fraction of nondissociated molecules on the surface). The left-hand side of Eq. (6.139) is proportional to the rate of adsorption because σ is proportional to the number of "vacant sites." That number is determined by the number of anions "not blocked" by cations.

The rise in cation concentration at the surface monolayers, resulting in blocking of the anions, is caused by the electrostatic interaction. In view of the comments above, the Poisson-Boltzmann equation (6.5) now reduces to a simple form:

$$\frac{d^2\psi}{dx^2} = - (4\pi/\epsilon)ec_\infty \exp(-e\psi/kT) \quad (6.140)$$

where c_∞ is the cation concentration in the bulk phase with which the film is in contact. Making use of the Boltzmann equation

$$c = c_\infty \exp(-e\psi/kT) \quad (6.141)$$

we can recast the first integral of Eq. (6.140) in a form that does not explicitly contain the potential ψ :

$$(2\pi/\epsilon kT)\sigma^2 = c_1 - c_0 = c_0 \tan^2(h/2d_0) \quad (6.142)$$

where

$$d_0 = \frac{1}{e} \sqrt{\frac{\epsilon kT}{2\pi c_0}} = \sqrt{\frac{2c_\infty}{c_0}} d_D \quad (6.143)$$

denotes a length that can be much less than the thickness d_D of ionic atmospheres in the bulk of the solution if the cation concentration c_0 in the symmetry plane is much greater than c_∞ ; this situation occurs at sufficiently small h .

Further simplification is achieved by considering only the limiting cases of small and moderately large thickness h . If

$$h/2d_0 \ll 1 \quad (6.144)$$

then $\tan(h/2d_0)$ can be replaced with its argument, and we find, after some elementary manipulations,

$$\sigma = ec_0 h/2 \quad (6.145)$$

It will be convenient for further analysis to rewrite Eq. (6.139) in a different form:

$$c_1/b + 1 = \sigma_0/\sigma \quad (6.146)$$

As the interlayer thickness diminishes, both concentrations c_0 and $c_1 > c_0$ increase. First we consider the case of both c_1 and c_0 remaining much less than a large constant b . Then it follows from Eq. (6.146) that $\sigma \approx \sigma_0$, and from Eq. (6.145) we find

$$c_0 \approx 2\sigma_0/eh \quad (6.147)$$

Formula (6.17), applied to the distribution (6.147), immediately yields a "Langmuir" expression for disjoining pressure:

$$\Pi_e = kT(c_0 - c_\infty) \quad (6.148)$$

(though the correct derivation of this formula is fundamentally different from Langmuir's). Taking into account that at sufficiently small h the concentration $c_0 \gg c_\infty$, we obtain from (6.147) and (6.148)

$$\Pi_e \approx kTc_0 \approx kT \frac{2\sigma_0}{eh} \quad (6.149)$$

However, this expression is not the limiting law. At still smaller h the concentration c_1 finally grows to values at which the assumed condition reverses, $c_1 >> b$, and $c_1 \approx c_0$ by (6.142). Then we find from (6.146) and (6.145) that

$$\sigma = b\sigma_0/c_1 \approx b\sigma_0/c_0 \quad (6.150)$$

$$c_0 \approx \sqrt{\frac{2b\sigma_0}{eh}} \quad (6.151)$$

and from (6.148)

$$\Pi_e \approx kTc_0 \approx kT\sqrt{2b\sigma_0/eh} \quad (6.152)$$

In the other limiting case, the argument of the tangent in (6.142) tends to $\pi/2$ and, correspondingly, $c_0 \ll c_1$. However, we assume that again $c_0 \gg c_\infty$, and find

$$h = \pi d_0 \ll \pi d_D \quad (6.153)$$

whence

$$c_1 \gg c_\infty, \text{ i.e., } e\psi/kT \gg 1 \quad (6.154)$$

Now, in accord with the definition of d_0 , i.e., (6.143),

$$c_0 \approx (\pi/2)(\epsilon kT/e^2 h^2) \quad (6.155)$$

so that

$$\Pi_e \approx \pi \epsilon (kT)^2 / 2e^2 h^2 \quad (6.156)$$

The formula (6.156) so obtained coincides exactly with Langmuir's formula (6.35) derived for h much less than the $1/\kappa$, and of the dimensionless surface potential much greater than unity; these conditions are equivalent to (6.153) and (6.154).

An important feature of Eq. (6.152) is that Π_e is a function of the adsorption parameters σ_0 and b . As for σ_0 , with a dense, nearly saturated monolayer it falls in a narrow range of values. The range of b can be much wider. It is the greater, the easier the adsorbed molecules dissociate and the easier the cations transfer from the monolayer to the bulk of the film. The most effective in this respect in aqueous solutions are lithium ions, and then sodium ions owing to their large hydration energy.

Having evaluated the value of b , it is possible to establish by simple calculations that the transition from (6.156) to (6.149) and then to (6.152) is accompanied, as h diminishes, by a sharp increase in Π_e by several orders of magnitude. The disjoining pressure Π_e would reach even greater values if h diminished at constant charge. However, this mode is incompatible with equilibrium conditions, and thus cannot be responsible for long-term stability of, for instance, black soap films.

6.11. EXPERIMENTAL VERIFICATION OF THE THEORY OF ELECTROSTATIC INTERACTION

There have been many experimental studies confirming the validity of the theory of electrostatic repulsion for the range of electrolyte concentrations and double-layer potentials in which the Poisson-Boltzmann equation holds. Paradoxical though this may sound, the first evidence of its correctness is found in the results of Derjaguin and Kussakov [55] obtained in 1936-1937 in experiments with equilibrium wetting films before the theory was developed [1]. Later, a number of authors [56] measured equilibrium thickness of wetting films of very dilute electrolyte solutions on quartz and mica surfaces and reported results in agreement with those of [55] in the range of thickness about $0.1 \mu\text{m}$ and greater. In this range, molecular forces are negligibly small compared with the electrostatic repulsion, so that the pressure created in the film indeed corresponds to the ionic component of disjoining pressure.

A considerable number of direct measurements of surface forces as a function of distance between surfaces have been re-

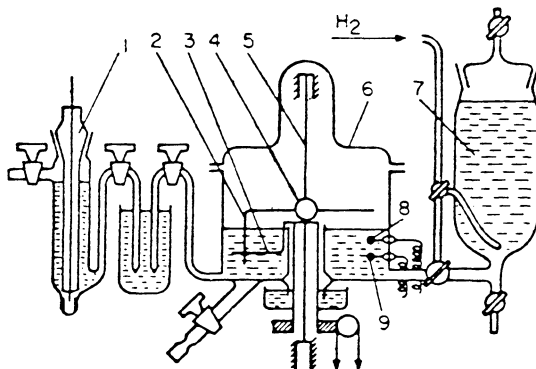


Fig. 6.24. Schematic representation of the set-up of Derjaguin and Voropaeva [62]: 1) reference electrode; 2, 3) platinum fibers; 4) mirror; 5) suspension; 6) hermetically sealed cell; 7) reservoir with electrolyte; 8, 9) platinum electrodes for polarization of fibers.

ported recently. The experiments included transparent [27, 28, 57] and opaque specimens [26, 58]. These studies were extended to the range of still thinner interlayers in which the measured forces are a sum of several components (at least two) of comparable intensity, viz., the ionic and molecular components. It was found that most of the data could be interpreted by taking into account just these two components. Occasionally this interpretation was valid until the surfaces were in contact. At small distances it was sometimes necessary to take into account the mechanism of surface charge formation. In certain cases the repulsive forces exceeded, at very small distances below 30-50 Å, the forces that are expected when double ion layers overlap [26, 59]. These "excess" forces are the structural forces treated later (Chapter 7).

Even before it became possible to measure repulsive forces between charged surfaces in electrolyte solutions as functions of distance, Derjaguin and Voropaeva measured force barriers between crossed metal wires [60-62]. The force barrier preventing the adhesion of crossed metal wires in electrolyte solutions was determined by a specially designed setup [60] shown in Fig. 6.24. A metal filament 1, 300 µm in diameter, was fixed on an elastic suspension 3 of a torsion balance. The second metal filament 2 perpendicular to the first was moved toward (or away from) the filament 1 until they were in contact, as indicated by a jumpwise equalization of the filament potentials. The maximum angle of torsion of the suspension 3 was measured by a photoelectric cell recording the angle of rotation of the mirror 4; it gave a measure of the force barrier. Electrochemical cleaning of the filaments was

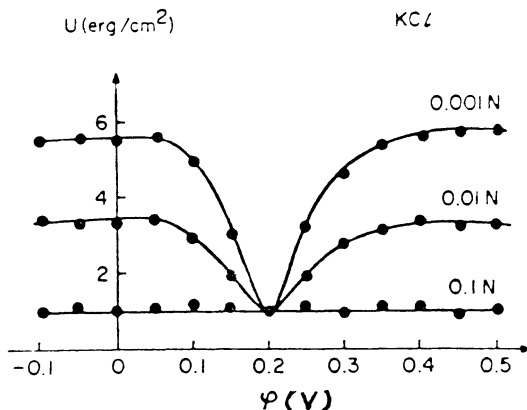


Fig. 6.25. Barrier height as a function of potential of platinum fibers in KCl solutions [62].

carried out in 1 N solution of sulfuric acid by means of additional electrodes which also served to polarize the filaments to a prescribed potential. The electrochemical potential was measured with respect to the reference electrode 7.

The results obtained with this instrument were reported in detail in [61-63]. Figure 6.25 shows the force barrier recorded in KCl solutions, plotted as a function of potential of the platinum filaments. The measured values of force acting on filaments were converted by formula (2.49) into the specific free energy (per unit area) of interaction between plane-parallel plates of the same material. It is clear from Fig. 6.25 that the potential barrier ψ_{\max} between the plates (i.e., the force barrier between the filaments) is symmetrical with respect to the potential 0.2 V, which is close to the point of zero charge. In accordance with the DLVO theory, as the potential increases, the force barrier asymptotically tends to a limiting value depending on the electrolyte concentration. However, at the point of zero charge the force barrier did not vanish, in contradiction to the theory. Furthermore, the barrier did not drop to zero at high electrolyte concentration c , also in contradiction to the DLVO theory. Similar results were obtained by Derjaguin and Rabinovich [64] by means of a more sensitive and less complicated experimental setup shown in Fig. 6.26. With this system, it was possible not only to check and extend the results for platinum filaments reported in [60-62], but also to study the barrier between gold filaments. A bifilar suspension made of metal filaments 1 stretched by two weights 4 and 5 and a glass rod 2 was mounted in a glass cell with an electrolyte. The suspension was in neutral equilibrium, so that practically no restoring torque appeared when the rod 2 was rotated. The lower parts of the crossed filaments were in the field of a permanent magnet. When a current

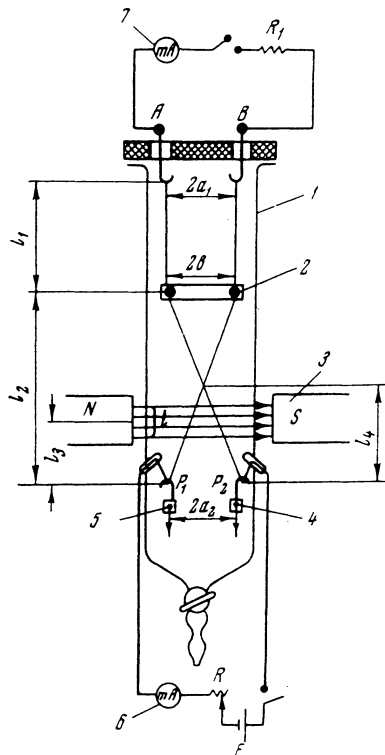


Fig. 6.26. Schematic representation of the Derjaguin-Rabinovich setup [64]: 1) bifilar suspension; 2) glass rod; 3) magnet; 4, 5) platinum weights; 6, 7) milliammeters; A, B) electrodes.

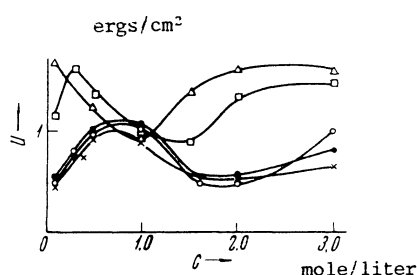


Fig. 6.27. Potential barrier between gold fibers as a function of electrolyte concentration: Δ) CsCl; □) RbCl; •) KCl; ×) NaCl; ○) LiCl [64].

was passed through the filaments, the Ampere force so generated rotated the suspension and brought the filaments together, until the barrier was overcome, producing a current jump in the microammeter 7. The force barrier N equals the Ampere force. It was calculated by means of the formula

$$N = JB\ell\ell_3/\ell_4$$

where J is the electric current, B is the magnetic induction, and the geometric characteristics ℓ , ℓ_3 , and ℓ_4 are indicated in Fig. 6.26. The bifilar suspension used in [64] made it possible to eliminate the need to calibrate the instrument.

Figure 6.27 plots the force barrier between gold filaments as a function of concentration of 1-1 electrolytes. In high concentrations the barrier is independent of potential, which proves the non-electrostatic nature of the forces involved. Similar curves $V^{\max}(c)$ were obtained for platinum filaments [60-64]. Figure 6.27 demonstrates that the height of the barrier depends on the cation species; therefore, the forces appearing in concentrated electrolyte solutions seem to be related to the hydration of ions. So far no quantitative theoretical explanation has been found for these forces.

The values of force barrier measured in dilute electrolyte solutions far from the point of zero charge can be used to calculate the Hamaker constant A because the Derjaguin-Landau formula (6.61) can be regarded as valid at such concentrations and potentials. (An attempt of this sort, made in [61, 62], failed because of a mistake that crept into calculations, but the correct calculation was made in [65].) The idea was to take into account just the molecular V_m and the electrostatic V_e forces. The first is calculated by means of formula (6.20):

$$V_m = -A/12\pi H^2 \quad (6.157)$$

where A is the Hamaker constant, and H is the distance between the planes. The electrostatic component at high potentials is found by using (6.61) and (6.51), for $\psi_1 \rightarrow \infty$:

$$V_e = \frac{8nkT}{\kappa} \left[\frac{2}{k_1} E(k_1) - \left(\frac{1}{k_1} - k_1 \right) K(k_1) - 2 \right] \quad (6.158)$$

$$\kappa H = 2k_1 K(k_1) \quad (6.159)$$

where n is the concentration of ions of one sign of charge in the solution (in cm^{-3}), κ is the reciprocal Debye radius, $K(k_1)$ and $E(k_1)$ are elliptic integrals of the first and second kind, respectively, with the modulus $k_1 = I/\cosh(z\epsilon\psi_d/2kT)$, and ψ_d is the potential in the symmetry plane. Taken together with the extremum condition, Eqs. (6.157)-(6.159) yield the following equation:

TABLE 6.1. Hamaker Constant A Calculated from the Experimentally Determined Height of Force Barrier

Substance	Electrolyte	Concentration, mole/liter	$A \cdot 10^{12}$ erg
Platinum	KCl	$1 \cdot 10^{-3}$	1.2
	KCl	$1 \cdot 10^{-2}$	1.6
	MgSO ₄	$6 \cdot 10^{-4}$	0.9
	MgSO ₄	$2 \cdot 10^{-3}$	0.8
Gold	KCl	$1 \cdot 10^{-3}$	4.1

$$\kappa V^{\max} / 4nkT = (1/k_1)[4E(k_1) - 4k_1 - 3(1 - k_1^2)K(k_1)] \quad (6.160)$$

Having calculated k_1 from Eq. (6.160) by using the height of the barrier V^{\max} found experimentally, we can find the Hamaker constant A. This means that the derivative of $V(H)$ must be set equal to zero:

$$4nkT(1/k_1^2 - 1) = A/6\pi H^3 \quad (6.161)$$

and then Eq. (6.159) must be used.

Equation (6.160) becomes especially simple if $k_1 \ll 1$, i.e., if the barrier is high and the potential ψ_d also reaches a relatively high value at the extremum. As was shown in [65], in this case

$$k_1 = \pi/8(\alpha + 1) \quad (6.162)$$

where $\alpha = \kappa V^{\max} / 16nkT$. The constant A can then be calculated by the formula [65]

$$A = 3\pi^5 V^{\max} / 16\kappa^2 \alpha (\alpha + 1) \quad (6.163)$$

In the opposite case of a moderately high barrier V^{\max} (V^{\max} being a fraction of 1 erg/cm²) we have to solve Eq. (6.160) numerically and then determine A from Eqs. (6.161) and (6.159). The results of such calculations of A from the experimental values of V^{\max} are listed in Table 6.1. These results are reasonably good as to order of magnitude, and are in satisfactory agreement both with the theoretical calculations and with later experimental studies of the stability of gold sols [67].

REFERENCES

1. B. V. Derjaguin, Izv. Akad. Nauk SSSR, Ser. Khim., No. 5, 1153 (1937); Acta Physicochim. URSS, 10, 333 (1939).
2. I. Langmuir, J. Chem. Phys., 6, 885 (1938).
3. A. J. Babchin, J. Colloid Interface Sci., 49, 390 (1974).
4. B. V. Derjaguin, Kolloidn. Zh., 37, 1015 (1975); J. Colloid Interface Sci., 56, 492 (1976).
5. G. Bell and S. Levine, J. Colloid Interface Sci., 56, 218 (1976).
6. I. E. Tamm, Foundations of the Theory of Electricity, Mir, Moscow (1979).
7. B. V. Derjaguin, Trans. Faraday Soc., 36, 203, 730 (1940); Kolloidn. Zh., 6, 291 (1940).
8. B. V. Derjaguin and L. D. Landau, Acta Physicochim. URSS, 14, 633 (1941); Zh. Eksp. Teor. Fiz., 11, 802 (1941).
9. E. J. W. Verwey and J. Th. G. Overbeek, Theory of the Stability of Lyophobic Colloids, Elsevier, Amsterdam (1948).
10. H. R. Kruyt (ed.), Colloid Science. Irreversible Systems, Vol. 1, Elsevier, Amsterdam (1952).
11. B. V. Derjaguin, Usp. Khim., 48, 675 (1979).
12. Y. Ikeda, J. Phys. Soc. Jpn., 8, 49 (1953).
13. P. Debye and E. Hückel, Phys. Z., 24, 873 (1938).
14. B. V. Derjaguin and N. V. Churaev, Kolloidn. Zh., 37, 1075 (1975); Dokl. Akad. Nauk SSSR, 222, 554 (1975).
15. B. V. Derjaguin, Discuss. Faraday Soc., 18, 85 (1954); Kolloidn. Zh., 16, 425 (1954).
16. B. V. Derjaguin and V. G. Levich, Dokl. Akad. Nauk SSSR, 98, 985 (1954).
17. V. P. Smilga, Kolloidn. Zh., 22, 615 (1960).
18. O. F. Devereux and P. L. de Bruyn, Interaction of Plane Parallel Double Layers, M.I.T. Press, Cambridge, Massachusetts (1963).
19. G. M. Bell and G. C. Peterson, J. Colloid Interface Sci., 41, 542 (1972).
20. S. Usui, J. Colloid Interface Sci., 44, 107 (1973).
21. A. N. Frumkin and A. V. Gorodetskaya, Zh. Fiz. Khim., 12, 511 (1938); A. N. Frumkin, Trans. Faraday Soc., 36, 79 (1940).
22. P. Bergmann, P. Low-Beer, and H. Zocher, Z. Phys. Chem., A181, 301 (1938).
23. V. M. Muller, Kolloidn. Zh., 38, 704 (1976).
24. V. M. Barboi, Kolloidn. Zh., 25, 385 (1963).
25. V. M. Muller, in: Research in Surface Forces, Vol. 3, Consultants Bureau, New York (1971), p. 236; Kolloidn. Zh., 31, 427 (1969).
26. Ya. I. Rabinovich, B. V. Derjaguin, and N. V. Churaev, Adv. Colloid Interface Sci., 16, 63 (1982).
27. R. M. Pashley, Adv. Colloid Interface Sci., 16, 57 (1982).
28. J. N. Israelachvili, Adv. Colloid Interface Sci., 16, 31 (1982).

29. G. Frens, Reversibility of Irreversible Colloids, Thesis, Univ. of Utrecht (1968); G. Frens and Th. G. Overbeek, J. Colloid Interface Sci., 38, 376 (1972).
30. E. P. Honig and P. M. Mul, J. Colloid Interface Sci., 36, 258 (1971).
31. V. M. Muller, in: Surface Forces in Thin Films and Stability of Colloids, Nauka, Moscow (1974), p. 245.
32. B. V. Derjaguin and I. I. Abrikossova, Discuss. Faraday Soc., 18, 24 (1954); D. Tabor, J. Colloid Interface Sci., 58, 2 (1977); E. D. Shchukin, E. A. Amelina, and V. V. Yaminski, Colloids and Surfaces, 2, 221 (1981).
33. B. V. Derjaguin, Kolloid Z., 69, 155 (1934); Zh. Fiz. Khim., 6, 1306 (1935).
34. L. N. McCartney and S. Levine, J. Colloid Interface Sci., 30, 345 (1969).
35. S. S. Dukhin, N. M. Semenikhin, and L. M. Shapinskaya, Dokl. Akad. Nauk SSSR, 193, 385 (1970).
36. S. S. Dukhin, B. V. Derjaguin, and N. M. Semenikhin, Dokl. Akad. Nauk SSSR, 192, 357 (1970).
37. N. E. Hoskin and S. Levine, Philos. Trans. R. Soc. London, A248, 449 (1956).
38. R. Hogg, T. W. Healy, and D. W. Fuerstenau, Trans. Faraday Soc., 62, 1638 (1956).
39. G. Wilemski, J. Colloid Interface Sci., 88, 111 (1982).
40. V. V. Karasev, N. A. Krotova, and B. V. Derjaguin, Dokl. Akad. Nauk SSSR, 88, 777 (1953).
41. E. I. Kats, Zh. Eksp. Teor. Fiz., 60, 1172 (1971).
42. I. S. Zhiguleva and V. P. Smilga, in: Surface Forces in Thin Films and Stability of Colloids, Nauka, Moscow (1974), p. 220.
43. Yu. I. Yalamov, in: Research in Surface Forces, Vol. 2, Consultants Bureau, New York (1966), p. 104.
44. P. Richmond, J. Chem. Soc., Faraday Trans. II, 71, 1154 (1975).
45. F. S. Kaplan, I. F. Efremov, and O. G. Us'yarov, loc. cit., Ref. 42, p. 171.
46. F. S. Kaplan and O. G. Us'yarov, Kolloidn. Zh., 36, 258 (1974).
47. F. S. Kaplan and O. G. Us'yarov, Kolloidn. Zh., 36, 672 (1974).
48. P. Richmond, J. Chem. Soc., Faraday Trans. II, 70, 1066 (1974).
49. B. V. Derjaguin and V. M. Muller, Dokl. Akad. Nauk SSSR, 225, 601 (1975).
50. V. M. Muller and B. V. Derjaguin, Kolloidn. Zh., 38, 1117 (1976).
51. V. M. Muller and B. V. Derjaguin, Izv. Akad. Nauk SSSR, Ser. Khim., No. 8, 1710 (1982); Colloids Surfaces, 6, 205 (1983).
52. V. M. Muller, G. L. Kuzmina, G. A. Martynov, and I. V. Bulatova, Kolloidn. Zh., 38, 480 (1976).
53. V. M. Muller, and B. V. Derjaguin, Dokl. Akad. Nauk SSSR, 228, 645 (1976); J. Colloid Interface Sci., 61, 361 (1977).
54. B. W. Ninham and V. A. Parsegian, J. Theor. Biol., 31, 405 (1971).

55. B. V. Derjaguin and M. M. Kussakov, Izv. Akad. Nauk SSSR, Ser. Khim., No. 5, 741 (1936); No. 5, 1119 (1937).
56. A. Scheludko, *Colloid Chemistry*, Elsevier, Amsterdam-London-New York (1966), p. 197; A. D. Read and J. A. Kitchener, J. Colloid Interface Sci., 30, 391 (1969); T. D. Blake and J. A. Kitchener, J. Chem. Soc., Faraday Trans. I, 68, 1435 (1972); M. P. Aronson and H. M. Princen, J. Colloid Interface Sci., 52, 345 (1975); Colloid Polymer Sci., 256, 140 (1978); H. J. Schulze and Chr. Cichos, Z. Phys. Chem., 251, 145, 252 (1972).
57. J. N. Israelachvili and B. W. Ninham, J. Colloid Interface Sci., 58, 14 (1977); J. N. Israelachvili, Faraday Discuss. Chem. Soc., 65, 20 (1978); J. N. Israelachvili and G. E. Adams, J. Chem. Soc., Faraday Trans. I, 74, 975 (1978).
58. Ya. I. Rabinovich, Kolloidn. Zh., 39, 1094 (1977); B. V. Derjaguin, Ya. I. Rabinovich, and N. V. Churaev, Nature, 272, 313 (1978).
59. R. M. Pashley, J. Colloid. Interface Sci., 83, 531 (1981).
60. T. N. Voropaeva, B. V. Derjaguin, and B. N. Kabanov, Dokl. Akad. Nauk SSSR, 128, 981 (1959).
61. T. N. Voropaeva, B. V. Derjaguin, and B. N. Kabanov, Kolloidn. Zh., 24, 396 (1962).
62. B. V. Derjaguin, T. N. Voropaeva, B. N. Kabanov, and A. S. Titiyevskaya, J. Colloid Interface Sci., 19, 113 (1964).
63. B. V. Derjaguin, Pure Appl. Chem., 10, 375 (1965).
64. B. V. Derjaguin and Ya. I. Rabinovich, Kolloidn. Zh., 31, 47 (1969); Dokl. Akad. Nauk SSSR, 179, 1373 (1968).
65. B. V. Derjaguin, V. M. Muller, and Ya. I. Rabinovich, Kolloidn. Zh., 41, 304 (1969).
66. V. M. Muller and N. V. Churaev, Kolloidn. Zh., 36, 492 (1974); V. A. Parsegian and G. H. Weiss, J. Colloid Interface Sci., 81, 285 (1981); H. Krupp, W. Schnabel, and G. Walter, J. Colloid Interface Sci., 39, 421 (1972).
67. N. M. Kudryavtseva, A. A. Baran, and B. V. Derjaguin, Kolloidn. Zh., 39, 1070 (1977).

Chapter 7

THE STRUCTURE OF BOUNDARY LAYERS OF LIQUIDS AND THE STRUCTURAL COMPONENT OF DISJOINING PRESSURE

The DLVO theory (Chapter 8) cannot explain all the known facts about the stability of colloids and thin liquid films. There are certain discrepancies that might tentatively be ascribed to "solvation" of the surfaces of particles. Solvation implies formation of boundary layers of special molecular structure, different from that of the bulk liquid.

This idea arose from the observation that the discrepancies are particularly marked with polar materials. The interaction of lyophilic surfaces in polar liquids cannot be reduced to the net effect of dispersion forces and double-layer forces. Forces of a "third kind," associated with a modification of the structure in boundary layers of solvents, were first reported in [1-4].* Later, these forces became known as structural forces, or the structural component of disjoining pressure [5].

We shall begin by outlining the experimental evidence for a special structure in boundary layers of polar liquids. Various physical methods have been employed to investigate the structure of liquid boundary layers. First, there are spectroscopic methods (NMR, IR, and UV spectrosopies, birefringence) that are capable of measuring differences in the mobility of molecules, in their orientation and mutual arrangement, and in interaction energy. Second, measurements have been made (even earlier) on the viscosity and density of liquids in thin layers and fine pores. Third, their dielectric permittivity, specific heat capacity, and heat and temperature of phase transitions have been determined.

A mass of experimental data is now available. Besides establishing the existence of special boundary layers, the data can give

*See also B. V. Derjaguin, Discuss. Faraday Soc., No. 42, 317 (1966).

quantitative estimates of the physical properties and thickness of the layers in various liquids. The long-range structuring influence of hydrophilic surfaces in water is particularly strong, and will therefore be discussed first. The data given below refer to polymolecular interlayers that can be treated as a part of the liquid phase affected by surface forces. (We shall not consider here the properties of adsorbed monolayers.)*

7.1. STRUCTURAL CHANGES IN THIN INTERLAYERS AND BOUNDARY LAYERS OF WATER

Water differs from other polar liquids in having strong, oriented intermolecular hydrogen bonds, which are responsible for a number of well-known anomalies of its bulk properties. As a result of the network of hydrogen bonds, the changes produced in the arrangement of water molecules within the boundary layer by active sites on the surface decay gradually with distance from this surface; sometimes it is appreciable at distances up to 100 Å and even farther. Active sites are surface atoms or groups capable of forming hydrogen bonds with water molecules, or certain adsorbed ions. The same sites are known to be responsible for the formation of the adsorbed monolayer of water molecules that are fixed most strongly, for instance by the surface of hydrophilic quartz [6-8]. The structure of boundary layers (and hence their properties) essentially depend on the specific arrangement of active sites on the surface, and on their number per unit area of the interface. Consequently, the structure of boundary layers of water can be different on the seemingly same surface of fused quartz, depending on the number and arrangement of surface hydroxyls, adsorbed ions, and impurity molecules.

Derjaguin and Zorin [9] discovered that water and some other polar liquids can form polymolecular adsorption layers on hydrophilic surface of glass at low undersaturation (at $p/p_s \geq 0.95$). The isotherms intersected the saturation axis at a finite film thickness h on the order of tens of angstroms. Since the isotherms obtained and the $h-(p/p_s)$ curves could not be explained by the net effect of the electrostatic and dispersion forces, it was assumed that the stability of such water films is related to the changes in their structure and to the appearance of the structural component of disjoining pressure [5]. Later Pashley and Kitchener [10] repeated the experiments of Derjaguin and Zorin and demonstrated that the thickness h of polymolecular water layers depends critically on the quartz surface cleaning procedure used, and on its hydrophilic properties. The cleaner the quartz surface was and the more hydrophilic it was made, the thicker were the polymolecu-

*See also B. V. Derjaguin, Chem. Scr., 9, 97 (1976); Pure Appl. Chem., 52, 1163 (1980); J. Offic. l'Union Int. Chim. Pure Appliq., 10, 375 (1965).

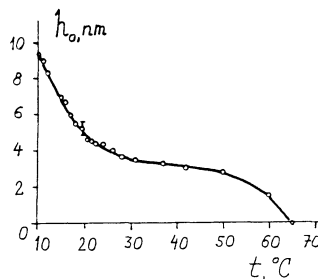


Fig. 7.1. Effect of temperature on thickness h_0 of polymolecular adsorption water films on the surface of fused quartz at $p/p_S \approx 1$.

lar water films (with thicknesses of several hundred molecular monolayers) in equilibrium with undersaturated vapor. The equilibrium film thickness was sharply reduced by decreasing the number of surface hydroxyls or by contaminating the surface with hydrophobizing impurities, at the same experimental conditions.

Independent confirmation of the structural nature of the effect was supplied by the high sensitivity of the thickness of polymolecular adsorbed water layers on quartz to temperature [11, 12]. Figure 7.1 clearly shows that as temperature increases, film thickness h decreases. The explanation is a partial destruction or weakening of the network of H-bonds responsible for the structural long-range forces. A similar effect was reported by Perevertaev and Metsik [13] for water films on mica.

An increase in temperature from 15 to 65°C (Fig. 7.1) could not affect appreciably the electrostatic and molecular forces; their temperature dependence is slight. Dissolution of substrates and surface gel formation at the surface do increase as temperature rises; however, this would result not in thinner films but in their further stabilization, in contrast to the actual results. Other independent measurements confirm that the special structure of boundary layers is destroyed by increasing temperature. Thus, thermo-osmotic flow of water in fine-pore glasses [14] ceases at $t \geq 70^\circ\text{C}$. It will be shown in Chapter 11 that thermo-osmosis develops because boundary water layers participating in the flow have a changed enthalpy owing to their special structure.

Structural modifications in boundary water layers are also confirmed by the study of flow in narrow quartz capillaries [15, 16]. Capillaries made of high-purity fused quartz (more than 99.99% SiO_2) have molecularly a smooth surface and strictly cylindrical shape, because of the high rate at which the heated tubes are stretched. Capillaries can be drawn with bore radius from tens to hundredths of a micrometer, several meters long. Capillary segments 5-7 cm long are used to measure viscosity. One end

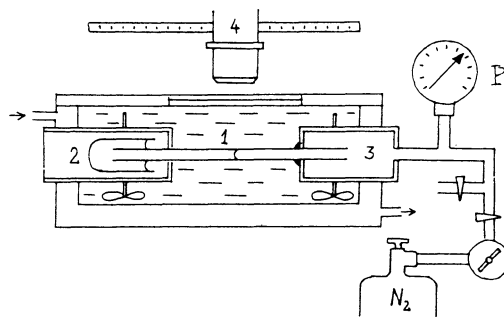


Fig. 7.2. Schematic diagram of thermostated set-up for measuring the viscosity of liquids in narrow capillaries.

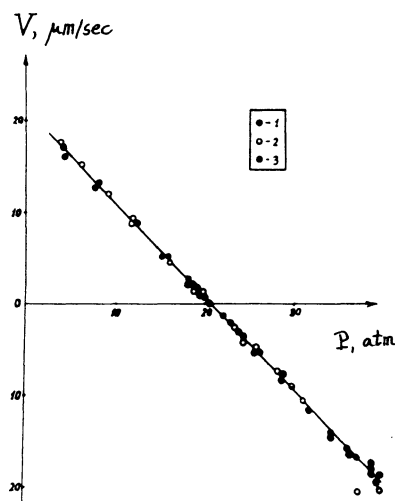


Fig. 7.3. Velocity of meniscus advance v as a function of gas pressure P in a capillary $r = 0.069 \mu\text{m}$ for water (1) and for aqueous solutions of KCl with concentrations 10^{-4} N (3) and $1.4 \cdot 10^{-3} \text{ N}$ (2) at 20.5°C .

of a capillary 1 (see Fig. 7.2) is dipped into an ampule 2 with the selected liquid, and the other end is in a chamber 3 with a gas (nitrogen) at a pressure P above the atmospheric pressure. The meniscus recedes when $P > P_c$, where P_c is the capillary pressure, and advances when $P < P_c$. The meniscus displacement velocity v is

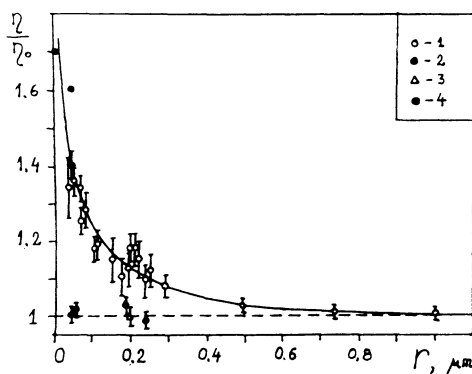


Fig. 7.4. Relative viscosity η/η_0 of water (1), benzene (2), and CCl_4 (3) as a function of capillary radius r ; filled circles (4) plot the data obtained by Tovbina [20] for water in silica gel pores.

measured by a microscope 4. No hysteresis of the contact angle is observed when the meniscus recedes ($v < 0$) or when it advances ($v > 0$) along a previously wetted surface: the plots of $v(P)$ for the advancing and receding meniscus are linear and identical (Fig. 7.3). The velocity v is measured along a short segment of the capillary $\Delta l \ll l$, where l is the length of the capillary bore filled with the liquid.

The mean velocity of a liquid in a capillary is calculated by using the Poiseuille equation

$$\eta = r^2(P - P_c)/8\pi l \quad (7.1)$$

The value of P_c is given by the intercept of the line $v(P)$ on the pressure axis (Fig. 7.3). The radius of the capillary is measured by means of a nonpolar reference liquid completely wetting the quartz surface, by the method of maximum pressure of the meniscus at the endface of the capillary. The constancy of the radius along the length of the capillary was controlled by measuring the capillary pressure of a nonpolar liquid at different points of the bore.

The results of viscosity measurements at 20-21°C are shown in Fig. 7.4, where capillary radii r are marked on the abscissa axis, and the relative viscosity η/η_0 along the ordinate axis. Here η_0 is the viscosity of the bulk liquid at the same temperature. It is clear from this figure that in capillaries with $r < 0.5 \mu\text{m}$ the viscosity of water is raised: the ratio η/η_0 becomes greater than 1. At the same time, the viscosity of the nonpolar liquids, benzene

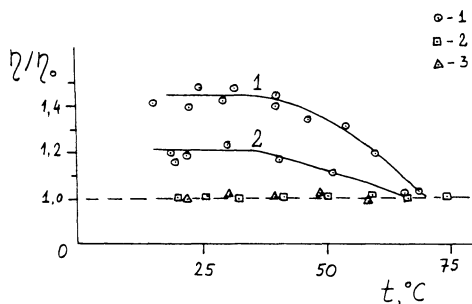


Fig. 7.5. Temperature dependence of relative viscosity η/η_0 of water in capillaries with radii $r = 0.05$ (1) and $0.17 \mu\text{m}$ (2). The symbols on curve 3 refer to benzene and CCl_4 in the same capillaries.

and CCl_4 , in the same capillaries remains at the bulk value. The effect cannot be associated with electroviscosity because the measured values of η did not change when electrolyte concentration was varied by three orders of magnitude, in the range from the triply distilled water (conductivity $1.5 \cdot 10^{-6} \Omega^{-1} \cdot \text{cm}^{-1}$) to KCl solutions with concentration up to $1.4 \cdot 10^{-3}$ mole/liter (Fig. 7.3). These measurements were made in the same capillary with $r = 0.069 \mu\text{m}$, at the same length of liquid column, $l = 4.2 \text{ cm}$. The theory of electroviscosity (also called electro-osmotic counterflow) predicts that an increase in electrolyte concentration from 10^{-6} to 10^{-4} mole/liter in a capillary with $r = 0.069 \mu\text{m}$ must produce an apparent drop in viscosity by a factor of roughly 2 [17]. The absence of the effect of electroviscosity can be explained by specific features of viscosity measurement in the method of meniscus displacement by small distances (on the order of 10^{-3} cm). No appreciable flow potential can develop under these conditions because the volume of the displaced liquid is extremely small ($\approx 10^{-14} \text{ cm}^3$).

As temperature increases, the departure of the mean viscosity of water from the bulk value diminishes (see Fig. 7.5). At a temperature near 70°C , when the thickness of so-called α -films of water on quartz reduces to one monolayer (see Fig. 7.1), the departure of the viscosity of water from the bulk value disappears, even in very thin capillaries. The disappearance of the effect at elevated temperatures also completely excludes an explanation in terms of electroviscosity because the surface potential of quartz is a weak function of temperature. The largest increase in the viscosity of water, recorded at 20°C in the narrowest capillaries ($r = 0.03\text{-}0.05 \mu\text{m}$), comes to 35-40% (Fig. 7.4).

The mean viscosity of water in finely porous glasses with mean pore radius from 20 to 100 Å is found to be increased by a factor of 1.5-2. These estimates were obtained by comparing filtration rates for water and the nonpolar CCl_4 (whose viscosity in fine pores was assumed unaltered) [18]. Similar results were obtained by comparing filtration rates of water in porous glasses at temperatures from 20 to 70°C [14, 19]. By assuming that water viscosity reaches its bulk value at 70°C, it was possible to evaluate its departure from the bulk value at 20°C. It was shown that, as in experiments with individual capillaries, increased temperature results in a gradual vanishing of the differences between the viscosity of water in fine pores and that in the bulk.

The measurements of diffusion rates of different molecules and ions through fine pores of silica gels, carried out by Tovbina [20], and also measurements of the mobility of water molecules in these systems, carried out by NMR techniques, both point to increased viscosity of water in narrow pores. Low [21] showed that, as pore size in clays diminishes, the Newtonian viscosity of water increases exponentially. This conclusion generalizes the results of measurements carried out by three different methods: measurements of filtration rate at different temperature, measurements of self-diffusion of water molecules (by neutron scattering), and measurements of transport rate of water molecules labeled with a radiotracer (tritium). All measurements carried out by the NMR technique with water in fine pores of clays, silica gels, and porous glasses reveal a certain orientation of water molecules by the surface and a reduction in their mobility [20, 22-30]. This is confirmed by the magnetic resonance not only of protons but also of O^{17} nuclei when the interference of paramagnetic impurities is successfully suppressed [26]. Measurements in the systems mentioned above make it possible to evaluate the thickness h_s of boundary layers; they reach 10^{-6} cm, with higher estimates for more hydrophilic surfaces [29]. Correlation times of molecular motion in boundary layers are found to be several times greater than in bulk water, in good agreement with the experiments discussed above, in which enhanced viscosity of water in thin layers was established.

Conversely, NMR does not reveal polymolecular boundary layers on such surfaces as AgI [31], and points to h_s below 20 Å for polystyrene latex [32]. This is confirmation of the sensitivity of thickness and structure of boundary layers to the state and properties of solid surfaces.

Another manifestation of altered viscosity in boundary layers is the discrepancy between the bulk viscosity and the mean (or effective) viscosity of flow through narrow pores in finely dispersed powders. The simplest method of detecting abnormal boundary layer viscosity, developed by Derjaguin and Zakhavaeva [33-35], is based on this effect. They measured the filtration coefficient of aqueous solutions of electrolytes and carbon tetrachloride through bentonite

clay (with specific surface area $35 \text{ m}^2/\text{g}$) and quartz sand of different degrees of dispersion. Special measures were taken to eliminate the possible effects of swelling of bentonite clay and of shrinkage of quartz sand on the results. A comparison of the experimental filtration coefficients (K_1) with those calculated by means of the Kozeny-Carman formula using the bulk viscosity value (K) demonstrated that the viscosity of CCl_4 was in all cases identical to the bulk value. With water the experimental filtration coefficient was less than the calculated one by a factor of three, indicating that the boundary layer viscosity is substantially greater than the bulk viscosity.

This effect is suppressed by adding high concentrations of electrolytes ($C \geq 1 \text{ mole/liter}$ with NaCl), which means destruction or contraction of boundary layers with special structure. Neither is this increment ($K > K_1$) observed in the filtration of water through sand layers with particle size above $5 \mu\text{m}$. If the observed effects were caused by electrical double layers, viscosity would reach the bulk value already at $C = 0.1 \text{ mole/liter}$, where the Debye radius becomes comparable to the thickness of the Stern layer. However, the ratio K/K_1 still remained high at this concentration, about 2.5.

These conclusions were further supported by experiments with KCl solutions filtered through nonselective glass membranes with rigid pore structure [18]. The experiments revealed a gradual decrease in the viscosity of water with increasing concentration of the electrolyte, and showed that the viscosity tends to that of the bulk solution at $C = 2 \text{ mole/liter}$. Viscosity was also determined by comparing the filtration coefficients of aqueous solutions with that of nonpolar CCl_4 . The mean diameter of glass pores found from filtration rates of CCl_4 was about 100 \AA . These results can be explained by assuming that, as the concentration of ions increases, their effect on the structure of water is enhanced, weakening the long-range influence of the hydrophilic surface of glass and silicates.

Specific properties of boundary layers are most pronounced at low temperature, in agreement with the data shown in Figs. 7.1 and 7.5. In frozen materials the long-range surface forces result in the formation of nonfreezing liquid interlayers between ice and solid surface, with thickness sharply increasing as temperature approaches the melting point of bulk water, T_0 . Clearly, these nonfreezing interlayers must have a structure different from that of bulk water. The thickness of nonfreezing interlayers has been obtained as a function of temperature for different solid surfaces [36-42]. Figure 7.6 plots the thickness of nonfreezing water interlayers h_s , determined by NMR techniques, as a function of temperature for frozen water dispersions of hydrophobic Teflon, hydrophilic Aerosil, and clays [41]. The curves show that as the solid surface

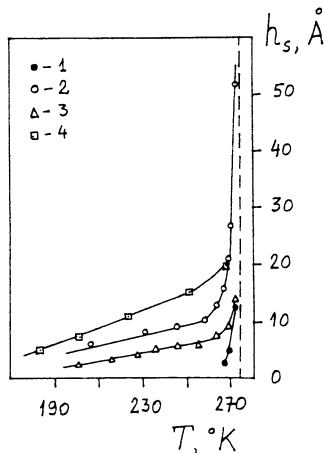


Fig. 7.6. Temperature dependence of the thickness of nonfreezing water interlayers h_s for frozen dispersions of Teflon (1), Aerosil (2), Na-montmorillonite (3), and Ca-kaolinite (4).

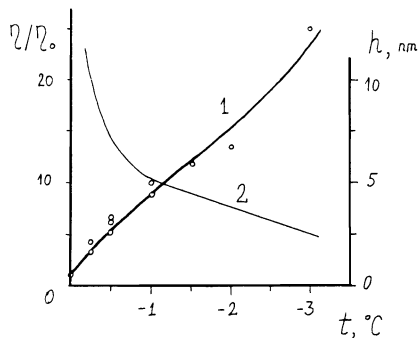


Fig. 7.7. Temperature dependence of relative viscosity η/η_0 (1) and thickness (2) of nonfreezing thin water interlayers between ice and a molecularly smooth surface of fused quartz.

becomes more hydrophilic, the thickness of nonfreezing liquid layers grows. Presumably, the nonfreezing liquid can be identified with the structurally altered boundary layers previously discussed.

At a temperature of -1°C , h_s reaches 40–50 Å. Similar results are obtained for nonfreezing water films on ice and for nonfreezing polymolecular adsorbed films of water (see Section 11.7). Thus, at

-0.3°C, the thickness of nonfreezing adsorbed water films on molecularly smooth surfaces of quartz capillaries is $h_s \approx 100 \text{ \AA}$ [43].

The viscosity of nonfreezing interlayers of water, determined by measuring the displacement of ice columns in cylindrical capillaries [44-46], was found to be substantially greater than the viscosity η_0 of bulk (supercooled) water at the same temperature. Figure 7.7 shows the obtained temperature dependence of η/η_0 (curve 1). The values of η were found from the equation of viscous flow in the interlayer,

$$\eta = (h/V)(\nabla P r / 2)$$

where V is the displacement velocity of the ice column driven by a gas pressure gradient ∇P in a capillary with radius r . The thickness of nonfreezing interlayers as a function of temperature, $h_s(t)$ (curve 2), was plotted by using published data [41, 43].

These curves show that deviations from bulk viscosity grow with decreasing temperature (and, hence, with decreasing thickness of the interlayers), pointing to gradually increasing departure of the structure of nonfreezing boundary layers from that of bulk water. The values obtained for viscosity are close to those calculated in [40] from the self-diffusion coefficient of water molecules measured in an NMR study of the water molecules' mobility in liquid-like films on the surface of ice. All these results support the conclusion of the enhancement of the structure-inducing long-range effect of surface forces at reduced temperatures.

Not only viscosity but also the density of liquid water is found to be changed in narrow pores. The first reliable evidence of this effect was reported in [47], which was a study of the thermal expansion of water that filled (in vacuum) the pores of a silica gel powder compressed to a porosity $m \approx 0.5$. A highly dispersed silica gel was pressed into a cylindrical Invar chamber 1 (see Fig. 7.8a) at a pressure 1000 atm. The chamber was then covered by a stainless-steel lid 2. A flanged branch 3 with a copper disk radiator 4 was soldered to the lid. The lid was soldered to the cylinder with a tin solder. After this, a Kovar tube 5, soldered to a calibrated glass capillary 6 (0.3 mm in diameter), was soldered on the inside to the branch 3. The capillary joined a sphere 7 to a tube 8 having a bottleneck for sealing the unit off after evacuation. A tube 9 was used to fill the system with water after evacuating it to a pressure of 10^{-4} mm Hg . This operation was conducted by breaking off the end of the tube 9 after dipping it into previously degassed water. The amount of water in the system was determined by weighing. The necessary position of the meniscus in the capillary was set by evaporating the water. By varying the temperature of the cylinder with silica gel, it was possible to monitor the displacement of the meniscus in the capillary and

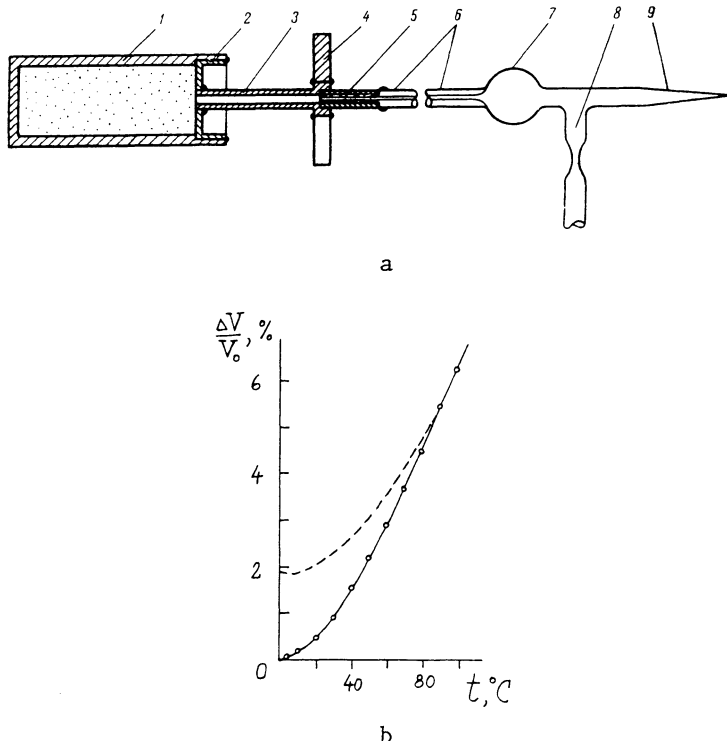


Fig. 7.8. a) Setup for studying thermal expansion of water in narrow pores; b) the results of the experiment with water in narrow pores of silica gel powder.

then calculate the variation of the volume of water in the pores of the silica gel. The minimum of specific volume, which in bulk water lies at +4°C, was not observed in this system. When the same method was used to analyze thermal expansion of heavy water D_2O , the minimum-volume temperature was found to be shifted from +10 to +6°C [48].

Similar results were obtained in a study of the expansion of ordinary and heavy water in the pores of TiO_2 powder [49]. For technical reasons, these measurements could not be conducted at temperatures above 20°C; consequently, the absolute densities of pore water could not be determined. Later, the thermal expansion of water in interstitial pores of a silica gel powder was measured in a wider temperature range from 0 to 90°C [50]. The results are plotted in Fig. 7.8, in which the volume of pore water is given as a function of temperature (solid curve). The dashed curve plots temperature dependence of the volume of bulk water whose amount was chosen for the two curves to merge in the temperature range from 70

to 90°C, demonstrating the identical behavior of the curves. By superposing the two curves at 70-90°C it was possible to evaluate the absolute density of water in narrow pores at any temperature, on the basis of the divergence of the curves below this range. Thus, at 0°C the water in thin pores had a density of 1.02 g/cm³. However, silica gel particles had inner pores.* Consequently, it is not clear so far what effective pore size must be put to correspond with this density and how the volume of water in the pores actually behaves as a function of temperature. The gap width between porous particles of silica gel was about $r = 50 \text{ \AA}$; to some extent this width characterizes the state of water in the powders investigated.

A greater increase in the density of water, approximately by 10%, was found in microporous zeolite NaX ($r \approx 3.5 \text{ \AA}$). Van Gils [52] detected by pycnometric measurements an increased density of boundary water layers at glass surface at 25°C. In contrast, water in narrow pores of clays [53-55] has a density several percent lower than that of bulk water. This effect can perhaps be ascribed to adsorbed cations influencing the structure of water. The departures of water density from bulk values are felt only at distances less than 50-70 Å from the surface of clay particles. As in all cases discussed above, increased temperature reduced the deviations from the bulk water density. The change in density being relatively small, no appreciable difference is observed, within experimental error, in refractive index of thin ($h \approx 70 \text{ \AA}$) polymeric adsorption water films on quartz [56], and of thin ($50 < h < 300 \text{ \AA}$) water interlayers between closely spaced mica sheets [57].

In order to evaluate the structural anisotropy of thin interlayers of water and other liquids, Greene-Kelly and Derjaguin [58, 59] employed a method based on measuring changes in birefringence of montmorillonite produced by its swelling in certain liquids. An oriented clay flake was placed in a recess in a slide. A cover glass was carefully slid over the specimen after pouring in the liquid. When swelling was completed, after up to 48 h, the path length difference was determined by a Séenarmont compensator of a polarization microscope in sodium-D light, and the birefringence B was calculated. The birefringence of water films formed by inter-crystalline swelling was then calculated by means of the Wiener formula, which makes it possible to find B as a function of swelling S, under the assumption that liquid interlayers retain isotropic optical properties of the bulk phase. The solid curve in Fig. 7.9, representing the swelling of Na-montmorillonite in NaCl solutions of different concentrations, plots b (calculated by Wiener's formula) as a function of S. The experimental results are shown by circles. The spread of data occurs because each circle represents an individual specimen. The difference ΔB between the ordinates of

*Such pores are absent in the aerosil powders; see B. V. Derjaguin et al., Kolloidn. Zh., 49, 17 (1987); Colloid Surf. Sci., in press.

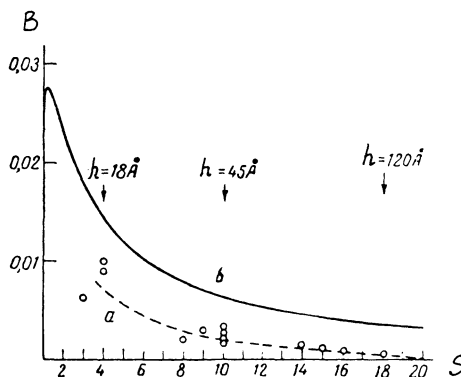


Fig. 7.9. B as a function of S: a) experimental data; b) calculations by Wiener's formula.

the solid and dashed curves gives a measure of the birefringence of water films as a function of their thickness h determined from x-ray diffraction data.

It was found that as h grows from 45 to 120 Å, or as S changes from 10 to 18 (when the concentration of NaCl correspondingly diminishes), the birefringence ΔB of water films drops from 0.004 to 0.003. Because of some uncertainty in the birefringence of the montmorillonite specimen (for details see [58, 59]), Wiener's curve can be brought closer to the abscissa axis while retaining the hyperbolic shape. The lowest possible position of Wiener's curve (even if of low probability) gives for ΔB the value +0.002 identical for all thicknesses from 45 to 120 Å. This points not only to a certain optical anisotropy of water interlayers but also to either its constancy or small variation in the stated thickness range. Calculations also show that the Kerr effect on ionic double layers in these interlayers cannot account for more than 10% of the observed birefringence.

Thin interlayers of water in Na-montmorillonite also have a lowered static permittivity [60-63]. Thus, $\epsilon_0 = 23-25$ for interlayers 50-80 Å thick [60], much less than the bulk value for water ($\epsilon_0 = 80$). At increased temperatures, the static permittivity of thin interlayers grows and approaches the bulk level. Hoexstra and Doyle [61] reported $\epsilon_0 = 35-40$ for the permittivity of thin interlayers ($h = 15-18$ Å) of water in montmorillonite. As the interlayers thinned to 5-6 Å, ϵ_0 dropped to 3-4. Heyde et al. [62] observed substantially lowered permittivity of water in narrow pores ($d \approx 15-20$ Å) of cellulose acetate membranes. According to the data of Dushchenko and Romanovsky [63], the permittivity of water filling narrow pores of silica gels is $\epsilon_0 = 40$ for mean pore radius $r = 40$ Å and $\epsilon_0 = 24$ for $r = 13$ Å pores.

Special properties of boundary water layers are revealed also in a different solvent power of water, owing to a modification of its structure. Earlier, the reduced solvent power was widely used to determine the amount of "bound water" in disperse systems [63a, b]. Sucrose, glucose, and certain alcohols were often used as indicators unable to penetrate into the bound water. Derjaguin [63c] developed the theory of nonsolvent volume, based on the concept of the field of surface forces repelling the solute molecules from the boundary layer. The modern form of this theory is discussed in Chapters 5 and 11 (Section 11.1).

In boundary water layers adjacent to a silica surface the intermolecular hydrogen bonds are strengthened. This is confirmed by a shift of the IR absorption band (in the region of O-H stretching vibrations) in thin α -films toward longer wavelengths [64, 65]. The conclusion agrees with the observed increase of density in thin interlayers. Similar shifting of absorption bands is observed in foam films for water located close to the hydrophilic parts of surfactant molecules stabilizing the film [66].

The structure of boundary water layers in clays can be affected by adsorbed ions and the ions in the pore moisture. In these systems IR spectra point to a weakening of intermolecular bonding compared with bulk water [67], in agreement with the reduced density of water in narrow pores of clay [53]. A decrease in water density at the points of contact between coagulated clay particles is confirmed by a reversible decrease in the volume of degassed suspension when stirring transforms the gel to sol [68].

These results demonstrate the various physical methods to reveal changes in the properties of water in thin interlayers ($h \leq 100 \text{ \AA}$). There is no doubt that the long-range structural influence of the surface goes beyond the first two layers of water molecules. The effects are the stronger, the more hydrophilic the surface, the lower the temperature, and the lower the electrolyte concentration.

7.2. BOUNDARY LAYERS WITH LIQUID-CRYSTAL STRUCTURE

Boundary layers with special properties are formed not only in water but also in other polar liquids. Especially well-pronounced effects leading to formation of boundary liquid-crystal structures have been observed with molecules having benzene rings, monosubstituted products of benzene; also with ethyl and octyl esters of benzoic acid [69]. Early studies of nitrobenzene films on the surface of glass powder particles (lyophilized by glow discharge) indicated that nitrobenzene forms boundary phases with thickness $h_s \approx 0.1 \mu\text{m}$ [70, 71]. It was found that at thicknesses

below 0.1 μm the specific heat of nitrobenzene films C_2 was independent of thickness and was approximately 8% below the bulk specific heat C_1 of nitrobenzene.

This difference between the properties of thin films and the bulk phase of nitrobenzene pointed to a structure quite different from that in the bulk. Practical independence of C_2 of film thickness was an indication that this special structure is homogeneous. It was logical to interpret these data as corroborating the hypothesis [3, 9, 11] of the existence of boundary phases with uniform properties, separated from the bulk phase by an abrupt interface. The properties of the liquid are assumed to undergo a jump across this "interface." Thick nitrobenzene films ($h > 0.1 \mu\text{m}$) had a two-layer structure, consisting of a boundary-phase layer of thickness h_s at the solid interface and a bulk liquid layer. This entails a complicated temperature dependence of heat capacity of films. If the thickness of the boundary phase h_s in a two-layer film were independent of temperature, the heat capacity of a nitrobenzene film with mass M would be

$$Q = (M - m)C_2 + mC_1$$

where m is the mass of the bulk-phase layer of the film.

However, the experimental data do not obey this simple relation for thick films ($h > h_s$), indicating that at increased temperatures the thickness of the boundary-phase layer diminishes. Hence, the thermal effect of the layer-by-layer transition of the boundary phase in the bulk liquid must also be taken into account in the expression for Q . The apparent heat capacity then is

$$Q = (M - m)C_2 + mC_1 + \lambda(\partial m / \partial T) \quad (7.2)$$

where λ is the specific heat of the phase transition. When the film thickness is below the thickness h_s of the boundary-phase layer, not only $m = 0$ but also $\partial m / \partial T = 0$ and, hence $Q = MC_2$. If we choose as the initial state a film with mass M and thickness $h < h_s$ at a given temperature T , and measure Q at gradually increasing values of T , then first Q equals MC_2 , and only after $h_s(T)$ decreases to h will Q be given by Eq. (7.2). Experiments confirmed this prediction; a transition from $Q(T) = MC_2$ to Eq. (7.2) was indeed observed. By using Kirchhoff's equation

$$d\lambda/dT = C_1 - C_2$$

we can rewrite Eq. (7.2) in the form

$$d(m\lambda)/dT = Q - MC_2$$

Integration gives

$$m\lambda = \int_{T_0}^T (Q - MC_2) dT \quad (7.2')$$

where T_0 is the temperature of "homogenization" at which $M = h_s S$ (S being the surface area of nitrobenzene films) and at which $m = 0$ and $dm/dT = 0$, i.e., T_0 is the temperature of the jumpwise transition from formula $Q = MC_2$ to (7.2).

Formula (7.2) could be applied to films of unequal thickness, with correspondingly unequal temperatures of homogenization, i.e., unequal T_0 . By taking, for instance, two such films with masses M and M_1 , it was possible to find, for equal T and, as a result equal λ and h_s , the values of $m\lambda$ and $m_1\lambda$, where m_1 is the mass of the bulk phase in the second film at the same temperature T :

$$m\lambda = \int_{T_0}^T (Q - MC_2) dT$$

$$m_1\lambda = \int_{T_{10}}^T (Q - M_1C_2) dT \quad (7.3)$$

and

$$m = M - Sh_s(T) \text{ and } m_1 = M_1 - Sh_s(T) \quad (7.4)$$

Therefore, $m - m_1 = M - M_1$, where $M - M_1$ is given by the experimental situation. These equations gave the value of $\lambda(T)$. By experimenting not with two but with n films of different thickness, it was possible to combine them pairwise and determine $\lambda(T)$ in the whole experimental temperature range by a similar method. Then an averaged curve $\lambda(T)$ could be plotted. However, it proved more convenient to find $\lambda(T)$ from the integral of Kirchhoff's equation:

$$\lambda = \int (C_1 - C_2) dT + \text{const} \quad (7.2'')$$

where the integration constant could be chosen by using the known values of λ found from Eqs. (7.3) and (7.4) at a certain temperature T . By using the values of $m\lambda$ found from (7.3) and $\lambda(T)$ found from (7.2''), it was possible to determine $m(T)$ and, hence,

$$h_s(T) = (M - m)/\rho S$$

where ρ is the density of the liquid.

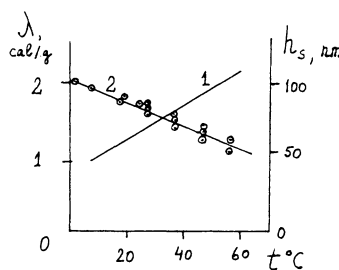


Fig. 7.10. Temperature dependence of the heat of transition λ of the nitrobenzene boundary phase to the bulk phase (curve 1), and of boundary phase layer thickness h_s (curve 2).

Figure 7.10 shows the averaged temperature dependence of the heat λ of phase transition (curve 1) and the temperature dependence of the equilibrium thickness h_s of the boundary phase (curve 2). Although the values of λ and h_s obtained are not considered as very accurate, similar values of h_s were later obtained in optical measurements. Furthermore, λ is of the same order of magnitude as the specific heat of transition of liquid-crystal-like phases to isotropic liquid (e.g., 0.6 cal/g for para-azoxyanisole), thus supporting the suggested concept of boundary phases and supporting the reliability of the results.

A study of the birefringence (B) of nitrobenzene boundary layers gave further evidence that their structure is indeed ordered: the longer axes of molecules are oriented perpendicularly to the surface of glass [72-74]. Birefringence was measured in a narrow gap between black glass plates opaque for visible light. A beam of polarized light passed parallel to the walls of the gap, so that B could be measured in a gap about 1 mm long to within $\Delta n = n_0 - n_e \approx 10^{-4}$. The layer of nitrobenzene in the gap was two-phase, comprising optically anisotropic layers of a boundary phase close to the surfaces with isotropic bulk nitrobenzene in the middle part of the gap, whose width H could be varied from 2 to 20 μm . This optical system was modeled for calculations by a five-layer dielectric waveguide. Boundary phases were modeled as uniaxial crystals with the optical axis directed perpendicularly to the surface of the glass walls. The interlayer of bulk nitrobenzene and the glass plates were regarded as isotropic dielectrics. Figure 7.11 shows the temperature dependence of Δn and of the thickness h_s of the boundary phase. As with water, both Δn (characterizing structural modifications) and h_s (characterizing the long-range surface effects) diminish with increasing temperature.

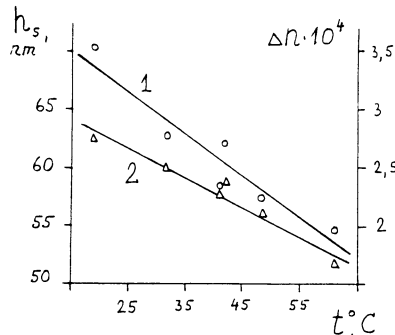


Fig. 7.11. Temperature dependence of boundary phase thickness h_s of nitrobenzene at a glass surface (curve 2), and of boundary phase birefringence Δn (curve 1).

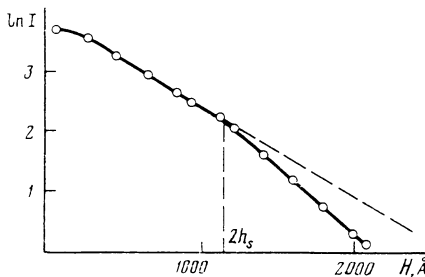


Fig. 7.12. Intensity I of UV radiation ($\lambda = 262$ nm) transmitted by a nitrobenzene interlayer as a function of interlayer thickness H .

A much simpler and direct method of studying optical properties of boundary layers was developed later [75, 76].* It consists in measuring the attenuation of the intensity of ultraviolet radiation J transmitted through a liquid interlayer between two quartz plates, as a function of interlayer thickness H . The quartz surfaces were lyophilized by treatment in hot bichromate mixture in sulfuric acid. The measurements were conducted by the method of local spectrometry of a wedge-shaped liquid interlayer which was scanned by a collimated beam of polarized UV light (beam width ≈ 0.01 cm). The resultant curve gave $\log J$ as a function of H .

Two linear segments on this curve (see Fig. 7.12) demonstrated the constancy of absorption coefficient $\mu = d \ln J / dH$ throughout the bulk of the liquid with another constant value in the layers at the walls. A sharp bend on the curve $J(H)$ at $H \approx 1000$ Å pointed to an

*See also B. V. Derjaguin, in: *Fluid Interfacial Phenomena*, C. T. Cronton, ed., Wiley, New York (1986), p. 739.

abrupt interface between bulk liquid and boundary liquid. Hence, the boundary phase thickness is obviously about $1000/2 = 500 \text{ \AA}$. In the boundary phase, μ is less than the absorption coefficient of the bulk phase μ_0 ; this is an indication of a homeotropic orientation of nitrobenzene molecules in the boundary layer.

With μ determined, it was possible to calculate the parameter of structural ordering of nitrobenzene molecules in the boundary phase, $S = 1 - (\mu/\mu_0) = 0.27 \pm 0.01$ at 295 K. The quantity $S = \frac{1}{2}(3<\cos^2 v> - 1)$ is known to characterize the mean value of cosine of the angle v between the longer axis of the molecule and the normal to the substrate [77, 78].

The formation of boundary phases was also observed in other polar substituted benzenes. The following data were obtained [79] for S and h_S (in \AA), respectively: aniline 0.29, 590; acetophenone 0.31, 620; parachlorotoluene 0.28, 530; ethyl esters 0.14, 470; octyl esters of benzoic acids 0.24, 630. An enhanced lyophilicity of the substrate after treatment in a hydrogen flame and in a glow discharge plasma increases both S and h_S . Increased temperature produced the opposite effect. Treatment of the activated surface of glass and quartz with a dilute solution of hydrofluoric acid resulted in a deactivation of the surface: indeed, boundary layers of nitrobenzene and other polar liquids ceased to form.

The structure of boundary phases of polar substituted benzene is less developed than that of true liquid-crystalline nematic phases. In these S may come to 0.3-0.4 at the phase transition temperature, and to 0.8 at lower temperatures [77, 78]. The possibility of formation of liquid-crystalline boundary structures in polar liquids with asymmetric planar molecules (including a benzene ring) was postulated because the values of S obtained are close to those for nematic liquid crystals. It could be supposed that boundary phases in such liquids differ from nematic substances by lower values of the parameter S , spatial restriction, and mechanism of formation. As surface forces rapidly diminish with increasing distance from the surface, it is logical to expect that the orientational ordering induced by them in the boundary layer cannot be uniform, and must decrease away from the substrate; but this assumption is in contradiction to the experimental data. On the other hand, if we assume that here, as in the case of liquid crystals, the predominant factor is the presence of intermolecular interactions, then the limited thickness of the boundary phase and its abrupt interface on contact with bulk liquid are not explained. Presumably, both surface forces and forces of intermolecular interaction within the boundary phase play important roles in the formation of the liquid-crystal phase.

Let us consider the main concepts of the theory of the nematic liquid crystal state developed by Maier and Saupe [78], as applied

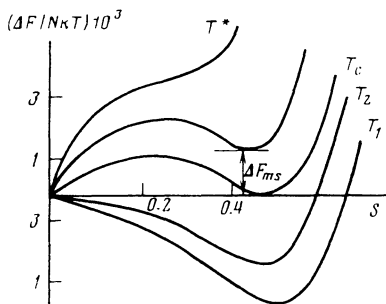


Fig. 7.13. $\Delta F/NkT$ as a function of S , calculated by Eq. (7.2); $T_1 < T_2 < T_c$.

in [69] to the problem discussed above. According to this theory, the main factor stabilizing the liquid-crystalline state is the dipole-dipole component of dispersion forces. Maier and Saupe considered the expressions for the orientational component of the potential energy of molecules in the mean field approximation and obtained the following expression for the free energy of the orientationally ordered phase:

$$\begin{aligned} \Delta F = NkT &[\frac{1}{2}BS(S + 1) \\ &- \ln \int_0^1 \exp(-\frac{3}{2}BS \cos^2 \theta_i) d \cos \theta_i] \end{aligned}$$

where N is Avogadro's number, k is the Boltzmann constant, T is the temperature, S is the order parameter, θ_i is the angle between the longer axis of the i -th molecule and the director, and $B = A/kT v_m^2$, where A is a constant and v_m is the molar volume. The free energy ΔF calculated by means of this equation is plotted in Fig. 7.13 as a function of S for different temperatures. When $T < T_c$ (T_c being the temperature of the nematic-isotropic liquid phase transition), the curve $\Delta F(S)$ has a single minimum corresponding to the nematic bulk phase with a well-defined order parameter S . At $T = T_c$ the minimal value of ΔF becomes zero, corresponding to the equality of the energies of the nematic (for $S = 0.44$) and the isotropic (for $S = 0$) phases coexisting in thermodynamic equilibrium.

At $T > T_c$ and $S > 0$, all values of ΔF are positive; the region around a minimum at some $S > 0$ obviously corresponds to metastable states of the liquid-crystal phase, separated by a potential barrier from the isotropic state more stable under these conditions. At a certain temperature T^* even this shallow minimum disappears, and the liquid-crystalline state becomes completely unstable.

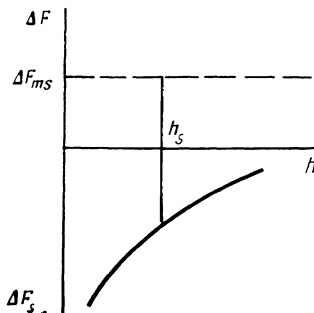


Fig. 7.14. A schematic, illustrating the possibility of formation of liquid-crystal boundary structures.

Only a metastable liquid-crystalline state stabilized by a field of surface forces seems to be allowed for liquids of the type of monosubstituted derivatives of benzene. This possibility is illustrated in Fig. 7.14, where the dashed line is the value of ΔF_{ms} (see Fig. 7.13) corresponding to the region of metastability. The solid curve shows the free energy ΔF_s due to long-range surface forces, as a function of distance to a solid lyophilic substrate. At a distance h_s from the substrate $\Delta F_{ms} + \Delta F_s = 0$. Then the net free energy is negative at $h < h_s$, and the boundary liquid-crystal phase is stable. At $h > h_s$ only the bulk isotropic liquid can be stable. At $h = h_s$ the liquid-crystalline and isotropic states co-exist, and this determines the thickness h_s of the boundary liquid-crystalline phase.

This simple model gives a qualitative explanation, first of the structural homogeneity of the boundary phase and, second, of the abrupt interface between the boundary phase and the bulk liquid. It is seen in Fig. 7.13 that, in accord with the experiments, the model predicts for the liquid-crystalline boundary phase a lower-order parameter than for ordinary nematic liquid crystals. As temperature rises, ΔF_{ms} must increase, resulting (as shown in Fig. 7.14) in reduced thickness of the boundary phase. This conclusion is indeed confirmed in experiments. The metastable states of nematic liquid crystals (at $T > T_c$), stabilized by the surface force field, were observed experimentally [80, 81], supporting the correctness of the theory outlined above.

Other methods also reveal boundary layers at lyophilic surfaces in monosubstituted derivatives of benzene. Thus, Peschel and Schnorrer [82] demonstrated that the viscosity of halogenated benzene in interlayers with $h < 500 \text{ \AA}$ between hydroxylated quartz surfaces is greater than normal. This increase in viscosity was found in a relatively narrow temperature range around the melting point.

Some concurrent reduction in the permittivity of thin interlayers was also found [83]. The maximum of structural repulsive forces due to overlapping of boundary layers is observed in the same temperature range. Thus, viscosity and structural disjoining pressure Π_s reach their maxima at -8°C for chlorobenzene, 0°C for iodobenzene, and $+3^\circ\text{C}$ for bromobenzene.

Michnewitsch et al. [84-87] proved the existence of the boundary layers of supercooled polar betol (2-naphthyl salicylate) and piperine (1-piperylpiperidine), up to $1 \mu\text{m}$ in thickness, close to a glass surface. The special structure manifested itself in an inhibited formation of crystallization nuclei in boundary layers oriented by the surface, in comparison with the bulk of the same liquid. The surface activity could be lowered by treating the glass with a solution of hydrofluoric acid or by covering it with a thin layer of collodion. A pulsed magnetic field destroyed the oriented structure of thin betol layers at the walls [87]. It was assumed that the viscosity of these boundary layers of supercooled betol was anomalously high. This conclusion was recently confirmed by Mezhidov and Mezhidov [88], who measured the rate of advance of the crystallization interface in supercooled diphenylamine, thymol, and betol as a function of capillary radius (varied in these experiments from $4 \mu\text{m}$ to 15 mm).

7.3. BOUNDARY LAYERS OF NONPOLAR LIQUIDS

Simple, nonpolar liquids, including liquids with spherically symmetric molecules, also form boundary layers with a modified structure. However, the thickness of boundary layers in such liquids does not exceed several molecular layers. The structural modifications result in intensive density oscillations, as demonstrated by Monte Carlo and molecular dynamics calculations [89-100]. In contrast to the systems discussed in the preceding section, this effect is purely molecular and stems only from the finite size of molecules. The local density oscillates with a period close to the diameter d_0 of molecules modeled by rigid spheres, and with an amplitude that decays away from the solid wall. Oscillations are not so strongly pronounced for diatomic (nonspherical) molecules, because of a richer variety of molecular arrangements in the layers adjacent to the surface [98].

Microoscillations of density are also revealed by oscillations in the force of interaction between surfaces when they are brought close enough for the oscillatory boundary layers to overlap. Force oscillations were experimentally detected in liquids with large molecules. This was successfully done by Israelachvili and his co-workers [101, 102] by the method of crossed cylinders, for thin interlayers of octamethylcyclotetrasiloxane ($d_0 \approx 10 \text{ \AA}$) and cyclohex-

ane ($d_0 \approx 6 \text{ \AA}$) between mica surfaces. The oscillating forces were observed when interlayer thickness h was below 100 \AA in the first, and below 50 \AA in the second of these liquids.

Specific properties of boundary layers have also been observed at a macroscopic level in a number of nonpolar liquids (with non-spherical molecules). Thus, Findenegg et al. [103, 104] and Parfitt and Tideswell [105] carried out dilatometric measurements of the density of liquid alkanes concurrently with measuring their wetting heat in graphitized carbon black powders and found that the density of these liquids in narrow pores exceeded the bulk value. Cyclohexane was used as a reference liquid, for which it was assumed that its density in the pores remains unchanged. Density deviations increased on approaching the melting point T_0 . These results could be interpreted as a formation of several ordered layers of molecules, packed closer than in the bulk, and oriented with their long axis parallel to the substrate. Density deviations increased with the number of carbon atoms in the alkane molecule. As temperature was increased, the density of pore liquid tended to that in the bulk. The thickness of octadecane and hexadecane boundary layers, whose density was increased by 10% on the average, was about $h_s = 9\text{-}10 \text{ \AA}$ at $T \rightarrow T_0$ [103]. Similar results were obtained for alkanes on cleavage surfaces of an ionic crystal NiCl_2 [100]. Numerical calculations by Sullivan et al. [107] confirmed that the probability of elongated molecules aligning parallel to a solid wall increases with increasing length of the molecules. Direct confirmation of the special properties of boundary layers were obtained by means of the blow-off technique developed by Derjaguin, Karasev, and Zakhavaeva [108-110]. The results of systematic studies of the viscosity profile of boundary layers formed in various liquids are discussed in the following section.

7.4. THE STUDY OF BOUNDARY LAYERS OF LIQUIDS BY THE BLOW-OFF TECHNIQUE

The "blow-off" method was developed as early as 1948-1952 [108-110]. It remains the only method of layer-by-layer study of boundary layers, viz., of layer-by-layer measurements of viscosity of a liquid on a smooth solid surface. The first estimates of boundary layer thickness were obtained by this method [108-116]. The results of these and other studies led to the concept of "boundary phases" [3, 9, 11], whose properties, as a first approximation, are homogeneous; at a certain distance from the substrate surface these phases undergo a jumpwise transition to the isotropic bulk liquid phase. The idea of the blow-off technique is as follows. A layer of a nonvolatile liquid 1 to be studied, with thickness greater than 10 μm , is placed on one wall of a plane-parallel gap 2 (Fig. 7.15) with gap width $H = 0.2 \text{ mm}$. A uniform flow 3 of

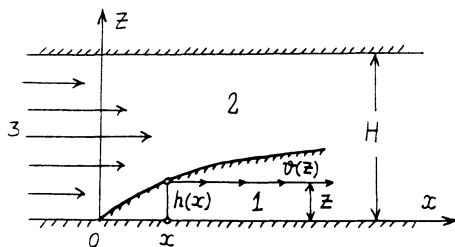


Fig. 7.15. Schematic arrangement of layer-by-layer measurements of liquid viscosity by the blow-off technique.

gas (nitrogen) is pumped through this gap and causes a streamline flow of the liquid film, which takes on the shape of a wedge with the angle gradually diminishing with the time of blow-off. The shear stress F in the film is everywhere the same because the tangential force applied to the surface of the liquid by the gas flow is uniform and bulk forces in the liquid layer are absent.

If the viscosity η of the boundary layer is assumed to depend solely on the distance z to the solid substrate (regardless of the distance to the outer surface of the layer), then the law of Newtonian viscous flow, viz.,

$$F = \eta(z) \frac{dv}{dz}$$

shows, after integration, that the velocity of displacement of the layers is a function of a single variable, the distance z . It follows then that the flow of elementary layers of liquid, parallel to the substrate, is analogous to the motion of individual cards when a pack is cut (with uniform strain), and that the flow of each plane layer of the liquid is one-dimensional. By substituting for z in Newton's equation the local layer thickness h , and x/τ for velocity v , where x is the path covered by a point A during the time τ of blowing (see Fig. 7.15), we arrive at the formula

$$\eta(z = h) = F\tau \frac{dh}{dx} \quad (7.5)$$

This formula yields the viscosity η as a function of distance $z = h$ from the solid substrate, in terms of the slope dh/dx of the profile of the film subjected to blow-off.

Obviously, if there is no special boundary viscosity, i.e., if η is constant, the layer of liquid after an exposure to blow-off will be wedge-shaped, bounded from above by an inclined plane. This

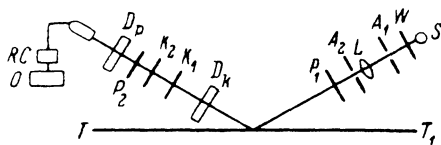


Fig. 7.16. Schematic diagram of the setup for measuring film thickness.

was the case observed for Vaseline oil (i.e., a paraffin of high molecular weight) that has been most thoroughly cleaned to remove polar impurities (by employing a platinum catalyst at an elevated temperature, by a method suggested by Prof. S. Yu. Elovich). But in many cases the bounding surface is not planar, revealing altered viscosity of the boundary layer. Measurements are necessarily limited to nonvolatile liquids. Depending on the nature of the liquid and of the solid wall, the layer thickness can vary substantially. In polymer liquids and solutions the change in viscosity could be traced up to 7-8 μm from the solid wall. However, in low-molecular-weight liquids and ordinary oils the corresponding thickness was much smaller, about 10^{-5} cm. Consequently, the requirements for the optical methods of measuring film thickness and wedge profile are quite different for different objects of study. With polymers sufficient information can be obtained by photographing equal-thickness fringes produced when the film is illuminated by monochromatic light [109].

A more sensitive and accurate method of determining thickness must be employed to study ordinary liquids and oils. A method based on determining the parameters of optical polarization of light reflected by different parts of the film was found to meet these requirements. However, the need to determine thickness at different parts of a film of nonuniform thickness made it impossible to use conventional polarization goniometers and standard wide-beam observation methods. Also, narrowing the incidence beam while retaining its small angular aperture reduced the reflected light intensity to such a degree that accurate measurements of polarization became unfeasible. This difficult experimental problem was solved by developing a special modulation-based analysis of reflected polarized light, using a photomultiplier and an oscilloscope. For details we refer the reader to original publications [108] and describe here only the principle of the setup (Fig. 7.16) and the experimental procedure.

A slit A_1 is illuminated by a mercury lamp S (with ac current supply) through a filter W transmitting the line $\lambda = 579$ nm; the beam is projected onto the experimental film TT_1 through an objective lens L (A_2 is the objective aperture, P_1 is an iodoquinine polaroid, and P_2 is a polaroid revolving around the axis coinciding

with the reflected beam at a frequency of about 1 Hz). The modulated light falls on a photomultiplier whose output voltage is preamplified by an RC amplifier with an RC filter and fed to a CRT oscillograph O indicating the presence or absence of photocurrent modulation. K_1 and K_2 are two $\lambda/4$ -plates; the principal axes of K_1 are at 45° to the incidence plane, and the K_2 plate is in the read-off graduated dial; D_k and D_p are two plates, 1-cm thick, cut out of Iceland spar parallel to the optical axis. D_p is a depolarizer introduced to suppress the effect of photocathode sensitivity to the direction of polarization, and D_k is a "coherence suppressor" introduced to eliminate the coherence of the \parallel and \perp components of the beam. In order to eliminate modulation, with the coherence suppressor in the "on" position, it is necessary and sufficient to orient the depolarizer P_1 at the azimuth at which the \parallel and \perp components of the reflected beam are equal. With the coherence suppressor in the "off" position, it is necessary and sufficient for the elimination of the reappearing modulation of photocurrent to orient the axes of the plate K_2 acting as the analyzer, at the azimuth angle of 45° to the polarization plane of the light transmitted through K_1 . Further calculations with the azimuth angles so obtained are standard [108].

The measurement procedure used was as follows. After the film deposited on the surface of a stainless-steel plate was subjected to a blow-off exposure during a time τ , the setup was dismantled, the plate with the film was mounted on micrometer slide, and the thickness of the film was successively measured at different points of the plate by shifting the slide. The graph of this thickness gave the film profile. Films of some liquids and solutions were not very stable and tended to decay into droplets. For these a different procedure of recording the film profile was developed. Thickness was then measured not after blowing, but in the course of the blow-off exposure at a fixed spot separated by a distance x_0 from the wetting boundary whose position was regularly checked. Accordingly, the top of the blow-off chamber was made of a transparent material.

The version of this technique in which an oil film covered the lower surface of a glass prism that formed the lid of the blow-off chamber proved especially convenient because a short time sufficed for the optical measurements. Total internal reflection was observed with oblique incidence of polarized light, so that the amplitudes of the components with oscillations parallel and perpendicular to the incidence plane remained unchanged, but a nonzero phase shift appeared between them. This phase shift was altered by the presence of the film, and the increment gave a measure of film thickness. The advantage of this version is that only one azimuth angle, instead of two angles in the standard procedure, is required in the measurements.

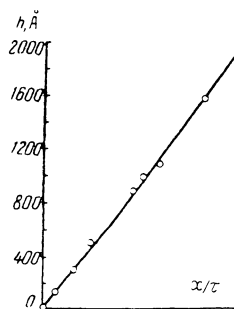


Fig. 7.17. Thickness profile of a purified Vaseline oil film on a metal substrate.

In order to normalize the thickness data obtained in this second variant of the blow-off method, to the form reconstructing the velocity profile at a solid wall (as in the first variant), it was sufficient to plot the thickness h measured at a time instant τ after blowing was started, as a function of $v = x_0/\tau$. Obviously, the abscissa gives the velocity of the layer at a distance $z = h$ from the wall. Therefore, this graph directly gives the velocity profile.

To measure the boundary viscosity at a metal surface, the total reflection prism was replaced with another prism, such that the beam transmitted through its base was at the most favorable incidence angle to the surface under study. The rays reflected at the glass surface, or multiple reflections in the gap, were removed by a slit diaphragm. Film thickness was measured by the same method as described earlier.

Figure 7.17 gives the velocity profile of pure Vaseline oil, obtained by the blow-off technique, on a highly polished metal surface that had been cleaned in gas discharge. Clearly, the viscosity is strictly constant down to a thickness on the order of 10^{-7} cm.

Figure 7.18 shows the profile of amyl sebacate on steel. The curve clearly shows an enhanced viscosity at small thickness; at 150 Å it transforms jumpwise into constant viscosity of the bulk phase. The velocity profile in a layer of butyl palmitate on a layer of hexadicarboxylic acid about 75 Å thick, covering the stainless-steel surface, reveals a more complex behavior (Fig. 7.19). The viscosity of the liquid at the substrate is sharply reduced, presumably because of the horizontal alignment of the molecules. Farther from the surface the viscosity is considerably enhanced, and reaches the bulk value (but not jumpwise) around $h = 1000$ Å.

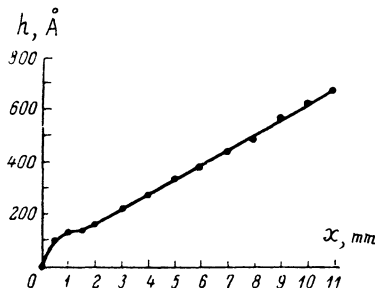


Fig. 7.18. Thickness profile of amylo sebacic ester film after exposure to blowing off.

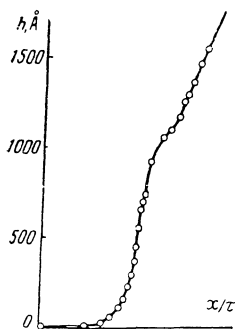


Fig. 7.19. Thickness profile of butyl palmitic ester after exposure to blowing off.

A number of polar liquids with long-chain molecules form quite thick boundary layers. The method of filming the motion of interference fringes in the film in the course of blowing was successfully employed in such cases [112]. By comparing the spacing between interference fringes close to and far from the wetting boundary, it was possible to see clearly that the boundary viscosity was several times greater than that in the bulk, even at distances from the substrate on the order of 0.5-1 μm . The results obtained by this technique are listed in Table 1.

Undoubtedly, the boundary viscosity increases or decreases owing to a specific orientation of molecules in the liquid (horizontal or vertical alignment). As we know from observations with the flow of polymers and from the behavior of liquid crystals, orientation parallel to the flow reduces viscosity, while that perpendicular to the flow increases it [77, 78].

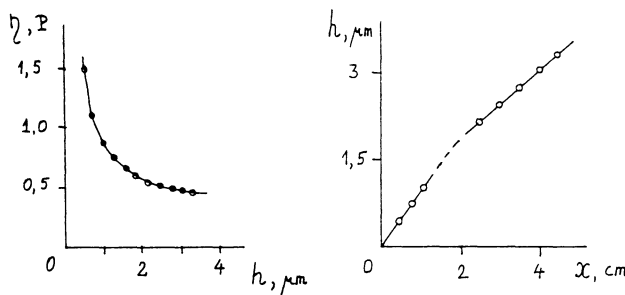


Fig. 7.20. a) Layer-by-layer viscosity η of vinypol ($M = 600$) as a function of distance h to metal substrate ($t = 20^\circ\text{C}$); b) thickness profile of a 0.05% vinypol solution ($M = 3850$) in turbine oil at 20°C .

TABLE 7.1. Boundary Viscosity: Experimental Data

Compound, its molecular mass M	Ratio of boundary viscosity η to bulk viscosity η_0
Tetraethoxyhexane, $M = 262$	0.8
Tributoxybutane, $M = 274$	1.1
Pentaethoxyoctane, $M = 334$	1.25
Tetrabutoxyhexane, $M = 374$	1.5
Hexaethoxydecane, $M = 406$	2.5

Figure 7.20a plots viscosity η calculated from Eq. (7.5) as a function of distance to the metal surface, for a vinypol (vinyl ester polymer, $M = 600$) film. The curve shows that viscosity drastically increases at the surface of the metal, the effect of the surface being felt out to a distance of several micrometers.

Enhanced viscosity of boundary layers is also observed for vinypol solutions in turbine oil. As an example, Fig. 7.20b gives the profile $h(x)$ of a turbine oil film with an admixture of 0.05% vinypol ($M = 3850$). In this case the viscosity of the boundary layer with thickness $h \leq 1 \mu\text{m}$ is approximately twice that of the bulk liquid beyond the $2 \mu\text{m}$ of the layer contiguous to the wall. An interesting feature of these solutions is the existence of a region of unstable film thickness (between 1 and $2 \mu\text{m}$), in which films tend to separate into droplets. As will be shown in Chapter 10,

this phenomenon is of a general nature; it reflects the formation of a transition layer between the layer with modified structure directly at the substrate surface and the bulk phase. When the film thickness increases and approaches the transition layer thickness, the sign of the structural component of disjoining pressure is reversed (from $\Pi_s > 0$ to $\Pi_s < 0$). When $\Pi_s < 0$, in a certain range of thickness the films become unstable (provided other components make a much smaller contribution than Π_s), break into droplets, and cover the surface of a thinner, more stable α -film (see Chapter 10, Fig. 10.5). This phenomenon was first observed in water [9]. As seen from Fig. 7.20b, it is also observed in polymer solutions.

The flow of pure turbine oil (as was used as a solvent in the above experiments) shows a pattern sharply different from that of polymers dissolved in this oil. The film profile in turbine oil is a perfect wedge, demonstrating that viscosity remains constant up to the oil-substrate interface. This result proves the reliability of the method, and bears out the discovery of viscosity anomalies in the boundary layers of polymers.

Surprisingly, the data obtained on viscosity anomalies in boundary layers, in spite of being painstakingly proved and despite their considerable importance for colloid and surface science, have not received, even now, the attention they deserve. There have been a number of attempts at refuting them, often citing an early paper by Bastow and Bowden [118] in which the error in thickness determination was as large as 0.1-0.2 μm (cf. [111]). Bascom and Singletary [119] demonstrated, as was shown in [120], that the blow-off technique can indeed yield erroneous results if one mistakenly chooses conditions in which the rate of blow-off is made so low that the displacement of the wetting boundary along or counter to the air flow affects the results. On the contrary, our measurements included monitoring of the position of the wetting boundary; the data were reported only when this boundary did not move. If the stability of the wetting boundary was insufficient, then the measurement procedure was shortened by taking the second variant of the method: observation of the thinning of the film in the course of the blow-off exposure at a film segment located 1-2 cm from the wetting boundary. The stationary position of this boundary was especially apparent when the motion of interference fringes in the course of blow-off was observed on the movie film [121].

Another paper claiming to show no special viscosity in thin films is that of Lyklema et al. [122] which tested the formula for the thickness of a liquid layer; the layer was drawn together with monolayers from a tenside solution when a soap film was formed. Lyklema et al. demonstrated the validity of Frankel's formula [122a] which relates film thickness to the rate of film drawing.

It differs from the formula derived earlier by Derjaguin [123] in having a factor 2 (because the film-gas interfaces are tangentially immobilized by a dense monolayer of surfactant). The formula gave correct results when the viscosity of the water interlayer used in calculations was taken as that of the bulk liquid η_0 . However, this is not surprising because a careful analysis of the capillary-hydrodynamic derivation of the formula [124] clearly shows that the thickness of the layer that is drawn out is in fact determined by the mean viscosity of the solution in the zone in front of the "entrance" into the emerging soap film, and not by the viscosity of the solution inside the film after it has been formed. Therefore, a different method is needed to determine this last viscosity.

Only data on the effect of solid substrates on the boundary viscosity have been reported to date, both in the absence and presence of adsorbed monolayers on the interface. No information is available on the possible effect of monolayers at a liquid-gas interface on the viscosity of the liquid; it would be interesting to fill this gap.

Unfortunately, the viscosity of water and other volatile liquids cannot be measured by the blow-off techniques because of the masking influence of evaporation. However, the theory of the method for moderately volatile liquids has been developed recently, and the first, promising results obtained [125]. (As mentioned in Section 7.1, other techniques have proved that the viscosity of water in boundary layers is substantially altered.)

New compounds have recently been studied [115, 116], notably polydimethylsiloxane (PMS) liquids with bulk viscosity $5 < \eta_0 < 2000$ cSt (at 20°C), and a number of oligosiloxanes (OS) in which the methyl groups with silicon atoms were substituted partially or totally by ethyl, phenyl, chlorophenyl, or other groups. Figure 7.21 shows flow velocity profiles in PMS films of different molecular mass on steel substrate. The feature shared by all these curves is the presence of three segments differing in profile slope and, hence, in viscosity of the corresponding liquid layers. Thus, viscosity is greatly reduced in the 20-30 Å layer at the wall, but exceeds the bulk layer η_0 by 30-40% in the layer from 20-30 to 150-200 Å. The layer beyond 150-200 Å has the bulk viscosity. These data can be explained in terms of shifted conformational equilibrium of PMS molecules in the force field of the solid substrate. Presumably, the anomalously low viscosity in the layers contiguous to the steel surface appears because of uncoiling of molecular coils and subsequent orientation of the straightened chains parallel to the substrate surface. Since a monolayer of uncoiled PMS molecules is only 5.6 Å "thick," it appears that the region of reduced viscosity is formed by several monolayers of horizontally aligned molecules. These layers, bounded by methyl groups, must easily slide along one another. The field of surface forces weakens

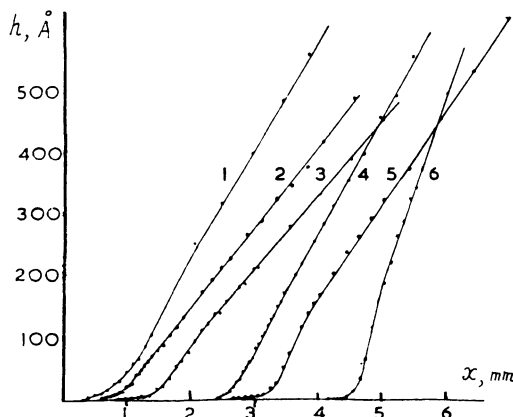


Fig. 7.21. Thickness profiles of PMS films of different molecular mass with narrow molecular weight distribution. Bulk viscosity $\eta_0 = 5$ (1), 10 (2), 25 (3), 70 (4), 400 (5), 2000 cSt (6).

in layers more distant from the substrate, so that the ordering of the boundary layer is lost. The orientation of molecules still having an uncoiled conformation becomes chaotic, and viscosity correspondingly increases. Further weakening of the surface force field leads to a gradual transition to bulk viscosity at distances greater than 150–200 Å.

If PMS has a wide molecular weight distribution, fractionation is observed, i.e., boundary layers are enriched with heavier fractions having a larger adsorption energy. The competition of these two processes (ordering of the horizontally aligned linear molecules, and growth of concentration of the high-molecular-weight component) explains the transition from a reduced viscosity directly at the surface to an enhanced viscosity at some distance from it. This conclusion was proved in experiments with PMS mixtures of different molecular mass [115].

The molecular weight distribution in PMS spreads as a result of external factors, such as thermal oxidation and photooxidation. The study of such PMS by the blow-off technique made it possible to monitor the changes in viscosity profile produced in the material [126]. The introduction of polar or bulky substituting groups for methyl groups is known to reduce the intramolecular mobility of oligosiloxanes [127]. Consequently, the complete set of conformational transformations, typical of PMS, cannot be realized in such systems. In fact [128], no intermediate layer with increased viscosity, as found in PMS, is observed in OS films containing various polar groups. The distribution of polar groups along the

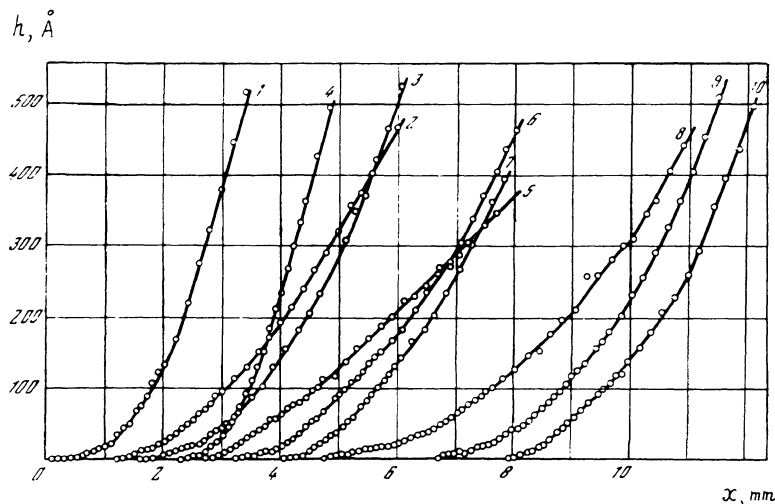


Fig. 7.22. Thickness profiles of OS films containing ethyl (1), methyl chlorophenyl (2), trifluoropropyl (3-5), thienyl (6-9), and chlorothienyl siloxy units (10).

chain in OS molecules facilitates their horizontal alignment along a solid substrate, and reduces viscosity. Also, stronger intermolecular interaction helps to transfer the effect of the force field of the solid substrate to considerably larger distances than in PMS. As a result, as seen in Fig. 7.22, in some samples the thickness of the reduced viscosity layer reaches 350-400 Å. The formation of slip planes at a distance of 20-30 Å from the substrate in certain OS samples (curves 2, 3, 6, 9) can be related to surface fractionation enhanced by an increased adsorbability of molecules of these oligomers.

The evidence summarized in this chapter shows, beyond doubt, that all liquids can form boundary layers with structure modified in comparison with the bulk state. The phenomenon depends on specific properties of the structure of the bulk liquid, especially on polarity, temperature, the presence of dissolved molecules and ions, and on the composition and state of the solid surface. For simple liquids it has proved possible to analyze the effects of these factors theoretically [89-99]. For polar liquids and liquids with intermolecular hydrogen bonds such calculations are only now appearing in the literature [129-131]. The difficulties stem from the inadequate state of the theory of associated liquids.

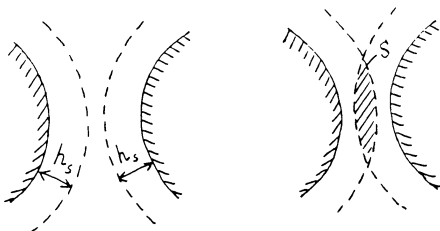


Fig. 7.23. Formation of the structural component of disjoining pressure when the thickness of a liquid interlayer between bodies diminishes: a) position of particles prior to overlapping of boundary layers with thickness h_s ; b) after boundary layers overlap.

7.5. THEORY OF THE STRUCTURAL COMPONENT OF DISJOINING PRESSURE

As long as the thickness of a liquid interlayer or film is greater than the total thickness of boundary layers with special structure, the effect of these layers may lead only to changes in the electrostatic and molecular components of disjoining pressure. Indeed, a change in the dissolving capability of boundary layers of a liquid and in their permittivity can alter the distribution of ions in the electrical double layer, both in the Stern layer and in the diffuse layer. Structural modifications in boundary layers will produce corresponding changes in the frequency dependence of permittivity $\epsilon(i\xi)$, resulting in its anisotropy and hence affecting the dispersion forces.

However, the main effects due to the formation of boundary layers occur when these layers overlap (Fig. 7.23). In this situation a change in the thickness of the interlayer entails a restructuring of the liquid and a change in the Gibbs free energy $G_s(h)$ in the system [132]. Here G_s refers only to the part of the free energy that is related to overlapping of boundary layers of the solvent. Clearly, a change in interlayer thickness h can also lead to changes in the work of electrostatic G_e and molecular G_m force.

Through the definition

$$\pi_s(h) = -(\partial G_s / \partial h)_T$$

a change in G_s caused by a change in h must be accompanied by the appearance of a force of structural repulsion or attraction, which

was named in [5] "the structural component $\Pi_S(h)$ of disjoining pressure." In an isothermal process

$$dG_S = dH_S - T dS_S$$

where dH_S is the change in enthalpy and dS_S is the change in entropy of the system. The term dH_S is mostly determined by the increment in the energy of intermolecular bonds in the interlayer, and dS_S mostly by the changes in the ordering of molecular arrangement. The values of H_S and S_S being independent of h in that region where the boundary layers do not overlap, the magnitude and sign of dG_S/dh depend on the changes of dH_S and dS_S in the overlap zone S , shown by hatching in Fig. 7.23. This zone covers the structurally modified part of the liquid. Obviously, the volume of the zone of structural modification depends on the degree of overlapping of boundary layers. The calculation of $G_S(h)$ must also take into account that the overlapping is accompanied by a transition of a part of the structured volume of the liquid into the bulk state. For the simplified model of interaction (Fig. 7.23) that assumes the homogeneous structure of the boundary layer and its modification solely within the hatched zone S , this means that the volume of the liquid with boundary layer structure is reduced by an amount equal to the volume of the overlap zone S . The calculated free energy of the system G_S must take into account both the transition of this part of the liquid into bulk state and the structural changes in the zone of overlapping. Depending on how G_S changes when the interlayer thins out, the structural forces can be repulsive, $\Pi_S > 0$ (when $\partial G_S / \partial h < 0$), or attractive, $\Pi_S < 0$ (when $\partial G_S / \partial h > 0$); this was already mentioned earlier, for instance by Eley, who discussed the interaction between hydrated protein molecules [133].

Attempts at quantitative calculations of the structural component of disjoining pressure in polar liquid interlayers involve a number of simplifying assumptions. One of the first was made by Marčelja and Radić [134], who employed the expansion of free energy introduced by Landau in the theory of phase transitions of the second kind [135], and later was frequently employed in the theory of the liquid-crystalline state [77, 78]. The order parameter η is defined in these cases in such a way that it is zero in a disordered (isotropic) bulk phase and nonzero (positive or negative) in the ordered phase. The sign of η determines the direction of the molecule (or a dipole) with respect to a chosen axis. In the case discussed below the axis x was directed normally to the surfaces bounding a flat liquid interlayer. Marčelja and Radić considered the range $|\eta| \ll 1$ and thus retained only two terms in the expansion of specific free energy:

$$g(x) = g_0 + \alpha \eta^2(x) + c(\partial \eta / \partial x)^2 \quad (7.6)$$

where g_0 is the free energy per unit volume of isotropic bulk phase, x is the coordinate measured off the middle of the interlayer, α and c are constants; $\eta(x)$, the order parameter, is a function of distance from the bounding surfaces of the interlayer. In the framework of this model, the molecules differ in direction and in the angle at which their axes are tilted with respect to the axis x . The order parameter η is assumed to be positive when the direction of a molecular axis or its projection coincides with the positive direction of the axis x and negative in the opposite case. As was shown by Landau [135], the first-order term in the expansion (7.6) is identically zero if the states with $\eta = 0$ and $\eta \neq 0$ have different symmetries; this is the case we consider here because $\eta = 0$ corresponds to the isotropic phase and $\eta \neq 0$ to the ordered phase.

Marčelja and Radić introduced a certain constant degree of ordering of liquid molecules at the surfaces of an h -thick interlayer,

$$\eta(h/2) = -\eta(-h/2) = |\eta_0|$$

and then, minimizing the specific free energy of the interlayer per unit area,

$$G_s = \int_{-h/2}^{h/2} [g(x) - g_0] dx \quad (7.7)$$

and using the equation $\Pi_s = -(\partial G_s / \partial h)$, derived the following expression for the structural component of disjoining pressure:

$$\Pi_s(h) = K / \sinh^2(h/2\ell) \quad (7.8)$$

where $\ell = \sqrt{c/\alpha}$ is a parameter with the physical meaning of correlation length, and $K = 4\alpha\eta_0^2$. For sufficiently thick symmetrical interlayers with $h > \ell$, (7.8) transforms into an exponential dependence of structural repulsive forces on interlayer thickness:

$$\Pi_s(h) = K \exp(-h/\ell) \quad (7.9)$$

Marčelja and Radić obtained the following constants of this equation from experiments with thin ($h \approx 20 \text{ \AA}$) water interlayers between lecithin layers: $K = 10^{11} \text{ dyn/cm}^2$ and $\ell \approx 2 \text{ \AA}$. The theory developed by Marčelja and Radić is based on several simplifications. It ignores the change in density of the liquid due to changed order parameter, and rather arbitrarily imposes boundary conditions. Furthermore, the order parameter itself is not related to any concrete physical property of molecules. Ninham [136] treated $\eta(x)$ as the polarization of the dielectric $P(x)$ induced by the electric field E_0 produced by monolayers of adsorbed dipole molecules ori-

ented perpendicularly to the surface. Then η_0 is interpreted as the surface polarization $P_0 = \alpha E_0$, where α is the polarizability of the medium, and the constant K equals $2\epsilon_0 P_0^2/\alpha$, where ϵ_0 is the static permittivity of the liquid. Despite its greatly simplified model of the phenomenon of structural repulsion, the theory of Marčelja and Radić gives a qualitatively correct dependence of Π_s on h , in good agreement with available experimental results [137-140].

The interpretation of the order parameter $\eta(x)$ as the state of polarization $P(x)$ of water layers was further elaborated first in a subsequent paper by Gruen and Marčelja [140a] and then by Ruckenstein and Schiby [140b]. Ruckenstein and Schiby took into account the dependence of polarization in the surface layer of water molecules on interlayer thickness, using the methods of electrostatics theory. $\Pi_s(h)$ is a complicated function of h at small interlayer thickness; but at large thickness ($h \gg \ell$) it can again be approximated by an exponential (7.9) with a characteristic length ℓ , which for water equals 2.4 Å. The number of cations adsorbed per unit surface area of the interlayer affects the magnitude of the preexponential factor K . The effect of deformation of hydrated shells of adsorbed cations is taken into account at small separations between interlayer surfaces.

Jönsson and Wennerström [140c] proposed that the structural repulsion between the interfaces of a water layer separating hydrocarbon phases is caused by image forces due to the adsorption of dipole molecules of amphoteric phospholipids at interlayer surfaces. They showed that, with a high degree of ordering in the arrangement of dipoles within adsorption layers, the isotherm $\Pi_s(h)$ obeys the exponential law (7.9) with the characteristic length ℓ about 1 Å. If there is no correlation in the arrangement of dipole molecules, the decay of Π_s with increasing interlayer thickness is described by a power law.

The forces of structural interaction can be calculated fairly rigorously for simple liquids in terms of the hard spheres model. This can be done by numerical Monte Carlo or molecular dynamics calculations. The pressure P of such a liquid (usually assumed to obey the Lennard-Jones potential of intermolecular forces) at the walls of a flat thin interlayer is found as the derivative of the free energy of an ensemble of molecules with respect to the interlayer thickness h . It is also assumed that the thin interlayer is in equilibrium with the bulk liquid whose pressure is P_0 . The difference $P(h) - P_0 = \Pi(h)$, minus the molecular component $\Pi_m < 0$, now gives the structural component of disjoining pressure,

$$\Pi_s(h) = P(h) - P_0 - \Pi_m$$

and we can plot a theoretical isotherm $\Pi_s(h)_T$ for a simple liquid [141-144].

Overlapping of boundary layers in simple liquids with oscillating density produces oscillations of Π_S with a period equal to the diameter d_0 of spherical molecules. Oscillations decay as interlayer thickness increases. The maximum values of Π_S may even exceed the molecular attractive force Π_m , so that the resultant is repulsion between interlayer surfaces ($\Pi(h) > 0$). Oscillations in the interaction force stem from the thermodynamic gain in filling the interlayer with an integral number of molecular layers, and from the instability of "fractional" states. As a result, if h is a multiple of d_0 , the interlayer resists both thinning and thickening. Thus, it is thermodynamically stable, corresponding to those segments of the isotherms where $\partial\Pi_S/\partial h < 0$. Otherwise, the interlayer tends to transform to a different thickness that is an integral multiple of d_0 , by thinning or thickening. Such states are unstable: $\partial\Pi_S/\partial h > 0$. The force necessary to remove the last two monolayers of molecules, whose binding to each of the surfaces of the interlayer is the strongest, is especially large [143].

As the interlayer thickness increases, the amplitude of the oscillating forces decays because the molecule-substrate binding energy decreases. Oscillations practically vanish when $h > 10d_0$, and the function $\Pi(h) = \Pi_S(h) + \Pi_m(h)$ corresponds to the law describing the dispersion attractive forces across the interlayer: $\Pi(h) \approx \Pi_m(h)$. The discreteness of the molecular structure is no longer felt, and the function $\Pi(h)$ obeys the law $\Pi \propto 1/h^3$ describing nonretarded dispersion forces, even at relatively small thickness. If the molecules are nonspherical, for instance diatomic, the oscillations of structural repulsive forces are less pronounced [98] owing to the destruction of the strictly layer-by-layer arrangement of such molecules whose packing depends not only on their size but also on their possible mutual orientations. Such forces, oscillating owing to the discreteness in structure, can also be classified as structural forces because they appear when boundary layers of a liquid overlap. However, they should not be confused with structural long-range forces that arise because of the modified macroscopic properties of the liquid (treated as a continuous medium) in overlapping boundary layers.

Nevertheless, these two approaches can partially overlap; as particles move closer, or films and interlayers become thinner, the effects of discreteness must inevitably come to the fore. These effects may become predominant at interlayer thickness $h \leq 20 \text{ \AA}$, which in some cases corresponds to the position of the coagulation barrier, or to the primary potential well, or to the equilibrium thickness of wetting films. Chan, Mitchell, Ninham, and Pailthorpe [145, 146] combined the microscopic formalism of the theory of simple liquids with the macroscopic theory of dispersion forces. They took into account the effect of the altered density of boundary liquid layers in a thin interlayer on the force of dispersion interaction between the surfaces bounding this interlayer. Calcula-

tions were carried out for the Lennard-Jones liquid. The interaction between its molecules and a hard (absolutely rigid and smooth) structureless wall appears as an attractive potential inversely proportional to the cube of distance. If the interaction between the molecules and the walls is weaker than the intermolecular one, the density of the liquid at the interfaces is reduced. In this case, the interfaces of the nonhomogeneous interlayer undergo a dispersion attraction much greater than the dispersion attraction across a homogeneous interlayer without boundary layers. The energy of attraction $G(h)$ decreases exponentially, with a characteristic length $\ell = 1.5d_0$, in the range $h \leq 10d_0$. In contrast to the hard-spheres model of the liquid, here the oscillations of the interaction force are much reduced. The asymptotic solution for large interlayer thickness gives an expression for $G(h)$ containing, in addition to the term describing the conventional dispersion attraction across a homogeneous liquid interlayer and proportional to $1/h^2$, also a "structural" term proportional to $1/h^3$ (not related to electromagnetic retardation). Numerical estimates for a water interlayer between hydrocarbon phases shows that the contribution of the "structural" term, also leading to attractive forces, becomes predominant when $h < 10-20d_0$. This approach ignores the principal structural effect, viz., the restructuring of the network of intermolecular hydrogen bonds in boundary water layers.

In principle, a transition to structural repulsive forces is possible when the molecules of a liquid strongly interact with interlayer surfaces. However, the parameters of the Lennard-Jones liquid were chosen in such a manner that the liquid was near its critical state, owing to a low energy of intermolecular bonds. Consequently, calculations of repulsion were impossible here [145, 146]. Presumably, this effect could be observed in polar liquids strongly interacting with substrates; however, the necessary calculations could not be carried out. Both attractive and repulsive structural forces are possible if one surface of the interlayer interacts with the molecules strongly and another weakly — for instance, with wetting films, one surface being a liquid-gas and the other a liquid-solid interface.

The effect of nonuniform distribution of density in a thin liquid interlayer can be evaluated qualitatively with a simpler model [147], which assumes that the surfaces of the interlayer are lined with homogeneous boundary layers about d_0 thick, of density greater or less than the density of the liquid in the remaining part of the interlayer ($thickness h \gg 2d_0$). Calculations of the energy of dispersion interaction in such a five-layer system give the following expression for the energy of interaction between surfaces separated with a liquid interlayer:

$$G(h) = -\frac{A_{131}}{12\pi h^2} \left[1 - \frac{4d_0}{h} \frac{(A_{13} - A_{33})}{A_{131}} \right] =$$

$$= - \frac{A_{131}}{12\pi h^2} \left(1 - C \frac{d_0}{h} \right) \quad (7.10)$$

Here A_{131} is the Hamaker constant for the dispersion attraction of identical surfaces 1 in a bulk liquid 3, and A_{13} and A_{33} are the corresponding vacuum Hamaker constants. Evidently, the second term of this equation is analogous to the "structural" term in the first of the theories outlined [145, 146]. This demonstrates that the structural effect in the theories discussed above [145, 147] is, in fact, reduced to the effect produced on the forces of dispersion interaction in multilayer systems by the alternation of layers with different density. (Obviously, this effect cannot give an adequate description of the structural long-range interaction in polar liquids. It is totally inappropriate for liquids with directional intermolecular hydrogen bonds where not only distances between molecules but also their mutual orientation and the number and energy of bonds per molecule play an essential role). If $A_{33} > A_{13}$, i.e., if the interaction between liquid molecules via dispersion forces between themselves is stronger than that with the wall, the second term of Eq. (7.10) is positive, indicating that "structural" effects enhance the attraction. Otherwise, when $A_{33} < A_{13}$, the "structural" repulsion somewhat reduces the forces of dispersion attraction. Ninham's evaluations show [136] that, for instance, for a water interlayer between oil phases the value of C in Eq. (7.10) is ≈ 30 . This gives a correction to the Hamaker constant A_{131} of about 30% already at a distance $h \sim 100d_0$. At $h < 30d_0$, the "structural" repulsion can overcome the dispersion attraction. However, so far nobody has reported stable films of pure water between oil phases. It seems, therefore, that Eq. (7.10) reflects a possible qualitative tendency of variation of dispersion forces in a water interlayer rather than a significant physical reality.

A few theoretical studies have been reported on thin water interlayers. Antonchenko, Davydov, and Ilyin [131] carried out numerical Monte Carlo calculations, with the Rowlinson potential used to describe intermolecular interactions in water. This potential includes, in addition to the Lennard-Jones potential, the Coulomb interaction between four effective electric charges in each water molecule. Two positive charges $q = +0.328e$ are located at hydrogen atoms at a distance of 0.8743 \AA from the oxygen atom. Two negative charges $q = -0.328e$ are located at a distance of 0.25 \AA from the center of the oxygen atom along the line perpendicular to the plane of the molecule. These charges approximate to the distribution of maximum electron density around the nucleus of the oxygen atom. The interaction between the charges of two water molecules gives an approximate description of the intermolecular hydrogen bonding. The distribution of the centers of mass of water molecules within a flat water interlayer with $h = 10 \text{ \AA}$ was calculated for hydrophobic walls of the interlayer - i.e., not interacting with water mol-

ecules and only preventing them from leaving the interlayer. It was concluded that water forms a laminated structure in a thin interlayer, the planes of the molecules being mostly oriented parallel to the walls. Four layers of molecules are formed within the interlayer, the density in the middle portion being greater, and that at the walls lower than bulk water.

The strengthening of hydrogen bonds in the layers of water molecules arranged in parallel to the surfaces of the interlayer may result in anomalously high proton conductance of thin interlayers. Similar results, also based on the Rowlinson intermolecular potential, were obtained by Christou et al. [130] for water interlayer with thickness $h = 20.6 \text{ \AA}$, sandwiched between hydrophobic surfaces. The density and the number of intermolecular bonds were again found to be reduced in water layers at the walls. Gruen et al. [129] analyzed the structure of water in a thin interlayer ($h = 31.4 \text{ \AA}$) between surfaces, simulating the structure of the basal plane in mica, by the method of molecular dynamics. Each surface was composed of 16 oxygen atoms, 6 silicon atoms, and 2 Al atoms located at their appropriate crystallographic sites. The surface was made electrically neutral by placing Na^+ counterions above Al^- ions. The interlayer consisted of 81 dipolar water molecules interacting via a well-known Stillinger-2 potential, also modeling the hydrogen bonding [148]. The water molecule-mica surface interaction was modeled by the Lennard-Jones and the electrostatic potentials. The ordered arrangement of dipoles was found to decay with increasing distance from the surface. The density at the interface was lowered, and that at the middle of the interlayer slightly increased in comparison with the bulk value. However, these are only preliminary results because the analyzed system was not in total equilibrium. A hypothesis was advanced [129] that the special structure of boundary water layers arises because of the formation of a surface layer of oriented dipoles that polarize more remote layers of the liquid by their electric field.

7.6. EXPERIMENTAL ISOTHERMS OF THE STRUCTURAL COMPONENT OF DISJOINING PRESSURE

First experimental isotherms $\Pi_S(h)$ of the structural component of disjoining pressure were obtained by Derjaguin and Zorin [9] who studied the polymolecular adsorption of vapor of polar liquids on a flat glass surface. The film thickness h was measured ellipsometrically, and the film disjoining pressure Π was found from the equilibrium relative vapor pressure p/p_s :

$$\Pi = (RT/v_m) \ln(p_s/p) \quad (7.11)$$

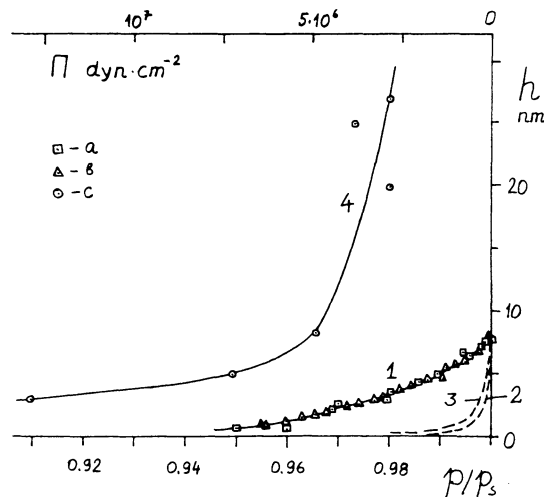


Fig. 7.24. Disjoining pressure isotherms of water α -films on the surface of glass and quartz.

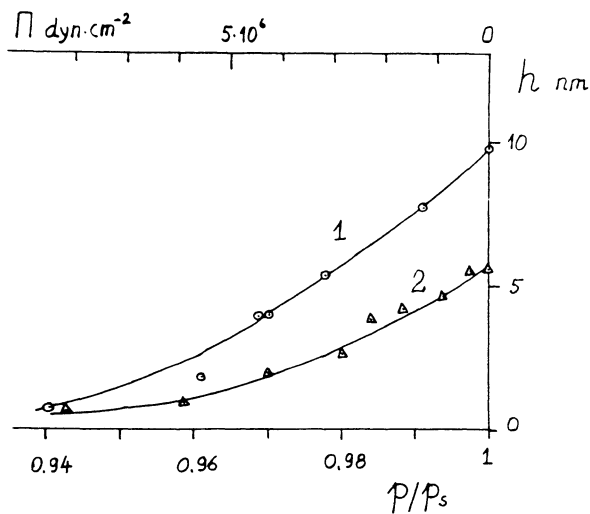


Fig. 7.25. Disjoining pressure isotherms of n-hexyl (1) and n-butyl (2) alcohols on a glass surface.

where R is the gas constant, T is the temperature, and v_m is the molecular volume of the liquid. As an example, Fig. 7.24 shows $h-(p/p_s)$ isotherms obtained by Derjaguin and Zorin [9] for water films (curve 1, squares a), and Fig. 7.25 gives such isotherms for films of hexyl alcohol (curve 1) and butyl alcohol (curve 2) on glass. The behavior of these isotherms, i.e., of measured thick-

ness h as a function of vapor pressure p/p_s , and, correspondingly, of disjoining pressure Π , could not be explained by the effect of either molecular forces (Fig. 7.24, curve 2) or electrostatic forces (curve 3), or by their combined action. Interpretation of the results had to resort to the structural repulsive forces between film interfaces $\Pi_S > 0$ due to a modified structure of polar liquids in films thinner than 100 Å. Structural modification in α -films of water on quartz was directly confirmed by IR spectroscopic studies [64, 65]. The isotherms obtained in thin films fit quite well the exponential dependence of Π_S on h given by Eq. (7.9). A solid curve 1 in Fig. 7.24 and curves 1 and 2 in Fig. 7.25 were calculated by using this equation, with the following values for the parameter K (dyn/cm²) and ℓ (Å), respectively: for water, $9.94 \cdot 10^7$, 23.2; for hexyl alcohol, $3.36 \cdot 10^7$, 26.6; for butyl alcohol, $3.42 \cdot 10^7$, 16.6.

Later, Hall [56] reported similar h -(p/p_s) isotherms for α -films of water on quartz (Fig. 7.24, curve 1, triangles b). Pashley and Kitchener [10] obtained, after a very careful cleaning of crystalline quartz surfaces, disjoining pressure isotherms pointing to much greater thickness of adsorbed water films (Fig. 7.24, curve 4, circles c). These results are even less amenable to explanations ignoring the concept of structural repulsive force enhanced by hydrophilization of the quartz surface. Estimates of the contribution of various forces, made later by Pashley [149], support this conclusion.

In order to describe isotherms of polymolecular adsorption of vapor of a number of liquids on flat substrates, Adamson et al. [150, 152], who obtained the isotherms ellipsometrically, used an empirical equation including two exponential terms, one positive and the other negative, responsible for structural forces. The parameters of the empirical equation were determined by comparing it with experimental isotherms in the range $p/p_s \leq 1$. The approximation of the empirical isotherms (after the parameters had been determined) in the range $p/p_s > 1$ made it possible to find the theoretical values of contact angle, using the Frumkin-Derjaguin equation. The calculated angles were in good agreement with experimental values reported for the same system [152].

Structural repulsive forces are found not only in films on the surface of solids but also in thin symmetrical liquid interlayers. This was first pointed out by Derjaguin [1-3]. The contact of approaching particles was modeled with freshly drawn molecularly smooth quartz fibers crossed at right angles [153]. The fibers were brought to contact in a number of liquids, including water and aqueous electrolyte solutions. The fibers did adhere strongly, as would be anticipated if there were a deep primary minimum on the potential curve. The electrostatic repulsive force would be suppressed by a sufficiently high concentration of electrolyte. Hence,

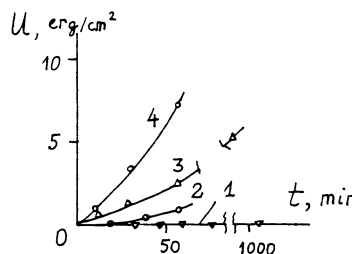


Fig. 7.26. Adhesion energy of polymers (cellulose esters) as a function of contact time in water at 20°C: 1) cellulose acetate and hydrated cellulose; 2) ethylcellulose; 3) nitrocellulose; 4) benzylcellulose.

the high force barrier preventing adhesion could be explained only in terms of repulsive forces of a different type, viz., the structural forces.

In a number of cases (but not always) it was discovered that boundary layers undergo slow decay with time, presumably because overlapping leads to destabilization. At any rate, the force of adhesion appreciably increased with the time of contact, the growth being more rapid at increased temperatures, and tending to a certain equilibrium limiting value. Increased electrolyte concentration also intensified the decay of hydrated water layers.

The same technique was then applied to study the interaction between crossed quartz fibers ($d \approx 100 \mu\text{m}$) with thin films of various substances deposited on the fiber surface by condensation or vacuum deposition [154]. The method substantially widened the range of materials that could be investigated. Thus, the interaction between surfaces of various polymers, deposited from suitable solutions by a drainage technique, was studied [155]. After a volatile solvent was removed, a uniform solidified polymer film was left on the surface of a fiber. As an example, Fig. 7.26 shows the measured energy of adhesion of a number of polymer films in water, as a function of duration of contact. Each point on the curves shows adhesion energy measured after the fibers were kept in water, slightly pressed together, for a time τ . The measured adhesive force N was converted into adhesion energy per unit area U of plane-parallel surfaces of the same physical nature, by using the formula [156]

$$N = 2\pi\sqrt{R_1 R_2} \cdot U$$

where R_1 and R_2 are the fiber radii (together with the deposited films). Figure 7.26 demonstrates that the most hydrophilic hydrated cellulose, and also cellulose acetate (curve 1), do not evince any adhesive forces no matter how long the contact duration. In contrast to this, other less hydrophilic polymers (curves 2-4), especially benzylcellulose (curve 4), have adhesion energy steadily growing with the duration of contact. Simple calculations show that the slow rate of growth of adhesive force between fibers simply cannot be ascribed to a retarded thinning of the liquid interlayer due to viscosity. The only remaining hypothesis is that the reason is a slow modification of the structure of the interlayer, accompanied by thinning and (possibly) a change in the magnitude of the structural forces. This hypothesis agrees with the fact that increased temperature accelerates the development of adhesion, which is also accelerated by adding an electrolyte.

Later, the crossed-fibers technique was used to measure the forces of electrostatic and dispersion interaction between thin ($d \approx 300 \mu\text{m}$) smooth platinum and gold filaments in solutions of various electrolytes [157, 158]. The height of the force barrier was measured as the force necessary to establish electrical contact of slowly approaching filaments. The results were in good agreement with DLVO theoretical estimates in low-concentration solutions. However, repulsive forces, not predicted by this theory, were unexpectedly observed in more concentrated solutions. These forces did not vanish either at the point of zero charge or at even higher concentrations (above 0.1 mole/liter). It can be conjectured that neutral boundary layers with a structure different from that of the bulk solution are also formed in high-concentration electrolyte solutions. This is an example of a different mechanism of boundary-layer structuring that is not related to the structure of the solvent (water) itself. A microscopic heterogeneity of high-concentration solutions, in which separately associated ions and molecules of the solvent form distinct clusters, may play a certain role in this effect. The layers at the interface subjected to the field of surface forces may be enriched with one species of clusters, forming a boundary layer. This hypothesis agrees with the known experiments on reverse-osmosis separation of aqueous electrolyte solutions (see Chapter 11). Even highly concentrated solutions ($C \geq 1 \text{ mole/liter}$) are partially retained by hydrophilic fine-pore membranes, pointing to a reduced concentration of the electrolyte in narrow pores, and to a predominant adsorption of water molecules by the membrane surface.

Similar effects of structural repulsion at high electrolyte concentrations (greater than 0.1 mole/liter) were observed in flat interlayers of aqueous Na_2SO_4 solutions between a glass surface and a mercury meniscus [159]. The equilibrium interlayer thickness was measured ellipsometrically. The disjoining pressure of the interlayer was found from the pressure of a bulk solution in equilibrium

with the interlayer, the pressure being controlled and measured by a differential mercury pressure gauge. As the electrolyte concentration was raised from $C = 0.003$ to $C = 0.1$ mole/liter, the interlayer thickness h dropped from 600-700 Å to 200 Å, in qualitative agreement with electrostatic theory. The quantitative discrepancies can be explained by postulating structural forces operating simultaneously. The presence of these forces is confirmed by the rupturing of water interlayers, i.e., their jumpwise thinning to 120-130 Å. The thickness of these films was not affected by a polarization of the mercury and by changes in surface charge, pointing to a non-electrostatic nature of stability. This thickness is quite close to other estimates of the thickness of water boundary layers at silicate surfaces. At a higher concentration of electrolytes (above 0.1 mole/liter) the equilibrium interlayer thickness again increases up to 500-600 Å; but this happens because of structural effects of a different nature, mentioned above.

Peschel et al. [139, 161] confirmed the existence of structural repulsion in water interlayers between highly polished surfaces (roughness about 20-30 Å) of a quartz plate and a high-curvature-radius lens. Israelachvili et al. [137, 138, 162] demonstrated the presence of structural repulsive forces in water interlayers between crossed cylinders (of radius of about 1 cm) covered with molecularly smooth mica sheets. Rabinovich et al. [140] also measured structural repulsive forces in interlayers of aqueous electrolyte solutions at the contact area of glass or quartz fibers having a smooth, fused surface, and crossed at right angles. The methods of directly measuring the long-range surface forces, developed in these laboratories, made it possible to single out structural forces against the background of simultaneously operating molecular Π_m and electrostatic Π_e forces in interlayers. The isotherm $\Pi_s(h)$ of structural forces is found from the difference between the experimental values of disjoining pressure $\Pi(h)$ and the theoretically calculated isotherms $\Pi_m(h)$ and $\Pi_e(h)$. Usually the structural forces are appreciable at $h \leq 70$ -80 Å, where their contribution to the total isotherm $\Pi(h)$ becomes substantial because of a steeper exponential growth with diminishing interlayer thickness.

Three sets of points, a, b, and c in Fig. 7.27, plot the logarithm of the specific energy of structural repulsion G_s between flat quartz surfaces, as a function of separation h for interlayers of aqueous solutions of different concentration [141]. The values of $G_s(h)$ are directly measurable in crossed-fibers experiments because, according to Derjaguin's equation [156], the force of interaction for fibers of identical radius R_0 , crossed at right angles, is

$$F(h) = 2\pi R_0 G(h)$$

Figure 7.27 shows that in the range of small thickness h , G_s decreases almost exponentially.

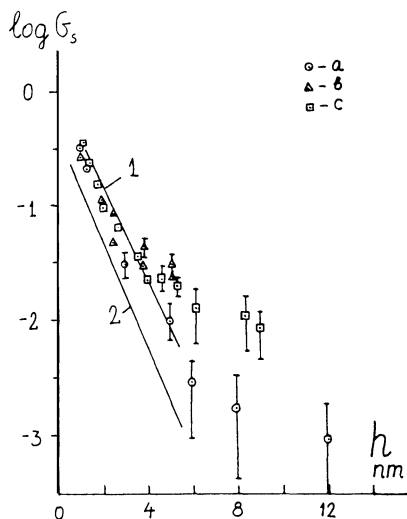


Fig. 7.27. Energy of structural repulsion G_s as a function of thickness h of water interlayers between quartz surfaces ($t = 25^\circ\text{C}$). KCl concentration: 10^{-2} (a), 10^{-3} (b), and 10^{-4} (c) mole/liter. Curves 1 and 2: data of Peschel et al. [139] for aqueous NaCl solutions: 10^{-4} (1) and 10^{-3} (2) mole/liter. G_s is expressed in erg/cm^2 .

By using the definition $\Pi_s = -(\partial G_s / \partial h)$, we can find the constants in Eq. (7.9) for the exponential isotherm $\Pi_s(h)$ of the structural component. For water interlayers these constants are $K = 1.4 \cdot 10^7 \text{ dyn/cm}^2$ and $\ell = 8.5 \text{ \AA}$. This is quite close to the results reported by Israelachvili and Adams [138] for water interlayers between mica surfaces: $K = 10^8 \text{ dyn/cm}^2$ and $\ell = 10 \text{ \AA}$. These values of K and ℓ do not differ greatly from the corresponding values for water films on quartz, suggesting that the nature of forces is common in the two systems. Lines 1 and 2 in Fig. 7.27 plot the results of Peschel et al. [139], with the experimental isotherms $\Pi_s(h)$ converted here into the values of $G_s(h)$. These lines are obviously in good agreement with our experimental data. The authors reported the following parameters of the experimental isotherms: $K = 9.7 \cdot 10^6 \text{ dyn/cm}$ and $\ell = 10.5 \text{ \AA}$ (for line 1) and $K = 7.3 \cdot 10^6 \text{ dyne/cm}^2$ and $\ell = 10.1 \text{ \AA}$ (for line 2). It is thus apparent that despite the different experimental techniques and surfaces (these were always sufficiently hydrophilic) the structural repulsive forces invariably undergo a steep exponential growth in the region of small distances, with a characteristic length ℓ about 10 \AA . Increasing the concen-

tration of a 1-1 electrolyte to 0.01 mole/liter produced a small effect in interlayers with $h < 50 \text{ \AA}$. It was shown in Sec. 7.1 that boundary water layers begin to decay intensively only at higher concentrations of electrolytes. Israelachvili and Adams also mention a low sensitivity of structural forces to the change in the concentration of a 1-1 electrolyte from 0.001 to 0.01 mole/liter [138]. However, this conclusion seems to hold only for the most structurally modified part of the boundary layer, nearest to the solid surface. As seen in Fig. 7.27, the behavior of structural forces becomes concentration-dependent at distances $h > 50 \text{ \AA}$: their long-range character is more pronounced in dilute solutions. Actually, the error of measurements and computations sharply increases in this range of distances, so that there is some uncertainty about the apparent concentration effect. Peschel et al. [139] also reported some weakening of the structural repulsive forces, caused by increasing the concentration of a 1-1 electrolyte (see lines 1 and 2 in Fig. 7.27). The characteristic length ℓ diminished in these experiments from 10 to 7.5 \AA as the concentration grew to 1 mole/liter. However, a substantial spread in the values of ℓ obtained again leaves room for doubt whether a concentration dependence has been established.

All the above studies indicated the range of structural forces to be $h \leq 70\text{--}80 \text{ \AA}$. This is the distance at which structural forces can be experimentally discriminated from the background of electrostatic and molecular forces. In fact, a number of difficulties are encountered in attempts at correct separation of structural forces. The main obstacle is the possible lack of accuracy in theoretical calculations of electrostatic forces as functions of interlayer thickness $\Pi_e(h)$. These calculations necessarily involve a choice of assumptions of the dependence of the potential ψ and charge Q of the surfaces on h . Usually one chooses the assumption of constant potential. But in real situations this assumption need not always hold. Therefore, a more rigorous theory of electrostatic forces will be needed for further elaboration of the isotherm of structural forces acting in thin water interlayers. This can be achieved only by taking into account the mechanism of surface charging and the effect of overlapping both of diffuse ionic layers and of boundary layers of the solvent on the adsorption of ions and on the dissociation of surface ionogenic groups. Thus, after Pashley modified his method of calculating the electrostatic component of disjoining pressure in electrolyte interlayers [163], the structural force isotherms $\Pi_s(h)$, which in previous papers were found from the difference $\Pi_s = \Pi - \Pi_m - \Pi_e$, had to be essentially modified. In the case of mica, Pashley is inclined to trace the observed structural repulsive forces not to the effect of a hydrophilic surface as such on the solvent's structure but to the effect of hydration of ions adsorbed on the surface. However, there can be no sharp discrimination between "structure"- and "hydration"-induced effects. Indeed, the K^+ ions that cover the surface of mica by a

dense layer ($2 \cdot 10^{14}$ ions/cm²) [i.e., before it is immersed in water - Editor] also constituted active centers (in the sense of interaction with water molecules) capable of modifying the structure of boundary layers to a considerable depth, up to 50-70 Å. Hence, the effect as a whole cannot be reduced solely to the hydrate shell of the K⁺ ion whose radius does not exceed one to two layers of water molecules. The long-range effect can be produced only by a collective but not additive influence of active surface centers on the structure of water.

We have already mentioned that the shape of the calculated isotherms $\Pi_s(h)$ essentially depends on the assumption chosen for the calculation of the electrostatic component $\Pi_e(h)$. Peschel et al. [139, 161], Israelachvili and Adams [138], and Rabinovich, Derjaguin, and Churaev [140] assumed that $\psi = \text{const}$. This was the condition under which the isotherms $\Pi_s(h)$ shown in Fig. 7.27 were obtained. Pashley also found appreciable "hydration" forces in the case $\psi = \text{const}$ [164]. The only exception is made for the conductivity water: the experimental isotherms are then compared with the calculations of Π_e for $Q = \text{const}$. This was taken as a basis for concluding that there are no structural forces in conductivity water. However, a comparison of $\Pi(h)$ with $\Pi_e(h)$ assuming $\psi = \text{const}$ gives weaker but nevertheless appreciable structural repulsive forces for pure water as well. Structural forces are detected at interlayer thickness $h \leq 60-70$ Å, and the $\Pi_s(h)$ isotherm gives the exponential decrease of these forces with increasing h , with a characteristic length $\ell = 8-10$ Å, i.e., the same ℓ as for glass and quartz. Under the assumption $Q = \text{const}$ we also obtained [140] structural repulsive forces, although of lower magnitude and smaller range, for glass fibers in aqueous 0.001 mole/liter solution of KCl.

Recently, Pashley [163] made an attempt to improve the calculations of $\Pi_e(h)$ for water interlayers between mica surfaces by taking into account the ion-exchange mechanism of surface charge formation. Pashley used the law of mass action and the Boltzmann equation for the description of ionic adsorption, taking into account the difference in radii r_0 of hydrated cations. With the ion exchange included, the situation became intermediate between the cases $\psi = \text{const}$ and $Q = \text{const}$. This changed the isotherms of "hydration" forces $\Pi_s(h)$ by diminishing their range to 20-30 Å in comparison with the case of $\psi = \text{const}$. However, this theory, being based on a number of assumptions and employing r_0 as an adjustment parameter, can hardly be regarded as universal. Further search for more general and rigorous solutions is necessary. At the same time, it is desirable to study experimentally the surface charge of the specimens used for direct determination of surface forces, at different thickness of the separating interlayer, for instance by electrokinetic methods.

An analysis of experimental data obtained by Pashley for mica [163, 164] leads to a conclusion that structural "hydration" forces increasing exponentially when $h \rightarrow 0$, with a characteristic length 8-10 Å, were detected in all experiments (except the single one with the conductivity water) when interlayer thickness was below 60-70 Å. These results do not differ in any way (except the name given to the force) from those obtained in experiments with quartz and glass [139, 140], indicating the general structure-related nature of the effect.

As in [139, 140], Pashley found that at increased electrolyte concentrations the range of "hydration" forces was slightly reduced and that they decrease more steeply (the value of ℓ was reduced). A decrease in pH in Pashley's experiments [164] diminished the structural repulsive forces, while an increase in pH substantially increased both their range (up to 100 Å) and their characteristic length ℓ (up to 15 Å). Pashley interpreted this observation as the effect of substitution of weakly hydrated H_3^+O ions by strongly hydrated K^+ or Na^+ ions, intensified at higher pH. However, a more plausible explanation is that at increasing pH the potential-determining OH ions are adsorbed at the mica surface, bringing its state closer to that of the hydrophilic surface of quartz and thus increasing Π_s . Pashley was able to show in a recent paper [165] that the law describing the decay of "hydration" repulsive forces F_s with increasing interlayer thickness h of aqueous solutions of Li, Na, K, and Cs chlorides between mica surfaces is more complicated:

$$F_s/R_0 = A_1 \exp(-h/D_1) + A_2 \exp(-h/D_2) \quad (7.12)$$

where R_0 is the radius of mica surfaces, and A_1 , A_2 , D_1 , and D_2 are empirical constants. The effect of "hydration" forces becomes appreciable at electrolyte concentrations above a certain critical concentration C_c . Thus, $C_c = 10^{-4}$ mole/liter in KCl, and $C_c = 6 \cdot 10^{-2}$ mole/liter in LiCl.

By Pashley's conjecture, "hydration" forces are caused by dehydration of ions on approaching surfaces. We are of the opinion, however, that these forces are a particular case of the structural forces, when overlapping boundary layers of water interact in the vicinity of cations adsorbed on the surfaces.

Hydrophobization of mica surface by the adsorption of cation-active surfactant resulted in the reversal of sign of structural forces; Pashley and Israelachvili [166] detected experimentally extra attractive forces (in excess of $\Pi_e + \Pi_m$), several times greater than the molecular forces, at short distances. One possible explanation of this effect is that boundary water layers formed at hydrophobic surfaces have a structure different from that at hydrophilic surfaces. Among the phenomena based on such structural mod-

ifications in water in the neighborhood of hydrophobic segments of molecules are the well-known effects of hydrophobic interaction [67].*

The possibility of both structural repulsion $\Pi_S > 0$ (or hydrophilic interaction) and structural attraction $\Pi_S < 0$ (or hydrophobic interaction) was first discussed by Derjaguin and Churaev [5]. Israelachvili and Pashley confirmed in a recent paper [168] the existence of long-range "hydrophobic" attraction between hydrophobized mica surfaces. They demonstrated that the hydrophobic attractive forces depend only weakly on electrolyte concentration and on the pH of the solution, and also obey the exponential law of diminishing force (with a reversed sign of force, $\Pi_S < 0$) with a characteristic length $\ell \approx 10 \text{ \AA}$. The range of these forces is about 100 \AA . The functions $\Pi(h)$ were analyzed in these experiments on model systems, so that it was possible to obtain reasonably reliable quantitative data on structural forces.

In colloids the structural component of disjoining pressure produces deviations from the DLVO theory since the theory takes into account only electrostatic and molecular forces. Thus, hydrophilic colloids, such as silica in water, become anomalously stable owing to the action of structural forces [169-173]. This effect is especially noticeable in acidic media, where the surface potential of silica is low. By using the DLVO theory, Chernoberezhsky et al. [173] were able to evaluate the thickness of boundary layers of water, $h_s = 60-150 \text{ \AA}$, in agreement with the model experiments described above. Glazman et al. [174-178] demonstrated that the stability of sols stabilized with nonionogenic surfactants stems from structural forces that result from the overlapping of boundary water layers formed at the hydrophilic segments of the surfactant molecules, directed into the continuous medium. The special structure of boundary layers is produced here by the interaction between water molecules, not directly with the surface of the sol particles, but indirectly, via surfactant molecules adsorbed on this surface. The stabilizing action of boundary water layers structured by the adsorbed layers of nonionogenic surfactants has been established for gold hydrosol [179] and for graphite suspensions in water [180]. Similar effects are found in free films stabilized by surfactants [181-183].

Baran et al. investigated the effect of boundary water layers on the stability of hydrophobic sols stabilized with water-soluble polymers [184-187]. It was shown in this work that as temperature increases, the boundary layers of water are destroyed, reducing the repulsive forces between particles and lowering the stability of the sol. Clay systems whose platelet-shaped particles are separated with thin flat water interlayers constitute a convenient object for studying the effect of surface forces. In carefully arranged experiments with these systems it is also possible to detect

*See also B. V. Derjaguin and Ya. I. Rabinovich, Surf. Colloids, in press.

structural repulsive forces. Thus, Barclay and Ottewill [188] applied pressure to clay and found that repulsive forces between clay particles increased more sharply than would follow from the DLVO theory, when water interlayers thinned to $h \leq 50 \text{ \AA}$. Barclay and Ottewill suggested that these additional forces are caused by the solvation of the clay particle surface.

Low et al. [189-191] conducted a systematic study of swelling in montmorillonite clays subjected to loading. The swelling pressure is, in fact, the averaged disjoining pressure of water interlayers in clay, corresponding to a certain interlayer thickness. This thickness can be found from the equilibrium moisture content W in the clay. The empirical equation relating Π and W is exponential. Its form coincides with that of Eq. (7.9) for the structural component of disjoining pressure. By combining the measurements of swelling pressure $\Pi(W)$ and of heat of wetting for different initial moisture content in the clay, Oliphant and Low [191] were able to calculate the thermodynamic functions of thin water interlayers. An analysis of their dependence on moisture content led to a conclusion that the factor determining the magnitude of swelling pressure is the structural modification in thin water interlayers, and that this is a long-range effect. The independence of structural repulsion in clays of the amount of adsorbed ions, discovered by Low et al. [192], makes it possible to conclude that the repulsion is a result not of "hydration" of ions but of structural modifications in boundary water layers [5]. Parsegian [193, 194] reports data on structural repulsive forces [also following the same exponential law (7.9)] acting in a thin water interlayer ($h \leq 30 \text{ \AA}$) between bilayers of phospholipids (PL). These forces balance out the molecular attraction of PL bilayers at $h = 27.5 \text{ \AA}$, when $\Pi_m + \Pi_s = 0$. The structuring of water in interlayers was ascribed to polar hydrophilic groups of PL. It was this set of data [194] that Marčelja and Radić used to calculate for the first time the constants of Eq. (7.9) [134].

Structural repulsive forces are found not only in water and aqueous solutions but also in alcohols and their mixtures [195, 196]. However, here the thickness of boundary layers is smaller, and structural repulsive forces are found only when $h \leq 20 \text{ \AA}$.

The liquid boundary layers with special structure are thus a well-proven physical reality. Overlapping of such layers belonging to approaching surfaces gives rise to repulsive or attractive forces, depending on the type of structural features and on the specific changes in the structure of the liquid in the overlap zone. Structural forces can become especially important in very thin interlayers in which their contribution to the interaction can become dominant. Although a number of aspects of the structural interaction have not been adequately studied yet, the exponential

equation (7.9) with experimentally determined parameters K and ℓ can be used to describe them as a first approximation. Experiments with well-characterized surfaces are particularly required.

REFERENCES

1. B. V. Derjaguin and M. M. Kusakov, Izv. Akad. Nauk SSSR, Ser. Khim., No. 5, 741 (1936); No. 5, 1119 (1937).
2. B. V. Derjaguin and M. M. Kusakov, Acta Physicochim. URSS, 10, 25, 153 (1939).
3. B. V. Derjaguin, in: Proceedings of the 3rd USSR Conference on Colloid Chemistry, Izd. Akad. Nauk SSSR, Kiev (1952), p. 26.
4. B. V. Derjaguin, in: Advances of Colloid Chemistry, Nauka, Moscow (1973).
5. B. V. Derjaguin and N. V. Churaev, Dokl. Akad. Nauk SSSR, 207, 572 (1972); J. Colloid Interface Sci., 49, 249 (1974).
6. A. V. Kiselev and V. I. Lygin, Usp. Khim., 31, 351 (1962); A. V. Kiselev, Discuss. Faraday Soc., 52, 14 (1971).
7. A. C. Zettlemoyer, F. J. Micale, and K. Klier, in: Water in Disperse Systems, Plenum Press, New York (1975), p. 249.
8. A. C. Zettlemoyer and H. H. Hsing, J. Colloid Interface Sci., 55, 637 (1976); 58, 263 (1977).
9. B. V. Derjaguin and Z. M. Zorin, Zh. Fiz. Khim., 29, 1755 (1955); Proceedings of the 2nd International Congress of Surface Activity, Vol. 2, Butterworths, London (1957), p. 145.
10. R. M. Pashley and J. A. Kitchener, J. Colloid Interface Sci., 71, 491 (1979).
11. G. F. Ershova, Z. M. Zorin, and N. V. Churaev, Kolloidn. Zh., 37, 208 (1975).
12. B. V. Derjaguin, Z. M. Zorin, N. V. Churaev, and V. A. Shishin, in: Wetting, Spreading, and Adhesion, J. F. Padday (ed.), Academic Press, London (1977), p. 201.
13. V. D. Perevertaev and M. S. Metsik, Kolloidn. Zh., 28, 254 (1966).
14. P. A. Voznyi and N. V. Churaev, Kolloidn. Zh., 39, 264 (1977); P. A. Voznyi, V. P. Dushchenko, and N. V. Churaev, in: Surface Forces in Thin Films, Nauka, Moscow (1979), p. 109.
15. N. V. Churaev, V. D. Sobolev, and Z. M. Zorin, in: Thin Liquid Films and Boundary Layers, Academic Press, London (1971), p. 213.
16. B. V. Derjaguin, B. V. Zhelezny, Z. M. Zorin, V. D. Sobolev, and N. V. Churaev, in: Surface Forces in Thin Films and Stability of Colloids, Nauka, Moscow (1974), p. 90.
17. B. V. Derjaguin and N. V. Churaev, Dokl. Akad. Nauk SSSR, 169, 396 (1966); in: Research in Surface Forces, Vol. 3, Consultants Bureau, New York (1971), p. 261.
18. V. I. Lashnev, V. D. Sobolev, and N. V. Churaev, Teor. Osn. Khim. Tekhnol., 10, 926 (1976).

19. N. E. Khadakhane, V. D. Sobolev, and N. V. Churaev, *Kolloidn. Zh.*, 42, 911 (1980).
20. Z. M. Tovbina, in: *Research in Surface Forces*, Vol. 3, Consultants Bureau, New York (1971), p. 20.
21. P. F. Low, *Soil Sci. Soc. Am.*, 40, 500 (1976); 43, 651 (1979).
22. J. Clifford and S. M. A. Lecchini, in: *Wetting*, No. 25, p. 174, *Soc. Chem. Industry*, London (1967).
23. V. V. Mank, Z. E. Suyunova, Yu. I. Tarasevich, and F. D. Ovcharenko, *Dokl. Akad. Nauk SSSR*, 202, 117 (1972).
24. D. E. Woessner, in: *Mass Spectrometry and NMR Spectroscopy in Pesticide Chemistry*, Plenum Press, New York (1974), p. 279.
25. F. D. Ovcharenko, A. G. Brekhunets, V. V. Mank, and I. N. Pereverzeva, *Kolloidn. Zh.*, 36, 1177 (1974).
26. V. I. Kvividze and A. V. Krasnushkin, *Dokl. Akad. Nauk SSSR*, 222, 388 (1975).
27. E. Almagor and G. Belfort, *J. Colloid Interface Sci.*, 66, 146 (1978).
28. F. D. Ovcharenko, *Physicochemical Mechanics and Lyophilic Properties of Disperse Systems*, Naukova Dumka, Kiev, No. 11 (1979), p. 5.
29. Yu. I. Tarasevich, *Khim. Tekhnol. Vody*, 2, 99 (1980).
30. P. A. Sermon, *J. Chem. Soc., Faraday Trans. I*, 76, 885 (1980).
31. D. D. Eley, H. J. Hey, and C. K. Rix, *J. Colloid Interface Sci.*, 65, 592 (1978).
32. J. Clifford, J. Oakes, and G. J. T. Tiddy, in: *Thin Liquid Films and Boundary Layers*, Academic Press, London (1971), p. 175.
33. B. V. Derjaguin, N. N. Zakhavaeva, and A. M. Lopatina, *Inzh.-Fiz. Zh.*, 3, 66 (1960).
34. B. V. Derjaguin, N. N. Zakhavaeva, and A. M. Lopatina, in: *Research in Surface Forces*, Vol. 1, Consultants Bureau, New York (1963), p. 162.
35. B. V. Derjaguin and N. N. Zakhavaeva, *Bull. RILEM*, 27, 27 (1965).
36. W. Drost-Hansen, *J. Colloid Interface Sci.*, 25, 131 (1967).
37. D. M. Anderson, *J. Colloid Interface Sci.*, 25, 174 (1967).
38. N. H. Fletcher, *Rep. Prog. Phys.*, 34, 913 (1971).
39. D. M. Anderson and A. R. Tice, *Ecol. Stud.*, 4, 107 (1973).
40. V. I. Kvividze, V. F. Kiselev, A. B. Kurzaev, and L. A. Ushakova, *Surf. Sci.*, 44, 60 (1974).
41. V. I. Kvividze and A. B. Kurzaev, in: *Surface Forces in Thin Films*, Nauka, Moscow (1979), p. 211.
42. G. R. Enikeeva, N. K. Andreev, F. D. Ovcharenko, A. G. Bratunets, and M. G. Zarínov, *Dokl. Akad. Nauk SSSR*, 246, 136 (1979).
43. B. V. Derjaguin, N. V. Churaev, V. D. Sobolev, and S. S. Barer, *J. Colloid Interface Sci.*, 84, 182 (1981).
44. O. A. Kiseleva, S. N. Klad'ko, V. D. Sobolev, and N. V. Churaev, *Kolloidn. Zh.*, 37, 1220 (1975).
45. S. S. Barer, B. V. Derjaguin, O. A. Kiseleva, V. D. Sobolev, and N. V. Churaev, *Kolloidn. Zh.*, 39, 1039 (1977).

46. S. S. Barer, N. V. Churaev, B. V. Derjaguin, O. A. Kiseleva, and V. D. Sobolev, *J. Colloid Interface Sci.*, 74, 173 (1980).
47. V. V. Karasev, B. V. Derjaguin, and E. N. Efremova, *Kolloidn. Zh.*, 24, 471 (1962).
48. V. V. Karasev, B. V. Derjaguin, and E. N. Khromova, in: *Research in Surface Forces*, Vol. 3, Consultants Bureau, New York (1971), p. 25.
49. B. V. Derjaguin, V. V. Karasev, and E. N. Khromova, *J. Colloid Interface Sci.*, 78, 274 (1980); *Kolloidn. Zh.*, 42, 808 (1980).
50. B. V. Derjaguin, N. V. Churaev, and Z. M. Zorin, *Izv. Akad. Nauk SSSR, Ser. Khim.*, No. 8, 1698 (1982).
51. B. Kh. Rakhmukov, I. I. Seliverstova, V. V. Serpinsky, and A. A. Fomkin, *Izv. Akad. Nauk SSSR, Ser. Khim.*, No. 11, 2419 (1979).
52. G. E. Van Gils, *J. Colloid Interface Sci.*, 30, 272 (1969).
53. D. M. Andersen and P. F. Low, *Soil Sci. Soc. Am. Proc.*, 22, 99 (1958).
54. W. F. Bradley, *Nature*, 183, 1614 (1969).
55. C. T. Deeds and H. van Olphen, *Adv. Chem. Ser.*, No. 33, 332 (1961).
56. A. C. Hall, *J. Phys. Chem.*, 74, 2742 (1970).
57. J. Israelachvili, *Nature Phys. Sci.*, 229, 85 (1971).
58. D. Green-Kelly and B. V. Derjaguin, *Dokl. Akad. Nauk SSSR*, 153, 638 (1963); *Trans. Faraday Soc.*, 60, 449 (1964).
59. D. Green-Kelly and B. V. Derjaguin, in: *Research in Surface Forces*, Vol. 2, Consultants Bureau, New York (1966), p. 117.
60. B. V. Derjaguin, N. A. Krylov, and V. F. Novik, *Dokl. Akad. Nauk SSSR*, 193, 126 (1970); in: *Surface Forces in Thin Films and Stability of Colloids*, Nauka, Moscow (1974), p. 164.
61. P. Hoexstra and W. T. Doyle, *J. Colloid Interface Sci.*, 36, 513 (1971).
62. M. E. Heyde, C. R. Peters, and J. E. Anderson, *J. Colloid Interface Sci.*, 50, 467 (1975).
63. V. P. Dushchenko and I. A. Romanovsky, *Zh. Fiz. Khim.*, 44, 1479 (1970).
- 63a. A. V. Dumansky, *Kolloid-Z.*, 65, 178 (1933).
- 63b. A. V. Dumansky, *Lyophilicity of Disperse Systems*, Izd. Akad. Nauk SSSR, Kiev (1960).
- 63c. B. V. Derjaguin, *Kolloidn. Zh.*, 5, 257, 605 (1939).
64. G. F. Ershova, Z. M. Zorin, and N. V. Churaev, *Kolloidn. Zh.*, 41, 19 (1979).
65. G. F. Ershova, Z. M. Zorin, A. V. Novikova, and N. V. Churaev, in: *Research in Surface Forces*, Nauka, Moscow (1979), p. 168.
66. K. Rödel, *Tenside*, 18, 141 (1981).
67. J. Salle de Chou, P. F. Low, and C. B. Roth, *Clays Clay Miner.*, 28, 111 (1980).
68. D. M. Anderson, G. F. Leaming, and G. Sposito, *Science*, 141, 1040 (1963).

69. B. V. Derjaguin, Yu. M. Popovsky, and B. A. Altoiz, *Kolloidn. Zh.*, 44, 843 (1982).
70. Yu. M. Popovsky and B. V. Derjaguin, *Dokl. Akad. Nauk SSSR*, 159, 897 (1964); 175, 385 (1967).
71. Yu. M. Popovsky, in: *Research in Surface Forces*, Vol. 3, Consultants Bureau, New York (1971), p. 120.
72. B. V. Derjaguin, Yu. M. Popovsky, and G. P. Silenko, *Dokl. Akad. Nauk SSSR*, 207, 1153 (1972); 239, 828 (1978).
73. Yu. M. Popovsky, G. P. Silenko, V. G. Zaremba, and L. V. Sokol'skaya, in: *Surface Forces in Thin Films and Stability of Colloids*, Nauka, Moscow (1974), p. 28.
74. Yu. M. Popovsky and G. P. Silenko, in: *Surface Phenomena in Liquids*, Leningrad. Gos. Univ., Leningrad (1975), p. 49.
75. Yu. M. Popovsky and B. A. Altoiz, *Kolloidn. Zh.*, 43, 1177 (1981).
76. B. V. Derjaguin, Yu. M. Popovsky, and B. A. Altoiz, *Dokl. Akad. Nauk SSSR*, 262, 853 (1982).
77. P. G. De Gennes, *The Physics of Liquid Crystals*, Clarendon Press, Oxford (1974).
78. S. Chandrasekhar, *Liquid Crystals*, Cambridge Univ. Press, Cambridge (1977).
79. B. V. Derjaguin, Yu. M. Popovsky, and B. A. Altoiz, *J. Colloid Interface Sci.*, 96, 492 (1983).
80. M. Hitoshi and K. Shunsuke, *Appl. Phys. Lett.*, 35, 4 (1979).
81. P. Sheng, *Phys. Rev. A*, 26, 1610 (1982).
82. G. Peschel and R. Schnorrer, *Ber. Bunsenges. Phys. Chem.*, 78, 1286, 1294 (1974).
83. G. Peschel, K. H. Adlfinger, and R. Schnorrer, in: *Chemie, phys. Chemie und Anwendungstechnik der grenzflächenaktiven Stoffe*, Carl Hanser Verlag, München (1973), p. 403.
84. G. L. Michnewitsch and I. F. Browko, *Acta Physicochim. URSS*, 8, 103 (1938); 9, 795 (1938).
85. G. L. Michnewitsch and E. N. Owtschinikowa, *Acta Physicochim. URSS*, 11, 603 (1939).
86. G. L. Michnewitsch and E. N. Owtschinikowa, *Proceedings of the Odessa Univ., Fizika*, Vol. 2 (1940), p. 63.
87. G. L. Michnewitsch, V. P. Efimova, and V. G. Zaremba, in: *Growth of Crystals*, Izd. Akad. Nauk SSSR (1957), p. 199; *Kolloidn. Zh.*, 24, 488 (1962); G. L. Michnewitsch and V. G. Zaremba, *Kolloidn. Zh.*, 24, 491 (1962).
88. V. Kh. Mezhidov and S. Kh. Mezhidov, *Kolloidn. Zh.*, 45, 349 (1983).
89. A. G. Grivtsov, *Dokl. Akad. Nauk SSSR*, 190, 868 (1970); in: *Fundamental Problems in the Theory of Physical Adsorption*, Nauka, Moscow (1970), p. 352.
90. B. Borštník and A. Ažman, *Mol. Phys.*, 30, 1565 (1975); *Z. Naturforsch.*, 33A, 1557 (1978).
91. D. Henderson, F. F. Abraham, and J. A. Barker, *Mol. Phys.*, 31, 1291 (1976).

92. S. Toxvaerd and E. Praestgaard, *J. Chem. Phys.*, 67, 5291 (1977).
93. D. E. Sullivan and G. Stell, *J. Chem. Phys.*, 69, 5450 (1978).
94. A. J. C. Ladd and L. V. Woodcock, *J. Phys.*, C11, 3565 (1978).
95. A. C. Grivtsov, in: *Heterogeneous Crystallization from the Gas Phase*, Nauka, Moscow (1978), p. 100.
96. I. Snook and W. van Megen, *J. Chem. Phys.*, 70, 3099 (1979).
97. M. J. Grimson, G. Rickayzen, and P. Richmond, *Mol. Phys.*, 39, 61, 1455 (1980).
98. M. J. Grimson and P. Richmond, *J. Chem. Soc., Faraday Trans. II*, 76, 1478 (1980).
99. V. Ya. Antonchenko, V. V. Ilyin, and N. N. Makovsky, *Dokl. Akad. Nauk SSSR*, A11, 69 (1981).
100. J. Fischer, *Ber. Bunsenges. Phys. Chem.*, 85, 1041 (1981).
101. R. G. Horn and J. N. Israelachvili, *Chem. Phys. Lett.*, 71, 192 (1980); *J. Chem. Phys.*, 75, 1400 (1981).
102. H. K. Christenson, R. G. Horn, and J. N. Israelachvili, *J. Colloid Interface Sci.*, 88, 79 (1972).
103. G. H. Findenegg, *J. Colloid Interface Sci.*, 35, 249 (1971).
104. K. Harmut, W. V. Rybinski, and G. H. Findenegg, *J. Colloid Interface Sci.*, 59, 301 (1977); R. Löring and G. H. Findenegg, *J. Colloid Interface Sci.*, 84, 355 (1981).
105. G. D. Parfitt and M. W. Tideswell, *J. Colloid Interface Sci.*, 79, 518 (1981).
106. M. Grosse-Rhode and G. H. Findenegg, *J. Colloid Interface Sci.*, 64, 374 (1978).
107. D. E. Sullivan, R. Barker, G. G. Gray, W. B. Streett, and K. E. Gubbins, *Mol. Phys.*, 44, 597 (1981).
108. V. V. Karasev and B. V. Derjaguin, *Dokl. Akad. Nauk SSSR*, 62, 761 (1948); *Kolloidn. Zh.*, 15, 365 (1953); *Zh. Fiz. Khim.*, 33, 100 (1959).
109. B. V. Derjaguin and N. N. Zakhavaeva, in: *Research in High-Molecular-Weight Compounds*, Izd. Akad. Nauk SSSR, Moscow (1949), p. 223.
110. B. V. Derjaguin and V. V. Karasev, *Dokl. Akad. Nauk SSSR*, 101, 289 (1955); in: *Proceedings of the 2nd International Congress of Surface Activity*, Vol. 2, Butterworths, London (1957), p. 531.
111. B. V. Derjaguin, V. V. Karasev, N. N. Zakhavaeva, and V. P. Lazarev, *Zh. Tekh. Fiz.*, 27, 1976 (1957); *Wear*, 1, 277 (1958).
112. B. V. Derjaguin, N. N. Zakhavaeva, S. V. Andreev, and A. M. Khomutov, *Kolloidn. Zh.*, 24, 289 (1962); *Fnzh.-Fiz. Zh.*, 5, 92 (1962).
113. B. V. Derjaguin, N. N. Zakhavaeva, S. V. Andreev, A. A. Milovidov, and A. M. Khomutov, in: *Research in Surface Forces*, Vol. 1, Consultants Bureau, New York (1963), p. 110.
114. N. N. Zakhavaeva, B. V. Derjaguin, A. M. Khomutov, and S. V. Andreev, in: *Research in Surface Forces*, Vol. 2, Consultants Bureau, New York (1966), p. 156.

115. B. V. Derjaguin, V. V. Karasev, I. A. Lavygin, I. I. Skorokhodov, and E. P. Khromova, Dokl. Akad. Nauk SSSR, 187, 846 (1969); Spec. Discuss. Faraday Soc., No. 1, 98 (1970); in: Research in Surface Forces, Vol. 4, Consultants Bureau, New York (1975), p. 188.
116. B. V. Derjaguin, V. V. Karasev, I. A. Lavygin, I. I. Skorokhodov, and E. N. Khromova, in: Polymer Composite Materials, No. 10 (1981), p. 51.
117. B. V. Derjaguin, V. V. Karasev, and Z. M. Zorin, in: Academician I. P. Lazarev. Memorial Volume, Izd. Akad. Nauk SSSR, Moscow (1956).
118. S. Bastow and F. Bowden, Proc. R. Soc. London, A151, 220 (1935).
119. W. D. Bascom and C. R. Singleterry, J. Colloid Interface Sci., 66, 559 (1978).
120. B. V. Derjaguin, V. V. Karasev, and E. N. Chromova, J. Colloid Interface Sci., 66, 573 (1978).
121. P. Neogi, J. Colloid Interface Sci., 89, 358 (1982).
122. J. Lyklema, P. C. Scholten, and K. J. Mysels, J. Phys. Chem., 69, 116 (1965).
- 122a. K. J. Mysels, K. Shinoda, and S. Frankel, Soap Films: Studies of Their Thinning, Pergamon Press, London (1959).
123. B. V. Derjaguin, Zh. Eksp. Teor. Fiz., 15, 9 (1945); Acta Phys. Chim. URSS, 20, 6 (1945); C. R. Acad. Sci. USSR, 39, 13 (1943).
124. B. V. Derjaguin and S. M. Levi, Physical Chemistry of Depositing Thin Films on a Moving Substrate, Izd. Akad. Nauk SSSR, Moscow (1959); Film Coating Theory, Focal Press, London-New York (1964).
125. B. V. Derjaguin, V. V. Karasev, V. M. Starov, and E. N. Khromova, Kolloidn. Zh., 39, 664 (1977); J. Colloid Interface Sci., 67, 465 (1978).
126. B. V. Derjaguin, V. V. Karasev, I. A. Lavygin, I. I. Skorokhodov, and B. N. Khromova, in: Surface Forces in Thin Films and Stability of Colloids, Nauka, Moscow (1974), p. 25.
127. I. A. Lavygin, I. I. Skorokhodov, M. V. Sobolevsky, D. V. Nazarova, M. B. Lotarev, O. I. Kudinova, and B. V. Voropaeva, Vysokomol. Soedin., A42, 90 (1976).
128. B. V. Derjaguin, V. V. Karasev, I. A. Lavygin, I. I. Skorokhodov, and E. N. Khromova, in: Surface Forces in Thin Films, Nauka, Moscow (1979), p. 124.
129. D. W. R. Gruen, S. Marčelja, and B. A. Pailthorpe, Chem. Phys. Lett., 82, 315 (1981).
130. N. I. Christou, J. S. Whitehouse, D. Nicholson, and H. C. Parsonsage, Faraday Symp. Chem. Soc., No. 16, 139 (1981).
131. V. Ya. Antonchenko, A. S. Davydov, and V. V. Flyin, Preprint of the Institute of Theoretical Physics, IT8-82-113 V, Kiev (1982).
132. B. V. Derjaguin and N. V. Churaev, Croat. Chem. Acta, 50, 187 (1977).

133. D. D. Eley, Trans. Faraday Soc., 42B, 125 (1946).
134. S. Marčelja and N. Radić, Chem. Phys. Lett., 42, 129 (1976).
135. L. D. Landau and E. M. Lifshitz, Statistical Physics, Addison-Wesley, Reading, Mass. (1958).
136. B. W. Ninham, J. Phys. Chem., 84, 1423 (1980).
137. J. N. Israelachvili, Faraday Discuss. Chem. Soc., No. 65, 20 (1978).
138. J. N. Israelachvili and G. E. Adams, J. Chem. Soc., Faraday Trans. I, 74, 975 (1978).
139. G. Peschel, P. Belouschek, M. M. Müller, M. R. Müller, and R. König, Colloid Polymer Sci., 260, 444 (1982).
140. Ya. I. Rabinovich, B. V. Derjaguin, and N. V. Churaev, Adv. Colloid Interface Sci., 16, 63 (1982); Izv. Akad. Nauk SSSR, Ser. Khim., No. 8, 1743 (1982).
- 140a. D. W. R. Gruen and S. Marčelja, J. Chem. Soc. Faraday Trans. II, 79, 225 (1983).
- 140b. E. Ruckenstein and D. Schiby, Chem. Phys. Lett., 95, 435, 439 (1983).
- 140c. B. Jönsson and H. Wennerström, J. Chem. Soc., Faraday Trans. II, 79, 19 (1983).
141. W. van Megen and I. Snook, J. Chem. Soc., Faraday Trans. II, 75, 1095 (1979).
142. J. E. Lane and T. H. Spurling, Chem. Phys. Lett., 67, 107 (1979).
143. I. K. Snook and W. J. van Megen, J. Chem. Phys., 75, 4738 (1981).
144. V. Ya. Antonchenko, V. V. Ilyin, N. N. Makovsky, A. N. Pavlov, and V. P. Sokhan, Preprint ITP-82-43E, Kiev (1982).
145. D. Y. C. Chan, D. J. Mitchell, B. W. Ninham, and B. A. Pailthorpe, J. Chem. Soc., Faraday Trans. II, 74, 1098, 1116 (1978).
146. D. Y. C. Chan, D. J. Mitchell, B. W. Ninham, and B. A. Pailthorpe, Mol. Phys., 35, 1669 (1978); J. Chem. Soc., Faraday Trans. II, 75, 556 (1979).
147. D. J. Mitchell, B. W. Ninham, and B. A. Pailthorpe, J. Colloid Interface Sci., 64, 194 (1978).
148. F. H. Stillinger and A. Rahman, J. Chem. Phys., 60, 1545 (1974).
149. R. M. Pashley, J. Colloid Interface Sci., 80, 153 (1981).
150. A. W. Adamson and I. Ling, Adv. Chem., No. 43, Washington, D.C. (1964).
151. M. E. Tadros, P. Hu, and A. W. Adamson, J. Colloid Interface Sci., 49, 184 (1974).
152. A. W. Adamson, Physical Chemistry of Surfaces, 4th ed., Wiley-Interscience, New York (1982).
153. B. V. Derjaguin and A. D. Malkina, Kolloidn. Zh., 12, 431 (1950); Discuss. Faraday Soc., No. 18, 24 (1954).
154. B. V. Derjaguin, N. I. Moskвитин, and M. F. Futran, in: Proceedings of the 3rd USSR Conference on Colloid Chemistry, Izd. Akad. Nauk SSSR, Moscow (1956), p. 285.

155. B. V. Derjaguin and A. S. Titiyevskaya, Dokl. Akad. Nauk SSSR, 50, 307 (1945).
156. B. V. Derjaguin, Kolloid-Z., 69, 155 (1934); Zh. Fiz. Khim., 6, 1306 (1935).
157. T. N. Voropaeva, B. V. Derjaguin, and B. N. Kabanov, Dokl. Akad. Nauk SSSR, 128, 981 (1959); Kolloidn. Zh., 24, 396 (1962).
158. B. V. Derjaguin and T. N. Voropaeva, J. Colloid Interface Sci., 19, 113 (1964).
159. B. V. Derjaguin, A. V. Gorodetskaya, A. S. Titiyevskaya, and V. N. Yashin, Kolloidn. Zh., 23, 535 (1961).
160. G. Peschel, K. H. Adlfinger, and G. Schwartz, Naturwissenschaften, 61, 215 (1974).
161. G. Peschel and P. Belouschek, Prog. Colloid Polym. Sci., 60, 108 (1976); Z. Phys. Chem. (BRD), 108, 145 (1977).
162. J. N. Israelachvili, Philos. Mag., A43, 753 (1981).
163. R. M. Pashley, J. Colloid Interface Sci., 83, 531 (1981).
164. R. M. Pashley, J. Colloid Interface Sci., 80, 153 (1981).
165. R. M. Pashley, Adv. Colloid Interface Sci., 16, 57 (1982).
166. R. M. Pashley and J. N. Israelachvili, Colloids Surfaces, 2, 169 (1981).
167. C. Tanford, *The Hydrophobic Effect*, Wiley-Interscience, New York (1973).
168. J. Israelachvili and R. Pashley, Nature, 300, 341 (1982).
169. L. H. Allen and E. Matijević, J. Colloid Interface Sci., 31, 287 (1969); 33, 420 (1970).
170. R. D. Harding, J. Colloid Interface Sci., 35, 172 (1971).
171. Yu. P. Klementova, L. F. Kirichenko, and Z. Z. Vysotsky, in: *Surface Forces in Thin Films and Disperse Systems*, Nauka, Moscow (1972), p. 67; in: *Research in Surface Forces*, Vol. 4, Consultants Bureau, New York (1975), p. 60.
172. Yu. M. Chernoberezhsky, E. V. Golikova, and L. V. Malinovskaya, in: *Surface Forces in Thin Films and Stability of Colloids*, Nauka, Moscow (1974), p. 249.
173. Yu. M. Chernoberezhsky, G. F. Girfanova, L. M. Labunets, and E. V. Golikova, in: *Surface Forces in Thin Films*, Nauka, Moscow (1979), p. 67.
174. Yu. M. Glazman and M. E. Krasnokutskaya, Kolloidn. Zh., 27, 815 (1965); 28, 847 (1966); in: *Research in Surface Forces*, Vol. 3, Consultants Bureau, New York (1971), p. 189.
175. Yu. M. Glazman and G. I. Fuks, in: *Advances in Colloid Chemistry*, Nauka, Moscow (1973), p. 140.
176. Zh. G. Blashchuk and Yu. M. Glazman, in: *Research in Surface Forces*, Vol. 4, Consultants Bureau, New York (1975), p. 72.
177. Yu. Glazman, Croat. Chem. Acta, 52, 115 (1979).
178. G. D. Botsaris and Yu. M. Glazman, J. Dispers. Sci. Technol., 3, 67 (1982).
179. B. V. Derjaguin, N. M. Kudryavtseva, and I. Ya. Malikova, Dokl. Akad. Nauk SSSR, 216, 1319 (1974).
180. A. P. Tikhonov and E. G. Kirillova, Kolloidn. Zh., 44, 163 (1982).

181. B. V. Derjaguin, A. S. Titiyevskaya, and V. Kh. Vybornova, *Kolloidn. Zh.*, 22, 398 (1961).
182. A. Scheludko, *Adv. Colloid Interface Sci.*, 1, 391 (1967).
183. A. Scheludko, *Annuaire de l'Université de Sofia, fac. de Chimie*, Vol. 62, Sofia (1969), p. 47.
184. A. A. Baran, I. M. Solomentseva, V. V. Mank, and O. D. Kurilenko, *Dokl. Akad. Nauk SSSR*, 207, 363 (1972).
185. I. M. Solomentseva, A. A. Baran, G. P. Kiselev, and O. D. Kurilenko, *Kolloidn. Zh.*, 35, 699 (1973).
186. A. A. Baran and I. M. Solomentseva, *Kolloidn. Zh.*, 36, 1035 (1974).
187. A. A. Baran, I. M. Solomentseva, and O. D. Kurilenko, *Kolloidn. Zh.*, 37, 219 (1975).
188. L. M. Barclay and R. H. Ottewill, in: *Thin Liquid Films and Boundary Layers*, Academic Press, London (1971), p. 88.
189. P. F. Low and J. F. Margheim, *Soil Sci. Soc. Am. J.*, 43, 473 (1979).
190. P. F. Low, *Soil Sci. Soc. Am. J.*, 44, 667 (1980).
191. J. L. Oliphant and P. F. Low, *J. Colloid Interface Sci.*, 89, 366 (1982).
192. B. E. Viani, P. F. Low, and B. E. Roth, *J. Colloid Interface Sci.*, 96, 229 (1983).
193. V. A. Parsegian, *Adv. Colloid Interface Sci.*, 16, 49 (1982).
194. D. M. Le Neveu, R. P. Rand, and V. A. Parsegian, *Nature*, 259, 601 (1976); *Biophys. J.*, 18, 209 (1977).
195. G. Peschel and P. Belouschek, *Z. Naturforsch.*, A35, 869 (1980).
196. G. Peschel, P. Belouschek, and S. Erfle, in: *7th International Conference on Non-Aqueous Solutions*, Vol. 1, Regensburg (1980), p. 5.

Chapter 8

THE DERJAGUIN—LANDAU—VERWEY— OVERBEEK (DLVO) THEORY OF STABILITY OF LYOPHOBIC COLLOIDS

The most impressive achievement of the theory of surface forces has been its successful solution of the classical problem of colloid stability. The combination of long-range electrostatic and molecular forces provided the basis for a quantitative explanation of the stability of lyophobic colloids and the role played by electrolytes in their destabilization.

Lyophobic sols are colloids whose particles interact relatively weakly with the molecules of the dispersion medium. Consequently, interaction between particles is mainly through forces of electrostatic repulsion (when ionic atmospheres overlap) and dispersion forces. This concept was suggested as early as 1932 by Kallman and Willstätter [1]. It formed the basis of the theory of slow coagulation of weakly charged and high-dispersion colloids developed by Derjaguin [2, 3]. The stability of these dispersions is ascribed to a virtually zero rate of coagulation, though they are metastable.

Later, the theory of stability was generalized to include strongly charged colloids [4]. Subsequently, it was further generalized and presented in detail in a monograph [5].* Nowadays this theory is commonly referred to as the DLVO theory (for Derjaguin—Landau—Verwey—Overbeek).

8.1. EFFECTS OF ELECTROLYTES ON LYOPHOBIC COLLOIDS

A peculiar feature of lyophobic colloids is their dual response to electrolytes. On the one hand, the presence of small amounts of certain potential-determining ions in the dispersion medium is

*See also B. V. Derjaguin, Theory of Stability of Colloids and Thin Films, Nauka Moscow (1986), p. 205.

necessary for the whole lyophobic system to be stable against aggregation. On the other hand, the introduction of somewhat greater amounts of a low-molecular-weight electrolyte into a stable sol usually results first in slow and then, after passing a threshold, or critical, concentration, in fast coagulation of the sol. In fact, it is just this behavior of a sol in response to an electrolyte that is regarded as sufficient for classifying it as "lyophobic." In contrast, lyophilic colloids require a high concentration of electrolytes for coagulation — of the order of several moles per liter. A critical analysis of older theories and of empirical relations developed by March, Freundlich, Langmuir, Wolfgang Ostwald, Tezak, and others that explained the aggregative destabilization of lyophobic sols by electrolytes can be found in papers [2-4, 6, 7], in monographs [5, 8], and in textbooks of colloid chemistry [9].

The DLVO theory is based on the assumption that lyophobic sols are fundamentally unstable, and their persistence is kinetic in nature. In other words, the "stable state" must be interpreted as a "frozen" condition with practically zero rate of coagulation. In contrast to ordinary molecular or true solutions, the stability of lyophobic sols is due to long-range surface forces that present a potential energy barrier high enough to either greatly reduce or even completely prevent collisions between particles. Therefore, the most important theoretical problem is to analyze the force and potential curves obtained by a superposition of electrostatic repulsion and molecular attraction.

An analysis of the curves for pair interactions of particles in ordinary dilute dispersions gave the following results [4]. If an electrolyte solution is not too dilute, the interaction between particles at large and small distances is always dominated by attractive forces with a power-law dependence on the distance between surfaces (see Chapter 4). Indeed, the molecular component of disjoining pressure and the corresponding term of the free energy of interaction in a very narrow gap between two parallel plates are [10]

$$\Pi_m = - A / 6\pi h^3 \quad (8.1)$$

$$V_m = - A / 12\pi h^2 \quad (8.2)$$

where A is the Hamaker constant. The rings method* gives for two identical spheres with radius a

$$U_m = - a A / 12H \quad (8.3)$$

where H is the shortest distance between the surfaces. An expansion of the Hamaker formula [11] and Lifshitz's macroscopic theory [12, 13] also gives this formula. If electromagnetic retardation is

*B. V. Derjaguin, Kolloid Z., 69, 155 (1934).

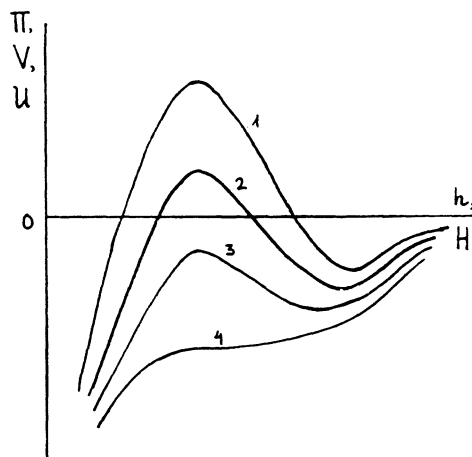


Fig. 8.1. Force or energy of interaction as a function of separation between surfaces (see explanation in the text).

taken into account, the exponent with distance in the above formulas increases by unity.

Under certain conditions the forces of electrostatic repulsion can prevail at intermediate distances between particles. These forces are exponential (see Chapter 6) everywhere except at short distances (less than the Debye length) where a power law may operate [Langmuir's formula (6.35), Chapter 6]. However, here the dependence on distance h is not as steep as for molecular interaction. Thus, the electrostatic pressure is proportional to h^{-2} while the molecular pressure is proportional to h^{-3} . The situation is graphically plotted by a force or energy curve with two minima separated by a maximum (curve 1 in Fig. 8.1). A sufficiently high maximum corresponds to a kinetically stable (or "stable") state of a disperse system or a liquid film. An increase in electrolyte concentration results in either a decrease of surface electrostatic potential, owing to adsorption of counterions, or a contraction of the diffuse ion layer, or both effects simultaneously. In any case, this is accompanied by a lowering of the repulsion barrier and reduction of the kinetic stability. A slow-rate coagulation of the sol starts (curve 2 in Fig. 8.1). After a certain electrolyte concentration is reached, attractive forces become dominant, irrespective of the distance (curve 3), and high-rate reversible coagulation of the colloid sets in. Further increase in the concentration of the electrolyte leads to complete disappearance of the maximum on the diagram (curve 4), although this leaves the rate of coagulation practically unaffected.

8.2. KINETICS OF COAGULATION OF LYOPHOBIC COLLOIDS

The pattern outlined above gives only a qualitative description of the mechanism by which aggregative stability is destroyed; but it suggests a way of establishing a quantitative criterion of kinetic stability — by an analysis of coagulation kinetics and the calculation of coagulation rates.

The classical theory of the kinetics of irreversible coagulation of colloids was developed by Smoluchowski in 1917 [14], long before the DLVO theory was born. Its main shortcoming was that it ignored the spatial variation of interaction forces between colloidal particles. Hence, it could not relate coagulation rate to the parameters of the interaction potential. It was assumed that at the maximum rate of coagulation each encounter ("collision") of particles is "effective," i.e., produces irreversible adhesion or merging of the particles. Smoluchowski showed that the rate of change of the overall numerical concentration v of particles and aggregates (consisting of arbitrary numbers of identical original particles) is described by an equation that formally coincides with the equation of bimolecular reaction:

$$\dot{v} = -Kv^2 \quad (8.4)$$

In $1/v$ vs. t coordinates the solution of Smoluchowski's equation is a straight line:

$$v_0/v = 1 + t/T_{1/2} \quad (8.5)$$

where

$$T_{1/2} = 3\eta/4kTv_0 \quad (8.6)$$

is the coagulation half-time, η is the viscosity and T the temperature of the dispersion medium, and v_0 is the initial number of particles and aggregates per unit volume. In water at room temperature

$$T_{1/2} \approx 2 \cdot 10^{11}/v_0, \quad s \quad (8.7)$$

where v_0 is measured in cm^{-3} . This formula is largely supported by experimental data. For a quantitative description of "slow" coagulation, Smoluchowski formally introduced into the coagulation equation an efficiency factor $\alpha \leq 1$; α characterizes the fraction of collisions that result in new aggregates. The introduction of this factor is equivalent to increasing the coagulation half-time by a factor of $1/\alpha$.

The physical meaning of the collision efficiency factor was clarified by Derjaguin in [2] by employing a formula derived by Fuchs for the coagulation of aerosols [15]. As follows from this formula, mutual repulsion of particles must reduce the coagulation rate by a factor W , viz.,

$$W = \frac{2\alpha}{2\alpha} \int_{r_0}^{\infty} \exp[U(r)/kT] \frac{dr}{r^2} \quad (8.8)$$

where $U(r)$ is the interaction potential, and r is the center-to-center distance between particles. This gives $\alpha = 1/W$. Formula (8.8) is obtained by solving the equation for the stationary diffusion flux J of particles in a field of central forces $U(r)$ generated by the particles themselves.

8.3. COAGULATION CRITERIA

By using Eq. (8.8), it proved possible to explain qualitatively all specific features of the transition from kinetic stability to a slow, and then fast, coagulation when the electrolyte concentration in the solution increases [3]. Indeed, the presence of a barrier with height U_{\max} on the potential curve $U(r)$ makes possible an evaluation of the integral in (8.8) by the steepest descent method, so that in a crude approximation

$$W \sim \exp(U_{\max}/kT) \quad (8.9)$$

A high barrier then corresponds to $W \gg 1$ and, hence, the rate constant tends to zero. A reduced barrier height reduces W and increases the coagulation rate, and a vanishing barrier,

$$U_{\max} = 0 \quad (8.10)$$

corresponds to the practically maximal rate of coagulation, when $W \approx 1$. For small (Brownian) platelets the sticking will be the fastest if

$$V_{\max} = 0 \quad (8.11)$$

and for thin planar interlayers between solids the stability will break down spontaneously if

$$\Pi_{\max} = 0 \quad (8.12)$$

The stability of large non-Brownian particles with curved surface is destroyed if the force barrier between them vanishes:

$$F_{\max} = 0 \quad (8.13)$$

By virtue of relation (2.50), this condition is equivalent to (8.11). Starting with (8.8) and making use of expression (6.65) for the energy of repulsion of weakly charged particles, Derjaguin [3] quantitatively elaborated and gave a theoretical basis to a

well-known empirical Eilers-Korff rule that relates the electrokinetic potential ζ and the Debye radius l/κ at the coagulation threshold:

$$\zeta_c^2/\kappa_c = \text{const} \quad (8.14)$$

where the subscript c refers to the critical state. It was shown in [3] that the theoretical criterion (8.14) must have the following form:

$$\epsilon\psi_{1c}^2/A\kappa_c \approx 1 \quad (8.15)$$

The constant on the right-hand side of Eq. (8.14) thereby gains a definite physical meaning, being expressed through quantities determining the intensity of the electrostatic and molecular interaction between particles.

If the potential ψ_{1c} is identical for counterions with unequal valence z, then Eq. (8.15) yields the "law of z^2 " for the threshold concentration n_c of weakly charged sols [see formula (8.24)]. By using conditions (8.10)-(8.13) with the appropriate expressions for molecular forces (8.1)-(8.3) and for electrostatic repulsion (6.52) and (6.61) substituted into them, Derjaguin and Landau derived the well-known law of z^6 for maximum-charge sols [4]:

$$n_c = B \frac{\epsilon^3 (kT)^5}{A^2 e^6 z^6} \quad (8.16)$$

where z is the valence of a counterion. B is a numerical coefficient weakly dependent on the values of the co-ion; it changes by a factor of 1.5-2 in the transition from Brownian to non-Brownian particles, and is shape-dependent (different for platelet and spherical particles). Equation (8.16) gives a quantitative form to the classical Schulze-Hardy rule. The law of z^6 is borne out by tables compiled in [4, 5, 8, 16].

Later, Verwey and Overbeek [5, 8] analyzed the coagulation behavior, by calculations and by a graphical analysis of interaction curves, not only in strongly and weakly charged sols but also in dispersions composed of particles with arbitrary surface potential, assumed constant in the course of approach. The simplest way to find the coagulation threshold as a function of the potential ψ_1 of the diffuse ionic layer is to use the approximate relation for disjoining pressure Π_e or for the free energy V_e of interaction, derived by superposition of the potentials of isolated double layers (see Chapter 6). The energy V_e of two identical double layers in solutions of symmetrical electrolytes with valence z is given by formula (6.57) [5, 8]:

$$V_e = \frac{8\epsilon\theta^2\kappa}{\pi z^2 e^2} \gamma^2 \exp(-\kappa h) \quad (8.17)$$

where $\gamma = \tanh(ze\psi_1/4\theta)$, $\theta = kT$.

Each of the conditions of destabilization (8.10), (8.11), or (8.12) is a system of two equations. Thus, (8.11) is equivalent to the equations

$$V_e + V_m = 0 \quad (8.18)$$

and

$$dV_e/dh + dV_m/dh = 0, \text{ i.e., } \Pi_e + \Pi_m = 0 \quad (8.19)$$

By combining these equations and employing Eq. (9.2) (i.e., neglecting electromagnetic retardation), we arrive at the following equation:

$$h \frac{d \ln V_e}{dh} = \frac{d \ln V_m}{d \ln h} = -2 \quad (8.20)$$

that leads to a relation between the unknown critical concentration n_c and the equally unknown coordinate h_c of the maximum in the "critical" state. Indeed, by substituting V_e from (8.17) into (8.20), we obtain

$$(\kappa h)_c = 2 \quad (8.21)$$

The relation thus obtained is therefore independent of the potential ψ_1 in the superposition approximation that strictly holds at large values of κh . Now we make use of (8.21) to express h_c in Eqs. (8.17) for V_e and (8.2) for V_m in terms of the Debye length $1/\kappa$, equate V_e and $-V_m$ as follows from (8.18), take the square of the equality so obtained, recall the definition of the reciprocal Debye length (1.30),

$$\kappa^2 = 8\pi e^2 z^2 n / \epsilon \theta \quad (8.22)$$

and obtain the critical electrolyte concentration ($1/\text{cm}^3$) as an explicit function of the parameters of the system [5, 8]:

$$n_c \approx 107 \frac{\epsilon^3 (kT)^5}{z^6 e^6 A^2} \tanh \left(\frac{ze\psi_1}{4kT} \right) \quad (8.23)$$

The same dependence of n_c on the parameters of the system is found by applying criteria (8.12) or (8.10). The only difference is that for $\Pi_{\max} = 0$ the distance is $h_c = 3/\kappa_c$ and the numerical coefficient in (8.23) equals 166, while for $U_{\max} = 0$ the distance is $h_c = 1/\kappa_c$ and the coefficient 50.

At high potentials $ze\psi_1 \gg 4kT$ formula (8.23) immediately yields the limiting relation (8.16) because here $\tanh x \approx 1$. It can be readily found that in univalent electrolytes this relation holds for $\psi_1 \gtrsim 200-250$ mV. At low potentials the expansion $\tanh x \approx x$ gives

$$n_c \approx 0.42 \frac{\epsilon^3 k T \psi_1^4}{z^2 e^2 A^2} \quad (8.24)$$

This is completely equivalent to condition (8.15) if we take into account relation (8.22) between n_c and κ_c . As follows from (8.24), in weakly charged sols the "law of z^6 " must be replaced with the "law of z^2 " if the change in counterion valence does not affect the potential ψ_1 , and coagulation results from a strong contraction of ionic double layers (concentration coagulation). This dependence of n_c on z is indeed observed in some cases, although more often than not it points to coagulation involving the secondary minimum [17, 18].

Although the simple approximate formula (8.23) provides a faithful description of the basic features of the observed effects of electrolytes on coagulation sols, it raises a number of questions and objections. The two most important are:

- i) Will the conclusions change and, if so, how, if the problem is solved rigorously, with the exact expressions for U_e , V_e , and U_e given in Chapter 6?
- ii) Will the criterion change in the transition to a different mechanism of surface charge formation if the diffuse layer potential is not preserved during the approach of the particles? (This can be best clarified in the opposite extreme case of constant surface charge density σ .)

8.4. EXACT SOLUTION

As an example, let us consider how the stability criterion is obtained for platelet Brownian particles ($V_{max} = 0$) at $\psi_1 = \text{const}$ [19]. In Chapter 6 we found a parametric dependence of the energy of repulsion V^ψ [see (6.55)] on distance h expressed in Debye lengths [Eq. (6.30)]. This dependence has the following form [19]:

$$\begin{aligned} V^\psi = & \frac{4n\theta}{\kappa} \left\{ -\frac{2}{k}(1 - k^2)F(\varphi, k) + \frac{4}{k} \left[E(\varphi, k) - k \right. \right. \\ & \left. \left. + \tan \left(\frac{\pi}{4} - \frac{\varphi}{2} \right) \sqrt{1 - k^2 \sin^2 \varphi} \right] \right\} \end{aligned} \quad (8.25)$$

$$\langle h \rangle = 2kF(\varphi, k) \quad (8.26)$$

where $F(\varphi, k)$ and $E(\varphi, k)$ are elliptic integrals of the first and second kind, with modulus k and amplitude φ related to the potentials of symmetry plane ψ_d and of the diffuse layer boundary ψ_1 ,

$$k = 1/\cosh(ze\psi_d/2\theta) \quad (8.27)$$

$$\varphi = \arccos[\sinh(ze\psi_d/2\theta)/\sinh(ze\psi_1/2\theta)] \quad (8.28)$$

The independent variable is, therefore, the potential ψ_d ; at a fixed ψ_1 this potential determines the two parameters k and φ and the corresponding pair of values of V and h . The same parameters determine the value of disjoining pressure Π_e [see (6.52)]:

$$\Pi_e = 4n\theta(1/k^2 - 1) \quad (8.29)$$

By substituting h from (8.26) into (8.1), and then (8.1) and (8.29) into (8.19), and taking into account (8.22), we arrive at the following coagulation criterion [19, 20]:

$$n_c^\psi = \frac{72}{\pi} \frac{\epsilon^3 \theta^5}{A^2 e^6 z^6} k_c^2 (1 - k_c^2)^2 F^6(\varphi_c, k_c) \quad (8.30)$$

Here the dependence on the potential ψ_{1c} is "hidden" in the last three factors. The relation between φ_c and k_c in the critical state is found from the equation [19]

$$\begin{aligned} \frac{3}{4}(1 - k_c^2)F(\varphi_c, k_c) &= E(\varphi_c, k_c) - k_c \\ + \tan\left(\frac{\pi}{4} - \frac{\varphi_c}{2}\right)\sqrt{1 - k_c^2 \sin^2 \varphi_c} \end{aligned} \quad (8.31)$$

This is obtained by substituting (8.25), (8.26), and (8.29) into (8.20), taking into account that $dV_e/dh = -\Pi_e$. A number of solutions of this equation are listed in Table 8.1, together with the values of $\langle h \rangle_c$ and of the product $k_c^2(1 - k_c^2)F^6(\varphi_c, k_c)$. This table shows that $\langle h \rangle_c$ is a weakly increasing monotonic function of increasing ψ_1 ; but on the whole it is quite close to the value $\langle h \rangle_c = 2$ found above by means of the superposition approximation. This occurs because the potential in the symmetry plane is relatively low in the critical state, even for highly charged surfaces. It does not exceed $25 \times 2.442 \approx 60$ mV. In addition, the exact functional dependence $n_c^\psi(\psi_1)$ is quite close to the approximate one that includes $\tanh^4(ze\psi_1/40)$. The ratio of the approximate to the exact coagulation thresholds is almost independent of the potential ψ_1 .

Similar calculations were carried out for criteria (8.12) [20] and (8.10) [19]. A separate analysis was given in [19] of the case

TABLE 8.1. Solutions of Eq. (8.38) and Critical Concentrations

$\frac{ze\psi_{1c}}{kT}$	$\frac{ze\psi_{dc}}{kT}$	$(\kappa h)_c$	$\frac{72}{\pi} k_c^2 (1 - k_c^2) F_c^6$	$107 \tanh^4 \left(\frac{ze\psi_{1c}}{4kT} \right)$	$(5):(4)$
0	0	2.218	0	0	-
0.295	0.175	2.216	0.00244	0.00313	1.28
0.613	0.352	2.210	0.040	0.057	1.43
0.972	0.530	2.198	0.210	0.345	1.64
1.243	0.713	2.190	0.611	0.88	1.28
1.615	0.902	2.180	1.815	2.31	1.27
2.030	1.099	2.160	4.00	5.13	1.28
2.528	1.306	2.136	8.16	10.5	1.28
3.114	1.525	2.090	14.74	19.3	1.31
3.913	1.762	2.044	26.15	34.3	1.31
5.105	2.022	1.982	43.9	57.3	1.31
7.693	2.308	1.900	70.3	90.2	1.28
∞	2.442	1.858	84.1	107	1.27

of low ψ_1 where an exact analytical solution exists, and of the case $\psi_1 \gtrsim 50$ mV where a good parametric approximation (6.71) is possible. All the conclusions formulated above are confirmed also in these two cases. The main conclusion is that the hyperbolic tangent to the fourth power fits very well the curve $n_c^\psi(\psi_1)$ in all cases, but the corresponding coefficients deviate, although not seriously, from the predictions of the superposition formulas.

8.5. EFFECT OF CHARGING MECHANISM

In Chapter 6 we gave the exact expression for V_e , obtained in [21], valid for the calculation of the function $V_e(h)$ whatever the mechanism of surface charging. The same paper also demonstrated that the energy V_e can be expected to differ significantly for different mechanisms only at short distances of the order of one Debye length. These distances were found to be the shorter the higher the potentials of the isolated surfaces. The weakest repulsion corresponds to the condition $\psi_1 = \text{const}$, and the strongest to $\sigma = \text{const}$ [19]. Detailed tables illustrating this effect were also published by Honig and Mul [22].

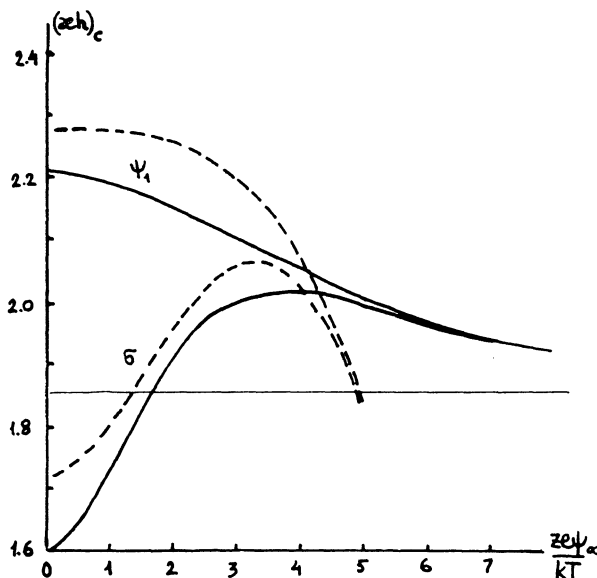


Fig. 8.2. Critical interlayer thickness as a function of surface potential. Upper curves correspond to a constant potential. Solid curves refer to [19] and dashed curves to [23]. The horizontal line gives the limiting value.

Exact analytical criteria of stability for flat and curved surfaces at $\sigma = \text{const}$ were also derived [19]. The calculated curves $n_c(\psi_{1\infty})$, where $\psi_{1\infty} = \psi_1(\infty)$ is the potential of an isolated double layer, were indistinguishable in all the cases analyzed, for $\psi_1 = \text{const}$ and for $\sigma = \text{const}$, when $z\psi_{1\infty} \gtrsim 100$ mV. For maximum-charge surfaces the criteria coincide exactly with those found by Derjaguin and Landau [4]. However, at $\sigma = \text{const}$ the coagulation thresholds for low potentials are approximately twice those at $\psi_1 = \text{const}$. The coagulation threshold can thus depend on the charging mechanism only if the double layer potential at the critical state does not exceed, say, $50/z$ mV. Later, Honig and Mul [22] and also Jones and Levine [23] came to this conclusion; the method used was an approximate calculation of repulsion energy at $\sigma = \text{const}$, leading to certain errors in the dependence of $(\langle h \rangle)_c$ on the potential of isolated double layer $\psi_{1\infty}$ (Fig. 8.2) but leaving the principal conclusion unchanged.

All the results obtained in [19] are plotted in Fig. 8.3; the curves show that the hyperbolic tangent representation can be used for coagulation thresholds in moderately and highly charged sols, after the exact limiting value of the required numerical constant has been previously established. In all the cases analyzed, the limiting z^6 behavior holds only when $z\psi_{1c} > 200$ mV. In order to

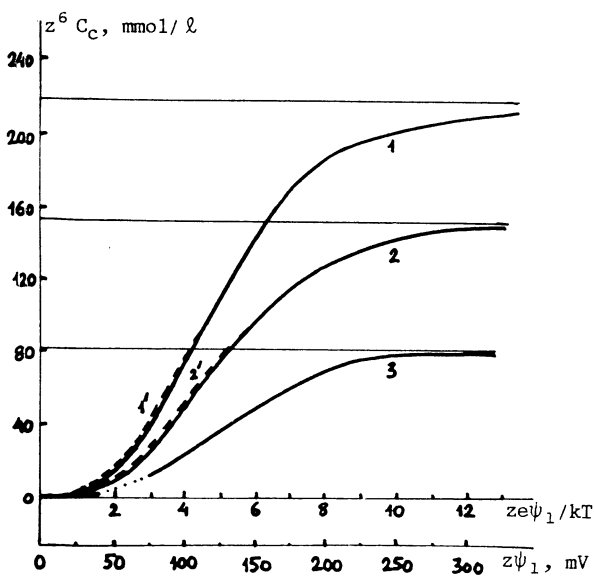


Fig. 8.3. Critical electrolyte concentration as a function of surface potential: 1, 1') flat particles, force barrier; 2, 2') spherical particles, force barrier, or platelet particles, potential barrier; 3) spherical particles, potential barrier. Curve 1' is plotted after [20], and the remaining curves after [19]. Solid curves correspond to a constant potential, and dashed curves to constant surface charge. Horizontal lines indicate the corresponding limiting values. (The results were found for $\epsilon = 80$, $kT = 4 \cdot 10^{-14}$ erg, $A = 2 \cdot 10^{-12}$ erg.)

explain why, in practice, this law holds at lower potentials (according to numerous experiments), it is necessary to assume that as a result of adsorption on the surface the diffuse layer potential ψ_1 is reduced in the transition to counterions with a higher valence z . Glazman [24] was the first to notice that if in critical conditions the equality $z\psi_{1c} = \text{const}$ holds, then the law of z^6 is strictly obeyed at the critical concentration not only in highly charged sols, but in weakly charged ones as well, and that in the latter case the Eilers-Korff rule holds, too [in the form (8.15) derived by Derjaguin]. In order to substantiate this possibility, Langmuir's adsorption isotherm for counterions was used, and it was concluded [25] that the required result can be obtained by stipulating an approximate equality of the adsorption constants for counterions of unequal charge and different species. Later Us'yarov [26] made a more detailed analysis of the conditions under which

$z\psi_{1c} = \text{const}$ [26]. Obviously, this equality can be expected to materialize only very approximately, because adsorption is specific.

Experimentally found coagulation thresholds are indeed known to deviate from the law of z^6 , and sometimes quite substantially.

8.6. FURTHER DEVELOPMENT AND VERIFICATION OF THE DLVO THEORY

A large number of papers devoted to the development of the DLVO theory appeared after it was first formulated [2-5, 8]: the development involved both dropping a number of restrictive assumptions and elaborating for conditions representing actual experiments on destabilization of hydrophobic colloids.

We shall analyze here only those papers that fall within the scope of this monograph. Certain aspects of the theory of the stability of lyophobic colloids were studied by Barboi: effects produced by the potential of the particles, co-ion charge, and electrolyte composition on coagulation thresholds [27]. These calculations were based on analyzing the balance of molecular attraction and electrostatic repulsion in systems composed of planar particles with fixed potential of diffuse double layer. The Brownian motion of particles was completely ignored. Conversely, Kligman and Glazman gave a detailed analysis of the kinetic aspects of stability [28]. Glazman, Barboi, and co-workers showed [29] that such phenomena as additivity, antagonism, and synergism observed in mixtures of ions can be explained, in principle, by a model of interacting planar particles, under certain assumption on the adsorbability of specific ions at the interface between the dispersion medium and the disperse phase. The observed experimental difference in the sensitivity of concentrated and dilute dispersions of the same composition to electrolytes led to the conclusion on the necessity of taking into account collective interactions in dispersions of high concentration [30]. The model suggested for this purpose [31] made it possible to interpret a number of observed effects. Nevertheless, the model cannot be regarded as universal because it simulates a high-concentration sol by a system, strictly periodic in one direction, of flat platelets of identical thickness, resembling accordion pleats, with interparticle distances depending on concentration of the disperse phase.

Recently, these ideas were developed further by statistical mechanics, and applied to the description of colloidal phase transitions [32] and to the properties of periodic colloidal systems formed in high-concentration dispersions of spherical and anisometric particles in water [18, 33]. It was found that many of these properties, not only static but dynamic as well, can be described quantitatively by the so-called DLVO potential, i.e., the

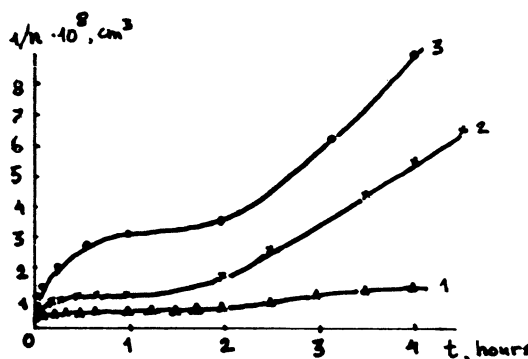


Fig. 8.4. The reciprocal particle concentration as a function of time. Blue gold sol, KCl electrolyte: 1) $5 \cdot 10^{-3}$; 2) $1 \cdot 10^{-2}$; 3) $2 \cdot 10^{-2}$ mole/liter [37].

algebraic sum of the potentials of the molecular and electrostatic interactions (Chapters 4 and 6), using the conventional or appropriate modified techniques of statistical mechanics. However, we shall omit these interesting topics from this monograph.

Derjaguin and Smilga were the first to analyze theoretically the effect of electromagnetic retardation, discussed in Chapter 4, on coagulation of maximally charged sols [34]. They demonstrated that in this case the valence of counterions affects the threshold concentration n_c less strongly than the Derjaguin-Landau law of z^6 predicts [see formula (8.16)]. As a result of retardation, n_c is inversely proportional to the fourth, not the sixth, power of counterion charge ze :

$$n_c \sim \epsilon^2 (kT)^3 / B z^4 e^4 \quad (8.32)$$

[B is the constant of retarded molecular force, Eq. (4.25)]. The experimentally observed dependence of n_c on z for polyvalent ions is stronger than that prescribed by (8.32). In [34] this is ascribed to an enhanced adsorbability of these ions and to the corresponding reduction in the charge and potential of the particles. Rabinovich carried out a theoretical analysis of the retardation effect for particles with arbitrary charge [35]. He concluded that a substantial difference between theoretical estimates of n_c , taking retardation into account or neglecting it, can be expected only for electrolytes containing three- and four-valent counterions.

An important experimental advance was the development by Derjaguin and Vlasenko of the flow ultramicroscope, utilized by Kudryavtseva in direct measurements of the number concentration of particles and of concentration changes caused by coagulation in de-

stabilized hydrosols of gold and AgI [36, 37]. This technique made it possible to establish that Smoluchowski's linear time dependence (8.5) for the reciprocal particle concentration holds (approximately) only in the rapid coagulation phase. In slow coagulation the kinetic curves had a complicated shape, often being S-shaped (Fig. 8.4). In some cases concentration ceased to change, completely or temporarily, soon after coagulation started. It was concluded from these experiments [37] that horizontal segments on kinetic curves point to a dynamic equilibrium of coagulation and peptization. The net rate of change in the number of particles at the initial stage is, by the law of mass action,

$$\frac{dv_1}{dt} = -K_1 v_1^2 + K_2 v_2 \quad (8.33)$$

where v_1 and v_2 are the concentrations of single particles and doublets, and K_1 and K_2 are the corresponding rate constants for aggregation and disaggregation. The transition from a temporary equilibrium to a subsequent rapid coagulation was explained in [37] by the greater stability of aggregates composed of three or more particles than of doublets.

These ideas were later developed in a series of papers [38] devoted to a theory of reversible aggregation of particles at the secondary potential well discussed above (see Fig. 8.1). Verwey and Overbeek suggested in 1948 [5] using as a quantitative estimate of the degree of this aggregation the quantity

$$\Delta n = n_0 \int 4\pi r^2 \exp\left[-\frac{U(r)}{kT}\right] dr \quad (8.34)$$

in which n_0 is the concentration of initial particles, and the integration is carried out over the region of the secondary minimum. The quantity Δn is the number of particles that on average are associated with any of the particles of the disperse phase, assuming that the distribution density of the disperse phase around a given particle in equilibrium is described by the Boltzmann law. This definition means that for a low degree of association this is also the fraction of associated particles in the dispersion. Verwey and Overbeek suggested an equality

$$n \geq 0.1 \quad (8.35)$$

as the condition of coagulation at the secondary minimum; but the number at the right-hand side was chosen only intuitively. (In a later monograph [8], Overbeek reviewed only the experimental facts supporting the argument of secondary aggregation with respect to coarse particles larger than 1 μm .)

It was also shown [38] how the coagulation criterion at the secondary minimum can be rigorously derived on the basis of generalized equations of coagulation kinetics, taking into account possible decay of the aggregates produced. The threshold concentration n_c was found to depend only very weakly on the particle potential; but it is an explicit function of concentration of the disperse phase and particle size, represented by an approximate formula

$$n_c \propto \frac{\varepsilon(kT)^3}{z^2 e^2 A^2 \alpha^2} \log^2 \left(\frac{1}{\alpha^3 n_0} \right) \quad (8.36)$$

Us'yarov and Rabinovich [39, 40] came to similar conclusions. Muller [41] analyzed the kinetics of aggregation at both potential minima simultaneously, and derived the kinetic coefficients relating the aggregation and disaggregation probabilities to the parameters of the DLVO potential.

REFERENCES

1. H. Kallman and M. Willstätter, *Naturwissenschaften*, 20, 952 (1932).
2. B. V. Derjaguin, *Izv. Akad. Nauk SSSR, Ser. Khim.*, No. 5, 1153 (1937); *Acta Physicochim. URSS*, 10, 333 (1939).
3. B. V. Derjaguin, *Trans. Faraday Soc.*, 36, 203, 730 (1940); *Kolloidn. Zh.*, 6, 291 (1940); 7, 285 (1941).
4. B. V. Derjaguin and L. D. Landau, *Acta Physicochim. URSS*, 14, 633 (1941); *Zh. Eksp. Teor. Fiz.*, 11, 802 (1941); reprinted: *Zh. Eksp. Teor. Fiz.*, 15, 663 (1945).
5. E. F. Verwey and J. Th. G. Overbeek, *Theory of the Stability of Lyophobic Colloids*, Elsevier, Amsterdam (1948).
6. S. Levine and E. Matijević, *J. Colloid Interface Sci.*, 23, 188 (1967); *Nature*, 197, 1196 (1963).
7. B. V. Derjaguin, *Usp. Khim.*, 48, 675 (1979).
8. H. R. Kruyt (ed.), *Colloid Science. Irreversible Systems*, Vol. 1, Elsevier, Amsterdam (1952).
9. S. Voyutsky, *Colloid Chemistry*, Mir, Moscow (1978), p. 316; D. A. Fridriksberg, *Textbook of Colloid Chemistry*, Khimiya, Leningrad (1975), p. 247; E. D. Shchukin, A. V. Pertsov, and E. A. Amelina, *Colloid Chemistry*, Mosk. Gos. Univ., Moscow (1982); Yu. G. Frolov, *Textbook of Colloid Chemistry. Surface Phenomena and Disperse Systems*, Khimiya, Moscow (1982), p. 325.
10. J. H. de Boer, *Trans. Faraday Soc.*, 32, 10 (1936).
11. H. C. Hamaker, *Physica*, 4, 1058 (1937).
12. E. M. Lifshitz, *Zh. Eksp. Teor. Fiz.*, 29, 94 (1955).
13. I. E. Dzyaloshinskii, E. M. Lifshitz, and L. P. Pitaevskii, *Zh. Eksp. Teor. Fiz.*, 37, 229 (1959); *Usp. Fiz. Nauk*, 73, 381 (1961); *Adv. Phys.*, 10, 165 (1961).

14. M. Smoluchowski, *Z. Phys. Chem.*, 92, 129 (1917).
15. N. Fuchs, *Z. Phys.*, 89, 736 (1934).
16. W. Ostwald, *Kolloid-Z.*, 88, 1 (1939).
17. I. F. Efremov and O. G. Us'yarov, *Usp. Khim.*, 45, 875 (1976).
18. I. F. Efremov, Periodic Colloid Structures, in: *Surface and Colloid Science*, E. Matijević (ed.), Vol. 8, Chap. 2, Wiley, New York (1975).
19. V. M. Muller, in: *Research in Surface Forces*, Vol. 3, B. V. Derjaguin (ed.), Consultants Bureau, New York (1971), p. 236; *Kolloidn. Zh.*, 31, 427, 548 (1969).
20. V. M. Barboi, *Kolloidn. Zh.*, 25, 385 (1963).
21. V. M. Muller, in: *Surface Forces in Thin Films and Stability of Colloids*, Nauka, Moscow (1974), p. 245.
22. E. P. Honig and P. M. Mul, *J. Colloid Interface Sci.*, 36, 258 (1971).
23. J. E. Jones and S. Levine, *J. Colloid Interface Sci.*, 30, 241 (1969).
24. Yu. M. Glazman, *Kolloidn. Zh.*, 24, 275 (1962).
25. V. M. Barboi, Yu. M. Glazman, and I. M. Dykman, *Kolloidn. Zh.*, 24, 382 (1962).
26. O. G. Us'yarov, *Kolloidn. Zh.*, 37, 79 (1975); *Dokl. Akad. Nauk SSSR*, 230, 381 (1976).
27. V. M. Barboi, *Kolloidn. Zh.*, 25, 385 (1963); 26, 409 (1964); 27, 494 (1965).
28. F. I. Kligman and Yu. M. Glazman, in: *Research in Surface Forces*, Vol. 3, B. V. Derjaguin (ed.), Consultants Bureau, New York (1971), p. 198.
29. V. M. Barboi, Yu. M. Glazman, and I. M. Dykman, *Kolloidn. Zh.*, 23, 376, 381 (1961); Yu. M. Glazman and E. F. Zhel'vis, *Kolloidn. Zh.*, 24, 405 (1962); V. M. Barboi and Yu. M. Glazman, in: *Research in Surface Forces*, Vol. 3, B. V. Derjaguin (ed.), Consultants Bureau, New York (1967), p. 183.
30. E. F. Zhel'vis and Yu. M. Glazman, *Kolloidn. Zh.*, 29, 196 (1967).
31. B. V. Barboi, V. M. Barboi, Yu. M. Glazman, and I. M. Dykman, *Kolloidn. Zh.*, 31, 660 (1969); in: *Research in Surface Forces*, Vol. 4, B. V. Derjaguin (ed.), Consultants Bureau, New York (1975), p. 39.
32. G. A. Martynov and V. M. Muller, *Dokl. Akad. Nauk SSSR*, 207, 370 (1972); *Kolloidn. Zh.*, 36, 687 (1974).
33. I. Langmuir, *J. Chem. Phys.*, 6, 885 (1938); L. Onsager, *Ann. N. Y. Acad. Sci.*, 51, 627 (1949); P. A. Hiltner and I. M. Krieger, *J. Phys. Chem.*, 73, 2386 (1969); S. Hachisu and Y. Kobayashi, *J. Colloid Interface Sci.*, 42, 342 (1972); W. van Megen and J. Snook, *J. Colloid Interface Sci.*, 57, 40, 47 (1976).
34. B. V. Derjaguin and V. P. Smilga, *Dokl. Akad. Nauk SSSR*, 153, 377 (1963); *Kolloidn. Zh.*, 26, 589 (1964).
35. Ya. I. Rabinovich, *Kolloidn. Zh.*, 41, 881, 889 (1979).

36. B. V. Derjaguin, G. Ja. Vlasenko, A. I. Storozhilova, and N. M. Kudryavtseva, *J. Colloid Sci.*, 17, 605 (1962); B. V. Derjaguin and N. M. Kudryavtseva, *Kolloidn. Zh.*, 26, 61 (1964).
37. B. V. Derjaguin and N. M. Kudryavtseva, in: *The Law of Mass Action. A Centenary Volume*, Universitetsforlaget, Oslo (1964), p. 79.
38. G. A. Martynov and V. M. Muller, *Dokl. Akad. Nauk SSSR*, 207, 370, 1161 (1972); in: *Research in Surface Forces*, Vol. 4, B. V. Derjaguin (ed.), Consultants Bureau, New York (1975), p. 3; *Kolloidn. Zh.*, 34, 716 (1972); V. M. Muller, *Kolloidn. Zh.*, 40, 885 (1978).
39. O. G. Us'yarov and M. V. Serebrovskaya, in: *Research in Surface Forces*, Vol. 4, B. V. Derjaguin (ed.), Consultants Bureau, New York (1975), p. 51.
40. Ya. I. Rabinovich, *Kolloidn. Zh.*, 43, 78 (1981).
41. V. M. Muller, in: *Surface Forces in Thin Films*, Nauka, Moscow (1979), p. 30.

Chapter 9

THE THEORY OF HETEROFOAGULATION IN LYOPHOBIC SYSTEMS

An analysis of binary mixtures of particles belonging to different classes meets with additional difficulties when the particles differ in charge and potential. The difference may lie not only in the magnitude but also in the sign of charge; for instance, the points of zero charge of the two dispersed materials may fall on different sides of the value of pH of their common dispersion medium. As a result, the interaction between particles is not necessarily repulsive.

There is, however, another factor — less evident but not less important — that distinguishes heterodispersions from homodispersions. It was shown [1-5] (see Chapter 4) that the constant A of molecular interaction between two bodies of different nature through a liquid continuous phase can be positive (corresponding to the attraction between particles) or negative (corresponding to repulsion).

The theory of stability of such nonidentical bodies in electrolyte solutions can be constructed by analogy to the procedure used in the preceding chapter. In this way the theory was developed by one of us [2] in 1954. The problem proved more complicated technically than that of destabilization of homodispersions. Nevertheless, the principle of the solution again lies in analyzing the force or potential diagrams, taking into account electrostatic and dispersion forces. A high barrier indicates stability, and its disappearance adhesion. Let us consider the conclusions that follow from the theory in the cases in which dispersion forces correspond to attraction ($A > 0$) and to repulsion ($A < 0$).

9.1. DESTABILIZATION CRITERIA FOR HETERO DISPERSIONS WITH POSITIVE HAMAKER CONSTANT

If the dispersion interaction between two particles of different nature results in attraction between them, the force or potential barrier preventing their coagulation or adhesion can exist only if the charges on the particles are of like sign. Two main electrolyte-induced destabilization modes can be singled out (Chapter 8). The first occurs when the electrostatic potential of particles decreases below a certain critical value ψ_c satisfying Eq. (8.22) [6]:

$$\epsilon \psi_c^2 / \kappa_c A = \text{const} \quad (9.1)$$

in which ϵ is the static permittivity of the medium, and κ_c is the reciprocal Debye length at the critical electrolyte concentration leading to destabilization. This is the so-called neutralization coagulation. Secondly, coagulation can occur at a high surface potential of particles, as a result of contraction of ionic double layers when electrolyte concentration increases to a critical value n_c given by equality (8.23) [7]:

$$n_c = \text{const} \frac{\epsilon^3 (kT)^5}{A^2 e^6 z^6} \quad (9.2)$$

where k is the Boltzmann constant, T is the absolute temperature, e is the electron charge, and z is the counterion valence. This is called concentration coagulation. When two nonidentical particles with unequal potentials ψ_1 and ψ_2 interact, it is interesting to establish the conditions of adhesion caused either by contraction of double layers such that the high values of both potentials ψ_1 and ψ_2 are preserved ($\psi_1 < \psi_2$), or by reduction of one (ψ_1) or both potentials. Let us analyze each of these modes separately, taking, for simplicity, the interaction of flat double layers in symmetric binary electrolytes.

Case 1. High Potentials. Obviously, the formulas for the explicit dependence of interaction energy and disjoining pressure on distance (derived in Section 6.8 by the linear approximation) cannot be used here either for a quantitative or a qualitative analysis because they are valid only for weakly charged surfaces. However, the necessary equations can be readily obtained in the general theory developed in Chapter 6. The calculations that follow are based on the first integral of the Poisson-Boltzmann equation (6.7) and the formula for disjoining pressure (6.12).

By introducing the notations

$$u = ze\psi/\theta, \xi = \kappa x,$$



$$\left. \begin{aligned} \kappa &= (8\pi e^2 z^2 n / \varepsilon \theta)^{1/2}, \quad \theta = kT \\ w &= -C/n\theta \end{aligned} \right\} \quad (9.3)$$

where n is the concentration and z the valence of the electrolyte, and C is the integration constant in Eq. (6.7), we rewrite these two equations in the following form:

$$\left(\frac{du}{d\xi} \right)^2 = 2(\cosh u - 1) - w \quad \left(\begin{array}{l} u_1 \leq u \leq u_2 \\ 0 \leq \xi \leq \kappa h \end{array} \right) \quad (9.4)$$

$$\Pi_e = n\theta w \quad (9.5)$$

We are considering the case of like-sign charged surfaces illustrated in Fig. 9.1a, b showing how the potential distribution ψ (a) and disjoining pressure Π_e (b) in the interlayer change when its thickness diminishes (see also Figs. 6.15 and 6.12). When potentials are unequal, the curve $\Pi_e(h)$ has a maximum Π_e^{\max} corresponding to an interlayer thickness h_{\max} . For interlayers with $h > h_{\max}$ the curve $\psi(x)$ has a minimum $\psi = \psi_m$ at $x = x_m$ (curve 1 in Fig. 9.1a) and hence, Eq. (9.4) can be solved by elliptic integrals in complete analogy to the procedure of deriving (6.30) for identical double layers. We then find

$$\kappa h = k[F(\varphi_1, k) + F(\varphi_2, k)] \quad (9.6)$$

$$w = 4(1/k^2 - 1) \quad (9.7)$$

where

$$F(\varphi, k) = \int_0^\varphi d\varphi / \sqrt{1 - k^2 \sin^2 \varphi} \quad (9.8)$$

is an elliptic integral of the first kind with modulus k and amplitude φ ,

$$k = 1/\cosh(u_m/2), \quad u_m = ze\psi_m/\theta \quad (9.9)$$

$$\varphi_1 = \arccos[\sinh(u_m/2)/\sinh(u_1/2)] \quad (9.10)$$

$$\varphi_2 = \arccos[\sinh(u_m/2)/\sinh(u_2/2)] \quad (9.11)$$

In Chapter 6 it was shown that Π_e reaches a maximum at an interlayer thickness h_{\max} at which $\psi_m = \psi_1$ (i.e., $u_m = u_1$), $x_m = 0$ (curve 2 in Fig. 9.1a) and, hence, by (9.10), $\varphi_1 = 0$ and $F(\varphi_1, k) = 0$. As follows from (9.9), (9.11), (9.7), and (9.6),

$$k_{\max} = 1/\cosh(u_1/2) \quad (9.12)$$

(Here and below the subscript max indicates that a quantity is taken at $\Pi = \Pi_e^{\max}$ and $h = h_{\max}$)

$$\varphi_2 = \varphi_{\max} = \arccos [\sinh(u_1/2)/\sinh(u_2/2)] \quad (9.13)$$

From the earlier assumption $u_1 < u_2$

$$w_{\max} = 4 \sinh^2(u_1/4) \quad (9.14)$$

$$\kappa h_{\max} = k_{\max} F(\varphi_{\max}, k_{\max}) \quad (9.15)$$

As the interlayer thins further, repulsion is replaced with attraction. The thickness h_0 at which this conversion occurs corresponds to the point $\Pi_e = 0$ in Fig. 9.1b. Integration of Eq. (9.4) with $w = 0$ (curve 3 in Fig. 9.1a) is carried out as in the derivation of Eq. (1.31) in Chapter 1, and we find

$$\kappa h_0 = \ln [\tanh(u_2/4)/\tanh(u_1/4)] \quad (9.16)$$

If the potentials u_1 and u_2 are low, formulas (9.16), (9.15), and (9.14) transform to the corresponding formulas (6.85), (6.87), and (6.88) derived in Chapter 6.

As follows from the formulas derived above, the interaction between two strongly but unequally charged surfaces can essentially depart from that in the symmetrical case only at very low values of κh . Indeed, at high dimensionless potentials u_1 and u_2 both hyperbolic tangents in (9.16) are close to unity, and the logarithm of their ratio, equal to κh_0 , tends to zero:

$$\kappa h_0 \approx 2(e^{-u_1/2} - e^{-u_2/2})$$

A simple calculation proves that at $\psi_1 = 100$ mV and $\psi_2 = 150$ mV the thickness h_0 is one sixth of the Debye screening length, and at $\psi_1 = 150$ mV and $\psi_2 = 200$ mV it is only one sixteenth of it. This is also the tendency for h_{\max} in (9.15) in which the modulus k_{\max} tends, by (9.12), to zero as the lower potential u_1 increases:

$$k_{\max} \approx 2 \exp(-u_1/2)$$

and at $k_{\max} \rightarrow 0$ the elliptic integral $F(\varphi_{\max}, k_{\max}) \approx \varphi_{\max}$ [see (9.8)]. At any rate, it never exceeds $\pi/2$ [this follows from (9.13)]. Therefore, if both potentials ψ_1 and ψ_2 are high, the difference between them can affect only the adhesive force between particles and the constraints on their reseptization but not the condition of onset of rapid coagulation and adhesion (corresponding to $\kappa h \approx 3$) derived in the preceding chapter and given by Eq. (9.2).

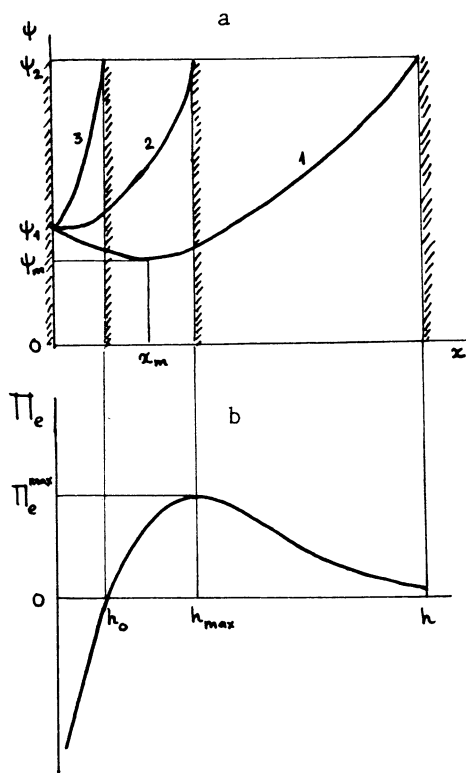


Fig. 9.1. Potential distribution (a) and electrostatic disjoining pressure (b) as functions of the thickness of interlayer between charged surfaces of like sign.

Case 2. One of the Potentials Is Low. The formulas derived above make it possible to analyze adhesion of two particles due to a fall in one of the potentials, ψ_1 . As an example, we choose

$$u_2 \gg 1 \gg u_1 \quad (9.17)$$

The adhesion of two flat surfaces can occur if the force barrier between them vanishes. Evidently, this condition corresponds to that value of Π_e whose abscissa lies to the right of the maximum on the $\Pi_e(h)$ curve in Fig. 9.1b (i.e., at $h > h_{\max}$). The curve $\psi(x)$ then has a minimum ψ_m (curve 1 in Fig. 9.1a) meeting an obvious inequality

$$u_m < u_1 \ll 1 \quad (9.18)$$

In this case Eq. (9.6) relating the interlayer thickness h parametrically to potentials u_1 , u_2 , and u_m can be transformed to an explicit relation between these quantities. At high u_2 the angle φ_2 in (9.11) tends to $\pi/2$, and the integral $F(\varphi_2, k)$ can be written, as shown in [8] [see Eq. (6.51)], in the form

$$F(\varphi_2, k) \approx K(k) - 1/k \sinh(u_2/2) \quad (9.19)$$

where $K(k)$ is a total elliptic integral of the first kind. By inequality (9.18), the modulus k defined by (9.9) is

$$k \approx 1 - u_m^2/8 \quad (9.20)$$

quite close to unity. But at $k \rightarrow 1$

$$K(k) \approx \ln(4/k'), k' = (1 - k^2)^{1/2} \quad (9.21)$$

(see [9]). As follows from (9.21) and (9.20), $k' = u_m/2$, and hence,

$$\kappa(h - x_m) = kF(\varphi_2, k) \approx \ln(8/u_m) - 1/\sinh(u_2/2) \quad (9.22)$$

If we take into account that both potentials u_m and u_1 are low, it can be readily shown that the second term on the right-hand side of Eq. (9.6) is

$$\kappa x_m = kF(\varphi_1, k) \approx \ln(u_1/u_m + \sqrt{(u_1^2/u_m^2) - 1}) \quad (9.23)$$

This can be done via definitions (9.9) and (9.10); but a simpler way is to integrate Eq. (9.4) in the range $u_m \leq u \leq u_1 \ll 1$, i.e., to integrate along curve 1 in Fig. 9.1a on the left of x_m . Taking into account (9.7) and (9.20), the equation is simplified to

$$du/d\xi = -\sqrt{u^2 - u_m^2} \quad (9.24)$$

and its integral is indeed Eq. (9.23). By adding up Eqs. (9.22) and (9.23) and neglecting the weak dependence of (9.22) on high potential u_2 , we obtain

$$\kappa h \approx \ln(8/u_m) + \ln(u_1/u_m + \sqrt{(u_1^2/u_m^2) - 1}) \quad (9.25)$$

The condition satisfied at the critical state is (8.19), and it is equivalent to two equations:

$$d \ln \Pi_e / d \ln (\kappa h) \Big|_{\kappa h = (\kappa h)_c} = -3 \quad (9.26)$$

and

$$\Pi_e = -\Pi_m \quad (\Pi_m = A/6\pi h_c^3 = A\kappa_c^3/6\pi(\kappa h)_c^3) \quad (9.27)$$

In addition, by (9.20), (9.18), (9.7), and (9.4),

$$\Pi_e \approx n\theta u_m^2 \quad (9.28)$$

Therefore, if the potential u_1 is known, we can first determine the dimensionless coordinate $(\kappa h)_c$ of the force barrier from Eqs. (9.25)–(9.28), and with it the corresponding value of u_m necessary to calculate the electrostatic repulsion Π_e in the critical state. Then, making use of (9.27), we find the critical value of the Debye length $1/\kappa_c$ and, finally, the critical (threshold) concentration n_c of the electrolyte from (9.3), i.e., we find the required stability criterion. By substituting (9.28) into (9.26) and into (9.27), we obtain

$$\left[u_m \frac{d(\kappa h)}{du_m} \right]_c = - \frac{2}{3} (\kappa h)_c \quad (9.29)$$

$$3\varepsilon\theta^2 u_m^2 (\kappa h)_c^2 = 4A\kappa_c z^2 e^2 \quad (9.30)$$

where we took into account that, by (9.3),

$$\kappa_c^2 = 8\pi e^2 z^2 n_c / \varepsilon\theta \quad (9.31)$$

The substitution of κh from Eqs. (9.25) and (9.29) yields

$$\frac{3}{2} \left(1 + \frac{p}{\sqrt{p^2 - 1}} \right) - \ln p - \ln(p + \sqrt{p^2 - 1}) = \ln \left(\frac{8}{u_1} \right) \quad (9.32)$$

This equation determines the relation between the ratio $p \equiv u_1/u_m$ and the potential u_1 in the critical state. Its solution is plotted in Fig. 9.2, showing that p is close to 1 if $u_1 < 0.3$. With p and u_1 known, we can find $u_m = u_1/p$ and then obtain the required criterion by means of (9.25) and (9.30). Setting for simplicity $p \approx 1$, i.e., assuming $u_m \approx u_1$ (this state is close to that in which $\Pi_e = \Pi_{\max}$), we find

$$(\kappa h)_c \approx \ln(8/u_1) \quad (9.33)$$

$$A\kappa_c / \varepsilon\psi_{1c}^2 \approx \frac{3}{4} \ln^3(8\theta/ze\psi_{1c}) \quad (9.34)$$

This last relation resembles the refined Eilers-Korf rule (9.1) for adhesion of particles charged to the same potential ψ_1 . However, in this particular case the right-hand side of Eq. (9.34) is greater at low values of ψ_{1c} than in Eq. (9.1), where it is of the order of unity. Hence, the critical potential at which adhesion occurs is less, other conditions being equal, in asymmetric systems than in symmetric ones.

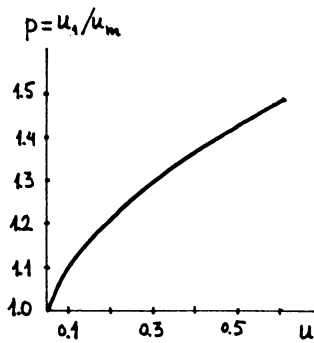


Fig. 9.2. Relationship between u_1 and u_m given by Eq. (9.32).

Case 3. Low Potentials. If the adhesion of two surfaces occurs as a result of a decrease in both potentials ψ_1 and ψ_2 , the stability threshold will be obtained by substituting into condition (9.26) Eq. (6.83) for Π_e , derived in Chapter 6 on the basis of the linearized Poisson-Boltzmann equation:

$$\Pi_e = \frac{\epsilon \kappa^2}{8\pi} \frac{2\psi_1\psi_2 \cosh \kappa h - (\psi_1^2 + \psi_2^2)}{\sinh^2 \kappa h} \quad (9.35)$$

In contrast to the symmetrical case in which the critical state is described by the equation

$$\left(\frac{\kappa h}{2}\right)_c \tanh \left(\frac{\kappa h}{2}\right)_c = \frac{3}{2} \quad (9.36)$$

[8], whose solution $(\kappa h)_c = 3.24$ is independent of the potential $\psi_1 = \psi_2$, in asymmetrical cases the solution $(\kappa h)_c$ is evidently dependent on the ratio $p_1 = \psi_2/\psi_1$, in accord with the following equation:

$$\frac{(\cosh y - 1)[y(\cosh y - 1) - 3 \sinh y]}{2y \cosh y - 3 \sinh y} = \frac{(p_1 - 1)^2}{2p_1} \quad (9.37)$$

where $y = (\kappa h)_c$. For this reason, it is impossible to derive a rigorous simple stability criterion of the type of the Eilers-Korff equation (9.1). However, we can make use of the fact that $(\kappa h)_c$ depends on $p_1 = \psi_2/\psi_1$ rather weakly. Thus, while at $p_1 = 1$ Eq. (9.37) [or (9.36)] gives the solution $(\kappa h)_c = 3.24$ (already mentioned), at $p_1 = 3$ we find $(\kappa h)_c \approx 3.4$, and at $p_1 = 5$ $(\kappa h)_c \approx 3.6$. This dependence is weak because the values of $(\kappa h)_c$ are relatively large, so that (as was shown in Chapter 6) Π_e obeys an approximate exponential relation (6.84):

$$\Pi_e \approx \frac{\epsilon \kappa^2}{2\pi} \psi_1 \psi_2 e^{-\kappa h} \quad (9.38)$$

By substituting (9.38) into criterion (9.26) we immediately find $(\kappa h)_c = 3$ irrespective of ψ_1 and ψ_2 . From this result and Eq. (9.38), and following the procedure outlined above, we readily obtain the following approximate formula:

$$A\kappa_c / \epsilon \psi_1 \psi_2 \approx \text{const} \quad (9.39)$$

whose right-hand side is indeed a weak function of the ratio ψ_2/ψ_1 . Usui was able to show [10], on the basis of accurate tabulated data of Devereux and de Bruyn [11], that this formula indeed gives a good description of the relation between the critical values of ψ_1 , ψ_2 , and κ .

Case 4. Adhesion of Convex Surfaces. All the results derived above can be readily generalized to the case of adhesion of convex surfaces. The rings method (see Chapter 2) is used to calculate the energy of electrostatic interaction between flat double layers by integrating the disjoining pressure, by analogy to the procedure employed in Chapter 6. However, the manipulations are very cumbersome: we state here only that, for the case $A > 0$, $u_2 \gg 1 \gg u_1$, criterion (9.34) is replaced with a similar criterion having a more complicated right-hand side. The result retains a similarity to Eq. (9.1).

9.2. DESTABILIZATION CRITERIA FOR DISPERSIONS WITH A NEGATIVE HAMAKER CONSTANT

The dispersion interaction between particles of different nature in a liquid medium can result in their repulsion ($A < 0$). If at the same time the particles have high like-sign charges (even if their potentials are different), it follows from the arguments of the preceding section that both the electrostatic component and the resultant disjoining pressure are positive at all distances. (In principle, Π_e can become negative at very small thickness h of the liquid interlayer, but then the molecular repulsive forces, being inversely proportional to h^3 , suppress the interaction of double layers.) If at least one of the potentials ψ_1 is relatively low (or has the sign opposite to that of ψ_2), repulsion is predominant in that case also, both at small and at large distances. Nevertheless, as seen from Fig. 9.3, the total pressure Π plotted as a function of distance at $\psi_1 \neq \psi_2$ can have at certain conditions a minimum with depth Π_{\min} , preceded by a maximum with height Π_{\max} . If the external force is sufficient to overcome the barrier Π_{\max} , the system moves to the energy minimum corresponding to a thickness $h = h^*$ marked in Fig. 9.3. Obviously, in this situation Π_{\min} is the adhesion force.

Case 1. Charged Surfaces of Like Sign. A change in composition and concentration n of the electrolyte and in potentials ψ_1 and ψ_2 simultaneously affects Π_{\max} and Π_{\min} . If the electrolyte concentration is low, and the potentials ψ_1 and ψ_2 are of like sign but are not too close in magnitude, then Π reaches its maximum at a relatively large interlayer thickness, on the order of the Debye length $1/\kappa$ (as already discussed in Section 9.1, case 1). Equation (9.15) dictates that, in addition, at least one of the potentials must be low, i.e., not higher than approximately 50 mV. As an example, let us consider a system with the following parameters: $\psi_1 = 25 \text{ mV}$, $\psi_2 = 150 \text{ mV}$, $n = 10^{-3} \text{ mole/liter}$, and $|A| = 10^{-13} \text{ erg}$. Here $(\kappa h)_{\max} \approx 1.4$, i.e., $h_{\max} \approx 140 \text{ \AA}$, $\Pi_e^{\max} \approx 24 \cdot 10^3 \text{ dyn/cm}^2$, $\Pi_m(h_{\max}) \approx 0.5 \cdot 10^3 \text{ dyn/cm}^2$. Therefore, Π_{\max} can be calculated by using (9.4) and (9.14), neglecting the van der Waals forces, and using the formula

$$\Pi_{\max} \approx \Pi_e^{\max} = 4n\theta \sinh^2(u_1/2) \quad (9.40)$$

If n and ψ_1 (i.e., u_1) are small, the "activation" barrier is not high and adhesion occurs easily. As n and ψ_1 increase, the barrier Π_{\max} grows while Π_{\min} diminishes and vanishes when n reaches a certain concentration n_c .

The condition under which adhesion is completely prevented can be established by the same equations (9.26) and (9.27) as before. However, in this case we have to use for Π_e , instead of the particular equation (9.28), the general equation (9.5) whose substitution into (9.26) gives

$$[d(\kappa h)/d \ln w]_c = \frac{1}{3}(\kappa h)_c \quad (9.41)$$

In order to find the dependence of κh on w we integrate Eq. (9.4) from $x = 0$ to $x = h$ in that range of thickness where $\Pi_e < 0$ and, hence, $w < 0$ (i.e., in the range $h < h_0$ in Fig. 9.1). The result is

$$\xi = \kappa h = \int_{u_1}^{u_2} \frac{du}{\sqrt{4 \sinh^2 \left(\frac{u}{2} \right) - w}} \quad (9.42)$$

For simplicity, we assume that $u_2 \gg 1$ and $u_1 \ll 1$, and can replace (9.42) with

$$\kappa h \approx \int_0^\infty \frac{du}{\sqrt{4 \sinh^2 \left(\frac{u}{2} \right) + w'}} - \int_0^{u_1} \frac{du}{\sqrt{u_2 + w'}} \quad (9.43)$$

where $w' = -w > 0$. By taking integrals in (9.43) and evaluating the elliptic integral appearing thereby, using (9.21), we obtain

$$\kappa h \approx \ln 8 - \ln(u_1 + \sqrt{u_1^2 + w'}) \quad (9.44)$$

Substituting this into (9.41) we find (taking into account that $w = -w'$)

$$\frac{3}{2} \left(1 - \frac{u_1}{\sqrt{u_1^2 + w'_c}} \right) + \ln(u_1 + \sqrt{u_1^2 + w'_c}) \approx \ln 8 \quad (9.45)$$

If we assume that the solution of this equation $w'_c > 1$ (for $u_1 \ll 1$), we can set $u_1 = 0$ everywhere in (9.45). Then

$$\ln 8 - \frac{1}{2} \ln w'_c \approx \frac{3}{2}$$

so that indeed

$$w'_c \approx 64 \exp(-3) \approx 3 > 1 \quad (9.46)$$

and by (9.44)

$$(\kappa h)_c \approx 3/2 \quad (9.47)$$

By substituting $w'_c = -w_c$ and $(\kappa h)_c$ into Eqs. (9.5) and (9.27), we arrive at the following condition of no adhesion:

$$\frac{A' \kappa_c^3}{6\pi\theta n_c} \approx \left(\frac{3}{2}\right)^3 \cdot 64 \exp(-3) \approx 11 \quad (9.48)$$

where $A' = -A$, and κ_c and n_c are related through (9.31). Hence, in the case $1 \gg u_1 > 0$, adhesion is impossible if

$$n > n_c \approx 2.5 \frac{\varepsilon^3 \theta^5}{A^2 e^2 z^6} \quad (9.49)$$

Case 2. Charged Surfaces of Unlike Signs. If $u_1 < 0 < u_2$, w is always negative and at small n there is always a sort of "force well." In order to clarify the details of this variant, let us consider the simplest limiting case:

$$u_2 \gg 1, -u_1 \gg 1 \quad (9.50)$$

It corresponds to situations shown in Figs. 6.10 and 6.12 (curves 2). Integration of Eq. (9.5) gives

$$\kappa h = \int_{u_1}^{u_2} \frac{du}{\sqrt{2(\cosh u - 1) + w'}} \approx \int_{-\infty}^{\infty} \frac{du}{\sqrt{2(\cosh u - 1) + w'}} \quad (9.51)$$

so that κh reduces to a complete elliptic integral of the first kind with a modulus k dependent on w' . An evaluation of this integral gives

$$\kappa h \approx 2 \ln(8/\sqrt{w'}) \quad (9.52)$$

By substituting (9.52) into (9.41), we obtain

$$(\kappa h)_c \approx 3 \quad (9.53)$$

and hence, as in the preceding case,

$$w'_c \approx 3 \quad (9.54)$$

The corresponding critical concentration is

$$n_c = 160 \frac{\epsilon^3 \theta^5}{e^6 z^6 A^2} \quad (9.55)$$

so that adhesion ceases at $n > n_c$. For convex surfaces the stability criterion differs from (9.55) only by a numerical factor.

Therefore, the stability criteria (9.2) and (9.55) have identical form for strongly charged surfaces and differ only in numerical factors. However, adhesion criteria are given in these two cases by inequalities with opposite "polarity." Adhesion or coagulation of particles of different nature can be caused not by adding but by diluting the electrolyte, i.e., by increasing the Debye length. In this particular case dilution results in an increased range of attraction between surfaces. This inversion of the Schulze-Hardy rule (9.2) (derived in [7]) was first obtained by Derjaguin in [2]. Examples of this type of coagulation were observed by Frumkin et al. [12], who studied the adhesion of mercury droplets to glass in dilute electrolyte solutions.

The stability criterion for weakly charged surfaces of unlike signs can be obtained from the same formulas and equations that were employed for a similar purpose in the preceding section. The same arguments yield a simple approximate criterion [10]:

$$|\kappa_c A / \epsilon \psi_1 \psi_2| = \text{const} \quad (9.56)$$

As in the case analyzed above, here coagulation sets in (in contrast to the case $\psi_1 \psi_2 > 0$) when the ionic strength of the solution diminishes, i.e., when $\kappa < \kappa_c$.

In order to find the adhesive force at a given concentration and for known functions $\Pi_e(h)$ and $\Pi_m(h)$, it is first necessary to determine the position of the force-well minimum h_{\min} from the equation

$$d\Pi_e/dh + d\Pi_m/dh = 0 \quad (9.57)$$

In the case under consideration, adhesion is produced by electrostatic attractive forces between unlike-sign charged surfaces at very small distances where these forces must be quite strong, so that the dependence $\Pi_e(h)$ can be found by calculating the integral (9.42) [or (9.51)] at $w' \gg 1$; the result is

$$\kappa h \approx (u_2 - u_1)/\sqrt{-w} \quad (9.58)$$

Finding now w from (9.58) and substituting it into (9.5), we make use of the definition of κ , (9.3), and obtain

$$\Pi_e \approx -\epsilon(\psi_2 - \psi_1)^2/8\pi h^2 < 0 \quad (9.59)$$

recalling that

$$\Pi_m = -A/6\pi h^3 > 0, \quad A < 0 \quad (9.60)$$

The coordinate of the minimum is found from (9.59), (9.60), and (9.57):

$$h_{min} = -2A/\epsilon(\psi_2 - \psi_1)^2 \quad (9.61)$$

Evidently, h_{min} is independent of electrolyte concentration. In water, for $A = -10^{-12}$ erg,

$$h_{min} \approx 300/(u_2 - u_1)^2 \quad (\text{\AA})$$

so that if $|\psi_2 - \psi_1| \approx 150$ mV (i.e., for $|u_2 - u_1| \approx 6$), we have $h_{min} \approx 8-9$ Å. The required adhesive force is obtained by substituting the value of h_{min} from (9.61) into (9.59) and (9.60), and adding the results algebraically:

$$|\Pi_{min}| = \frac{\epsilon^3(\psi_2 - \psi_1)^6}{96\pi A^2}, \quad \psi_1 \psi_2 < 0 \quad (9.62)$$

For $A = -10^{-12}$ erg and $|\psi_2 - \psi_1| = |\psi_2| + |\psi_1| = 150$ mV, the adhesive force is $|\Pi_{min}| \approx 2.5 \cdot 10^7$ dyn/cm².

9.3. DEVELOPMENT AND VERIFICATION OF THE THEORY

The theory presented in the preceding sections was mostly developed by Derjaguin [2]. It was later further developed by a number of authors [10, 11, 13-15]. Interaction between surfaces with prescribed surface charge density [15-17] and between two surfaces one of which has a constant charge density and another a constant

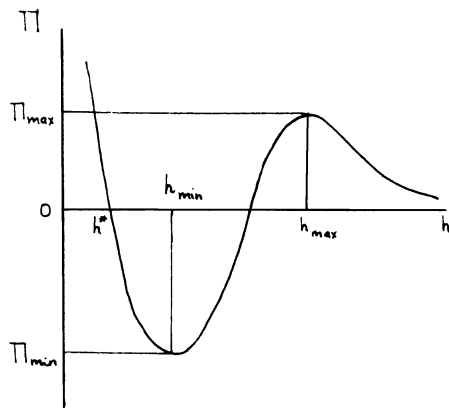


Fig. 9.3. Net disjoining pressure $\Pi = \Pi_e + \Pi_m$ as a function of interlayer thickness in the case $A < 0$.

surface potential [18] was analyzed. Devereux and de Bruyn, and Honig and Mul published tables for the energy of electrostatic interaction between nonidentically charged surfaces in symmetrical electrolytes at constant potentials [11] and constant surface charge densities [19], and Smilga gave an analysis for an arbitrary mixture of electrolytes [20]. Interaction at low potentials, first discussed in [21], was later studied in more detail [10, 14, 22].

The theory was experimentally verified in a number of papers. Thus, the inverted Schulze-Hardy rule was confirmed by Chernoberezhsky et al. [23]. A rigorous quantitative comparison of the theory and experimental data is not easy, mainly because of the difficulties in determining the effective surface potential of the particles. The results of interest in this respect are those of model experiments in which adhesion of two mercury droplets polarized to different potentials [24], and of mercury droplets and glass [25], was studied. The disjoining pressure of the electrolyte interlayer between glass and polarized mercury droplets was analyzed in [26]. The theory of heterocoagulation was tested and borne out again by studying the adhesion of dispersed particles to a rotating disc [27]. Taken together, the theories of homo- and heterocoagulation explained the effect of selective coagulation in which the growing aggregates contain particles of only one kind but no particles of different kind. In this case three distinct critical concentrations are possible: two of them correspond to the coagulation thresholds of each of the sols in the mixture, and the third corresponds to formation of aggregates of unlike particles.

Obviously, the description of heterocoagulation kinetics meets with considerably greater difficulties than does homocoagulation. However, here, too, a certain progress has been achieved, on the

basis of the results obtained in [2] and outlined above. Thus, Hogg et al. [14] and Muller [28] determined how kinetic equations are modified in heteroaggregation, and how the "mean" coefficient of retardation of aggregation must be calculated in a mixed dispersion. It is necessary to allow for three known pair potential energies of the interaction, two of them corresponding to the interaction between particles of the original homodispersions, and the third corresponding to the interaction of particles of different nature; the volume fractions of each homodispersion of the mixture must also be taken into account.

Heteroaggregation covers a wider range of phenomena than homo-aggregation (which constitutes a particular case of the former). Furthermore, heteroaggregation provides the foundation of such important practical processes as flotation [29], filtration of polluted water [30], dyeing, adhesion of biological cells, and many others. Therefore, heteroaggregation theory definitely deserves still further attention [31].

REFERENCES

1. H. C. Hamaker, *Physica*, 4, 1058 (1937).
2. B. V. Derjaguin, *Discuss. Faraday Soc.*, 18, 85 (1954); *Kolloidn. Zh.*, 16, 425 (1954).
3. I. E. Dzyaloshinsky, E. M. Lifshitz, and L. P. Pitayevsky, *Zh. Eksp. Teor. Fiz.*, 37, 229 (1959); *Usp. Fiz. Nauk*, 73, 394 (1961).
4. B. V. Derjaguin, B. V. Zheleznyi, and A. P. Tkachev, *Dokl. Akad. Nauk SSSR*, 206, 1146 (1972); H. J. Schulze and Chr. Cichos, *Z. Phys. Chem.*, 145, 251 (1972); H. Sonntag, N. Buske, and M. Fruhner, *Kolloid-Z. Z. Polym.*, 250, 330 (1972); P. M. Kruglyakov, *Kolloidn. Zh.*, 36, 145 (1974).
5. N. V. Churaev, *Kolloidn. Zh.*, 36, 287 (1974); C. G. van Oss, D. R. Absalom, and A. W. Neumann, *Colloids Surfaces*, 1, 45 (1980); J. Visser, *Adv. Colloid Interface Sci.*, 15, 157 (1981).
6. B. V. Derjaguin, *Trans. Faraday Soc.*, 36, 203, 730 (1940); *Kolloidn. Zh.*, 6, 291 (1940).
7. B. V. Derjaguin and L. D. Landau, *Acta Physicochim. URSS*, 14, 633 (1941); *Zh. Eksp. Teor. Fiz.*, 11, 802 (1941); reprinted: *Zh. Eksp. Teor. Fiz.*, 15, 663 (1945).
8. V. M. Muller, in: *Research in Surface Forces*, Vol. 3, B. V. Derjaguin (ed.), Consultants Bureau, New York (1971), p. 236; *Kolloidn. Zh.*, 31, 427 (1969).
9. H. B. Dwight, *Tables of Integrals and Other Mathematical Data*, Macmillan, New York (1961).
10. S. Usui, in: *Progress in Surface and Membrane Science*, Vol. 5, J. F. Danielli, M. D. Rosenberg, and D. A. Cadenhead (eds.), Academic Press, New York (1972), p. 223.

11. O. F. Devereux and P. L. de Bruyn, *Interaction of Plane-Parallel Double Layers*, M.I.T. Press, Cambridge, Mass. (1963).
12. A. V. Gorodetskaya, A. N. Frumkin, and A. S. Titiyevskaya, *Zh. Fiz. Khim.*, 21, 675 (1947).
13. O. F. Devereux and P. L. de Bruyn, *J. Chem. Phys.*, 37, 2147 (1962); *J. Colloid Sci.*, 19, 302 (1964).
14. R. Hogg, T. W. Healy, and D. W. Fuerstenau, *Trans. Faraday Soc.*, 62, 1638 (1966).
15. R. J. Pugh and J. A. Kitchener, *J. Colloid Interface Sci.*, 35, 656 (1971).
16. G. R. Wiese and T. W. Healy, *Trans. Faraday Soc.*, 66, 490 (1970).
17. S. Usui, *J. Colloid Interface Sci.*, 44, 107 (1973).
18. G. Kar, S. Chander, and T. S. Mika, *J. Colloid Interface Sci.*, 44, 347 (1973).
19. E. P. Honig and P. M. Mul, *J. Colloid Interface Sci.*, 36, 258 (1971).
20. V. P. Smilga, *Kolloidn. Zh.*, 22, 615 (1960).
21. B. V. Derjaguin and V. G. Levich, *Dokl. Akad. Nauk SSSR*, 98, 984 (1954).
22. A. Bleier and E. Matijević, *J. Colloid Interface Sci.*, 55, 510 (1976); *J. Chem. Soc., Faraday Trans. I*, 74, 1346 (1978).
23. Yu. M. Chernoberezhsky, E. V. Golikova, and T. F. Girfanova, in: *Surface Forces in Thin Films and Stability of Colloids*, Nauka, Moscow (1974), p. 256; Yu. M. Chernoberezhsky and E. V. Golikova, *Kolloidn. Zh.*, 36, 115 (1974).
24. A. Watanabe and R. Gotoh, *Kolloid-Z. Z. Polym.*, 191, 36 (1963); A. Watanabe, M. Matsumoto, and R. Gotoh, *Kolloid-Z. Z. Polym.*, 201, 147 (1965).
25. S. Usui, T. Yamasaki, and J. Shimoizaka, *J. Phys. Chem.*, 71, 3195 (1967); S. Usui and T. Yamasaki, *J. Colloid Interface Sci.*, 29, 629 (1969).
26. B. V. Derjaguin, A. V. Gorodetskaya, A. S. Titiyevskaya, and V. N. Yashin, *Kolloidn. Zh.*, 23, 535 (1961).
27. J. K. Marshall and J. A. Kitchener, *J. Colloid Interface Sci.*, 53, 342 (1966); G. E. Clint, J. H. Clint, J. M. Corkill, and T. Walker, *J. Colloid Interface Sci.*, 44, 121 (1973); T. Dabros and J. Czarnecki, *J. Colloid Interface Sci.*, 53, 335 (1975); W. J. Whek, D. Gidaspow, and D. T. Wasan, *J. Colloid Interface Sci.*, 59, 1 (1977); D. C. Prieve and E. Ruckenstein, *J. Colloid Interface Sci.*, 60, 337 (1977).
28. V. M. Muller, *Kolloidn. Zh.*, 37, 894 (1975).
29. B. V. Derjaguin and V. D. Samygin, *Kolloidn. Zh.*, 26, 179 (1974); B. V. Derjaguin, S. S. Dukhin, and N. N. Rulev, *Kolloidn. Zh.*, 38, 251, 1015 (1976).
30. S. S. Dukhin, O. D. Kurilenko, and V. D. Grebenyuk, *Kolloidn. Zh.*, 37, 859 (1975).
31. B. V. Derjaguin and S. S. Dukhin, *Bull. Inst. Min. Met.*, 1961, No. 651, *Trans.*, 70, Part 5, 221 (1960); Part 10, 569 (1960-1961); in: *Surface and Colloid Science*, Plenum Press, New York, Vol. 13 (1984), p. 71.

Chapter 10

WETTING FILMS

Wetting films are crucially important in many technologies and natural processes. Flotation, detergency, wetting, and spreading require an understanding of wetting films. Their properties also influence the physical and mechanical properties of porous bodies, and the mechanism and kinetics of mass and energy transfer processes in them. For instance, the moisture transfer processes in soil and ground, in buildings and other porous materials, the processes of drying and moistening, capillary impregnation, and capillary condensation all involve wetting films. The thickness, viscosity, and stability of wetting films largely control the rates of these processes.

10.1. DISJOINING PRESSURE OF WETTING FILMS

By "wetting films" is meant liquid films covering the surface of a condensed body. In contrast to foam and emulsion films, wetting films are asymmetric: one surface is bounded by a solid or liquid phase, the other by a gas.

At any interface there are transition layers within which intensive properties and composition of the liquid differ from those in the bulk. The pressure tensor is anisotropic in interfacial transition layers. Its normal component P_N is constant and equals, for planar films, the pressure P in the gas phase. But the tangential component is a function of distance from the dividing interface, $P_T = P_T(z)$.

A film is here designated "thick" if its thickness exceeds the sum of thicknesses of the boundary layers at the film/substrate and film/gas interfaces. The middle part of a thick film has the properties and the pressure of the bulk phase:

$$P_0 = P_N = P \quad (10.1)$$

We shall consider mainly "thin" films, whose thickness is less than the sum of thicknesses of interfacial layers, so that these layers overlap. Consequently, there is no separating interlayer, with bulk liquid properties, between the interfacial layers. The normal component of pressure tensor P_N is still equal to the pressure of the gas phase P , but differs from the pressure P_0 in the bulk liquid phase from which the film was formed while thinning out locally. The difference $P_N - P_0$ gives the disjoining pressure of the film:

$$\Pi = P_N - P_0 = P - P_0 \quad (10.2)$$

The concept of disjoining pressure of thin films and interlayers was introduced in [1-3].

Disjoining pressure is a function of the degree of overlapping of interfacial layers and, hence of film thickness h . The disjoining pressure isotherm [i.e., the function $\Pi(h)T$] is a thermodynamic characteristic of a thin liquid film.

The Gibbs excess free energy G per unit area of a film can be defined, at constant pressure in the bulk phase P_0 , constant temperature T , and constant chemical potentials μ_i and electric potentials of the film/gas and film/substrate interfaces, respectively, ψ_g and ψ_s , on the basis of the disjoining pressure isotherm $\Pi(h)$:

$$G(h) = - \int_{\infty}^h \Pi(h) dh \quad (10.3)$$

At the conditions given above the value of G is equal to the work of thinning the film in a reversible isobaric-isothermal process from $h = \infty$ to a finite thickness h . Clearly [4],

$$\Pi(h) = -(\partial G / \partial h)_{P_0, T, \mu_i, \psi_g, \psi_s} \quad (10.4)$$

The quantity extracted directly from a physical experiment with thin films is the disjoining pressure. Methods of measuring it are given in Section 10.2. The theoretical calculation of various components of the Gibbs free energy for wetting films is considerably more complicated than a direct calculation of the disjoining pressure as such.

The minimum of the function $G(h)$, determining the state of stable equilibrium, corresponds to the condition $\partial^2 G / \partial h^2 > 0$. As follows from Eq. (10.4), this yields the condition of stability of wetting films [2]:

$$\partial \Pi / \partial h < 0 \quad (10.5)$$

A specific form of the isotherm $\Pi(h)$ is determined by the contribution of surface forces of different nature. As a first approximation, this contribution can be considered additive:

$$\Pi(h) = \Pi_e(h) + \Pi_m(h) + \Pi_s(h) + \Pi_a(h) + \Pi_c(h) \quad (10.6)$$

Here Π_e is the electrostatic component of disjoining pressure caused by the overlapping of diffuse ionic layers at the charged surfaces of the film (or of only one charged surface, usually at the substrate), Π_m is the molecular component due to the dispersion forces between the substrate and the liquid film, Π_s is the structural component of disjoining pressure due to the overlapping of the interfacial layers of the liquid with a structure modified in comparison with the bulk phase, Π_a is the adsorption component of disjoining pressure due to the overlapping of diffuse adsorption layers of neutral solute molecules, and Π_c is the component due to a "steric" interaction between adsorption layers of surfactants or polymers.

In some cases it is sufficient to take into account only some of these components. For example, it is common practice to restrict the analysis for lyophobic colloids and wetting films to only two components of disjoining pressure, the molecular Π_m and the electrostatic Π_e . When wetting films are stabilized by adsorption layers of nonionic surfactants or polymers, in some cases it is sufficient to take into account only molecular forces and steric repulsion, i.e., only two components, Π_m and Π_c .

The accuracy of the theoretical prediction of disjoining pressure isotherms of wetting films $\Pi(h)$ depends most of all on how well one knows the frequency dependence of permittivity $\epsilon(i\xi)$ of the substrate and the film (this being necessary for calculating Π_m and Π_a), and also the potentials of its surfaces (required for calculating Π_e). Unfortunately, at present calculations of the other components of disjoining pressure cannot be carried out with sufficient reliability, so that usually the isotherms $\Pi(h)$ must be found experimentally.

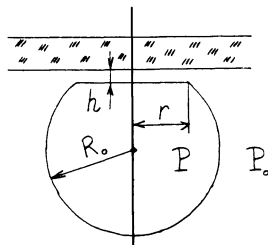


Fig. 10.1. The bubble method of determining the disjoining pressure isotherms of wetting films.

10.2. EXPERIMENTAL METHODS OF DETERMINING THE DISJOINING PRESSURE ISOTHERMS OF WETTING FILMS

Several techniques have been used to determine the isotherms $\Pi(h)$ experimentally. The first study was used by Derjaguin and Kussakov [2]; gas bubbles of different radii R_0 were floated up and approached a horizontal smooth plate (Fig. 10.1). When the approach of a bubble was sufficiently slow, and the contact area radius r sufficiently small, a planar film with thickness h was formed after some time, in equilibrium with the bulk liquid phase surrounding the bubble. (If these conditions are not met, a "dimple" is formed, slowing down the establishment of equilibrium.)

The radius r is determined by the equality of the pressure squeezing the captive bubble up according to Archimedes' principle, to the pressure acting on a circular planar film:

$$\frac{4}{3}\pi R_0^3 g(\rho_g - \rho_l) = \frac{2\sigma}{R_0} \pi r^2 \quad (10.7)$$

where ρ_g and ρ_l denote the density of the gas and liquid, respectively, and g is the gravitational acceleration.

This equality shows that bubbles are relatively slightly deformed if they are not too large because the ratio r/R_0 is directly proportional to R_0 . Experiments with very small bubbles are hampered by the dissolution of gas compressed within a bubble. Moreover, this reduces the film area, thereby making difficult the measurement of its thickness. Consequently, the range of conveniently measured bubbles was restricted to $10^{-2} < R_0 < 10^{-1}$ cm [2].

The disjoining pressure of a planar film is found from Eq. (10.1) in which $P = (2\sigma/R_0) + P_0$ corresponds to the gas pressure in the bubble, and P_0 to the pressure of the bulk liquid phase surround-

ing the bubble. The substitution of these values of P and P_0 into (10.1) yields

$$\Pi = 2\sigma/R_0 = \Delta P_k \quad (10.8)$$

where ΔP_k is the capillary pressure of the bubble.

The values of Π were found by measuring under a microscope the radius R_0 of an equilibrium bubble, for the known value of the surface tension σ of the liquid. Film thickness was found by a monochromator, by recording the wavelength of the illuminating beam until a dark ($h_1 = \lambda_1/4n$) or light ($h_2 = \lambda_2/2n$) fringe around a uniformly illuminated (and hence planar) film disappeared. Here λ_1 and λ_2 are the corresponding wavelengths, and n is the refractive index of the liquid. Simultaneous measurement of Π and h for bubbles with different radii gives the segment of the disjoining pressure isotherm in the range of positive values of Π from $\sim 10^3$ to $\sim 10^4$ dyn/cm².

This technique was later refined in order to improve accuracy and widen the range of $\Pi(h)$ measurements. First Derjaguin and Kus-sakov [2], and later Read and Kitchener [6, 7] and Blake [8, 9] introduced holders with which a bubble could be slowly brought into contact with a plate from above. By using a holder it became possible to fix a bubble accurately with respect to a substrate. The time necessary to reach equilibrium, i.e., the time of formation of a planar film, range from 10 min for the smallest bubbles ($R_0 \approx 0.2$ cm) to several hours for large bubbles ($R_0 \approx 2.2$ cm).

Since the bubbles are deformed by the holder, the capillary pressure ΔP_k had to be found from the radius of curvature of the bubble surface near the film. This was achieved by measuring the distance between interference fringes in monochromatic light illuminating the film and meniscus. At the same time, the film thickness was measured from the relative intensity of light reflected by the film I/I_0 (where I_0 is the intensity of the incident light), assuming that the liquid refractive index in the film equals the bulk value. However, the measurement error could be as high as 10% because of a nonuniform illumination of the film and errors in measuring I_0 . This measurement technique was successfully applied to films thicker than 0.1λ (where λ is the light wavelength), i.e., for $h \geq 300$ Å. The accuracy of determining Π was better, about 2%.

The next step in developing the experimental method was to reject the use of individual bubbles and to form the films between two menisci [10] or between a meniscus at the end of a tube and a plate [11-14]. Aronson and Princen [15, 16], by increasing the gas pressure in the tube, first formed at its end a spherical meniscus and then, by lifting the plate by a micrometric screw and bringing it into a contact with the meniscus, produced a film with

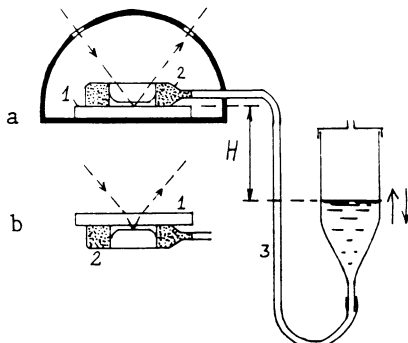


Fig. 10.2. Schematic diagram of the technique for determining the disjoining pressure isotherms of wetting films on opaque (a) and transparent (b) solid substrates: the liquid is pulled out by suction through a channel in a porous filter.

a radius $r \leq 0.01$ cm. By slowly bringing together the meniscus and the plate it was possible to produce and observe even metastable films. The time to establish an equilibrium of the film and meniscus was about 1 h.

The disjoining pressure Π of the film was determined, as in earlier work [2], from the capillary pressure of the meniscus in equilibrium with the flat film, $\Pi = \Delta P_k$. The value of ΔP_k was found from the profile of the meniscus given by the interference pattern, by means of the formulas derived by Scheludko et al. [17] and taking into account the effect of gravity [15].

The thickness of the film was measured photometrically, from the intensity of reflected light. The accuracy of measurement was increased by means of a method, developed by Scheludko and Manev [18], of measuring the reflected intensity by a fiber lightguide 150 μm in diameter. This made possible the scanning of I/I_0 at different parts of the film, to monitor the uniformity of its thickness. Tubes of different radii were used to carry out measurements with different $\Pi = \Delta P_k$ and to obtain the $\Pi(h)$ isotherms. Aronson and Princen [15, 16] obtained in this manner the isotherms $\Pi(h)$ for water films on a quartz plate in the range of Π from 300 to 1500 dyn/cm².

The transition to cells with a porous filter [19, 20] first suggested by Mysels to investigate free films [21] and refined by Scheludko and Exerova [22] helped to extend further the range of disjoining pressure in which isotherms $\Pi(h)$ of wetting films could be obtained.

A circular wetting film is formed (Fig. 10.2) on a flat substrate 1 to which a microporous filter 2 with a cylindrical hole is clamped [19]. A flexible polyethylene pipe 3 connects the filter filled with the test liquid to a vessel 4 that can be moved vertically by a micrometric device. The disjoining pressure of a wetting film is given by the distance H to the level of the liquid and is equal to

$$\Pi = \Delta P_k = (\rho_l - \rho_g)gH \approx \rho_l gH$$

where ΔP_k is the capillary pressure of the bulk-liquid meniscus surrounding the film. The quantity H is measured by a cathetometer. The accuracy in determining Π is about 1 dyn/cm².

The maximum pressure Π that could be produced in this method is determined by the size of pores in the filter (usually 5-10 μm). However, more often (for poorly volatile liquids) the limiting factor is a steeply increasing time required to reach equilibrium between the meniscus and film, owing to increasing viscous resistance of the film as its thickness diminishes. As a result, this study was practicable only for $\Pi \leq 10^4$ dyn/cm² [19, 23].

By moving the vessel up and down, it is checked that the results are independent of the direction of approach to equilibrium. The time required to reach equilibrium for film thicknesses $h \approx 100$ Å, with the diameter of the bore in the filter 3-5 mm, was found to be several hours. The time factor limits the practicability of the method to film thickness $h \geq 50$ Å.

The film thickness was measured by means of an ellipsometer. In this way it was possible to measure the thickness of wetting films both on transparent (Fig. 10.2b) and on opaque substrates (Fig. 10.2a), for instance metals. The accuracy of measuring thickness by the micropolarization method [24] was about 3 Å. This method is also convenient for working with very thin films because it has practically no limitations when $h \rightarrow 0$. Ellipsometry is known to work quite well even with adsorbed monolayers.

When wetting films of solutions are studied by this method, the time required to establish the film-meniscus equilibrium is determined not only by the rate at which mechanical equilibrium (equality of pressures) is reached for the film and the meniscus, but also by the time necessary for reaching total thermodynamic equilibrium associated with the exchange of solute components. This occurs because the chemical potential and the concentration of the solution in the film are functions of its thickness. The outflow of liquid leading to establishing mechanical equilibrium is mainly determined by hydrodynamics; but mass transfer is limited by the usually slower process of diffusion. Consequently, the time necessary to reach total thermodynamic equilibrium in multicomponent films may be much longer than in one-component liquids.

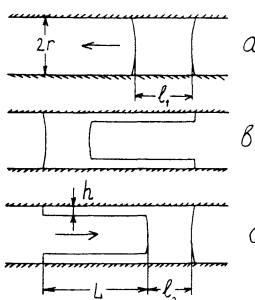


Fig. 10.3. The capillary technique of determining the disjoining pressure isotherms of wetting films.

The suction technique was also used by Sonntag et al. [25, 26] to study wetting liquid films on the surface of another liquid, immiscible with the first. Hydrocarbon films on a water surface were obtained, for example, by sucking out the oil through a capillary sealed into the wall of a hollow cylinder and packed with sintered quartz powder. The level of water in the cell was maintained by a micrometer screw. The thickness of the film was varied by applying external gas pressure, and measured by the intensity of light reflected by the film.

The thickness of films of low-volatility liquids can also be measured by the spreading technique [27]. The idea of the method (Fig. 10.3) is to slowly move a column of liquid in a capillary (Fig. 10.3a) so that the column leaves behind a wetting film on the capillary surface. After the column is moved forward a certain distance (Fig. 10.3b), it is returned to the original position (Fig. 10.3c). This last operation is necessary to eliminate the effect of possible tapering of the capillary. By measuring the length of the column in its initial position, $\Delta l = l_1 - l_2$, it is possible to determine the volume of liquid in the film and its mean thickness $h = \Delta l \cdot r / 2L$, where r is the capillary radius and L is the length of the film.

Since the thickness of the film left behind the moving meniscus depends on the velocity of its advance v [28], measurements are conducted at different v and then the function $h(v)$ is extrapolated to $v = 0$, which gives the thickness $h(0)$ of the film in equilibrium with the meniscus. The accuracy of measuring film thickness is the better, the longer the distance L and the smaller the capillary radius. With capillary radii from 10^{-5} to 10^{-2} cm it is possible to obtain isotherms in a wide range of values of $\Pi = \sigma/r$: from $5 \cdot 10^6$ to $8 \cdot 10^3$ dyn/cm². The method fails for volatile liquids because of evaporation from the column and condensation of the vapor on the whole surface of the capillary.

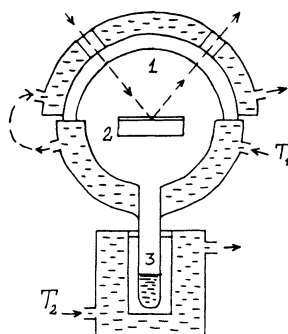


Fig. 10.4. The adsorption technique of determining the disjoining pressure isotherms of films of volatile liquids.

The range of still smaller thicknesses becomes accessible by adsorption methods of forming films (of volatile liquids) on flat substrates [24, 29]. The disjoining pressure of a polymolecular adsorption film in equilibrium with vapor is determined from the condition of equal chemical potentials of molecules μ in the liquid ($\mu = -\Pi v_m$) and the gas ($\mu = RT \ln p/p_s$) phases:

$$\Pi = -\frac{RT}{v_m} \ln \frac{p}{p_s} \quad (10.9)$$

Here v_m is the molar volume of the liquid, and p/p_s is the relative vapor pressure.

The relative vapor pressure p/p_s is fixed by maintaining different temperatures T_1 and T_2 in chamber 1 (Fig. 10.4) containing the plate 2 and in the cell with the experimental liquid 3, with $T_1 > T_2$. If the temperature difference $T_1 - T_2$ is maintained to within 0.02° , it is possible to achieve an accuracy of p/p_s of about 0.002, so that measurements can be carried out practically up to saturation, i.e., up to $p/p_s = 0.99-0.995$, or, according to Eq. (10.9), up to $\Pi \approx 10^6 \text{ dyn/cm}^2$. The combination of a porous filter and adsorption techniques thus makes it possible to cover practically the whole range of values of Π .

Saturated salt solutions can also be used to produce different relative vapor pressures. By choosing solutions whose saturated vapor pressure is a weak function of temperature it is possible to lessen the requirements on the accuracy of thermostating. However, to plot an isotherm it is necessary to employ a number of different solutions and replace them successively in the adsorption setup. This method of fixing p/p_s was used, for example, by Pashley and Kitchener [30], who designed a "one-piece" setup (with no ground-glass joints) with windows to transmit the ellipsometer beam.

As a result, they were able to measure polymolecular adsorption on the surface of an extremely well-cleaned quartz substrate in the absence of vacuum oil vapor.

If adsorption takes place on a stack of a large number of parallel plates, it is possible to measure the total thickness of adsorption films by the absorption of IR radiation (in the range of substrate transparency) [31]. This technique gave good agreement with the ellipsometrically measured polymolecular water films on quartz. (The number of plates was 20, the thickness of a single adsorption layer of water down to 40 Å.) Measurements were conducted at the wavelength $\lambda_m = 3.05 \mu\text{m}$, on thin plates of fused quartz with low bulk content of hydroxyl groups (below 0.12%). The absorption coefficient of bulk water was used to calculate film thickness.

The thickness of adsorption films can be determined with good accuracy by the quartz transducer method, based on the shift in the resonant frequency of an oscillating plate of piezoelectric quartz on whose surface the vapor adsorbs [32-34]. In order to obtain adsorption isotherms on a metal substrate, it has to be deposited in vacuum onto the surface of quartz. The thickness of the adsorbed layer of the liquid is determined by the formula

$$h = \Delta m / \rho S$$

where Δm is the increment in the mass, determined by the shift in the resonant frequency of piezoelectric quartz, ρ is the adsorbate density assumed to be equal to that of the bulk liquid, and S is the surface area covered by the film. The greatest difficulties are encountered in determining the actual surface area S , especially for films whose thickness is comparable to, or less than, the characteristic size of surface roughness. The roughness factor $K = S/S_g$ (where S_g is the geometric surface area of a plate) is either assumed equal to 1, thus overestimating the values of h , or estimated from the monolayer adsorption of an inert gas. For example, the value of K measured from argon adsorption was about 1.3 for an optically polished piece of piezoelectric quartz.

The method of acoustic interference proved successful for measuring the thickness of wetting helium films 10 to 250 Å thick on cleavage surfaces of crystals [35].

Adsorption onto porous or powdered solids can be measured by a standard balance technique; but capillary condensation is an obstructing factor. To eliminate this effect, it is possible to employ, for example, systems composed of a large number of parallel plates [31] or a set of identical capillaries of regular shape, open at both ends. By such means it was possible to measure, for example, the thickness of helium films on the inner surface of

about 100 polymer filters with the diameter of straight cylindrical pores of about $0.2 \mu\text{m}$ [36]. Such filters are obtained by irradiating a polymer film with a penetrating flux of charged particles (ions) and then etching out the invisible tracks [37]. The diameter of the cylindrical channels so formed is determined by the etching time.

Hauxwell and Ottewill [38] studied the polymolecular adsorption films of hydrocarbons on a water surface by measuring the surface tension of the latter. The amount of adsorption was then calculated from the Gibbs equation as a function of relative pressure of the hydrocarbon vapor.

All of the above methods are static, and valid for disjoining pressure isotherms of stable, even if metastable, equilibrium of a film (i.e., when $\partial\Pi/\partial h < 0$). Scheludko et al. [39-44] developed a dynamic method that yields $\Pi(h)$ curves in the instability range (when $\partial\Pi/\partial h > 0$) and in the range $\Pi < 0$, by measuring the rate of spontaneous thinning of the film. The method is based on the Reynolds equation relating the rate of decrease of the thickness of a circular interlayer between two solid bodies to the applied pressure difference ΔP :

$$\frac{d(1/h^2)}{dt} = \frac{16}{3\eta r^2} \Delta P \quad (10.10)$$

where t is time, η is the viscosity of the liquid, and r is the radius of the flat interlayer.

The hydrodynamic pressure in the flowing film is [45]

$$P_h = P - \Pi \quad (10.11)$$

where P is the pressure applied to the surface of the flat film, and Π is its disjoining pressure. At equilibrium

$$P_h = P - (P - P_0) = P_0$$

and the hydrodynamic pressure in the film equals the pressure in the surrounding bulk phase.

When the equilibrium is disturbed or impossible, the equality $P_h = P_0$ breaks down. The liquid flows from the film into the bulk phase (if $P_h > P_0$) or from the bulk phase into the film (if $P_h < P_0$). Since $P_0 = P - \Delta P_k$, where ΔP_k is the capillary pressure of the meniscus surrounding the film, the pressure difference ΔP in Eq. (10.10) is

$$\Delta P = P_h - P_0 = \Delta P_k - \Pi$$

When $\Delta P_k = \Pi_0$, i.e., at equilibrium, the flow vanishes. With a concave meniscus, $\Delta P_k > 0$ and the disjoining pressure of an equilibrium film is positive: $\Pi_0 > 0$. When $\Delta P_k > 0$ and $\Pi < \Pi_0$, the pressure difference $\Delta P > 0$ drives the flow of liquid from the film, thereby reducing its thickness.

By measuring the intensity of light reflected by the film it was possible to monitor the mean thickness of the film as a function of time [i.e., it gave $h(t)$]. By using Eq. (10.10), it was then possible to find ΔP as a function of h , and then $\Pi = \Delta P_k - \Delta P$ as a function of h , i.e., to obtain the segment of the isotherm in the region of instability. In these measurements the capillary pressure of the meniscus ΔP_k must be maintained constant or independently controlled.

By using this technique, Scheludko and Exerova [39-41] obtained the isotherm $\Pi_m(h)$ for unstable ($\Pi_m < 0$) free films of aqueous solutions, and Scheludko and Platikanov obtained it for benzene films on mercury, unstable at large film thickness [42]. Later, Schulze [46] applied this technique to determine the isotherm of unstable n-octane films on the surface of a quartz single crystal.

One shortcoming of the dynamic method is the assumption, used in calculations with Eq. (10.10), that the film remains plane-parallel in the process of thinning. Actually, viscous resistance in a flowing film must result in a gradient of hydrodynamic pressure and, hence, in a gradient of film thickness. Deviations of the film geometry from the plane-parallel model are the greater, the larger the film radius and the more intensive the flow (i.e., the greater the pressure difference ΔP).*

Nevertheless, at the present time the dynamic method is the only one for studying $\Pi(h)$ in the states in which wetting films are absolutely unstable. Consequently, further development of the theory of this method is of great interest.

For metastable films whose transformation to a more stable state is opposed by a potential barrier (when $\partial\Pi/\partial h < 0$), measurements are facilitated with films of small area. The error introduced into the dynamic method by departures from the plane-parallel geometry of the films is also reduced when the film radius decreases.

10.3. DISJOINING PRESSURE ISOTHERMS OF WETTING FILMS FORMED BY VARIOUS LIQUIDS

The form of the disjoining pressure isotherms $\Pi(h)$ is determined by the nature of surface forces. Which of the components of

*Another shortcoming is the assumption that the film viscosity equals the bulk viscosity.

disjoining pressure is dominant depends on the properties and composition of the liquid and on the lyophilicity and structure of the solid substrate. Only one of these components, viz., the molecular component (Π_m), is always present. Other components may be effective to different extents, depending on the charge of film surfaces, the polarity of the liquid, its composition, and adsorption of dissolved components.

The forces with the longest range are the electrostatic forces. Their characteristic range is on the order of the Debye length $1/\kappa$, and in dilute solutions of a 1-1 electrolyte (10^{-6} - 10^{-7} mole/liter) amounts to $0.3\text{-}1 \mu\text{m}$. Consequently, thick films of water and aqueous electrolyte solutions ($h > 500 \text{ \AA}$) are stable mainly through the Π_e component of disjoining pressure. This is confirmed by a high sensitivity of the corresponding part of the isotherm to the concentration and valence of the electrolyte, since they determine the value of $1/\kappa$.

Obviously, the magnitude and contribution of the Π_e component depend mainly on the charge of the surfaces of the film or substrate. Temperature has little effect on Π_e , because usually the energy of dissociation of the surface ionogenic groups is high and the adsorption potentials of ions is usually large in comparison with kT .

The effect of the dispersion forces may become appreciable in the range $h < 500 \text{ \AA}$, and their contribution is enhanced by large differences between the permittivity $\epsilon(i\xi)$ of the liquid and the substrate.

The forces of structural repulsion may come into play in the range of thickness around 100 \AA , and grow sharply as the film thickness diminishes below this figure. The radius of action of these forces strongly depends on the lyophilic properties of the substrate. Pashley and Kitchener demonstrated [30] that with very good wetting the characteristic radius of these forces may reach several hundred angstroms. Even the smallest traces of contaminants that tend to hydrophobize the substrate reduce substantially the characteristic radius of structural long-range forces, so that they vanish or even change sign in the case of poor wetting.

Structural repulsion is not only associated with changed solvent structure close to a solid; it also arises with structured water layers at adsorbed ions or polar groups of surfactant molecules adsorbed on the substrate [47-49]. Here the effect of the structural component of disjoining pressure can be revealed already when the outer hydrated parts of the adsorption layers of the surfactant come into contact. This increases the range of structural forces by the thickness of the adsorption layer of the surfactant.

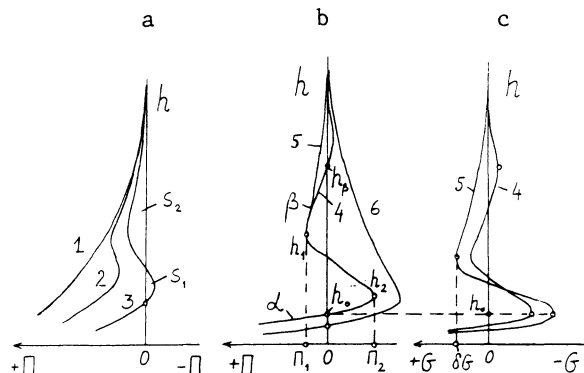


Fig. 10.5. Different types of isotherm $\Pi(h)$ (curves a and b) and $G(h)$ (curve c) of wetting films.

In some cases the adsorption component Π_a can overcome the effect of molecular forces Π_m at small film thickness [50]. The range of the steric component of disjoining pressure is comparable to the thickness of adsorption layers of surfactants or polymers.

Figure 10.5 is a qualitative illustration of typical $\Pi(h)$ isotherms. Curves 1-3 correspond to complete wetting. This situation occurs when the area S_1 bounded by the isotherm in the range $\Pi < 0$ is less than the area S_2 in the range $\Pi > 0$. Isotherms 4 and 5 correspond to partial wetting, when the bulk liquid forms a finite contact angle $\theta_0 > 0$ with the equilibrium film (here $S_1 > S_2$). The stable states of films correspond to those segments of isotherms for which $\partial\Pi/\partial h < 0$, in accord with condition (10.5). For instance, the stable film thickness for isotherm 5 is in the ranges $h > h_1$ (the β -branch of the isotherm), and $h < h_2$ (the α -branch). The range of thickness from h_1 to h_2 corresponds to instability of the film, since here $\partial\Pi/\partial h > 0$.

For S-shaped isotherms (curves 2-5) each value of pressure corresponds, in a certain interval of disjoining pressure (e.g., from 0 to $\Pi = \Pi_1$, curves 4 and 5), to two possible thicknesses of the film, belonging to the α - and β -branches of the isotherm, respectively. The α -branch of the isotherm corresponds to the thermodynamic stability of wetting films. The upper β -branch of the isotherm corresponds to a metastable state. This follows from an analysis of the dependence of excess free energy ΔG on film thickness h plotted in Fig. 10.5 on the basis of Eq. (10.3) for isotherms 4 and 5. This graph shows that the minimum values of ΔG lie in the range of α -films.

The equilibrium of the meniscus and the wetting film is determined by condition (10.8): $\Pi = \Delta P_k$. When $\Delta P_k = 0$ (i.e., the me-

niscus surface is flat), $\Pi = 0$ and the thickness of the equilibrium α -film equals h (Fig. 10.5a, b). Films with this thickness can be in equilibrium with the saturated vapor of the bulk liquid, at $p/p_s = 1$. This is not possible for β -films (isotherms illustrated by curve 5) because $h \rightarrow \infty$ when $\Pi \rightarrow 0$. However, if the isotherm has a more complex shape (curve 4, Fig. 10.5b), i.e., if it penetrates twice into the range of negative values of Π and has two regions of thickness instability, the bulk liquid at $\Delta P_k = 0$ can also be in equilibrium with a metastable β -film of thickness h_β .

In the region of supersaturation $p/p_s > 1$, α -films can exist in equilibrium only with a convex meniscus (e.g., with a droplet), i.e., when $\Delta P_k < 0$. The film thickness then slightly exceeds h_0 , as seen in Fig. 10.5b.

Metastable β -films can undergo a spontaneous transition to a more stable state of α -films. This process is accompanied by overcoming a potential barrier δG (Fig. 10.5c) and is realized by rupture of a thick β -film separating into droplets distributed on the surface of the retained α -film. The breakdown of a β -film into droplets was observed in the earliest experiments with wetting films of water on glass [2] and mercury [51]. The liquid flows out of droplets through the α -film to the meniscus where the pressure is reduced or, with volatile liquids, the droplets evaporate and recondense on the concave surface of the meniscus or on the surface of the α -film over which the vapor pressure is reduced.

The transition $\beta \rightarrow \alpha$ is spontaneous. It occurs randomly as a result of thermal fluctuations of film thickness, generating nuclei of the more stable α -phase in the metastable β -film. Thus, Schulze [52] obtained in 218 experiments a nearly Gaussian distribution of rupturing thicknesses of wetting films of an aqueous solution of dodecylamine (10^{-5} mole/liter) at pH 6 on quartz. Film thicknesses immediately before the rupturing were measured by recording the intensity of light reflected by the film. The surface area of the film was maintained nearly constant ($r = 90 \pm 10 \mu\text{m}$) by a slight variation of capillary pressure, in order to eliminate the effect of this factor on the probability of rupturing.

The probability of formation of a critical nucleus of the α -phase depends on the capillary pressure of the meniscus $\Delta P_k = \Pi$, which is in equilibrium with the film, and on the film surface area. The closer the disjoining pressure Π to the critical value Π_1 (Fig. 10.5b) and, hence, the lower the potential barrier, the more rapid the transition $\beta \rightarrow \alpha$ and the less stable the β -film. The rupturing thickness of wetting films under various external conditions and with additives of electrolytes and surfactants was extensively studied in connection with research into flotation. The rupture of β -films increases the contact angle and improves the adhesion of a gas bubble to a mineral particle.

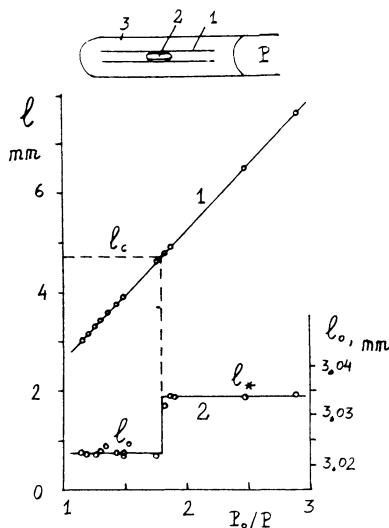


Fig. 10.6. The effect of the surface area of β -films of water covering quartz surface, on their stability.

An increase in film area increases the probability of formation of a critical nucleus and film rupturing. The dependence of stability of β -films on film area was investigated in [53-61]. In early experiments [54, 55], β -films of water were observed to rupture when they were slowly extended at constant disjoining pressure Π and constant temperature. The experiment involved thin quartz capillaries with radii r from 1 to 100 μm . A capillary 1 with a gas bubble 2 was placed in a tube 3 filled with the same liquid (Fig. 10.6). If the bubble length l is sufficiently small, $l < l_c$, the surface of the capillary in the gap between two menisci is covered with a metastable β -film. A slow gentle pumping of air out of the tube 3 caused the bubble to extend, thereby increasing the area of the wetting β -film, $S = 2\pi rl$. Curve 1 in Fig. 10.6 plots the bubble length l as a function of decreasing pressure P_0/P .

After each step of decreasing pressure P , the invariance of the initial length of the bubble l_0 was checked by restoring pressure to the initial level P_0 . For nonpolar benzene and CCl_4 , exhibiting complete wetting on quartz, changes of the bubble length were invariably reversible. Wetting films of these liquids did not rupture and were always stable, thus conforming to isotherm 1 in Fig. 10.5.

The situation was different for water. The initial length of the bubble cannot be restored after exceeding a certain critical length l_c . Figure 10.6 shows that at $l = l_c$ the length changes

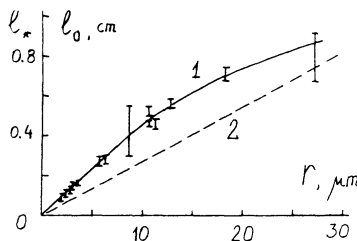


Fig. 10.7. The limiting length l_* of wetting β -films of water as a function of capillary radius r .

jumpwise and takes on a new constant value l_* , slightly greater than l_0 : $l_* > l_0$. At constant gas pressure P_0 this can be explained only by a change in the capillary pressure of the meniscus in equilibrium with the film. The transition is from equilibrium of the meniscus with a β -film (when $\theta_0 = 0$) to equilibrium with an α -film forming a finite contact angle $\theta_0 > 0$ with the meniscus of the bulk liquid in the capillary. The mean value of θ_0 over 20 measurements for α -films on quartz was $22 \pm 6^\circ$.

Figure 10.7 shows the results obtained for l_* as a function of the capillary radius which determines the value of the disjoining pressure of a film $\Pi = \sigma/r$, where σ is the surface tension. Curve 1 gives the data obtained in experiments with bubbles [54]. The dashed line 2 is given for comparison. It generalizes numerous data on the limiting length l_* of β -films obtained by observing the rate of evaporation of water from quartz capillaries with radii greater than $1 \mu\text{m}$ [53-55]. The value of $l_c = l_*$ was found from the length of a β -film left behind the meniscus receding when water evaporated from the capillary. At a certain distance from the meniscus, i.e., precisely at l_c , the β -film ruptured and transformed into an α -film. By observing water evaporation from capillaries with different radii, $l_c = l_*$ was obtained as a function of $\Pi = \sigma/r$.

Figure 10.8 shows the results of similar experiments in capillaries of still smaller radius $r \leq 1 \mu\text{m}$ [57], which made it possible to improve the value of the critical capillary radius $r = r_c$. β -Films do not form at all in capillaries with radii smaller than r_c . Obviously, only an α -film can be in equilibrium with the meniscus when $r \leq r_c$. This value of the radius determines the critical disjoining pressure Π_1 (Fig. 10.5), equal to $\Pi_1 = \sigma/r_c = 3 \cdot 10^6 \text{ dyn/cm}^2$.

Other methods of studying the stability of wetting films with different surface area were developed by Us'yarov et al. [58-61]. Several hundreds of cylindrical capillaries with different radii

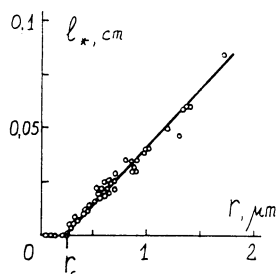


Fig. 10.8. The length l_* of wetting β -films as a function of radius r of narrow quartz capillaries, obtained by measuring water evaporation rate.

($r = 0.1\text{--}1.2 \text{ mm}$), filled with an electrolyte solution, contained gas bubbles of different lengths. The capillaries were scanned over 3 days, under a microscope. The rupturing of β -films was detected by the appearance of microscopic droplets on the segment of the capillary between two menisci. It was shown that rupturing is statistical in nature, and can be characterized by the mean lifetime τ_c of the β -film. The critical disjoining pressure Π_1 was found from the value of the capillary radius within which more than 95% of all β -films ruptured within this time interval.

In another series of experiments [58] the area of films was gradually increased by shifting the gas bubble into the narrower part of a conical capillary, which at the same time slightly increased the disjoining pressure. The rupturing of a β -film was detected by a jumpwise increase in the electric resistance of the film. These measurements were carried out with electrolyte solutions at $C \geq 5 \cdot 10^{-3}$ mole/liter, a concentration that made it possible to measure the thickness of films by electrical conductance until they broke down. Qualitatively, the dependence of the limiting area of films $S = 2\pi r l$ on the capillary radius r was the same as shown in Fig. 10.8. The higher the positive disjoining pressure, the smaller the area of stable β -films. The values of Π extrapolated to $S = 0$ obviously point to the impossibility of forming β -films and are equal to the critical disjoining pressure Π_1 . The value of Π_1 for films of electrolyte solutions was smaller than for pure water, and approximately equal to $5 \cdot 10^3 \text{ dyn/cm}^2$.

Figure 10.9 shows lifetimes τ_c of β -films as a function of pH of a CaCl_2 solution (curve 1) at constant ionic strength of 10^{-3} gram-equivalent per liter [60, 61]. A decrease in the pH, reducing the potential of the quartz surface, leads to rapid rupturing of β -films. Addition of cation-active cetyltrimethylammonium bromide (CTAB) (curve 2) also substantially reduced the stability of β -films.

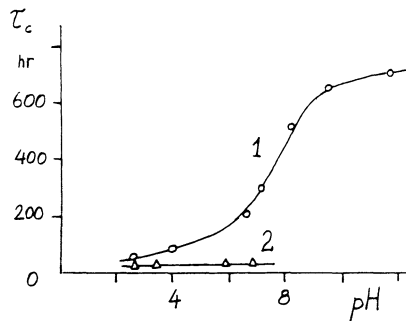


Fig. 10.9. Mean lifetime τ_c of β -films as a function of the pH of an aqueous electrolyte solution (1) and of the same solution with CTAB added (2).

Aronson and Princen [16] measured critical concentrations C_c of alkyltrimethylammonium bromides (C_nTAB) causing the rupture of β -films on quartz (at pH 6). The value of C_c diminished as the length of the alkyl chain increased: from $C_c \approx 10^{-6}$ mole/liter for $n = 5$ to $C_c < 10^{-13}$ mole/liter for $n = 16$.

Blake and Kitchener [8] observed rupturing of water β -films on hydrophobized surfaces of quartz at $h < 600 \text{ \AA}$ for films with diameter of about 0.1 mm. Schulze [62] showed that the critical thickness of rupturing of water films on hydrophobized quartz increases with increasing concentration of dodecylamine. The transition from relatively stable states of β -films to a rapid loss of stability took place at $C_c \approx 5 \cdot 10^{-6}$ mole/liter.

We can now analyze the experimental disjoining pressure isotherms and compare them with theory. Figure 10.10 plots all the data available at present [2, 3, 6, 8, 15, 16, 63] on wetting films of water and aqueous solutions of 1-1 electrolytes ($C \leq 10^{-5}$ mole/liter) on silicate surfaces (glass, quartz, mica). The solid curve 1 represents the equation for the electrostatic component $\Pi_e(h)$ of disjoining pressure [64] valid at low electrolyte concentration and high substrate potential:

$$\Pi_e(h) = \frac{\pi \epsilon_0}{8} \left(\frac{kT}{ez} \right)^2 \frac{1}{h^2} \quad (10.12)$$

where ϵ_0 is the static permittivity of water, e is the electron charge, $z = 1$ is the valence of an ion, k is the Boltzmann constant, T is the temperature.

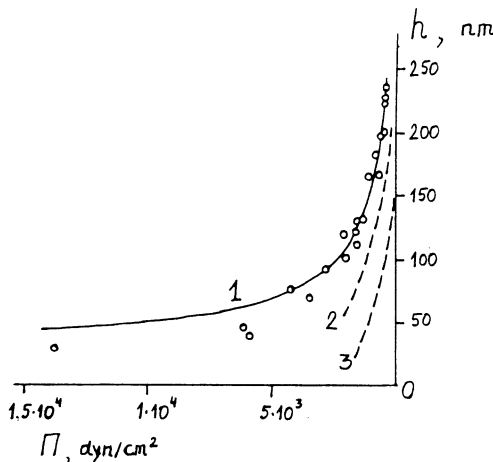


Fig. 10.10. Experimental disjoining pressure isotherms of β -films of water on silicate surfaces.

We see from a comparison of experimental points and curve 1 that Eq. (10.12) gives a satisfactory description of experimental results for films with $h > 500 \text{ \AA}$. This situation arises because the potential of silicate surfaces at $C \leq 10^{-5} \text{ mole/liter}$ is about -150 mV , i.e., is sufficiently high. A small (and also negative) potential of the film surface (about -30 mV [65]) leaves the behavior of isotherms in the range of large film thickness practically unaffected. Deviations appear at $h < 500 \text{ \AA}$ and may be caused both by this charge and by molecular forces.

The wetting of quartz by water is usually partial, so that the data in Fig. 10.10 refer to the β -branch of the isotherm (see curve 5 in Fig. 10.5b). The β -films usually rupture at thicknesses from 400 to 700 \AA . An increase in the concentration of an indifferent electrolyte reduces the potentials of film surfaces, thereby causing the experimental isotherms (dashed curves 2 and 3 in Fig. 10.10) to deviate from Eq. (10.12) (curve 1) valid only at high potentials. Curves 2 and 3 are plotted for two concentrations of a 1-1 electrolyte, $C = 10^{-4}$ and $10^{-3} \text{ mole/liter}$, on the basis of data given in Fig. 10.11 which plots the thickness of films of aqueous solutions, measured at constant disjoining pressure and different solution concentrations [7, 15, 63]. A decrease in film thickness with increasing electrolyte concentration is caused by a decrease both in the surface potentials and in the Debye radius of diffuse ion layers. In this concentration range isotherms must be calculated by using exact solutions of the theory of electrostatic and molecular forces.

Frumkin and Gorodetskaya [51] reported that the adhesion of hydrogen bubbles in water and aqueous solutions of Na_2SO_4 to the

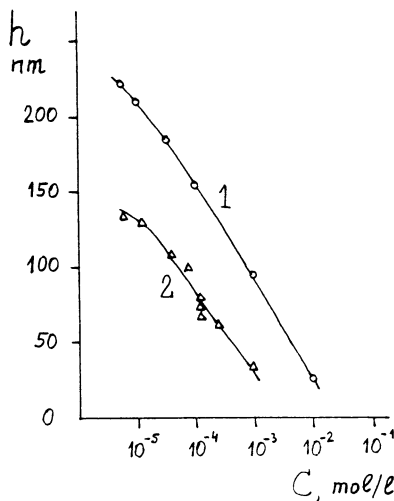


Fig. 10.11. The thickness h of β -films as a function of concentration C (in mole/liter) of an aqueous KCl solution at a constant disjoining pressure $\Pi = 430 \text{ dyn/cm}^2$ (1) and $\Pi = 1450 \text{ dyn/cm}^2$ (2).

surface of mercury diminished with decreasing concentration of the electrolyte and increasing charge of mercury surface. Obviously, adhesion was weakened by an increase in the thickness of β -films. An analogy thus appears in the behavior of β -films of water on the surfaces of dielectrics and metals.

It should be mentioned, however, that even exact numerical calculations of the isotherms of electrostatic forces in films $\Pi_e(h)$ do not always manifest a good agreement with experimental data. The reason for this may be that these calculations operate with values of the ζ -potential found from electrokinetic measurements, not with those of the ψ -potential required for the theory of the Π_e component. Consequently, in a number of cases the experimental isotherms $\Pi_e(h)$ are used to solve the inverse problem: to find the ψ -potentials of the surfaces of the film from the known experimental values of Π_e and h .

The second reason for possible departures of experimental isotherms from the theory of the Π_e component at film thickness below 300-500 Å lies in the growing importance of molecular forces $\Pi_m(h)$. Calculations of $\Pi_m(h)$ for such systems as aqueous solutions on silicate surfaces are quite difficult because the spectral characteristics of substrates and solutions with various compositions have

not been studied adequately. The result is a substantial spread in the values of the Hamaker constants used by different authors. Moreover, electromagnetic retardation, which can be appreciable in water films already when $h \geq 50 \text{ \AA}$ (see Chapter 4), was rarely taken into account in calculating the Π_m component. Consequently, at the present time quantitative calculations of the Π_e and Π_m components for wetting films of aqueous solutions cannot be rigorous.

Nevertheless, the behavior of experimental isotherms is given a good qualitative description by the theory of heterocoagulation and the DLVO theory (see Chapters 8 and 9). This signifies that the main physical factors underlying the formation of thick ($h \geq 400-500 \text{ \AA}$) wetting films of water and aqueous solution are clear, in principle. Quantitative calculations require that spectral characteristics be further elaborated and the methods of determining the potentials of film surfaces be improved.

For instance, it is possible to explain in the framework of these theories how β -films lose stability when the solution pH is lowered to 2-3, i.e., when the isoelectric state of quartz surface is reached (Fig. 10.9). On the contrary, an increase in the pH raising the potential of quartz surface by adsorption of potential-determining OH ions stabilizes the β -films of aqueous solutions.

Adsorption of polyvalent cations (e.g., Al^{+3}) on the surface of a substrate reduces its negative potential. Consequently, β -films of such solutions ($C \approx 10^{-5}$ mole/liter) either have a much smaller thickness in comparison with solutions of 1-1 electrolytes, or are unstable (at still higher concentrations) [2, 7, 52].

The adsorption of ionogenic surfactants produces an especially strong effect on the stability of β -films. In this case it is important on which of the surfaces of the film the surfactant is adsorbed. Thus, the adsorption of cation-active $C_n\text{TAB}$ on a film/gas interface results (when the negative charge of the quartz surface is conserved) in heterocoagulation, i.e., in the attraction of oppositely charged surfaces of the film [16, 66]. The electrostatic component of disjoining pressure changes sign and becomes negative. As a result, the β -branch of the isotherms is not realized (curve 6, Fig. 10.5b). In this case the only stable state is that of thin α -films. This change in the shape of an isotherm, caused by a change in the sign of the Π_e -component, simultaneously leads to an increase in contact angle.

The decisive role of electrostatic forces in the stability of thick β -films of aqueous solutions is demonstrated especially well in that their thickness is practically independent of hydrophilic properties of the surface. Thus, Blake and Kitchener [8] reported observation of metastable β -films (at $\Pi = 300 \pm 20 \text{ dyn/cm}^2$) with thickness of 2350 \AA on the original hydrophilic surface of quartz,

and 2200 Å-thick β -films under the same conditions on a surface hydrophobized by trimethylchlorosilane. They explained this result by nearly identical values of the ζ -potential for the hydrophilic and hydrophobic quartz, producing practically identical forces of electrostatic repulsion.* Aronson and Princen showed [15] that a nonionogenic surfactant $C_{12}EO_8$ (10^{-4} - 10^{-5} mole/liter) added to water hydrophobizes the quartz surface but again leaves the β -branch of the isotherm practically unaffected. The adsorption of anion-active surfactants enhancing the negative charge of quartz surface and/or of film/gas interfaces increases the thickness of β -films and widens the range in which they are stable [63]. These qualitative conclusions following from the theory of surface forces give a good explanation also of the results discussed above on rupture thickness of β -films.

Let us analyze now the factors providing the stability of thin α -films of water. In contrast to β -films for which the adequately studied Π_e and Π_m components are dominant, a theoretical interpretation of α -isotherms meets with difficulties. This is caused, first, by lack of a rigorous theory of the structural component $\Pi_s(h)$ (see Chapter 7).

Most of the experimental isotherms of α -films of water were obtained by ellipsometric techniques of measuring the thickness of polymolecular films formed as a result of adsorption of water vapor on flat surfaces of glass, quartz, or mica. Very few measurements were carried out on α -films formed immediately after thinning and rupturing of β -films. The obvious reason is that in experiments with β -films thickness was determined by measuring the intensity of reflected light, i.e., by a method that fails for thin α -films which usually are thinner than 100 Å.

Figure 10.12 compares the results of measuring the thickness of α -films obtained by various authors [29-31, 67-70]. The distinctive feature of α -isotherms is a much steeper (nearly exponential) dependence of disjoining pressure on film thickness. For instance, for isotherm 3 (Fig. 10.12) the value of $(-\partial\Pi/\partial h)$ at $h \approx 50$ Å is approximately 10^{17} dyn/cm³. Such values of the derivative cannot be explained, say, by molecular forces because otherwise the Hamaker constant

$$A = -(-\partial\Pi/\partial h)2\pi h^4$$

would have to be set equal, in magnitude, to $\approx 10^{-7}$ erg, which is five to six orders of magnitude greater than its possible value. This slope of isotherm cannot be explained by electrostatic forces either. For a 1-1 electrolyte and $h = 50$ Å calculations by means of Eq. (10.12) yield values of $(-\partial\Pi/\partial h)$ not exceeding $5 \cdot 10^{12}$ dyn/cm³, which is four orders of magnitude lower than experimental data.

*The rupture at $h < 600$ Å of these β -films is perhaps due to the hydrophobic attraction.

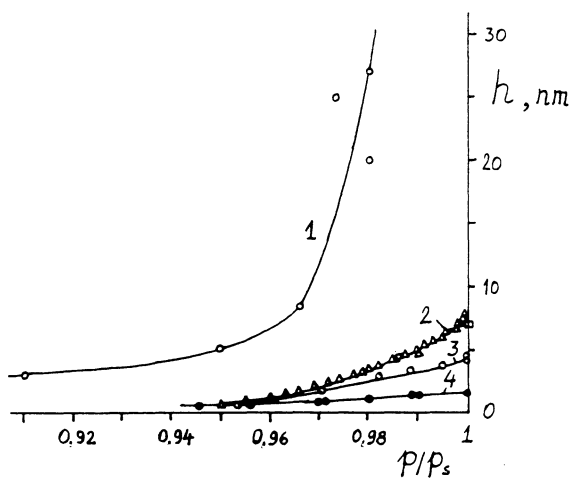


Fig. 10.12. Experimental disjoining pressure isotherms for α -films of water on quartz.

The impossibility of describing the behavior of α -isotherms in the framework of the theory of molecular and ion-electrostatic forces made it necessary to postulate that the stability of α -films has a different physical nature, connected with changes in water structure within a thin layer close to a hydrophilic solid substrate. The results of research into the structure of thin water layers, supporting this assumption, were given in Chapter 7. There is reason to believe, therefore, that the α -branch of the isotherm is mostly caused by the structural component of disjoining pressure, $\Pi_s(h)$.

A comparison of the curves in Fig. 10.12 with the corresponding values of contact angle θ_0 measured on the same substrate shows that α -isotherms shift upward when wetting improves. Therefore, better hydrophilic properties of a substrate result in increasing the range of the forces of structural repulsion. This may be caused by a long-range influence of the substrate, forcing on the boundary layers of water a certain degree of modification, the greater, the larger the number of active centers on the surface (centers capable of forming hydrogen bonds with water molecules). The difficulty in developing a quantitative theory of the Π_s component consists precisely in a high sensitivity of the structure of boundary water layers (and, consequently, of the depth of the zone of structural modification) to hydrophilic properties of the substrate. Pashley and Kitchener [30] have applied what seems to be the most elaborate method of cleaning the surface of quartz, producing complete wetting ($\theta_0 = 0$), and obtained α -films with thickness of 200-300 Å at $p/p_s = 0.97-0.975$ (curve 1, Fig. 10.12). Even the minutest contam-

ination of quartz surface, resulting in its feeble hydrophobization, or a partial dehydroxylation, reduces the thickness of α -films (at the same values of p/p_s) down to 30-50 Å (curves 2 and 3). Thus, the isotherm marked as curve 2 is obtained under ordinary conditions when the contact angle of water on quartz is $\theta_0 = 10-20^\circ$ [31]. Methylation of quartz surface ($\theta_0 = 90^\circ$) results in a further reduction of thickness of α -films [68-70]. Ellipsometric analysis of water adsorption on a Teflon surface (curve 4) gives similar results [69]. Adsorption of surfactants, resulting in a change in hydrophilic properties of the substrate, may produce an analogous effect.

The data on the temperature dependence of the thickness of α -films of water [68], discussed in Chapter 7 (see Fig. 7.1), offer a direct confirmation of the structural nature of stability of these films. As already mentioned, the Π_e and Π_m components of disjoining pressure are hardly sensitive to temperature. Therefore, a sharp drop in the thickness of α -films as a result of a rise in temperature can be explained only by destruction of a special structure of boundary layers of water when the thermal motion of molecules is intensified. When temperature increases to 80°C, water is known to behave as an ordinary liquid because the network of intermolecular hydrogen bonds is destroyed. Earlier Perever-tayev and Metsik observed that the thickness of α -films of water on the surface of cleaved mica diminished when temperature was increased from 20 to 50°C [71].

It is difficult to explain repulsive forces on the order of $\Pi \approx 3 \cdot 10^6$ dyn/cm² when the surfaces of a film are spaced by about 300 Å (curve 1, Fig. 10.12) without introducing structural long-range forces, as Pashley's consideration of possible alternative explanations indicated [72].

We should not ignore the fact that isotherms of α -films could be affected to some extent by leaching and dissolving of substrates (which is pronounced for glass and mica), as well as the formation (however slow) of a gel layer on quartz surface in contact with water [73]. However, the contribution of the Π_s component to the shape of α -isotherms seems to be the main factor. An increase in temperature can be expected to intensify dissolution and gel formation and to increase (not decrease) the thickness of films because of osmotic and steric effects; Fig. 7.1 shows that increasing temperature invariably results in reducing the thickness of α -films.

Derjaguin and Zorin [29] demonstrated experimentally that α -isotherms intersect the thickness axis and pass into the range of negative values of disjoining pressure. This means that at a certain film thickness $h = h_0$, the structural component Π_s changes sign (Fig. 10.5b). This could be caused by a complex structure of the boundary water layer near a hydrophilic surface. Derjaguin et al. [74] and later Drost-Hansen [75] suggested that water layers adja-

cent to a surface are better ordered, and molecules in this layer are more strongly bound to each other than they are in the bulk liquid. A transient layer (referred to as "partially melted") with a lower degree of ordering and intermolecular bonds partially disrupted in comparison with the bulk state is formed between the ordered layer mentioned above and the bulk water. The overlapping of these "partially melted" layers in the course of thinning of a film may result in attractive structural forces ($\Pi_s < 0$) that can be replaced, as film thickness further diminishes, by repulsive structural forces ($\Pi_s > 0$). Obviously, this hypothesis needs testing and refining.

However, it is not in contradiction with the known experimental facts on sign reversal of the thermomechanical effect [74] at increasing pressure gradient, and the reversal of direction of thermo-osmotic flow in thinner layers with diminishing pore size [76, 77] (see Chapter 9, Section 9.6).

We have mentioned already that in some cases the isotherms of α -films may be affected by the formation of a gel layer on the surface of quartz on prolonged exposure to water (longer than several days) [73]. The gel layer develops as a result of loosening of the surface of quartz by penetrating water molecules and because of adsorption of dissolved molecules of silicic acid.

In order to clarify the role played by the gel layer in the stability of α -films, α -isotherms were recorded under conditions in which the formation of the gel layer was a result of hydrothermal treatment of quartz plates in the autoclave [78]. Figure 10.13 shows the isotherms of polymolecular adsorption of water vapor on a hydrothermally treated surface (curves 1 and 2) and on the original quartz surface (curve 3). The relative vapor pressure was varied by means of saturated solutions of various salts. Film thickness was measured by absorption of IR radiation.

The curves show that the presence of a gel layer on a hydrothermally treated surface shifts the isotherm upward by about 25–30 Å. This value characterizes the thickness of the surface layer of gel because even a considerable drop in p/p_s did not decrease the thickness of water layer strongly bound to the fine-pore gel. It must be emphasized that the measured thickness characterizes precisely the layers of gel water because thickness measurements were carried out by absorption of IR radiation in the range of stretching OH vibrations. But the thickness of the gel layer, taking into account the silicic acid it contained, could be greater than 30 Å. As we find from Fig. 10.13, at $p/p_s > 0.9$ polymolecular adsorption of water vapor begins on the gel layer. The behavior of α -isotherms of water on the surface of the gel layer is approximately the same as on the original quartz surface.

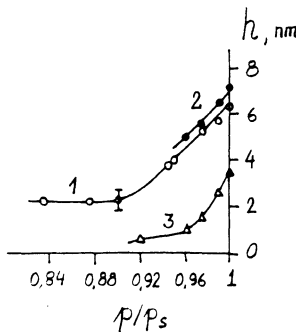


Fig. 10.13. Isotherms of polymolecular adsorption $h(p/p_s)$ of water on the gel-layer surface (curves 1 and 2), and on the initial quartz surface (curve 3).

We also see from Fig. 10.13 (curve 3) and Fig. 10.12 that, in the absence of a gel layer, the thickness of the water film on the quartz surface tends to a monolayer at $p/p_s \leq 0.9$. Kiselev and Kvividze [96] have demonstrated that clusters of water molecules separated by "dry" areas are formed on the surface at the value of adsorption that formally corresponds to one monolayer coverage. The clusters merge when film thickness exceeds 10 \AA , when the film can already be regarded as a continuous polymolecular coating, i.e., as a truly wetting film. Films with smaller thickness must be classified as adsorption films. The adsorption isotherm of such films is determined, in contrast to wetting films, by short-range forces, and mostly by the forces of covalent and hydrogen bonding between water molecules and substrate atoms.

Let us now consider the experimental results obtained for wetting films of nonpolar liquids.

By determining adsorption from the shift in the resonance frequency of a piezoelectric quartz plate coated with a 3000-\AA gold layer, Lando et al. [34] found that $\Pi(h)$ isotherms for polymolecular films of benzene, CCl_4 , octane, and cyclohexane are of the type $\Pi \propto 1/h^2$ in the range of h from 30 to 170 \AA . The law of molecular forces $\Pi \propto 1/h^3$ was observed to hold for $h < 30 \text{ \AA}$. Lando and co-workers suggested that departures from this law in the range of large thicknesses are caused by a possible deviation of the frequency dependence of permittivity $\epsilon(i\xi)$ in the surface layers of the metal from the bulk values. However, this behavior of frequency dependence would rather change the Hamaker constant than the law of interaction. More probably, the cause of departures was the roughness of the metal layer deposited on the surface of quartz. When film thickness is much less than the height of surface rough-

ness relief Δ , the influence of roughness is revealed only via the roughness coefficient, and this factor cannot modify the law of interaction but can only change the value of measured thickness. When h is comparable to Δ , surface roughness becomes capable of changing the shape of isotherms as well, the type of changes being dependent on the shape of asperities [96].

The same method of shift in resonance frequency was applied to obtain the isotherm for n-heptane on carefully polished surface of piezoelectric quartz without a metal coating [32]. The isotherm was found to fit extremely well the law $\Pi_m = -A_0/6\pi h^3$ in the range of thickness from 30 to 100 Å, with the Hamaker constant $A_0 = -2.3 \times 10^{-12}$ erg. However, this value of the constant is approximately an order of magnitude greater than the theoretical prediction ($A_0 = -1.6 \cdot 10^{-13}$ erg); no explanation of the discrepancy has been found so far.

The discrepancies discussed above probably originate in peculiarities of measurements on piezoelectric quartz. It is known that measurements by other techniques give a good fit to the law $\Pi \propto 1/h^3$, corresponding to the interaction of the film with the substrate due to molecular forces. This holds for the polymolecular low-temperature adsorption of nitrogen and of a number of other inert gases (argon on graphite, helium on quartz, as well as on glass, polymers, and fluorite crystals) [35, 36, 80-82].

The data obtained by direct measurements of thickness of wetting films for nonpolar liquids on smooth substrates are especially important in connection with the discrepancies mentioned above. Thus, very good quantitative agreement of $\Pi(h)$ isotherms with the results of calculations by means of the exact equation of the molecular forces theory were obtained for helium films on atomically smooth cleavage surfaces of crystals of alkaline-earth fluorites by acoustic interference techniques in the thickness range from 10 to 250 Å [35]. The functions $\epsilon(i\xi)$ for helium and substrate materials (CaF_2 , SrF_2 , and BaF_2) were obtained by using the technique of Ninham and Parsegian [83] on the basis of spectral data. Detailed data are known for fluorites in the range of quantum energies up to 50 eV. Three main resonance frequencies were used for helium: $\omega_c = 3.22 \cdot 10^{16}$, $3.74 \cdot 10^{16}$, and $1.2 \cdot 10^{17}$ rad/s. The combination of the exact theory of Lifshitz and reliable spectral data yielded an excellent agreement with the experiment. Sabisky and Anderson [35] also believe that deviations from the Lifshitz theory for helium films, reported in other papers, were caused by surface roughness of specimens.

Kussakov and Titiyevskaya [84] applied the bubble method [2] and obtained the isotherms of disjoining pressure for wetting films of a number of nonpolar liquids on steel, long before the publica-

tion of the above-cited papers. The optical interference method of measuring the film thickness used in [84] made the measurements possible only for $h \geq 400 \text{ \AA}$. For films 400-800 \AA thick the isotherms were in a satisfactory agreement with the law $\Pi_m = -B/h^4$ representing the fully retarded molecular forces. The values of B extracted from experimental data are in good agreement with the theoretical values [85]. Thus, the experimentally obtained B for a hexane film on steel is $B = -1.7 \cdot 10^{-19} \text{ erg}\cdot\text{cm}$, while theory gives $B = -1.6 \cdot 10^{-19} \text{ erg}\cdot\text{cm}$. A somewhat smaller value $B = -1.5 \cdot 10^{-19} \text{ erg}\cdot\text{cm}$, again not very different from the theoretical value, was obtained for cyclohexane. In the same work [84] the authors found that the thickness of wetting n-octane films decreased in a regular manner as the refractive index of the substrate was reduced from that of steel to diamond and quartz, in good agreement with the theory of molecular forces (see Chapter 4).

Blake [9] measured the thickness of wetting n-decane and n-octane films on a polished surface of Al_2O_3 by recording the intensity of light reflected by the film. Good agreement with the results of numerical calculations via the exact equation of the Lifshitz dispersion forces was obtained for films with thickness from 300 to 800 \AA . The difference between the theoretical and experimental values of Π did not exceed 1-2%.

In an earlier paper Blake et al. [86] obtained, by the balance technique, the adsorption isotherm of n-decane vapor on oxidized surface of aluminum foils. The thickness of oxide layer was not less than 50 \AA . In the range of film thickness from 5 to 20 \AA the isotherm satisfied the law $\Pi_m = -A_0/6\pi h^3$ with the Hamaker constant A_0 greater than the theoretical value calculated by the Gregory equation [87], $A_0 = -4.7 \cdot 10^{-20} \text{ J}$, by only 15%. Deviations from the law of inverse cubes appeared at $h \geq 25 \text{ \AA}$; possibly, this was caused by the effect of the metallic substrate or the effect of surface roughness of oxidized foil that start at such thicknesses ($h \approx \Delta$).

Ellipsometric techniques applied to wetting films made it possible to move into the range of h smaller than in Kussakov's and Blake's experiments. Figure 10.14 shows $\Pi(h)$ isotherms obtained by removing the liquid from a solid substrate by suction through a porous filter (Fig. 10.2) [19, 20, 23]. Curve 1 describes wetting films of tetradecane on polished steel, and curve 2 on glass. Filled circles were obtained when the film approached equilibrium while its thickness diminished, and unfilled circles while it increased. The curves show that the isotherms obtained are indeed equilibrium isotherms because both filled and unfilled circles lie on the same curve.

The Hamaker constants calculated from the slope of the plots are $A_0 = -7.3 \cdot 10^{-13} \text{ erg}$ for the metal substrate and $A_0 = -4.8 \cdot 10^{-14}$

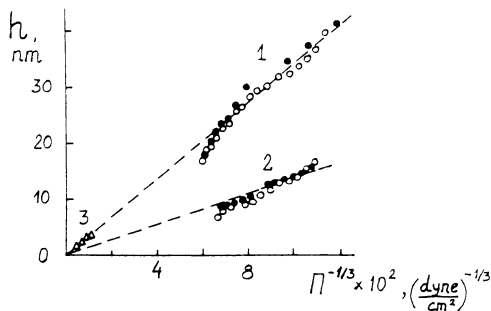


Fig. 10.14. Isotherms of the disjoining pressure $\Pi(h)$ of tetradecane films on the polished surface of steel (1) and glass (2). Curve 3 is characteristic of the polymolecular adsorption of n-hexane on steel. The values of Π are given in dyn/cm².

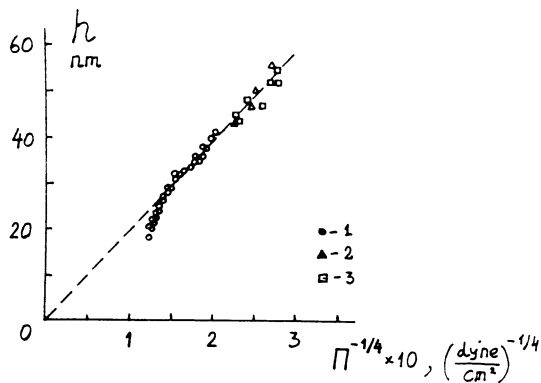


Fig. 10.15. Isotherms of the disjoining pressure $\Pi(h)$ of the films of tetradecane (1), cyclohexane (2), and n-heptane (3) on the steel surface. The values of Π are given in dyn/cm².

erg for the dielectric (glass). These values are smaller than the theoretical ones by a factor of two to three. In the case of glass, spectral data are lacking, so that $\epsilon(i\xi)$ was calculated by using the absorption spectrum of quartz and the Kramers-Krönig equation [85]. The function $\epsilon_3(i\xi)$ for tetradecane was calculated by using a single UV absorption band. The calculated values of constants were $A_0 = -1.5 \cdot 10^{-12}$ erg for the metal and $A_0 = -1.3 \cdot 10^{-13}$ erg for quartz.

The discrepancies between experimental and theoretical values of A_0 are possibly associated with the effects of electromagnetic

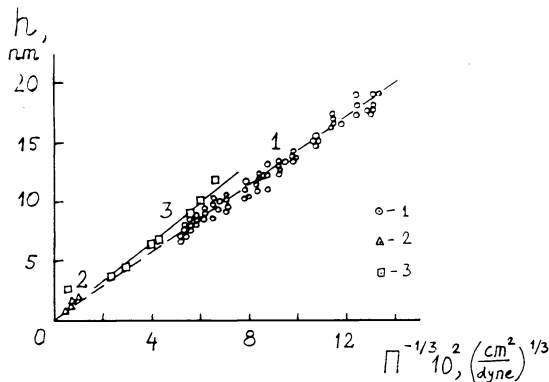


Fig. 10.16. Isotherms of the disjoining pressure $\Pi(h)$ of tetradecane films on the surfaces of mica (1) and quartz capillaries (3). Curve 2 illustrates the polymolecular adsorption of n-hexane on the mica surface.

retardation and of surface roughness of polished glass and steel. Electron-microscopic study demonstrated that the mean depth of the network of scratches was $\Delta = 120 \text{ \AA}$ on glass and $\Delta = 150 \text{ \AA}$ on steel.

Figure 10.15 gives the curve $\Pi(h)$ for the steel substrate, replotted in different coordinates. It shows that for $h \geq 300 \text{ \AA}$ the data fit better the law of fully retarded forces $\Pi_m = -B/h^4$. The constant $B = -1.6 \cdot 10^{-19} \text{ erg} \cdot \text{cm}$ found from this graph is close to the theoretical value $B = -1.75 \cdot 10^{-19} \text{ erg} \cdot \text{cm}$. The data of Kussakov and Titiyevskaya [84] for cyclohexane on steel also fit satisfactorily the same straight line. This occurs because the values of ε_{30} are nearly equal for tetradecane (2.04) and cyclohexane (2.05).

It is seen in Fig. 10.14 that the law $1/h^3$ is not valid in the range of h from 170 to 270 \AA (curve 1). This is caused by the transition to fully retarded forces at $h > 270 \text{ \AA}$, and by the effect of surface roughness Δ that is felt at $h < 270 \text{ \AA}$. The law $1/h^3$, which could hold in the range of thickness $h \leq 200 \text{ \AA}$, is hidden behind roughness effects.

This is one of the main differences between the studies of free and wetting films. With the former the surfaces retain molecular smoothness, while in the latter the surface roughness may be unavoidable. This factor is always present in actual cases, with very rare exceptions. Consequently, the law $1/h^3$ is often observed to fail in the range of thickness comparable to the size of surface roughness Δ .

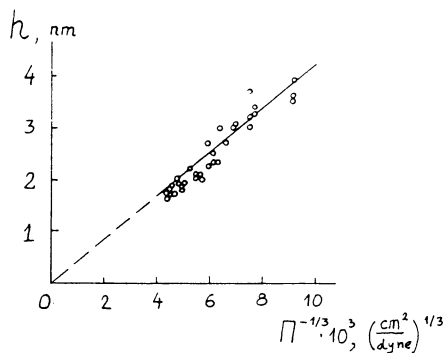


Fig. 10.17. Isotherm of the polymolecular adsorption of n-hexane on the polished steel surface.

The above conclusion is confirmed by the observation that, as a rule, the law $\Pi \sim 1/h^3$ holds quite well on molecularly smooth substrates (mica, surface-melted quartz) and for thinner films (when $h \ll \Delta$). Thus, Fig. 10.16 shows Zheleznyi's data [27] for tetradecane films obtained by the spreading technique (see Fig. 10.3) on the surface of freshly drawn quartz capillaries (curve 3), as well as $\Pi(h)$ isotherms for tetradecane films on molecularly smooth surface of mica (curve 1) [20, 23]. In the latter case we used the same method of suction through a porous filter as in the experiments whose results were plotted in Figs. 10.14 and 10.15. As seen from Fig. 10.16, the law $1/h^3$ holds well in the whole range of thickness, down to very small h . The experimental Hamaker constant is fairly close to the theoretical value for tetradecane films in capillaries ($A_0 = -0.8 \cdot 10^{-14}$ erg and $A_0 = -1.3 \cdot 10^{-14}$ erg, respectively), and the values of the constant coincide for films on mica ($A_0 = -0.5 \cdot 10^{-13}$ erg).

The law of nonretarded molecular forces $\Pi \propto 1/h^3$ is also observed to give a good fit to the data for polished steel ($\Delta \approx 150 \text{ \AA}$), but only for films with $h \ll \Delta$ [88]. These results were obtained for polymolecular adsorption films of n-hexane by ellipsometry. Figures 10.14 (curve 3) and 10.17 demonstrate that the graph is linear in the range of h from 20 to 40 \AA ($h \ll \Delta$), passing through the origin of the coordinate system, with $A_0 = -1.4 \cdot 10^{-12}$ erg. This value falls fairly close to the theoretical value of the constant $A_0 = -1.9 \cdot 10^{-12}$ erg.

The theory of molecular forces also adequately describes [89, 90] the stability of alkane films on water surface as a function of chain length, experimentally studied by Hauxwell and Ottewill [38] and later by Sonntag et al. [25, 26].

Therefore, when the macroscopic theory of molecular forces is applied correctly, i.e., when exact solutions and reliable spectral data are used, it is found to agree with the experimental data for wetting films of a number of nonpolar liquids on smooth surfaces and for films whose thickness is much greater or much less than the characteristic height of surface roughness.

Sonntag et al. [25, 26] investigated the stabilization of wetting aqueous films on a liquid substrate (oil) due to the steric component of disjoining pressure when a surfactant is added. In contrast to this situation, oil films on water can be stabilized by dispersion forces alone. It was found that films with refractive index below 1.4 (up to n-octane) can be stable.

Very little is known about the stability of wetting films formed by mixtures of mutually soluble liquids. Kussakov and Titiyevskaya [84] demonstrated that 10^{-3} mole/liter of caprylic acid added to heptane sharply increases the thickness of films at the same value of disjoining pressure. This cannot be explained in terms of the theory of molecular forces because this admixture does not appreciably alter the static permittivity of the liquid ($\epsilon_{30} = 2.04$ for heptane, $\epsilon_{30} = 1.91$ for caprylic acid). It can be assumed that nonuniform distribution of caprylic acid across the film led to the rise of the positive adsorption component of disjoining pressure, $\Pi_a(h)$ (see Chapter 5).

10.4. WETTING FILMS ON NONFLAT SURFACES

Let us consider now the stability of wetting films on nonflat surfaces of constant curvature, viz., cylindrical and spherical surfaces. Particular cases are wetting films on the surface of cylindrical and spherical pores, on fibers, and on spherical particles.

The equilibrium of a film on a curved surface of a solid with the vapor or with a capillary meniscus at a capillary pressure ΔP_k is given by the equation that takes into account both the capillary and the surface forces [3, 91, 92]:

$$P_k(K) + \Pi(h) = - \frac{RT}{v_m} \ln \frac{P}{P_s} = \Delta P_k \quad (10.13)$$

where P_k is the capillary pressure in the film, depending on the surface curvature K , and Π is the disjoining pressure which depends only on film thickness. If $h \ll r$, where r is the radius of curvature of the substrate, it is sufficient to use in Eq. (10.13) the isotherm $\Pi(h)$ of disjoining pressure for flat films.

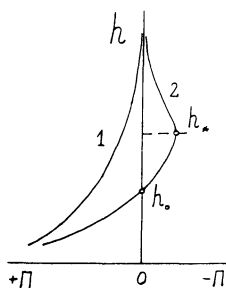


Fig. 10.18. Change in the disjoining pressure isotherm when passing over from the plane surface (curve 1) to the wetting film on the outer surface of a cylinder (curve 2).

Consider first films on convex solid surfaces: a spherical particle and a cylindrical fiber of constant radius $r = \text{const}$. Equation (10.13) is then rewritten in the form [93]

$$-m\sigma/(r + h) + \Pi(h) = \phi(h) = \Delta P_k \quad (10.14)$$

where $m = 1$ for the film on a cylinder and $m = 2$ for the film on a sphere.

We refer to $\phi(h)$ as the normalized isotherm of disjoining pressure. As follows from (10.13), at $p/p_s = 1$, when $\phi(h) = 0$, a film on a convex surface has, even in the case of complete wetting, a finite thickness h_0 determined by the condition

$$\Pi(h_0) = m\sigma/(r + h_0)$$

(see Fig. 10.18). This situation was also discussed by Broekhoff [94].

The condition of stability for a film on a convex surface is written in the form [93]

$$(\partial\phi/\partial h) < 0 \text{ or } \partial\Pi/\partial h < -m\sigma/(r + h)^2 \quad (10.15)$$

The constraint (10.15) is stronger than the condition $\partial\Pi/\partial h < 0$ for flat films. This means that, other conditions being equal, films on a convex surface are less stable than flat films. Thus, with complete wetting, when flat films (curve 1, Fig. 10.18) are stable regardless of thickness, a film on a convex surface (curve 2) becomes unstable when $h \geq h^*$ and h^* can be evaluated, for example, for the isotherm $\Pi_m = -A_0/6\pi h^3$. By taking the derivative $\partial\Pi_m/\partial h$ and equating it to the right-hand side of Eq. (10.15), we find

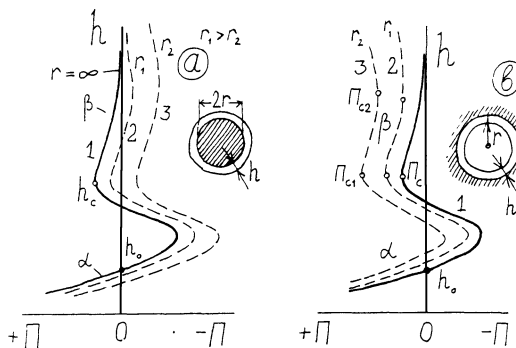


Fig. 10.19. Isotherms of the disjoining pressure of the wetting films on the surfaces of threads (a) and the internal surface of capillaries (b) of different radii.

$$h_* = C + \sqrt{C(C + 2r)} \quad (10.16)$$

where $C = (-A_0/8\pi m\sigma)^{1/2}$.

For instance, assuming $A_0 = -3 \cdot 10^{-12}$ erg and $\sigma = 23$ dyn/cm for films on a quartz fiber ($m = 1$), we obtain $h_* = 1700 \text{ \AA}$ for $r = 10^{-5}$ cm. Films with thickness greater than h_* become unstable and rupture, necessarily undergoing a transition to a more stable state of a thin film. In the supersaturation range these films ($h_* > h > h_0$) can be in equilibrium with droplets on a fiber or sphere.

For S-shaped isotherms of flat films (Fig. 10.5) corresponding to partial wetting, the isotherms $\Phi(h)$ for films on fibers have the shape outlined in Fig. 10.19a. Here curve 1 corresponds to the flat-film isotherm $\Pi(h)$, and curves 2 and 3 correspond to $\Phi(h)$ isotherms on fibers of decreasing radius. Curves $\Phi(h)$ are obtained by shifting the $\Pi(h)$ isotherm by a quantity $m\sigma/(r + h)$, as prescribed by Eq. (10.14). The graphs show that as the radius of the fiber or sphere diminishes, the thickness of equilibrium α -films at the same values of Π or p/p_s decreases and the range of metastable β -films (curve 3) vanishes (at sufficiently small r). The value of the critical disjoining pressure Π_c also decreases in this sequence.

The equation of equilibrium for films on a concave surface, for instance on the inner surface of a cylindrical capillary, has the following form [93]:

$$\frac{\sigma}{(r - h)} + \Pi(h) = \Phi(h) = -\frac{RT}{V_m} \ln \frac{P}{P_s} = \Delta P_k \quad (10.17)$$

The corresponding stability equation is written as follows:

$$\frac{\partial \Phi}{\partial h} < 0 \text{ or } \frac{\partial \Pi}{\partial h} < -\sigma/(r - h)^2 \quad (10.18)$$

In contrast to convex surfaces, in this case the value of radius r limits the film thickness. However, even before h reaches the value of r , the necessity arises of taking into account the interaction of the local segment of the film not only with the immediately adjacent segment of the wall but with other segments of the capillary surface as well [97]. For this reason, hereafter we consider only capillaries with sufficiently large radii, satisfying the condition $h \ll r$.

Figure 10.19b shows how an S-shaped isotherm of a flat film (curve 1) is transformed in the case of a wetting film on the inner surface of a capillary when its radius diminishes (curves 2 and 3). In contrast to convex surfaces, in this situation the range of β -film instability falls into the range of undersaturation ($\Pi > 0$). An interesting feature of the $\Phi(h)$ isotherms is that β -films become unstable not only when vapor pressure is lowered (at $\Pi \leq \Pi_{c1}$) but also when the second critical pressure is exceeded (at $\Pi \geq \Pi_{c2}$). In some cases (Fig. 10.19b, curve 3), metastable β -films can be formed only in a limited range of capillary radii, $r_2 > r > r_1$, corresponding to intermediate values of disjoining pressure: $\Pi_{c1} < \Pi < \Pi_{c2}$, where $r_1 = \Pi_{c1}/\sigma$ and $r_2 = \Pi_{c2}/\sigma$. Only α -films are stable in capillaries with larger radii.

This explains the results of Zorin and Sobolev [95], who observed that only thin α -films ($h \approx 50-60 \text{ \AA}$) were formed in capillaries with $r \geq 0.4 \text{ \mu m}$, while much thicker films ($h \approx 300-400 \text{ \AA}$), which can represent only the β -branch of isotherms, formed in capillaries of smaller radii. The effect is thus traced to the curvature of the surface of the wetting film.

Two distinct cases of loss of stability are possible for wetting films on the inner surface of a capillary. The first corresponds to the instability of a β -film with respect to a more stable state of α -films. This $\beta \rightarrow \alpha$ transition can be realized only with partial wetting, and occurs spontaneously, being accompanied by thinning of the film. The corresponding critical disjoining pressure equals Π_{c1} (Fig. 10.19).

The second case corresponds to film instability with respect to the formation of capillary condensate. It is associated with the geometry of a capillary and is realized when the film thickness increases to a certain limit corresponding to the second critical pressure Π_{c2} . When this limit is approached, fluctuations of film thickness are enhanced, so that the film closes up and the capillary bore fills up with the liquid.

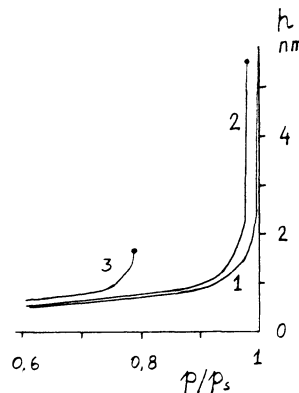


Fig. 10.20. An example of calculation of the isotherms of polymolecular adsorption on the plane surface (1) and the internal surface of capillaries having $r = 100 \text{ nm}$ (2) and $r = 10 \text{ nm}$ (3).

Isotherms $\Phi(h)$ for liquids completely wetting the concave surface of a capillary have the form shown in Fig. 10.20. Here curve 1 is the isotherm of a flat film, and curves 2 and 3 are $\Phi(h)$ isotherms in capillaries with successively smaller radii. Calculations were carried out for the same values of A_0 and σ as in the example discussed above. The cutoff of the isotherms at $p/p_s = 0.98$ (curve 2) and at $p/p_s = 0.79$ (curve 3) corresponds to the loss of film stability when the constraint (10.18) is violated. The loss of stability results in filling the capillary with the condensate. The critical film thicknesses at which this occurs are 18 \AA (curve 3) and 55 \AA (curve 2), much smaller than the respective capillary radii, $r = 100 \text{ \AA}$ and $r = 1000 \text{ \AA}$. The condition $h \ll r$ of the applicability of Eq. (10.13) was thus satisfied in the whole physically realizable range of film thickness.

As seen from Fig. 10.20, at equal values of p/p_s the reduction in capillary radius increases the thickness of wetting films but makes the range in which they are stable narrower.

The equations obtained for equilibrium, (10.14) and (10.17), make it possible to calculate the isotherms $h - (p/p_s)$ and the ranges of stable states of wetting films on fibers, spherical particles, and internal surface of capillaries for flat-film isotherms of arbitrary type, including isotherms obtained experimentally.

REFERENCES

1. B. V. Derjaguin and E. V. Obukhov, *Acta Physicochim. URSS*, 5, 1 (1936).
2. B. V. Derjaguin and M. M. Kussakov, *Acta Physicochim. URSS*, 10, 25, 153 (1939).
3. B. V. Derjaguin, *Kolloidn. Zh.*, 17, 207 (1955).
4. B. V. Derjaguin, *Kolloidn. Zh.*, 39, 1139 (1977); in: *Modern Theory of Capillarity*, Academie Verlag, Berlin (1981), p. 35.
5. "Definitions, terminology, and symbols in colloid and surface chemistry," *Pure Appl. Chem.*, 31, 579 (1972).
6. A. D. Read and J. A. Kitchener, *Wetting*, Soc. Chem. Ind., No. 25, London (1967), p. 300.
7. A. D. Read and J. A. Kitchener, *J. Colloid Interface Sci.*, 30, 391 (1969).
8. T. D. Blake and J. A. Kitchener, *J. Chem. Soc., Faraday Trans. I*, 68, 1435 (1972).
9. T. D. Blake, *J. Chem. Soc., Faraday Trans. I*, 71, 192 (1975).
10. B. V. Derjaguin, A. S. Tityevskaya, I. I. Abrikossova, and A. D. Malkina, *Discuss. Faraday Soc.*, No. 18, 24 (1954); *Proceedings of the 2nd International Congress of Surface Activity*, Vol. 1, Butterworths, London (1957), p. 211.
11. B. V. Derjaguin, A. V. Gorodetskaya, A. S. Tityevskaya, and V. N. Yashin, *Kolloidn. Zh.*, 23, 535 (1961).
12. A. Scheludko and D. Platikanov, *Kolloid-Z.*, 175, 150 (1961).
13. D. Platikanov, *J. Phys. Chem.*, 68, 3619 (1964).
14. A. Scheludko, S. Tschaljowska, and A. Fabrikant, in: *Thin Liquid Films and Boundary Layers*, Academic Press, London (1971), p. 215.
15. M. P. Aronson and H. M. Princen, *J. Colloid Interface Sci.*, 52, 345 (1975).
16. M. P. Aronson and H. M. Princen, *Colloid Polymer. Sci.*, 256, 140 (1978).
17. D. Exerova, I. Ivanov, and A. Scheludko, *Ann. Univ. Sofia, Fac. Chem.*, 56, 157 (1961).
18. A. Scheludko and E. Manev, *Trans. Faraday Soc.*, 64, 1123 (1968).
19. V. A. Shishin, Z. M. Zorin, and N. V. Churaev, *Kolloidn. Zh.*, 39, 400, 520 (1977).
20. B. V. Derjaguin, Z. M. Zorin, N. V. Churaev, and V. A. Shishin, in: *Wetting, Spreading, and Adhesion*, Academic Press, London (1978), p. 201.
21. K. J. Mysels, *J. Phys. Chem.*, 68, 3441 (1964).
22. D. Exerova and A. Scheludko, *Dokl. Bolg. Akad. Nauk*, 24, 47 (1971).
23. B. V. Derjaguin, Z. M. Zorin, N. V. Churaev, and V. A. Shishin, in: *Surface Forces in Thin Films*, Nauka, Moscow (1979), p. 148.
24. B. V. Derjaguin and Z. M. Zorin, *Zh. Fiz. Khim.*, 29, 1010 (1955).

25. H. Sonntag, N. Buske, and B. Unterberger, *Kolloid-Z. Z. Polym.*, 248, 1016 (1971).
26. H. Sonntag, N. Buske, and H. Fruhner, *Kolloid-Z. Z. Polym.*, 250, 330 (1972).
27. B. V. Derjaguin, B. V. Zheleznyi, and A. P. Tkachev, *Dokl. Akad. Nauk SSSR*, 206, 1146 (1972).
28. B. V. Derjaguin and S. M. Levi, *Film Coating Theory*, Focal Press, New York-London (1964).
29. B. V. Derjaguin and Z. M. Zorin, *Zh. Fiz. Khim.*, 29, 1755 (1955); *Proceedings of the 2nd International Congress of Surface Activity*, Vol. 2, Butterworths, London (1957), p. 145.
30. R. M. Pashley and J. A. Kitchener, *J. Colloid Interface Sci.*, 71, 491 (1979).
31. G. F. Ershova, Z. M. Zorin, and N. V. Churaev, *Kolloidn. Zh.*, 41, 19 (1979).
32. W. H. Wade and L. J. Slutsky, *J. Chem. Phys.*, 40, 3394 (1964).
33. D. Lando and L. J. Slutsky, *Phys. Rev.*, 2B, 2863 (1970).
34. D. Lando, J. F. Bohland, and W. C. Hahn, *J. Phys. Chem.*, 77, 1969 (1973).
35. E. S. Sabisky and C. H. Anderson, *Phys. Rev.*, A7, 790 (1973).
36. T. P. Chen, M. J. Di Pirro, A. A. Gaeta, and F. M. Gasparini, *J. Low Temp. Phys.*, 26, 927 (1977).
37. S.-T. Hwang and K. Kammermeyer, *Membranes in Separations*, Wiley-Interscience (1975).
38. F. Hauxwell and R. H. Ottewill, *J. Colloid Interface Sci.*, 34, 493 (1970).
39. A. Scheludko, *Kolloid-Z.*, 155, 39 (1957).
40. A. Scheludko, *Dokl. Akad. Nauk SSSR*, 123, 1074 (1958).
41. A. Scheludko and D. Exerova, *Dokl. Akad. Nauk SSSR*, 127, 149 (1959); *Kolloid-Z.*, 165, 148 (1959); 168, 24 (1960).
42. A. Scheludko and D. Platikanov, *Dokl. Akad. Nauk SSSR*, 138, 415 (1961).
43. A. Scheludko, D. Exerova, and D. Platikanov, *Kolloidn. Zh.*, 25, 606 (1963).
44. A. Scheludko, *Adv. Colloid Interface Sci.*, 1, 391 (1967).
45. B. V. Derjaguin and N. V. Churaev, *J. Colloid Interface Sci.*, 66, 389 (1978).
46. H. J. Schulze, *Naturwissenschaften*, 59, 119 (1972).
47. Yu. M. Glazman and M. E. Krasnokutskaya, *Kolloidn. Zh.*, 27, 815 (1966); 28, 847 (1966); in: *Research in Surface Forces*, Vol. 3, Consultants Bureau, New York (1971), p. 189.
48. J. G. Blashuk and Yu. M. Glazman, in: *Research in Surface Forces*, Vol. 4, Consultants Bureau, New York (1975), p. 72.
49. G. D. Botsaris and Yu. M. Glazman, *J. Dispersion Sci. Technol.*, 3, 67 (1982).
50. B. V. Derjaguin and N. V. Churaev, *J. Colloid Interface Sci.*, 62, 369 (1977).
51. A. N. Frumkin and O. Gorodetskaya, *Zh. Fiz. Khim.*, 12, 511 (1938).

52. H. J. Schulze, *Colloid Polymer Sci.*, 253, 730 (1975).
53. B. V. Derjaguin, N. V. Churaev, and I. G. Ershova, *Dokl. Akad. Nauk SSSR*, 182, 132 (1968).
54. M. M. Viktorina, B. V. Derjaguin, I. G. Ershova, and N. V. Churaev, *Dokl. Akad. Nauk SSSR*, 200, 1306 (1971).
55. N. V. Churaev, B. V. Derjaguin, and I. G. Ershova, in: *Research in Surface Forces*, Vol. 4, Consultants Bureau, New York (1975), p. 165.
56. Z. M. Zorin, A. V. Novikova, A. K. Petrov, and N. V. Churaev, in: *Surface Forces in Thin Films and Stability of Colloids*, Nauka, Moscow (1974), p. 94.
57. N. V. Churaev, A. V. Novikova, A. K. Petrov, and Z. M. Zorin, *J. Colloid Interface Sci.*, 48, 374 (1974).
58. V. Ya. Volkova, C. V. Nerpin, and O. G. Us'yarov, in: *Collected Papers in Agrophysics*, No. 32, Gidrometeoizdat, Leningrad (1971), p. 184.
59. E. E. Voznaya, E. D. Taevere, and O. G. Us'yarov, *Kolloidn. Zh.*, 39, 1144 (1977).
60. O. G. Us'yarov, in: *Surface Forces in Thin Films*, Nauka, Moscow (1979), p. 159.
61. N. P. Tantsura and O. G. Us'yarov, *Kolloidn. Zh.*, 43, 375 (1981).
62. H. J. Schulze, *Colloid Polymer Sci.*, 254, 438 (1976); 256, 1037 (1978); in: *Surface Forces in Thin Films*, Nauka, Moscow (1979), p. 165.
63. H. J. Schulze and Chr. Cichos, *Z. Phys. Chemie DDR*, 251, 252 (1972).
64. B. V. Derjaguin and L. D. Landau, *Acta Physicochim. URSS*, 14, 633 (1941); *Zh. Eksp. Teor. Fiz.*, 11, 802 (1941); 15, 633 (1945).
65. D. Exerova and M. Zaharieva, in: *Research in Surface Forces*, Vol. 4, Consultants Bureau, New York (1975), p. 253.
66. Z. M. Zorin, V. P. Romanov, and N. V. Churaev, *Kolloidn. Zh.*, 41, 1066 (1979); *Colloid Polymer Sci.*, 257, 968 (1979).
67. A. C. Hall, *J. Phys. Chem.*, 74, 2742 (1970).
68. G. F. Ershova, Z. M. Zorin, and N. V. Churaev, *Kolloidn. Zh.*, 37, 208 (1975).
69. P. Hu and A. W. Adamson, *J. Colloid Interface Sci.*, 59, 605 (1977).
70. G. F. Ershova, Z. M. Zorin, A. V. Novikova, and N. V. Churaev, in: *Surface Forces in Thin Films*, Nauka, Moscow (1979), p. 168.
71. V. D. Perevertayev and M. S. Metsik, *Kolloidn. Zh.*, 28, 254 (1966).
72. R. M. Pashley, *J. Colloid Interface Sci.*, 78, 246 (1980).
73. N. V. Churaev, I. P. Sergeeva, V. D. Sobolev, and B. V. Derjaguin, *J. Colloid Interface Sci.*, 84, 451 (1981).
74. B. V. Derjaguin, Yu. Shutor, S. V. Nerpin, and M. A. Arutyunyan, *Dokl. Akad. Nauk SSSR*, 161, 147 (1965).

75. W. Drost-Hansen, Ind. Eng. Chem., 61, 10 (1969); J. Colloid Interface Sci., 58, 251 (1977).
76. P. A. Voznyi and N. V. Churaev, Kolloidn. Zh., 39, 264, 438 (1977).
77. B. V. Derjaguin and N. V. Churaev, Croat. Chem. Acta, 50, 187 (1977).
78. G. F. Ershova and N. V. Churaev, Kolloidn. Zh., 41, 1176 (1979).
79. V. M. Starov and N. V. Churaev, Kolloidn. Zh., 39, 1112 (1977).
80. R. W. Cranston and F. A. Inkley, Adv. Catal., 9, 143 (1957).
81. D. A. Payne, K. S. W. Sing, and D. H. Turk, J. Colloid Interface Sci., 43, 287 (1973).
82. W. A. Steele, J. Colloid Interface Sci., 75, 13 (1980).
83. B. W. Ninham and V. A. Parsegian, J. Chem. Phys., 52, 4578 (1970).
84. M. M. Kussakov and A. S. Titiyevskaya, Dokl. Akad. Nauk SSSR, 28, 333 (1940).
85. N. V. Churaev, Kolloidn. Zh., 36, 318, 323 (1974).
86. T. D. Blake, J. L. Cayias, W. H. Wade, and J. A. Zerdecki, J. Colloid Interface Sci., 37, 678 (1971).
87. J. Gregory, Adv. Colloid Interface Sci., 2, 396 (1970).
88. Z. M. Zorin, N. V. Churaev, and V. A. Shishin, Kolloidn. Zh., 40, 986 (1978).
89. P. Richmond, B. W. Ninham, and R. H. Ottewill, J. Colloid Interface Sci., 45, 69 (1973).
90. N. V. Churaev, Kolloidn. Zh., 37, 730 (1975).
91. B. V. Derjaguin, V. M. Starov, and N. V. Churaev, Kolloidn. Zh., 38, 875, 1082 (1976).
92. N. V. Churaev, V. M. Starov, and B. V. Derjaguin, J. Colloid Interface Sci., 89, 16 (1982).
93. V. M. Starov and N. V. Churaev, Kolloidn. Zh., 40, 909 (1978).
94. J. C. P. Broekhoff and B. G. Linsen, in: Physical and Chemical Aspects of Adsorbents and Catalysts, B. G. Linsen (ed.), Academic Press, London (1970), p. 23.
95. V. D. Sobolev and Z. M. Zorin, in: Research in Surface Forces, Vol. 3, Consultants Bureau, New York (1971), p. 30.
96. V. I. Kvividze and V. F. Kiselev, Zh. Strukt. Khim., 8, 221 (1967).
97. B. V. Derjaguin and N. V. Churaev, J. Colloid Interface Sci., 54, 157 (1976).

Chapter 11

SURFACE FORCES

IN TRANSPORT PHENOMENA

Previous chapters have shown how the field of long-range surface forces alters the composition and properties of liquids in the neighborhood of interfaces. Clearly, these changes must also affect mass transfer processes to some extent. Among the better known transport processes due to surface charge are the electrokinetic phenomena. However, these phenomena will not be discussed in this book because they have been thoroughly reviewed in recent monographs [1-3]. We begin this chapter with a treatment of less well-known phenomena, viz., capillary osmosis and diffusiophoresis, first analyzed by Derjaguin [4]. Then we treat the thermo-osmosis and thermocrystallization flow of liquids.

11.1 CAPILLARY OSMOSIS

It was shown in Chapter 5 that a diffuse structure can form not only in ionic atmospheres but also in adsorption layers of neutral molecules in solutions. The molecules of the diffuse part of the adsorption layer are found to be, like ions, sufficiently mobile to be entrained by a flow of liquid. Transfer of ions of a diffuse layer by the flow or, conversely, entrainment of liquid by the ions of a diffuse layer in an electric field, cause the various electrokinetic phenomena [1-3]. By analogy, there are parallel phenomena caused by capillary osmosis (first pointed out in [4]), viz., the flow of a liquid due to a concentration gradient of the solute (an analog of electro-osmosis) and the transfer of the diffuse-layer molecules by the flow of the liquid (reverse osmosis) resulting in a concentration difference (an analog of streaming potential). Conversely, the experimental observations of capillary-osmotic effects

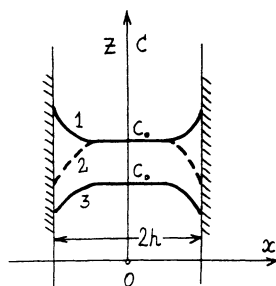


Fig. 11.1. Concentration distribution in a solution at the walls of a wide gap of width $2h$, with diffuse adsorption layers not overlapping.

(capillary osmosis or reverse osmosis) are themselves direct confirmation of the diffuse nature of adsorption layers. Surface forces change the equilibrium concentration of the solution: the concentration at the walls can be either greater than the bulk value C_0 (Fig. 11.1, curve 1) or less than C_0 (dashed curve 2). The latter case is the so-called negative adsorption in which the molecules of the solvent interact with the solid surface more strongly than the molecules of the solute.

In dilute solutions the change in concentration $C(x)$ along the normal to the wall causes a gradient of osmotic pressure,

$$dp_0/dx = RT[d(C - C_0)/dx]$$

which is balanced out at equilibrium by the corresponding gradient of hydrostatic pressure dp/dx in the layers of the solution adjacent to the walls. The additional constraint is $p_0 + p = P$, where P is the pressure in the bulk liquid. The extension of the diffuse adsorption layer along the x axis and the distribution of solute concentration $C(x)$ within this layer depend on solvent composition and on the field of surface forces. Curve 3 in Fig. 11.1 illustrates how concentration distribution changes when C_0 diminishes. A comparison of curves 1 and 3 shows that a concentration gradient along the z axis in the bulk solution (in the absence of a pressure gradient in the bulk solution, i.e., at $\partial p/\partial z = 0$) results in nonbalanced tangential pressure gradients $\partial p/\partial z \neq 0$. When the pore width $2h$ is much greater than the thickness of diffuse adsorbed layers, the flow that appears can be treated as the slippage of the liquid at the wall.

The velocity v_{co} of slippage at the wall is found from the Navier-Stokes equation:

$$\frac{\partial p}{\partial z} = RT \frac{d(C - C_0)}{dz} = - \frac{\partial}{\partial x} \left(\eta \frac{dv}{dx} \right) \quad (11.1)$$

Following an earlier procedure [4], we assume that, by virtue of the Boltzmann equation, C is proportional to C_0 and that the viscosity η of the liquid is constant. Then Eq. (11.1) can be rewritten in the following form:

$$\frac{RT}{\eta} \left(\frac{C - C_0}{C_0} \right) \frac{dC_0}{dz} = - \frac{d^2 v}{dx^2} \quad (11.2)$$

Integrating twice and taking into account that for $h \rightarrow \infty$ the tendencies are $dv/dx \rightarrow 0$ and $v \rightarrow v_{co}$, we find [4] that

$$v_{co} = - \frac{RT\xi}{\eta} \frac{dC_0}{dz} \quad (11.3)$$

where

$$\xi = \int_0^\infty \frac{C - C_0}{C_0} dx \quad (11.4)$$

Equation (11.3) gives the velocity of the capillary-osmotic slip in dilute nonionic solutions. Here ξC_0 is the moment of adsorption with respect to the slip plane. The quantity $\sqrt{\xi}$ characterizes the extension of the diffuse adsorption layer.

Solutions obtained by other methods [5], including that based on thermodynamics of irreversible processes [6], yield the same form of Eq. (11.3) for the capillary-osmotic slip.

Let us consider two reservoirs separated by a porous membrane of thickness ℓ , filled with a solution at uniform temperature T and with uniform composition. By using a well-known expression for the production of entropy [7] in the isothermal flow of a non-electrolyte solution driven by a pressure difference Δp and concentration difference ΔC_i and, hence, by the difference in chemical potential $\Delta \mu_i$ of the components 1 and 2 of the solution in the reservoirs, we obtain [6]

$$I_1 = L_{11} \Delta \mu_1 + L_{12} \Delta \mu_2 + L_{13} \Delta p \quad (11.5)$$

$$I_2 = L_{21} \Delta \mu_1 + L_{22} \Delta \mu_2 + L_{23} \Delta p \quad (11.6)$$

$$V = L_{31} \Delta \mu_1 + L_{32} \Delta \mu_2 + L_{33} \Delta p \quad (11.7)$$

where $I_i = I_{0i} - C_i V$ characterizes the flux of the i -th component minus its transfer as a whole at the mean center-of-mass flow velocity V , and

$$\Delta\mu_i = (\partial\mu_i/\partial C_i)_P \Delta C_i$$

The subscript 1 marks the solute, and 2 marks the solvent. The phenomenological coefficients L_{ik} obey the Onsager relation:

$$L_{12} = L_{21}, \quad L_{13} = L_{31}, \quad L_{23} = L_{32} \quad (11.8)$$

Capillary osmosis can be characterized by the flux of the liquid driven by the gradient of chemical potential at $\Delta p = 0$. With this constraint the flow velocity V is

$$V = L_{13}\Delta\mu_1 + L_{23}\Delta\mu_2 \quad (11.9)$$

The coefficients L_{13} and L_{23} can be found from (11.5) and (11.6), taking the fluxes $(I_1)_c$ and $(I_2)_c$ under the condition $\Delta\mu_1 = \Delta\mu_2 = 0$. Then $L_{13} = (I_1)_c/\Delta p$ and $L_{23} = (I_2)_c/\Delta p$. The fluxes $(I_1)_c$ and $(I_2)_c$ are called transferred masses. They can be calculated if the distribution of component concentrations at the pore walls is given. In wide pores, where diffuse layers do not overlap, and for low concentration of the solution, in which the change in the chemical potential of the solvent is negligible ($\Delta\mu_2 \approx 0$), we obtain

$$V = L_{13}\Delta\mu_1 = (I)_c \Delta\mu_1 / \Delta p \quad (11.10)$$

Obviously, when solution concentration in the pores is constant and equal to the bulk concentration C_0 in the reservoirs, the flow of the liquid does not affect the solution concentration in the reservoirs. But if the solution concentration at the pore walls is altered, the solution flowing out of one of the reservoirs will have a mean concentration $C \neq C_0$, and the solution flowing into the second reservoir will have a correspondingly changed concentration. This excess of the solute mass transferred through a planar pore with width much greater than the diffuse layer thickness within which the concentration is altered, is precisely $(I)_c$. It is given, per unit length of the pore, by the formula

$$(I)_c = 2 \int_0^\infty v(x)[C(x) - C_0]dx \quad (11.11)$$

In the sense outlined above, the velocity profile at the walls of wide pores can be considered linear: $v(x) = x\Delta p/2\eta l$. By substituting this value of $v(x)$ into (11.11) and then (11.11) into (11.10), and taking into account that $\Delta\mu = RT\Delta C/C_0$, we obtain

$$V = \frac{\Delta C R T h}{\eta l} \int_0^\infty \frac{C(x) - C_0}{C_0} x dx \quad (11.12)$$

This expression is identical to (11.3), recalling that $v_{co} = -V/h$ and $\Delta C/\ell = dC_0/dz$.

In order to calculate the velocity of the capillary-osmotic slip one has to know the value of ξ , which depends on concentration distribution $C(x)$ at a specific surface. A quantitative determination of ξ can be carried out in nonionic solutions when the interaction between solute molecules and the surface results solely from dispersion forces. In this case, ξ can be calculated in the framework of the macroscopic theory of dispersion forces [8] (see Chapter 5 for details).

In the general case the concentration distribution at a wall can be found from the Boltzmann equation

$$C(x) = C_0 \exp(-U/kT) \quad (11.13)$$

where $U(x)$ is the potential energy of a solute molecule in the force field at the wall. In the case of dispersion forces [8]

$$U(x) = \frac{\hbar}{16\pi^2 x^3} \int_0^\infty \frac{\Delta_{32}}{\varepsilon_2} \left(\frac{\partial \varepsilon_{12}}{\partial N} \right) d\omega \quad (11.14)$$

where \hbar is Planck's constant, and

$$\Delta_{32} = (\varepsilon_3 - \varepsilon_2)/(\varepsilon_3 + \varepsilon_2)$$

where ε_3 and ε_2 are the permittivities of the wall and solvent, respectively, being functions of cyclic frequency ω (see Chapter 4). The derivative $(\partial \varepsilon_{12}/\partial N)_{N=0}$ is found from the equation [8]

$$\varepsilon_{12} = \varepsilon_2 + (\partial \varepsilon_{12}/\partial N)_{N=0} N \quad (11.15)$$

that relates the permittivity ε_{12} of the solution to its concentration N (molecules/cm³) and to the permittivity ε_2 of the solvent. Equation (11.15) holds at low solution concentration; this constraint is typical for the theory of capillary osmosis. Equation (11.14) is obtained on the basis of the macroscopic theory of non-retarded dispersion forces. In the case under consideration this is a good approximation because, as a rule, the extension of diffuse nonionic adsorbed layers does not exceed 10^{-6} cm.

If the concentration gradient dC_0/dz is nonzero, the convective capillary-osmotic flow is accompanied by solute diffusion. Then the continuity condition for the stationary flow of the liquid and for the flow of the solute yields [3]

$$v = \text{const}, \quad v_{co}C_0 - D \frac{dC_0}{dz} = \text{const} \quad (11.16)$$

Various conditions of stationary mass transfer are possible, depending on the longitudinal Peclet number $Pe = v_{co}\ell/D$, where ℓ is the thickness of the porous body, and D is the diffusion coefficient. If $Pe \ll 1$, the concentration distribution $C(z)$ is mostly determined by diffusion, and integration of Eq. (11.16) gives a linear concentration profile. The condition $v_{co} = \text{const}$ then leads to $dC_0/dz = \text{const}$ and to the already known expression for the velocity of the capillary-osmotic slip:

$$v_{co} = -\frac{RT\xi}{\eta} \frac{\Delta C}{\ell} \quad (11.17)$$

where ΔC is the concentration difference between the end sections of the channel. The total flux of the solute is

$$j = \left(\frac{RT\xi}{\eta} + D \right) \frac{\Delta C}{\ell} \quad (11.18)$$

The capillary-osmotic flow can accelerate or slow down the diffusion, depending on the sign of ξ (which, in turn, is determined by the sign of adsorption).

If the Peclet number is not small, the solution of Eq. (11.16) at boundary conditions $z = 0$, $C_0 = C_1$ and $z = \ell$, $C_0 = C_2$ gives the following equation for solute flux [9]:

$$j = v_{co} \frac{C_1 \exp(Pe) - C_2}{\exp(Pe) - 1} \quad (11.19)$$

This flux produces an exponential distribution of concentration $C(z)$, and the slip velocity must vary along the flow, in contradiction with the continuity condition law $v_{co} = \text{const}$. However, this merely indicates that the convective flow is determined in this case not only by the slip but also by the viscous flow driven by the arising pressure gradient $\partial P/\partial z$ that maintains the constancy of the total flux. It is readily shown that if $Pe \gg 1$, Eq. (11.19) transforms to a simple equation in which the flux is determined solely by the slip velocity:

$$j = C_1 v_{co} \quad (11.20)$$

Measurements of the rate of capillary osmosis meet with least difficulties if $Pe \gg 1$. However, in practice this condition is not easy to satisfy, so that the equation normally used for processing the results is (11.19).

Capillary osmosis effects were experimentally studied [9] in a setup schematically shown in Fig. 11.2. A membrane 1 of porous glass (mean pore radius $r \approx 10 \mu\text{m}$) separated the volumes 2 and 3 in which unequal solution concentrations were maintained. A tube 4

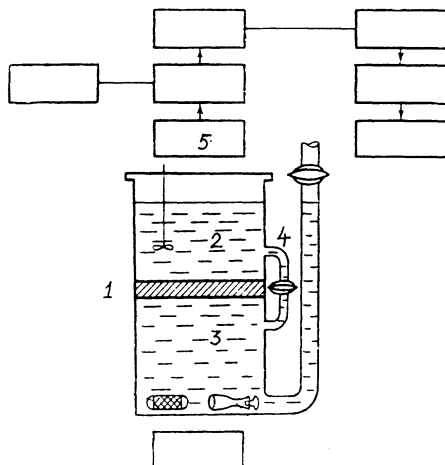


Fig. 11.2. Schematic arrangement of the setup for studying capillary osmosis by the radiotracer technique.

(with relatively large diffusion resistance) bypassed the membrane and thus eliminated the convective transfer due to pressure difference. Mass transfer from one reservoir into another could appear only as a result of diffusion through the membrane and of capillary-osmotic flow, as covered by Eq. (11.19). A radiotracer technique was employed to measure the solute flux. The number of radioactive labeled molecules transferred from one reservoir into another was measured by a β -emission detector 5, mounted above the surface of the solution with lower concentration. Preliminary calibration served to convert the measured radioactivity J of the solution into concentration C .

The results of one series of experiments with aqueous solutions of ethyl alcohol are shown in Fig. 11.3. The graph plots the radioactivity J of the solution as a function of time. The linearity of the curves shows that the mass flux j is stationary. The slip velocity v_{co} could be found by converting the values of J to C and making use of Eq. (11.19).

The ratio of the capillary-osmotic flux j_{co} (curves 1 and 2) to the diffusion flux $j_d = D \Delta C / l$ (curve 3) in experiments with water-ethyl alcohol mixtures was 3.3 in a No. 5 Schott filter at $\Delta C = 10\%$ and a mean solution concentration in the pores $C_m = 5\%$ (curve 2). In these experiments the filters separated pure water ($C = 0$) from 10% alcohol solution. When the mean solution concentration was raised to $C_m = 55\%$ with the same concentration difference $\Delta C = 10\%$, the relative capillary-osmotic flow rate was observed to increase: the ratio j_{co}/j_d rose to 8 (curve 1). This

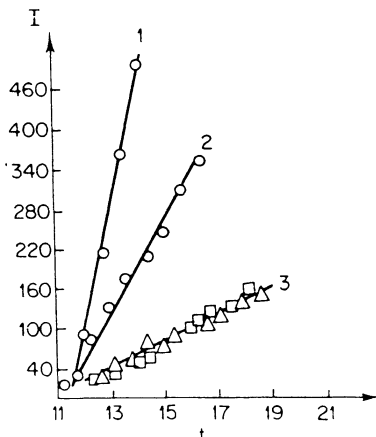


Fig. 11.3. Concentration I (in pulses/min) of the radioactive tracer in the upper part of the cell as a function of time t (in h), for ethanol solution in water. Schott filter No. 5. 1) $C_1 = 60\%$, $C_2 = 50\%$; 2) $C_1 = 10\%$, $C_2 = 0$; 3) $C_1 = C_2 = 10\%$.

time the filter separated solutions with concentrations of 50 and 60%. In aqueous solutions of acetic acid the ratio j_{CO}/jd was 1.5-1.95 at a mean solution concentration in the pores from 5-10%.

The situation with capillary osmosis in ionic solutions is more complicated owing to electrokinetic phenomena caused by the concentration dependence both of the ζ -potential and of the Debye radius $1/\kappa$, which determines the extension of diffuse ionic layers. In deriving the equation for the velocity of the capillary-osmotic slip in electrolyte solutions it is necessary to take into account the contributions of the diffuse layers formed by two types of particle, viz., anions and cations. For binary dilute solutions, Eq. (11.17) takes the following form [9, 10]:

$$v_{CO} = - (z_- \xi_+ + z_+ \xi_-) \frac{RT \Delta C}{\eta l} \quad (11.21)$$

where ξ_+ and ξ_- are the adsorption moments of ions with respect to the slip plane, and z_+ and z_- are the valences of the ions. The expressions for ξ are substantially simplified with low and high ζ -potentials ($|\zeta| \ll 25$ mV and $|\zeta| \gg 25$ mV [9, 10]).

A more precise solution of the problem of capillary osmosis in electrolytes [11] demonstrated that the following approximate expression gives quite good accuracy both for symmetrical and asymmetrical (2-1 and 1-2) electrolytes:

$$v_{co} \approx - \frac{\epsilon_0 \zeta^2 \Delta C}{32\pi\eta C_0 l} \quad (11.22)$$

This expression shows that, in contrast to the velocity of electro-osmosis (which is proportional to ζ), the capillary-osmotic slip velocity in electrolytes is proportional to the square of the ζ -potential, and its direction is independent of the sign of ζ .

When the concentration difference ΔC at the endfaces of a porous body or of a single capillary is kept constant, the capillary-osmosis flux not only involves the diffusion of the electrolyte, but also produces a potential difference $\Delta\varphi$ of diffusion origin, provided the ions have unequal mobilities ($D_+ \neq D_-$):

$$\Delta\varphi_d = \frac{RT \Delta C (D_+ - D_-)}{FC_0 (z_+ D_+ + z_- D_-)} \quad (11.23)$$

As a result of this potential difference, the electrolyte is made to flow electro-osmotically at a velocity

$$v_e = \frac{FC_0 z_+ z_- (\xi_- - \xi_+)}{\eta} \frac{\Delta\varphi}{l} = \frac{\epsilon_0 \zeta}{4\pi\eta} \frac{\Delta\varphi}{l} \quad (11.24)$$

In the general case, the velocity of capillary osmosis v_{co} and that of electro-osmosis v_e , driven by $\Delta\varphi_d$, are of the same order of magnitude. In order to eliminate the effect of the electro-osmotic flow on the velocity of the capillary-osmotic flow, electrodes must be placed into reservoirs separated by a membrane and then electrically connected.

The phenomenon of capillary osmosis in electrolytes was investigated [12] with the same setup (Fig. 11.2) in Na_2SO_4 solutions with concentrations from 0.001 to 0.5 mole/liter. These experiments directly measured the difference between the levels of the liquid in the capillaries communicating with the reservoirs, which were separated by a sintered glass membrane with mean pore radius about 2.5 μm . The capillary-osmotic and electro-osmotic pressures made the liquid rise in the capillary communicating with

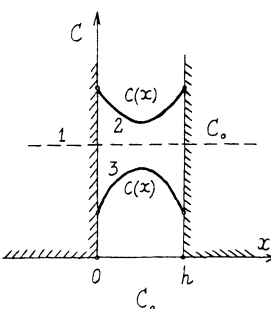


Fig. 11.4. Concentration distribution of a solution across a thin plane-parallel gap, with diffuse adsorption layers overlapping.

the lower volume, where the electrolyte concentration was higher. The quantity $(v_{co} + ve)$ was calculated by using Eqs. (11.22) and (11.24), taking into account the rate of electrolyte filtration through the membrane due to the difference between the liquid levels that developed. The theoretically calculated values of $(v_{co} + ve)$ were found to be an order of magnitude lower than the experimental ones. This could be caused by polarization effects or by underestimation of the values of the ζ -potential used in the calculations. Furthermore, the experiment did not always strictly conform to the constraints of low solution concentration and low concentration gradient, required for the approximate theory of capillary osmosis.

The case of fine pores in which diffuse adsorption layers of neutral molecules can overlap (Fig. 11.4) must be treated separately. Here the concentration $C(x)$ is not equal anywhere within the h -wide pore to the bulk solution concentration C_0 , shown by the dashed line 1. The concentration $C(x)$ is greater than C_0 at all points of the pore volume if the solute is positively adsorbed (curve 2), and is below C_0 for negative adsorption (curve 3). The problem of calculating the capillary-osmotic flow in fine pores can be solved, as in [6, 7], by the methods of nonequilibrium thermodynamics. The phenomenological coefficient L_{13} [see Eq. (11.10)] determining the velocity of capillary osmosis can be found (as was shown above on the basis of the Onsager relation) from the expression for the mass transfer of solute at $\Delta C = 0$.

Calculations were carried out for slit pores with width h and length l [13]. Assuming the Poiseuille velocity profile and assuming the viscosity of the solution to be independent of concentration, we obtain

$$v_{co} = \frac{RT \Delta C}{2\eta h \ell C_0} \left[\int_0^h (h-x)C(x)x dx - C_0(h^3/6) \right] \quad (11.25)$$

At $h \rightarrow \infty$, this equation transforms to Eqs. (11.3) and (11.12) derived for wide pores. If there is no adsorption, i.e., at $C(x) = C_0 = \text{const}$, the integral in (11.25) equals $(h^3/6)$, so that $v_{co} = 0$. The direction of the capillary-osmotic flux depends on the magnitude of the ratio $C(x)/C_0$. If $C(x) > C_0$, i.e., with positive adsorption, the liquid flows toward the lower concentration, and if $C(x) < C_0$, it flows toward the higher-concentration solution. If the fine pores are completely inaccessible to the solute molecules (i.e., with "semipermeable" membranes) and $C(x) = 0$, the capillary-osmotic flow of the solvent is simply the Poiseuille flow driven by the difference of osmotic pressure in the solution, $\Delta\pi = RT \Delta C$:

$$v_{co} \approx -h^2 RT \Delta C / 12\eta \ell \quad (11.26)$$

Quantitative calculations with Eq. (11.25) require the function $C(x)$ to be known. The distribution of concentration $C(x)$ across the section of a slit pore for solutions whose molecules interact with the wall surface through dispersion forces was obtained in [14, 15]:

$$\begin{aligned} C(x) &= C_0 \exp \left\{ \left(\frac{\delta^3}{4\pi kT} \int_0^\infty \Delta_{32} \Delta'_{12} d\omega \right) \left[\frac{1}{x^3} + \frac{1}{(h-x)^3} \right] \right\} \\ &= C_0 \exp \left\{ \frac{\delta^3 A_0}{kT} \left[\frac{1}{x^3} + \frac{1}{(h-x)^3} \right] \right\} \end{aligned} \quad (11.27)$$

where Δ_{32} has the same meaning as in Eq. (11.14); $\Delta'_{12} = (\epsilon_1 - \epsilon_2)x / (\epsilon_1 + 2\epsilon_2)^{-1}$; and δ is the radius of a solute molecule. This equation takes into account the interaction between solute molecules and the two surfaces of a slit pore. It was shown [16] that the assumption of independent (additive) contribution of the field of each of the surfaces to the total interaction energy U , used in deriving this equation, holds sufficiently well.

As seen from Eq. (11.27), the magnitude and sign of changes in solution concentration $C(x)$ in narrow pores in comparison to bulk concentration C_0 depend on pore width h and on the physical characteristics of the "solution-membrane" system. If $\epsilon_3 > \epsilon_2$ and $\epsilon_1 > \epsilon_2$ (in the frequency interval essential for the dispersion interaction, $\omega \approx 10^{16} \text{ rad/s}$), the exponent of the exponential is positive ($\Delta_{32} > 0$ and $\Delta'_{12} > 0$) and $C(x) > C_0$. Hence, positive adsorption occurs if the polarity of the solvent (ϵ_2) is less than that of the solute (ϵ_1) and of the membrane (ϵ_3). Negative adsorption will be obtained if the solvent is more polar than the solute ($\epsilon_2 > \epsilon_1$) or the material of the membrane ($\epsilon_2 > \epsilon_3$). If both conditions are

satisfied ($\varepsilon_2 > \varepsilon_1$ and $\varepsilon_2 > \varepsilon_3$), the adsorption will be positive because, in this case, Δ_{32} and Δ_{12} have like signs ($\Delta_{32} < 0$ and $\Delta_{12} < 0$).

By applying the macroscopic theory of dispersion forces to nonionic solutions, it is possible to predict the change in solution concentration in narrow pores and the direction and magnitude of the capillary-osmotic flux given by Eq. (11.25). Thus, for a quartz membrane and octane solution in tetradecane it was found that $A_0 = -0.056kT$ (A_0 is a certain constant of dispersion forces) [17]. This constant corresponds to octane concentration at the wall of a slit pore reduced by a factor of about 2 compared with C_0 . As a first approximation the polarity of a component can be characterized by its refractive index n ($\varepsilon \approx n^2$). The quartz-octane-tetradecane system satisfies the condition of negative adsorption: $n_2 > n_1$ and $n_2 < n_3$, where $n_2 = 1.446$ (tetradecane), $n_1 = 1.397$ (octane), and $n_3 = 1.46$ (quartz). The concentration reduction was thus caused by a lower polarity of the solute (octane) as compared to that of the solvent (tetradecane). This conclusion was confirmed by experiments. Thus, Cleland [18] demonstrated that the concentration of the less polar component of the solution was reduced in microporous Vicor glass ($n_3 = 1.55$), viz., the concentration of CCl_4 ($n_1 = 1.46$) in benzene ($n_2 = 1.5$) and that of *n*-heptane ($n_1 = 1.37$) in CCl_4 ($n_2 = 1.46$).

Equations (11.13) and (11.27) can be used for a description of concentration distribution both at single surfaces and in narrow pores because capillary osmosis calculations deal only with the mobile part of the adsorption layer. It is to this (diffuse) part within the reach of the long-range surface forces that the theory of dispersion forces can be correctly applied. The adsorption of the first molecular layer is known to be substantially affected by short-range forces not covered by the macroscopic theory of dispersion forces. Calculations of flow of liquids usually assume that the first molecular layer is fixed, this assumption being the physical basis of the boundary condition typical for hydrodynamics: the nonslip constraint. The only exception is the case of lyophobic surfaces at which slippage is possible [19-23]. This effect can be quite noticeable in pores less than 1 μm wide [23].

11.2. REVERSE OSMOSIS

The phenomenon of reverse osmosis consists in the appearance of a concentration difference in a solution flowing through pores whose walls preferentially adsorb solution components. The concentration difference is produced by mass fluxes $(I_1)_c$ and $(I_2)_c$ [see Eqs. (11.5), (11.6), and (11.11)] characterized by phenomenological coefficients L_{13} and L_{23} . The cross-coefficients L_{31} and L_{32} ,

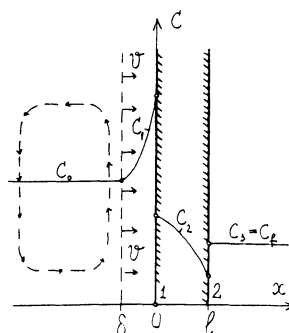


Fig. 11.5. Model for the calculation of the mass transfer by reverse osmosis in microporous membranes.

equal to L_{13} and L_{23} , respectively, characterize the effect of capillary osmosis analyzed in the preceding section.

As follows from (11.10) and (11.12), at $\Delta C = 0$ the mass flux of solute in a dilute solution in wide pores is

$$j_{\Delta C=0} = \frac{I_C}{l} = \frac{L_{13}}{l} \Delta p = - \frac{C_0 \xi}{\eta} \frac{\Delta p}{l} \quad (11.28)$$

Changing the concentration of a solution by forcing it under pressure through a microporous membrane is widely used nowadays for water desalination, for raising the concentration of various solutions, and for extracting desired components from waste water [24-27]. The reverse osmosis technologies often prove more economical than evaporation and distillation, which consume energy for heating and vaporization of the liquid. However, the boundary conditions corresponding to practical applications of the membrane method differ from those chosen in deriving Eq. (11.28) in that $\Delta C \neq 0$. Furthermore, as in cases treated earlier, here we have to take into account additionally the diffusion of solute molecules, the effect of concentration polarization at the inflow to the membrane, and the capillary-osmotic counterflow produced when $\Delta C \neq 0$.

Let us consider a flat microporous homogeneous membrane with thickness l through which a solution to be separated is forced by a pressure difference ΔP . Upstream of the membrane the solution has a constant concentration C_0 (Fig. 11.5). Membranes employed for the separation of solutions have negative adsorption of the solute. (In principle, positively adsorbing membranes can also be used, but their separating efficiency is much lower [28, 29].) Consequently, the concentration of the effluent solution C_f is reduced: $C_f < C_0$. The effect of separation is usually characterized by the rejection coefficient φ :

$$\varphi = 1 - C_f/C_0 \quad (11.29)$$

The separation of solutions by forcing them by pressure through membranes is the reverse of capillary osmosis (which is liquid flow driven by a concentration difference) — hence the name "reverse osmosis" [24-27], although reverse capillary osmosis might be a more logical term.

To solve the problem of separation by reverse osmosis is to obtain an expression for φ , reflecting the physical properties of the "membrane-solution" system and external conditions. The variables are flow velocity v , temperature, intensity of mixing in the solution entering the membrane, and the method of collecting the effluent solution. The exposition of the reverse osmosis theory that follows is based on an approach developed in our publications [28-30],* yielding many of the solutions obtained earlier [24-27] as particular cases.

In comparison with other types of membrane (ion-exchange and nonporous membranes, ultrafilters), reverse-osmosis membranes are characterized by a low surface charge density, small pore size ($r \approx 20-30 \text{ \AA}$), and negative solute adsorption through long-range surface forces. Consequently, the model of noncharged pores can be used for first-approximation calculations. Because of the small pore size and uncertain pore geometry, it is expedient to simplify the analysis by introducing the mean velocity of liquid flow v/m through the pores (m being the membrane porosity), mean diffusion coefficients of the solute in the pore volume D_m , mean concentration C , and mean potential of molecule-pore surface interaction $\phi = U/kT$. The mean values of D_m and ϕ were determined for a number of models of porous structures (cylindrical and planar pores) in [28-30].

In order to accelerate the collection of the enriched component, the separated solution is pumped along the entrance surface of the membrane. Turbulent mixing maintains a practically constant concentration C_0 at a certain distance δ from the membrane. A layer with thickness δ at the membrane surface (Fig. 11.5) remains laminar, and the distribution of solution concentration within this layer is determined by the convective flow velocity v perpendicular to the membrane. The flow is driven by the hydrostatic head ΔP and by diffusion of the enriched component back into the bulk solution. The formation of a nonmixed layer, whose thickness δ depends on the intensity of turbulence, results in concentration polarization, i.e., in formation of a layer of increased concentration $C_1 > C_0$ at the upstream surface of the membrane.

As shown above, the mean solution concentration in narrow, negatively adsorbing, pores is lower than the concentration outside the membrane pores. Any slow laminar flow of the solution ($v \approx 0.001-$

*See also our paper in Prog. Surf. Membr. Sci. 14, 69 (1981).

0.01 cm/s) cannot disturb the equilibrium produced at the solution-membrane interface by the field of surface forces because the adsorption potentials of molecules (and especially those of ions) are on the order of several times kT . Therefore, the concentration must change jumpwise across the entrance surface of the membrane, from $C_1(0)$ to $C_2(0) < C_1(0)$; by Eq. (11.13),

$$C_2(0) = C_1(0) \exp(-\phi) = C_1(0)/\gamma \quad (11.30)$$

where γ is the equilibrium distribution coefficient.

Likewise, the solution concentration increases jumpwise across the opposite face of the membrane, from $C_2(l)$ to $C_3(l) = C_f > C_2(l)$:

$$C_2(l) = C_3(l) \exp(-\phi) = C_3(l)/\gamma = C_f/\gamma \quad (11.31)$$

The distribution coefficient $\gamma = \gamma_0 \gamma_a (C_0)$, where γ_0 is the value of γ for an infinitely dilute solution, and $\gamma_a (C_0)$ is the activity coefficient of the bulk solution. With rare exceptions, the deviations in γ_a from unity for the solution in the pores can be neglected because in good reverse-osmosis membranes the pore concentration is lower than the bulk solution concentration by approximately two orders of magnitude. Boundary conditions (11.30) and (11.31) represent an approximation; end effects in the pores and the field of surface forces at the bounding surfaces of the membrane cause the transition from $C_1(0)$ to $C_2(0)$ and that from $C_2(l)$ to $C_3(l)$ to be not ideally abrupt but to occur in a certain transition zone of thickness Δ . However, it was already shown [29, 30] that if $\Delta \ll l$, the effect of these transition zones again reduces to the same equations (11.30), (11.31). The thickness Δ is on the order of the range of surface forces ($\Delta \approx 10^{-6}$ cm): the membrane thickness l is generally on the order of 10^{-4} cm; hence the ratio (Δ/l) is generally small.

The problem of stationary flow of the solution through the membrane can be solved on the basis of the equations of convective diffusion for three zones: 1) laminar layer $-\delta < x < 0$, 2) membrane $0 < x < l$, and 3) effluent solution $l < x < \infty$ (Fig. 11.5):

$$j_1 = vC_1(x) - D_0 \frac{\partial C_1}{\partial x} \quad (11.32)$$

$$j_2 = vC_2(x) - D_m \frac{\partial C_2}{\partial x} \quad (11.33)$$

$$j_3 = vC_3(x) - D_0 \frac{\partial C_3}{\partial x} \quad (11.34)$$

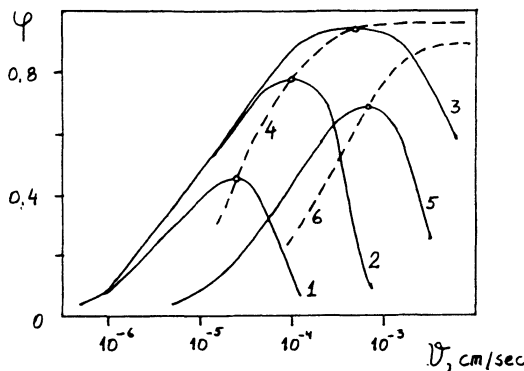


Fig. 11.6. Theoretically calculated dependence of selectivity φ on flow velocity v of the solution ($D_0 = 10^{-5} \text{ cm}^2/\text{s}$, $D_m = 5 \cdot 10^{-6} \text{ cm}^2/\text{s}$, $\ell = 0.02 \text{ cm}$). 1) $\gamma = 25$, $\omega = D_0 \ell / D_m \delta = 0.1$; 2) $\gamma = 25$, $\omega = 0.5$; 3) $\gamma = 25$, $\omega = 8$; 4) $\gamma = 10$, $D_m / \ell = 10^{-3} \text{ cm/s}$.

where D_0 is the diffusion coefficient for the bulk solution. By using the flow continuity condition $j_1 = j_2 = j_3$, which also leads to $C_3(x) = \text{const} = C_f$ and boundary conditions (11.30) and (11.31), we arrive at the following expression for rejection:

$$\varphi = 1 - \{1 + (\gamma - 1)[1 - \exp(-v\ell/D_m)] \exp(-v\delta/D_0)\}^{-1} \quad (11.35)$$

The solutions of this problem obtained earlier neglected the important effect of concentration polarization. As seen from (11.35), selectivity of a membrane is substantially reduced if the efficiency of turbulent mixing is diminished (i.e., if δ is large). Equation (11.35) transforms to familiar solutions [24, 25, 31-33] if mixing is ideal (and thus, of course, unattainable in practice), i.e., if $\delta = 0$.

It is also possible to give a more strict physicochemical characterization to the parameters introduced in earlier theories, for instance, "reflection coefficient" σ and "solute permeability" P_s . As follows from (11.35), $\sigma = 1 - (1/\gamma)$ and $P_s = D_m / \ell \gamma$ are both functions of the distribution coefficient γ that has a clear physical meaning.

Figure 11.6 shows the rejection φ , calculated by means of Eq. (11.35), plotted as a function of filtration velocity v . The curves show that the efficiency of separation reaches a maximum at a certain flow velocity. At decreased v the selectivity of a membrane is reduced because the diffusion transfer through the membrane increases. When $v \rightarrow 0$, $\varphi \rightarrow 0$: diffusion levels off the concentration difference, and $C_f \rightarrow C_0$. When the flow velocity exceeds a cer-

tain optimal value, separation becomes less effective owing to the buildup of concentration polarization, i.e., owing to slower removal of the enriched component from the membrane. (A high flow velocity can also disturb the equilibrium at the boundary separating the bulk solution from the solution in the adjacent pores of the membrane.) The less effective the mixing, the lower the $\varphi(v)$ curves. As follows from Eq. (11.35), high separation can be achieved only if $\delta \leq l/4$ and if the internal Peclet number $Pe = vl/D_m \approx 2$. The shape of the theoretically obtained curves $\varphi(v)$ is well supported by experimental data.

Actual reverse-osmosis membranes (e.g., of cellulose acetate) consist of a separating layer with very narrow pores and a support with much wider pores to provide mechanical strength. The solution of Eqs. (11.29)-(11.34) for a two-layer membrane shows that its selectivity depends on which side of the membrane faces the inflow [34]. The best separation is achieved when the flow enters the active layer of the membrane. In the reverse arrangement the wide-pore layer of the membrane increases the thickness δ of the non-mixed layer. The advanced theory of reverse osmosis transport has made it possible to obtain quantitative results also for membranes shaped into hollow fibers [35].

The selectivity depends on solution concentration via its dependence on $\gamma(C) = \gamma_0(C)\gamma_a(C)$ and $D_0 = D_0(C)$. As seen from Eq. (11.35), φ must decrease when γ_0 , the activity coefficient γ_a , and the diffusion coefficient D_0 diminish with increasing concentration of the solution. This is indeed confirmed in experiments. The effect of the capillary-osmotic counterflow was analyzed in [28-30]. This counterflow must be taken into account in calculating the pressure difference ΔP necessary to pump the solution at the optimal flow rate prescribed by Eq. (11.35). Calculation of the laminar layer thickness δ is a separate problem resolved by hydrodynamic methods [24-27]. The derived equations are strictly valid for non-ionic one-component solutions. They can also be used for electrolytes in which no electric field appears. This corresponds to two conditions: $\gamma_+ = \gamma_-$ and $D_+ = D_-$ (e.g., these conditions hold approximately in aqueous solutions of KCl). If these conditions are not satisfied, charge builds up on the membrane (even if its intrinsic surface charge was zero) because oppositely charged ions enter the pores in unequal amounts ($\gamma_+ \neq \gamma_-$), and an electric field appears. Furthermore, if $D_+ \neq D_-$, an electric potential difference $\Delta\varphi_d$ of diffusion origin is generated (when $\Delta C \neq 0$).

The theory of separating electrolyte solutions [29] is developed in the same manner, but separately for fluxes of different ions, with terms $z_i C_i (d\varphi/dx)$ added to Eqs. (11.32)-(11.34) (where z_i is the valence of the i -th ion). The electric field is found by using additionally the Poisson equation. The boundary conditions are supplemented with the condition of electric neutrality of the

bulk solution and the condition of continuity of the normal component of induction. The solution yields the same expression (11.35) for the rejection of reverse osmosis membranes with respect to electrolyte solutions, but with redefined distribution coefficient γ and diffusion coefficient D . For membranes with thickness much greater than the reciprocal Debye radius of the pore solution, and for binary electrolytes, we have

$$\gamma = (\gamma_+^{z_+} \gamma_-^{z_-})^{1/(z_+ + z_-)}, D = \frac{(1/z_+) + (1/z_-)}{(D_+/z_+) + (D_-/z_-)} \quad (11.36)$$

This equation shows, for example, that membrane selectivity can be enhanced by introducing into the electrolyte certain ions with high γ_i . If these ions are retained by the membrane, then the electric field that develops will cause the retention of ions of the opposite charge, even if the latter ions were not retained or positively adsorbed by the membrane ($\gamma \leq 1$). Thus, the effective value of γ in a symmetrical 1-1 electrolyte with $\gamma_+ = 100$ and $\gamma_- = 0.1$ is $\gamma = \sqrt{\gamma_+ \gamma_-} \approx 3.3 > 1$; i.e., the electrolyte will be partially enriched at the membrane.

In conclusion, we must discuss the methods of quantitative evaluation of the distribution coefficients $\gamma_i = \exp(\phi_i)$ that enter Eq. (11.35) as parameters. The values of ϕ_i can be found for binary mixtures of nonpolar liquids on the basis of the macroscopic theory of dispersion forces [28-30]. Thus, the mean values of γ_i in the slit pore model are found by means of Eq. (11.27):

$$\frac{1}{\gamma_i} = \exp(-\phi_i) = \frac{1}{h} \int_{\delta}^{h-\delta} \exp\left\{ \frac{\delta^3 A_9}{kT} \left[\frac{1}{x^3} + \frac{1}{(h-x)^3} \right] \right\} dx \quad (11.37)$$

where h is the width of the pore.

When $\gamma = \exp \phi$ is calculated for electrolyte solutions, complications arise because the electrostatic interaction of ions with the membrane must be taken into account. In accordance with Glückauf's hypothesis [24], the main factor here is presumably the change in the intrinsic energy of ions in their transition from the bulk aqueous solution with ϵ_0 to the membrane phase with a considerably lower static permittivity $\epsilon_m < \epsilon_0$. This assumption was experimentally confirmed by Heyde et al. [36], who measured distribution coefficients of different ions in cellulose acetate membranes. The results obtained for γ were found to be in good qualitative agreement with calculations by the Bjerrum-Larsson theory:

$$\ln \gamma \sim \frac{z_+ z_- e^2}{2kT R_m} \left(\frac{1}{\epsilon_m} - \frac{1}{\epsilon_0} \right) \quad (11.38)$$

where e is the electron charge and R_m is the radius of the ion. As this equation predicts, γ increases with increasing ion valence [36].

Sourirajan [37], and later Dukhin and Yaroshchuk [38], proposed to calculate the change in the Born energy of the ion when it is transferred from the bulk solution to a narrow pore in which the structure of the liquid is modified in comparison with the bulk phase and has a lower static permittivity $\epsilon_p < \epsilon_0$. In contrast to Glückauf's hypothesis, the membrane is treated as a heterogeneous system consisting of a liquid in narrow pores, where $\epsilon = \epsilon_p$, and the membrane material as such, with $\epsilon = \epsilon_m$. In this case, in addition to the change in the Born energy of the ion,

$$\phi_b = \frac{(ez)^2}{2RkT} \left(\frac{1}{\epsilon_p} - \frac{1}{\epsilon_0} \right) \quad (11.39)$$

we have to take into account the effect of image forces because $\epsilon_p \neq \epsilon_m$. In contrast to (11.39), the change in the ion energy associated with image forces Φ_c is a function of distance from the ion to the pore wall. In the model of a planar pore with width h ,

$$\Phi_c(x) = \frac{(ez)^2}{4kT\epsilon_p} \left(\frac{\epsilon_p - \epsilon_m}{\epsilon_p + \epsilon_m} \right) \left(\frac{1}{x} + \frac{1}{h-x} \right) \quad (11.40)$$

Equations (11.39) and (11.40) make it possible to evaluate Φ and compare the results with experimental data obtained for real reverse osmosis membranes. Assuming $\epsilon_0 = 80$, $\epsilon_m = 3$ (for cellulose acetate and glass), and $\epsilon_p = 20$ for moisture in narrow pores of $20-30 \text{ \AA}$ [39-41], we find for univalent ions ($R \approx 1.7 \cdot 10^{-8} \text{ cm}$) in membranes with slit pores ($h = 20 \text{ \AA}$): $\Phi_b \approx 5.2 \text{ kT}$ and $\Phi_c \approx 1.5 \times kT$. These last values are obtained by averaging $\Phi_c(x)$ over the pore cross section. The contribution of the force of dispersion attraction of the ion ($\Phi_d \approx -0.05 \text{ kT}$) was negligibly small. Calculations demonstrate that the main contribution to Φ and γ for ions is made, in agreement with the hypothesis suggested in [38], by the change in the Born energy of the ions. However, Eq. (11.39), gives only an approximate evaluation of this energy because it is based on the assumption of homogeneous dielectric properties of the liquid in the pore. Yaroshchuk recently analyzed the possibility of further refinement in calculations of Φ_b taking into account the inhomogeneity of thin interlayers [42].

In order to find a relation between γ and rejection φ of reverse osmosis membranes we shall simplify Eq. (11.35). Let us find the maximum values $\varphi = \varphi_m$ realized in the case of ideal mixing of the solution ($\delta \rightarrow 0$) and high flow velocity ($v\ell/D_m \gg 1$). Transformations yield

$$\varphi_m \approx 1 - 1/\gamma \quad (11.41)$$

By substituting $\gamma = \exp \phi$, corresponding to the change only in the Born energy ($\phi \approx 5.2$), we obtain $\varphi_m \approx 0.995$. This is close to the rejection of the best reverse osmosis membranes [24-27]. Therefore, theoretical estimates of membrane rejection for electrolyte solutions appear to be quite reasonable.

With mixtures of nonionic polar liquids rejection calculations are more complicated. Suggestions have been made to use comparative evaluations of the energy of intermolecular hydrogen bonds, Taft's and Hammett numbers [37], and the difference in adsorption energy of components on the basis of Rebinder's rule [27]. So far, quantitative calculations are not yet possible here because the theory of polar liquids has not been sufficiently developed. Solvation effects occur in ionic systems also, but there this factor is probably dominated by a stronger influence of electrostatic forces.

Evidently, further progress in the theory of long-range structural forces (Chapter 7) will largely determine the possibility of performing rigorous theoretical calculations of membrane rejection.

11.3. DIFFUSIOPHORESIS

The phenomenon of diffusiophoresis occupies the same place with respect to capillary osmosis as electrophoresis does with respect to electro-osmosis. Diffusiophoresis is defined as the transport of particles in a concentration field due to the formation of diffuse (and mobile) adsorption layers of neutral molecules or ions formed at the surface of the particles. This phenomenon was first predicted theoretically and then established experimentally by Derguin [4]. Obviously, in the simplest case the diffusio-phoresis rate is simply equal to the rate of capillary osmosis but with opposite sign. Consequently, the same equations serve to find the diffusiophoresis velocity.

Experiments carried out to measure the velocity of diffusiophoresis [4] are schematically represented in Fig. 11.7. A vertical concentration gradient of sucrose (or glucose) was created in a pipe CC about 10 cm in height by connecting the lower end of the pipe with a large reservoir B containing a sucrose solution of a high concentration, and the upper end with the pure solvent in the reservoir A. The solvent was a water-methyl alcohol mixture at a concentration giving a solution density 0.97 g/cm^3 . Japan wax beads with density 0.945 g/cm^3 and radii from 0.1 to 1.5 mm were placed in the middle part of the cylinder CC. At the beginning of the experiment, when the whole sucrose concentration difference was limited to a narrow zone in the middle of the tube, all beads, regardless of their radii, were floating at almost the same height

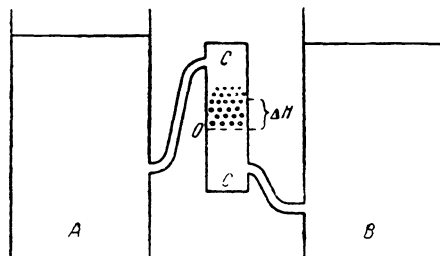


Fig. 11.7. Schematic arrangement of the setup for experimental study of diffusiophoresis of polydisperse wax particles.

within this zone. In the course of diffusion the zone of transient concentrations spreads wider, and a certain distribution of beads, according to their radii, was formed along the tube. The stationary state of the diffusion field was reached after several hours; subsequently, the distribution of beads along the tube became stationary. This steady state could remain unchanged for several days. The difference in height between beads of the smallest and largest diameters (occupying the highest and the lowest positions) reached 10 mm. The diffusiophoretic force F acting on the surface of the beads was directed upward in this case, toward lower solution concentrations. This force F lifted the beads to a height ΔH with respect to the level at which the density of the solution was equal to that of the beads, ρ_0 .

In order to find the height of the equilibrium position of a bead, we have simply to equate F to the resultant of weight and buoyancy forces:

$$F = \frac{4}{3}\pi r^2 g(\rho - \rho_0) \quad (11.42)$$

where r is the bead radius, g is the acceleration of gravity, and ρ is the density of the solution at height ΔH .

On the other hand, F can be found from Eq. (11.3) for the velocity of capillary-osmotic slip, taken with reversed sign:

$$v_{co} = \frac{RT\xi}{\eta} \frac{dC_0}{dz} \quad (11.43)$$

By Stokes's law, the diffusiophoretic force necessary to drive the motion at this velocity is

$$F = 6\pi r \eta v_{co} = 6\pi r RT \xi \frac{dC_0}{dz} \quad (11.44)$$

Assuming the solution density to be a linear function of height, we obtain

$$\rho - \rho_0 = \text{grad } \rho \Delta H = \frac{dp}{dz} \Delta H$$

This readily gives the formula for ΔH , if $\rho - \rho_0$ is replaced with its expression from (11.42), and F with (11.44). The resulting equation

$$\Delta H = \frac{9RT\xi}{gr^2} \frac{dC_0}{dp}$$

provides the interpretation of the practical results. The values of ΔH must increase with decreasing radius of particles. The sign of the effect (particles moving toward lower concentrations) indicates that the adsorption of sucrose on the particle surface is negative.

One recent application of diffusiophoresis is the coating of various solid surfaces from colloidal solutions [43, 44]. A more detailed analysis of diffusiophoresis in electrolytes (the system more often used in applications) can be found in the monograph of Dukhin and Derjaguin [2, 3]. Diffusiophoresis may also be responsible for the repulsion of small particles by live cells, because the cells generate around themselves a concentration field with gradient diminishing away from the cell as a result of material exchange with the surrounding continuous medium [45]. The range of such repulsive forces may reach several tens of micrometers.*

11.4. THERMO-OSMOSIS, THE MECHANOCALORIC EFFECT, AND THERMOPHORESIS

The phenomenon of thermo-osmosis, defined as the flow of a liquid, driven by a temperature gradient, through capillaries or porous bodies, appears because the specific enthalpy of the liquid in boundary layers and thin pores differs by ΔH from the bulk value. The isothermal flow of liquid layers with an altered enthalpy is known to produce an "excess" heat flux, generating a temperature gradient in the direction of flow. By the laws of nonequilibrium thermodynamics [7], the reverse effect must also exist, viz., the flow of the liquid (at zero pressure difference) due to a temperature gradient; this is what is called thermo-osmosis. Thermo-osmosis was discovered and analyzed theoretically and experimentally by Derjaguin and Sidorenkov [46]. The theory of thermo-osmosis and other thermokinetic phenomena was developed in [46] on the basis of nonequilibrium thermodynamics.

*In other papers [B. V. Derjaguin and M. V. Golovanov, J. Colloids Surfaces, 10, 77 (1984); Kolloidn. Zh., 48, 248 (1986); Dokl. Akad. Nauk SSSR, 272, 479 (1983)] this is given another explanation.

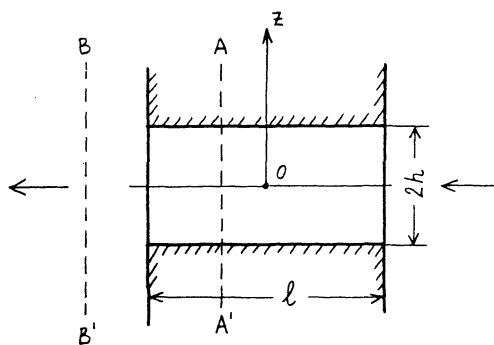


Fig. 11.8. Model for the calculation of the velocity of thermo-osmotic flow.

Let us consider a liquid filling two reservoirs separated by a porous membrane, with pressure difference ΔP and temperature difference ΔT maintained between the reservoirs. The rate of entropy production in the stationary mass and heat transfer across this membrane, for a single-component liquid, is

$$\psi = Q \Delta P + W \frac{\Delta T}{T} \quad (11.45)$$

where Q is the volume material flux (in cm^3/s) and W is the heat transfer flux (in erg/s). Sufficiently intensive stirring maintains a uniform temperature distribution in each reservoir. Consequently, the transferred heat must be released (or absorbed) at a rate W at the surfaces of the membrane or, rather, at the openings of the capillaries passing through this membrane. The form of the dissipative function chosen in (11.45) imposes the following system of kinetic equations:

$$Q = \beta_{11} \Delta P + \beta_{12} \frac{\Delta T}{T} \quad (11.46)$$

$$W = \beta_{21} \Delta P + \beta_{22} \frac{\Delta T}{T} \quad (11.47)$$

where β_{ik} are phenomenological coefficients. The coefficient β_{11} characterizes the isothermal flow of liquid due to the pressure difference, and β_{22} characterizes heat conduction in the system at $\Delta P = 0$.

In order to arrive at concrete results, we assume that all pores are plane-parallel slits with gap width $2h$, small in comparison with slit width B , in which the velocity of the liquid is everywhere perpendicular to the partition surfaces (Fig. 11.8). The overall perimeter of the pores will be denoted by $L = 2B$.

In order to determine β_{21} , consider the situation at the mouths of the "capillaries" where the flow emerges from the membrane. The isothermal heat flux across the section AA' within the membrane (Fig. 11.8) is

$$H_0 Q + B \int_{-h}^{+h} \Delta H(z) v(z) dz$$

where H_0 is the specific enthalpy of the liquid in the bulk, ΔH is its excess (or defect) in layers at the walls, and $v(z)$ is the linear flow velocity. The axis z is perpendicular to the pore walls, and $z = 0$ corresponds to the middle of the pore. Integration is carried out over that area of the section AA' at the walls where ΔH is nonzero.

Obviously, the isothermal heat-transfer flux across a section BB' outside the partition equals $H_0 Q$. The difference between the amount of heat isothermally transferred across the two sections BB' and AA' and that liberated at the membrane surface equals the transferred heat $W = W_0$ (at $\Delta T = 0$):

$$W_0 = B \int_{-h}^{+h} \Delta H(z) v(z) dz \quad (11.48)$$

By neglecting a possible inhomogeneity of viscosity η in boundary layers (i.e., assuming $\eta = \text{const}$), we can postulate a parabolic velocity profile described by Poiseuille's law:

$$v(z) = - \frac{(h^2 - z^2)}{\eta} \frac{\Delta P}{\ell}$$

where ℓ is the membrane thickness. By substituting this expression for $v(z)$ into Eq. (11.48) we find

$$W_0 = - \frac{B \Delta P}{\eta \ell} \int_{-h}^{+h} \Delta H(z) (h^2 - z^2) dz \quad (11.49)$$

Taken together with Eq. (11.47), the last equation yields the required coefficient β_{21} which, by the Onsager relations [7], equals β_{12} :

$$\beta_{21} = \beta_{12} = - \frac{B}{\eta \ell} \int_{-h}^{+h} \Delta H(z) (h^2 - z^2) dz \quad (11.50)$$

For the coefficient $\beta_{21} = \beta_{12}$ to be calculated, we need to know the distribution of $\Delta H(z)$ in boundary layers. First consider the simplest case of wide gaps for which h is much greater than the thickness h_s of the boundary layer with altered enthalpy. Here the velocity profile within the layer h_s can be assumed linear: $v(z) = -2hz \Delta P / \eta l$. Taking into account that only the boundary layers with thickness h_s contribute to the integral in Eq. (11.50), we obtain

$$\beta_{21} = \beta_{12} \approx -\frac{4Bh}{\eta l} \int_0^{h_s} \Delta H(z) z dz = -\frac{2Lh}{\eta l} J \quad (11.51)$$

The integral J can be called the moment of the boundary layer excess enthalpy. If ΔH denotes the mean, or effective, value of the excess enthalpy, then $J = \Delta H \cdot h_s^2 / 2$, so that

$$\beta_{21} = -\frac{Lhh_s^2 \overline{\Delta H}}{\eta l} = -\frac{Sh_s^2 \overline{\Delta H}}{\eta l} \quad (11.52)$$

where $S = hL = 2hB$ is the cross-sectional area of the plane-parallel pore. Since $\beta_{21} = \beta_{12}$, at $\Delta P = 0$ and $h \gg h_s$ the thermo-osmotic flow Q_0 is

$$Q_0 = -2SJ \frac{\nabla T}{T} \quad (11.53)$$

where ∇T is the temperature gradient. In wide pores the flux Q_0 is proportional to the cross-sectional area of the pore because the flow velocity changes only within a narrow layer adjacent to the wall, and produces a "thermo-osmotic slippage" at a velocity

$$v_0 = \frac{Q_0}{S} = -\frac{2J}{\eta} \frac{\nabla T}{T} = \chi \frac{\nabla T}{T} \quad (\text{cm/s}) \quad (11.54)$$

where $\chi = -2I/\eta$ (in cm^2/s) is the thermo-osmotic slip coefficient, or thermo-osmosis coefficient

As seen from the formulas for Q_0 and v_0 , the thermo-osmotic flux points to lower temperatures if $J > 0$, and to higher temperatures if $J < 0$. The sign of the integral follows from the sign of enthalpy change ΔH in boundary layers. Intermolecular forces being usually strengthened in single boundary layers at an interface with a lyophilic wall, their enthalpy must be lowered; consequently, the thermo-osmotic flow in wide lyophilic pores must be directed to a hotter region.

A number of other effects, in addition to isothermal heat transfer W_0 and thermo-osmosis Q_0 , follow from Eqs. (11.46) and (11.47). Thus, if the thermo-osmotic flux is exactly balanced by a reversed filtration flux (when $Q = 0$), Eq. (11.46) gives the

ratio of the pressure difference ΔP to the temperature difference ΔT in stationary conditions:

$$\left(\frac{\Delta P}{\Delta T}\right)_{Q=0} = - \frac{\beta_{12}}{\beta_{11}T} \quad (11.55)$$

This equation expresses the so-called thermomechanical effect — a stationary pressure difference arising as a result of a temperature gradient.

Another condition of a stationary state in the system (for $W_0 = 0$) can be obtained from Eq. (11.47) if the heat flux due to the viscous flow of the liquid with an altered enthalpy is assumed balanced out by heat conduction through the porous membrane:

$$\left(\frac{\Delta T}{\Delta P}\right)_{W=0} = - \frac{\beta_{21}T}{\beta_{22}} \quad (11.56)$$

This state can be realized if the reservoirs, separated by a porous partition, are adiabatically insulated. Equation (11.56) describes the mechanocaloric effect — a stationary temperature difference ΔT caused by a liquid flow driven by a pressure difference ΔP . The temperature difference is produced as a result of heat absorption (if $\Delta H > 0$) or liberation (if $\Delta H < 0$) at the entrance of the liquid into (and of the reverse effect at the emergence of the liquid from) the capillaries of the porous body because the liquid undergoes a transition from the bulk to the boundary phase, and vice versa.

As with electrokinetic and capillary-osmotic phenomena, thermo-kinetics also provides analogs of electrophoresis and diffusio-phoresis, viz., the thermophoresis of lyophilic particles in a polar liquid. The thermophoretic velocity is described by the same equation (11.53) as that of thermo-osmotic slip, taken with reversed sign.

In general, thermokinetic phenomena can be described quantitatively if we know the distribution of ΔH across the interlayer. At present there are adequately developed theories of electrostatic and molecular forces that are employed to find the electric potential distribution responsible for electrokinetic phenomena, or to find the concentration distribution responsible for capillary-osmotic phenomena; but no counterparts of these theories are yet available for calculating structural modifications of liquids. Certain simplifications are thus unavoidable. For instance, Eq. (11.52) is used for wide pores, when $h \gg h_S$. As seen from (11.55), the thermomechanical effect is small in wide pores (when β_{11} is large). This means that even small random pressure variations can bring about considerable difficulties in measuring the thermo-osmotic flow rate. For this reason most of the studies in thermo-

osmosis have been carried out with microporous objects. However, the condition $h \gg h_s$ postulated in deriving Eq. (11.51) is then violated. Instead, we can use another simplifying assumption, viz., that ΔH is constant over the whole cross section of a narrow pore, i.e., use a certain effective mean value $\overline{\Delta H} = \text{const.}$

By using the parabolic velocity profile instead of (11.50), we obtain for the same plane-parallel pore model

$$\beta_{21} = \beta_{12} = -2Lh^3 \overline{\Delta H} / 3\eta\ell \quad (11.57)$$

Correspondingly, the mean thermo-osmotic flow rate $q_0 = Q_0/S$ is given by the following equation:

$$q_0 = - \frac{2h^2 \overline{\Delta H}}{3\eta} \frac{\nabla T}{T} = x \frac{\nabla T}{T} \quad (11.58)$$

The thermo-osmotic coefficient x in the narrow pore model, giving the proportionality factor between thermo-osmotic velocity and temperature gradient ∇T , then takes the form

$$x = -2h^2 \overline{\Delta H} / 3\eta \quad (\text{cm}^2/\text{s}) \quad (11.59)$$

It is also easy to find the coefficient of isothermal filtration β_{11} in the plane-parallel pore model (Fig. 11.8). By comparing the expression for the isothermal flux driven by a pressure difference ΔP ,

$$Q_P = B \int_{-h}^{+h} v(z) dz = - \frac{B \Delta P}{\eta\ell} \int_{-h}^{+h} (h^2 - z^2) dz = - \frac{Lh^3 \Delta P}{3\eta\ell}$$

with the expression $Q_P = \beta_{11} \Delta P$, we find

$$\beta_{11} = -Lh^3 / 3\eta\ell \quad (11.60)$$

From this expression, taken together with (11.55) and (11.56), we obtain, for instance, that in the chosen model of narrow pores the thermomechanical pressure is

$$(\Delta P / \Delta T)_{Q=0} = -2 \overline{\Delta H} / T \quad (11.61)$$

Therefore, by measuring the thermomechanical pressure in narrow pores we can directly evaluate the mean increment of specific enthalpy. Equation (11.61) does not include pore size because both the thermo-osmotic flow rate q_0 and filtration flow rate $q_P = Q_P/S = -h^2 \Delta P / 3\eta\ell$ are proportional to h^2 .

The experimental results reported for thermo-osmotic flow in relatively wide-pore bodies are rather contradictory. Thus, the

thermo-osmotic flux in porous glass specimens with mean pore radius $r \approx 1 \mu\text{m}$ [46] and in glass capillaries ($r \approx 10-15 \mu\text{m}$) [47] was directed toward the colder end, indicating the enhanced enthalpy of water boundary layers. It was conjectured on this basis that not the whole boundary layer but only its peripheral part makes the major contribution to the thermo-osmotic flow (see Chapter 7). No thermo-osmotic flow could be observed, within experimental error, for rouge (Fe_2O_3) and corundum polishing powders with particle size about $0.1 \mu\text{m}$ [48]. However, a thermo-osmotic flow toward higher temperatures was observed in aqueous wetting films on glass [49-52], although in these experiments the velocity of thermo-osmotic flow was not directly measured but was found as a difference between the measured velocity of flow driven by a temperature gradient in the film and the theoretically calculated velocity of thermocapillary flow directed toward the colder end.

Measurements carried out in microporous systems (reverse osmosis membranes, clays, silica gels) [53-58] give less contradictory results. The thermo-osmotic flow of water was found to be toward the lower-temperature regions, and the thermo-osmosis coefficient X was from -10^{-8} to $-10^{-6} \text{ cm}^2/\text{s}$. As an example, we give here the results obtained with microporous glasses, i.e., systems with a rigid skeleton and low thermal expansion coefficient [57, 58]. These experiments gave, for the first time, the information on the dependence of thermo-osmotic velocity and thermo-osmosis coefficient on mean pore radius r (from 45 \AA to several μm), and on temperature gradient ∇T and mean specimen temperature T_m . The specimens of microporous glass were disks with diameter $D \approx 2.2 \text{ cm}$ and thickness ℓ about 1 mm . Mean pore radii r were determined from water vapor desorption isotherms [59]. The main structural characteristics of the specimens (mean pore radius r , porosity n , specific surface S_m) are listed in Table 11.1. In addition to porous glasses (specimens Nos. 1-4), two Schott filters (specimens Nos. 5 and 6) were used, cut into disks of the same size. Specimens are numbered in the order of increasing pore size.

A schematic arrangement of the setup used in the measurements is shown in Fig. 11.9. A specimen 1 was glued by an epoxy resin to a holder ring 2 made of Plexiglas. The ring was clamped with sealing gaskets between the flanges 3 of two parts of the setup made of Plexiglas. The working chambers 4 were filled with the liquid to be studied. Water pumped by two thermostats was circulated through coolant jackets 5. In some experimental runs a cryogenic pump was used to create a low mean temperature T_m . The liquid within the chambers was stirred by magnetically driven stirrers 6.

Platinum electrodes 7 and thermouple junctions 8 were placed at the specimen surface. The chambers 4 were connected with a bypass 9 that served to equalize pressure, prior to measuring the thermo-osmotic velocity by recording the displacement of menisci in

TABLE 11.1. Structural Characteristics of Porous Glass Specimens Used to Measure Thermo-Osmotic Velocity

Sample No.	$r, \text{ \AA}$	n	$S_m, \text{ m}^2/\text{g}$	$D, \text{ cm}$	$\ell, \text{ mm}$
1	45	0.322	89.7	2.2	1.02
2	83	0.331	79.7	2.2	1.07
3	100	0.333	52.5	2.2	0.89
4	550	0.362	22.8	2.2	0.96
5	$1.5 \cdot 10^4$	0.386	0.193	2.1	0.94
6	$4 \cdot 10^4$	0.391	0.168	2.2	1.02

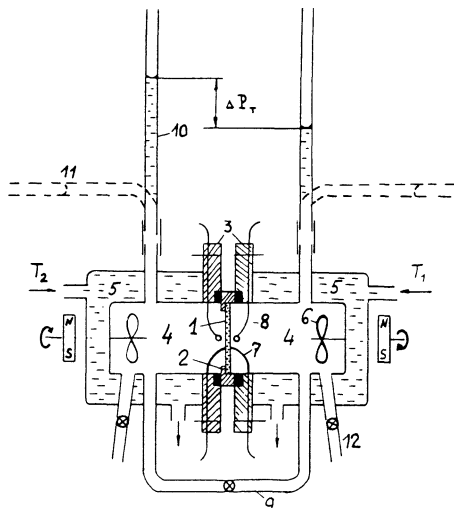


Fig. 11.9. Schematic arrangement of the setup for studying the thermo-osmotic flow of water in porous glass.

horizontal capillaries 11. With the bypass shut off, it was possible to measure the thermomechanical pressure difference by two vertical capillaries 10.

The main experiments were carried out with doubly distilled water. Measurements were conducted at different mean temperatures from 10 to 60°C and at temperature gradients ∇T from 20 to 300 deg/cm (corresponding to a temperature difference across a specimen

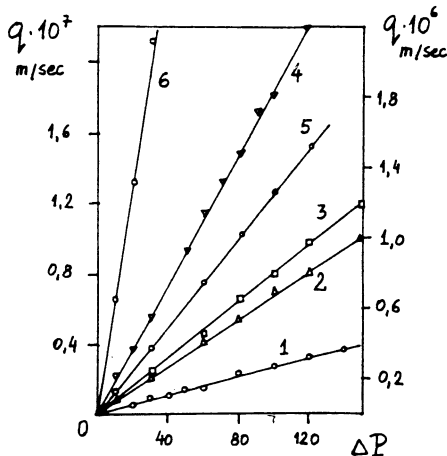


Fig. 11.10. q as a function of ΔP (in cm of water column) for six specimens of porous glass at 20°C. The numbers at the curves correspond to the numbers of the specimens in Table 11.1. Curves 1-4 refer to the left-hand ordinate axis, and curves 5 and 6 refer to the right-hand one.

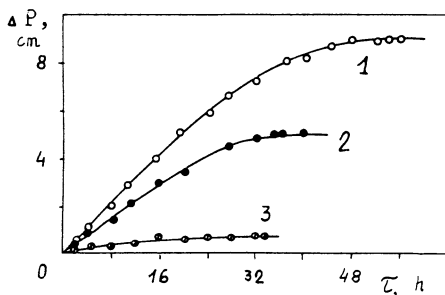


Fig. 11.11. ΔP (in cm of water column) as a function of time τ (in h) for the porous glass specimen No. 2 at different mean temperatures: 1) 20°C, $\nabla T = 166$ deg/cm; 2) 40°C, $\nabla T = 169$ deg/cm; 3) 60°C, $\nabla T = 178$ deg/cm.

from 2 to 30°). The thermo-osmotic rate q_0 (at $\Delta P = 0$) was found by measuring with a microscope the displacement of menisci in calibrated horizontal capillaries. The thermomechanical pressure differ-

TABLE 11.2. Thermo-Osmotic Coefficients Obtained from the Data on Thermomechanical Pressure (χ_1) and Thermo-Osmosis Rate (χ_2)

Specimen No.	Mean temperature T_m , K	ΔT , deg	∇T , deg/cm	$\chi_1 \cdot 10^6$, cm ² /s	$\chi_2 \cdot 10^6$, cm ² /s
1	313	13.0	127	-1.37	-1.48
2	293	17.8	166	-1.41	-1.36
2	313	18.1	169	-0.99	-0.95
2	333	19.0	178	-0.13	-0.16
3	293	15.8	145	-0.82	-0.87

ence ΔP (at $Q = 0$) was found by measuring with a cathetometer the difference in meniscus heights in vertical capillaries. The same setup was used to measure filtration rates q_p and to obtain the coefficients β_{11} for all specimens. Figure 11.10 plots q_p as a function of ΔP (at $\Delta T = 0$) recorded at 20°C. The graphs $q(\Delta P)$ are linear and pass through the origin, confirming the constancy of filtration coefficients and the validity, in these systems, of the viscous flow equations of Newtonian liquids. The value of β_{11} decreases monotonically with decreasing mean pore size.

Figure 11.11 shows the result of measuring thermomechanical pressure in the same specimen No. 2 at different mean temperatures T_m . The stationary, time-independent levels of ΔP are reached the sooner, the higher the temperature (and, hence, the lower the liquid viscosity in the pores). By measuring the stationary value of ΔP (Fig. 11.11) and knowing the mean temperature T_m and the coefficient β_{11} , it was possible to find from Eq. (11.55) the thermo-osmotic coefficient χ at a given temperature difference $\Delta T \approx 17^\circ$:

$$\chi = -KT(\Delta P/\Delta T)_{Q=0} \quad (11.62)$$

correspondingly, the filtration coefficient $K = 4\beta_{11}/\pi D^2$ of the specimens was measured at different temperatures. It was also possible to find the coefficient χ from Eq. (11.58) directly from the thermo-osmotic rate q_o , after vertical calibrated capillaries were replaced with horizontal ones. Table 11.2 lists the results of comparative measurements of χ by these two methods. It shows that the results yielded by the two methods are quite close, confirming the reliability of the method employed.

Figures 11.12 and 11.13 plot the thermo-osmotic rate q_o as a function of temperature gradient ∇T and as a function of mean specimen temperature T_m . In accord with the theory of thermo-osmosis, the dependences $q_o(\nabla T)$ obtained are linear in the whole range of ap-

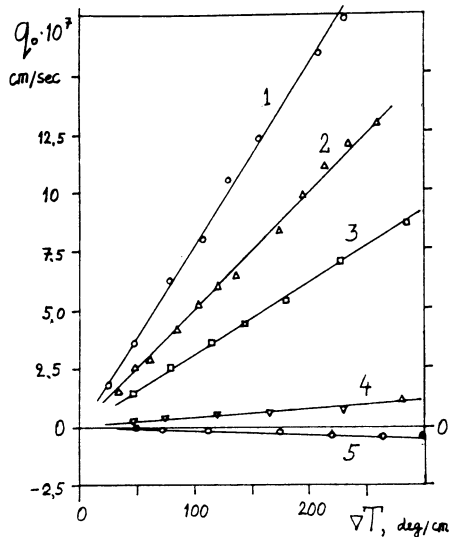


Fig. 11.12. Thermo-osmosis rate q_0 as a function of temperature gradient ∇T . Numbers at the curves correspond to the numbers of the specimens in Table 11.1.
 $T_m = 293$ K.

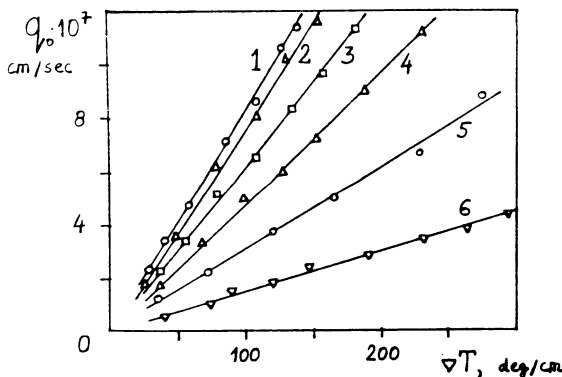


Fig. 11.13. Thermo-osmosis rate in specimen No. 1 of porous glass as a function of temperature gradient at different mean temperatures T_m : 1) 288; 2) 293; 3) 303; 4) 313; 5) 323; 6) 333 K.

plied gradients and pass through the origin. In a wide-pore specimen No. 5 the thermo-osmotic flow was directed to higher temperatures (Fig. 11.12), indicating that, in agreement with the predic-

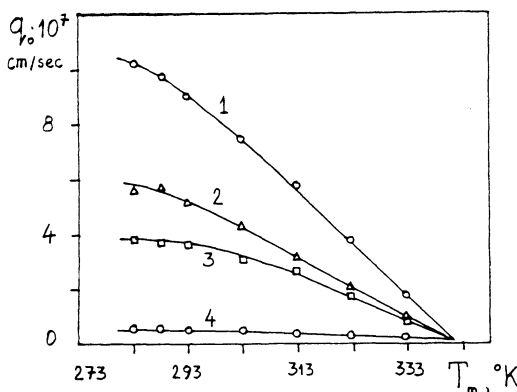


Fig. 11.14. Thermo-osmosis rate q_0 as a function of mean temperature T_m at a constant temperature gradient $\nabla T = 120$ deg/cm in porous glass specimens: 1) No. 1; 2) No. 2; 3) No. 3; 4) No. 4.

tions, the specific enthalpy of single boundary layers was reduced. No thermo-osmotic flow was detected, within experimental error, in sample No. 6, which had still wider pores. As the pore size is diminished, the direction of thermo-osmosis is reversed and the absolute values of thermo-osmotic coefficient χ increase. Possibly the mean values of $\Delta H > 0$ grow in thinner pores because of the overlap of boundary layers and owing to structural modifications in water within the overlap zone.

As the temperature increases, the deviations of specific enthalpy from the bulk value diminish, as with other properties of boundary layers (see Chapter 7). This conclusion follows from the graphs of $q_0(\nabla T)$ in Fig. 11.13. The thermo-osmotic rate measured in the same specimen monotonically diminishes with increasing mean temperature T_m . This effect is even more pronounced in Fig. 11.14, which shows similar results for four samples of porous glass. The thermo-osmotic rate is sharply reduced when the mean temperature rises from 10 to 60°C, and $\chi \rightarrow 0$ at temperatures above 60°C. An abrupt drop in the absolute value of χ was also observed after hydrophobization of the surface of porous glass; this result indicates that the effect was linked with the hydrophilicity of the surface, determining the depth to which the structure of water in boundary layers is modified (for details see Chapter 7).

Thermo-osmotic flow was also observed in another polar liquid, viz., methyl alcohol, although with lower absolute values of χ . As in water, the thermo-osmotic flux of alcohol in the porous glass specimen No. 2 was directed toward lower-temperature layers. The thermo-osmotic coefficient obtained for water in microporous glass

($r = 45-100 \text{ \AA}$) is of the order $\chi = -10^{-6}$ to $-10^{-7} \text{ cm}^2/\text{s}$. This is close to the values of χ already known in other microporous hydrophilic bodies. Thus, in a high-density cellulose acetate membrane $\chi \approx -10^{-7} \text{ cm}^2/\text{s}$, with χ diminishing, as in porous glasses, when the pore size increases [56]. In a cellophane membrane with a higher permeability, χ was only -10^{-9} to $-10^{-10} \text{ cm}^2/\text{s}$ [53]. In microporous clays $\chi = -3 \cdot 10^{-8} \text{ cm}^2/\text{s}$ [54]. A higher absolute value of χ was reported for bentonite: $\chi = -5 \cdot 10^{-6} \text{ cm}^2/\text{s}$ [55]. This situation with the orders of magnitude of χ and its sign is unlikely to be coincidental. Presumably, it is explained by the small pore size and strong hydrophilicity of the surface in porous glasses, membranes, and clays.

Equations (11.59) and (11.61) make it possible to evaluate the change in mean specific enthalpy of liquids in narrow pores. Assuming the half-width h of a pore to be approximately equal to its radius r , and setting $\eta = 0.02 \text{ P}$ [the viscosity of water in narrow pores of porous glass being enhanced by a factor of 1.5-2 (see Chapter 7)], we obtain that in specimen No. 1 of porous glass at 10°C (Table 11.1), $\Delta H = 3.6 \cdot 10^5$; in specimen No. 2, $\Delta H = 6.4 \cdot 10^4$; and in specimen No. 3, $\Delta H = 2.8 \cdot 10^4 \text{ erg/cm}^3$. It should be mentioned for comparison that the specific heat of melting of bulk water exceeds the highest of the above values of ΔH by a factor of about 10^4 . This means that relatively very small changes in the specific enthalpy of boundary layers are sufficient to produce a measurable thermo-osmotic flow of water in narrow pores. We can also conclude that measuring the thermo-osmotic flow rate provides a sensitive method of detecting structural modifications in water within thin layers and pores.

Owing to the high surface electrical conductivity of micro-porous materials, electrokinetic effects in them are rather weak [1-3, 60-62, 72]. Consequently, no appreciable flow potentials are generated by the flow of a liquid. Thus, short-circuiting of the electrodes in the experiments described above with thin porous glasses (Fig. 11.9) did not noticeably affect either the filtration rate or the thermo-osmotic rate. Mass transfer is most sensitive to electrokinetic effects when $kh \approx 1$ [1-3, 60-62] (k being the reciprocal Debye radius and h either the pore half-width or the film thickness). In water ($k = 10^4-10^5 \text{ cm}^{-1}$) these phenomena are most pronounced at h about $0.1-1 \mu\text{m}$. For such pores, as well as for wider ones ($h \approx 10 \mu\text{m}$), any theory of nonisothermal mass transfer in porous bodies with charged surface must take into account the charge transfer, in addition to heat transfer. The dissipative function involving the entropy production rate is then written in the following form, instead of (11.45) [63]:

$$\psi = Q\Delta P + W\frac{\Delta T}{T} + JVE \quad (11.63)$$

where earlier notations are retained: J for the electric current, and ∇E for the gradient of electric potential.

The following system of equations is obtained from Eq. (11.63) for specific mass flux q (in cm/s), specific heat flux W (in $\text{erg/cm}^2 \cdot \text{s}$), and electric current i (in A/cm^2):

$$q = \alpha_{11} \nabla P + \alpha_{12} (\nabla T/T) + \alpha_{13} \nabla E \quad (11.64)$$

$$w = \alpha_{21} \nabla P + \alpha_{22} (\nabla T/T) + \alpha_{23} \nabla E \quad (11.65)$$

$$i = \alpha_{31} \nabla P + \alpha_{32} (\nabla T/T) + \alpha_{33} \nabla E \quad (11.66)$$

New phenomenological coefficients α_{ik} , whose physical meaning needs clarification, appear in these conditions. The dimensionality of α_{ik} is different from that of β_{ik} : $\alpha_{ik} = \beta_{ik}/S$, where S is the cross-sectional area of the specimen. The coefficients $\alpha_{13} = \alpha_{31}$ characterize the familiar electrokinetic phenomena – electro-osmosis and flow potential, respectively; and α_{33} characterizes the electrical conductivity of the system. Hence, only two coefficients, $\alpha_{23} = \alpha_{32}$, describing two interrelated thermoelectric effects, are new.

Consider the transfer of heat $W_e = \alpha_{23} \nabla E$ (under the conditions $\Delta P = 0$ and $\Delta T = 0$). It is composed of heat transferred by electro-osmosis flow of the liquid polarized in the electric double layer, and the difference between heat transferred by anions, Q_- , and that transferred by cations, Q_+ , in the electric field ΔE [64]. Further calculations of the phenomenological coefficients will be restricted to the same model of a plane-parallel pore with gap width $2h$. In this case,

$$W_e = \alpha_{23} \nabla E = \frac{1}{h} \int_0^h \Delta H_e(z) v(z) dz + \alpha_{33} (Q_+ - Q_-) \frac{\nabla E}{2F} \quad (11.67)$$

where F is the Faraday number.

We shall analyze only the effects associated with diffuse electric layers, so that the increments ΔH_e in specific enthalpy appear only because the liquid is polarized in the electric field within these layers. The velocity distribution $v(z)$ also differs from that discussed earlier. Here the velocity profile forms because water is entrained by ions in the electric field, i.e., the profile results from electro-osmosis.

Let us calculate the distribution $\Delta H_e(z)$ across a plane-parallel pore with gap width $2h$. We use the expression for the increment in free energy ΔG of an elementary volume of the solution produced by the polarization of the solvent in the field of the diffuse electric layer [65]:

$$\Delta G = \frac{\epsilon_0}{8\pi} \left(\frac{\partial \varphi}{\partial z} \right)^2 \quad (11.68)$$

where ϵ_0 is the static permittivity, and $\varphi(z)$ is the local value of the electric potential. The solution was obtained for the approximation of low potentials φ_0 of the pore surfaces, when the following expression for the potential distribution $\varphi(z)$ within the gap is valid [66]:

$$\varphi = \varphi_0 \frac{\cosh \kappa z}{\cosh \kappa h} \quad (11.69)$$

The relevant expression for the increment in specific enthalpy is found from the Gibbs-Helmholtz equation. As in [65, 67], we find

$$\Delta H_e(z) = \frac{1}{8\pi} \left(\frac{\partial \varphi}{\partial z} \right)^2 \left(\epsilon_0 + T \frac{\partial \epsilon_0}{\partial T} \right) = \frac{\alpha \epsilon_0 \kappa^2 \varphi_0^2}{8\pi} \frac{\sinh^2(\kappa z)}{\cosh^2(\kappa h)} \quad (11.70)$$

where $\alpha = 1 + (T/\epsilon_0)(\partial \epsilon_0 / \partial T)$.

The quantity α in water at $T = 283-293$ K is known to be about -0.4. Consequently, ΔH_e is negative: restriction of the mobility of water molecules due to polarization results in a reduced specific heat content of water.

The profile $v(z)$ of electro-osmotic velocity can be found from the Navier-Stokes equations, with conventional boundary non-slip condition and symmetry [60, 62]:

$$v(z) = \frac{\epsilon_0 \varphi_0}{4\pi\eta} \left(1 - \frac{\cosh \kappa z}{\cosh \kappa h} \right) \nabla E \quad (11.71)$$

By substituting into the heat transfer equation (11.69) the expressions for $\Delta H_e(z)$ from (11.70), and $v(z)$ from (11.71), we arrive at the following expression for the thermoelectric coefficient $\alpha_{23} = \alpha_{32}$:

$$\alpha_{23} = \alpha_{32} = \frac{\epsilon_0^2 \varphi_0^3 \kappa^2 \alpha}{64\pi^2 \eta} \psi(\kappa h) + \alpha_{33} \frac{(Q_+ - Q_-)}{2F} \quad (11.72)$$

where

$$\psi(\kappa h) = (\tanh \kappa h / \kappa h) + \tanh^2 \kappa h - 1 + (2 \tanh^3 \kappa h / 3 \kappa h)$$

The meaning of the cross thermoelectric effect defined by the coefficient α_{32} can now be explained. Equation (11.66) shows that α_{32} determines the current i generated when a temperature gradient VT is imposed (at $\nabla P = 0$ and $\nabla E = 0$). The current arises

because of the thermodiffusion of ions accompanied by thermal polarization of the diffuse electric layer.

Our problem is to analyze how the flow of liquids through pores in a temperature gradient ∇T at zero pressure difference ($\Delta P = 0$) is influenced by electrical effects, because this is the situation we encounter when measuring the rate of thermo-osmotic flow in porous bodies. However, in the presence of a diffuse electric layer we have to take into account not only the effect of the third term in (11.64) but also the increment in specific enthalpy due to polarization of the liquid in the electric field of the diffuse layer. In fact, the coefficients $\alpha_{12} = \alpha_{21}$ must now include the sum of enthalpy increments $\Delta H + \Delta H_e$. Further calculations will be concerned only with ΔH_e since the effects of changes in the specific enthalpy of boundary layers ΔH were already discussed in the preceding pages. The solution presented below is thus valid for a porous body with charged surface but without structurally modified boundary layers of the solvent.

The coefficient α_{21} will be found from the heat transfer equation (11.48) for the same model of the plane-parallel pore:

$$w_0 = \frac{W_0}{2Bh} = \frac{1}{h} \int_0^h \Delta H_e(z) v(z) dz = \alpha_{21} \nabla P \quad (11.73)$$

By substituting here the expression for $\Delta H_e(z)$ from (11.70) and using now the parabolic Poiseuille velocity profile for a viscous flow driven by a pressure gradient ∇P , we obtain the following expression for α_{21} :

$$\alpha_{21} = \alpha_{12} = - \frac{\epsilon_0 \varphi_0^2 \alpha}{32\pi\eta} f(\kappa h) \quad (11.74)$$

where

$$f(\kappa h) = - \frac{1}{2} \left[(\tanh \kappa h / \kappa h) + \frac{4}{3} (\kappa h)^2 (1 - \tanh^2 \kappa h) - (1 + \tanh^2 \kappa h) \right]$$

To distinguish this case from that analyzed above, here we can refer to the coefficient $\alpha_{12} = \alpha_{21}$ as the thermoelectro-osmotic coefficient, and denote it by χ_e .

Now compare the two components of the thermoelectro-osmotic flux. The first of them is described by the equation

$$q_{e1} = \alpha_{12} \frac{\nabla T}{T} = \chi_e \frac{\nabla T}{T} = - \frac{\epsilon_0 \varphi_0^2 \alpha f(\kappa h)}{32\pi\eta} \frac{\nabla T}{T} \quad (11.75)$$

The second component, q_{e2} , is produced by the electric field gradient ∇E due to the imposed temperature gradient ΔT . The gradient ∇E can be found from Eq. (11.66), taking into account the conditions of zero current ($i = 0$) and zero pressure difference ($\Delta P = 0$). It is under these conditions that flow rates of liquids in pores are measured when applying a gradient ∇T . From (11.66) we find

$$\nabla E_T = - \frac{\alpha_{32}}{\alpha_{33}} \frac{\nabla T}{T} \quad (11.76)$$

By substituting this expression for the thermally generated potential gradient ∇E_T into (11.64), we obtain for the second component

$$q_{e2} = \alpha_{13} \nabla E_T = - \frac{\alpha_{32} \alpha_{13}}{\alpha_{33}} \frac{\nabla T}{T} = \chi_{e2} \frac{\nabla T}{T} \quad (11.77)$$

Substituting here for α_{32} its expression from (11.72), and also the electrokinetic coefficients α_{13} and α_{33} known for the same model [60, 62], we find [63]

$$q_{e2} = \frac{\epsilon_0 \varphi_0^2 \alpha}{32\pi\eta} [\Phi(kh) + Q(kh)] \frac{\nabla T}{T} \quad (11.78)$$

where $\Phi(kh) = 4f(kh)[1 - (\tanh kh/kh)]/[2\eta\lambda(4\pi/\epsilon_0\varphi_0\kappa)^2 + (\tanh kh/kh) + \tanh^2 kh - 1]$; $Q(kh) = -4(Q_+ - Q_-)(1 - \tanh kh/kh)/F\varphi_0\alpha$, and λ is the electrical conductivity of the solution. To further simplify the calculations, we assume $Q_+ \approx Q_-$; i.e., we restrict the analysis to the effect of polarization of the liquid in the electric field of the diffuse layer. Then

$$q_{e2} = \chi_{e2} \frac{\nabla T}{T} = \frac{\epsilon_0 \varphi_0^2 \alpha}{32\pi\eta} \Phi(kh) \frac{\nabla T}{T} \quad (11.79)$$

A comparison of (11.75) and (11.79) shows that the fluxes q_{e1} and q_{e2} have opposite signs [the functions $f(kh)$ and $\Phi(kh)$ are everywhere positive] and are proportional to the squared surface potential of the porous body, i.e., are independent of the sign of φ_0 . The flux q_{e1} is directed toward the warmer side, and thus corresponds to $\chi_{e1} > 0$, and the flux q_{e2} toward the cooler side, and thus corresponds to $\chi_{e2} < 0$. Since χ_{e1} and χ_{e2} differ only in sign and in the magnitude of the functions $f(kh)$ and $\Phi(kh)$, it will be sufficient to discuss only the results of numerical calculations of these functions (Fig. 11.15). Figure 11.15 shows that at $kh < 1$ the thermoelectro-osmotic fluxes are small. This demonstrates that electric effects in narrow pores are negligible, and that "true" thermo-osmosis due to a modified structure of boundary layers of polar liquids is the dominant factor.

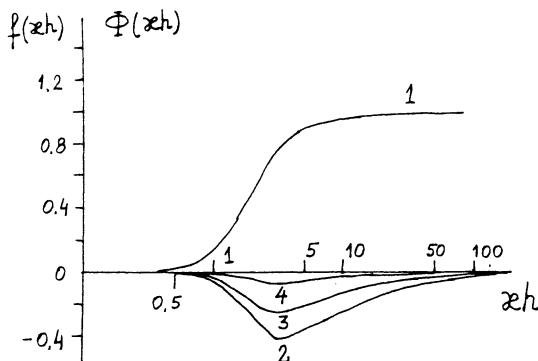


Fig. 11.15. Thermoelectro-osmotic coefficients χ_{e1} (curve 1) and χ_{e2} (curves 2-4) as functions of dimensionless width of planar pore, ϕh , at 25°C . 2) $\phi_0 = 150 \text{ mV}$; 3) 100 mV ; 4) 50 mV .

The main contribution in wide pores ($\phi h \geq 5$) is made by the thermoelectro-osmotic flux q_{e1} . The flux q_{e2} can also be appreciable in the range $\phi h \geq 1$, the higher the surface potential ϕ_0 . The possibility of simultaneous manifestation of different effects (χ , χ_{e1} , χ_{e2}) in wide-pore bodies explains the spread in magnitudes and signs of the experimentally measured effect. As follows from the above analysis, the differences could stem from unequal surface potentials ϕ_0 and unequal values of ϕh . Furthermore, the effect of ion thermodiffusion could also be appreciable. Calculations show that at $\phi h > 0.1$ (provided ϕ_0 is sufficiently high) this effect can exceed all other thermoelectro-osmotic components [63]. The sign of the function $Q(\phi h)$ in Eq. (11.78) depends on the sign of the difference $Q_+ - Q_-$ and on that of the surface potential ϕ_0 . These arguments show that the rate of the true thermosmosis due to a modified structure of boundary layers can be reliably measured only in microporous bodies, under the condition $\phi h \leq 0.1$, which for water corresponds to a pore size $2h \leq 500 \text{ \AA}$.

The presence of surface charge and solutes makes it considerably more difficult to interpret the data on thermo-osmotic rates, as was shown above. Moreover, they are often poorly reproducible owing to uncontrolled effects of electro-osmosis and capillary osmosis. In addition, the effect of thermal polarization [68] due to a finite thermal conductivity of the liquid in the reservoirs separated by a membrane may prove considerable. Consequently, the actual temperature difference across the membrane ΔT deviated from that measured in the bulk of the stirred liquid ΔT_b . If stirring is ineffective, ΔT can be less than ΔT_b by two orders of magnitude, reducing the value of χ and producing an apparently nonlinear de-

pendence of thermo-osmotic flow rate on ∇T . Although in some cases the rate of thermo-osmosis is influenced by electric charge and capillary osmosis effects, thermo-osmosis is not reducible solely to these effects that ignore the main cause of this phenomenon, viz., structural modifications in boundary layers of the liquid (see [46, 71, 69, 70].

Thermophoresis in liquids has been studied much less thoroughly than thermo-osmosis, because of the difficulties involved in correctly taking into account thermal conduction and Brownian motion (of small particles). McNab and Meisen [72] were able to measure the thermophoretic velocity of spherical latex particles about 1 μm in diameter, in water and hexane. A vertical temperature gradient was imposed on a dilute suspension filling a flat horizontal slit 0.3 cm wide. The lower part of the suspension was kept cooler in order to reduce convection. The velocity of thermophoresis v_t was found as the difference between the measured velocity of vertical displacement of particles in the thermal field and their Stokes settling velocity. The values of v_t were from 3-8 $\mu\text{m/s}$ for ∇T varied from 100 to 300 deg/cm. The thermophoretic motion of the particles went toward cooler layers, accelerating their settling. Only small differences in χ were observed between water and hexane. The dependence of v_t on ∇T so obtained was erroneously explained in [72] in terms of the theory of thermodiffusion of particles in gases; that is not valid for liquid media because it neglects the special structure of boundary layers of the liquid and the diffuse electric layer.

Thermo-osmotic flow related to the changed enthalpy of boundary layers is found not only in water but also (and in a very conclusive manner) in films of some organic liquids [73]. A film of low-volatility liquid was deposited on a metal substrate along which a temperature gradient was maintained. At the beginning of the experiment the film was wedge-shaped. The angle of the wedge became gradually smaller with time because the film spread out as a result of a thermocapillary flow directed toward the colder side. The evolution of the thickness and of the profile of the film was observed by monitoring the displacement of interference fringes created by monochromatic light illuminating the film from above. Films of nonpolar turbine oil had a rectilinear profile at any time (all interference fringes being equally spaced). The flow was driven only by thermocapillary forces applied to the surface of the film. They act like the tangential component of the air flow when boundary viscosity is measured by the blowoff technique (see Section 7.4). In contrast to oil, interference fringes in silicon polymer films and films of incompletely hydrated benzanthrone were observed to crowd toward the wetting boundary. The slope of the film surface at this boundary was steeper than it was far from the boundary. This effect clearly demonstrates that in thin layers of polymer liquids close to the walls (where they have a

changed specific enthalpy $\Delta H < 0$) there is a thermo-osmotic counterflow toward the warmer region.

Bykhovsky [74] analyzed the effect of thermo-osmosis on the spreading of a number of liquids over metals in a temperature gradient. When a droplet spreads over a specimen from its cooler to the warmer end, the boundary of the droplet stops at a certain distance. This is caused by the balancing of two oppositely directed flows, viz., the thermocapillary and thermo-osmotic flows. Calculations taking into account these fluxes, the hydrostatic pressure in the droplet, and the difference between interfacial energies at the substrate below the droplet and in front of the droplet boundary, made it possible to evaluate the product of the increment ΔH in specific enthalpy by boundary layer thickness h_s , and the thermo-osmotic coefficient χ . The thermo-osmotic flux in 2-octanol on a germanium surface was directed toward the warmer end: $\Delta H h_s = -37.2 \text{ erg} \cdot \text{cm/g}$, and $\chi \approx 2 \cdot 10^{-3} \text{ cm}^2/\text{s}$. Similar quantitative results were obtained for droplets of octanol, undecane, dodecane, and di-butyl phthalate on a titanium plate. We thus see that thermo-osmosis also plays an important role in nonisothermal spreading of liquids, including nonpolar liquids, on the surface of semiconductors and metals with high surface activity.

11.5. THERMOCRYSTALLIZATION FLOW IN THIN NONFREEZING INTERLAYERS

The flow in nonfreezing interlayers of water and other liquids due to a temperature gradient requires a special treatment. The existence of nonfreezing interlayers between ice and a solid surface as such is a phenomenon caused by surface forces. These interlayers are essentially a boundary phase of ice, with a structure so modified by surface forces that a transition from crystal to liquid state takes place. A salient feature is the formation of an interface between the ice and the nonfreezing liquid interlayer. The interlayer has a certain thickness h which is a function of temperature and pressure: $h = h(p, T)$. As $T \rightarrow T_0$, where T_0 is the melting point of ice, $h \rightarrow \infty$. As the temperature is lowered (at $T < T_0$), the thickness of nonfreezing interlayers diminishes. Thus, in water h does not exceed one monolayer thickness when $\Delta T = T_0 - T \gtrsim 15-20^\circ$. Consequently, the effects due to the presence of nonfreezing water in porous bodies are especially well pronounced at temperatures close to T_0 , i.e., in layers close to the freezing front.

The presence of nonfreezing water in hydrophilic porous bodies (soil, earth, construction materials) has been confirmed by various methods [75-80]. Unfortunately, the studies were mostly concerned with one equilibrium property: the amount of nonfreezing water or interlayer thickness as a function of temperature. Also, these data suffer from a considerable spread due to strong effects of

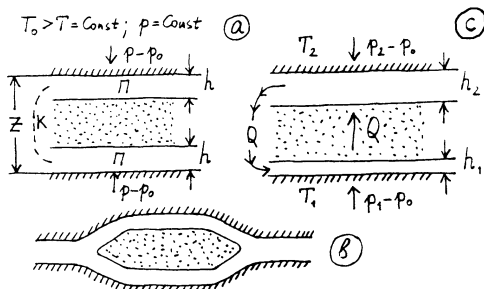


Fig. 11.16. Plane-parallel slit model of a pore filled with ice (a, c) and its real analog (b): an ice lens in a porous body.
 a) Equilibrium in the model at $T < T_0$; c) stationary state at $T_0 > T_2 > T_1$ and $p_2 > p_1$.

structural specificities, composition, and degree of hydrophilicity of the solid phase on the structure of water boundary layers.

Considerably less is known about the flow in nonfreezing interlayers subjected to pressure and temperature gradients. Although it has been reliably established that such flows do exist [76, 79, 81-85], the physical relationships and the transport mechanism have not been studied in sufficient detail. The existing theories of transport of nonfreezing moisture [79, 83-88] did not relate the flux intensities to the heat of the water-ice phase transition. We showed, however, that this is a decisive factor in the phenomenon [89].*

A quantitative solution of the problem of nonfreezing moisture transport under temperature and pressure gradients requires a treatment of the interrelated mass and energy fluxes in terms of non-equilibrium thermodynamics. In order to bring out the principal physical mechanism of the phenomenon, let us consider a plane-parallel gap model of the pore space, shown in Fig. 11.16a. Here an ice platelet is sandwiched between parallel solid walls. The ice is separated from the walls by nonfreezing water interlayers of thickness h . The model corresponds to a deformable porous body because the spacing $z \gg h$ between the pore walls can change in response to external pressure. The upper and lower interlayers are connected through nonfreezing communication channels K . A real situation corresponding to this is, for instance, an ice lens in a widened pore (see Fig. 11.16b). Such wider segments are connected by narrower pores where boundary layers overlap and water does not freeze. These narrower pores and the system of liquid interlayers form nonfreezing communicating channels in the proposed model.

*See also B. V. Derjaguin and N. V. Churaev, Cold Regions Sci. Technol., 12, 57 (1986).

The system shown in Fig. 11.16a is in equilibrium at a constant temperature $T < T_0$ and at equal pressure exerted by the walls (gravity is neglected). The equilibrium thickness of nonfreezing interlayers is determined by the hydrostatic pressure p in the interlayer and the temperature in the liquid:

$$h = h(p, T) \quad (11.80)$$

Inverting this relation we can write

$$T = T(p, h) \quad (11.81)$$

Here T is the temperature of phase equilibrium, depending both on p and on h . This relation generalizes the concept that the curves $T = T(p)$ are different for open ($h \rightarrow \infty$) and for closed ($h \rightarrow 0$) crystal faces [90].

An excess external pressure $p - p_0$ applied to an interlayer is balanced out by its disjoining pressure Π , which is a function of interlayer thickness and temperature (see Chapter 2):

$$p - p_0 = \Pi = \Pi(h, T) \quad (11.82)$$

where p_0 is the pressure in the bulk (supercooled) liquid phase with which the interlayer is, or could be, in equilibrium. At a given temperature T_i and pressure p_0 , Eqs. (11.80) and (11.82) determine the equilibrium thickness h_i as that at the intersection point of two $h(p)$ curves given by these equations. In turn, this point corresponds to equilibrium values of p_i and Π_i . The pressure p_i is transmitted through the liquid to the ice platelet, which is at rest when $\Delta p = 0$, since on both sides it is subjected to the same equilibrium pressure p_i . In what follows we assume that the isolated element of the ice platelet (Fig. 11.16a) is bounded on the sides by an ideal adiabatic surface, and that the friction between these surfaces and the ice is zero. In real conditions this corresponds to a "floating" ice lens (Fig. 11.16b).

Now we disturb the equilibrium in the system by creating a small temperature difference $\Delta T = T_2 - T_1$ or a small pressure difference $\Delta p = p_2 - p_1$ in the interlayers, or both differences simultaneously (Fig. 11.16c). The disturbance starts the heat and mass exchange between the interlayers, accompanied by melting of ice at one surface and crystallization of water at the other. Now we assume that the temperatures T_1 and T_2 are constant across the walls bounding the gap. Then the rates of the phase transitions are controlled only by the mass transfer processes and by heat conduction in the ice platelet. Let us consider the stationary process that finally sets in. The mass flux Q in the liquid phase along the communicating channels is exactly equal to the counter-flux in the ice, $Q = \rho_s q_s$, where ρ_s is the density of ice, and q_s

is the velocity of the vertical displacement of the ice platelet (Fig. 11.16c). The force applied per unit area of the ice platelet must be balanced out by an equal and oppositely directed pressure difference Δp . Thus, ice moves upward at $p_2 > p_1$, and the liquid flows along communication channels from the upper to the lower interlayer, bringing about mass circulation.

Let us find the production of entropy S in this model (per unit time t and unit area of the ice platelet):

$$\frac{dS}{dt} = q_s \frac{\Delta p}{T} + W \frac{\Delta T}{T^2} \quad (11.83)$$

The first term on the right-hand side contains the specific work of the force applied to the ice platelet and displacing it at a constant velocity q_s . The second term characterizes the entropy production due to the heat absorbed per unit time by a unit surface area of ice at a temperature T , and to the heat liberated by a unit area of the other surface of ice at a temperature lower by ΔT than T . The following kinetic equations can be written on the basis of expression (11.83) for entropy production in the irreversible heat and mass transfer process:

$$q_s = \alpha_{11} \Delta p + \alpha_{12} \frac{\Delta T}{T} \quad (11.84)$$

$$W = \alpha_{21} \Delta p + \alpha_{22} \frac{\Delta T}{T} \quad (11.85)$$

The first of these equations describes the rate of mass transfer in the ice, $q_s = Q/\rho_s$, and the second describes the rate of heat transfer W in the model system. The coefficient α_{11} characterizes the resistance to ice displacement, determined by the hydrodynamic resistance of communication channels and interlayers. If $h \ll z$, the coefficient α_{22} can be assumed equal to the thermal conductivity of ice.

The cross-coefficients α_{12} and α_{21} , equal by the Onsager relations, determine two interrelated effects: mass flux $q = q_0$ (at $\Delta p = 0$) driven by a temperature gradient, and isothermal heat flux $W = W_0$ (at $\Delta T = 0$) driven by a pressure gradient. The heat flux W_0 is called the heat transfer. It has been suggested to call the mass flux q_0 , first introduced in [89], the "thermocrystallization mass flux." The magnitudes of the coefficients α_{12} and α_{21} are determined by the physical properties and the geometry of the model system. In order to calculate $\alpha_{12} = \alpha_{21}$, let us write the expression for heat transfer W_0 . Obviously, it equals the product of the isothermal mass flux rate and the heat of the water-ice phase transition L :

$$W_0 = \alpha_{11} \Delta p \rho_s L \quad (11.86)$$

The flow of the liquid from one interlayer into another is accompanied by isothermal heat transfer because the specific enthalpy of thin water interlayers differs by ΔH from the bulk value. Consequently, in the general case L must be supplemented by ΔH , i.e., we have to take into account the effect of thermo-osmotic flow discussed in the preceding section. However, the heat of the water-ice phase transition being a more powerful source-sink, the effect of thermo-osmosis is negligible because $L \gg \Delta H$ ($L \approx 3 \cdot 10^9$ erg/g, $\Delta H \approx 3 \cdot 10^5$ erg/g).

As follows from Eq. (11.85),

$$W_0 = \alpha_{21} \Delta p \quad (11.87)$$

By comparing (11.86) and (11.87), we find

$$\alpha_{12} = \alpha_{21} = \alpha_{11} \rho_S L \quad (11.88)$$

By introducing this expression for α_{12} into Eq. (11.84), we rewrite q_s in the following form:

$$q_s = \alpha_{11} (\Delta p + \rho_S L \frac{\Delta T}{T}) \quad (11.89)$$

The last equation shows, among other things, that the rate of the thermocrystallization flux

$$q_0 = \alpha_{11} \rho_S L \frac{\Delta T}{T} \quad (11.90)$$

is determined by the phase transition heat L , justifying the name suggested for this flux [89].

As we see from the solutions obtained, the disjoining pressure of thin interlayers does not enter explicitly the equations of mass transfer (11.84) and (11.90). Disjoining pressure affects the flow in nonfreezing interlayers through the coefficient α_{11} in Eq. (11.90). This coefficient is a function of interlayer thickness h which, in turn, is determined by the disjoining pressure isotherm $\Pi(h)$. As a result, flux rates q_s and q_0 depend on the shape of the isotherm $\Pi(h)$.

One more aspect needs clarification. For this purpose we compare two systems - one in which a thin water interlayer contacts two solid (non-ice) phases, and the other where one of the solid phases is ice. If $p - p_0 \neq \Pi(h)$, the liquid in the first system flows out of the interlayer (at $p - p_0 > \Pi$) or into it (at $p - p_0 < \Pi$). The rate of the isothermal flow of thin liquid layers is found here from the familiar equation (Chapter 2)

$$Q = \alpha \rho (\Delta p - \Delta \Pi) \quad (11.91)$$

where the difference $\Delta p - \Delta \Pi$ is the hydrostatic pressure difference across the considered element of the thin layer, α is the hydrodynamic resistance coefficient of the interlayer within this element, and ρ is the density of the liquid.

If the liquid flows from a thin interlayer sandwiched between two solid non-ice walls into the bulk phase, then $\Delta p = p - p_0$, where p_0 is the pressure in the bulk phase, and $\Delta \Pi = \Pi$. Thus, the rate of mass transfer Q for two circular plates of radius R_0 (which is equal to the amount of liquid flowing through the area $2\pi R_0 h$ per unit time) is given by the Reynolds equation:

$$Q = \frac{\rho h^2}{3\eta R_0} (p - p_0 - \Pi) \quad (11.92)$$

The expression for the coefficient α is found by comparing (11.91) and (11.92):

$$\alpha = \frac{h^2}{3\eta R_0} \quad (11.93)$$

Evidently, α is a function of thickness h and extension R_0 of the liquid interlayer, and of viscosity η . For an equilibrium to be set up in a system of solid (non-ice) plates, the liquid must flow out of the interlayer (or into it) until such a thickness h is reached that the applied external pressure $p - p_0$ becomes exactly equal to the disjoining pressure $\Pi(h)$.

When one of the plates consists of ice, and the interlayer liquid is the nonfreezing water, the equilibrium interlayer thickness can also be reached in another way: through a partial melting of the ice or through crystallization of excessive water. This gives an additional degree of freedom in the system. If the hydrodynamic resistance of the interlayers is considerable, equilibrium may be reached much faster via phase transitions than via viscous flow. If the communication channels connecting the interlayers h_2 and h_1 are blocked, the equilibrium thickness $h_i(p_0, T_i)$ will be rapidly reached in each of the interlayers as a result of melting of ice or crystallization of water. This thickness will be practically uniform if the hydrodynamic resistance of the interlayers is negligibly small compared with that of the communication channels. In this case there will develop a stationary mass exchange between interlayers, owing to the imposed gradient ∇T and the pressure difference prescribed by Eqs. (11.80) and (11.82). By Eq. (11.82), this pressure difference can be replaced in Eqs. (11.84), (11.85), and (11.89) with the equivalent difference between disjoining pressures. (We assume that the pressure p_0 in the bulk phase is identical in the two interlayers.) If the mass exchange is controlled by the hydrodynamic resistance of the interlayers h_2 and

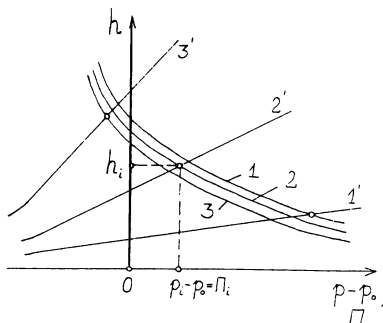


Fig. 11.17. Anticipated shape of the isotherms $h(\Pi)$ (curves 1-3) and $h(p - p_0)$ (curves 1'-3') of nonfreezing water interlayers. The numbers at the curves refer to temperatures $T_1 < T_2 < T_3 < T_0$.

h_1 , their thickness cannot be constant along the gap surface, and thus departs from the equilibrium value at any given T and p_0 . The profile of the interlayers along the gap surface is determined by the shape of the isotherms (11.80) and (11.82).

Since nonfreezing interlayers have a structure different from that of the bulk liquid (and this is, in fact, the reason for non-freezing in contact with ice), $\Pi(h)$ is mostly determined by the structural component Π_s of disjoining pressure (Chapter 7). However, an additional effect of the electrostatic component Π_e due to the surface charge on ice [91] and on the solid substrate cannot be excluded. The isotherms $\Pi(h)$ and $h(p)$ are schematically plotted in Fig. 11.17 for several values of $T < T_0$. In plotting these curves we took into account that the differences between $\Pi(h)$ isotherms are small in a relatively narrow temperature range around T_0 , i.e., in the range where the flow of nonfreezing moisture is appreciable. These isotherms slightly shift downward in Fig. 11.17 because at higher temperatures the same interlayer thickness corresponds to slightly lower disjoining pressure owing to a degradation of the special structure of boundary layers (see Chapter 7). The shape of the $\Pi(h)$ curves shown in Fig. 11.17 follows from the known shape of the $\Pi_s(h)$ isotherms for α -films of water (see Chapter 10).

The $h(p)$ isotherms must be much more sensitive to temperature. In order to find their dependence on temperature, we use an identity

$$\left(\frac{\partial h}{\partial p}\right)_T \left(\frac{\partial p}{\partial T}\right)_h \left(\frac{\partial T}{\partial h}\right)_p = -1 \quad (11.94)$$

from which we obtain

$$\left(\frac{\partial h}{\partial p}\right)_T = - \left(\frac{\partial h}{\partial T}\right)_p \left(\frac{\partial T}{\partial p}\right)_h \quad (11.95)$$

At $p_0 = \text{const}$ the derivative $(\partial T / \partial p)_h$ can be assumed equal to $(\partial T / \partial p)_h = -T_0 / \rho_S L$, which gives the temperature of the phase equilibrium as a function of pressure $p - p_0$ on a closed crystal face [90]. It has already been mentioned [see Eq. (11.81)] that the dependence of the phase equilibrium temperature on pressure $T(p)$ is different for an open crystal face ($h = \infty$) and for a closed face contacting a solid substrate through an equilibrium liquid interlayer of a small finite thickness h .

Ice in pores is in contact with thin nonfreezing interlayers subjected to an excess external pressure $p - p_0$, so that the relevant equation here is Eq. (11.81) for a closed crystal face. Then we obtain, instead of (11.95),

$$\left(\frac{\partial h}{\partial p}\right)_T = \frac{T_0}{\rho_S L} \left(\frac{\partial h}{\partial T}\right)_p \quad (11.96)$$

The dependence $h(T)$ is rather insensitive to changes in pressure p , so that we are justified in assuming $(\partial h / \partial T)_p = \text{const}$. Recalling that $(\partial h / \partial T)_p > 0$ [77-80], we obtain practically linear plots $h(p)$, increasing with increasing p . However, as $T \rightarrow T_0$, the values of $(\partial h / \partial T)_p$ increase steeply (see Fig. 7.6 in Chapter 7), and the slope of the $h(p)$ isotherms must correspondingly grow with increasing temperature.

The equilibrium thickness of a nonfreezing interlayer is determined by the intersection point of the isotherms $h(p - p_0)$ and $h(\Pi)$ for $p - p_0 = \Pi$ (Fig. 11.17). Each given temperature $T = T_i$ and pressure p_0 establishes a single possible thickness h_i of the equilibrium interlayer and the corresponding hydrostatic pressure $p_i = \Pi_i + p_0$. Deviations from T_i or p_0 disturb the equilibrium, and the ice platelet either grows or melts. For instance, this means that stationary states of the system shown in Fig. 11.16c, realized with high hydrodynamic resistance of communication channels, are possible, but not at arbitrary values of ΔT and Δp . At fixed ΔT and p_0 only quite definite values of h_2 , p_2 and h_1 , p_1 set in, i.e., a quite definite pressure difference Δp is formed. If Δp deviates from the value fixed by the conditions of local equilibrium in each of the interlayers, the thickness of the ice platelet must change and, hence, the stationary state of the system is perturbed.

A comparison of consecutive positions of intersection points in Fig. 11.17 shows that as the temperature increases, the thickness of nonfreezing interlayers grows and the disjoining pressure developed in them diminishes. The absolute value of interlayer thickness depends on the shape of the $\Pi(h)$ isotherms. The higher the isotherm $\Pi(h)$ in Fig. 11-17, the larger the equilibrium interlayer thick-

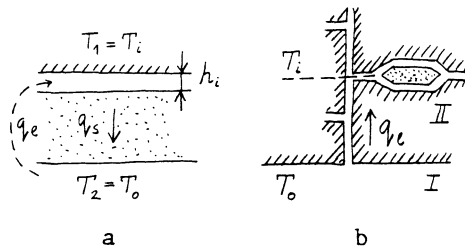


Fig. 11.18. The plane-parallel pore model (a) and its real analog (b) in the problem of mass exchange between unfrozen I and frozen II zones of a porous body.

ness reached at a given temperature. The coefficient α_{11} being a function of h (for low hydrodynamic resistance of communication channels), the kinetics of mass exchange in frozen materials also substantially depend on the shape of the $\Pi(h)$ isotherms. In frozen porous bodies it can be possible to realize a negative disjoining pressure, especially at $T \rightarrow T_o$. This follows from the already known fact (see Chapter 10) that the $\Pi_s(h)$ isotherms of water α -films intersect the thickness axis (Fig. 11.17). Therefore, nonfreezing interlayers can produce not only a repulsive (at $\Pi > 0$) but also an adhesive, attractive effect (at $\Pi < 0$) on the particles of the solid phase of porous bodies.

We have discussed the mass exchange phenomena taking place in nonfreezing interlayers within a single planar pore filled with ice. This model can be readily generalized to another important case corresponding to mass transfer between the unfrozen and frozen zones of a porous body (such as soil). In order to describe this situation, it is sufficient to assume the following conditions for one of the interlayers (Fig. 11.18a):

$$\Pi_2 = p_2 - p_0 = 0, \quad T_2 = T_o, \quad h_2 \rightarrow \infty \quad (11.97)$$

This model corresponds to a real situation shown in Fig. 11.18b. Here temperature T_o separates the unfrozen zone I from the overlaying zone II where ice lenses coexist with nonfreezing interlayers at $T < T_o$. The temperature of interlayers above and below a lens can be assumed identical because the lens thickness is small compared with the distance from the lens to the unfrozen zone. Consequently, mass exchange between the unfrozen and frozen zones can be calculated by using Eq. (11.89) rewritten for this special case (Fig. 11.18a):

$$q_s = \alpha_{11} \left[-(p_i - p_0) + \rho_s L \frac{(T_o - T_i)}{T_o} \right] \quad (11.98)$$

where T_i and p_i are the temperature and hydrostatic pressure in the i -th layer of the soil. Since the coefficient α_{11} is determined in this case by the hydrodynamic resistance of communication channels, the quantities p_i and h_i correspond to their equilibrium values at the intersection point of the isotherms $h(p - p_0)$ and $h(\Pi)$ at $T = T_i$. As seen from Fig. 11.17, increasing the temperature results in decreasing h_i and in increasing the pressure $p_i - p_0 = \Pi_i > 0$ acting on the walls bounding the lens in the pore.

If the positive disjoining pressure Π_i developed in the i -th interlayer exceeds the strength of the porous material, this material undergoes deformations, and the pore fills up with ice at the expense of moisture arriving through nonfreezing communication channels. As the density and counterpressure of the compacted soil increase, the rate of growth of the ice lens diminishes and drops to zero when the condition $p_i - p_0 = \Pi_i$ is reached. Consequently, ice lenses must be formed with maximum probability in weakened regions of the porous body. This conclusion is in good agreement with the results and conclusions reported in [83, 84]. Compaction of the soil, eliminating loose regions in the structure, diminishes the probability of ice lens formation and suppresses the effects of frost heaving. If the temperature is lowered to -15 to -20° , liquid interlayers become so thin that ice cements the particles of the porous body together, and the strength of the body is enhanced [92]. Consequently, frost heaving reaches its maximum at temperatures slightly below T_0 . At this temperature the pressure developed Π_i is sufficiently large, while interlayer thickness h_i is not yet so small as to obstruct the inflow of liquid moisture to the growing ice lenses. This explains the results of a number of experiments in which frost heaving of soil was observed to reach a maximum at temperatures above -4 to -5° [77, 83-85].

However, there is one essential difference between the schematics in Figs. 11.18a and 11.18b. In the model in Fig. 11.18a the stationary state corresponds to a downward motion of the ice layer as a whole at a velocity $q_s = \text{const}$, accompanied by a reverse flow of liquid moisture toward the nonfreezing interlayer. In the porous body model (Fig. 11.18b) a stationary state is realized through a constant inflow of liquid through nonfreezing communication channels, feeding the growing ice phase in the pores. In this case, $q_s = \text{const}$ corresponds to a linear growth rate of the ice interlayer (lens) in the pore undergoing deformation. For the process to be stationary, it is necessary that the disjoining pressure Π_i developed in the interlayer deform the soil at a constant rate. This can occur, for instance, in a viscous flow of structures without their destruction, or in viscoplastic flow.

When a positive disjoining pressure, capable of causing frost heaving, develops in interlayers, the first two terms of Eq. (11.98) have opposite signs because $T_0 - T_i > 0$ and $p - p_0 = \Pi_i >$

0. This means that, in addition to a thermocrystallization mass inflow ($q_s > 0$) there is a counterflow driven by the developing disjoining pressure $\Pi_i > 0$ of the interlayers. Obviously, the maximum disjoining pressure $\Pi_i > 0$ building up in the interlayers is reached at $q_s = 0$ when the counterfluxes cancel each other out, and ice lenses cease to grow. The maximum disjoining pressure developed in nonfreezing interlayers can be found from Eq. (11.98) if we set $q_s = 0$:

$$\Pi_{\max} = p_{\max} - p_0 = \rho_s L \frac{T_0 - T_i}{T_0} \quad (11.99)$$

This equation coincides with the expression for the maximum crystallization pressure, i.e., the pressure at a closed growing crystal face, derived from equations of equilibrium thermodynamics [90]. The conclusions reached above follow from a more rigorous analysis of nonequilibrium processes in terms of nonequilibrium thermodynamics.

By substituting (11.101) into (11.100) we find

$$q_s = \alpha_{11}(-p_i + p_{\max}) = \alpha_{11}(-\Pi_i + \Pi_{\max}) \quad (11.100)$$

When $p_i < p_{\max}$, the flux of liquid moisture is directed from the unfrozen zone I to the zone II, and feeds the growth of ice lenses. When $p_i > p_{\max}$, the flow direction is reversed. Ice lenses then melt away in the field of the applied external pressure. The difference $p_{\max} - p_i$ is the greater the lower T_i . However, lowering the temperature simultaneously increases the thickness of non-freezing interlayers, and this must diminish the value of α_{11} . Hence, the curve $q_s(T)$ must go through a maximum. This prediction is in good agreement with observations indicating that the growth of ice lenses is the most rapid in layers with temperature not below -5 to -3°C [77, 83-85].

Unfortunately, the number of experiments that enable us to test directly the theory of thermocrystallization mass transfer is very limited. The best in this respect are the results published by Vignes and Dijkema [93], who devised a novel technique. They were able to carry out, in well-controlled conditions, measurements of the growth rate of ice, fed by water sucked through a narrow slit capillary (acting as a nonfreezing communication channel) from the bulk liquid phase, which was kept at a temperature $T_w > T_0$. The experimental conditions obviously satisfy both the model schematically shown in Fig. 11.18b and Eq. (11.98). Water and the non-freezing interlayer of thickness h_1 separating it from the chamber walls are kept at a temperature $T_1 = T_i < T_0$. The thickness of the water layer at the ice meniscus surface in the capillary is infinite: $h_2 = \infty$. The temperature T_2 over the meniscus is that of the water-ice phase equilibrium, i.e., $T_2 = T_0$. It was for this reason that

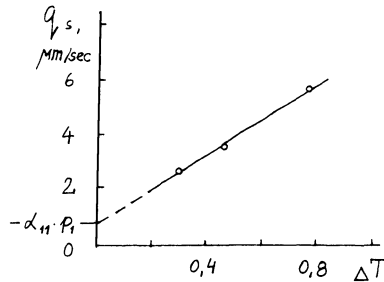


Fig. 11.19. Growth rate q_s of the ice phase as a function of $\Delta T = T_0 - T_1$, plotted from the data of [93].

Vignes and Dijkema [93] found the growth rate of ice phase, $q_s = Q/\rho_s$, to be independent of T_w . In agreement with Eq. (11.98), the flux q_s is a function of the difference between the temperature of ice in contact with the nonfreezing interlayer T_1 , and the temperature T_0 of ice meniscus in equilibrium with the bulk water. With T_0 being constant, q_s could depend only on T_1 . This conclusion is borne out by experimental data [100].

The temperature difference $T_w - T_0$ could produce an additional thermo-osmotic flux of water through the slit capillary. The negligible effect of the bulk water temperature T_w on q_s , reported in [100], only confirms that ΔH was negligibly small in comparison with the water-ice phase transition heat L . If we assume that the ice-water surface at the entrance into the capillary has negligible curvature, we can set $T_0 = 273$ K. It is then possible to plot the data of Vignes and Dijkema [93] in the form $q_s = f(\Delta T)$, where $\Delta T = T_0 - T_1$. Figure 11.19 shows that the graph is linear, in agreement with Eq. (11.98). The intercept of this line on the axis q_s at $\Delta T = 0$ is the segment $q_p = -\alpha_{11}(p_1 - p_0) = -\alpha_{11}\Pi_1 = 0.7 \cdot 10^{-4}$ cm/s. Hence, $p_1 < p_0$, i.e., the pressure in the interlayer is lower than in the bulk water. The negative disjoining pressure $\Pi_1 < 0$ in the interlayer can be explained in terms of the effect, already mentioned, of the isotherm $\Pi(h)$ intersecting the thickness axis (Fig. 11.17), because in the experiments that we analyze here T_1 never considerably deviated from T_0 .

The value of the disjoining pressure Π_1 can be found from the slope of the linear dependence $q_s(\Delta T)$: $A = dq_s/d(\Delta T)$; by Eq. (11.98), $A = \alpha_{11}\rho_s L/T_0$. Assuming $L = 3.34 \cdot 10^9$ ergs/g, $T_0 = 273$ K, and $\rho_s = 0.917$ g/cm³ in the equation

$$q_p/A = -\Pi_1 T_0 / \rho_s L \quad (11.101)$$

we obtain $\Pi_1 = -1.2 \cdot 10^6$ dyn/cm². For α -films on quartz this value of the disjoining pressure corresponds to α -film thickness h_0 about

50 Å at 20°C and about 100 Å at 10°C (see Chapter 7, Fig. 7.1). Let us estimate the thickness h_1 of a nonfreezing interlayer, using the obtained values of q_p and Π_1 to find the coefficient $\alpha_{11} = -q_p/\Pi_1 = 6 \cdot 10^{-11} \text{ cm}^2 \cdot \text{s/g}$, and then Eq. (11.93). Taking $\eta \approx 0.02 \text{ P}$ and $R_0 = 0.5 \text{ cm}$ (the radius at the base of the ice cone), we find that at -0.5° the interlayer thickness is about 130 Å, quite close to h_0 . This shows that the forces decisive in determining the thickness of nonfreezing interlayers originate at the quartz substrate. It is then clear how large the effect of hydrophilicity of the surface of the particles in porous bodies can be. Incidentally, a drop in the hydrophilicity of the substrate reduces the thickness of α -films [94] (for details see Chapter 10), and also reduces the thickness of nonfreezing interlayers [80].

Recently Biermans, Dijkema, and De Vries [95] obtained an experimental confirmation of Eq. (11.98). The method they used was, in principle, the same as in the preceding paper [93]. They showed that water inflow toward ice ceased (i.e., $q_s = 0$) at a pressure on the ice $P = \Delta T/K \text{ atm}$, where $K = 0.083 \text{ deg/atm}$ and ΔT is the water-ice temperature difference. The difference ΔT was varied from 0.02 to 0.05° . The ice was separated from water by a microporous filter that acted as a nonfreezing communication channel. Equation (11.98) predicts that the thermocrystallization flux must vanish at a pressure on ice $P = p_{\max} - p_0$ given by Eq. (11.99). By substituting into this equation $p_s = 0.91 \text{ g/cm}^2$, $L = 3.34 \cdot 10^9 \text{ erg/g}$, and $T_0 = 273 \text{ K}$, we obtain the theoretical estimate $K = 0.09 \text{ deg/atm}$, quite close to the experimental value given above. Also in agreement with Eq. (11.98), the rate of moisture inflow to the ice was the greater, the higher the temperature difference ΔT . It reached its maximum at zero pressure on ice, i.e., at $P = 0$. Unfortunately, further quantitative comparison of the experimental results with the theory is not possible because the coefficient α_{11} is unknown. (It depends on the conduction of nonfreezing communication channels: narrow pores of the filter and narrow nonfreezing interlayers between ice and filter surface.)

Consequently, frost cracking of porous bodies (and, in particular, frost heaving of soil) is caused by the disjoining pressure developed by thin nonfreezing water interlayers and by their thermocrystallization flow. The rate of growth of the ice phase is determined by the water-ice phase transition heat, by the temperature gradient, and by water conductance of nonfreezing communication channels. As follows from Eq. (11.99) for the water-ice system, after the values of p_s , L , and T_0 are entered into it, a reduction in temperature by 1° corresponds to the increment in the maximum crystallization pressure by about 10 atm, close to Hoekstra's data for high-dispersion soils [96]. Increased hydrodynamic resistance of nonfreezing communication channels, resulting in reduced values of α_{11} , reduces the ice growth rate. Indeed, lowering the water conductivity of soil by introducing surfactants [97], by hydro-

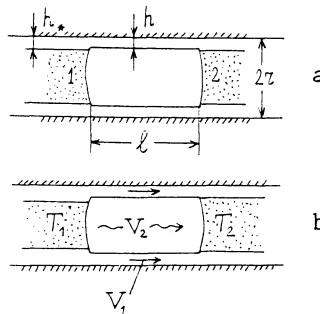


Fig. 11.20. Model for the calculation of the thermocrystallization flow of nonfreezing films at the segment between ice menisci in a capillary: a) at equilibrium, $T_1 = T_2$; b) mass exchange at $T_1 > T_2$.

phobization [98], and by reducing the particle size, thereby contracting the interfacial surface and the content of nonfreezing moisture, resulted in decreasing the effect of frost heaving [96, 99], in agreement with Eq. (11.98). Likewise, frost heaving is reduced, in agreement with the theory developed above, when the strength of the porous body is enhanced or when a consolidating load is applied [83-85, 100].

The theory outlined above thus describes the phenomenon of frost heaving far better than that proposed by Everett and Haynes [101, 102], who related the effect to the pressure difference at the curved ice-water interface. Loch and Miller demonstrated [103] that actual pressures exceed those calculated by this theory, which in general fails for planar ice layers, being unable to explain the build-up of pressure leading to frost cracking.

The theory developed above of thermocrystallization transport is valid not only for completely water-saturated porous bodies but also gives an adequate description of the flow of nonfreezing films in pores free of ice [104, 105]. As an example, consider two ice menisci in a cylindrical capillary, modeling a pore, separated by a gas-filled gap of length ℓ (Fig. 11.20). The surface of the capillary within this segment is covered with a nonfreezing adsorption film of thickness h . Ice and the internal surface of the capillary are separated by nonfreezing interlayers of thickness $h_* \neq h$. In isothermal conditions (Fig. 11.20a) the films, interlayers, and ice are in equilibrium. If a constant temperature gradient $VT = (T_1 - T_2)/\ell > 0$ is imposed on the model system (Fig. 11.20b), the thermocrystallization flow in the film and the vapor diffusion toward the colder end set in. In order to calculate the film flux,

we use the same systems of equations (11.84), (11.85) of nonequilibrium thermodynamics.

An isothermal film flow driven by a pressure difference Δp in the direction from 1 to 2 (Fig. 11.20a) would be accompanied by ice melting at the meniscus 1 and by the crystallization of the excess water brought in by the film flow to the meniscus 2. Consequently, the transferred heat W_0 is obviously equal to the product of the isothermal flux rate $q_p = \alpha_{11}\Delta p$ and the water-ice phase transition heat $\rho_S L$. Therefore, as in the case of nonfreezing interlayers, discussed above,

$$W_0 = \alpha_{11}\rho_S L \Delta p \quad \text{and} \quad \alpha_{12} = \alpha_{21} = \alpha_{11}\rho_S L$$

This leads to the equation of thermocrystallization flow in a non-freezing film, analogous to (11.90):

$$q_T = \alpha_{11}\rho_S L (\nabla T / T) \quad (11.102)$$

For wetting films the coefficient α_{11} is

$$\alpha_{11} = h^2 / 3\eta \quad (11.103)$$

By substituting (11.103) into (11.102), we obtain the flux across a unit cross-sectional area of the film [104, 105]:

$$Q_T = q_T \rho = \frac{\rho h^2 \rho_S L}{3\eta} \frac{\nabla T}{T} \quad (\text{g/cm}^2 \cdot \text{s}) \quad (11.104)$$

where ρ is the density of liquid water.

The thermocrystallization flow of the film results in the following displacement rate V_f of ice menisci:

$$V_f = \frac{2\pi r h Q_T}{\pi r^2 \rho_S} = \frac{2\rho h^3 L}{3\eta r} \frac{\nabla T}{T} \quad (\text{cm/s}) \quad (11.105)$$

where r is the capillary radius.

The displacement rate of the menisci as a result of vapor transport between these menisci can be written as follows:

$$V = \frac{DM}{\rho_S RT} \frac{\Delta p_S}{\ell}$$

where D is the vapor diffusion coefficient, Δp_S is the difference between saturated vapor pressures over ice menisci 1 and 2, M is the molar mass of water, and R is the gas constant. By making use of the Clapeyron-Clausius equation $\Delta p_S = \rho_V L_v (\Delta T / T)$, we obtain

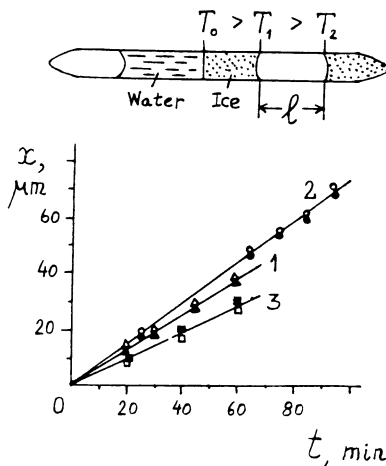


Fig. 11.21. a) Schematic diagram of the filling of the capillary with water.
 b) Displacement of ice menisci in quartz capillaries in a constant temperature gradient $\nabla T = 3.8 \text{ deg/cm}$: 1) capillary radius $r = 10.7 \mu\text{m}$, $l = 0.486 \text{ cm}$, mean film temperature $T = -1^\circ\text{C}$; 2) $r = 9.8 \mu\text{m}$, $l = 0.1 \text{ cm}$, $T = -0.28^\circ\text{C}$; 3) $r = 10.3 \mu\text{m}$, $l = 0.081 \text{ cm}$, $T = -0.27^\circ\text{C}$.

$$V_v = \frac{DM\rho_v Lv}{\rho_s RT} \frac{\nabla T}{T} \quad (11.106)$$

where ρ_v is the vapor density, and L_v is the sublimation heat (in ergs/g).

The ratio of the thermocrystallization flux to the vapor flux is

$$\frac{V_f}{V_v} = \frac{2ph^3\rho_s LRT}{3\eta r DM\rho_v Lv} \quad (11.107)$$

These equations were tested in experiments [104, 105] with quartz capillaries in which ice menisci were separated with an air bubble, corresponding to the model schematically represented in Fig. 11.20. The experiments were carried out on a setup similar to that used earlier to study the thermocapillary flow in wetting films [106]. Figure 11.21a shows how the capillary was filled with doubly distilled water. Water in the capillary was frozen by abruptly lowering the temperature to -35 to -40°C . Then a constant

temperature gradient $\nabla T = 3.8 \pm 0.1 \text{ deg/cm}$ was created and maintained by gradually raising the end temperatures of the plate and the capillary with thermojunctions. The temperature difference that was finally achieved was such that the point at the ice melting temperature $T_0 = 273 \text{ K}$ was close to, and to the left of, the ice meniscus at a temperature T_1 (Fig. 11.21a). The length l of the air bubble between the ice menisci was small (0.1-0.4 cm) so that the temperature of both menisci differed only slightly from T_0 . This was necessary to make the film flow effect most pronounced. Indeed, the thickness of nonfreezing interlayers is known to be the greater the closer the temperature is to T_0 [80].

The experiments consisted in measuring, with a horizontal comparator, the recession rate of the left-hand ice meniscus and the advance rate of the right-hand ice meniscus, as a result of vapor transfer and film flow in the capillary. Figure 11.21b plots the coordinates x of the two ice menisci as a function of time t . Unfilled circles, triangles, and squares represent the receding, and filled ones the advancing, ice menisci. These two sets of experimental points are close to each other, indicating negligible mass loss and the stationary character of mass transfer. The rate of stationary mass transfer $V = dx/dt$ was found from the graphs $x(t)$. The velocity V_v of displacement of ice meniscus due to vapor diffusion was calculated by using Eq. (11.106). In determining the value of D we took into account that the air pressure in the gap between the menisci was below the atmospheric pressure, owing to the method of sealing the left-hand end of the capillary (Fig. 11.21a) [104, 105].

Let us assume, as a first approximation, that the flows of vapor and film liquid are independent, so that V_f can be found as the difference between the measured velocity V and the velocity of ice meniscus displacement V_v due to evaporation: $V_f = V - V_v$. Then, for $\nabla T = 3.8 \text{ deg/cm}$, $T \approx 272 \text{ K}$, $\rho_s L = 3.6 \cdot 10^2 \text{ J/cm}^3$, $\rho = 1 \text{ g/cm}^3$, and for known r , it is possible to find the surface film thickness h from Eq. (11.105). For the viscosity of water in the film we use the known viscosity value for nonfreezing interlayers at the same mean temperature [107]. The thickness of polymolecular adsorption films on quartz surface between ice menisci was found in a number of experimental runs to lie from 100-120 Å, which is close to the thickness of water α -films (see Chapter 10) on quartz. However, it is necessary to take into account the possible effects of the thermo-osmotic and thermocapillary flows in the film on the rate of mass transfer between the ice menisci. Clearly, the effect of thermo-osmosis is negligible in the presence of a stronger thermocrystallization flow because the heat effect of the boundary layer-bulk water transition (see Section 11.4) is much less than the melting heat.

Let us compare the thermocapillary flux in the film with the thermocrystallization flux, by using Eq. (11.105). The ratio V_t/V_f is then

$$\frac{V_t}{V_f} = \frac{3T}{2hpL} \left(-\frac{\partial\sigma}{\partial T} \right) \quad (11.108)$$

Setting again $L = 3.6 \cdot 10^2$ J/g, $T \approx 272$ K, and $\partial\sigma/\partial T = -1.5 \cdot 10^2$ N/m·deg, we find that for film thickness $h \approx 10^{-6}$ cm the contribution of the thermocapillary flow does not exceed 2%. When the film thickness reduces to $h = 10^{-7}$ cm, the contribution of the thermocapillary flow grows to 20%. However, hydrodynamic calculations become hardly valid for films of such thickness.

The main mechanisms of mass transfer in frozen porous materials containing ice, nonfreezing interlayers, water films, and a gas phase are, therefore, the vapor diffusion and the thermocrystallization flow of nonfreezing moisture. The relative contributions of vapor diffusion and thermocrystallization flow in the film to the net flux depend on capillary radius. Indeed, this follows from the expression for the ratio V_f/V_v given by Eq. (11.107). Using the standard physical parameters of water and assuming for the viscosity of film moisture $\eta = 0.1$ P [107], we obtain for a temperature close to the melting point T_0 and $h \approx 10^{-6}$ cm that

$$\frac{V_f}{V_v} = \frac{8.65 \cdot 10^{-4}}{r} \quad (11.109)$$

where r is measured in cm.

This equation shows that the thermocrystallization film flow is the dominant mechanism of transport in thin pores, with $r \leq 1$ μm . Conversely, the main mechanism of mass exchange between isolated ice menisci in large pores with $r \geq 100$ μm is vapor diffusion. In the experimentally investigated case (Fig. 11.21), the ratio V_f/V_v was nearly 1 for $r \approx 10$ μm .

Rigorous quantitative solutions of the problems discussed above can be found if the dependences of $\Pi(h, T)$, $h(T, p)$, and $\eta(h, T)$ are determined (h and η denoting the thickness and viscosity of the nonfreezing interlayers between ice and a solid surface, or of nonfreezing films). At the present time only the dependences $h_x(T)$ [80] and $\eta(T)$ [107, 108] are known, for certain solid substrates.

REFERENCES

1. S. S. Dukhin and B. V. Derjaguin, "Electrokinetic phenomena," in: *Surface and Colloid Sciences*, Vol. 7, E. Matijevic (ed.), Wiley, New York (1974), p. 335.
2. S. S. Dukhin, *Electric Conduction and Electrokinetic Properties of Disperse Systems*, Naukova Dumka, Kiev (1975).
3. S. S. Dukhin and B. V. Derjaguin, *Electrophoresis*, Nauka, Moscow (1976).
- 3a. See also R. J. Hunter, *Zeta Potential in Colloid Science*, Academic Press, London (1981).
4. B. V. Derjaguin, G. P. Sidorenkov, E. A. Zubashchenko, and E. V. Kiseleva, *Kolloidn. Zh.*, 9, 335 (1947).
5. M. M. Milekhina, *Kolloidn. Zh.*, 23, 173 (1961).
6. B. V. Derjaguin and S. S. Dukhin, *Dokl. Akad. Nauk SSSR*, 159, 401, 636 (1964); in: *Research in Surface Forces*, Vol. 3, Consultants Bureau, New York (1971), p. 286.
7. S. R. de Groot and P. Mazur, *Non-Equilibrium Thermodynamics*, North-Holland, Amsterdam (1962).
8. B. V. Derjaguin, I. E. Dzyaloshinski, M. M. Koptelova, and L. P. Pitaevski, *Discuss. Faraday Soc.*, 40, 246 (1965).
9. B. V. Derjaguin and M. M. Koptelova, *Kolloidn. Zh.*, 31, 692 (1969); in: *Surface Forces in Thin Films and Disperse Systems*, Nauka, Moscow (1972), p. 169; in: *Research in Surface Forces*, Vol. 4, Consultants Bureau, New York (1975), p. 153.
10. B. V. Derjaguin, S. S. Dukhin, and M. M. Koptelova, *Kolloidn. Zh.*, 31, 359 (1969).
11. V. M. Muller, *Kolloidn. Zh.*, 40, 259 (1978).
12. B. V. Derjaguin, M. M. Koptelova, V. M. Muller, and K. P. Tikhomolova, *Kolloidn. Zh.*, 39, 1060 (1977).
13. N. V. Churaev, *Kolloidn. Zh.*, 42, 295 (1980).
14. B. V. Derjaguin and N. V. Churaev, *Kolloidn. Zh.*, 37, 1075 (1975).
15. B. V. Derjaguin and N. V. Churaev, *J. Colloid Interface Sci.*, 62, 369 (1977).
16. B. V. Derjaguin and N. V. Churaev, *J. Colloid Interface Sci.*, 87, 543 (1982).
17. V. M. Starov and N. V. Churaev, *Teor. Osn. Khim. Tekhnol.*, 14, 509 (1980).
18. R. Cleland, *Trans. Faraday Soc.*, 62, 336 (1966).
19. D. M. Tolstoi, *Dokl. Akad. Nauk SSSR*, 85, 1089, 1329 (1952).
20. A. B. Basset, *A Treatise on Hydrodynamics*, Vol. 2, Dover, New York (1961).
21. J. Happel and H. Brenner, *Low Reynolds Number Hydrodynamics*, Noordhoff, Gröningen (1973).
22. A. N. Somov, *Kolloidn. Zh.*, 44, 160 (1982).
23. N. V. Churaev, V. D. Sobolev, and A. N. Somov, *J. Colloid Interface Sci.*, 97, 574 (1984).
24. N. Lakshminarayanaiah, *Transport Phenomena in Membranes*, Academic Press, New York (1969).

25. S. Sourirajan, *Reverse Osmosis*, Logos, London (1970).
26. H. Klonsdale and H. E. Podall (eds.), *Reverse Osmosis Membrane Research*, New York (1972); [cf. H. E. Podall, *Recent Dev. Separ., Sci.*, 2, 171 (1972) - Editor.]
27. Yu. I. Dytnerovsky, *Reverse Osmosis and Ultrafiltration*, Khimiya, Moscow (1978).
28. G. A. Martynov, V. M. Starov, and N. V. Churaev, *Kolloidn. Zh.*, 42, 489, 657 (1980).
29. B. V. Derjaguin, N. V. Churaev, and G. A. Martynov, *J. Colloid Interface Sci.*, 75, 419 (1980).
30. B. V. Derjaguin, N. V. Churaev, G. A. Martynov, and V. M. Starov, *Khim. Tekhnol. Vody*, 3, 99 (1981).
31. O. Kedem and A. Katchalsky, *Biochim. Biophys. Acta*, 27, 229 (1958); *J. Gen. Physiol.*, 45, 143 (1961).
32. K. S. Spiegler and O. Kedem, *Desalination*, 1, 311 (1966).
33. E. H. Bresler, E. A. Mason, and R. P. Wendt, *Biophys. Chem.*, 4, 229 (1976).
34. V. M. Starov and N. V. Churaev, *Kolloidn. Zh.*, 43, 698 (1981).
35. N. V. Churaev and V. M. Starov, *J. Colloid Interface Sci.*, 89, 77 (1982).
36. M. E. Heyde, C. R. Peters, and J. E. Anderson, *J. Colloid Interface Sci.*, 50, 467 (1975).
37. S. Sourirajan, *Pure Appl. Chem.*, 50, 593 (1978).
38. S. S. Dukhin and A. E. Yaroshchuk, *Kolloidn. Zh.*, 44, 884 (1982).
39. V. P. Dushchenko and I. A. Romanovsky, *Zh. Fiz. Khim.*, 44, 1479 (1970).
40. P. Hoexstra and W. T. Doyle, *J. Colloid Interface Sci.*, 36, 513 (1971).
41. B. V. Derjaguin, N. A. Krylov, V. F. Novik, and G. V. Goncharov, in: *Surface Forces in Thin Films and Stability of Colloids*, Nauka, Moscow (1974), p. 164.
42. A. E. Yaroshchuk, *Kolloidn. Zh.*, 45, 140 (1983).
43. B. V. Derjaguin, S. S. Dukhin, and A. A. Korotkova, *Kolloidn. Zh.*, 40, 643 (1978).
44. B. V. Derjaguin, S. S. Dukhin, Z. R. Ulberg, and T. V. Kuznetsova, *Kolloidn. Zh.*, 42, 464 (1980); *Izv. Akad. Nauk SSSR, Ser. Khim.*, No. 8, 1729 (1982).
45. M. V. Golovanov and B. V. Derjaguin, *Kolloidn. Zh.*, 41, 649 (1979); *Dokl. Akad. Nauk SSSR*, 272, 479 (1983).
46. B. V. Derjaguin and G. P. Sidorenkov, *Dokl. Akad. Nauk SSSR*, 32, 622 (1941).
47. B. V. Derjaguin, Yu. Shutor, S. V. Nerpin, and M. A. Arutyunyan, *Dokl. Akad. Nauk SSSR*, 161, 147 (1965).
48. J. Reekie, *Nature*, 156, 367 (1945).
49. B. V. Derjaguin and M. K. Mel'nikova, in: *Festschrift Volume on the 70th Birthday of Academician A. F. Ioffe*, Izd. Akad. Nauk SSSR, Moscow (1950), p. 482.
50. B. V. Derjaguin and M. K. Mel'nikova, *Highway Res. Board*, No. 40, *Natl. Acad. Sci., Wash.* (1958), p. 43.

51. A. P. Ershov and N. V. Churaev, *Teor. Osn. Khim. Tekhnol.*, 3, 583 (1969).
52. B. V. Derjaguin, A. P. Ershov, and N. V. Churaev, in: *Surface Forces in Thin Films and Disperse Systems*, Nauka, Moscow (1972), p. 160; in: *Research in Surface Forces*, Vol. 4, Consultants Bureau, New York (1975), p. 142.
53. R. Haase and C. Steiner, *Z. Phys. Chem.*, 21, 270 (1959); 44, 301 (1965).
54. C. Dirksen, *Soil Sci. Soc. Am. Proc.*, 33, 821 (1969).
55. R. S. Srivastava and I. P. Abrol, *Indian J. Chem.*, 7, 1121 (1969).
56. M. S. Dariel and O. Kedem, *Isr. Atom. Energy Commis.*, No. 1262, 105 (1971); *J. Phys. Chem.*, 79, 336 (1975).
57. P. A. Voznyi and N. V. Churaev, *Kolloidn. Zh.*, 39, 264, 438 (1977).
58. P. A. Voznyi, V. P. Dushchenko, and N. V. Churaev, in: *Surface Forces in Thin Films*, Nauka, Moscow (1979), p. 109.
59. V. P. Dushchenko, M. S. Panchenko, I. A. Romanovsky, and I. B. Slinyakova, *Inzh.-Fiz. Zh.*, 15, 653 (1968).
60. N. V. Churaev and B. V. Derjaguin, *Dokl. Akad. Nauk SSSR*, 169, 396 (1966); *Kolloidn. Zh.*, 28, 751 (1966).
61. C. L. Rice and R. Whitehead, *J. Phys. Chem.*, 69, 4017 (1965).
62. N. V. Churaev and B. V. Derjaguin, in: *Research in Surface Forces*, Vol. 3, Consultants Bureau, New York (1971), p. 220.
63. N. V. Churaev, B. V. Derjaguin, and P. P. Zolotarev, *Dokl. Akad. Nauk SSSR*, 183, 1139 (1968).
64. R. Haase, *Thermodynamik der irreversiblen Prozesse*, Dr. Dietrich Steinkopff Verlag, Darmstadt (1963).
65. B. V. Derjaguin, *Kolloidn. Zh.*, 6, 291 (1940); *Trans. Faraday Soc.*, 36, 203 (1940).
66. B. V. Derjaguin, *Izv. Akad. Nauk SSSR, Ser. Khim.*, 5, 1153 (1937); *Acta Physicochim. URSS*, 10, 333 (1939).
67. H. Frölich, *Theory of Dielectrics, Dielectric Constant and Dielectric Loss*, Clarendon Press, Oxford (1949).
68. F. Belucci, *J. Membr. Sci.*, 9, 285 (1981).
69. C. Carr and K. Sollner, *J. Electrochem. Soc.*, 109, 616 (1962).
70. Y. Kobatake and H. Frijuta, *J. Chem. Phys.*, 41, 2963 (1964).
71. S. K. Sanyal and M. Adhikari, *J. Indian Chem. Soc.*, 59, 460 (1982).
72. G. S. McNab and A. Meisen, *J. Colloid Interface Sci.*, 44, 339 (1973).
73. V. V. Karasev, B. V. Derjaguin, and E. N. Efremova, in: *Research in Surface Forces*, Vol. 2, Consultants Bureau, New York (1966), p. 150.
74. A. I. Bykhovsky, *Spreading*, Naukova Dumka, Kiev (1983).
75. P. V. Vershinin, B. V. Derjaguin, and N. V. Kirilenko, *Izv. Akad. Nauk SSSR, Ser. Geogr. Geofiz.*, 13, 108 (1949).
76. A. A. Ananyan, in: *Current Status of the Concept of Bound Water in Rock*, Izd. Akad. Nauk SSSR, Moscow (1963), p. 59; in: *Surface Forces in Thin Films and Dispersion Systems*, Nauka, Moscow (1972), p. 269; in: *Research in Surface Forces*, Vol.

- 4, Consultants Bureau, New York (1975), p. 240; *Kolloidn. Zh.*, 40, 1165 (1978).
77. Z. A. Nersesova and N. A. Tsytovich, Laboratory Study of Frozen Soil, No. 3, Izd. Akad. Nauk SSSR, Moscow (1957), p. 14.
78. B. N. Dostavalo^v and V. A. Kudryavtsev, Fundamentals of Permafrost Soil Science, Mosk. Gos. Univ., Moscow (1967).
79. L. V. Chistotinov, Moisture Migration in Freezing Water-Non-Saturated Soils, Nauka, Moscow (1973).
80. A. B. Kurzaev, V. I. Kvividze, and V. F. Kiselev, Biofizika, 20, 544 (1975); in: Bound Water in Dispersion Systems, No. 4, Mosk. Gos. Univ., Moscow (1977), p. 156.
81. A. R. Jumikis, Highway Res. Board, No. 40, 179 (1958); Highway Res. Rec., No. 209, 86 (1967); in: Second International Conference on Permafrost Soil Science, Yakutsk (1973), p. 305.
82. J. W. Cary and H. F. Mayland, *Soil Sci. Soc. Am. Proc.*, 36, 549 (1972).
83. V. A. Kudryavtsev, E. D. Ershov, and V. G. Cheverev, in: Second International Conference on Permafrost Soil Science, No. 4, Yakutsk (1973), p. 125; *Vestn. Mosk. Gos. Univ., Geol.*, No. 5, 26 (1973).
84. E. D. Ershov, E. Z. Kuchukov, and I. A. Komarov, Sublimation of Ice in Disperse Rock, Mosk. Gos. Univ., Moscow (1975).
85. A. S. Katysheva, Bulletin of Agrophysics Research, Agrofiz. NII VASKhNIL, Leningrad, No. 21, 8 (1974); No. 24, 14 (1975); No. 26, 58 (1976).
86. A. M. Globus and S. V. Nerpin, *Dokl. Akad. Nauk SSSR*, 133, 1422 (1960).
87. M. Vignes-Adler, *J. Colloid Interface Sci.*, 60, 162 (1977).
88. R. R. Gilpin, *J. Colloid Interface Sci.*, 68, 235 (1979).
89. B. V. Derjaguin and N. V. Churaev, *J. Colloid Interface Sci.*, 67, 391 (1978); *Kolloidn. Zh.*, 42, 842 (1980).
90. V. Ya. Khaimov-Mal'kov, in: Growth of Crystals, Vol. 2, Izd. Akad. Nauk SSSR, Moscow (1959), p. 5.
91. V. P. Romanov, E. A. Nechaev, and G. V. Zvonareva, *Kolloidn. Zh.*, 38, 1009 (1976).
92. V. M. Moskvin, M. M. Kapkin, A. N. Savitsky, and V. N. Yav-makovsky, Concrete for Construction in Severe Climatic Conditions, Stroizdat, Leningrad (1973).
93. M. Vignes and K. M. Dijkema, *J. Colloid Interface Sci.*, 49, 165 (1974).
94. G. F. Ershova, Z. M. Zorin, and N. V. Churaev, *Kolloidn. Zh.*, 37, 208 (1975); 41, 19 (1979).
95. M. Biermans, K. M. Dijkema, and D. A. De Vries, *J. Hydrol.*, 37, 137 (1978).
96. P. Hoekstra, *Soil Sci. Soc. Am. Proc.*, 33, 512 (1969).
97. B. D. Kay and W. S. Scott, *Can. J. Soil Sci.*, 53, 421 (1973).
98. G. H. Brandt, *Highway Res.*, No. 393, 30 (1972).
99. G. D. Voroshilov, in: Second International Conference on Permafrost Soil Science, No. 4, Yakutsk (1973), p. 74.

100. T. N. Zhestkova, in: *Permafrost Research*, No. 13, Mosk. Gos. Univ., Moscow (1973), p. 205.
101. D. H. Everett, *Trans. Faraday Soc.*, 57, 1541 (1961).
102. D. H. Everett and J. M. Haynes, *Bull. RILEM*, No. 27, 31 (1965).
103. P. G. Loch and P. D. Miller, *Soil Sci. Soc. Am. Proc.*, 39, 1036 (1975).
104. S. S. Barer, O. A. Kiseleva, V. D. Sobolev, and N. V. Churaev, *Kolloidn. Zh.*, 43, 627 (1981).
105. B. V. Derjaguin, N. V. Churaev, V. D. Sobolev, and S. S. Barer, *J. Colloid Interface Sci.*, 84, 182 (1981).
106. O. A. Kiseleva, Ya. I. Rabinovich, V. D. Sobolev, and N. V. Churaev, *Kolloidn. Zh.*, 41, 1074 (1979).
107. S. S. Barer, N. V. Churaev, B. V. Derjaguin, O. A. Kiseleva, and V. D. Sobolev, *J. Colloid Interface Sci.*, 74, 173 (1980).
108. H. H. G. Jellinek, *J. Colloid Interface Sci.*, 25, 192 (1967).

CONCLUSION

We hope that it is now clear how some of the components of surface forces have been given a thorough theoretical foundation. Their effects in colloid systems and liquid films can be calculated with sufficient accuracy for practical purposes. This is mainly true for molecular and electrostatic forces. The difficulties that still remain here reflect the insufficient knowledge of the spectral characteristics of the interacting bodies, especially in the frequency range around 10^{16} rad/s, which is the region that gives the main contribution to the dispersion interaction. Difficulties also appear when the theory of dispersion forces is applied to interlayers of very small thickness (less than 15-20 Å), for here the discreteness of molecular structure becomes a significant factor. The problem of calculating the surface charge in the theory of electrostatic forces still awaits a complete solution.

Further progress is needed in the theory of the adsorption component of disjoining pressure – in particular, to account for the effects of solvation. Equally desirable is a direct experimental testing of the theory. Indeed, we regard this as the most urgent aim of our research.

The theory of the structural component of disjoining pressure in polar liquids and in liquids with intermolecular hydrogen bonding is still in its infancy. In all likelihood, progress will be made by methods of computer simulation – molecular dynamics and Monte Carlo techniques.

In our opinion, it is extremely important now, especially for practical applications, to expand the studies (first of all, with

model systems) of mass exchange processes in colloid systems, micro-porous materials and films, where the mechanism and kinetics of the phenomena are largely determined by surface forces. By introducing the disjoining pressure isotherms of thin interlayers and films into the appropriate calculations of mass transfer, it will be possible to pass from a purely phenomenological to a strictly quantitative description based on molecular-kinetic models of the phenomena.

Progress in surface forces research has been very rapid in recent years. Consequently, when this book is published, it will not mention many a paper that may be known to readers by that time. The authors hope to correct this shortcoming, as well as other less apparent defects, which are unavoidable in a first attempt at covering such a wide field of investigations, in later editions.

INDEX

- Adhesion between beads, 50
Adhesion of particles to plates, 39
Adsorption by dispersion forces, 154-157
at interacting surfaces, 157-158
Alkanes on carbon black, 253
Attractive forces between bodies
chromium, 129, 130
Langmuir-Blodgett multilayers, 136
mica, 131-134
quartz, 94-96, 129
stearic acid monolayers, 135
thallium halides, 96
wires (metals, etc.), 136-141
- Birefringence of water in montmorillonite, 242-243
Bjerrum-Larsson theory, 386
Black films, theory of, 82
secondary, 219
"Blow-off" technique, 253-264
principle of, 253-255
refined method, 255-257
thickness profile of amyl sebacate, 257-258
of butyl palmitate, 258
velocity profile of Vaseline oil, 257
- Boundary layers of betol, piperine, diphenylamine, and thymol, 252
of nonpolar liquids, 252-253
oscillations of density, theory of, 252
indicated by force measurements, 252-253
- Capillary osmosis, *see under Transport phenomena*
Conclusion (summing up), 433-434
Contact angle, 75, 81, 340, 341, 343, 350, 351
Convective diffusion, 383
Cyclohexane boundary layers, 252-253
- Debye length, 12, 339, 346
radius, 386
Density of water in narrow pores, 240-242
Derjaguin-Landau-Verwey-Overbeek theory, *see under DLVO theory*
Diffuse adsorption layers, nonionic, 151
Diffusion in boundary layers, 237
Diffusiophoresis, *see under Transport phenomena*
Discreteness of charge, effect on interactions, 210-218
Disjoining pressure, 25-51
adsorption component, theory of, 151-172
and contact angle, 59
at curved surfaces, 39-40
definition, 27-31
electrostatic component, 173-230
approximate formulas, 185-189
at constant charge or constant potential, 181-183

- Disjoining pressure
electrostatic component
(continued)
identical layers, 179-181
in asymmetrical electrolytes, 183-185
methods of calculating, 173-178
experimental studies, 271-283
alcohol on glass, 272
between hydrophobic surfaces, 280-281
by crossed-fibers method, 274-275
effect on colloid stability, 281
in clays, 281-282
in electrolyte solutions, 275-280
in phospholipid bilayers, 282
influence of cations, 278-280
water on glass and quartz, 272, 273
in films under gravity, 40-44
in free films, 218-222
in wetting films, 328-359
isotherm, 29
negative, 27, 29
refinement of definition, 36-40
steric component, 152
structural component, theory of, 264-271
theoretical oscillations in, 268, 269
Dispersion constants for water, quartz, etc., 118
Dispersion forces
London's theory, 98
between macroscopic bodies
by summation method, 98-100
comparison of theory and experiment, 106, 128-146
Hamaker's theory, 98-99, 101
Lifshitz's theory, 100-106
theories, 98-106
between solids, direct measurements, 88-98
historical background, 85-88
in surface science, 85-171
Dispersion function from spectral data, 114-118
- DLVO theory of colloid stability, 293-310
conditions for reversible coagulation, 307
effect of charging mechanism, 302-305
effect of retardation, 306
exact solution, 300-302
further developments, 305-308
Dzyaloshinsky-Lifshitz-Pitayevsky theory, 109-110
- Eilers-Korff rule, 298, 304
Electrical double layers, 8-19
at curved surfaces, 15
Debye-Hückel approximation, 12-13
diffuse part, 9-16
discreteness of charge effect, 16
formation and structure, 8-9
formed by ionogenic groups, 18
Gouy-Chapman theory, 10-11
Grahame model, 18-19
interacting, *see under Interaction*, and *under DLVO theory*
Langmuir formula, 15
planar, exact formulas, 13-15
Stern theory, 16-17
tests of models, 18-19
Electrostatic charges on glass, etc., 93
Electroviscosity, 236
"Film elasticity," 41
Five-layer systems, interactions in, 123-126
Flow through narrow pores, 237-238
Flow-ultramicroscope, 306-308
Free energy of interacting electrical double layers, 189-193
Free films
exchange of volatile components, 71-73
local fluctuations in, 69
stable, 74
stepped, 74-76
theory of measurement of disjoining pressure in, 76-82

- Force measurements: methods
beads, 139
cantilevered spring (Overbeeck-Sparnaay), 107
crossed fibers (Rabinovitch et al.), 136-137
electronic microbalance (Derjaguin-Abrikossova), 91-93
in liquids (Rabinotich: Israelachvili-Adams), 142
jump method, 131
mica cylinders (Tabor-Winterton), 131-135
vibration methods, 130, 133
- Frost heaving of soil, 418, 421, 422
- Hamaker constant, 99, 111, 353, 354, 355, 358
from force barrier, 226-227
- Heterocoagulation, 311-325
applications, 325
at constant charge, 323-324
conditions for adhesion, 315-317, 319, 322
dispersions with negative Hamaker constant, 319-323
dispersions with positive Hamaker constant, 312-319
experimental checks, 324
kinetics of, 324-325
later developments, 323-324
theory, 311-324
- Heterointeraction of double layers, 198-210
- Hydration of ions, effect on force barrier, 226
- Ice lenses, 411, 417, 418, 419
- Image force, 7
- Ionized surfaces
bodies with curved surfaces, 46-51
dissimilar double layers, 198-210
spherical double layers, 193-197
tests of models, 18-19
- Interaction of double layer: experimental studies, 222-227
force barrier, with crossed wires, 223-227
- Interactions through an interlayer, 119-123
- Isodynamic curves, method of, 199-200
- Langbein's treatment of dispersion interactions, 124-125
- Langmuir's equations for interacting double layers, 179, 183, 186, 222
- Lebedev's theory of molecular forces, 85-86
- Lifshitz's theory of interaction of macroscopic bodies, 6-7, 100-106
current status of, 109-128
- Liquid-crystalline structure in boundary layers, 244-252
- London's theory of dispersion forces, 5, 98
- Lyophobic colloids, 293-324
coagulation criteria, 297-300
coagulation into secondary minimum, 307-308
coagulation kinetics, 296-297, 305
coagulation threshold, 298, 303, 305, 308
effect of electrolytes, 293-294
energy barrier, 294-295
periodic systems, 305
secondary minimum, 307-308
studied by flow ultramicroscope, 306-307
- Marangoni-Gibbs principle, 74
- Mechanocaloric effect, 394
- Molecular forces near interfaces, 4-8
- Nematic liquid-crystalline state, theory of, 249-251
- Nernst equation, 8

- Nitrobenzene boundary films, 244-249
 birefringence, 247-248
 heat capacity, 245-247
 liquid-crystalline structure, 244-249
 UV absorption, 248-249
- Nonfreezing water, 409, 410, 415, 416, 419, 421, 422, 425
- Octamethylcyclotetrasiloxane boundary layers, 252
- Poisson-Boltzmann equation, 10, 11
- Polar benzene derivatives, liquid-crystalline boundary layers of, 249-252
- Polymolecular adsorption of water, 353
- Pressure, disjoining, *see under* joining pressure
- Pressure distribution in interlayers, 33-36
- Quartz, dispersion properties of, 105-108
- Retardation, electromagnetic, 5, 98
- Retardation of dispersion force, 5, 98, 99, 106, 128, 133, 141, 142
- Reverse osmosis, *see under* Transport phenomena
- Roughness, *see* Surface roughness
- Rytov's theory of electromagnetic fluctuations, 101
- Schulze-Hardy rule, 298
- Secondary minimum, 307-308
- Smoluchowski's theory, 296
- "Solvation" of surfaces, 231
- Stabilization by dispersion force adsorption, 168-169
- Stern layer, 16-17
- Structural component of disjoining pressure, 231-283
- Structural forces, 223
- Surface energy, etc. (Gibbs), 4
- Surface energy of solids, 3
- Surface roughness, effect on interaction force, 134, 135, 139, 146
- Swelling pressure, 51
- Thin films
- between convex bodies, 55-57
 - between fluid bodies, 59-82
 - between parallel plates, 53-54
 - flow in, 44-45
 - thermodynamic theory of, 53-82
- Thermocrystallization flow, *see under* Transport phenomena
- Thermocrystallization mass flux, 412
- Thermodynamics of irreversible processes, 371-372, 380-381, 383, 391-393, 403, 412-413
- Thermoelectro-osmotic coefficient, 405, 407
- Thermokinetic phenomena, 394
- Thermomechanical effect, 394, 395
- Thermo-osmosis, 390-409
- Thermophoresis, 394, 408
- Transport phenomena
- capillary osmosis, 369-380
 - experimental studies, 374-376
 - in ionic solutions, 376-378
 - in very fine pores, 378-380
 - diffusiophoresis, 388-390
 - experimental scheme, 388-389
 - for coating, 390
 - in electrolytes, 390
 - possibly occurs in cells, 390
 - mechanocaloric effect, 394
 - reverse osmosis, 380-388
 - capillary osmotic counterflow, 385
 - distribution coefficients, 386-388
 - in electrolytes, 385-388
 - membranes, 381-388
 - technical uses, 381
 - surface forces in, 369-496
 - thermocrystallization flow in nonfreezing interlayers, 409-426
 - experimental studies, 419, 422, 424-426

- Transport phenomena
thermocrystallization flow in nonfreezing interlayers
(continued)
relation to disjoining pressure, 413, 415, 421
thermoelectric coefficient, 404
thermoelectro-osmotic co-efficient, 405, 407
thermokinetic phenomena, 394
thermomechanical effect, 394, 395
thermo-osmosis, 390-393, 395, 406, 408-409
experimental studies, 396-409
thermophoresis, 394, 408
- Viscosity of water in boundary layers, 234-237, 240
in nonfreezing interlayers, 240
- Viscosity in boundary layers, 258-263
silicone oils, 261-263
turbine oil, 260
vinypol solutions, 259
- Water
birefringence in montmorillonite, 242-243
density in microporous zeolite, 242
density in narrow pores, 240-242
IR spectrum in boundary layers, 244
nonfreezing interlayers, 238-240
permittivity in montmorillonite, 243
solvent power in boundary layers, 244
structural changes at surfaces, 232
effect of temperature, 233
effect on flow in narrow capillaries, 233-240
viscosity in boundary layers, 240
- Wetting films, 327-367
disjoining pressure in, 328-330
- Wetting films (continued)
disjoining pressure isotherms, 338-359
 α - and β -branches, 340-344
alkanes on alumina, 355
alkanes on steel, etc., 355, 356
alkanes on water, 358, 359
comparison of theory and experiment, 345-349
component forces, 339
dominance of electrostatic forces in thick films, 348-349
effect of surface roughness, 353, 354, 355, 357
for α -films, 349-352
helium on fluorides, 354
influence of gel layer, 352-353
nonpolar liquids, 353
relation to molecular forces, 347-348
relation to surface potential, 347
S-shaped, 340
tetradecane, etc. on steel, 355-357
tetradecane on quartz and mica, 357, 358
experimental techniques for study, 330-338
acoustic interference method, 336, 354
capillary method, 334
Derjaguin-Kussakov method, 330-331
developments in the Derjaguin-Kussakov method, 331-334
dynamic method, 337-338
other static methods, 336-337
quartz transducer method, 336, 353, 354
stack-of-plates method, 336
vapor adsorption methods, 335-337
in capillaries, 362-363
nonpolar liquids, 353-359
on concave surfaces, 361-363

Wetting films (continued)
on convex surfaces, 360-361
on flat surfaces, 359-363
relevance to various
processes, 327
stability of, 57-59
"thick" and "thin" films, 328
work of Derjaguin and
Kussakov, 222